α-L-Fucosylated precision glycomacromolecules for binding studies with viral and bacterial lectins

Inaugural-Dissertation

zur Erlangung des Doktorgrades
der Mathematisch-Naturwissenschaftlichen Fakultät
der Heinrich-Heine-Universität Düsseldorf

vorgelegt von

Katharina Susanne Bücher
aus Frankfurt am Main

Düsseldorf, September 2018

aus dem Institut für organische und makromolekulare Chemie
der Heinrich-Heine-Universität Düsseldorf

Gedruckt mit der Genehmigung der
Mathematisch-Naturwissenschaftlichen Fakultät der
Heinrich-Heine-Universität Düsseldorf

Referent: Prof. Dr. Laura Hartmann
Koreferent: Prof. Dr. Jörg Pietruszka

Tag der mündlichen Prüfung: 14.02.2019

Was wir wissen ist ein Tropfen,
was wir nicht wissen ein Ozean

(Isaac Newton)

Danksagung

Zunächst möchte ich mich bei meiner Professorin Dr. Laura Hartmann bedanken für die Möglichkeit an diesem interessanten Thema innerhalb des ViroCarb-Projektes zu arbeiten und meine Ergebnisse auf Konferenzen zu präsentieren. Darüber hinaus möchte ich mich für die regelmäßigen Diskussionen sowie den wissenschaftlichen und praktischen Gestaltungsfreiraum während meiner Arbeit bedanken.

Außerdem möchte ich mich bei meinem Mentor Prof. Dr. Jörg Pietruszka für die hilfreichen Ratschläge und die Begutachtung dieser Arbeit bedanken.

Meinen vielen Kooperationspartnern möchte hiermit ebenfalls danken, insbesondere Dr. Filip Kovacic und Nikolina Babic für die mELLA- und Biofilm-Assays und die gute Zusammenarbeit. Ein großer Dank geht an Dr. Charlotte Uetrecht und Hao Yan (Panda) für die umfangreichen nativen MS-Messungen sowie Prof. Dr. Thomas Peter, Robert Creutznacher und Dr. Alvaro Mallaragay für die NMR-Studien. Ebenso danke ich Dr. Grant Hansman, Kerstin Ruoff und Turgay Kilic für die Kristallographie-Studien, Dr. Andrea Grafmüller für die Kalkulationen, Jun.-Prof. Dr. Stephan Schmidt für die DLS-Messungen, Sabrina Weickert, Anna Rubailo und Prof. Malte Drescher für EPR-Messungen und Dr. Nicole Snyder für viele hilfreiche Tipps. Ein großes Dankeschön geht an meine Koautoren aus der Arbeitsgruppe von Prof. Hartmann, Tanja Freichel, Patrick Konietzny und meinen ehemaligen Masterstudenten Jan Dirks.

Ich danke Maria Beuer (NMR-Messungen) und Dr. Peter Tommes (MALDI-TOF-MS-Messungen) für die Flexibilität und hervorragende Messqualität sowie Michaela Kitza für ihre herzliche und hilfsbereite Art.

Last but not least, danke ich der Arbeitsgruppe von Prof. Hartmann für das gute Klima und die schöne Gruppenfahrt nach Holland. Dr. Stephen Hill danke ich für die ausgiebigen sprachlichen Korrekturen meiner Arbeit (thank you very much, Steven). Für besondere Hilfsbereitschaft, Kollegialität und gute Stimmung danke ich Christoph Gerke, Tanja Paul, Alexander Strzelczyk, Markus Giesler, Fawad Jacobi, Özgür Capar und Josip Stipanovic. Ich danke Sebastian Bauer für die vielen IT-Hilfsaktionen und Mischa Baier für den stetigen wissenschaftlichen Austausch und die schönen gemeinsamen Kooperationstreffen. Bei meinem Büronachbarn Peter Pasch möchte ich mich für die gute Atmosphäre bedanken, die mir das letzte Jahr erleichtert hat.

Allen voran möchte ich mich hiermit von Herzen bei meinen Eltern Christine Bücher und Prof. Dr. Karlheinz Bill bedanken für die vielseitige Unterstützung, die wertvollen Ratschläge und dafür, dass sie immer ein offenes Ohr haben.

Mein größter Dank geht an meinen Partner Felix Schossau für seine unbegrenzte und außergewöhnlich große Unterstützung in jeglicher Hinsicht, seine Liebe und sein festes Vertrauen in mich, was mich immer motiviert hat.

Publications in context of this thesis

- **Fucose-functionalized precision glycomacromolecules targeting human norovirus capsid protein**, Katharina Susanne Bücher, Hao Yan, Robert Creutznacher, Kerstin Ruoff, Alvaro Mallagaray, Andrea Grafmüller, Jan Sebastian Dirks, Turgay Kilic, Sabrina Weickert, Anna Rubailo, Malte Drescher, Stephan Schmidt, Grant Hansman, Thomas Peters, Charlotte Uetrecht, Laura Hartmann, *Biomacromolecules* **2018**, *19* (9), 3714–3724.

- **Monodisperse sequence-controlled α-L-fucosylated glycooligomers and their multivalent inhibitory effects on LecB**, Katharina Susanne Bücher, Nikolina Babic, Tanja Freichel, Filip Kovacic, Laura Hartmann, *Macromol. Biosci.* **2018**, *18,* 1800337 (1-8).

- **Heteromultivalent glycooligomers as mimetics of blood group antigens**, Katharina Susanne Bücher, Patrick Benjamin Konietzny, Nicole L. Snyder, Laura Hartmann*, Chem. Eur. J.* **2019**, *25* (13), 3301-3309.

Related presentations

- **Addressing multivalent interactions of α-L-fucosylated glycooligomers with Norovirus capsid protein**, K. Bücher, H. Yan, R. Creutznacher, A. Mallagaray, K. Ruoff, T. Kilic, G. Hansman, T. Peters, C. Uetrecht, L. Hartmann, 1. International Symposium on Glycovirology (2018), Schöntal, poster presentation.

- **Monodisperse fucosylated glycooligomers to investigate multivalent binding to LecB**, K. Bücher, L. Hartmann, 255th annual meeting of the ACS (American Chemical Society) (2018), New Orleans, USA, talk.

- **Sequence-defined α-L-fucose functionalized oligo(amidoamines) for binding studies with human Norovirus capsid protein**, K. Bücher, L. Hartmann, PhD-Symposium of FOR2327 ViroCarb of the DFG (Deutsche Forschungsgemeinschaft), Heinrich-Pette-Institut (2017), Hamburg, talk.

The work presented in this thesis has led to three first-author publications that are used as base for this thesis, resulting in a chapter-based work. The specific contributions on each publication is described immediately before the corresponding chapter.

Table of Contents

List of abbreviations

ADS	Alloc diethylenetriamine succinyl building block
AIDS	Acquired immune deficiency syndrome
AS	Aminoacid
ATRP	Atom transfer radical polymerization
BADS	*p*-(Azidomethyl)benzoyl diethylenetriamine succinyl building block
BB	Building block
BDS	Boc diethylenetriamine succinyl building block
Boc	*tert*-Butyloxycarbonyl
BOP	Benzotriazol-1-yl-oxy-tris(dimethylamino)phosphonium hexafluorophosphate
$CDCl_3$	Deuterated chloroform
CFRP	Controlled free radical polymerization
CRD	Carbohydrate recognition domain
CSP	Chemicla shift perturbation
CuAAC	Copper-catalyzed azide-alkyne cycloaddition
DCC	Dicyclohexylcarbodiimide
DCM	Dichloromethane
DDS	Double bond diethylenetriamine succinyl building block
DI	Dispersity index
DIPEA	Diisopropylethylamine
DLS	Dynamic light scattering
DMF	Dimethylformamide
DMSO	Dimethylsulfoxide
DNA	Desoxyribonucleic acid
D_2O	Deuterated water
iso-DTDS	*iso*-Di-triple bond diethylenetriamine succinyl building block
EDS	Ethylenedioxy-bis(ethylamine) succinyl building block
ELLA	Enzyme linked lectin assay
EGF	Epidermal growth factor
EPR	Electron paramagnetic resonance
ESI MS	Electrospry ionization mass spectrometry
EtOH	Ethanol
Fmoc	Fluorenylmethoxycarbonyl
FTLD	F-type lectin domain
Fuc	L-Fucose
FUT	Fucosyltransferase genes
Gal	Galactose
GalNAc	*N*-Acetyl-D-galactosamine
GDP-fucose	Guanosine-5´-diphospho-L-fucose
Glc	D-Glucose
GlcNAc	*N*-Acetyl-D-glucosamine
GTA	α(1,3)Galactoseaminyltransferase of antigen A
GTB	α(1,3)Galactosyltransferase of antigen B
HATU	1-[Bis(dimethylamino)methylene]-1*H*-1,2,3-triazolo[4,5-b]pyridinium-3-oxid hexafluorophosphate
HBGA	Histo-blood group antigen
HBTU	2-(1*H*-Benzotriazol-1-yl)-1,1,3,3-tetramethyluronium-hexafluorophosphat
Hex	Hexane
HF	Hydrofluoric acid
HMO	Human milk oligosacharide
HMPA	Hexamethylphosphoric acid triamide

HOBt	1-Hydroxybenzotriazole
HR-ESI	High resolution electrospray ionization
IC_{50}	Inhibitor concentration at half-maximal inhibition
IgM	Immunoglobulin M
ITC	Isothermal titration calorimetry
K_D	Dissoziation constant
Lac	D-Lactose
LacNAc	*N*-Acetyl-D-lactosamine
LAD II	Leukocyte adhesion deficiency type II
Le	Lewis
SLe	Sialyl-Lewis
MALDI-TOF-MS	Matrix-assisted laser desorption/ionization time-of-flight mass spectrometry
Man	D-Mannose
MD	Molecular dynamic
MDS	Methylsuccinyl diethylenetriamine succinyl building block
mELLA	Modified enzyme linked lectin assay
MeOH	Methanol
MNP	Magnetic nanoparticle
MS	Mass spectrometry
MUC-1	Mucin-1
NaOMe	Sodium methanolate
NEt_3	Triethylamine
NMP	Nitroxide-mediated polymerization
NMR	Nuclear magnetic resonance spectroscopy
NP	Nanoparticle
ODS	Octyl diamine succinyl building block
PAA	Polyacrylamide
PAMAM	Poly(amidoamine)
PEG	Polyethylene glycol
polyNIPAM	Poly(*N*-isopropylacrylamide)
PyBOP	Benzotriazol-1-yl-oxytripyrrolidinophosphonium-hexafluorophosphate
PyBrOP	Bromotripyrrolidinophosphonium hexafluorophosphate
RAFT	Reversible addition fragmentation chain transfer polymerization
RNA	Ribonucleic acid
RO(M)P	Ring opening (metatesis) polymerization
RP-HPLC	Reversed-phase high-performance liquid chromatography
RT	Room temperature
SA	Streptavidin
SDS	Sodium dodecyl sulfate
SI	Supporting informations
Sia	Sialic acid
$SiEt_3$	Triethylsilane
SPPS	Solid phase peptide synthesis
SPPoS	Solid phase polymer synthesis
SPR	Surface plasmon resonance spectroscopy
STD NMR	Saturation transfer difference nuclear magnetic resonance spectroscopy
TDS	Triple bond diethylenetriamine succinyl building block
TFA	Trifluoroacetic acid
TFA-OEt	Ethyl trifluoroacetate
TIPS	Triisopropylsilane, triisopropylsilyl group (in bound form)
TRIS	Tris(hydroxymethyl)aminomethane
UV/Vis	Ultraviolett/visible

1 Abstract

Carbohydrate-lectin interactions mediate a great number of important biochemical processes like inflammation, immune response, fertilization and blood group determination. Glycomimetics such as glycopolymers presenting several carbohydrate ligands on a synthetic scaffold have been shown to be useful tools to investigate carbohydrate-lectin interactions and learn more about the underlying multivalent binding mechanisms. Furthermore, glycomimetics have a great potential as modulators in biomedical applications such as in vaccination or biosensing or might serve as alternative antibiotics.

Previously Hartmann *et al.* introduced a new class of glycomimetics based on the solid phase synthesis of monodisperse, sequence-controlled glycooligo(amidoamines). Predominantly mannosylated and galactosylated glycooligomers were investigated to explore fundamental aspects of their multivalent binding behavior to the plant lectin Concanavalin A. However, multivalent carbohydrate-lectin interactions are also important in many adhesion and infection processes of pathogens.

Therefore, in the present work, the synthesis of glycooligo(amidoamines) has been extended to yield glycomimetics targeting two crucial pathogenic lectins; on the one hand the viral capsid protein P-dimer of human Norovirus, which represents the major cause of non-bacterial gastroenteritis worldwide. The second lectin is LecB, that is expressed by the hospital bacterium *Pseudomonas aeruginosa,* which often exhibits antibiotics resistances caused by the formation of dense biofilms. Both lectins bind fucosylated glycans on cell surfaces, most of all as part of the histo blood group antigens (HBGA).

Thus, fucosylated glycooligo(amidoamines) were synthesized for studies of their binding and inhibition behavior towards P-dimer and LecB. In order to address the lectins binding pockets (**a**) a series of homomultivalent fucosylated glycooligomers has been created and (**b**) a new double-clickable building block was developed for (**c**) the facilitated solid phase polymer synthesis of heteromultivalent fucosylated glycooligomers to mimic more complex glycan structures such as HBGA (see Figure 1).

The homomultivalent fucosylated glycooligomers were generated following previously established protocols of solid phase polymer synthesis (SPPoS) and Cu-mediated conjugation reaction using an alkyne-functionalized building block and an azide-functionalized α-L-fucose ligand. Glycooligomers with different valences (number of fucose side chains) with one up to six fucose units, with varying spacing exhibiting no or up to three ethyleneglycol-based spacer building blocks between the fucose units as well as with differing overall oligomer chain lengths ranging from four up to nine building blocks were successfully synthesized.

In addition, a new strategy for the construction of heteromultivalent glycooligomers was introduced by the development of the new functional double-clickable building block *iso*-DTDS. This building block exhibits a phenylene branching unit in the side chain with two alkyne groups in meta-positions of which one is equipped with a TIPS protecting group. This enables the consecutive attachment of different carbohydrates in high proximity to each other. *iso*-DTDS was successfully applied in SPPoS for the synthesis of heteromultivalent fucosylated glycooligomers as multivalent mimicry of more complex carbohydrates like HBGA (blood group antigens A and B and sLe[a]) as well as 2`fucosyllactose.

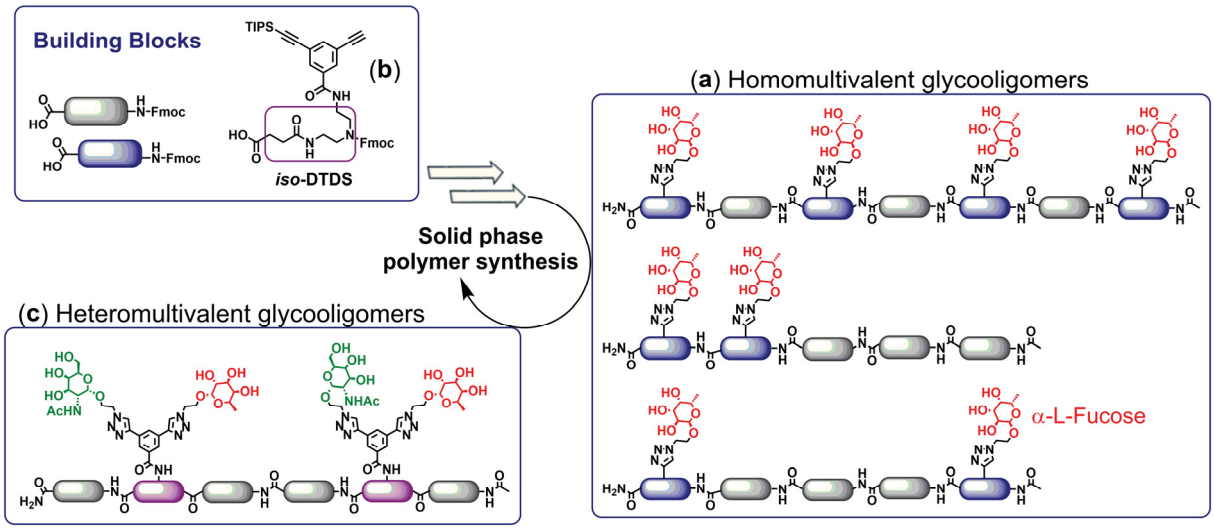

*Figure 1: Schematic representation of homomultivalent fucosylated glycooligomers (**a**), building blocks containing the generated iso-DTDS building block (**b**) and heteromultivalent fucosylated glycooligomers based on iso-DTDS (**c**).*

Both types of glycooligomers were then subjected to a number of binding studies in close collaboration with partners from virology and bacterial enzymology. First, looking at the interactions of homomultivalent fucosylated glycooligomers towards viral P-dimer, K_D-values of glycomimetics show that the binding towards P-dimer is about 2-3 times reduced in comparison to the natural ligand, the blood group B tetrasaccharide (HBGA B), as determined by native mass spectrometry (native MS) by Hao Yan and Dr. Charlotte Uetrecht. Although fucose is a very weak binder for P-dimer, results of epitope mapping by STD NMR experiments (saturation transfer difference NMR) (determined by Robert Creutznacher, Dr. Alvaro Mallagaray, Prof. Dr. Thomas Peters) as well as successful co-crystallization experiments of glycooligomers with P-dimer (performed by Kerstin Ruoff, Dr. Turgay Kilic, Dr. Grant Hansman) have shown that binding takes place with the fucose side chains and not with the scaffold or linker of the oligomer. However, the results suggest that all glycooligomers only use one fucose ligand to bind to one of the four known binding sites of P-dimer independent of the valence, spacing between fucose side chains and size of the glycooligomers.

A potential reason for this monovalent binding could be the flexibility of the oligo(amidoamine)-backbone structures leading to randomly coiled conformations as suggested by DLS measurements, performed by Jun.-Prof. Dr. Stephan Schmidt, and MD simulation, calculated by Dr. Andrea Grafmüller. However, also the protein receptor itself seems to hamper multivalent binding through potential structural changes upon ligand interaction.

Both homo- and heteromultivalent fucose-oligomers were tested for their binding to bacterial protein receptor LecB performing an inhibition-competition assay via surface plasmon resonance (SPR) measurements, that was specifically developed as part of this work. The results of binding studies with the homomultivalent structures showed that with increasing amount of fucose side chains the inhibitory effects on LecB are increased. The inhibitory potential of the glycooligomers was found to be about 2-3 times enhanced per fucose side chain compared to α-L-methylfucose describing a linear trend. The increased inhibitory effect of the fucosylated glycooligomers was further confirmed by ELLA assays, performed by Nikolina Babic and Dr. Filip Kovacic, who could also show the potential of fucosylated glycooligomers as inhibitors in LecB mediated biofilm formation.

When looking at the heteromultivalent HBGA mimetic glycooligomers, no improved inhibitory effects on LecB could be observed. Interestingly, the homomultivalent glycooligomer with four fucose units did not show better inhibition than the comparable homo- or heteromultivalent structures with only two fucose side chains. Thus, binding affinities do not benefit from the presentation of multiple fucose ligands in close proximity but rather from a higher number of ligands with larger spacing. Again, these findings support the design of next generation fucosylated glycooligomers as inhibitors of bacterial adhesion. The concept of introducing carbohydrate ligands in close proximity on the oligomeric backbone, either in homo- or heteromultivalent fashion, will further be explored also targeting other lectins such as bacterial FimH receptor.

2 Zusammenfassung

Kohlenhydrat-Lektin-Wechselwirkungen vermitteln eine Vielzahl wichtiger biochemischer Prozesse wie Entzündungen, Immunantwort, Befruchtung und Blutgruppenbestimmung. Glykomimetika wie zum Beispiel Glykopolymere, die mehrere Kohlenhydratliganden an einem synthetischen Gerüst präsentieren, haben sich als geeignete Werkzeuge zur Erforschung von Kohlenhydrat-Lektin-Wechselwirkungen und der zugrundeliegenden multivalenten Bindungsmechanismen herausgestellt. Darüber hinaus haben Glykomimetika großes Potenzial als Modulatoren in biomedizinischen Anwendungen beispielsweise als Impfstoffe oder Biosensoren oder könnten als alternative Antibiotika verwendet werden.

Hartmann *et al.* haben zuvor eine neue Klasse von Glykomimetika eingeführt, die auf der Festphasensynthese von monodispersen, Sequenz-kontrollierten Glykooligo(amidoaminen) basiert. Überwiegend mannosylierte und galactosylierte Glykooligomere wurden untersucht, um fundamentale Aspekte ihres multivalenten Bindungsverhaltens an das Pflanzenlektin Concanavalin A zu erforschen. Multivalente Kohlenhydrat-Lektin-Wechselwirkungen spielen jedoch auch eine große Rolle bei Adhäsions- und Infektionsprozessen von Pathogenen.

Daher wurde in der vorliegenden Arbeit die Synthese der Glykooligo(amidoamine) erweitert, um Glykomimetika zu erhalten, die zwei hoch-relevante pathogene Lektine ansteuern; zum einen das virale Kapsidprotein P-Dimer des humanen Norovirus, welches weltweit die Hauptursache für nicht-bakteriell erzeugte Gastroenteritis darstellt. Bei dem zweiten Lektin handelt es sich um LecB, welches von dem bakteriellen Krankenhauskeim *Pseudomonas aeruginosa* exprimiert wird, das häufig Antibiotikaresistenzen aufweist, die durch die Bildung dichter Biofilme verursacht werden. Beide Lektine binden fukosylierte Glykanstrukturen an Zelloberflächen, insbesondere als Bestandteil der Histoblutgruppenantigene (HBGA).

Daher wurden fukosylierte Glykooligo(amidoamine) für Studien zu ihrem Bindungs- und Inhibierungsverhalten gegenüber P-dimer und LecB hergestellt. Um die Bindungstaschen der Lektine anzusprechen wurde (**a**) eine Serie homomultivalenter fukosylierter Glykooligomere dargestellt und (**b**) ein neuer doppel-clickbarer Baustein entwickelt für (**c**) die erleichterte Festphasenpolymersynthese von heteromultivalenten fukosylierten Glykooligomeren, um komplexere Glykanstrukturen wie HBGA zu imitieren (siehe Abbildung 1).

Die homomultivalenten fukosylierten Glykooligomere wurden nach zuvor entwickelter Methoden für die Festphasenpolymersynthese (solid phase polymer synthesis – SPPoS) und die Cu-vermittelte Konjugationsreaktion hergestellt, unter Verwendung eines Alkin-funktionalisierten Bausteins und eines Azid-funktionalisierten α-L-Fukoseliganden. Glykooligomere mit unterschiedlichen Valenzen

(Anzahl der Fukoseeinheiten) mit einer bis zu sechs Fukoseeinheiten, mit variierenden Abständen mit null bis zu drei Ethylenglykol-basierten Abstandsbausteinen zwischen den Fukoseeinheiten sowie mit unterschiedlicher Gesamtlänge des Oligomergerüsts mit vier bis neun Bausteinen wurden erfolgreich synthetisiert.

Darüber hinaus wurde mit der Entwicklung des neuen funktionellen doppel-clickbaren Bausteins *iso*-DTDS eine neue Strategie zum Aufbau heteromultivalenter Glykooligomere eingeführt. Dieser Baustein weist als Seitenkette eine Phenylen-Verzweigungseinheit mit zwei Alkingruppen in *meta*-Position auf, eine davon ausgestattet mit einer TIPS-Schutzgruppe. Dies ermöglicht die aufeinanderfolgende Konjugation von unterschiedlichen Kohlenhydrateinheiten in großer Nähe zueinander. *iso*-DTDS wurde erfolgreich in der SPPoS angewendet, um heteromultivalente fukosylierte Glykooligomere als multivalente Mimetika komplexer Kohlenhydratstrukturen herzustellen, wie HBGA (Blutgruppenantigene A und B, sLe^a) und 2`Fukosyllaktose.

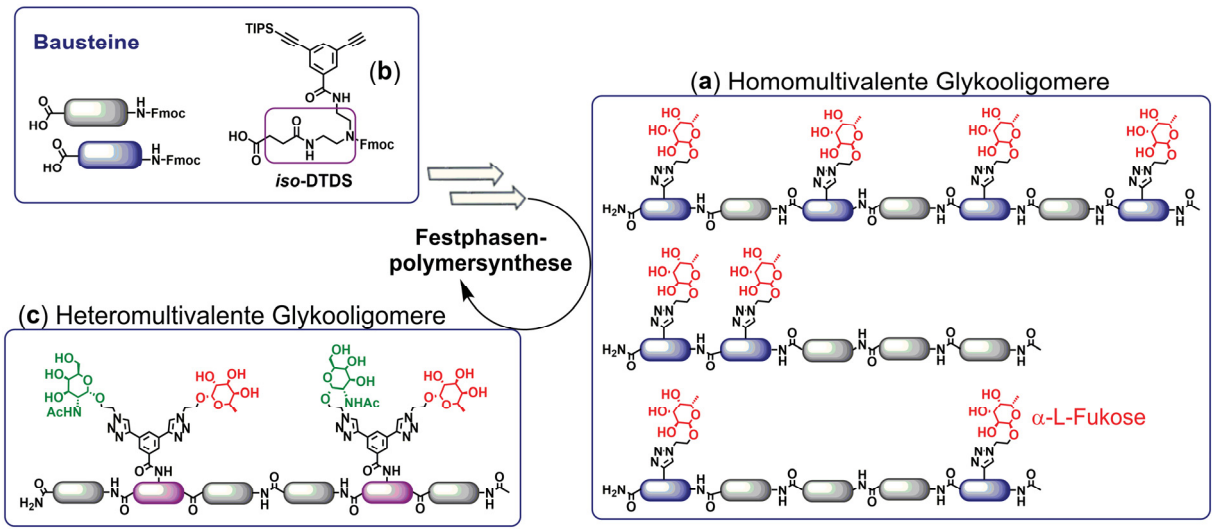

*Abbildung 1: Schematische Darstellung von homomultivalenten fukosylierten Glykooligomeren (**a**), Bausteinen, die den erzeugten iso-DTDS-Baustein enthalten (**b**) und heteromultivalente fukosylierte Glykooligomere auf Basis von iso-DTDS (**c**).*

Beide Arten von Glykooligomeren wurden anschließend in enger Zusammenarbeit mit Kooperationspartnern aus der Virologie und der bakteriellen Enzymologie in einer Reihe von Bindungsstudien untersucht. Betrachtet man zunächst die Wechselwirkungen der homomultivalenten fukosylierten Glykooligomere mit dem viralen P-dimer, zeigen die K_D-Werte der Glykomimetika eine 2-3 Mal reduzierte Bindung zum P-dimer im Vergleich zum natürlichen Liganden, dem Blutgruppentetrasaccharid B (HBGA B), was durch native Massenspektrometrie (native MS) von Hao Yan und Dr. Charlotte Uetrecht ermittelt wurde. Obwohl Fukose nur schwach an das P-dimer bindet, haben Ergebnisse von Epitopkartierungen mittels STD NMR (saturation transfer difference NMR) (bestimmt von Robert Creutznacher, Dr. Alvaro Mallagaray, Prof. Dr. Thomas Peters) sowie

erfolgreiche Co-Kristallisationen der Glykooligomere mit P-dimer (durchgeführt von Kerstin Ruoff, Dr. Turgay Kilic, Dr. Grant Hansman) gezeigt, dass die Bindung mit den Fukoseseitenketten und nicht mit dem Rückgrat oder dem Linker des Oligomergerüstes stattfindet. Jedoch zeigen die Resultate, dass alle Glykooligomere nur über einen Fukoseliganden an eine der vier bekannten Bindungstaschen des P-dimer binden, unabhängig von Valenz, Abstand zwischen den Fukoseseitenketten und Größe des Glykooligomers.

Eine mögliche Begründung für diese monovalente Bindung könnte die Flexibilität der Oligo(amidoamin)-Gerüststrukturen sein, die zu Random-Coil-Konformationen führen, was DLS-Messungen von Jun.-Prof. Dr. Stephan Schmidt und MD-Simulation, berechnet von Dr. Andrea Grafmüller, vermuten lassen. Jedoch scheint auch der Proteinrezeptor selbst die multivalente Bindung durch mögliche strukturelle Veränderungen bei der Ligandeninteraktion zu behindern.

Sowohl homo- als auch heteromultivalente Fukoseoligomere wurden auf ihre Bindung an den bakteriellen Proteinrezeptor LecB getestet, wobei ein Inhibitions-Kompetitionsassay mittels Oberflächenplasmonenresonanz-Messungen (SPR) durchgeführt wurde, der speziell im Rahmen dieser Arbeit entwickelt wurde. Die Resultate der Bindungsstudien mit den homomultivalenten Strukturen haben gezeigt, dass mit zunehmender Menge an Fukoseseitenketten die inhibitorischen Effekte gegenüber LecB verstärkt sind. Das inhibitorische Potential der Glykooligomere pro Fukose-Seitenkette ist etwa 2-3 Mal erhöht im Vergleich zu α-L-Methylfukose, einen linearen Trend beschreibend. Die verstärkte inhibitorische Wirkung der fukosylierten Glykooligomere wurde durch ELLA-Assays bestätigt, die von Nikolina Babic und Dr. Filip Kovacic durchgeführt wurden. Sie konnten ebenfalls das Potenzial der fukosylierten Glykooligomere als Inhibitoren der LecB-vermittelten Biofilmbildung zeigen.

Im Fall der heteromultivalenten HBGA-mimetischen Glykooligomere wurden keine verbesserten inhibitorischen Effekte auf LecB beobachtet. Interessanterweise zeigte das homomultivalente Glykooligomer mit vier Fukoseeinheiten keine bessere Inhibierung als die vergleichbaren homo- oder heteromultivalenten Strukturen mit nur zwei Fukoseseitenketten. Demnach profitieren die Bindungsaffinitäten nicht von der Präsentation mehrerer Fukose-Liganden in unmittelbarer Nähe, sondern eher von einer höheren Anzahl an Liganden mit größeren Abständen. Diese Ergebnisse unterstützen wiederum das Design fukosylierter Glycooligomere der nächsten Generation als Inhibitoren der bakteriellen Adhäsion. Das Konzept der Einführung von Kohlenhydratliganden in enger Nachbarschaft auf dem oligomeren Rückgrat, entweder in homo- oder heteromultiventer Weise, wird weiter erforscht werden und auch auf andere Lektine wie den bakteriellen FimH-Rezeptor abzielen.

3 General Introduction

3.1 Carbohydrate-lectin interactions – some basic information

Monosaccharides, amino acids, nucleotides and lipids are four essential basic structures in the construction of living systems. As monomers they can build up the most important biopolymeric structures such as polysaccharides, proteins and nucleic acids *e.g.* deoxyribose or ribose nucleic acid (DNA and RNA) or form supramolecular structures like lipid bilayers. These biopolymers are implicated with different cellular functions such as energy, stability, form, catalytic processes and encoding of information. In comparison to linear polypeptides or polynucleotides, oligo- and polysaccharides can be constructed not only linearly but also as branched structures due to the high variability in connectivity on different positions within a monosaccharide. The high amount of possible carbohydrate linkages results in increased structural combinations and so structural complexity. Today, it is well understood that carbohydrates do not only serve as an essential energy source and energy storage *e.g.* in the form of glucose or starch, but also are an important natural structural component *e.g.* cellulose as a key component of plant cell walls. Also, carbohydrates play key roles in information transfer, especially across membranes.[1] The crucial role of information transfer will be examined more carefully in this work.

Most cell membranes of pro- and eukaryotic cells are decorated by a dense layer of polysaccharides, oligosaccharides and glycoconjugates such as glycoproteins and glycolipids (see Figure 2). This so-called glycocalyx not only protects the cell but plays an important role for information exchange *e.g.* for intercellular cell-cell contacts, recognition and adhesion processes as well as signal transduction.[1,2] The presented carbohydrate structures can give specific signals to other cells or the environmental tissue. Additionally, many circulating proteins exhibit particular oligo- or polyglycans. Different glycosylation states are found to be characteristic for an organism, type and developmental stage of a cell or protein causing diverse contacts and signals for communication, immune response, inflammation, defense of cancer and infections, fertilization and erythrocyte blood group determination but also host-pathogen adhesion and infection.[1,3,4]

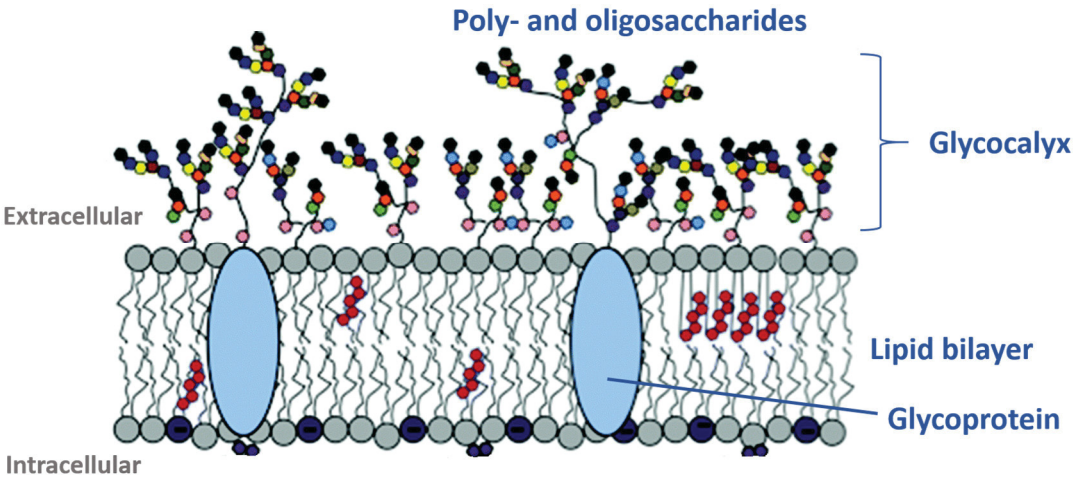

Figure 2: Schematic representation of glycocalyx, modified from literature[5].

Detection of such carbohydrate-based signals is realized by carbohydrate recognizing proteins called lectins (lat.: legere, to select). They exhibit conserved carbohydrate recognition domains (CRD) that feature a high specificity to certain carbohydrate ligands.[6,7] Carbohydrate-lectin interactions are usually weak and often display multivalent character. Indeed, multivalency in ligand-receptor binding is a fundamental mechanism in nature which modulates manifold biochemical processes.[7–10] In the case of lectins, interaction between one lectin binding pocket with one single carbohydrate ligand is often weak, but the collective interactions of multiple lectin binding sites (receptor) with multiple carbohydrates (ligand) can lead to a strong enhancement of the overall binding avidity. Avidity increases cannot only be realized by natural carbohydrate-based ligands but also through the development of artificial glycan mimetics where several carbohydrate ligands are presented on an artificial scaffold.

The following chapters will further elucidate the structure and biological function of carbohydrate ligands specifically focusing on the role of fucose and fucosylated glycans. Focus shall also be given to fucose-recognizing receptors followed by the use of precision glycomacromolecules as multivalent glycan mimetics.

3.2 Fucose and fucosylated glycans as carbohydrate ligands

Within the vast amount of different signals given by glycoconjugates predominantly seven monosaccharides account for the construction of lectin-relevant complex carbohydrates; these are galactose (Gal), *N*-acetylgalactosamine (GalNAc), glucose (Glc), *N*-acetylglucosamine (GlcNAc), mannose (Man), sialic acid (Sia) and fucose (Fuc).[1] Through the exposed position of fucose on glycan structures, it is one of the most important monosaccharide targets for recognition processes including cell-matrix and cell-cell contacts, adhesion as well as host-microbe interaction and forms the H-antigen

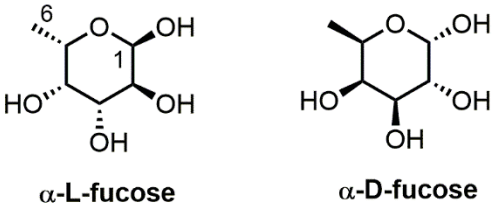

Figure 3: Fucose in α-L- and α-D-configuration.

substances, the basic compound of AB0 blood group determinants.[11–13] The fucosylation state of glycans determines developmental processes, signal cascades, immune responses and is an essential characteristic in many pathological appearances as in some cancers.[14,15] Different from other monosaccharides, fucose is a deoxyhexose lacking a hydroxyl group at 6-position (see Figure 3). This leads to a more hydrophobic character in comparison to other monosaccharides. Another important characteristic of fucose is its L-conformation in vertebrates, whereas all other monosaccharides exhibit the D-conformation. Resultantly L-fucose structurally corresponds to 6-deoxy-L-galactose.[11] Additionally, fucose is most often found in its alpha-anomeric form.[13]

Terminal fucosylation of glycoconjugates bound to glycoproteins and glycolipids on cell membranes as well as extracellular mucoproteins determines a variety of different (patho-)physiological processes. Fucosylation at *N*- and *O*-linked glycans of glycoproteins occurs posttranslationally, assisted by fucosyltransferases (gene products of FUT) with the precursor GDP-fucose.[12] Also direct transfer of L-fucose onto the hydroxyl groups of serine and threonine as protein amino acid residues is known. This so-called *O*-fucosylation can be found at epidermal growth factor (EGF) like domains.[12] Interestingly the degree of fucosylation of cell compartments in the gastrointestinal tract is recognized by specialized microorganisms.[16] *Bacteroides thetaiotamicron* that uses fucose as a carbon source reports the degree of fucosylation to the cells by activating crucial signaling cascades leading to the adjustment of fucosylation state on cells in the following.[12,17] A defective or missing fucosylation pattern can result in serious pathological disorders and diseases like cancer,[3,14,15,18] atherosclerosis or leukocyte adhesions deficiency type II (LAD II).[12,19]

3.2.1 Histo-blood group antigens (HBGA)

The terminal presentation of fucose on protein and lipid glycans exhibits a marker strategy to define and initiate diverse processes. One of the most well-known examples is the role of fucose in the AB0 blood group determining system. The responsible ABH blood group antigens represent complex fucosylated carbohydrate structures that are positioned especially on red blood cells and mucosal epithelial tissues of the gastrointestinal, respiratory and urinary tract, or in soluble form in saliva or

milk.[11–13] Bound to erythrocytes they are the most common substrates to define the blood group of each individual.[20] These antigens are recognized by immunoglobulins (IgM), specialized proteins of the immune system that can act against differing antigens leading to agglutination. As such blood group antigen presentation dictates the compatibility of blood serum in blood transfusions.[21] Though the detailed structures of both AB0 antigens and antibodies are well known and the mechanisms of binding and agglutination are widely studied, the biological function of this system is still unclear.

H antigen corresponds to blood group 0 and is created by addition of an L-fucose unit to a specified galactosylated unit forming an α(1,2)-linkage catalyzed by α-(1,2)fucosyltransferases.[11,12] In case of erythrocyte cell surfaces this fucosyltransferase is called H-transferase (gene product of FUT1). Soluble in saliva and on epithelial tissues the fucose attachment is catalyzed by the Secretor (Se) transferase (gene product of FUT2). The H antigen can act as a precursor for further modification by glycosyltransferases leading to A or B antigens (see Figure 4).[22] Attachment of a *N*-acetyl-α-D-galactosamine (α-D-GalNAc) unit to the H substance in an α(1,3)-linkage, which is catalyzed by α(1,3)galactosaminyltransferase (GTA), generates the A antigen. α(1,3)galactosyltransferase (GTB) catalyzes the transfer of an α-D-galactose, also with an α(1,3)-linkage, forming B antigen (see Figure 4). Blood group AB means that both A and B antigens are present. A very rarely occurring blood group type is the Bombay phenotype (hh) in which the concerned persons do not express the substance H (H antigen of blood group 0) due to lacking fucose.[23] This is due to mutations or deletions in genes FUT1 or FUT2 resulting in absent or inactive fucosyltransferases (H-transferase or Secretor transferase). Without the fucosylation step the transfer of galactose or *N*-acteylgalactosamine is also not possible, independent of the genotype. In case of a defective FUT2 the individuals are called non-secretors or secretor-negative because no antigen can be found in their saliva. The lack of AB0 antigens in soluble form or bound on tissues is not apparent but makes a difference in the infection rate with certain pathogens. It could be shown that non-secretors lacking the ABH antigens in the gastrointestinal mucosa are resistant to the infection of most Norovirus strains.[24,25] Individuals that have a functional secretor transferase are therefore called secretors or secretor-positive. Persons with Bombay phenotype express antibodies against A, B and even H antigen.

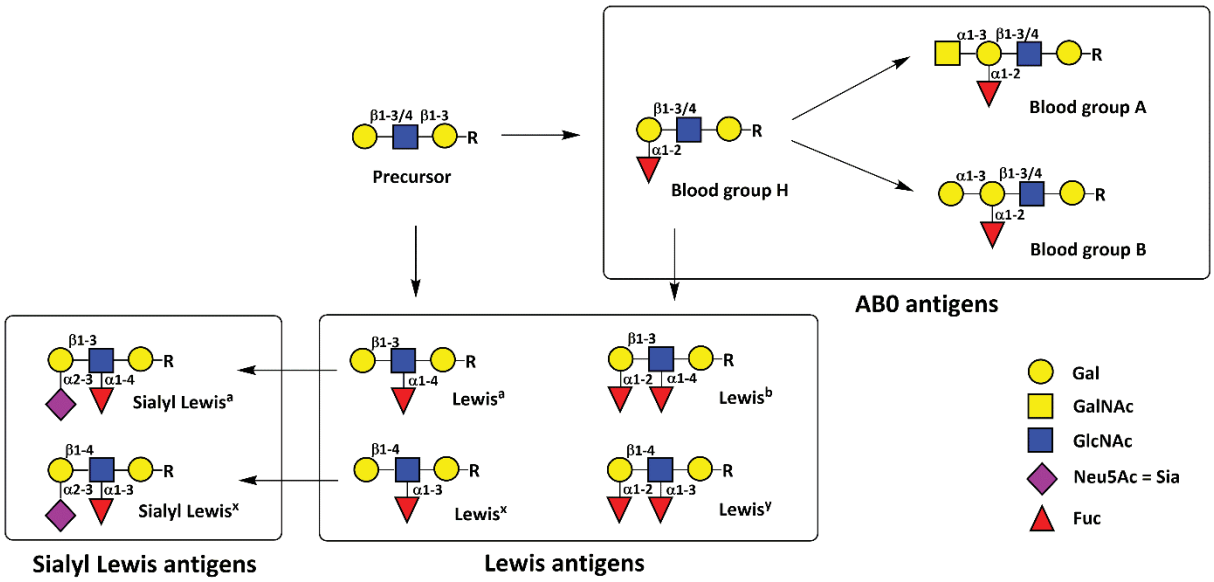

Figure 4: Schematic representation of AB0 and Lewis group antigens of HBGA.

Besides the ABH blood group antigens a second highly relevant group related to the HBGA are the Lewis antigens.[12,15] They can be differentiated in the four basic Lewis antigens (Le^a, Le^b, Le^x, Le^y) and two additionally sialylated Lewis antigens (SLe^x, SLe^a), differing in amount and connectivity of fucose units (see Figure 4). Many different fucosyltransferases catalyze the creation of Lewis antigens.[12] $Lewis^a$ (Le^a) is constructed by the addition of fucose via an α(1,4)-position linkage to a core *N*-acetyl-β-D-glucosamine (β-D-GlcNAc) bearing galactose with a β(1,3)-linkage. Whereas $Lewis^x$ (Le^x) exhibits a reversed substitution with galactose connected in β(1,4)-position and fucose linked in α(1,3)-position to GlcNAc. $Lewis^b$ (Le^b) derives from Le^a and $Lewis^y$ (Le^y) from Le^x by an additional fucosylation step at the galactose unit via an α(1,2)-linkage mediated by α(1,2)fucosyltransferase (FUT1). Instead of a secondary fucose unit, a sialic acid can be attached to the galactose of Le^a and Le^x forming sialyl-$Lewis^a$ (SLe^a) and sialyl-$Lewis^x$ (SLe^x) structures (see Figure 4).

3.3 Fucose-specific lectins

Lectins exhibit usually high specificity for particular carbohydrate structures as for instance fucose-specific lectins (F-type lectins or fucolectins) that feature distinct binding motifs for fucosylated glycoconjugates.[26,27,28] Fucolectins are a recently discovered type of lectins. Usually they have a F-type lectin domain (FTLD) with a binding site for fucose which is also calcium-mediated. This is further contributed by fucose itself that stabilizes the calcium ions by chelation with the vicinal hydroxyl groups at 2- and 3-position.[26] Besides the primary fucose binding sites extended carbohydrate binding sites can be found in some fucolectins for the interactions with additional carbohydrates of the blood group system.[27] F-type lectins can be found in pro- and eukaryotes as well as in viruses.[29] Two

important examples of F-type lectins are P-dimer from Norovirus and LecB from *Pseudomonas aeruginosa* and will be discussed more in detail in the following.

3.3.1 Norovirus and P-dimer

Norovirus (or Norwalk-like virus, originating from the first isolation in 1968 in Norwalk, Ohio) constitutes the predominant reason for epidemical outbreaks of acute non-bacterial gastroenteritis every year.[25] No vaccine or antiviral is known primarily due to difficulties in human Norovirus cultivation.[30] It is a highly infective non-enveloped virus that belongs to the *Caliciviridae* family.[31] The single-stranded positive sense RNA of Norovirus encodes for the viral RNA polymerase and two structural capsid proteins, the major protein VP1 (~60 kDa) and the minor protein VP2 (~20 kDa).[32] The function of VP2 is not well understood so far but is supposed to stabilize the viral capsid. The major structural protein VP1 consists of a S-domain (shell domain), responsible for the interior shell, and an extended P-domain (protruding domain) (see Figure 5 (b)). 180 copies of protein VP1 form the icosahedral virus capsid which is 35-39 nm in size (see Figure 5 (a)). The P-domains dimerize into 90 P-dimers that represent the crucial binding factors (see Figure 5 (c) and Figure 6).[33] Multiple binding pockets for fucosylated glycans are located in the cleft between two monomeric P-domains illustrating the importance of the dimeric form for P-protein's function (see Figure 5).[34] The interaction between P-dimer and HBGA, located on host cell surfaces, is suspected to be the first step of Norovirus infection process.[35,36]

Recent studies have shown that P-dimer exhibits four binding sites for HBGA.[37,38] The amino acids in the binding sites are strictly conserved providing a potential target for antivirals.[39]

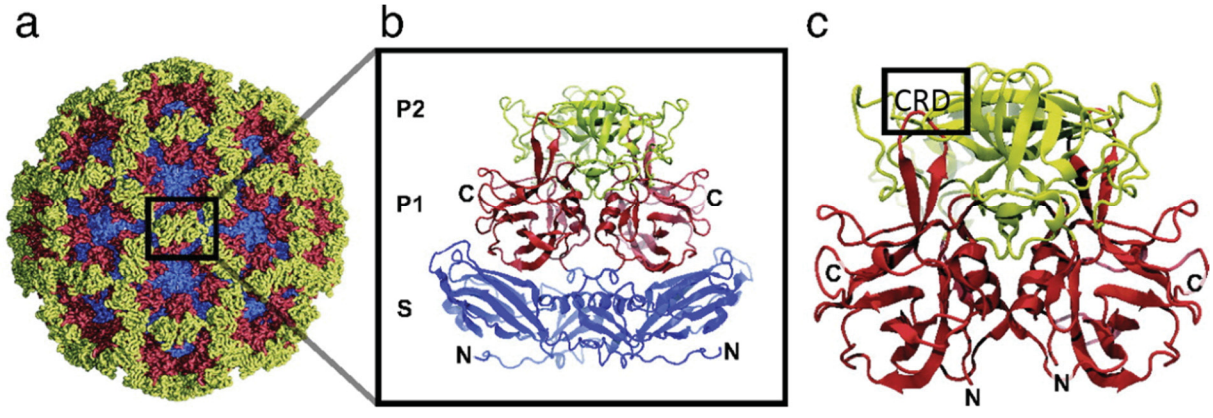

Figure 5: (a) Norovirus capsid structure formed by 90 VP1 dimers; (b) VP1 dimer in cartoon representation with S domains (blue), P1 domains (red) and P2 domains (yellow); (c) P-dimer with P1 and P2 domains and one carbohydrate recognition domain (CRD). Copyright (2008) National Academy of Sciences, U.S.A.[32]

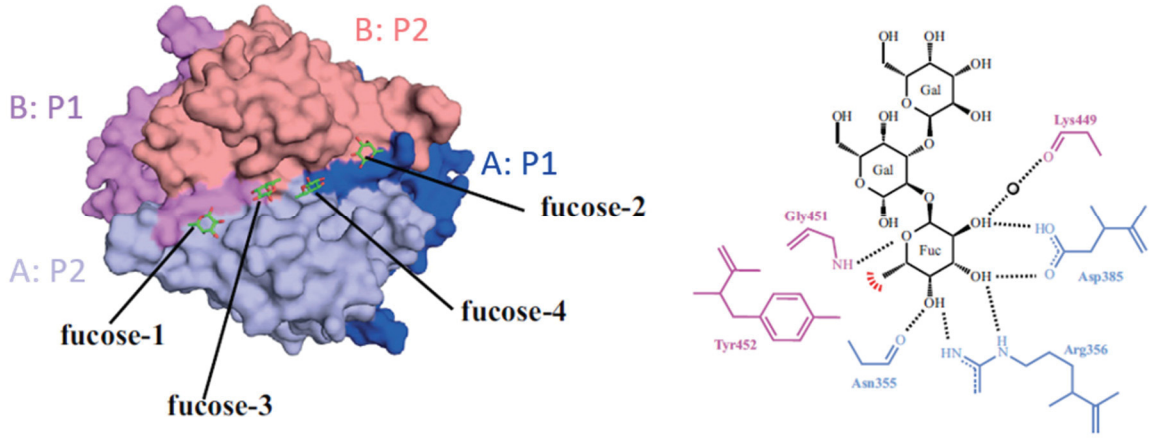

Figure 6: (Left) Surface representation of the X-ray crystal structure of human Norovirus P-dimer (GII.10) in complex with four fucose units. Subdomains P1 and P2 of P-domain monomers A and B are colored as follows: chain A (P1): blue, chain A (P2): light blue, chain B (P1): violet, chain B (P2): salmon. The four binding pockets are laying in the cleft between the P-domain monomers. (Right) Binding pocket 1 interacting with B-trisaccharide (30 mM) by hydrogen bonds with Asp, Arg, Asn, Lys and Gly as well as by hydrophobic interactions with the fucose methyl group. Modified from literature.[37]

The distances between the binding sites 1, 3, 4 and 2 of P-dimer have been estimated by crystal structures to be 11 Å (binding pockets 1 - 3), 17 Å (binding pockets 1 - 4) and 27 Å (binding pockets 1 - 2) (see Figure 6). It is known that terminal α-L-fucose is always involved in the binding to P-dimer in all human Norovirus strains and binds more intensely to the binding pockets than all other monosaccharides.[37] One hint was that most observed immunity against Norovirus infection was in secretor-negative individuals who lack the H substance on epithelial tissues.[24] Additional evidence is the protection of new-born children against Norovirus infection by circulating human milk oligosaccharides (HMO). Most likely fucosylated carbohydrates interact with the virus particles.[24,36] Fucose is a relatively weak binder for human Norovirus P-dimer. The dissociation constants of α-L-methylfucose towards P-dimer are around 2.4 ± 0.2 mM (K_{D1}) and 9.6 ± 0.1 mM (K_{D2}), respectively, for the first two binding sites and much lower for the binding sites 3 and 4.[38] It is thought that the attachment of α-L-methylfucose is a dose-dependent and step-wise process.

3.3.2 *Pseudomonas aeruginosa* and LecB

The opportunistic bacterium *Pseudomonas aeruginosa* is a rod-shaped, gram-negative pathogen discovered in 1900.[40] It represents one of the most problematic hospital-related pathogens due to its high viability in different environments and the often observed multi-resistance against currently used antibiotics. One main reason for resistance is the colonization of almost all kinds of human tissues and organs, forming dense biofilm formation. Biofilms reduces the efficacy of anti-bacterial agents, and so cannot be dispersed easily.[41,42] Especially in immune-suppressed patients (like those with cystic fibrosis, AIDS or cancer) the infection can lead to fatal complications and serious secondary diseases

like pneumonia or otitis externa. It could be shown that inhalation of a mixture of galactose and fucose in high amounts leads to a reduction of *P. aeruginosa* quantity in sputum of infected cystic fibrosis patients.[43] This can be explained by two multivalent lectins of *P. aeruginosa* namely LecA (PA-IL) and LecB (PA-IIL) that bind specifically on galactosylated and fucosylated glycans of the host cell surface.[10,44] LecA and LecB are assumed to play crucial roles in the human cell recognition and attachment as well as in biofilm generation and tissue damages. LecB shows a much higher specificity and affinity to fucosylated carbohydrate ligands in comparison to LecA.[45]

LecB is a homotetrameric C-type lectin with an overall size of 47 kDa (see Figure 7). The four binding pockets for fucose glycoconjugates exhibit distances of about 40-50 Å and can crosslink glycan structures from the host cell surface as well as polyglycans, secreted from the pathogen itself, within the biofilms.[41,47] In each binding pocket two Ca^{2+} ions are involved that interact with the three fucose hydroxyl groups (see Figure 7, right side). It is assumed that this explains the relatively high binding strength towards glycans in comparison to other carbohydrate-lectin interactions. The dissociation constant of L-fucose towards LecB is 2.9 µM. Affinity to mannose or fructose can also be observed but is much smaller. The highest binding to monosaccharides has been reported for α-L-methylfucose (K_D = 0.43 µM) and *p*-nitrophenyl-α-L-fucose.[48] LecB recognizes also oligosaccharides like the blood group antigens A, B, H, Le^x and Le^a with highest affinity observed for Le^a (K_D = 210 nM) that is supposed to be the natural ligand of LecB.[49] Furthermore it could be shown that human milk oligosaccharides prevent *P. aeruginosa* adhesion to the respiratory tract.[50]

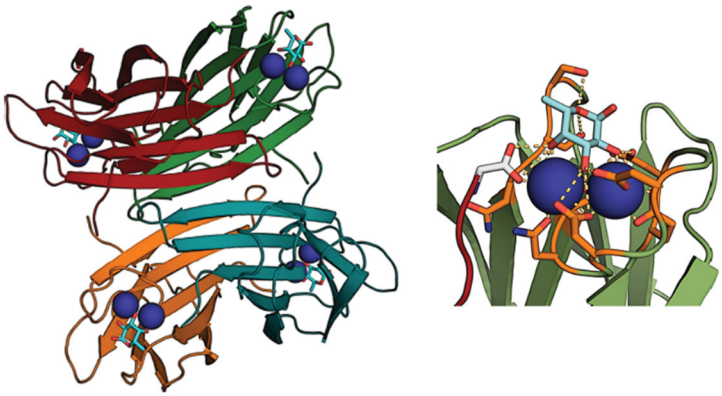

Figure 7: (Left) Cartoon representation of tetrameric LecB from Pseudomonas aeruginosa in complex with four L-fucose and eight calcium ions. (Right) zoom into one binding pocket. Reprinted with permission from[9,46]. Copyright (2015) American Chemical Society.

3.4 Multivalent glycomimetics

Natural oligosaccharide ligands are highly variable in terms of their composition, connectivity and size. Even small changes in their structure lead to different binding behaviors towards the recognizing receptors. Limited access to complex oligosaccharides and glycoconjugates – caused by synthesis, isolation and analysis difficulties – as well as the complexity of their multivalent binding behavior towards lectins display main challenges for the research of glycan-lectin interactions.[9,19,51] One alternative approach to gain deeper insights into the molecular mechanisms of multivalent carbohydrate-lectin interaction is the use of synthetic glycomimetics.[9,52,53,54] Mimetic displays are simplified models of their natural counterparts and provide useful information about structure-function relationships. Furthermore, synthetic multivalent glycomimetics can be designed by attaching several glycan motifs - often just monosaccharides - on an artificial backbone. This can contribute to higher binding avidities and potentially specificity towards their target receptors in comparison to the natural ligands, hence presenting a great potential for biomedical applications as biosensors or inhibitors.[55–57] Especially in viral and bacterial infections multivalent ligand binding might be a promising concept for potential therapeutics.[41,58,59]

The underlying mechanisms of multivalent interactions that lead to enhanced binding between lectin and multivalent glycomimetic can be described by several binding modes that usually happen simultaneously (see exemplarily Figure 8). For example, a multivalent ligand can bind to the binding sites of at least two different receptors. This bridging results in networks, clusters and aggregates that can precipitate and subsequently be observed by different techniques like turbidimetry or light scattering. This effect is referred to as the Cluster Glycoside Effect. Another important effect is chelation that describes the simultaneous attachment of at least two carbohydrates within the same ligand to two binding pockets of a single receptor. This effect is often correlated with an overall strong binding enhancement of approximately 10^3-10^6 orders of magnitude.[55] Chelate binding depends strongly on the chemical constitution of the ligand backbone, its flexibility and the distances between the presented ligand units. During statistical rebinding a first carbohydrate ligand that binds and rebinds in an equilibrium to a receptor can be replaced by another carbohydrate unit that is in close proximity to the first one on the same scaffold. Usually in a natural carbohydrate-lectin binding event several binding types play a role which makes the evaluation of multivalent binding even more complex. However, also parts of the multivalent ligand that are not directly involved in the binding process (scaffold or non-binding carbohydrates) can generate “indirect” binding effects such as hydrophobic interactions and macromolecular effects and can make further contacts. This can lead to an increased stability of the receptor-ligand complex due to their shielding effects to other ligands, what is known as sterical shielding (see Figure 8).

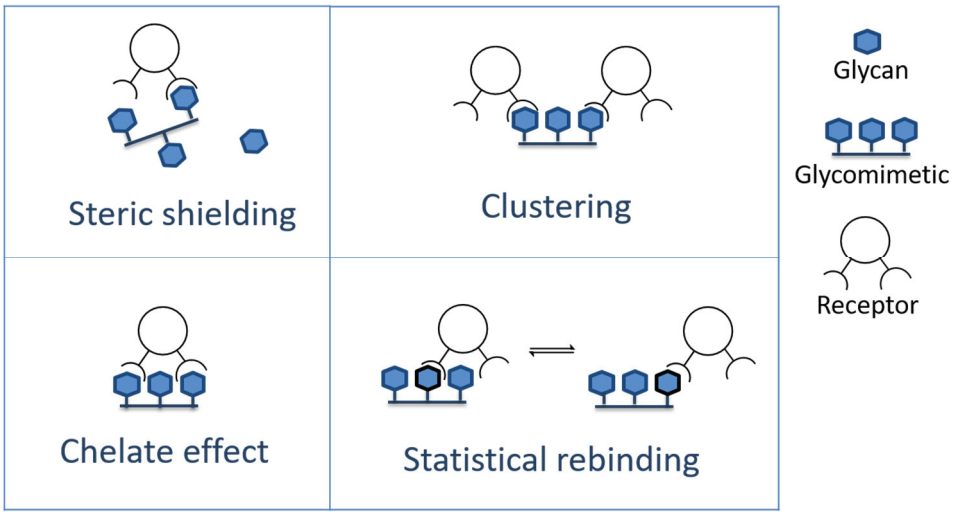

Figure 8: Exemplary schematic representation of four important theoretical multivalent binding modes.

Thus, in a glycomimetic, these factors need to be considered for the choice and design of the artificial scaffold. For example, the architecture and molecular weight as well as the valency (amount of carbohydrate units), distancing between glycans on the backbone and the resulting density of presented carbohydrates have been shown to strongly effect binding to a lectin receptor.[9,60] Additionally the bioactivity can suffer from choosing the "wrong" backbone or linker structures and the applicability of a glycomimetic in biomedicine depends strongly on any associated backbone toxicity.

Many different scaffolds have been explored for the design of glycomimetics with diverse backbone architectures such as linear, branched and dendritic structures. The synthetic strategies for these glycomimetics range from polymerization techniques and post-functionalization to step-wise growth of complex glycosylated macromolecules. Some important examples are shown schematically in Figure 9.

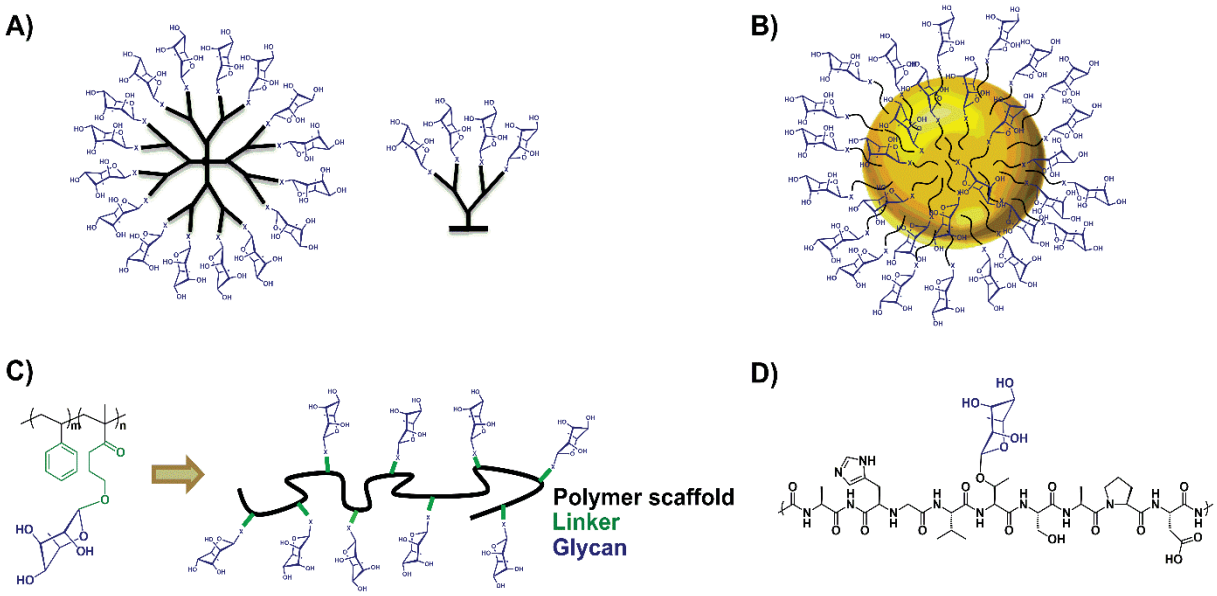

*Figure 9: Schematic representation of glycodendrimer and -dendron (**A**), glycosylated gold nanoparticle (**B**), glycopolymer (**C**), extract from glycopeptide of mucin-1 (MUC-1)[61] (**D**).*

An important mimetic class are glycosylated dendrimers that are characterized by a regularly branched composition and spherical shape with radial symmetry.[53,62] **Glycodendrimers** are most often monodisperse due to a repetitive, step-wise synthesis. A prominent example is the commercially available PAMAM-dendrimer that is composed of flexible poly(amidoamine)-chains bearing amino-end groups for further functionalization *e.g.* with glycans or next dendrimer generation formation.[63] An overall disadvantage of dendritic systems is their inflexible connectivity and secondary structure. Many examples are known for glycosylated dendritic systems, such as tetravalent pantaerythritol constructs, carbohydrate-centered glycoclusters or cyclopeptides that display interesting architectures for the investigation of carbohydrate-lectin interactions.[53,56,64] In addition, glycosylated dendrons (dendrimer arms) can be used for the attachment to surfaces like nanoparticles.[53,58]

Micro- and nanoparticles (NPs) are another type of scaffold used for the multivalent presentation of carbohydrates.[65,66] Many different materials for the construction of NPs are known as for example gold, magnetic materials (MNP) like iron or nickel and silica as well as polymeric materials like polyNIPAM or PEG.[67] Depending on the particle core material, carbohydrate ligands can be attached when exhibiting a suitable functional group by various conjugation methods such as amide bond formation, click chemistry or Michael addition reaction and even self-assembled NP complexes can be formed.[65,66]

Glycosylated polymers are usually linear structures of high molecular weight presenting a high number of carbohydrate ligands in their side chains.[68] Thereby they easily promote polyvalent binding when interacting with lectin receptors leading to large enhancement in binding. Glycopolymers can be synthesized either by the polymerization of glycomonomers or via post-functionalization methods (*e.g.*

by amide bond formation, copper(I)-catalyzed azide-alkyne cycloaddition (CuAAC) or thiol-ene click reactions) after generation of a suitable polymer-backbone.[52,68,69] A significant difference between glycopolymers and glycodendrimers or glycopeptides is their intrinsic molecular weight distribution, although (glyco-)polymers with very small dispersity indices (DI) are accessible *e.g.* by controlled free radical polymerization techniques (CFRP) like nitroxide-mediated polymerization (NMP), reversible addition fragmentation chain transfer polymerization (RAFT) or atom transfer radical polymerization (ATRP).[52,65,68,70]

Another important class of glycomimetic structures are **glycosylated peptides**.[71] The high chemical precision and monodispersity explains their potential for the investigation in basic research and applications in biomedical research. They can be used in sensing or as therapeutics, for example as antibiotic (*e.g.* vancomycin) or in immunotherapy,[61] also much research is focused on glycopeptide-based cancer and viral vaccinations.[61,72] Glycosylated peptides can be synthesized in solution phase reactions or – which is much more common – via solid phase peptide synthesis (SPPS) on a solid support using *N*-terminal protected amino acid as building blocks (see section 3.5 Solid phase peptide synthesis (SPPS)).[71] The attachment of carbohydrates can be performed before peptide elongation by conjugation to a suitable amino acid monomer or after backbone elongation onto functional groups of the amino acids in the chain on the solid support. Furthermore, hybrid glycopeptide systems can be formed possessing additional synthetic modifications at defined positions as for example an artificial linker structure,[73] an additional backbone conjunction or a non-natural spacer unit that can influence binding to crucial lectins. Such the reconstruction and modification of MUC1 (mucin-1), a highly glycosylated protein that has been found to be overexpressed on some cancer cells combined with an altered glycosylateion pattern, could help to develop mucin-anti-tumor vaccines (see Figure 9).[61] Glycopeptides can be applied to explore the influence of specific structural characteristics on carbohydrate-lectin binding and provide useful information about structure-function relationships. However, most glycopeptides suffer from high sensitivity against degradation by enzymes and can provoke immune responses.

Combining advantages of the glycopolymers and glycopeptides, Hartmann *et al* recently introduced a novel class of glycomimetics, the so-called **precision glycomacromolecules**.[74,75] These are based on an artificial scaffold assembled via stepwise addition of tailor-made building blocks on solid support. The created monodisperse, sequence-controlled oligo(amidoamine) backbone can then be used for the conjugation and multivalent presentation of carbohydrate ligands (see Figure 10). Controlled positioning of carbohydrates within the oligomeric backbones produces glycomimetics that are versatile tools for fundamental research but also generates compounds of great potential in different biotechnological and biomedical applications.[76,77]

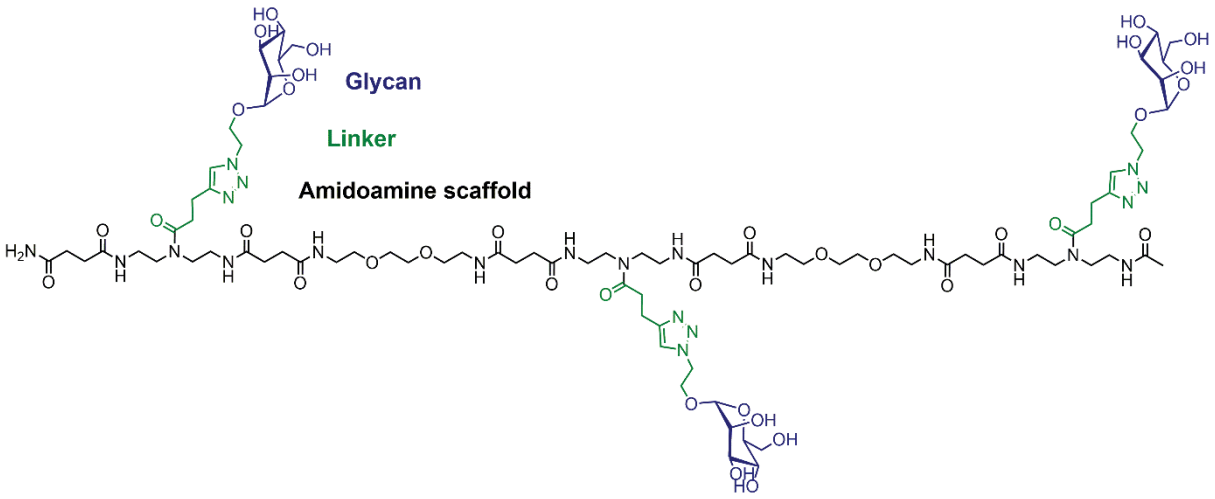

Figure 10: Example glycooligo(amidoamine) structure with mannose side chains (red) and triazole linker (green).

The following chapters will further elucidate the synthesis and applications of precision glycomacromolecules, first giving a general introduction into solid phase peptide synthesis (SPPS), which is the basis of later solid phase polymer synthesis (SPPoS) of glycooligo(amidoamines).

3.5 Solid phase peptide synthesis (SPPS)

Solid phase peptide synthesis (SPPS) was developed by Merrifield in the 1960s.[78] SPPS enables the efficient multistep synthesis of large peptide structures with defined composition in high amounts and purities. The solid support is characterized by resin particles that are often composed of polystyrene. Distinct functionalities on the solid support can be used as reactive anchor points for the subsequent covalent conjugation of the amino acids generating polypeptides. An important requirement to gain defined macromolecules is the completeness of each reaction step. As amide bond formation is not favored at room temperature,[79] activation of the acid group by coupling reagents is necessary. The amino acids are coupled with their *C*-terminal side (carboxyl group) to the amino groups of the growing chains on the resin (see Scheme 1). Therefore, the amino groups (*N*-terminus) of the amino acids need to be protected during the coupling step to avoid side reactions and the reduction of the amount of amino acid monomer that could be coupled to another unbound amino acid instead of the growing chain end on the resin. In this original form of SPPS the acid labile *tert*-butyloxycarbonyl group (Boc) was used as the *N*-protecting group.[80,81] Scheme 1 illustrates the most important reaction steps during SPPS as originally introduced by Merrifield.

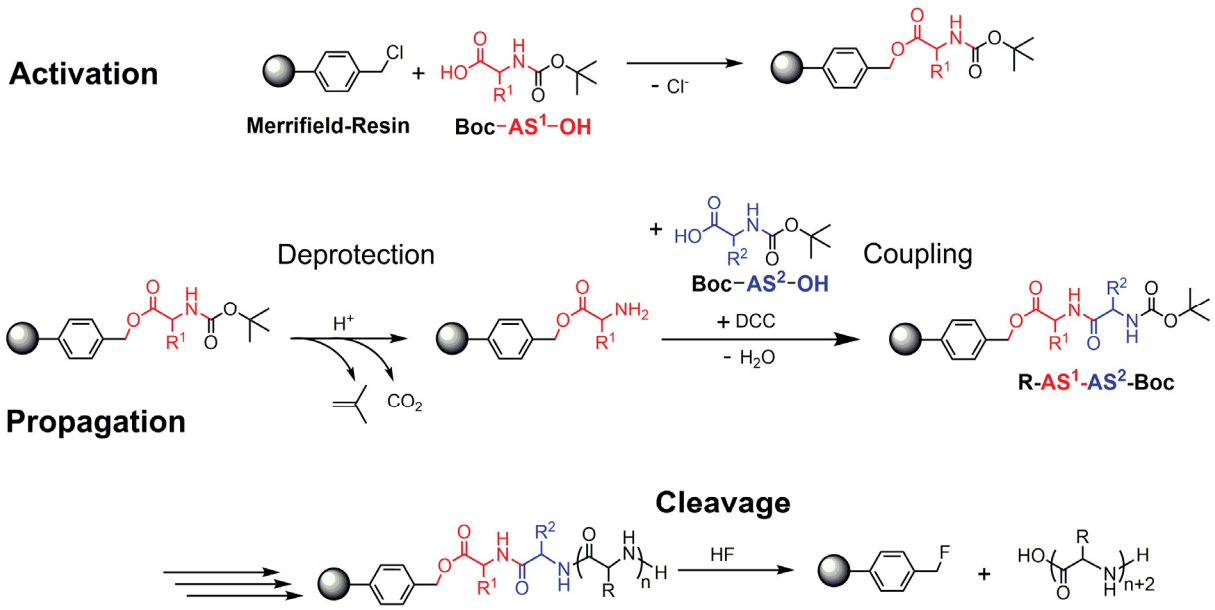

Scheme 1: Merrifield solid phase peptide synthesis in three phases containing activation of the Merrifield polystyrene resin (top), propagation of the bound peptide chain by alternating deprotection and coupling steps (middle) and acidic cleavage off the resin (bottom).

During the activation the first Boc-protected amino acid (HO-AS_1-Boc) is coupled to the surface functionalities of the polystyrene resin (Merrifield resin) in a nucleophilic substitution with chloride as leaving group. To make the coupled amino acid available for the next coupling step the protecting group needs to be removed, in this case the Boc-group is cleaved by a strong acid like trifluoroacetic acid (TFA) in DCM (deprotection step). After washing off the resin to remove all unreacted reagents and side products the coupling of the next amino acid to the unprotected amine of the previously coupled amino acid is applicable. The activation of the carboxylic acid (*C*-terminus) is accomplished by dicyclohexylcarbodiimide (DCC) as coupling reagent. DCC intermediate includes the acid (ester formation) and makes it more reactive for the nucleophilic attack of the amine.[82] Afterwards DCC is leaving the reaction as dicyclohexylurea, which is removed by the washing step between couplings. In alternating coupling and deprotection steps the elongation of the peptide chain on the resin is accomplished (propagation). The final product peptide is obtained after cleavage off the resin with hydrofluoric acid (HF).

The major advantage over solution phase reactions is the simple purification and potential isolation after each reactions step. All reagents can be washed off the resin and only the covalently bound product molecules remain on solid support until these are cleaved.[83] Thereby, high excess of reagents in every reaction step as well as multiple couplings to achieve full conversion are easily applicable. Today, SPPS is often performed fully automated using a peptide synthesizer. Furthermore, while the overall concept is still the same, many further improvements have been made since Merrifield

introduced his method. The following subchapters will highlight some of the important reagents that are applied in SPPS today and will also be relevant for SPPoS.

3.5.1 *N*-Terminal protecting groups

One of the critical aspects in SPPS is the use of *N*-terminal protecting groups to allow selective coupling of the amino acid onto the growing chain on the resin. Therefore, the amine protecting groups need to be stabile under coupling conditions of the amino acids on solid support, yet should be cleavable under conditions orthogonal to all other reaction steps (coupling or later cleavage from the support). Instead of the originally introduced Boc protecting group, more popular today is the use of fluorenylmethoxycarbonyl group (Fmoc). Fmoc is stable under acidic conditions and is cleaved by mild bases like secondary amines (usually achieved by a 20% solution of piperidine in dimethylformamide (DMF)). [80,81] The introduction of the Fmoc protecting group can be performed in aqueous sodium bicarbonate solution with the more reactive Fmoc-chloride (Fmoc-Cl) (see Scheme 2) or Fmoc-oxysuccinimide (Fmoc-OSu). An advantage of this basic cleavable amine protecting group is the characteristic UV-absorption of the cleaved side product at 295 nm that can be employed to determine the success of deprotection on solid support.

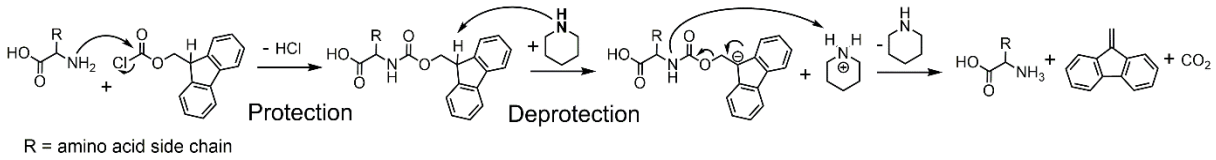

Scheme 2: Introduction (1) via Fmoc-Cl and removal (2) with piperidine of basis labile Fmoc-protecting group.

3.5.2 Solid support and linkers

The first described “Merrifield resin” was composed of polystyrene chains that are cross-linked with divinylbenzene (see Figure 11).[78] The chains are functionalized with methylenechloride residues for the elongation of desired products. Cross-linked polystyrene resins are still very often in use due to their high stability and availability with low costs. It usually exhibits a high degree of functionalization.

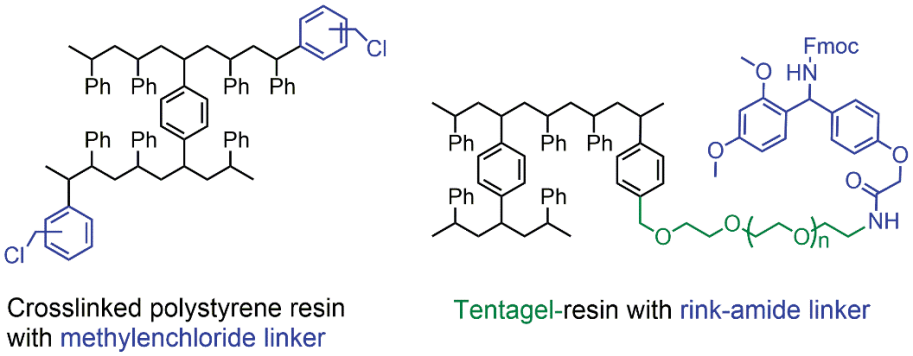

Figure 11: Extract of crosslinked polystyrene resin (Merrifield resin) with metyhlenechloride linker (left) and advanced Tentagel® resin with grafted PEG chains and rink-amide linker (right).

Both the polymeric structure as well as the type of functionalization was further developed and a great variety of different resins are commercially available nowadays. An example is the often used Tentagel® resin that is also constructed by cross-linked polystyrene and additionally contains PEG-chains that are grafted onto the polystyrene ("tentacle") (see Figure 11).[84] Advantageously the Tentagel® resins swells in both protic and aprotic solvents and so the reactive groups experience fewer sterical effects from the resin matrix. The capacity of functional groups is usually lower than for a standard polystyrene resin. Another often used resin is formed by polyacrylamides that are better soluble in polar solvents.[85] Additionally a range of linkers with various functional groups have been developed such as the acid-labile Rink-amide linker (see Figure 11). In the first step, the Fmoc protecting group is cleaved off to enable the coupling of a carboxylic acid of the first amino acid onto the amine functionality by amide bond formation. At the end of the synthesis the final cleavage of the product generates a carboxamide whereas the amine group is leaving the resin. The Rink-amide linker features high sensitivity in acidic environment due to the two electron-donating methoxy groups.[85] Other important linkers are the Wang linker or the Siber linker that also generates an amide end-group in the product or a traceless linker that does not transfer any functional group to the final product. Besides acidic cleavage the product can be cleaved off under various other conditions depending on the specific linker, as with basic-labile or even with photo-labile linkers.

3.5.3 Coupling reagents

In general, amide bond formation is slow and thermodynamically not favored (*e.g.* caused by salt formation) but can be facilitated by suitable coupling reagents that activate the acid group (*C*-terminus) to form a reactive ester or "activated ester".[79] The most important classes of coupling reagents in SPPS are carbodiimides, phosphonium salts and uronium salts that exhibit certain advantages for different coupling conditions and amino acid monomers.[86]

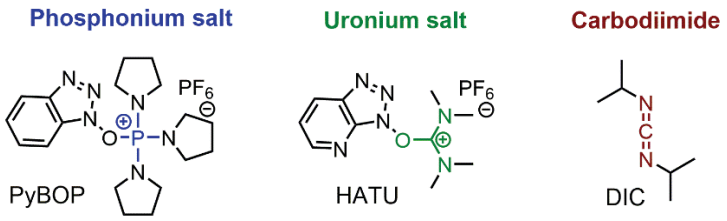

Figure 12: Important examples for the three main classes of coupling reagents. Phosphonium salts: PyBOP (left), uronium salts: HATU (middle) and carbodiimides: DIC (right).

Coupling with phosphonium and uronium reagents requires the addition of mild bases, like the often used Hünig's base or diisopropylethylamine (DIPEA), that deprotonate the acid group in the very first step. Additionally, the epimerization at the stereocenter of Cα-atom is a well-known problem in amide coupling reactions and can be avoided by additives like 1-hydroxybenzotriazole (HOBt, see Scheme 3). An alternative to HOBt is the less explosive Oxyma.[87] Important examples of the three main classes of coupling reagents are shown in Figure 12.

Today, mainly phosphonium salts are used as coupling reagents. The first phosphonium salt for SPPS coupling was benzotriazol-1-yl-oxytris(dimethylamino)phosphonium hexaflorophosphate (BOP).[86] Due to the carcinogenic effect of the byproduct hexamethylphosphoric acid triamide (HMPA) the less harmful benzotriazol-1-yl-oxytripyrrolidinophosphonium-hexafluorophosphate (PyBOP) was developed by substitution of the dimethylamino-groups with pyrrolidino-groups (see Figure 12). The good solubility in organic solvents and the ease in handling cause its frequent use. Further advances lead to several modifications, such as the relatively new coupling reagent bromotripyrrolidinophosphonium hexafluorophosphate (PyBrOP) where even the benzotriazolyl-oxy-residue is substituted to a bromide leading to better coupling results with secondary amines. Scheme 3 demonstrates the amide coupling mechanism supported by BOP.

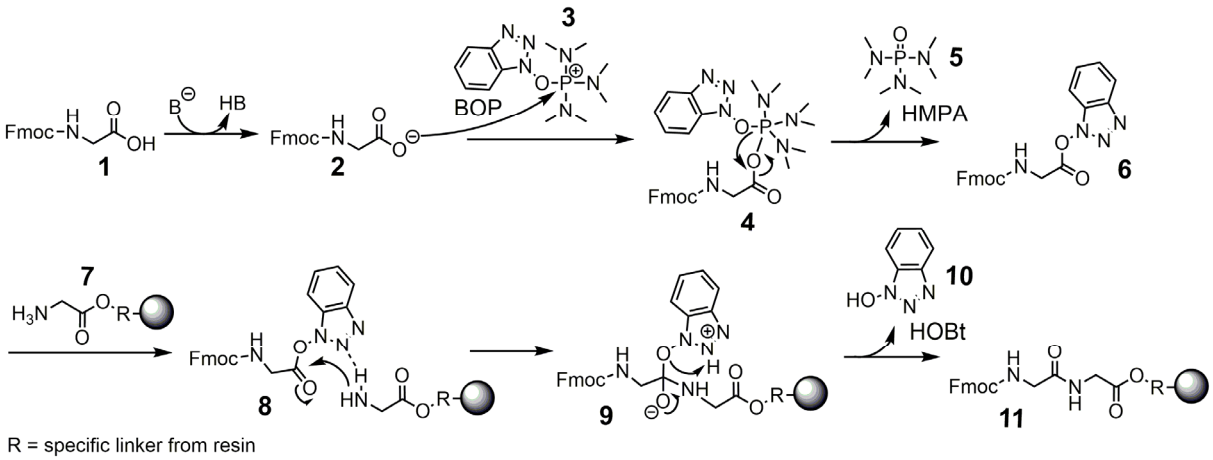

Scheme 3: Mechanism of phosphonium salt-guided amide bond formation between an Fmoc-protected amino acid and an amine group of a resin-coupled amino acid using BOP.

After deprotonation of the protected amino acid (**1**) the carboxylate (**2**) attacks the phosphonium ion (**3**) leading to the separation of the very stable phosphoramide derivative HMPA (**5**). The formed active ester (**6**) with HOBt stabilizes the transition state (**8** and **9**) with the amine group of the solid support (**7**). After separation of HOBt (**10**) the product amide (**11**) is formed.

Another important class of coupling reagent in SPPS are uronium salts such as 2-(1*H*-benzotriazol-1-yl)-1,1,3,3-tetramethyluronium hexafluorophosphate (HBTU) and *O*-(7-Azabenzotriazol-1-yl)-*N*,*N*,*N*',*N*'-tetramethyluronium hexafluorophosphate (HATU), where HBTU is sometimes preferred as it causes less racemization.[85,86] The uronium reagents can have two forms, the uronium salt or the less reactive iminium salt. The mechanism is very similar to the one of phosphonium salts previously shown in Scheme 3. Again, a base like DIPEA is required to deprotonate the acid and the carboxylate attacks the uronium carbon (instead of a phosphonium). An urea derivative is cleaved and the same HOBt-active ester is formed as is the case of phosphonium salts (see Scheme 3, **6**) that reacts with the amine group forming the desired product and HOBt.

3.6 Solid phase polymer synthesis (SPPoS)

Besides the use for the synthesis of peptides, solid phase strategies have today been implemented also for the synthesis of other biomacromolecules such as oligonucleotides and oligosaccharides.[88] Furthermore, fully synthetic macromolecules can be synthesized applying a stepwise assembly of building blocks on a solid support. Applying this concept L. Hartmann *et al* developed the synthesis of oligo(amidoamines) formed by tailor-made building blocks (BB) that bear a protected amine group as well as a carboxylic acid originating from diamines and di-acids for the introduction in solid phase polymer synthesis (SPPoS). Furthermore, these building blocks exhibit additional amine or amide groups and can act to either present additional functional groups or to be spacer units. This variability allows the BB to adjust length, hydrophilicity, branching and functionalization of the oligo(amidoamine) backbone.[75,89–93] Even switchable BBs have been introduced.[94,95] Figure 13 shows an example oligo(amidoamine) backbone structure on solid support carrying functional side chains.

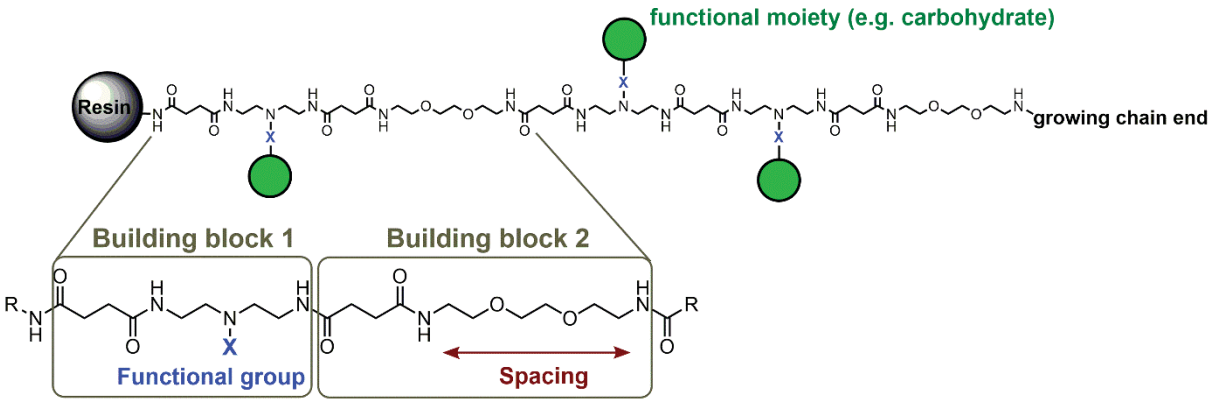

Figure 13: Exemplary oligo(amidoamine)-chain in SPPoS with functional and spacer building blocks (EDS) included.

3.6.1 Building blocks (BB)

Building blocks used in SPPoS are synthesized by precondensation of a diamine and a di-acid unit. Depending on the desired main or side chain functionality, different diamines and di-acids can be combined. However, for all BBs, the primary amine group for main chain elongation is protected with a Fmoc group. Figure 14 gives examples of BBs developed for SPPoS within the group. Generally, BBs are divided into two major classes – functional and spacer BBs. Functional BBs introduce different side chain motifs, *e.g.* an alkyne group for later attachment of azido-functionalized molecules as in TDS[75] or protecting groups for orthogonal cleavage on solid support and introduction of branching points as in ADS[89,91]. The azide-containing BADS is applicable with alkyne-functionalized molecules and MDS contains an additional protected acid group *e.g.* for Staudinger ligation. Other functional BBs are the acid labile Boc-functionalized BDS and the alkene-functionalized DDS for the conjugation of thiols via thiol-ene click reaction. Spacer BBs introduce different main chain motifs that can be used for controlled spacing of functional BBs in the oligomeric scaffold and furthermore can be introduced to vary chain length, molecular weight and solubility of the oligomer. Such ODS increases the hydrophobicity of the oligomer effecting hydrophobic interactions with lectins, whereas a shorter alkyl-spacer is introduced by SDS.[93] The ethyleneglycol-based spacer BB (EDS)[75] features good solubility in organic solvents as well as aqueous solutions and leads to high flexibility of the backbone.

***Footnote**:* Trivial names of building blocks (BB): TDS = triple bond diethylenetriamine succinyl-, ADS = alloc diethylenetriamine succinyl-, BADS = *p*-(azidomethyl)benzoyl diethylenetriamine succinyl-, MDS = methylsuccinyl diethylenetriamine succinyl-, BDS = Boc diethylenetriamine succinyl-, DDS = double bond diethylenetriamine succinyl-, ODS = octyl diamine succinyl-, EDS = ethylenedioxy-bis(ethylamine) succinyl-building block.

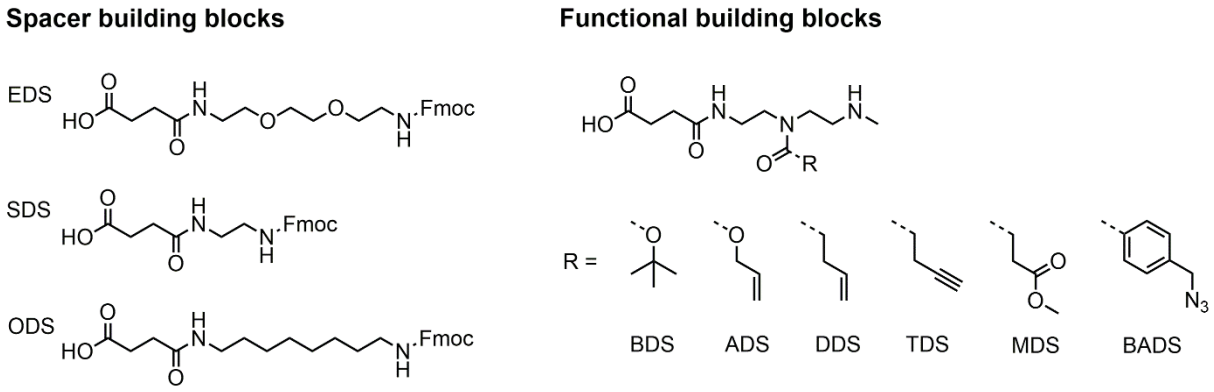

Figure 14: Several examples of developed spacer BB and functional BB for SPPoS. [75,89,92–96]

The synthesis of most functional BBs is based on a key intermediated. [92,96] In the following, the exemplary synthesis of TDS is shortly described (see Scheme 4).[75,89,91] The starting material is diethylene triamine (**1**) that reacts with trityl-chloride first and then with ethyl trifluoroacetate (TFA-OEt) for the protection of the two primary amines generating the key intermediate **2**. Afterwards 4-pentynoic acid **3** is coupled to the secondary amine forming an amide bond with PyBOP as coupling reagent and triethylamine (NEt_3) as base. The TFA protecting group of **4** is cleaved under basic conditions with K_2CO_3 and Fmoc is introduced using Fmoc-Cl producing **5**. Fmoc cannot be attached to the molecule at the beginning of the synthesis because it would not only react with the primary amine but also with the secondary amine that now is conjugated with the triple bond. At the end the trityl-protecting group is cleaved with TFA and triethylsilane ($SiEt_3$), as scavenger, generating the salt **6** that can afterwards react with succinic anhydride using triethylamine as base to form the product BB TDS (**7**).

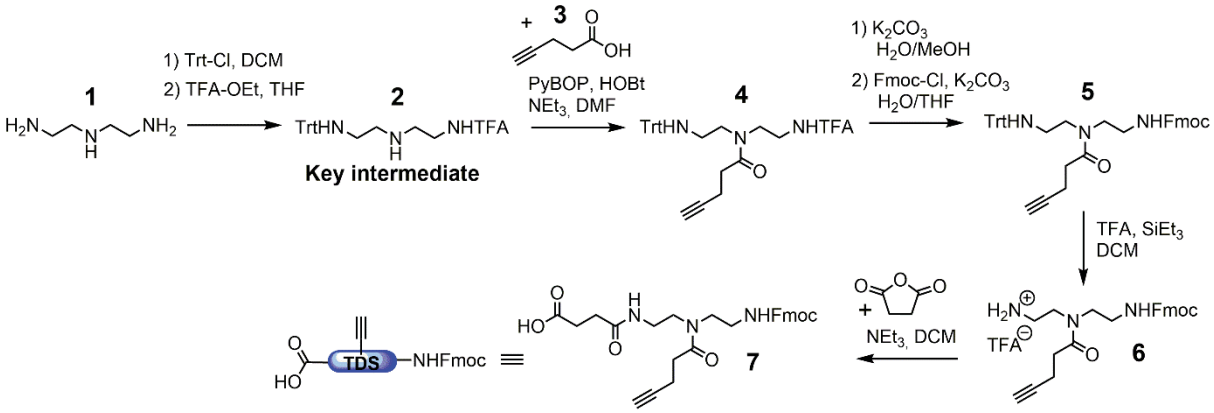

Scheme 4: Synthetic route of functional building block TDS.[75]

Following a similar strategy, spacer BBs such as EDS can be generated (see Scheme 5).

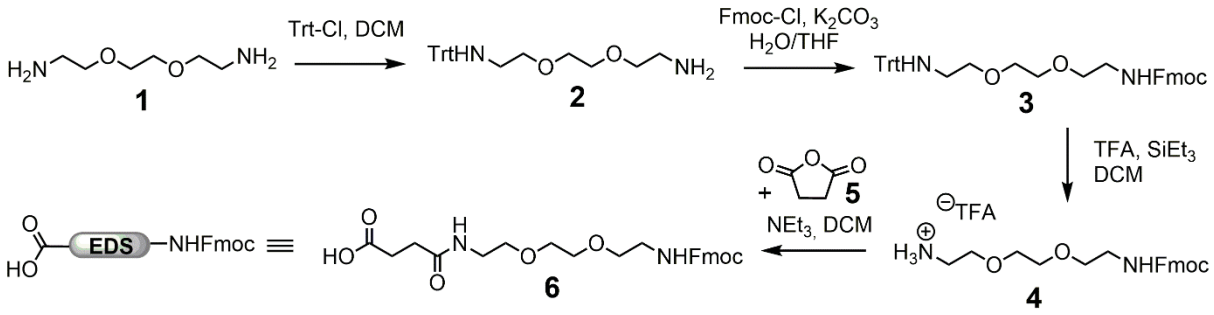

Scheme 5: Synthetic route of spacer building block EDS.[75]

In short, after protection of **1** with tritylchloride forming **2,** the Fmoc protecting group can be introduced directly to the second amine. After cleavage of the trityl group of **3** with TFA and $SiEt_3$ the TFA salt **4** can react with succinic anhydride (**5**) forming the spacer building block EDS (**6**).

3.6.2 Solid phase assembly of building blocks and ligand conjugation

With the toolbox of BBs in hand, the next step in SPPoS is the assembly of the oligo(amidoamine) scaffold on solid support (see Scheme 6). Following standard Fmoc-peptide coupling protocols, attachment of the first building block to the solid support (**a**) the successive Fmoc-deprotection (**b**) with piperidine (25% solution in DMF) and coupling of the next tailor-made BB, using usually PyBOP as coupling reagent and DIPEA as base, lead to the formation of suitable oligomer backbones. The last BB is usually capped with acetic anhydride (**c**) after Fmoc-deprotection to avoid side reactions during the following functionalization of side chains. The introduction of *e.g.* carbohydrate units along the oligomeric scaffold can be performed with different conjugation strategies and depends on the functional groups in the oligomer chain. The synthesis of glycosylated oligo(amidoamines) by solid supported polymer synthesis using TDS as functional BB and applying CuAAC for the conjugation of carbohydrate units is shown in Scheme 6 (**d**).[75] CuAAC is applied to conjugate an azidated carbohydrate to the alkyne previously introduced by TDS into the backbone on solid support. One of the advantages of performing the conjugation on solid support is the easy use of high excess of reagents and potential double couplings to realize full conversion. The other important advantage is the facile removal of all Cu residues, by a special washing protocol with DMF and DCM after complexation with dithiocarbamate.[97] CuAAC can be performed with an unprotected carbohydrate ligand, however, in most cases an acetyl-protected ligand is applied. Therefore, in the final step on resin acetyl-protected hydroxyl groups of coupled carbohydrate units are deprotected using NaOMe in methanol. Finally, the targeted structure can be cleaved off the resin (**e**). In case of rink-amide Tentagel®-resin cleavage is performed with 95% TFA with triisopropylsilane (TIPS) and DCM (1:1).

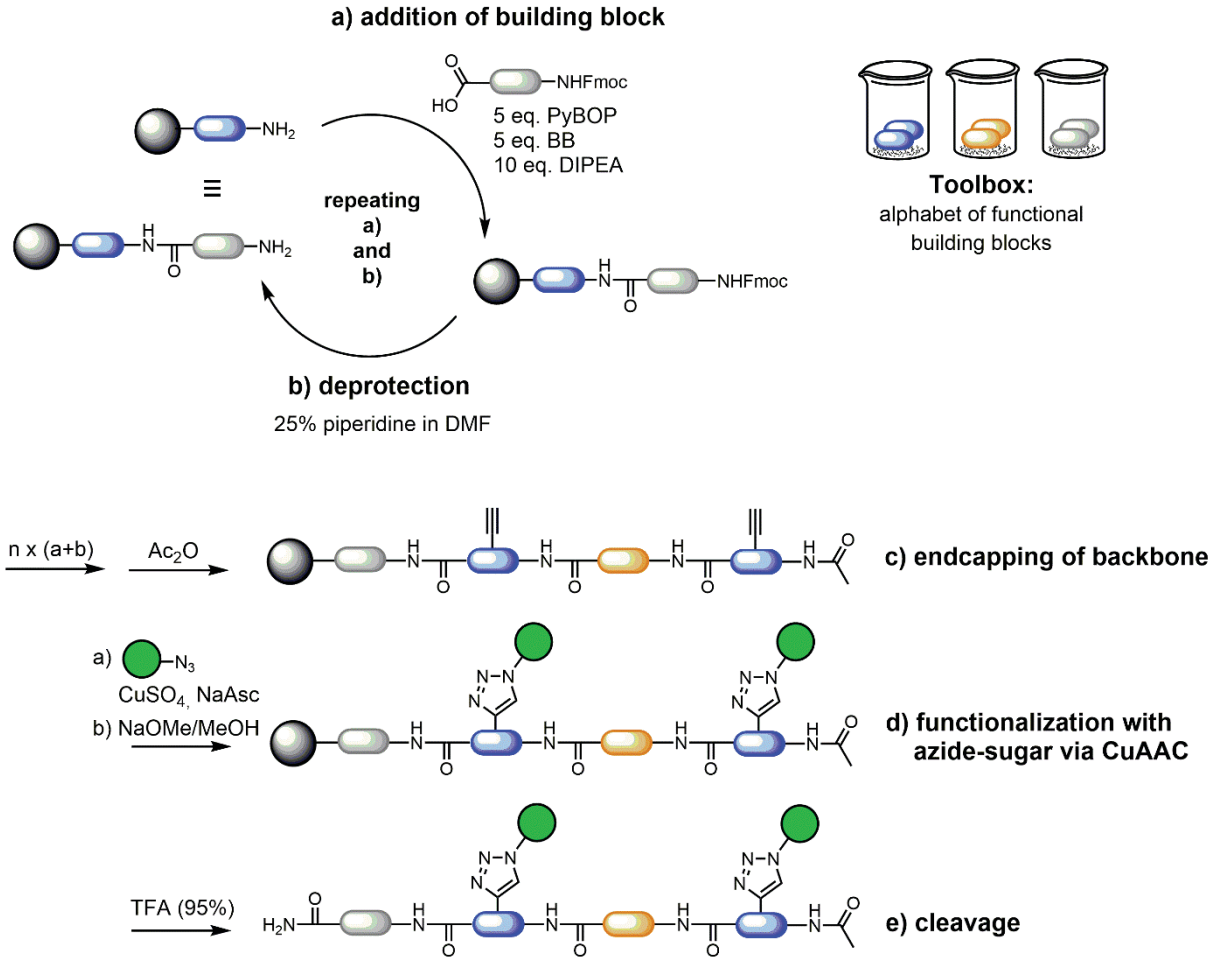

Scheme 6: SPPS of glycooligo(amidoamines) applying CuAAC.

The generated glycooligomers represent so called homomultivalent glycomimetics if only one type of carbohydrate is attached multiple times on the oligomeric scaffold. Homomultivalent glycooligomers can be achieved if the conjugation of carbohydrates is performed at the end of the synthesis and only one type of functional building block is used as shown in Scheme 6. Also the synthesis of glycooligomers that exhibit different carbohydrates at defined positions is possible. These constructs are called heteromultivalent glycooligomers and can be afforded by alternating deprotection/coupling and carbohydrate conjugation steps or during the introduction of different functionalities on the backbone suitable for orthogonal conjugation strategies with carbohydrates.[76,96]

Major focus has been devoted to the synthesis of heteromultivalent glycooligo(amidoamines) carrying different carbohydrate ligands in the side chains. Therefore, different conjugation strategies based on the different functional groups available from the functional building blocks have been established such as CuAAC, thiol-ene conjugation or Staudinger ligation.[75,89,91,92,96] In the following the mechanism of CuAAC will be shortly discussed, since it was also applied in this work.

The copper-catalyzed azide-alkyne cycloaddition reaction (CuAAC) was first described by Meldal *et al* and Sharpless *et al* simultaneously in 2001 and describes the regioselective cycloaddition reaction between an alkynylated with an azidated compound forming a 1,2,3-triazole linkage.[98] The copper-free connection between an alkyne and an azide was already described in 1893 and is known as Huisgen reaction.[99] It required high temperatures, long reaction times and was not stereoselective. The CuAAC reaction is very efficient with almost complete conversion at room temperature and satisfies the definition of a click reaction. It exhibits a high tolerance towards different conditions and substrates, though the Cu(I) species is sensitive to oxidation by air.[100] Therefore, reducing agents are used, usually sodium ascorbate. $CuSO_4$ can serve as the copper source. The proposed mechanism of the CuAAC reaction is shown in Scheme 7.[101]

The active Cu(I) species coordinates the alkyne group (**1** and **2**) and substitutes in the following the proton, whereupon a second Cu(I) coordinates the alkyne (**3**). The cycloaddition reaction now includes the second Cu(I) during the ring formation (see **5** and **6**) with the azide **4**. After formation of the triazole (**7**) the bound Cu(I) is substituted with a proton, generating the heterocycle **8** and the copper is available for the next reaction cycle.

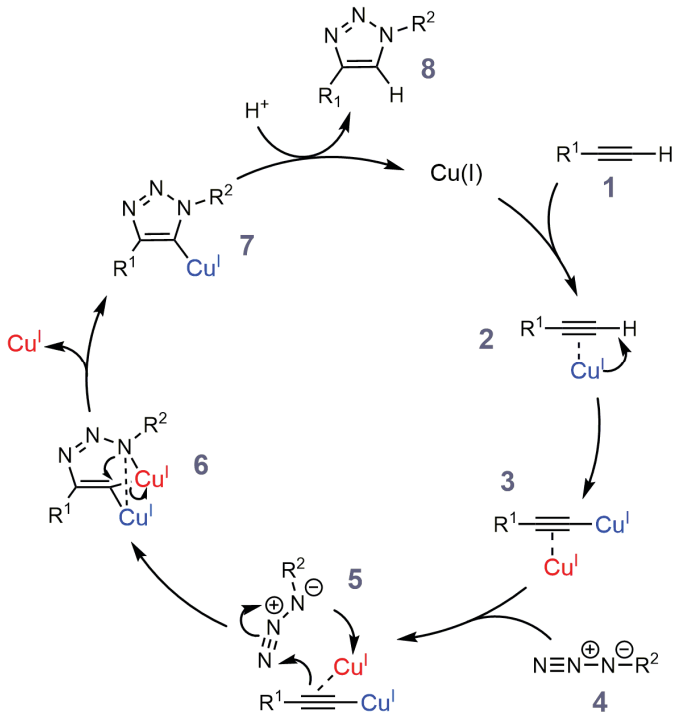

Scheme 7: Proposed di-copper-mechanism of Cu-catalyzed azide-alkyne cycloaddition click reaction (CuAAC).

3.7 References

[1] R. A. Dwek, *Chem. Rev.* **1996**, *96*, 683.

[2] P. M. Drake, W. Cho, B. Li, A. Prakobphol, E. Johansen, N. L. Anderson, F. E. Regnier, B. W. Gibson, S. J. Fisher, *Clin. Chem.* **2010**, *56*, 223.

[3] Y. J. Kim, A. Varki, *Glycoconj. J.* **1997**, *14*, 569.

[4] T. F. Orntoft, E. M. Vestergaard, *Electrophoresis* **1999**, *20*, 362.

[5] P. U. Atukorale, Y.-S. Yang, A. Bekdemir, R. P. Carney, P. J. Silva, N. Watson, F. Stellacci, D. J. Irvine, *Nanoscale* **2015**, *7*, 11420.

[6] a) I. J. Goldstein, C. E. Hayes, *Advances in Carbohydrate Chemistry and Biochemistry, Vol. 34,* (Eds.: R. S. Tipson, D. Horton), Academic Press, New York, **1978**, pp. 127–340; b) H. Rüdiger, *Chem. unserer Zeit* **1981**, *15*, 155.

[7] Y. C. Lee, R. T. Lee, *Acc. Chem. Res.* **1995**, *28*, 321.

[8] C. Fasting, C. A. Schalley, M. Weber, O. Seitz, S. Hecht, B. Koksch, J. Dernedde, C. Graf, E.-W. Knapp, R. Haag, *Angew. Chem.* **2012**, *124*, 10622.

[9] S. Cecioni, A. Imberty, S. Vidal, *Chem. Rev.* **2015**, *115*, 525.

[10] S. de Bentzmann, A. Varrot, A. Imberty, *Pseudomonas Methods and Protocols, Vol. 1149,* (Eds.: A. Filloux, J.-L. Ramos), Springer New York, **2014**, pp. 403–414.

[11] G. Péterszegi, I. Fodil-Bourahla, A.M. Robert, L. Robert, *Biomed. Pharmacother.* **2003**, *57*, 240.

[12] D. J. Becker, J. B. Lowe, *Glycobiology* **2003**, *13*, 41R–53R.

[13] G. F. Springer, P. Williamson, *Biochem. J.* **1962**, *85*, 282.

[14] R. Kannagi, *Glycoconj. J.* **1997**, *14*, 577.

[15] E. M. Vestergaard, H. O. Hein, H. Meyer, N. Grunnet, J. Jørgensen, H. Wolf, T. F. Ørntoft, *Clin. Chem.* **1999**, *45*, 54.

[16] A. R. Pacheco, M. M. Curtis, J. M. Ritchie, D. Munera, M. K. Waldor, C. G. Moreira, V. Sperandio, *Nature* **2012**, *492*, 113.

[17] L. V. Hooper, J. Xu, P. G. Falk, T. Midtvedt, J. I. Gordon, *Proc. Natl. Acad. Sci. USA* **1999**, *96*, 9833.

[18] E. Miyoshi, K. Noda, Y. Yamaguchi, S. Inoue, Y. Ikeda, W. Wang, J. H. Ko, N. Uozumi, W. Li, N. Taniguchi, *Biochim. Biophys. Acta, Gen. Subj.* **1999**, *1473*, 9.

[19] G. Wiederschain, *Glycobiology and Human Diseases*, Vol. 1, (Eds.: G. Wiederschain), CRC Press, **2016**, pp. 244-254.

[20] J. Finne, *Eur. J. Biochem.* **1980**, *104*, 181.

[21] W. T. J. Morgan, W. M. Watkins, *Br. J. Exp. Pathol.* **1953**, *34*, 94.

[22] a) F.-i. Yamamoto, H. Clausen, T. White, J. Marken, S.-i. Hakomori, *Nature* **1990**, *345*, 229 EP -; b) A. M. Slaney, I. E. Dijke, M. Jeyakanthan, C. Li, L. Zou, P. Plaza-Alexander, P. J. Meloncelli, J. A. Bau, L. L. Allan, T. L. Lowary et al., *Bioconjugate Chem.* **2016**, *27*, 705.

[23] E. J. Yunis, J. M. Svardal, R. A. Bridges, *Blood* **1969**, *33*, 124.

[24] L. C. Lindesmith, E. F. Donaldson, A. D. LoBue, J. L. Cannon, D.-P. Zheng, J. Vinje, R. S. Baric, *PLoS Med.* **2008**, *5*, e31.

[25] G. E. Rydell, E. Kindberg, G. Larson, L. Svensson, *Rev. Med. Virol.* **2011**, *21*, 370.

[26] G. R. Vasta, L. M. Amzel, M. A. Bianchet, M. Cammarata, C. Feng, K. Saito, *Front. Immunol.* **2017**, *8*, 1648.

[27] R. Bishnoi, I. Khatri, S. Subramanian, T. N. C. Ramya, *Glycobiology* **2015**, *25*, 888.

[28] a) J. Chen, S. Xiao, Z. Yu, *Fish Shellfish Immunol.* **2011**, *30*, 750; b) T. Haselhorst, T. Weimar, T. Peters, *J. Am. Chem. Soc.* **2001**, *123*, 10705.

[29] L. Cooling, *Clin. Microbiol. Rev.* **2015**, *28*, 801.
[30] E. Bartnicki, J. B. Cunha, A. O. Kolawole, Wobus C. E., *F1000Res* **2017**, *6*, 79.
[31] R. Chen, J. D. Neill, M. K. Estes, B. V. V. Prasad, *PNAS* **2006**, *103*, 8048.
[32] J.-M. Choi, A. M. Hutson, M. K. Estes, B. V. V. Prasad, *Proc. Natl. Acad. Sci. USA* **2008**, *105*, 9175.
[33] M. Tan, R. S. Hegde, X. Jiang, *J. Virol.* **2004**, *78*, 6233.
[34] a) S. Cao, Z. Lou, M. Tan, Y. Chen, Y. Liu, Z. Zhang, X. C. Zhang, X. Jiang, X. Li, Z. Rao, *J. Virol.* **2007**, *81*, 5949; b) B. Fiege, C. Rademacher, J. Cartmell, P. I. Kitov, F. Parra, T. Peters, *Angew. Chem. Int. Ed.* **2012**, *51*, 928.
[35] W. Nasir, M. Frank, A. Kunze, M. Bally, F. Parra, P.-G. Nyholm, F. Höök, G. Larson, *ACS Chem. Biol.* **2017**, *12*, 1288.
[36] H. Schroten, F.-G. Hanisch, G. S. Hansman, *J. Virol.* **2016**, *90*, 5855.
[37] A. D. Koromyslova, M. M. Leuthold, M. W. Bowler, G. S. Hansman, *Virology* **2015**, *483*, 203.
[38] A. Mallagaray, J. Lockhauserbäumer, G. Hansman, C. Uetrecht, T. Peters, *Angew. Chem.* **2015**, *127*, 12182.
[39] W. Liu, Y. Chen, X. Jiang, M. Xia, Y. Yang, M. Tan, X. Li, Z. Rao, *PLoS Pathog.* **2015**, *11*, e1005025.
[40] R. Hugh, E. Leifson, *Int. J. Syst. Evol. Microbiol.* **1964**, *14*, 69.
[41] A. V. Grishin, M. S. Krivozubov, A. S. Karyagina, A. L. Gintsburg, *Acta Naturae* **2015**, *7*, 29.
[42] a) C. Chemani, A. Imberty, S. de Bentzmann, M. Pierre, M. Wimmerová, B. P. Guery, K. Faure, *Infect. Immun.* **2009**, *77*, 2065; b) E. M.V. Johansson, S. A. Crusz, E. Kolomiets, L. Buts, R. U. Kadam, M. Cacciarini, K.-M. Bartels, S. P. Diggle, M. Cámara, P. Williams et al., *Chem. Biol.* **2008**, *15*, 1249.
[43] H.-P. Hauber, M. Schulz, A. Pforte, D. Mack, P. Zabel, U. Schumacher, *Int. J. Med. Sci.* **2008**, *5*, 371.
[44] N. Garber, U. Guempel, N. Gilboa-Garber, R. J. Royle, *FEMS Microbiol. Lett.* **1987**, *48*, 331.
[45] D. Avichezer, N. Gilboa-Garber, *FEBS Lett.* **1987**, *216*, 62.
[46] E. P. Mitchell, C. Sabin, L. Šnajdrová, M. Pokorná, S. Perret, C. Gautier, C. Hofr, N. Gilboa-Garber, J. Koča, M. Wimmerová et al., *Proteins* **2005**, *58*, 735.
[47] R. Loris, D. Tielker, K.-E. Jaeger, L. Wyns, *J. Mol. Biol.* **2003**, *331*, 861.
[48] C. Sabin, E. P. Mitchell, M. Pokorná, C. Gautier, J.-P. Utille, M. Wimmerová, A. Imberty, *FEBS Lett.* **2006**, *580*, 982.
[49] K. Marotte, C. Preville, C. Sabin, M. Moume-Pymbock, A. Imberty, R. Roy, *Org. Biomol. Chem.* **2007**, *5*, 2953.
[50] S. Perret, C. Sabin, C. Dumon, M. Pokorná, C. Gautier, O. Galanina, S. Ilia, N. Bovin, M. Nicaise, M. Desmadril et al., *Biochem. J.* **2005**, *389*, 325.
[51] B. Zeuner, C. Jers, J. D. Mikkelsen, A. S. Meyer, *J. Agric. Food Chem.* **2014**, *62*, 9615.
[52] G. Yilmaz, C. R. Becer, *Front. Bioeng. Biotechnol.* **2014**, *2*, 39.
[53] C. Muller, G. Despras, T. K. Lindhorst, *Chem. Soc. Rev.* **2016**, *45*, 3275.
[54] a) M. L. Huang, S. C. Purcell, S. Verespy III, Y. Wang, K. Godula, *Biomater. Sci.* **2017**, *5*, 1537; b) W.B. Turnbull, J.F. Stoddart, *Rev. Mol. Biotechnol.* **2002**, *90*, 231; c) S. Sattin, A. Bernardi, *Carbohydrate Chemistry: Design and synthesis of glycomimetics, Vol. 41*, (Eds.: A. P. Rauter, T. K. Lindhorst, Y. Queneau), The Royal Society of Chemistry, **2016**, pp. 1-25.
[55] J. M. Gargano, T. Ngo, J. Y. Kim, D. W. K. Acheson, W. J. Lees, *J. Am. Chem. Soc.* **2001**, *123*, 12909.
[56] N. Berthet, B. Thomas, I. Bossu, E. Dufour, E. Gillon, J. Garcia, N. Spinelli, A. Imberty, P. Dumy, O. Renaudet, *Bioconjugate Chem.* **2013**, *24*, 1598.
[57] R. J. Pieters, *Org. Biomol. Chem.* **2009**, *7*, 2013.

[58] B. Gerland, A. Goudot, G. Pourceau, A. Meyer, V. Dugas, S. Cecioni, S. Vidal, E. Souteyrand, J.-J. Vasseur, Y. Chevolot et al., *Bioconjugate Chem.* **2012**, *23*, 1534.
[59] C. Rademacher, J. Guiard, P. I. Kitov, B. Fiege, K. P. Dalton, F. Parra, D. R. Bundle, T. Peters, *Chem. Eur. J.* **2011**, *17*, 7442.
[60] a) J. E. Gestwicki, C. W. Cairo, L. E. Strong, K. A. Oetjen, L. L. Kiessling, *J. Am. Chem. Soc.* **2002**, *124*, 14922; b) J.-F. Lutz, *Sequence-Controlled Polymers*, Vol. 1, (Eds.: J.-F. Lutz), Wiley-VCH, Weinheim, **2018**, pp. 229.
[61] U. Westerlind, T. K. Lindhorst, *Beilstein J. Org. Chem.* **2012**, *8*, 804.
[62] a) E. Kolomiets, E. M. V. Johansson, O. Renaudet, T. Darbre, J.-L. Reymond, *Org. Lett.* **2007**, *9*, 1465; b) M. Fischer, F. Vögtle, *Angew. Chem.* **1999**, *111*, 934; c) H.-B. Mekelburger, W. Jaworek, F. Vögtle, *Angew. Chem.* **1992**, *104*, 1609.
[63] D. A. Tomalia, H. Baker, J. Dewald, M. Hall, G. Kallos, S. Martin, J. Roeck, J. Ryder, P. Smith, *Polym. J.* **1985**, *17*, 117.
[64] a) F. Morvan, A. Meyer, A. Jochum, C. Sabin, Y. Chevolot, A. Imberty, J.-P. Praly, J.-J. Vasseur, E. Souteyrand, S. Vidal, *Bioconjugate Chem.* **2007**, *18*, 1637; b) S. Sattin, A. Bernardi, *Carbohydrate Chemistry, Vol. 41*, (Eds.: A. P. Rauter, T. K. Lindhorst, Y. Queneau), The Royal Society of Chemistry, **2016**, pp. 1–25; c) N. Galanos, E. Gillon, A. Imberty, S. E. Matthews, S. Vidal, *Org. Biomol. Chem.* **2016**, *14*, 3476.
[65] Y. Wang, S. Quan, P. Kumar, R. Narain, *Glycopolymer Code - Synthesis of Glycopolymers and their Applications*: *Glyconanoparticles: Synthesis and biomedical applications,* Vol. 1, (Eds.: C. R. Becer, L. Hartmann), Royal Society of Chemistry, **2015**, pp. 196-214.
[66] J. M. de La Fuente, S. Penadés, *Biochim. Biophys. Acta, Gen. Subj.* **2006**, *1760*, 636.
[67] a) D. Pussak, D. Ponader, S. Mosca, S. V. Ruiz, L. Hartmann, S. Schmidt, *Angew. Chem. Int. Ed.* **2013**, *52*, 6084; b) D. Pussak, D. Ponader, S. Mosca, T. Pompe, L. Hartmann, S. Schmidt, *Langmuir* **2014**, *30*, 6142.
[68] S. R. S. Ting, G. Chen, M. H. Stenzel, *Polym. Chem.* **2010**, *1*, 1392.
[69] a) J. Guiard, B. Fiege, P. I. Kitov, T. Peters, D. R. Bundle, *Chem. Eur. J.* **2011**, *17*, 7438; b) M. Meldal, *Macromol. Rapid Commun.* **2008**, *29*, 1016.
[70] a) J. Chiefari, Y. K. Chong, F. Ercole, J. Krstina, J. Jeffery, T. P. T. Le, R. T. A. Mayadunne, G. F. Meijs, C. L. Moad, G. Moad et al., *Macromolecules* **1998**, *31*, 5559; b) B. M. Mandal, *Fundamentals of Polymerization*, Vol. 1, World Scientific, **2013**, pp. 468.
[71] D. Specker, V. Wittmann, *Glycopeptides and Glycoproteins: Synthesis, Structure, and Application*: Synthesis and application of glycopeptide and glycoprotein mimetics, Vol. 267 (Eds. V. Wittmann), Springer Verlag, Berlin, Heidelberg, **2007**, pp. 65-107.
[72] H. Xin, S. Dziadek, D. R. Bundle, J. E. Cutler, *Proc. Natl. Acad. Sci. USA* **2008**, *105*, 13526.
[73] A. Schierholt, M. Hartmann, T. K. Lindhorst, *Carbohydr. Res.* **2011**, *346*, 1519.
[74] L. Hartmann, E. Krause, M. Antonietti, H. G. Börner, *Biomacromolecules* **2006**, *7*, 1239.
[75] D. Ponader, F. Wojcik, F. Beceren-Braun, J. Dernedde, L. Hartmann, *Biomacromolecules* **2012**, *13*, 1845.
[76] D. Ponader, P. Maffre, J. Aretz, D. Pussak, N. M. Ninnemann, S. Schmidt, P. H. Seeberger, C. Rademacher, G. U. Nienhaus, L. Hartmann, *J. Am. Chem. Soc.* **2014**, *136*, 2008.
[77] F. Broecker, J. Hanske, C. E. Martin, J. Y. Baek, A. Wahlbrink, F. Wojcik, L. Hartmann, C. Rademacher, C. Anish, P. H. Seeberger, *Nat. Commun.* **2016**, *7*.
[78] R. B. Merrifield, *J. Am. Chem. Soc.* **1963**, *85*, 2149.
[79] C. A. G. N. Montalbetti, V. Falque, *Tetrahedron* **2005**, *61*, 10827.
[80] R. Behrendt, P. White, J. Offer, *J. Pept. Sci.* **2015**, *22*, 4.

[81] C. A. Chantell, M. A. Onaiyekan, M. Menakuru, *J. Pept. Sci.* **2012**, *18*, 88.
[82] J. J. Monagle, *J. Org. Chem.* **1962**, *27*, 3851.
[83] J. R. Dunetz, J. Magano, G. A. Weisenburger, *Org. Process Res. Dev.* **2016**, *20*, 140.
[84] R. Quarrell, T. D. W. Claridge, G. W. Weaver, G. Lowe, *Mol. Divers.* **1996**, *1*, 223.
[85] Lloyd-Williams, F. Albericio, E. Giralt*, Chemical Approaches to the Synthesis of Peptides and Proteins*, Vol. 1, (Eds.: P. Lloyd-Williams, F. Albericio, E. Giralt), CRC press, **1997**, pp. 177-198.
[86] A. El-Faham, F. Albericio, *Chem. Rev.* 2011, *111*, 6557.
[87] R. Subirós-Funosas, R. Prohens, R. Barbas, A. El-Faham, F. Albericio, *Chem. Eur. J.* **2009**, *15*, 9394.
[88] a) P. Sears, C.-H. Wong, *Science* **2001**, *291*, 2344; b) *Essentials of Chemical Biology*. *Structure and Dynamics of Biological Macromolecules, Chap. 2.3, 2.4*, (Eds.: A. D. Miller, J. Tanner John), Wiley & Sons, **2013**, pp. 102-118.
[89] F. Wojcik, S. Mosca, L. Hartmann, *J. Org. Chem.* **2012**, *77*, 4226.
[90] F. Wojcik, A. G. O'Brien, S. Götze, P. H. Seeberger, L. Hartmann, *Chemistry* **2013**, *19*, 3090.
[91] S. Mosca, F. Wojcik, L. Hartmann, *Macromol. Rapid Commun.* **2011**, *32*, 197.
[92] M. Baier, M. Giessler, L. Hartmann, *Chem. Eur. J.* **2018**, *24*, 1619-1630.
[93] S. Boden, K. G. Wagner, M. Karg, L. Hartmann, *Polymers* **2017**, *9*, 716.
[94] D. Ponader, S. Igde, M. Wehle, K. Marker, M. Santer, D. Bleger, L. Hartmann, *Beilstein J. Org. Chem.* **2014**, *10*, 1603.
[95] S. Wieczorek, S. Vigne, T. Masini, D. Ponader, L. Hartmann, A. K. H. Hirsch, H. G. Börner, *Macromol. Biosci.* **2015**, *15*, 82.
[96] T. Freichel, S. Eierhoff, N. L. Snyder, L. Hartmann, *J. Org. Chem.* **2017**, *82*, 9400.
[97] M. F. Ebbesen, D. Itskalov, M. Baier, L. Hartmann, *ACS Macro Lett.* **2017**, *6*, 399.
[98] a) H. C. Kolb, M. G. Finn, K. B. Sharpless, *Angew. Chem. Int. Ed.* **2001**, *40*, 2004; b) C. W. Tornøe, C. Christensen, M. Meldal, *J. Org. Chem.* **2002**, *67*, 3057.
[99] R. Huisgen, *Proc. Chem. Soc.* **1961**, 357.
[100] L. Liang, D. Astruc, *Coord. Chem. Rev.* **2011**, *255*, 2933.
[101] L. Zhu, C. J. Brassard, X. Zhang, P. M. Guha, R. J. Clark, *Chem. Rec.* **2016**, *16*, 1501.

4 Aims and Outlines

Carbohydrate-lectin interactions play a pivotal role for recognition and adhesion processes in nature. They are often determined by multivalent binding effects as single carbohydrate-lectin interactions are rather weak. The underlying mechanisms of multivalent carbohydrate binding are still not well understood but would provide new opportunities for the development of next generation carbohydrate-based therapeutics such as antibiotics or anticancer drugs.

The investigation of binding in carbohydrate-lectin interaction is often hampered by the demanding synthesis of complex natural glycoconjugates. Therefore, multivalent glycomacromolecules presenting more simplified carbohydrate motifs on a synthetic scaffold have been developed as glycomimetic models of their natural counterparts. Fortunately, only a relatively small amount of monosaccharides seems to build the main carbohydrate target structures with fucose being one of the most important binding motifs due to its exposed position in crucial complex carbohydrates like in histo blood group antigens (HBGA). Interestingly not only bacterial but also viral capsid proteins can bind fucosylated structures of HBGA as is the case for the two important fucose-binding pathogens, Norovirus and *Pseudomonas aeruginosa*.

Epidemic outbreaks of Norovirus infections cause many deaths every year due to serious gastroenteritis. The Norovirus capsid protein called P-dimer is suspected to be responsible for the main interactions with the host cell membrane during carbohydrate-binding leading to first steps of infection. P-dimer exhibits four non-equivalent binding pockets for HBGA located in the cleft formed by the protein-monomers where α-L-fucose seems to be always involved during successful binding. Recently a concentration-dependent multi-step binding process of α-L-methylfucose and HBGA has been discovered leading to the assumption that multivalent binding effects might play a role in the attachment of Norovirus capsid protein to the host cell surface. The opportunistic bacterium *Pseudomonas aeruginosa* is known to cause serious secondary infection in immune-suppressed patients. It forms very dense biofilms on almost all kinds of tissues and organs of the patient. LecB is a crucial lectin of *P. aeruginosa* that is supposed to be involved in the biofilm formation by adhesion towards fucosylated glycan structures on the human cell surfaces. Although several researchers have shown the potential blocking of LecB by fucosylated macromolecules, the mechanistic details in the binding process remain unclear.

Therefore, in this work, monodisperse fucosylated glycomacromolecules should be synthesized to investigate fundamental aspects of multivalent binding with lectins from Norovirus and *P. aeruginosa*. To allow for the investigation of structure-function relations, monodisperse sequence-controlled glycooligo(amidoamines) should be used as platform for the defined presentation of fucose side chains. These glycomimetics were first introduced by Hartmann *et al* and are accessible via the

step-wise assembly of tailor-made building blocks on solid support giving sequence-controlled oligo(amidoamine) scaffolds with precisely positioned functional side chains. These can then be used for the introduction of carbohydrates *e.g.* by copper-mediated click reaction leading to so-called precision glycomacromolecules.

Special focus should be devoted to the influence of valency (number of fucose ligands) and spacing between the fucose side chains on the binding and inhibition behavior towards lectins of interest. For that purpose, the synthesis of suitable backbones constructed by previously established tailor-made building blocks was required as well as the synthesis of alpha-functionalized L-fucose with an appropriate azide linker for the attachment onto the oligomeric scaffolds by CuAAC reaction.

To extend the structural realm of glycomacromolecules further and potentially enable enhanced binding towards the lectins of interest, heteromultivalent glycomacromolecules should be designed and synthesized mimicking histo blood group antigens (HBGA). For this goal, the synthesis of a new building block is necessary that enables the attachment of different carbohydrates in close proximity to each other. Besides α-L-fucose, anomerically pure azidated derivatives of α-D-galactose, *N*-acetyl-α-D-galactosamine, α-sialic acid and β-D-lactose with appropriate linkers need to be prepared for the attachment to the oligomeric scaffolds by CuAAC reaction.

The generated fucosylated glycooligomers should then be subjected to several binding studies with P-dimer and LecB in close collaboration with groups from virology and enzymology. To evaluate if the multistep process in binding of P-dimer to fucose-ligands is based on multivalent binding effects, the interactions of fucose-oligomers, exhibiting different structural characteristics such as varying valences, spacing between the fucose units and chain length, should be investigated by native mass spectrometry by Hao Yan and Dr. Charlotte Uetrecht, by saturation transfer difference (STD) NMR by Robert Creutznacher, Dr. Alvaro Mallagaray and Prof. Dr. Thomas Peters and by co-crystallization experiments by Kerstin Ruoff, Dr. Turgay Kilic and Dr. Grant Hansman. With these methods it is expected to get information about the binding behavior and strength between fucose-oligomers and P-dimer as by native MS and STD NMR studies dissociation constants (K_D) can be determined. In addition, the molecular details in binding could be evaluated by co-crystallization and epitope-mapping (NMR). Examining the influence of fucose-valences and spacing within fucose-oligomers on their inhibitory potential towards LecB and further biofilm formation inhibition-competition-assays should be performed by surface plasmon resonance spectroscopy (SPR). In addition, an enzyme-linked lectin assay (ELLA) should be performed by Nikolina Babic and Dr. Filip Kovacic. Both assays should be adapted to the system fucose-oligomer-LecB. With these methods it is expected to gain insights about structure-function-relations in binding towards and inhibition of LecB.

5 Publications

5.1 Fucose-functionalized precision glycomacromolecules targeting human norovirus capsid protein

Katharina Susanne Bücher, Hao Yan, Robert Creutznacher, Kerstin Ruoff, Alvaro Mallagaray, Andrea Grafmüller, Jan Sebastian Dirks, Turgay Kilic, Sabrina Weickert, Anna Rubailo, Malte Drescher, Stephan Schmidt, Grant Hansman, Thomas Peters, Charlotte Uetrecht, Laura Hartmann

Biomacromolecules **2018**, *19* (9), 3714–3724

DOI: 10.1021/acs.biomac.8b00829
Received 24 May 2018
Published online 2 August 2018
Published in print 10 September 2018

https://pubs.acs.org/doi/10.1021/acs.biomac.8b00829

Own Contribution (first author)

Synthesis of all building blocks and of azidoethyl-2,3,4-tri-*O*-acetyl-α-L-fucopyranoside, synthesis of all glycomacromolecules, characterization of all compounds by conducting HPLC-MS measurements and analyzing results of NMR, MALDI-TOF-MS and HR-ESI-MS, collaborative design of fucosylated glycomimetic structures, collaborative writing of the paper.

Biomacromolecules

Article

Cite This: Biomacromolecules 2018, 19, 3714−3724

pubs.acs.org/Biomac

Fucose-Functionalized Precision Glycomacromolecules Targeting Human Norovirus Capsid Protein

Katharina Susanne Bücher,[†] Hao Yan,[‡] Robert Creutznacher,[§] Kerstin Ruoff,[∥] Alvaro Mallagaray,[§] Andrea Grafmüller,[⊥] Jan Sebastian Dirks,[†] Turgay Kilic,[∥] Sabrina Weickert,[#] Anna Rubailo,[#] Malte Drescher,[#] Stephan Schmidt,[†] Grant Hansman,[∥] Thomas Peters,[§] Charlotte Uetrecht,*[,‡,¶] and Laura Hartmann*[,†]

[†]Heinrich-Heine-University Düsseldorf, Institute for Organic Chemistry and Macromolecular Chemistry, Düsseldorf, Germany

[‡]Heinrich Pette Institute, Leibniz Institute for Experimental Virology, Hamburg, Germany

[§]Institute of Chemistry and Metabolomics, University of Lübeck, Lübeck, Germany

[∥]Schaller Research Group at the University of Heidelberg and the DKFZ, Heidelberg, Germany and Department of Infectious Diseases, Virology, University of Heidelberg, Heidelberg, Germany

[⊥]Max-Planck-Institute of Colloids and Interfaces, Department of Theory and Bio-Systems, Potsdam, Germany

[#]University of Konstanz, Department of Chemistry and Konstanz Research School Chemical Biology, Konstanz, Germany

[¶]European XFEL GmbH, Schenefeld, Germany

Supporting Information

ABSTRACT: Norovirus infection is the major cause of nonbacterial gastroenteritis in humans and has been the subject of numerous studies investigating the virus's biophysical properties and biochemical function with the aim of deriving novel and highly potent entry inhibitors to prevent infection. Recently, it has been shown that the protruding P domain dimer (P-dimer) of a GII.10 Norovirus strain exhibits two new binding sites for L-fucose in addition to the canonical binding sites. Thus, these sites provide a novel target for the design of multivalent fucose ligands as entry inhibitors of norovirus infections. In this current study, a first generation of multivalent fucose-functionalized glycomacromolecules was synthesized and applied as model structures to investigate the potential targeting of fucose binding sites in human norovirus P-dimer. Following previously established solid phase polymer synthesis, eight precision glycomacromolecules varying in number and position of fucose ligands along an oligo(amidoamine) backbone were obtained and then used in a series of binding studies applying native MS, NMR, and X-ray crystallography. We observed only one fucose per glycomacromolecule binding to one P-dimer resulting in similar binding affinities for all fucose-functionalized glycomacromolecules, which based on our current findings we attribute to the overall size of macromolecular ligands and possibly to steric hindrance.

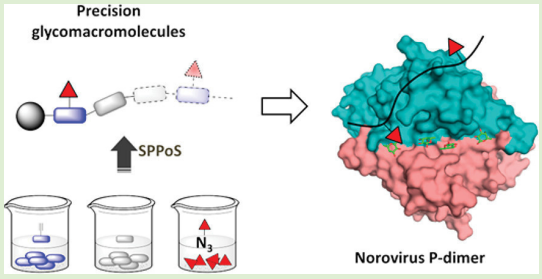

1. INTRODUCTION

Noroviruses (NoVs) belong to the *Caliciviridae* family and are the main cause of epidemic outbreaks of nonbacterial gastroenteritis worldwide. NoVs cluster in 7 main genogroups (termed GI-GVII) and these genogroups are further divided into numerous genotypes. The GII genotype 4 (GII.4) has caused several pandemics over the past decade and is by far the most clinically relevant.[1] Histo-blood group antigens (HBGAs) and the α-1,2-linked fucoside are well studied binding determinants for NoV.[2] The viral particles have icosahedral symmetry and contain 180 copies (90 dimers) of the major structural protein VP1 (~60 kDa). The VP1 is divided into shell (S) and protruding (P) domains. The P domain dimer (P-dimer) contains two HBGA binding sites.[3,4] These two HBGA pockets (termed fucose sites 1 and 2) are for the most part structurally conserved with genotypes, but are different among the genogroups.[4] Recently, a third and fourth α1,2-linked fucoside binding pocket (termed fucose sites 3 and 4) located between the two outer canonical binding sites were discovered by X-ray crystallography (Figure 1).[5−7] The atomic distances between the four-fucose binding pockets are estimated to be 11 Å (fucose sites 1 and 3), 17 Å (fucose sites 1 and 4) and 27 Å (pockets 1 and 2). It has been shown that the terminal α-L-fucoside moiety of HBGAs plays a key role in binding onto P-dimer for many NoV genotypes, where the responsible residues at binding pockets 1 and 2 are highly conserved.[8,9] However, the binding affinity to L-fucose is rather weak and in the low millimolar range. In order to increase

Received: May 24, 2018
Revised: July 31, 2018
Published: August 2, 2018

DOI: 10.1021/acs.biomac.8b00829
Biomacromolecules 2018, 19, 3714−3724

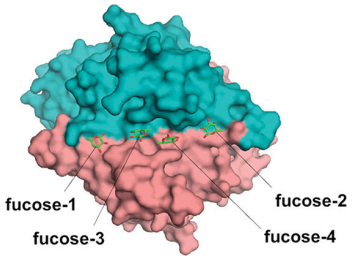

Figure 1. Structure of NoV GII.10 P-dimer (monomers A [teal] and B [salmon], surface representation) in complex with L-fucose (green sticks). Binding of L-fucose to the four binding sites in P-dimer was demonstrated to be a dose-dependent and stepwise process, in which pockets 1 and 2 displayed the highest affinities toward L-fucose.[5]

binding by avidity, multivalent structures presenting several fucose ligands can be used. Bundle et al. have shown that fucosylated polymers (60−100 kDa) had 10^6-fold enhanced binding to NoV-like particles.[10,11] However, little is known about the underlying mechanism of the ligand-virus binding and whether it is possible for a multivalent fucose-bearing ligand to bind simultaneously at all four binding sites.

Therefore, in this study, we report on the synthesis of a first generation of fucosylated precision glycomacromolecules and their use as multivalent model structures for the investigation of binding to NoV P-dimers. Precision glycomacromolecules were synthesized following previously established protocols for the stepwise assembly of tailor-made building blocks on solid support, giving an oligo(amidoamine) scaffold that allows for the conjugation of sugar ligands in the side chains.[12,13] By choosing the sequence of building blocks during solid phase assembly, the number and position of fucose ligands along the scaffold can be controlled. The binding of the fucosylated glycomacromolecules on NoV P-dimers were investigated with two different GII genotypes (GII.4 and GII.10) using a combination of native MS, STD NMR, and X-ray crystallography.

2. EXPERIMENTAL SECTION

2.1. Solid Phase Synthesis of Glycomacromolecules. The synthesis of glycomacromolecules was realized by solid phase polymer synthesis, based on previously established protocols by stepwise assembly of tailor-made building blocks, specifically an alkyne-functionalized building block (TDS) and an ethylene glycol building block (EDS; Scheme 1).[12−16] The resulting oligomer backbones were functionalized with fucose ligands on defined positions by using azido-functionalized α-L-fucopyranoside (Fuc-N_3) in a Cu-mediated alkyne−azide cycloaddition (CuAAC) on solid support (Scheme 1). The final target structures were cleaved from the resin and purified by preparative RP-HPLC leading to glycomacromolecules **1**−**9** (Figure 2; for details, cf. SI).

Scheme 1. General Synthetic Scheme for the Preparation of Precision Glycomacromolecules Presenting Fucose via Solid Phase Assembly of Tailor-Made Building Blocks[a]

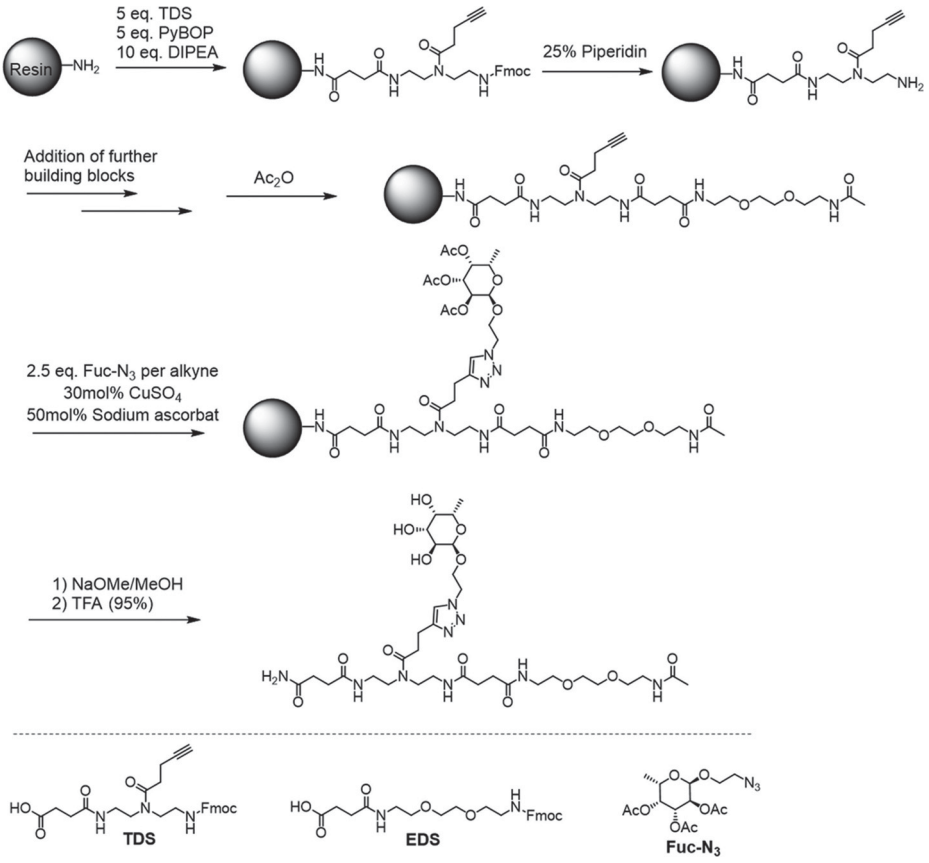

[a]Solid support was a Tentagel S RAM (rink amide) resin; for further details on the synthesis, see SI.

DOI: 10.1021/acs.biomac.8b00829
Biomacromolecules 2018, 19, 3714−3724

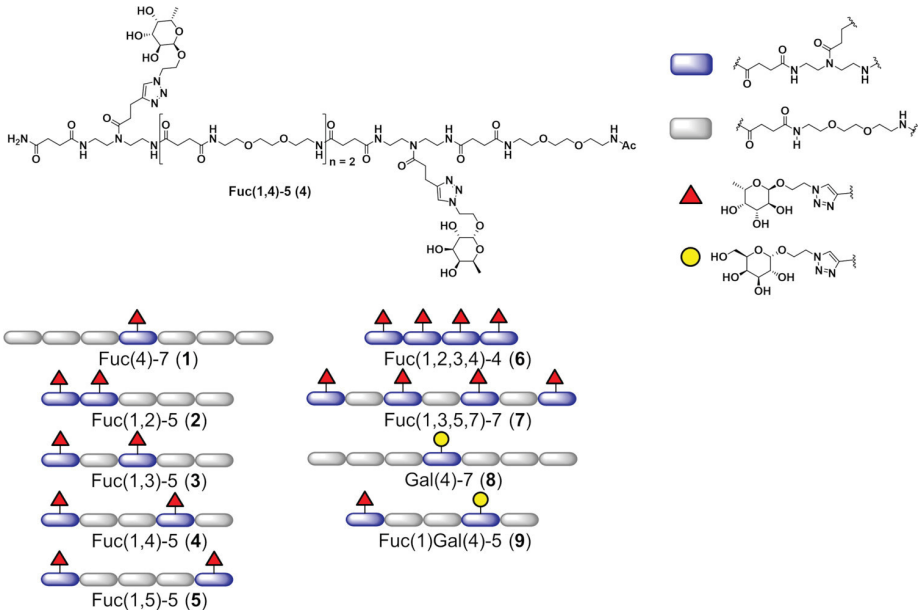

Figure 2. Overview of the structures of precision glycomacromolecules **1**−**9** presenting α-L-fucose and D-galactose.

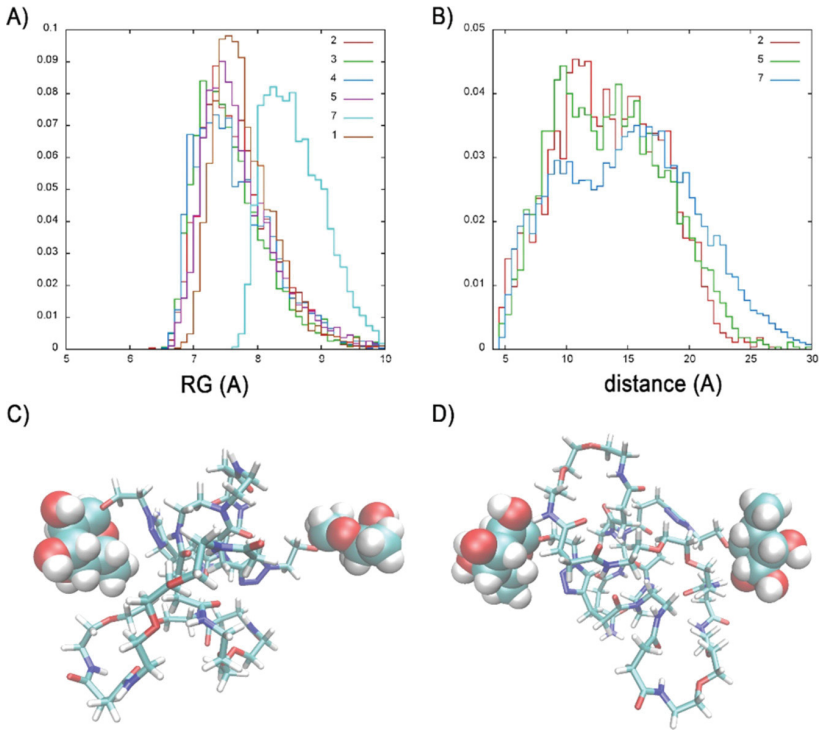

Figure 3. Glycomacromolecule simulations: (A) distribution of the radius of gyration for molecules **1**, **2**, **3**, **4**, **5**, and **7**; (B) distribution of the distance between fucose ligands for molecules **2** (purple), **5** (blue), and **7** (green); (C) snapshot of glycomacromolecule **2** and (D) snapshot of glycomacromolecule **5**.

3. RESULTS AND DISCUSSION

3.1. Design and Synthesis of Precision Glycomacromolecules. The focus of this study was the synthesis of fucose-presenting precision macromolecules and their use as multivalent model structures to investigate binding to NoV P-dimers. Two different GII genotypes (GII.4 and GII.10) were examined. We applied previously reported stepwise assembly of tailor-made building blocks on solid support, or so-called solid phase polymer synthesis,[12,13] for the sequence-controlled attachment of α-L-fucoside in the side chain of monodisperse oligo(amidoamine) scaffolds. Two different building blocks were used: (i) a hydrophilic spacer building block (EDS) and (ii) an alkyne-functionalized building block (TDS).[13,15] All building blocks possess a free carboxyl and an Fmoc-protected amine group allowing for chain elongation via standard Fmoc-

DOI: 10.1021/acs.biomac.8b00829
Biomacromolecules 2018, 19, 3714−3724

peptide coupling protocols. The sequence of building blocks during the chain elongation thereby gives the primary sequence of the macromolecular scaffold and allows for variations of the number and position of sugar ligands, as well as the overall length of the scaffold. After assembly of the scaffold, the alkyne side chains are conjugated with azido-functionalized α-L-fucoside or D-galactoside derivatives via Cu(I)-mediated 1,3-dipolar cycloaddition (CuAAC) to give the final precision glycomacromolecules (see Scheme 1). The azido-functionalized D-galactose was obtained following literature protocols[17] and used as anomeric mixture with an α/β-ratio of 1:4 as both anomers could serve as a negative control for binding. Azido-functionalized α-L-fucose derivative, 1-azidoethyl-2,3,4-tri-*O*-acetyl-α-L-fucopyranoside, was synthesized adapting a protocol applying H_2SO_4-silica catalyst for α-L-fucose with an azido ethyl linker (see SI).[18] Here, isolation of the α-anomer is important, since this is the "native type" of monosaccharide that binds onto the NoV P-dimer.[9]

Overall, nine precision glycomacromolecules were synthesized presenting up to four fucose ligands (Figure 2). As monovalent ligand (**1**), an oligomeric backbone with three EDS building blocks to each side of the fucose side chain was synthesized in order to account for a similar overall chain length in comparison to the other glycomacromolecules of this study. For divalent glycomacromolecules, a series with varying interligand distance going from zero to three EDS spacing building blocks between the fucose carrying building blocks was synthesized (**2**−**5**). Assuming an all-stretched conformation of the oligomeric backbone, the distance between two neighboring fucose ligands with no additional spacer building block would be ∼31 Å and thus correspond roughly to the distance between fucose sites 1 and 2 (∼27 Å).[11] However, we should rather assume a coiled structure of the glycomacromolecules in solution, since this coiled structure was previously discovered using fluorescence correlation spectroscopy.[12] To obtain insights into the conformation of fucosylated glycomacromolecules in solution, MD simulations were performed. Distance distributions of neighboring fucose ligands (center of mass of fucoses) for glycomacromolecules with different spacing range from approximately 10 to 20 Å (see Figure 3B). Thus, different spacing of ligands along the backbone does not become evident as differences in ligand spacing in the coiled conformation (Figure 3C,D). However, upon contact to a protein receptor, a change in the scaffold's conformation might occur to accommodate binding sites of the receptor.[19,20] Furthermore, MD simulations indicate that longer backbones lead to an increase in the radius of gyration of the overall glycomacromolecule (Figure 3A). Therefore, in order to keep the overall chain length constant, EDS building blocks were added to the backbone to obtain an overall chain length of five building blocks for all divalent macromolecules. Additionally, two tetravalent glycomacromolecules were synthesized having zero or one spacer building block between the sugar side chains (**6**, **7**). As control, a monovalent galactose functionalized glycomacromolecule (**8**) was synthesized as well as a first heterodivalent structure presenting one fucose and one galactose ligand (**9**).

The glycomacromolecules have been isolated as crude products after deprotection of the carbohydrate side chains and obtained after cleavage from the solid support with purities of 90−95% (analyzed by integration of UV signal at 214 nm using RP-HPLC). All glycomacromolecules were then further purified by ion exchange chromatography (quarternary ammonium, acetate form)[21] followed by semipreparative RP-HPLC and obtained with final purities ≥97% (analyzed by integration of UV signal at 214 nm using RP-HPLC; Table 1). All structures were confirmed by MS, HPLC, and NMR (see SI).

Table 1. Analytical Data Obtained for Precision Glycomacromolecules 1−9

Entry	Glycomacromolecule	MW (g/mol) calculated (meas.$[M+Na]^+$)[1]	Relative Purity[2](RP-HPLC)	R_h[3,4] (nm)
	Schematic structures			
1		1938.04 (1961.1)	98%	n.m.
2		1745.90 (1769.0)	98%	1.3±0.1
3	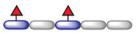	1745.90 (1769.0)	98%	n.m.
4		1745.90 (1769.0)	99%	n.m.
5		1745.90 (1769.0)	99%	1.2±0.04
6	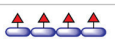	2052.01 (2075.0)	99%	1.2±0.1
7		2742.39 (2765.4)	97%	n.m.
8	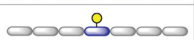	1954.04 (1977.1)	99%	n.m.
9		1761.90 (1784.9)	95%	1.3±0.1

[1]As determined by MALDI TOF MS as $[M + Na]^+$. [2]As determined by integration of UV-signal in RP LCMS for final products (gradient: water/acetonitrile (95:5) to water acetonitrile (1:1) in 30 min). [3]As determined by dynamic light scattering. [4]Buffer surrogate = 20 mM tetraethylammonium acetate (TEAA), 300 mM ammonium acetate (AmAc), pH 7, n.m. = not measured.

In order to analyze hydrodynamic size of the derived glycomacromolecules in solution, a light scattering study was performed. We observed that selected glycomacromolecules show hydrodynamic diameters of about 1.2−1.3 nm under buffered or high ionic strength conditions (see Table 1). These values are slightly larger than would have been expected based on the modeling data ($R_h = 0.665R_G$, for random coil polymers in θ conditions), but they still support an overall coiled conformation of the glycomacromolecules. Interestingly, when performing the measurement in the absence of salt (ultrapure water), we see the formation of aggregates of about 115 ± 15 nm in diameter. Since the overall solution is still optically transparent, we assume that the overall number of aggregates is rather small. However, to further confirm these findings additional experiments will be required, for example, cryo-TEM.

3.2. Binding Studies of Glycomacromolecules toward NoV GII.4 P-Dimer. *Native MS Measurements.* In order to obtain first insights into the potential multivalent binding of fucose-presenting glycomacromolecules to P-dimer, native MS measurements were performed using GII.4 P-dimers. In short, native MS employs nanoelectrospray ionization (ESI) to preserve noncovalent complexes in the gas phase and therefore allows analysis of the number of glycomacromolecules bound to the P-dimer protein.[6,22,23] Since binding affinities of P-dimers for glycans are low, the reference protein method is used to correct for unspecific clustering of ligands during the ESI process.[24] It has previously been shown that the size of the reference protein does not affect the unspecific clustering,[25] and we therefore chose cytochrome c to avoid any spectral

DOI: 10.1021/acs.biomac.8b00829
Biomacromolecules 2018, 19, 3714−3724

overlaps. As small ligands only marginally influence ionization efficiency, the peak areas of bound and unbound P-dimer can be translated into concentrations and the K_D be directly retrieved from the law of mass action. As is well described in the literature, multivalent ligands such as the precision glycomacromolecules can undergo different binding modes when binding to a multivalent protein.[26] In the native MS experiment, the intermolecular complex formation can be observed and particularly the stoichiometry of several ligands binding to one protein receptor can be detected.[27] Furthermore, it is possible to ramp ligand concentrations like in a titration to deduce cooperativity. In this case, we have analyzed 2−3 concentrations, which gave consistent K_D values (see Table 2), indicating no strong cooperative effects.

Table 2. Results of Native MS Measurements of Glycomacromolecules 1−9 as Well as HBGA B Tetrasaccharide as Positive Control Binding to GII.4 P-Dimer

Entry	Glycomacromolecule	K_{D1} (μM)[a]	Concentration glycomacromolecule (μM)		
			100	150	200
	Schematic structures		Maximum number of glycooligomers per P-dimer		
1		230 ± 50	1	1	1
2		310 ± 90	1	1	2
3		240 ± 60	1	2	2
4		340 ± 130	1	1	2
5		290 ± 90	1	1	2
6		380 ± 100	1		1
7		330 ± 80	1	1	1
8	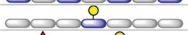	2400 ± 600	1	1	1
9		370 ± 90	1		1
HBGA B		110 ± 30	2	3	3

[a]Average value for the dissociation constant for the first glycomacromolecule bound, errors represent the standard deviation.

Figure 4 shows an exemplary mass spectrum after correction for unspecific clustering and normalization to the highest unbound protein peak recorded for glycomacromolecules **5** and **6** binding to GII.4 P-dimer at different concentrations. For higher concentrations (200 μM), it can be seen that up to two glycomacromolecules **5** can bind to GII.4 P-dimer at the concentrations tested (p2; Figure 4). From the experiment we cannot say, which of the fucose ligands binds to the protein or which of the protein binding sites is occupied. However, an apparent binding constant K_{D1} for the first binding event (p1) can be derived from the intensities of the different complexes giving an indication for the overall affinity of the glycomacromolecules toward GII.4 P-dimer.

Table 2 shows the data obtained for the series of glycomacromolecules using GII.4 P-dimers. Initially, we examined the negative control, the galactose carrying structure **8**. We observed some residual binding at higher concentration (SI) with weak binding affinities (K_{D1} = 2.4 ± 0.6 mM). Based on the available STD NMR data, we know there is no interaction between NoV and galactose (see also Figure 5). The observed binding therefore is considered a result from variation in electrospray quality or marginal backbone contribution. Signals of this residual binding do not exceed 10% including standard deviation for p1 and are therefore defined as threshold for stoichiometry determination. Next, the number of glycomacromolecules that can bind to GII.4 P-dimer in dependence of their valences was examined. We found that at the highest concentration evaluated, ligand-protein complexes with up to two glycomacromolecules per protein were detected for divalent systems **2**−**5**. This is in agreement with previous studies investigating the multivalent binding of glycomacromolecules based on similar scaffold showing formation of intermolecular complexes via ligand−receptor clustering.[12,16] All other glycomacromolecules show only binding of one glycomacromolecule per protein above

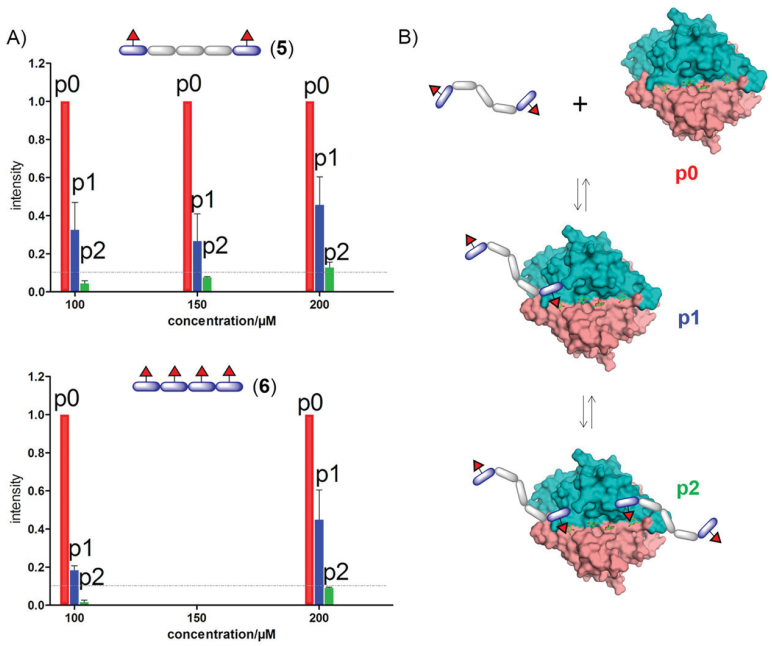

Figure 4. (A) Native MS results: interaction of NoV GII.4 P-dimer with glycooligomers **5** and **6** at indicated concentrations in 300 mM NH_4OAc and 20 mM TEAA pH 7; (B) proposed binding of divalent glycomacromolecule **5** with P-dimer (structures not to scale).

DOI: 10.1021/acs.biomac.8b00829
Biomacromolecules 2018, 19, 3714−3724

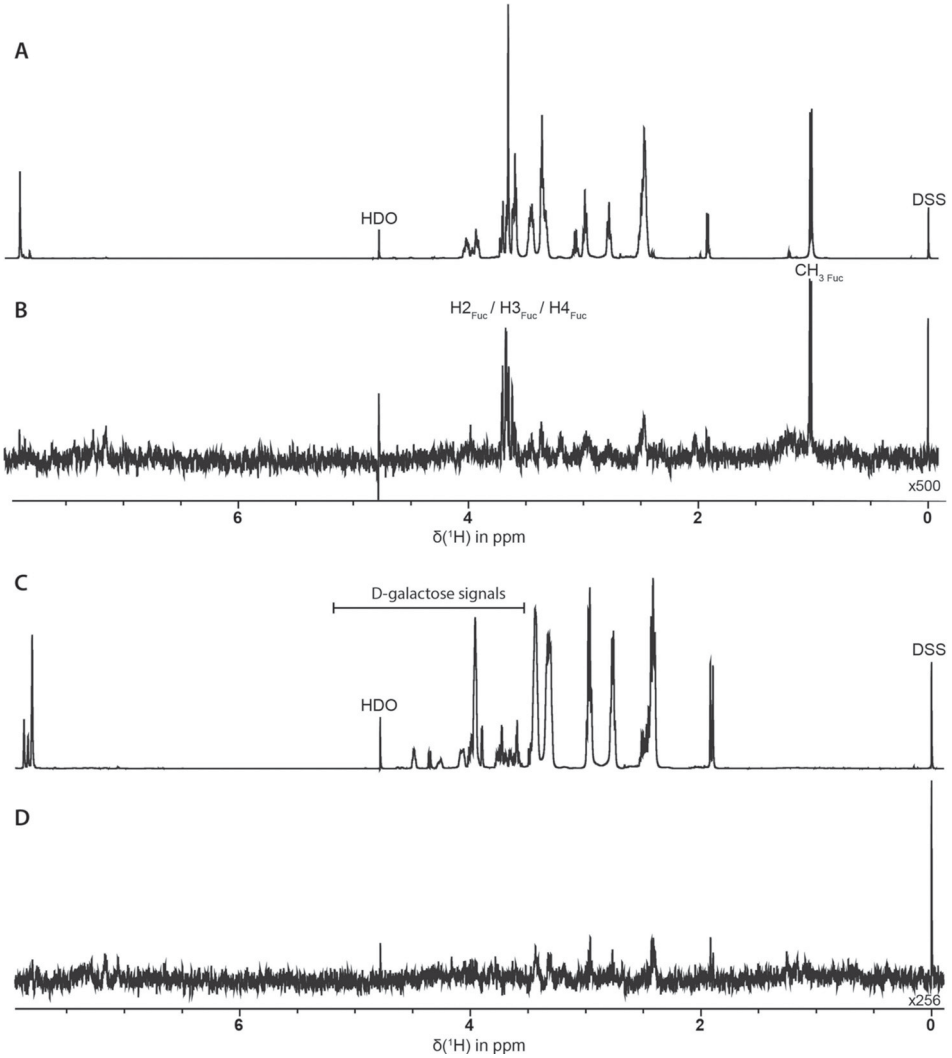

Figure 5. STD NMR spectra of glycomacromolecule **7** (B) and tetravalent galactose-functionalized glycomacromolecule **11** (see SI; D). Spectra were acquired on a Bruker AVIII 500 MHz NMR spectrometer. The concentration of glycomacromolecules **7** and **11** was 1 mM in each sample. STD spectra were obtained in the presence of 30 μM GII.4 P-dimers with a saturation time of 2 s. For more details, see Experimental Section. (A) Reference (off-resonance) ^{1}H NMR spectrum of glycomacromolecule **7**. (B) Difference spectrum of glycomacromolecule **7** in the presence of P-dimers. (C) Reference (off-resonance) ^{1}H NMR spectrum of **11**, (D) Difference spectrum of **11** in the presence of P-dimers. For display, the difference spectra (B) and (D) have been scaled by factors of 500 and 256, respectively, due to a different number of scans used in the experiments (see Experimental Section).

threshold. This is particularly interesting for the higher valent structures **6** and **7**, as they present four instead of two fucose units but show no enhanced binding and formation of only single ligand−protein complexes. We would have rather expected an increase in intermolecular complex formation due to higher statistical chance of ligand−receptor binding. Indeed, it has been shown for glycopolymers that higher-valent structures do not necessarily promote increased binding but that an increase in the number of sugar residues can also lead to a decrease in binding.[15] The underlying mechanisms of such findings are not fully understood but contributions could arise from increasing sizes of the ligands or decreased rotational freedom with increasing valency.

When we now look at the K_{D1} values derived from the native MS experiments (see Experimental Section), all fucose containing glycomacromolecules have similar affinities (K_{D1} of 200−400 μM). In order to compare K_{D1} values with known ligands of P-dimer, HBGA B tetrasaccharide type 1 was tested with GII.4 P-dimers. The natural ligand has a slightly higher affinity (K_{D1} of 110 ± 30 μM). The monosaccharide ligand, methyl α-L-fucopyranoside, could not be used as reference as the mass difference is too small to allow for resolution between bound and unbound species. If the glycomacromolecules would be able to address more than one binding site of P-dimer simultaneously in a chelate binding mode, we would expect an increase in affinity. We therefore conclude that only single fucose ligands per glycomacromolecule bind and no avidity effects are observed in the different multivalent structures as is also supported by the heterovalent species (**9**) behaving similar to the fucose only structures.

When considering simultaneous binding of different fucose residues of one glycomacromolecule, based on the ligand distances derived from the modeling and light scattering study, glycomacromolecules in their coiled conformation could

DOI: 10.1021/acs.biomac.8b00829
Biomacromolecules 2018, 19, 3714−3724

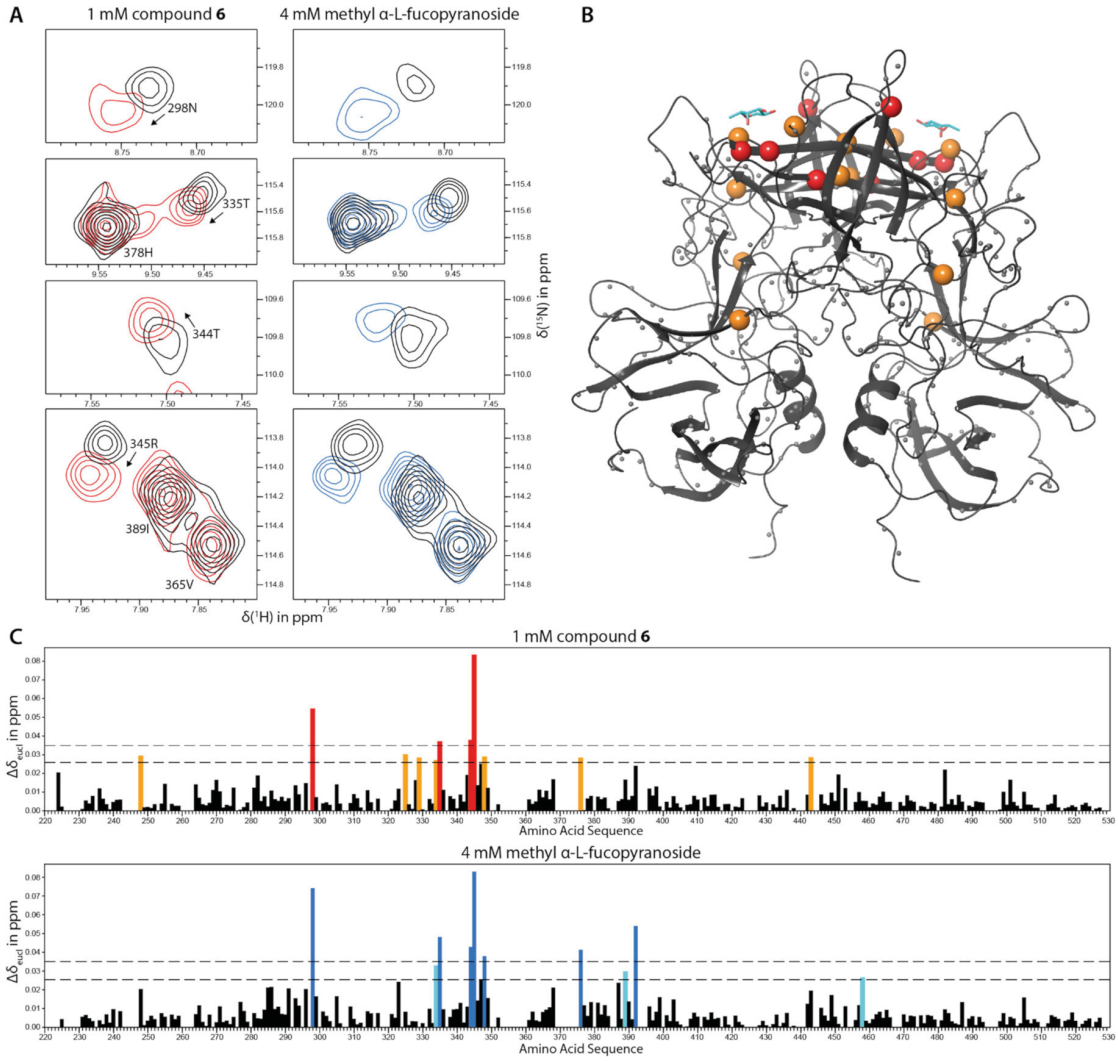

Figure 6. NMR chemical shift perturbation (CSP) experiments. CSPs are given as Euclidean distances $\Delta\delta$.[36] Selected regions from $^{1}H,^{15}N$-TROSY HSQC experiments (A) showing NH cross peaks of amino acids of uniformly $^{2}H,^{15}N$-labeled GII.4 P-dimer (black contours) and with Euclidean perturbations > $\mu + 3\sigma$ in the presence of 1 mM concentration of glycomacromolecule **6** (red contours). For comparison, to the right the same region of a $^{1}H,^{15}N$-TROSY HSQC spectrum of P-dimers (black contours) compared to a spectrum in the presence of 4 mM methyl α-L-fucopyranoside (blue contours) is shown. (B) CSPs are mapped on the crystal structure of the GII.4 P-dimer (pdb 4 × 06). For clarity, only the L-fucose residues (blue) of the B-trisaccharide ligands are shown. CSPs > $\mu + 2\sigma$ are highlighted in orange, CSPs > $\mu + 3\sigma$ are highlighted in red. Gray balls indicate perturbations below the significance threshold (2σ). (C) CSPs ($\Delta\delta$) of backbone NH signals. The upper panel shows the effect of glycomacromolecule **6**, and the lower panel refers to methyl α-L-fucopyranoside. 2σ (orange in the upper panel, light blue in the lower panel) and 3σ (red in the upper panel, blue in the lower panel) levels are visualized by dashed lines.

bridge binding site 1 with fucose binding sites 3 (also sites 2 and 4; see Figure 1). However, as previously discussed, this is not supported by similar K_{D1} values in native MS experiments. In principle, multivalent ligands based on flexible scaffolds such as the glycomacromolecules can also undergo a conformational change paying an entropic penalty in order to increase ligand-protein interactions.[19,20] Thereby, glycomacromolecules could theoretically also bridge the outer binding sites 1 and 4. To test this, divalent glycomacromolecule **4** was used in an electron paramagnetic resonance (EPR) experiment similar to previously described experiments by Wittmann and Drescher.[19] By the introduction of spin labels, here TEMPO side chains, at both ends of the glycomacromolecule (see SI for synthesis and characterization of resulting glycomacromolecule **10**), distances between these labels were analyzed in the absence and presence of P-dimer via double electron−electron resonance (DEER) spectroscopy (see SI for experimental setup).[28−30] No significant differences in the absence and presence of GII.4 P-dimer were observed suggesting that the conformational ensemble of the glycomacromolecule remains unaltered upon interaction with P-dimer (see SI).

Recent studies based on native MS[31] and simple docking[32] show that larger oligosaccharides such as blood group A or B tri- and tetrasaccharides do not bind into all four binding sites simultaneously. Along those lines, monovalent binding of glycomacromolecules could be attributed to steric effects resulting from the scaffold blocking binding of a second ligand. Since there are no indications of simultaneous binding of several fucose residues of the same glycomacromolecule, at this time, we cannot exclude the influence of other structural

DOI: 10.1021/acs.biomac.8b00829
Biomacromolecules 2018, 19, 3714−3724

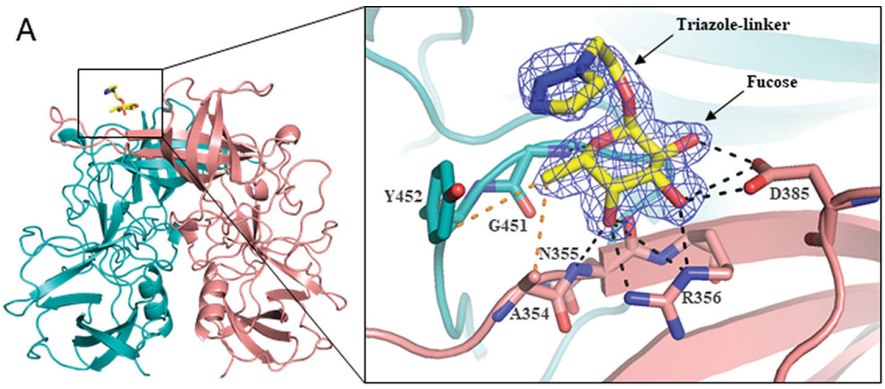

B

GII.10 Pdom [atom]	Type	Glycomacromolecule 6 [atom]	Type	Interaction	Distance (Å)
D385 [OD2]	H-Acceptor	KBA600 [O2]	H-Donor	Hydrogen Bond	2.62
D385 [OD1]	H-Acceptor	KBA600 [O3]	H-Donor	Hydrogen Bond	2.68
N355 [O]	H-Acceptor	KBA600 [O4]	H-Donor	Hydrogen Bond	2.68
R356 [NE]	H-Donor	KBA600 [O3]	H-Acceptor	Hydrogen Bond	2.77
R356 [NH2]	H-Donor	KBA600 [O4]	H-Acceptor	Hydrogen Bond	2.96
G451 [N]	H-Donor	KBA600 [O5]	H-Acceptor	Hydrogen Bond	2.99
N355 [N]	H-Donor	KBA600 [O4]	H-Acceptor	Hydrogen Bond	3.37
R356 [NE]	H-Donor	KBA600 [O4]	H-Acceptor	Hydrogen Bond	3.46
D385 [OD2]	H-Acceptor	KBA600 [O3]	H-Donor	Hydrogen Bond	3.47
A354	Alkyl	KBA600	Alkyl	Hydrophobic	3.65
Y452	Pi-Orbitals	KBA600	Alkyl	Hydrophobic	3.94

Figure 7. X-ray structure analysis of glycomacromolecules **6** cocrystallized with GII.10 P-dimer: (A) Asymmetric unit cell contained one P domain dimer and one glycomacromolecule **6**. The GII.10 P domain was subdivided into monomer chain A (salmon) and B (teal), while the glycomacromolecule is shown in yellow. Close-up view of the binding pocket of GII.10 P domain in complex with fucose ring and a linker structure of glycomacromolecule **6**. Hydrogen bond interactions are black lines and hydrophobic interactions are orange lines. The Omit map (mFo-DFc, blue mesh) is countered at 3.0 σ. (B) List of interactions where hydrogen bonds are between 2.5 and 3.5 Å, while hydrophobic interactions are between 3.6 and 5.3 Å. KBA is the code for glycomacromolecule **6** and the number 600 refers to the position of this ligand in the structure file.

parameters leading to an overall monovalent binding mode, such as an improper spacing of ligands along the scaffold or the conformational flexibility of the scaffold that are well-known to affect multivalent ligand−receptor binding.[12,19,26]

NMR Measurements Using GII.4 P-Dimers. In order to prove that ligand−receptor interactions observed in native MS are indeed based on binding of the fucose ligands attached to the macromolecular scaffold, we performed STD NMR experiments[33,34] as well as protein-based chemical shift perturbation (CSP) NMR experiments. In STD NMR experiments, proton transitions of the protein are saturated applying a low-power radio frequency (r.f.) field at a frequency that does not interfere with any of the ligand resonances. Best results are obtained by using a cascade of Gaussian-shaped low power r.f. pulses. In large proteins, slow tumbling allows for a process called spin diffusion that quickly distributes the saturation throughout the protein, and also toward ligands bound to it. Upon dissociation, ligands revert to fast tumbling and to associated altered relaxation properties allowing them to "store" the received saturation for a much longer period of time than in the slow tumbling protein-bound state. Therefore, a large excess of ligand over protein warrants a maximum accumulation of saturation transfer in the unbound state. Technically, the degree of saturation transfer is measured using difference spectra that are generated by subtracting NMR spectra with saturation from spectra without saturation transfer. STD NMR spectra discriminate binding ligands from nonbinding ligands, at the same time providing information on the binding epitope: Ligand protons closer to protons in the protein binding pocket show stronger STD signals than more remote protons. Performing a titration, STD NMR can be used to obtain dissociation constants K_D. The experiment is extremely well suited for the detection of low affinity binding and works best for low μM to mM K_D values.[35]

Precipitation of ligands in the presence of GII.4 P-dimers was a general problem, making it difficult to provide optimum conditions for STD NMR experiments. For instance, glycomacromolecule **1** led to precipitation at concentrations around 1 mM in the presence of a 30 μM solution of GII.4 P-dimers. Therefore, we were unable to obtain STD NMR titration curves that would have allowed determination of dissociation constants K_D. However, the experiments provided qualitative information about which parts of glycomacromolecules are in close contact with protons of the binding pocket. As an example, Figure 5 shows the STD NMR spectrum of glycomacromolecule **7** in the presence of GII.4 P-dimers. It is obvious that the fucose residues receive by far the largest amount of saturation whereas the backbone is almost "silent".

DOI: 10.1021/acs.biomac.8b00829
Biomacromolecules 2018, 19, 3714−3724

The spectra do not allow to conclude which of the fucose residues binds, or whether only one or more units of an individual glycomacromolecule attach to the protein.

As a negative control, we have recorded STD NMR spectra for tetravalent galactose-functionalized glycomacromolecule (**11**). As seen from Figure 5D, there is no response from the galactose units. Low intensity STD signals are only observed for the backbone, at the same order of magnitude as for glycomacromolecule **7**, nicely demonstrating that selective binding is mediated by fucose residues.

CSP NMR experiments usually employ the chemical shifts of backbone NH protons of a protein as probes sensing binding of ligand molecules, and at the same time mapping the binding pocket of the protein.[36] Interpretation of CSPs ideally requires a full assignment of all backbone NH resonances. As GII.4 P-dimers have a molecular weight of about 70 kDa this assignment is far from being trivial. Fortunately, we have recently succeeded in obtaining an almost complete backbone assignment of GII.4 P-dimers which will be published elsewhere (Biological Magnetic Resonance Data Bank, bmrb entry number 27445). Based on this assignment and employing $^{1}H,^{15}N$ TROSY HSQC spectra in the absence and presence of ligand, we were able to map the binding of glycomacromolecule **6** to GII.4 P-dimers, and to compare it to the binding of methyl α-L-fucopyranoside (Figure 6). Precipitation was a problem for CSP NMR experiments, too, although the experimental conditions were different from the ones applied for STD NMR. Therefore, CSP based titration experiments to obtain dissociation constants were not an option. Glycomacromolecule **6** was chosen as a prototypic glycomacromolecule to test in CSP experiments as glycomacromolecule **6** showed the most benign behavior under the given experimental conditions. From a comparison of CSPs observed for glycomacromolecule **6** versus methyl α-L-fucopyranoside as ligands, it is clear that glycomacromolecule **6** makes use of the same binding pockets as the methyl glycoside of fucose. This underscores that the scaffold presenting fucose residues makes little, if any contact with the protein. Most of the CSPs are associated with NH signals of amino acids in the binding pocket, as highlighted in Figure 6b. However, there are additional CSPs at remote positions in the backbone revealing the presence of long-range effects that are likely due to allosteric effects upon binding.

Overall, STD-NMR experiments support our finding that binding of L-fucose presenting glycomacromolecules to GII.4 P-dimers is mediated by the fucose residues and not by the backbone. Comparison of CSP NMR experiments in the presence of L-fucose versus glycomacromolecule **6** supports the finding that only one fucose residue per glycomacromolecule is involved in binding.

X-ray crystallography of GII.10 P-dimer and glycomacromolecules. Finally, to investigate further which parts of the glycomacromolecules mediate P-dimer binding, the glycomacromolecules **1**−**9** were examined for their binding to the GII.10 P-dimer using X-ray crystallography. The GII.10 P domain crystals were soaked with each of the glycomacromolecules **1**−**9** and further processed for data collection. All crystals diffracted between 1.9 and 1.4 Å resolution, which enables to unambiguously identify the ligands that bind in soaking experiments. Further analysis indicated that glycomacromolecules **1**, **2**, **7**, and **9**, as well as **8**, which was used as a negative control, yielded only apo structures with no electron density at any of the fucose binding sites. The fucosylated glycomacromolecules **3**, **4**, **5**, and **6** clearly showed electron density for one fucose moiety (Figure 7 and data not shown). The electron density of the triazole linker of these fucosylated glycomacromolecules was nicely defined with glycomacromolecule **6**, but less defined for other glycomacromolecules (data not shown). That is why; glycomacromolecule **6** was selected as a representative for the figure of the interaction between the fucose moiety of the glycomacromolecules and the GII.10 P domain. The ligand interactions in the crystal structure of the glycomacromolecule **6** are identical to those of the other glycomacromolecules (**3**, **4**, and **5**) and show no difference from the previously published fucose-P domain interactions.[37] The rest of the macromolecular scaffold is not detected, therefore not allowing us to conclude on any potential multivalent binding effects or orientation of the backbone, but again supporting the previous finding that fucose binds to the P domain.

4. CONCLUSION AND OUTLOOK

In summary, this study demonstrates the synthesis of a first generation of fucose-functionalized precision glycomacromolecules and their use as model structures to investigate multivalent binding modes of human norovirus P-dimer. Through the iterative addition of tailor-made building blocks following the previously established solid phase polymer synthesis, nine precision glycomacromolecules were synthesized varying the number of fucose ligands from one to four as well as the interligand spacing along the oligomeric backbone. Binding to P-dimer was analyzed using native MS, NMR, and X-ray crystallography. While native MS gives ligand-complex stoichiometry as well as affinities in terms of K_D values, STD NMR identifies portions of the macromolecular ligands in contact with the protein. In addition, protein-based chemical shift perturbation NMR directly provides access to the topology of the binding pocket. In combination of the methods affinities measured by native MS can be linked to interactions with the fucose ligands as further supported by X-ray crystallography. Taken together, with the structural definition and information on the glycomacromolecules as provided by their solid phase assembly as well as molecular modeling in combination with light scattering, a systematic approach was presented on deriving novel macromolecular ligands targeting P-dimer. However, we did not observe any evidence for binding of multiple fucose units from the same glycomacromolecules to the fucose binding sites on P-dimer, hence high affinity ligands were not yet achieved. Quite unexpectedly, with increasing number of fucose units, we observed no increase in intermolecular complex formation. Based on our current results, we attribute this finding to sterical effects where the overall size of the glycomacromolecules hampers binding to more than one binding site of the P-dimer, however, we cannot exclude other contributing factors as well. Therefore, we are now exploring other scaffolds for the multivalent presentation of fucose ligands reducing their hydrodynamic size, for example, by using branched instead of linear scaffolds.

■ ASSOCIATED CONTENT

Supporting Information

The Supporting Information is available free of charge on the ACS Publications website at DOI: 10.1021/acs.biomac.8b00829.

DOI: 10.1021/acs.biomac.8b00829
Biomacromolecules 2018, 19, 3714−3724

Information about materials and instrumentation, general synthetic methods, analytical data of compounds, additional data from binding studies, detailed procedures of native MS, NMR, X-ray crystallography, DLS and EPR measurements, protein expression, and setup of molecular dynamics (PDF).

AUTHOR INFORMATION

Corresponding Authors

*E-mail: charlotte.uetrecht@xfel.eu.
*E-mail: laura.hartmann@hhu.de.

ORCID

Andrea Grafmüller: 0000-0002-1671-3158
Sabrina Weickert: 0000-0002-5339-2779
Malte Drescher: 0000-0002-3571-3452
Stephan Schmidt: 0000-0002-4357-304X
Laura Hartmann: 0000-0003-0115-6405

Notes

The authors declare no competing financial interest.

ACKNOWLEDGMENTS

The authors thank the German Research Foundation (DFG) for financial support (FOR2327, Virocarb; DFG Pe494/12-1, HA 5950/5-1, UE 183/1-1). H.Y. received funding through a doctoral stipend from the University of Hamburg. C.U. acknowledges funding via Leibniz grant SAW-2014-HPI-4. The Heinrich-Pette-Institute, Leibniz Institute for Experimental Virology, is supported by the Freie und Hansestadt Hamburg and the Bundesministerium für Gesundheit (BMG). L.H. thanks the DFG for support through the large equipment Grant INST 208/735-1.

REFERENCES

(1) Lindesmith, L. C.; Donaldson, E. F.; LoBue, A. D.; Cannon, J. L.; Zheng, D.-P.; Vinje, J.; Baric, R. S. Mechanisms of GII.4 Norovirus Persistence in Human Populations. *PLOS Med.* **2008**, *5*, e31.

(2) Choi, J.-M.; Hutson, A. M.; Estes, M. K.; Prasad, B. V. V. Atomic resolution structural characterization of recognition of histo-blood group antigens by Norwalk virus. *Proc. Natl. Acad. Sci. U. S. A.* **2008**, *105*, 9175−9180.

(3) Tan, M.; Hegde, R. S.; Jiang, X. The P Domain of Norovirus Capsid Protein Forms Dimer and Binds to Histo-Blood Group Antigen Receptors. *J. Virol.* **2004**, *78*, 6233−6242.

(4) Rydell, G. E.; Kindberg, E.; Larson, G.; Svensson, L. Susceptibility to winter vomiting disease: A sweet matter. *Rev. Med. Virol.* **2011**, *21*, 370−382.

(5) Koromyslova, A. D.; Leuthold, M. M.; Bowler, M. W.; Hansman, G. S. The sweet quartet: Binding of fucose to the norovirus capsid. *Virology* **2015**, *483*, 203−208.

(6) Fiege, B.; Leuthold, M.; Parra, F.; Dalton, K. P.; Meloncelli, P. J.; Lowary, T. L.; Peters, T. Epitope mapping of histo blood group antigens bound to norovirus VLPs using STD NMR experiments reveals fine details of molecular recognition. *Glycoconjugate J.* **2017**, *34*, 679−689.

(7) Mallagaray, A.; Lockhauserbäumer, J.; Hansman, G.; Uetrecht, C.; Peters, T. Attachment of Norovirus to Histo Blood Group Antigens: A Cooperative Multistep Process. *Angew. Chem.* **2015**, *127*, 12182−12187.

(8) Hansman, G. S.; Biertümpfel, C.; Georgiev, I.; Mclellan, J.; Chen, L.; Zhou, T.; Katayama, K.; D Kwong, P. Crystal Structures of GII.10 and GII.12 Norovirus Protruding Domains in Complex with Histo-Blood Group Antigens Reveal Details for a Potential Site of Vulnerability. *J. Virol.* **2011**, *85*, 6687.

(9) Hansman, G. S.; Shahzad-ul-Hussan, S.; McLellan, J. S.; Chuang, G.-Y.; Georgiev, I.; Shimoike, T.; Katayama, K.; Bewley, C. A.; Kwong, P. D. Structural Basis for Norovirus Inhibition and Fucose Mimicry by Citrate. *J. Virol.* **2012**, *86*, 284−292.

(10) Guiard, J.; Fiege, B.; Kitov, P. I.; Peters, T.; Bundle, D. R. Double-Click" Protocol for Synthesis of Heterobifunctional Multivalent Ligands: Toward a Focused Library of Specific Norovirus Inhibitors. *Chem. - Eur. J.* **2011**, *17*, 7438−7441.

(11) Rademacher, C.; Guiard, J.; Kitov, P. I.; Fiege, B.; Dalton, K. P.; Parra, F.; Bundle, D. R.; Peters, T. Targeting Norovirus Infection—Multivalent Entry Inhibitor Design Based on NMR Experiments. *Chem. - Eur. J.* **2011**, *17*, 7442−7453.

(12) Ponader, D.; Maffre, P.; Aretz, J.; Pussak, D.; Ninnemann, N. M.; Schmidt, S.; Seeberger, P. H.; Rademacher, C.; Nienhaus, G. U.; Hartmann, L. Carbohydrate-Lectin Recognition of Sequence-Defined Heteromultivalent Glycooligomers. *J. Am. Chem. Soc.* **2014**, *136*, 2008−2016.

(13) Ponader, D.; Wojcik, F.; Beceren-Braun, F.; Dernedde, J.; Hartmann, L. Sequence-Defined Glycopolymer Segments Presenting Mannose: Synthesis and Lectin Binding Affinity. *Biomacromolecules* **2012**, *13*, 1845−1852.

(14) Ebbesen, M. F.; Itskalov, D.; Baier, M.; Hartmann, L. Cu Elimination from Cu-Coordinating Macromolecules. *ACS Macro Lett.* **2017**, *6*, 399−403.

(15) Gerke, C.; Ebbesen, M. F.; Jansen, D.; Boden, S.; Freichel, T.; Hartmann, L. Sequence-Controlled Glycopolymers via Step-Growth Polymerization of Precision Glycomacromolecules for Lectin Receptor Clustering. *Biomacromolecules* **2017**, *18*, 787−796.

(16) Igde, S.; Röblitz, S.; Müller, A.; Kolbe, K.; Boden, S.; Fessele, C.; Lindhorst, T. K.; Weber, M.; Hartmann, L. Linear Precision Glycomacromolecules with Varying Interligand Spacing and Linker Functionalities Binding to Concanavalin A and the Bacterial Lectin FimH. *Macromol. Biosci.* **2017**, *17*, 1700198.

(17) Geng, J.; Mantovani, G.; Tao, L.; Nicolas, J.; Chen, G.; Wallis, R.; Mitchell, D. A.; Johnson, B. R. G.; Evans, S. D.; Haddleton, D. M. Site-Directed Conjugation of "Clicked" Glycopolymers To Form Glycoprotein Mimics: Binding to Mammalian Lectin and Induction of Immunological Function. *J. Am. Chem. Soc.* **2007**, *129*, 15156−15163.

(18) Roy, B.; Mukhopadhyay, B. Sulfuric acid immobilized on silica: An excellent catalyst for Fischer type glycosylation. *Tetrahedron Lett.* **2007**, *48*, 3783−3787.

(19) Braun, P.; Nägele, B.; Wittmann, V.; Drescher, M. Mechanism of Multivalent Carbohydrate−Protein Interactions Studied by EPR Spectroscopy. *Angew. Chem., Int. Ed.* **2011**, *50*, 8428−8431.

(20) Hoshino, Y.; Nakamoto, M.; Miura, Y. Control of Protein-Binding Kinetics on Synthetic Polymer Nanoparticles by Tuning Flexibility and Inducing Conformation Changes of Polymer Chains. *J. Am. Chem. Soc.* **2012**, *134*, 15209−15212.

(21) Roux, S.; Zékri, E.; Rousseau, B.; Paternostre, M.; Cintrat, J.-C.; Fay, N. Elimination and exchange of trifluoroacetate counter-ion from cationic peptides: A critical evaluation of different approaches. *J. Pept. Sci.* **2008**, *14*, 354−359.

(22) Han, L.; Kitov, P. I.; Kitova, E. N.; Tan, M.; Wang, L.; Xia, M.; Jiang, X.; Klassen, J. S. Affinities of recombinant norovirus P dimers for human blood group antigens. *Glycobiology* **2013**, *23*, 276−285.

(23) Erba, E. B.; Zenobi, R. Mass spectrometric studies of dissociation constants of noncovalent complexes. *Annu. Rep. Prog. Chem., Sect. C: Phys. Chem.* **2011**, *107*, 199−228.

(24) Sun, J.; Kitova, E. N.; Wang, W.; Klassen, J. S. Method for Distinguishing Specific from Nonspecific Protein−Ligand Complexes in Nanoelectrospray Ionization Mass Spectrometry. *Anal. Chem.* **2006**, *78*, 3010−3018.

(25) Wang, W.; Kitova, E. N.; Klassen, J. S. Nonspecific Protein−Carbohydrate Complexes Produced by Nanoelectrospray Ionization. Factors Influencing Their Formation and Stability. *Anal. Chem.* **2005**, *77*, 3060−3071.

(26) Cecioni, S.; Imberty, A.; Vidal, S. Glycomimetics versus Multivalent Glycoconjugates for the Design of High Affinity Lectin Ligands. *Chem. Rev.* **2015**, *115*, 525−561.

DOI: 10.1021/acs.biomac.8b00829
Biomacromolecules 2018, 19, 3714−3724

(27) Uetrecht, C.; Heck, A. J. R. Modern Biomolecular Mass Spectrometry and its Role in Studying Virus Structure, Dynamics, and Assembly. *Angew. Chem., Int. Ed.* **2011**, *50*, 8248−8262.
(28) Pannier, M.; Veit, S.; Godt, A.; Jeschke, G.; Spiess, H. W. Dead-time free measurement of dipole−dipole interactions between electron spins. *J. Magn. Reson.* **2011**, *213*, 316−325.
(29) Milov, A. D.; Ponomarev, A. B.; Tsvetkov, Y. Electron-electron double resonance in electron spin echo: Model biradical systems and the sensitized photolysis of decalin. *Chem. Phys. Lett.* **1984**, *110*, 67−72.
(30) Jeschke, G. DEER Distance Measurements on Proteins. *Annu. Rev. Phys. Chem.* **2012**, *63*, 419−446.
(31) Ling, H.; Ruixiang, Z.; Michele, R. R.; Ming, T.; Elena, N. K.; Xi, J.; John, S. K. Quantifying the binding stoichiometry and affinity of histo-blood group antigen oligosaccharides for human noroviruses. *Glycobiology* **2018**, *28*, 1−11.
(32) Fiege, B.; Leuthold, M.; Parra, F.; Dalton, K. P.; Meloncelli; Peter, J.; Lowary; Todd, L.; Peters, T. Epitope mapping of histo blood group antigens bound to norovirus VLPs using STD NMR experiments reveals fine details of molecular recognition. *Glycoconjugate J.* **2017**, *34*, 679−689.
(33) Mayer, M.; Meyer, B. Group Epitope Mapping by Saturation Transfer Difference NMR To Identify Segments of a Ligand in Direct Contact with a Protein Receptor. *J. Am. Chem. Soc.* **2001**, *123*, 6108−6117.
(34) Mayer, M.; Meyer, B. Characterization of Ligand Binding by Saturation Transfer Difference NMR Spectroscopy. *Angew. Chem., Int. Ed.* **1999**, *38*, 1784−1788.
(35) Meyer, B.; Peters, T. NMR Spectroscopy Techniques for Screening and Identifying Ligand Binding to Protein Receptors. *Angew. Chem., Int. Ed.* **2003**, *42*, 864−890.
(36) Williamson, M. P. Using chemical shift perturbation to characterise ligand binding. *Prog. Nucl. Magn. Reson. Spectrosc.* **2013**, *73*, 1−16.
(37) Singh, B. K.; Leuthold, M. M.; Hansman, G. S. Human Noroviruses' Fondness for Histo-Blood Group Antigens. *J. Virol.* **2015**, *89*, 2024−2040.

DOI: 10.1021/acs.biomac.8b00829
Biomacromolecules 2018, 19, 3714−3724

Supporting Information

Fucose-functionalized precision glycomacromolecules targeting human norovirus capsid protein

Katharina Susanne Bücher[1], Hao Yan[2], Robert Creutznacher[3], Kerstin Ruoff[4], Alvaro Mallagaray[3], Andrea Grafmüller[5], Jan Sebastian Dirks[1], Turgay Kilic[4], Sabrina Weickert[6], Anna Rubailo[6], Malte Drescher[6], Stephan Schmidt[1], Grant Hansman[4], Thomas Peters[3], Charlotte Uetrecht[2,7] and Laura Hartmann[1*]*

[1]Heinrich-Heine-University Düsseldorf, Institute for Organic Chemistry and Macromolecular Chemistry, Düsseldorf, Germany

[2] Heinrich Pette Institute, Leibniz Institute for Experimental Virology, Hamburg, Germany

[3] Institute of Chemistry, University of Lübeck, Lübeck, Germany

[4] Schaller Research Group at the University of Heidelberg and the DKFZ, Heidelberg, Germany and Department of Infectious Diseases, Virology, University of Heidelberg, Heidelberg, Germany

[5] Max-Planck-Insitute of Colloids and Interfaces, Department of Theory & Bio-Systems, Potsdam, Germany

[6] University of Konstanz, Department of Chemistry and Konstanz Research School Chemical Biology, Konstanz, Germany

[7] European XFEL GmbH, Schenefeld, Germany

1. Synthesis of glycomacromolecules

1.1 Materials

Diethyl ether (with BHT as inhibitor, ≥ 99.8%), triisopropylsilane (TIPS) (98%), (+)-sodium-L-ascorbate (≥ 99.0%), citric acid (≥ 99.5%), D-galactose (≥ 99%), sodium diethyldithiocarbamat trihydrate, sodium methanolate (95%) and all deuterated solvents were all purchased from Sigma-Aldrich. *N*,*N*-Diisopropylethylamine (DIPEA) (≥ 99%) was purchased from Carl Roth. Methanol (100%), sulfuric acid (95-98%) and acetic anhydride (Ac_2O) (99.7%) were purchased from VWR Prolabo Chemicals. *N*,*N*-Dimethylformamide (DMF) (99.8%, for peptide synthesis), piperidine (99%), copper(II) sulfate (98%), 2-bromoethanole (97%), sodium azide (99%) and trityl chloride (98%) were purchased from Acros Organics. Dichloromethane (DCM) (99.99%) and acetonitrile (≥ 99.9%) were purchased from Fisher Scientific. Trifluoroacetic acid (TFA) (99%) was purchased from Fluorochem. Tentagel S RAM® (Rink Amide) resin was purchased from Rapp Polymere and had a loadin of 0.22 mmol, 0.23 mmol or 0.25 mmol of Fmoc-protected amine groups per gram of resin. L-Fucose was purchased from Jennewein Biotechnologie GmbH. Silica gel (60 M, 0.04-0.063 mm) was purchased from Machery-Nagel. Succinic anhydride was purchased from Carbolution. Benzotriazol-1-yl-oxytripyrrolidinophosphonium hexafluorophosphate (PyBOP) was purchased from NovaBiochem. The ion exchange resin (AG1-X8, quarternary ammonium, 100-200 mesh, acetate form) was purchased from BioRad. Syringe filters, 4 mm, 0.45 µm PTFE were purchased from Restek. Filter syringes with a polypropylene frit were purchased from Multisyntech GmbH.

1.2 Instrumentation

Nuclear magnetic resonance spectroscopy (NMR)

^{1}H NMR and ^{13}C NMR (600 MHz and 300 MHz) spectra were recorded on a Bruker AVANCE III – 300 and a Bruker AVANCE III – 600. Chemical shifts were reported in delta (δ) expressed in units of parts per million (ppm). As internal standard residual, non-deuterated solvent was used (δ 4.79 ppm for D_2O). STD NMR experiments were performed on a Bruker AV III 500 MHz NMR spectrometer equipped with a TCI cryogenic probe at 298 K.

Reverse-phase semi-preparative high-performance liquid chromatography (preparative RP-HPLC)

For purification of the final glycomacromolecules an Agilent 1200 HPLC System with a Varian Persuit semi-preparative column (C_{18}, 250x10.0 mm) was used at 25 °C. The solvent system used was water (**A**) and acetonitrile (**B**) and the glycomacromolecules were eluted with a linear water-acetonitrile gradient at a flow rate of 20 mL/min. The product fractions were combined and concentrated in vacuum. The glycomacromolecules were dissolved again in milliQ-water, filtered through syringe filters and lyophilized.

Reversed Phase - High Performance Liquid Chromatography - Mass Spectrometry (RP-HPLC/MS)

The purities of glycomacromolecules were determined by chromatograms recorded on an analytical RP-HPLC system (Agilent 1260 Infinity) using a Poroshell 120 EC-C18 (3.0×50 mm, 2.5 µm) RP column from Agilent at 25°C. The mobile phases used were H_2O/ACN (95/5) (**A**) and H_2O/ACN (5/95) (**B**), both mobile phases containing 0.1% formic acid. The instrument was coupled to a variable wavelength detector (VWD) that was set to 214 nm and was combined with a 6120 Quadrupole LC/MS with an electrospray ionization (ESI) source (operating in positive ionization mode in an *m/z* range of 200 to 2000). The measurements of glycomacromolecules were performed with a linear gradient starting with 100% of mobile phase **A** reaching 50% mobile phase **A** in 30 min. The flow rate was 0.4 mL/min. Analysis of UV and MS signals was realized with the OpenLab ChemStation software for LC/MS from Agilent Technologies.

High Resolution –Electrospray Ionization - Mass Spectrometry (HR-ESI/MS)

All HR-ESI/MS spectra were recorded on an Agilent 6210 ESI-ToF from Agilent Technologies (Santa Clara, CA, USA). The flow rate was 4 µL/min, the spray voltage was 4 kV and the desolvation gas was set to 15 psi (1 bar).

Matrix-Assisted Laser Desorption Ionization- Time Of Flight – Mass Spectrometry (MALDI-TOF-MS)

MALDI TOF MS spectra were recorded on a Bruker MALDI-TOF Ultraflex I system. The matrix was 2,5-dihydroxybenzoic acid (DHB) and was used in a 10 fold excess to the compound. Spectra were acquired either in linear mode for an *m/z* range of 1000-4000, calibrated with a protein mixture or in reflector mode for an *m/z* range 2000-20000 without calibration.

Freeze dryer

The lyophilization of glycomacromolecules was performed at -42 °C and 0.1 mbar with an Alpha 1-4 LD plus instrument from Martin Christ Freeze Dryers GmbH.

Peptide synthesizer

For automated synthesis of glycomacromolecule backbones a peptide synthesizer of the type CS136XT from CS Bio was used. The batch sizes were 0.1 mmol or 0.2 mmol. The protocols for automated synthesis were written with CSPEPM software from CS Bio.

1.3 General methods

1.3.1 Solid phase synthesis of glycomacromolecules

The batch sizes of macromolecule synthesis varied and are described for each macromolecule separately. As solid support for the SPPS of glycomacromolecules **1-9** was used a commercially available Tentagel S RAM® resin (Rink Amide). The elongation of the macromolecule backbones was proceeded by alternating coupling and Fmoc-deprotection steps at room temperature either hand-made in filter syringes or – in case of glycomacromolecules **6** and **8** – automated on a peptide synthesizer. The hand-coupled batches were proceeded in filter syringes with 10 mL (for batch sizes below 0.2 mmol) and 20 mL (for batch sized above 0.2 mmol) reaction volumes. The purification of final glycomacromolecules was performed with ion exchange resin with a ration of resin to macromolecule of 1g/0.1 according to literature with 1 g resin per 100 mg of macromolecule.[1]

The synthesis of macromolecules was proceeded as published previously and is described shortly in the following sections.[2] The heteromultivalent structure **9** was synthesized according to literature by sequential elongation and CuAAC reactions.[3]

Macromolecule elongation

The SPPS of glycomacromolecules is described exemplary for a batch size of 0.1 mmol. For other batch sizes all compounds were up- or downscaled according to the described equivalents.

General protocol for amine-deprotection and building block coupling

Before each synthesis the resin was swollen for 1 h in DCM at RT by shaking and washed 10 times with DMF afterwards.

The N^{α}-Fmoc-protecting group (of the resin or an already coupled building block) was cleaved by adding 5 mL of 25% piperidine solution in DMF. It was shaken for 30 min and the resin was washed 5 times with DMF. The procedure was repeated and the resin was washed 10 times with DMF.

The elongation of macromolecule backbones was realized by coupling the corresponding building block EDS (0.5 mmol, 235 mg) or TDS (0.5 mmol, 250 mg) in 5 equivalents excess in 3 mL DMF mixed with 5 equivalents of PyBOP (0.5 mmol, 260 mg) and 10 equivalents of DIPEA (1.0 mmol, 0.17 mL). The coupling solution was degassed for 1-2 min with nitrogen after adding of DIPEA and then added to the solid support. It was shaken for 1.5 h and the resin was washed 10 times with DMF afterwards.

After Fmoc-deprotection of the final primary amine with 5 mL of 25% piperidine in DMF (two times for 30 min) the macromolecule constructs were capped at the N-terminal side by adding 3 mL acetic anhydride to the resin. It was shaken for 15 min and washed 5 times with DMF. This procedure was repeated once and the resin was washed 5 times with DMF and 5 times with DCM.

The completeness of the elongation process was monitored via microcleavages with RP-HPLC/MS. The obtained macromolecule backbones were further functionalized with α-L-fucose or D-galactose (see section 1.1.2) on solid support and the final products were cleaved from the resin at the end.

α-L-Fucopyranoside functionalization via CuAAC on solid support

A mixture of 0.2 mmol (2 eq.) of 2-azidoethylpyranoside per alkyne group dissolved in 3 ml DMF and 9.9 mg (50mol%) sodium ascorbate per alkyne group in water (c = 33 mg/mL) was added to 0.1 mmol of resin loaded with EDS and TDS building blocks under N_2-atm. Then 4 mg (25mol%) per alkyne group of $CuSO_4$ were dissolved in water (c = 20 mg/mL), degassed and added to the resin. It was shaken overnight and afterwards the reaction mixture was pushed in a glas vial for storage and recovery of azidated carbohydrate. The resin with macromolecule attached was washed extensively with a 23 mM solution of sodium diethyldithiocarbamate in DMF, water, DMF and DCM until the DMF washing solution was no more colored from complexed cupper. For deacetylation of sugar units conjugated to the macromolecule on solid support was added 5 mL of 0.2 M NaOMe/MeOH solution. It was shaken for 45 min and the resin was then washed 3 times with MeOH and 3 times with DCM. The deacetylation was repeated and the washing steps were repeated three times.

The final cleavage of the glycomacromolecules was performed by adding 3 mL of the cleavage cocktail (95% TFA: 9.5 mL, DCM: 0.25 mL, TIPS: 0.25 mL) to the resin and allow it to react for 1.5 h. The cleavage solution was purged in cold Et_2O to precipitate the macromolecule, it was centrifuged and diethyl ether was decanted. The cleavage procedure was repeated and the mixture was shaken for 1 h. Then both product fractions were dried in nitrogen stream, dissolved in 5 mL MilliQ-water, combined and lyophilized overnight.

Azidated fucose protected with acetyl groups has been recovered from the reaction mixture after CuAAC reaction by extraction in 50 mL ethyl acetate with 50 mL of water (five times). The organic layer was dried over $MgSO_4$, filtered and the solvent was evaporated in vacuum.

Synthesis of spin-labeled glycomacromolecule 10

Backbone structure of spin-labeled glycomacromolecule was synthesized using EDS, TDS and the Boc protected non-proteinogenic amino acid dap (2,3-diamino propionic acid) as building blocks in a batch size of 0.3 mmol. After capping with acetic anhydride 0.1 mmol of the final backbone was functionalized with fucose by CuAAC as described previously. 0.05 mmol were further functionalized with TEMPO radicals on resin, applying the following protocol: the Boc protecting groups of included dap amino

acids were cleaved by adding 4 mL of a solution of HCl/Dioxane (0.4 M) to the resin twice (reaction times 5 min and 25 min) followed by addition of 10 mL of a solution of DIPEA in DCM (10%) twice. The resin was washed 12 times with DMF and 5 times with DCM. Subsequently 4-carboxy-TEMPO (5 eq.) was coupled via amide bond formation using PyBOP (5 eq.) and DIPEA (10 eq.) in 3 mL DMF for 1.5 h. The fucose side chains were deprotected as described before and the final product was cleaved off the resin, precipitated in diethyl ether. Ether was decanted and the product was dried in nitrogen stream and lyophilized. Final glycomacromolecules **10** was analyzed by ^{1}H NMR, HR-ESI-MS and RP-HPLC (for spectra see below).

1.3.2 Synthesis of 2-azidoethyl-2,3,4-tri-*O*-acetyl-α-L-fucopyranoside

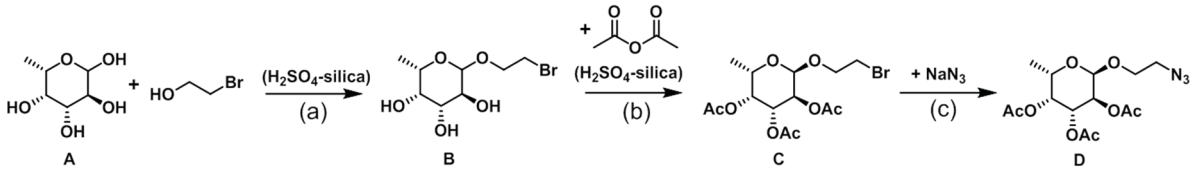

Scheme S1: Functionalization of L-fucose with azidoethyl-linker in α-position. (a) 65°C/6 h, (b) RT, 24 h; (c) DMF, 50°C/36 h.

Azidated α-L-fucose (**D**) was synthesized based on the synthetic strategy of Roy *et al.* who showed the Fischer glycosylation of several monosaccharides with a propargyl-linker predominantly in alpha position by using a silica catalyst with immobilized sulfuric acid.[4] The functionalization of L-fucose (**A**) with 2-bromoethanol as well as the protection of hydroxyl groups using acetic anhydride have been proceeded with this silica catalyst as shown in Scheme S1. Glycoside (**B**) was afforded in 59% yield with an α/β-ratio of 7:1. The anomeric mixture could be separated after acetylation (glycoside (**C**)) by silica gel column chromatography (toluene/ethyl acetate 50:1 - 8:1) and afforded the alpha-anomer in 48% yield in this reaction step. After azidation with NaN_3 (90% yield) the product glycoside (**D**) was obtained with an overall yield of 25%. The products were analyzed by ^{1}H- and ^{13}C NMR, TLC as well as ESI-MS.

Preparation of catalyst (H_2SO_4–silica)

The catalyst was produced as described in literature.[4] 10 g of silica gel was mixed with diethyl ether (50 mL) and conc. H_2SO_4 (3 mL) was added. The suspension was shaken for 5 min. The solvent was evaporated under reduced pressure. The remaining H_2SO_4-silica was then dried at 110°C for 3 h. The catalyst was used without further purification and activity was not determined.

2-Bromoethyl-α/β-L-fucopyranoside (B)

L-Fucose (**A**) (20 g, 122 mmol) was suspended in 2-bromoethanol (44 mL, 620 mmol, 5.1 eq.) and the mixture was stirred. After heating to 65 °C H_2SO_4–silica catalyst (0.61 g) was added and stirring was continued until all is dissolved (product formation). Due to unknown catalyst activity, more H_2SO_4-silica can be added if starting material is still visible in the mixture. After 6 h all the solid had dissolved and TLC (DCM/MeOH 7:1) showed complete conversion of L-fucose. After cooling to room temperature, the reaction mixture was stirred for 16 h. The crude mixture was separated with silica gel column chromatography. After eluting the excess of bromoethanol with pure DCM, the product was isolated with DCM/MeOH in a gradient solvent mixture (100:1 – 100:3). 19.49 g (71.89 mmol, 59%) of the product **B** was obtained as white to orange solid in an α/β-ratio of 7:1.

^{1}H NMR (300 MHz, Methanol-*d4*): δ [ppm] = 4.87 (d, ^3J = 2.7 Hz, 1H, H-1-α), 4.16 (q, ^3J = 6.4 Hz, 1H, H-5), 4.03-3.85 (m, 2H, OCH_2CH$_2$Br), 3.82-3.81 (m, 2H, H-2, H-3), 3.74-3.73 (m, 1H, H-4), 3.67-3.63 (m, 2H, CH_2-Br), 3.56-3.44 (m, β-protons), 1.33 (d, ^3J = 6.3 Hz, 0.5H, CH$_3$-β), 1.27 (d, ^3J = 6.6 Hz, CH$_3$-α). ^{13}C NMR (300 MHz, Methanol-*d4*): δ [ppm] = 105.0 (C-1-β), 100.8 (C-1-α), 73.6 (C-5), 71.6 (C-3), 69.9 (C-4), 69.7 (C-2), 68.0 (O-CH$_2$), 31.5 (CH$_2$-Br), 16.6 (CH$_3$). HR-ESI/MS*:* *m/z* calcd for $C_8H_{15}BrNaO_5$ 292.9995, found 292.9994. R_f = 0.54 (DCM/MeOH 7:1).

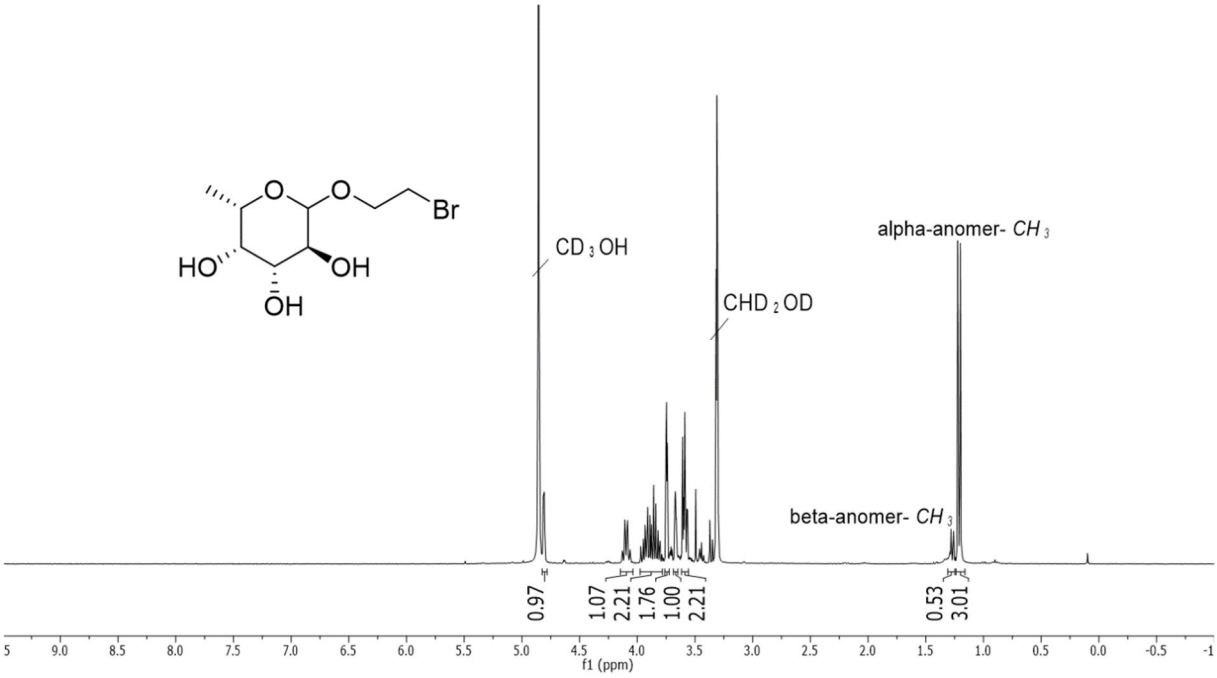

Figure S1: ^{1}H NMR (300 MHz, CD_3OD) of 2-bromoethyl-α/β-L-fucopyranoside (**B**).

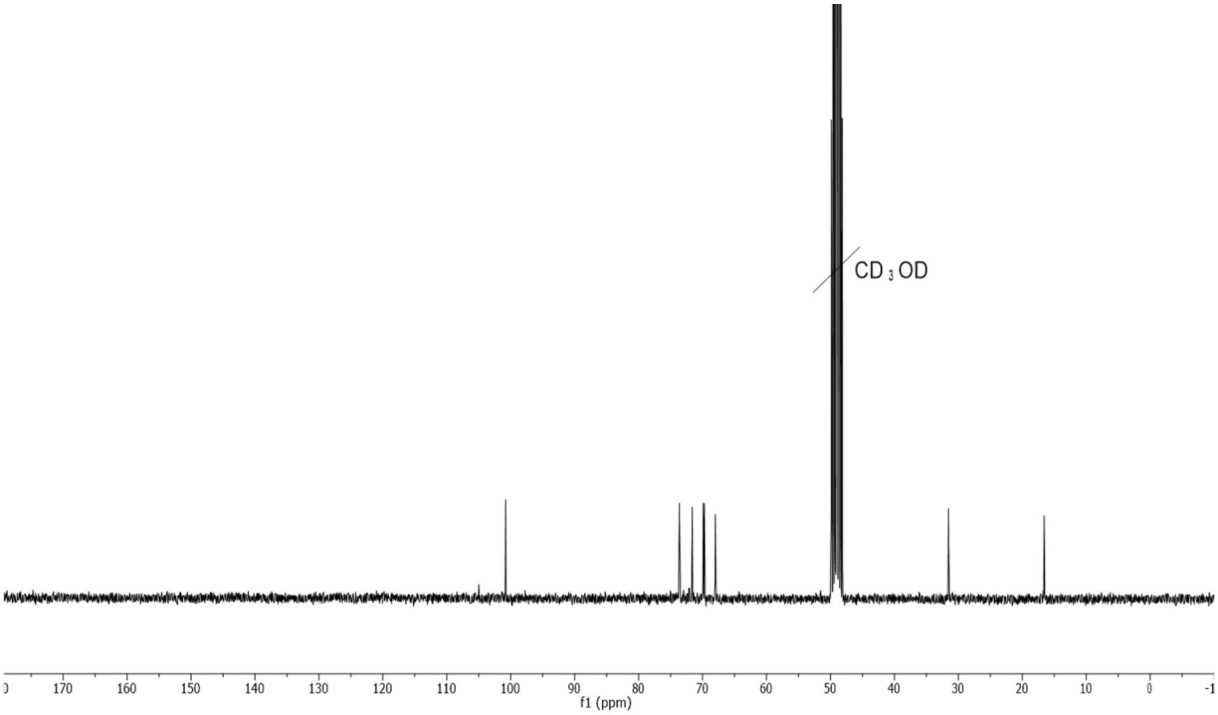

Figure S2: ^{13}C NMR (300 MHz, CD_3OD) of 2-bromoethyl-α/β-L-fucopyranoside (**B**).

2-Bromoethyl-2,3,4-tri-*O*-acetyl-α-L-fucopyranoside (C)

To a stirring mixture of 2-bromoethyl-α/β-L-fucopyranoside **B** (300 mg, 1.1 mmol) with acetic anhydride (4 mL, 42 mmol, 38 eq.) 10 mg H_2SO_4-silica catalyst were added. The mixture was stirred at

room temperature for 24 h. Completion of the reaction was monitored by TLC (ethyl acetate/toluene 2:8). The reaction mixture was diluted with DCM (20 mL) and washed sequentially with saturated aqueous $NaHCO_3$ solution and water twice. The extract was dried over $MgSO_4$ and concentrated in vacuum. The anomeric mixture was then separated by silica gel column chromatography using toluene/ethyl acetate (50:1 - 8:1) as eluent. 2,3,4-Tri-*O*-acetyl-1-*O*-(2-bromethyl)-α-L-fucose (**C**) was obtained after drying under vacuum as white solid (210 mg, 0.53 mmol) in 48%.

^{1}H NMR (300 MHz, $CDCl_3$): δ [ppm] = 5.37 (dd, $^{3,3}J$ = 10.3, 3.4 Hz, 1H, H-3), 5.31 (dd, $^{3,3}J$ = 3.4, 1.2 Hz, 1H, H-2), 5.14-5.07 (m, 2H, H-1, H-4), 4.25 (q, ^{3}J = 6.5, 1H, H-5), 3.98 (dt, $^{2,3}J$ = 11.6, 5.8 Hz, 1H, OCH_2CH$_2$Br), 3.80 (dt, $^{2,3}J$ = 11.6, 5.8 Hz, 1H, OCH_2CH$_2$Br), 3.49 (t, ^{3}J = 5.8 Hz, 2H, OCH$_2$CH_2Br), 2.16 (s, 3H, COCH_3), 2.08 (s, 3H, COCH_3), 1.99 (s, 3H, COCH_3), 1.14 (d, ^{3}J = 6.6 Hz, 3H, H-6). ^{13}C NMR (300 MHz, $CDCl_3$): δ [ppm] = 170.7 (O=C-CH$_3$), 170.2 (O=C-CH$_3$), 96.5 (C-1), 71.2 (C-4), 68.5 (C-5), 68.2 (C-2), 68.0 (C-3), 65.0 (O-CH$_2$), 30.3 (CH$_2$-Br), 21.0 (OC-CH$_3$), 20.8 (OC-CH$_3$), 16.0 (C-6). R_f (alpha) = 0.44 (toluene/ethyl acetate 4:1), R_f (beta) = 0.32 (toluene/ethyl acetate 4:1).

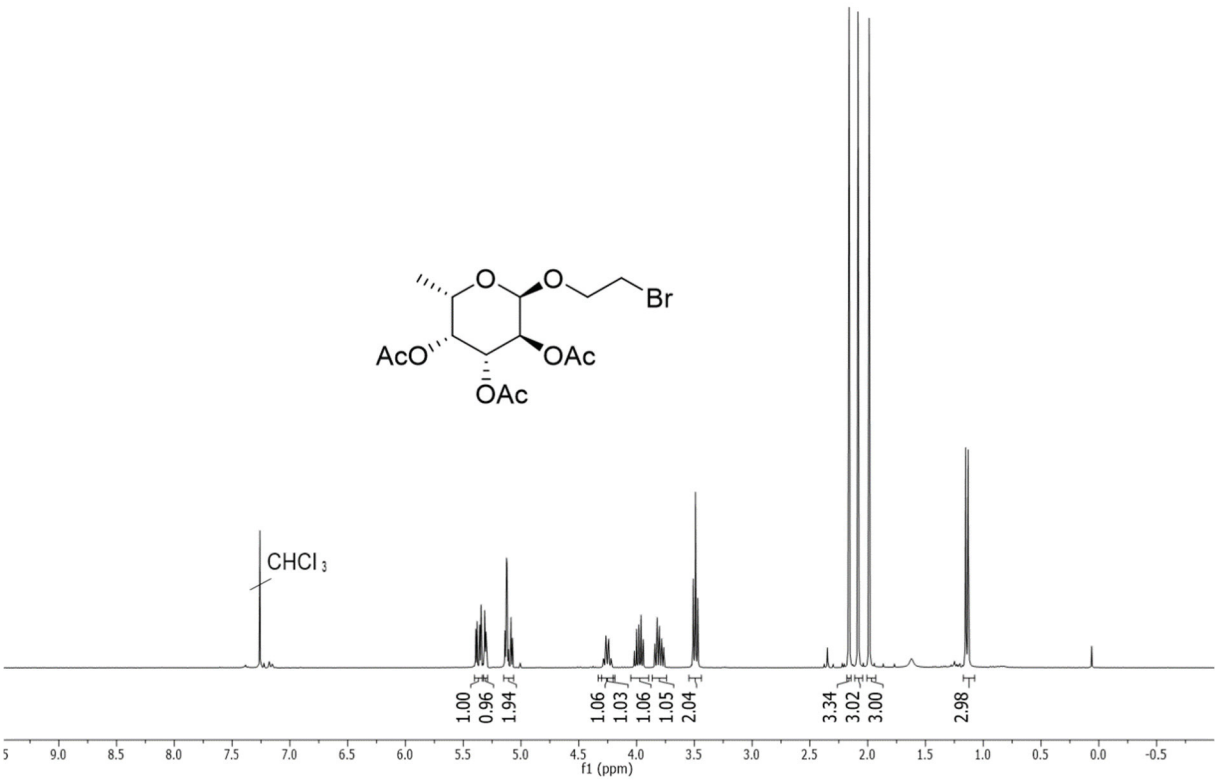

Figure S3: ^{1}H NMR (300 MHz, $CDCl_3$) of 2-bromoethyl-2,3,4-tri-*O*-acetyl-α-L-fucopyranoside (**C**).

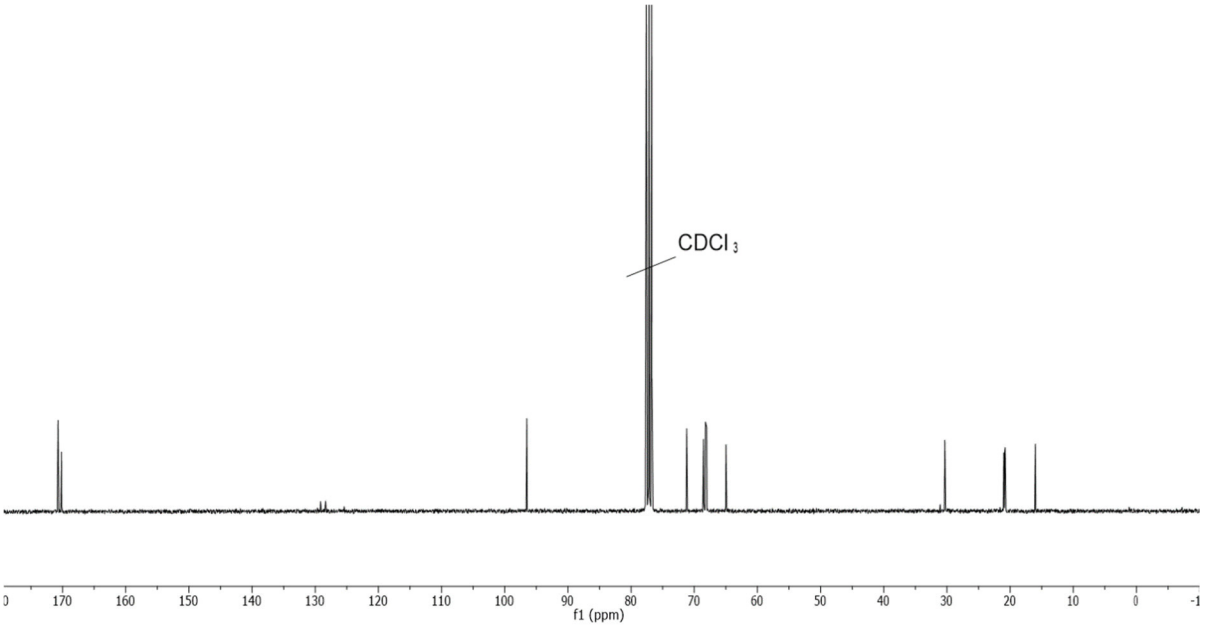

Figure S4: ^{13}C NMR (300 MHz, $CDCl_3$) of 2-bromoethyl-2,3,4-tri-*O*-acetyl-α-L-fucopyranoside (**C**).

2-Azidoethyl-2,3,4-tri-*O*-acetyl-α-L-fucopyranoside (D)

To a solution of 2 g (5 mmol) 2-bromoethyl 2,3,4-tri-*O*-acetyl-α-L-fucopyranoside (**C**) in 40 mL DMF was added 1.3 g sodium azide (20 mmol, 4 eq.) and the reaction mixture was stirred at 50 °C for 36 h. The reaction progress was monitored via TLC (Hex/ethyl acetate 4:3). 10 mL of water was added to the reaction mixture and it was concentrated to almost dryness under reduced pressure at 55°C (9 mbar). The obtained yellowish oil was dissolved in 100 mL ethyl acetate and extracted 3 times with 100 mL of water, 3 times with 100 mL of an aqueous saturated $NaHCO_3$ solution and again 3 times with 100 mL of water. The organic layer was dried over magnesium sulfate, filtered and concentrated to dryness under reduced pressure and finally in high vacuum. The product glycoside **D** was obtained as white crystals (1.61 g, 4.48 mmol, 90%).

^{1}H NMR (300 MHz, $CDCl_3$): δ [ppm] = 5.41-5.31 (m, 2H, H-3, H-2), 5.16-5.10 (m, 2H, H-1, H-4), 4.18 (dq, $^{3,3}J$ = 1.0, 6.6 Hz, 1H, H-5), 3.86 (ddd, $^{2,3,3}J$ = 10.7, 6.0, 3.4 Hz, 1H, OCH_2CH_2N$_3$), 3.61 (ddd, $^{2,3,3}J$ = 10.7, 6.8, 3.5 Hz, 1H, OCH_2CH_2N$_3$), 3.50-3.33 (m, 2H, OCH$_2$CH_2N$_3$), 2.17 (s, 3H, COCH_3), 2.08 (s, 3H, COCH_3), 1.99 (s, 3H, COCH_3), 1.15 (d, ^3J = 6.6 Hz, 3H, H-6). ^{13}C NMR (300 MHz, $CDCl_3$): δ [ppm] = 170.8 (O=*C*-CH$_3$), 170.7 (O=*C*-CH$_3$), 170.2 (O=*C*-CH$_3$), 96.6 (C-1), 71.2 (C-4), 68.1 (C-5), 68.0 (C-2), 67.3 (C-3), 64.8 (O-*C*H$_2$), 50.6 (*C*H$_2$-N$_3$), 21.0 (OC-*C*H$_3$), 20.8 (O=C-*C*H$_3$), 21.8

(O=C-*C*H$_3$), 16.0 (C-6). R_f (**4**) = 0.59 (Hex/ethyl acetate 4:3), R_f (starting material **3**) = 0.65 (Hex/ethyl acetate 4:3).

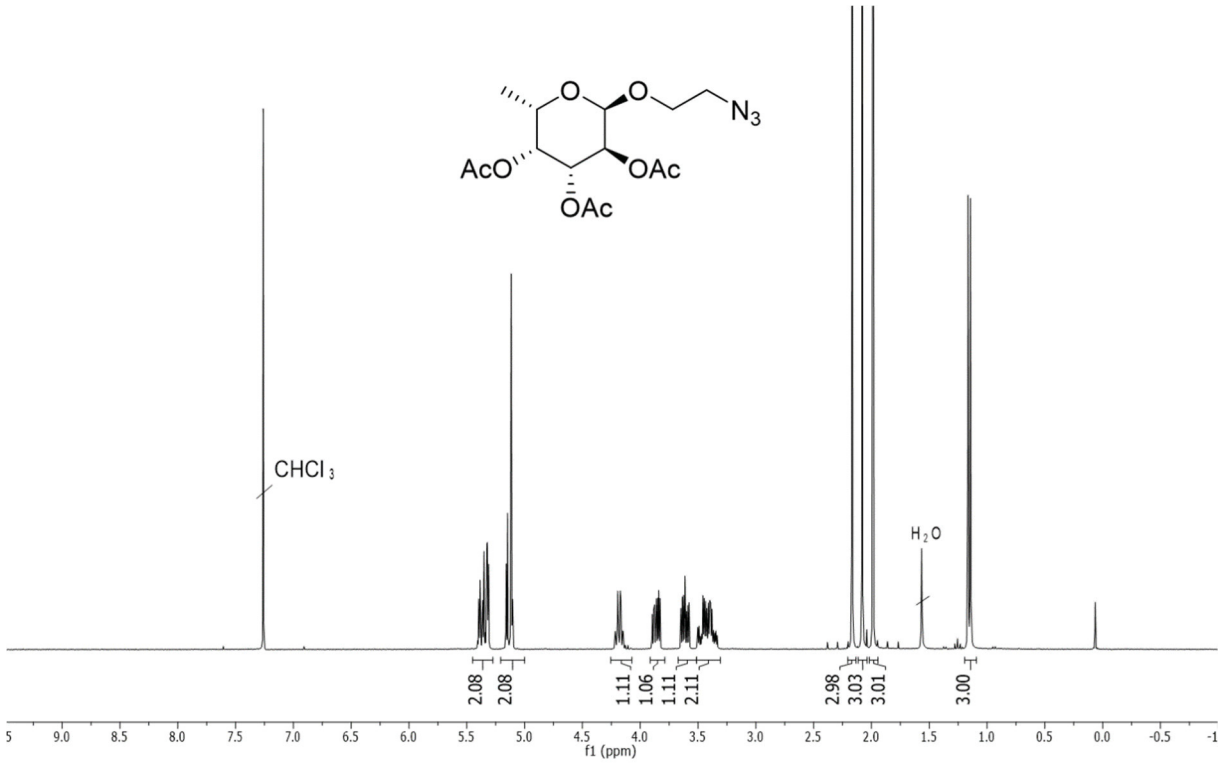

Figure S5: ^{1}H NMR (300 MHz, $CDCl_3$) of 2-azidoethyl-2,3,4-tri-*O*-acetyl-α-L-fucopyranoside (**D**).

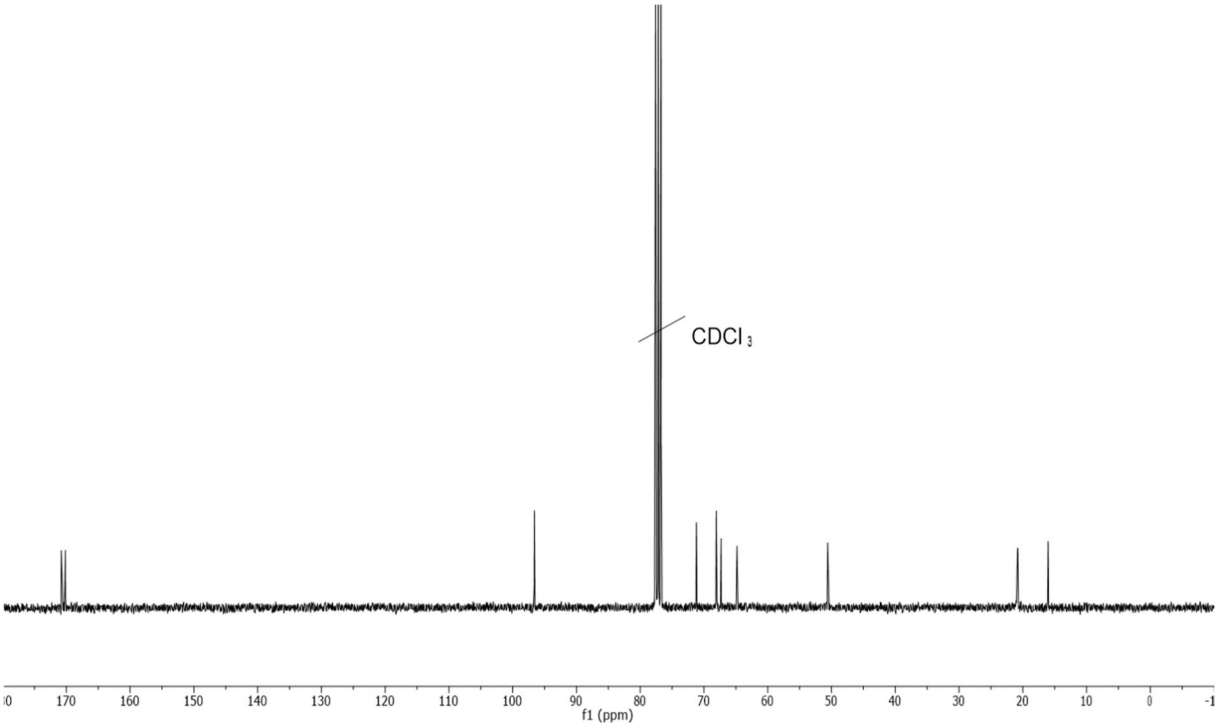

Figure S6: ^{13}C NMR (300 MHz, $CDCl_3$) of 2-azidoethyl-2,3,4-tri-*O*-acetyl-α-L-fucopyranoside (**D**).

2. Analysis of glycomacromolecules

Fuc(4)-7 (1)

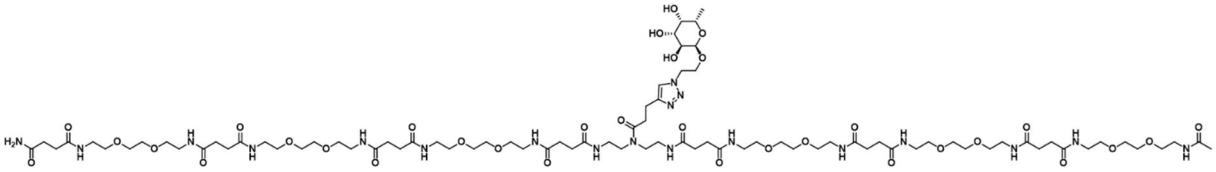

Compound **1** was synthesized in a batch size of 0.13 mmol. 80 mg (0.041 mmol) of crude product (260 mg) were purified by ion exchange resin and preparative RP-HPLC. The purified product **1** was obtained as lyophilized white powder (43 mg, 0.022 mmol, 55%).

^{1}H NMR (600 MHz, D_2O): δ [ppm] = 7.83 (s, 1H, N=N-N-C*H*), 4.76 (d, ^{3}J = 3.8 Hz, 1H, Fuc-H-1), 4.61-4.53 (m, 2H, N=N-N-CH_2), 3.97-3.93 (m, 1H, N=N-N-CH_2-CH_2), 3.86 (dt, $^{2,3}J$ = 10.8, 3.7 Hz, 1H, N=N-N-CH_2-CH_2), 3.67-3.58 (m, 27H, O-CH_2-CH_2-O, Fuc-H-2, Fuc-H-3), 3.56-3.53 (m, 25H, CH_2-O-$(CH_2)_2$-O-CH_2, Fuc-H-4), 3.41-3.37 (m, 4H, N-CH_2-CH_2-NH), 3.32-3.25 (m, 28H, O=C-NH-CH_2), 3.00 (q, ^{3}J = 6.6 Hz, 1H, Fuc-H-5), 2.92 (t, ^{3}J = 7.2 Hz, 2H, N-N=N-C-CH_2), 2.71 (t, ^{3}J = 7.3 Hz, 2H, N-N=N-C-CH_2-CH_2), 2.48-2.39 (m, 28H, O=C-CH_2-CH_2-C=O), 1.92 (s, 3H, O=C-CH_3), 0.95 (d, ^{3}J = 6.6 Hz, 3H, Fuc-H-6). MALDI TOF MS: *m/z* calcd for $C_{83}H_{147}N_{19}O_{33}$ $[M+Na]^+$ 1961.0; found 1961.1. HR-ESI/MS: *m/z* calcd for $C_{83}H_{147}N_{19}O_{33}$ (monoisotopic mass 1938.0409): $[M+3H]^{3+}$ 647.0209, found 647.0209. RP-HPLC: (gradient from 100% to 50% eluent A in 30 min, 25°C): t_R = 12.3 min, determined purity 98%.

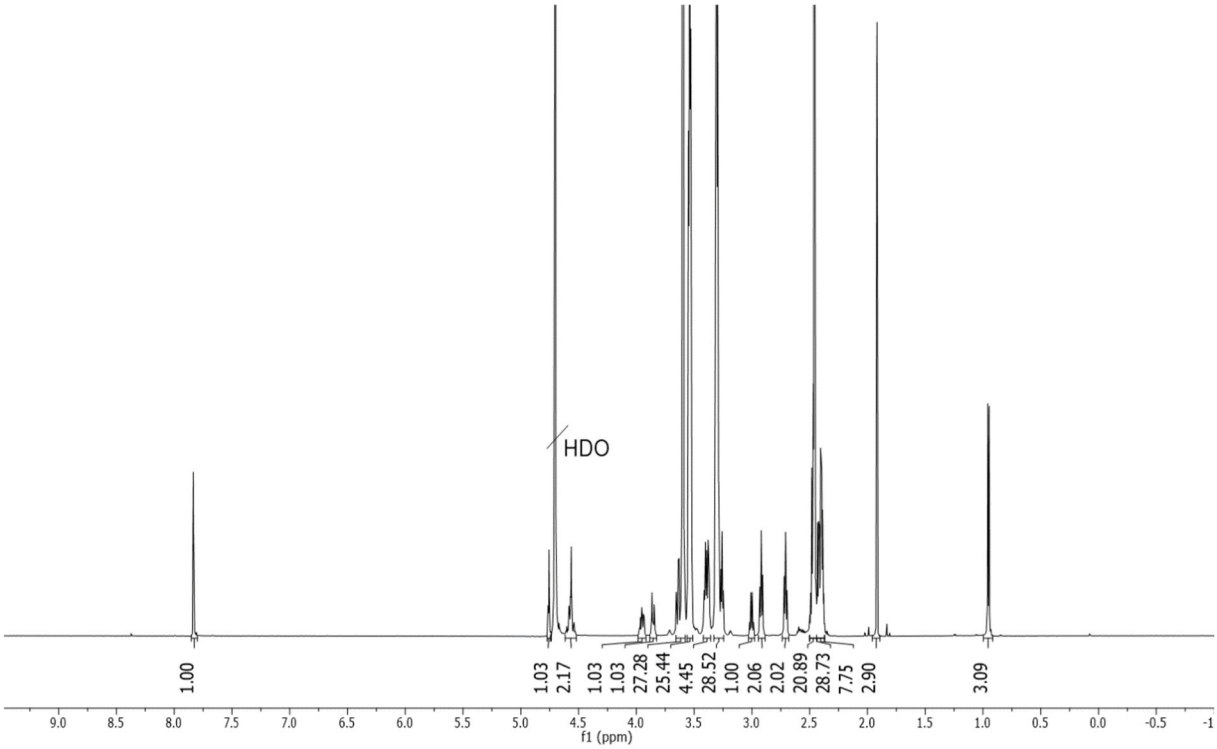

Figure S7: ^{1}H NMR (600 MHz, D_2O) of Fuc(4)-7 (**1**).

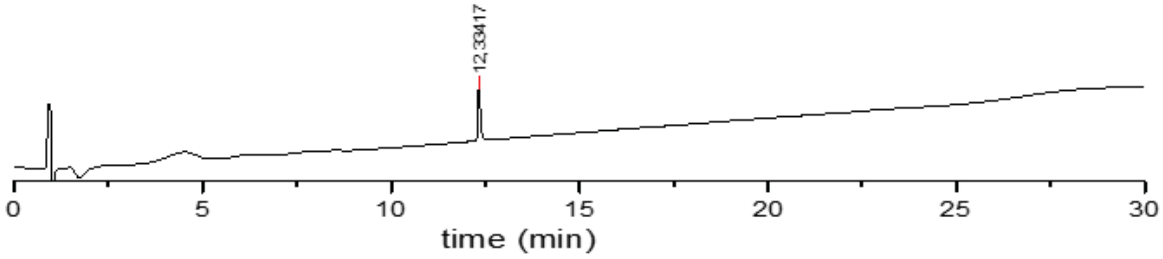

Figure S8: RP-HPLC spectra of Fuc(4)-7 (**1**).

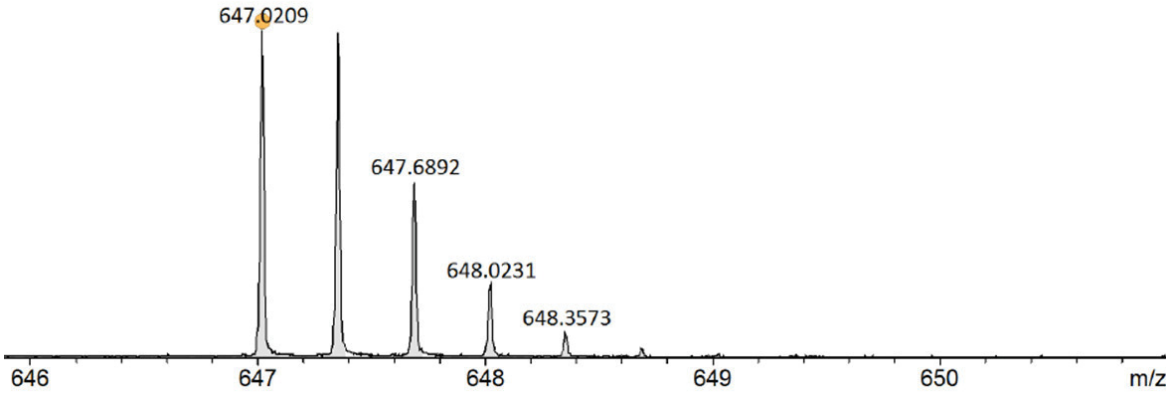

Figure S9: HR/ESI-MS spectra of Fuc(4)-7 (**1**).

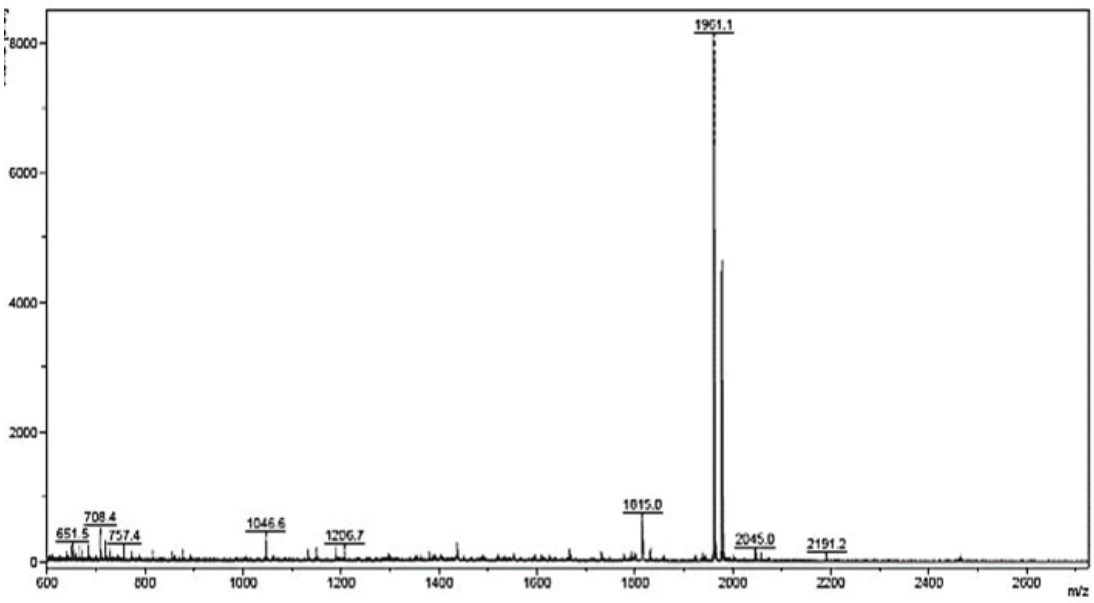

Figure S10: MALDI TOF MS spectra of Fuc(4)-7 (**1**).

Fuc(1,2)-5 (2)

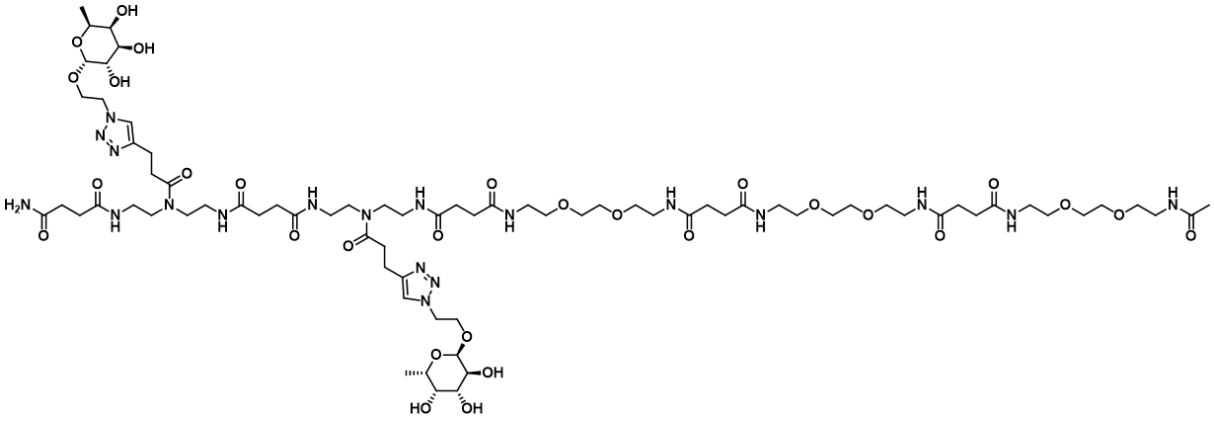

Compound **2** was synthesized in a batch size of 0.234 mmol. 232 mg (0.133 mmol) of crude product (292 mg) were purified by ion exchange resin and preparative RP-HPLC. The purified product **2** was obtained as lyophilized white powder (127 mg, 0.0727 mmol, 55%).

^{1}H NMR (600 MHz, D_2O): δ = 7.92 (s, 2H, N=N-N-C*H*), 4.84 (d, ^{3}J = 3.8 Hz, 2H, Fuc-H-1), 4.69-4.62 (m, 4H, N=N-N-CH_2), 4.05-4.01 (m, 2H, N=N-N-CH$_2$-CH_2), 3.94 (dt, $^{2,3}J$ = 10.8, 3.6 Hz, 2H, N=N-N-CH$_2$-CH_2), 3.73 (dd, $^{3,3}J$ = 10.3, 3.8 Hz, 2H, Fuc-H-2), 3.70-3.66 (m, 14H, O-CH_2-CH_2-O, Fuc-H-3), 3.64-3.61 (m, 14H, CH_2-O-(CH$_2$)$_2$-O-CH_2, Fuc-H-4), 3.49-3.45 (m, 8H, N-*CH*$_2$-CH$_2$-NH), 3.40-3.32 (m, 20H, O=C-NH-CH_2), 3.09 (q, ^{3}J = 6.6 Hz, 2H, Fuc-H-5), 3.00 (t, ^{3}J = 7.2 Hz, 4H, N-N=N-C-CH_2), 2.79 (t, ^{3}J = 7.3 Hz, 4H, N-N=N-C-CH$_2$-CH_2), 2.55-2.43 (m, 20H,

O=C-C*H*$_2$-C*H*$_2$-C=O), 2.00 (s, 3H, O=C-C*H*$_3$), 1.04 (d, ^3J = 6.67 Hz, 6H, Fuc-H-6). MALDI TOF MS*:* *m/z* calcd for $C_{74}H_{127}N_{19}O_{29}$ $[M+Na]^+$ 1768.89; found 1769.0. HR-ESI/MS: *m/z* calcd for $C_{74}H_{127}N_{19}O_{29}$ (monoisotopic mass 1745.9047): $[M+2H]^{2+}$ 873.9596, found 873,9589; $[M+3H]^{3+}$ 582.9755, found 582.9756. RP-HPLC: (gradient from 100% to 50% eluent A in 30 min, 25°C): t_R = 11.2 min, determined purity 98%.

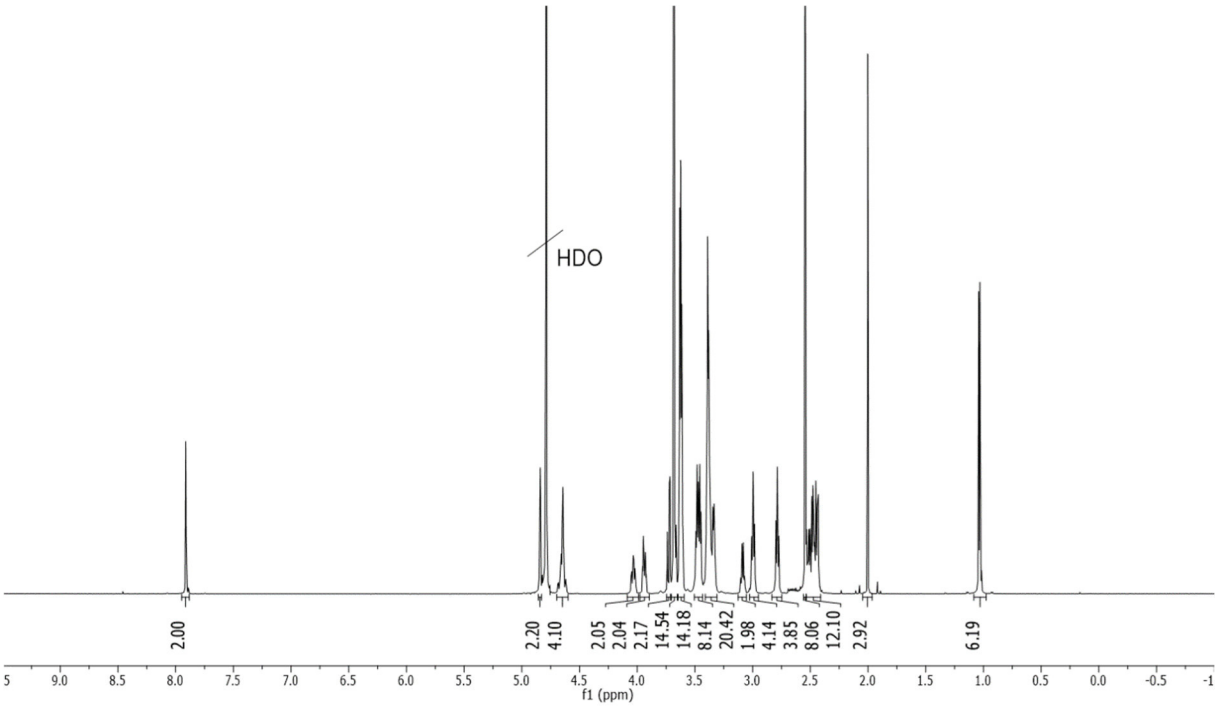

Figure S11: ^{1}H NMR (600 MHz, D_2O) spectra of Fuc(1,2)-5 (**2**).

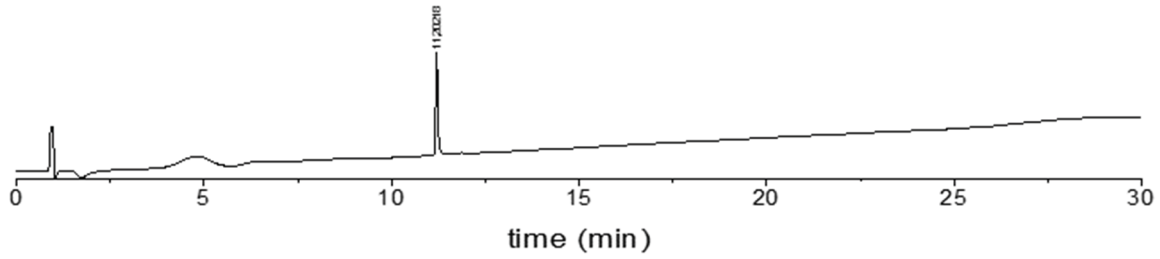

Figure S12: RP-HPLC spectra of Fuc(1,2)-5 (**2**).

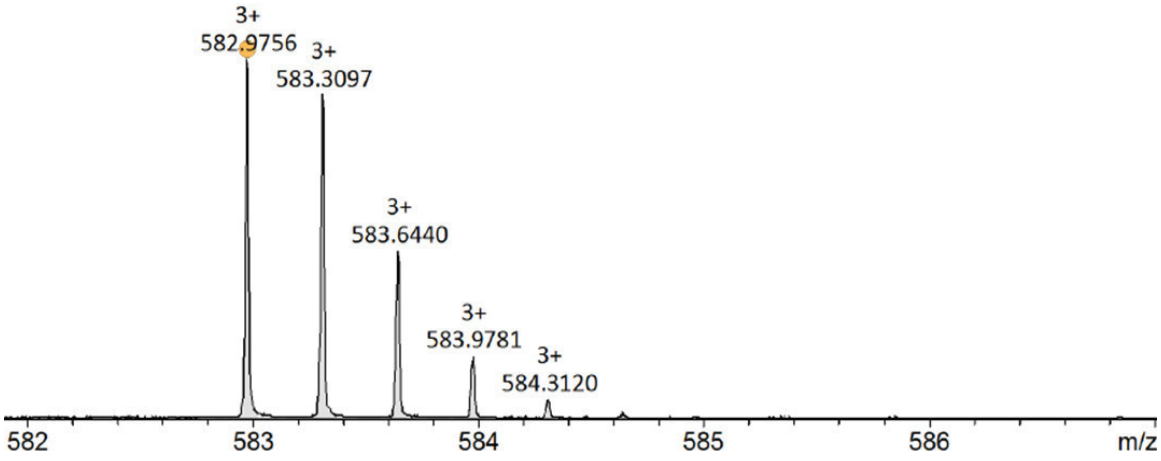

Figure S13: HR/ESI-MS spectra of Fuc(1,2)-5 (**2**).

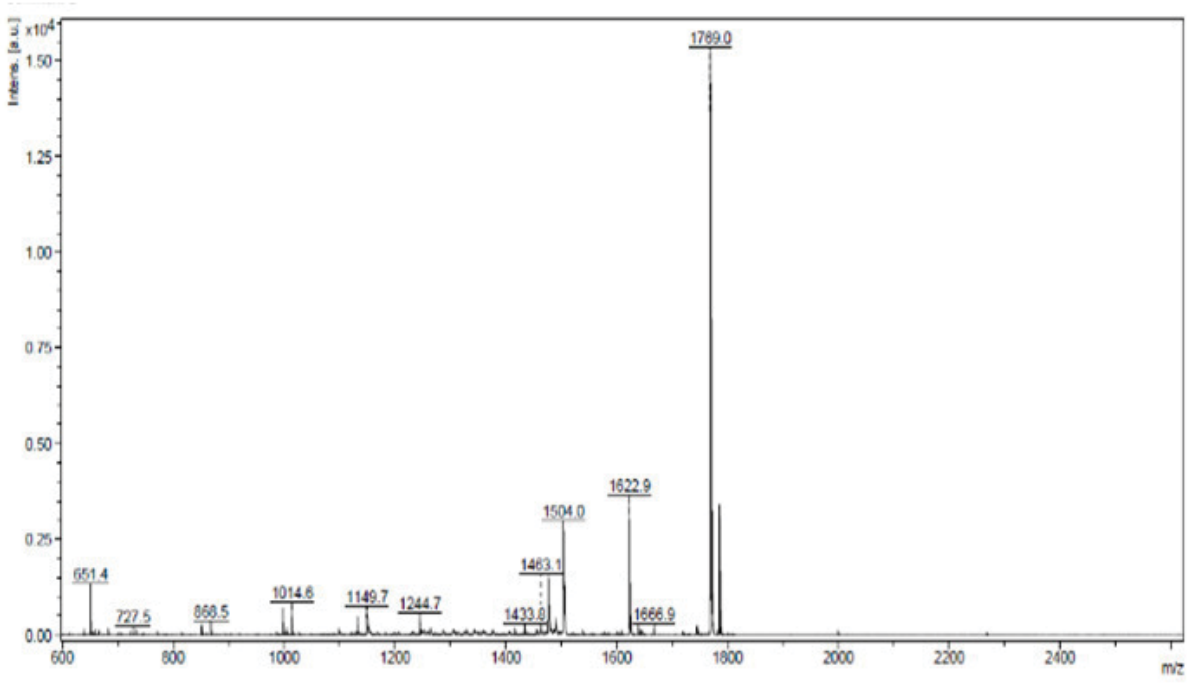

Figure S14: MALDI TOF MS spectra of Fuc(1,2)-5 (**2**).

Fuc(1,3)-5 (3)

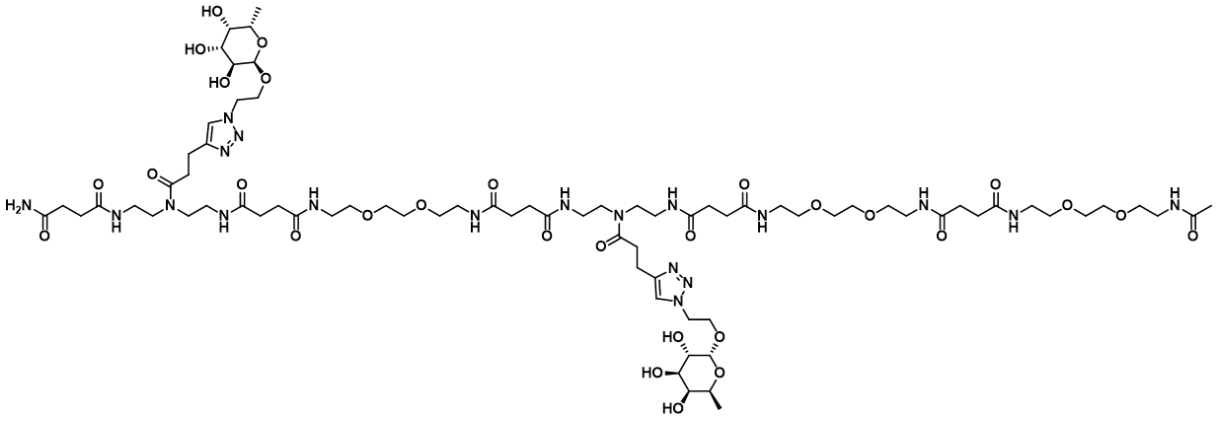

Compound **3** was synthesized in a batch size of 0.234 mmol. 248 mg (0.142 mmol) of crude product (283 mg) were purified by ion exchange resin and preparative RP-HPLC. The purified product **3** was obtained as lyophilized white powder (138 mg, 0.079 mmol, 56%).

^{1}H NMR (600 MHz, D_2O): δ = 7.92 (s, 2H, N=N-N-C*H*), 4.84 (d, ^{3}J = 3.8 Hz, 2H, Fuc-H-1), 4.69-4.62 (m, 4H, N=N-N-CH_2), 4.06-4.02 (m, 2H, N=N-N-CH_2-CH_2), 3.94 (dt, $^{2,3}J$ = 10.8, 3.7 Hz, 2H, N=N-N-CH_2-CH_2), 3.73 (dd, $^{3,3}J$ = 10.3, 3.8 Hz, 2H, Fuc-H-2), 3.70-3.65 (m, 14H, O-CH_2-CH_2-O, Fuc-H-3), 3.64-3.60 (m, 14H, CH_2-O-$(CH_2)_2$-O-CH_2, Fuc-H-4), 3.50-3.45 (m, 8H, N-*C*H_2-CH_2-NH), 3.40-3.33 (m, 20H, O=C-NH-CH_2), 3.09 (q, ^{3}J = 6.6 Hz, 2H, Fuc-H-5), 3.00 (t, ^{3}J = 7.2 Hz, 4H, N-N=N-C-CH_2), 2.79 (t, ^{3}J = 7.3 Hz, 4H, N-N=N-C-CH_2-CH_2), 2.54-2.46 (m, 20H, O=C-CH_2-CH_2-C=O), 2.00 (s, 3H, O=C-CH_3), 1.04 (d, ^{3}J = 6.6 Hz, 6H, Fuc-H-6). MALDI TOF MS*: m/z* calcd for $C_{74}H_{127}N_{19}O_{29}Na$ $[M+Na]^+$ 1768.9, found 1769.0. HR-ESI/MS: *m/z* calcd for $C_{74}H_{127}N_{19}O_{29}$ (monoisotopic mass 1745.9047): $[M+2H]^{2+}$ 873.9596, found 873.9591. RP-HPLC: (gradient from 100% to 50% eluent A in 30 min, 25°C): t_R = 11.2 min, determined purity 98%.

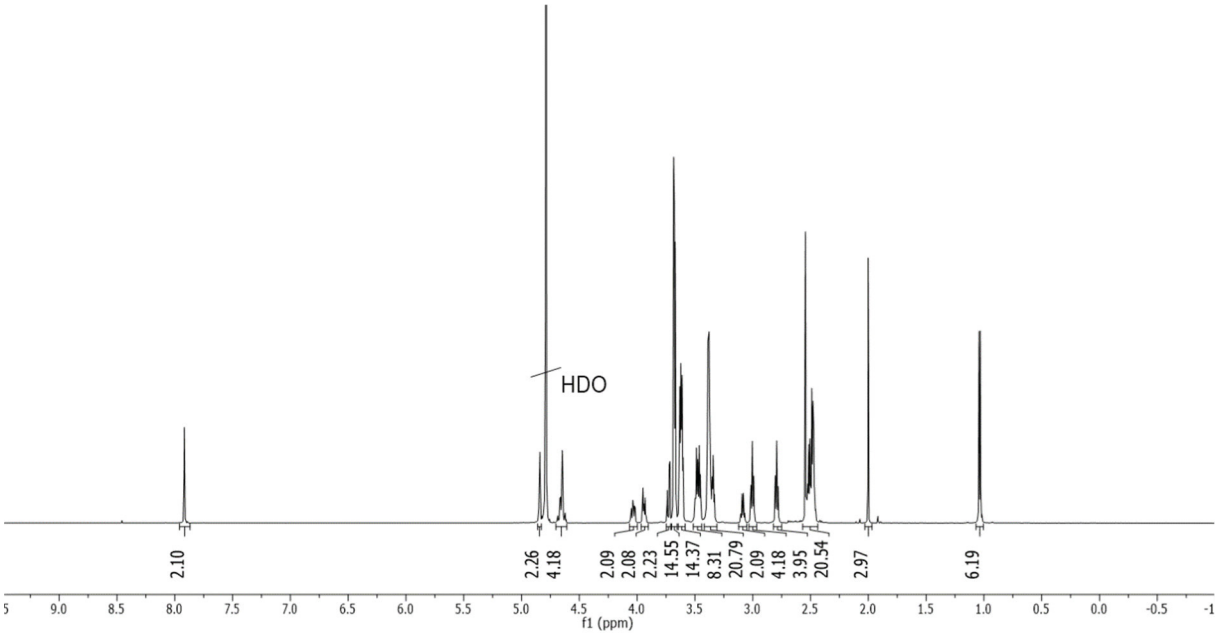

Figure S15: ^{1}H NMR (600 MHz, D_2O) spectra of Fuc(1,3)-5 (**3**).

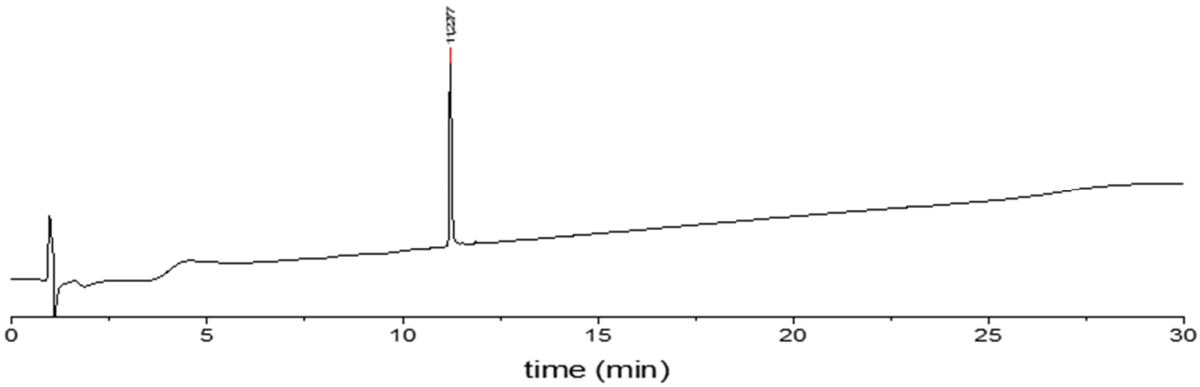

Figure S16: RP-HPLC spectra of Fuc(1,3)-5 (**3**).

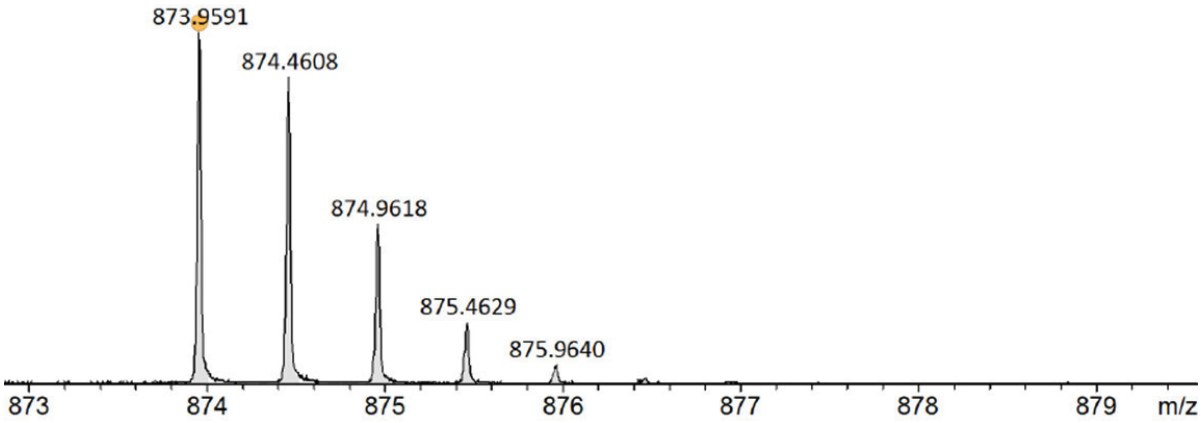

Figure S17: HR/ESI-MS spectra of Fuc(1,3)-5 (**3**).

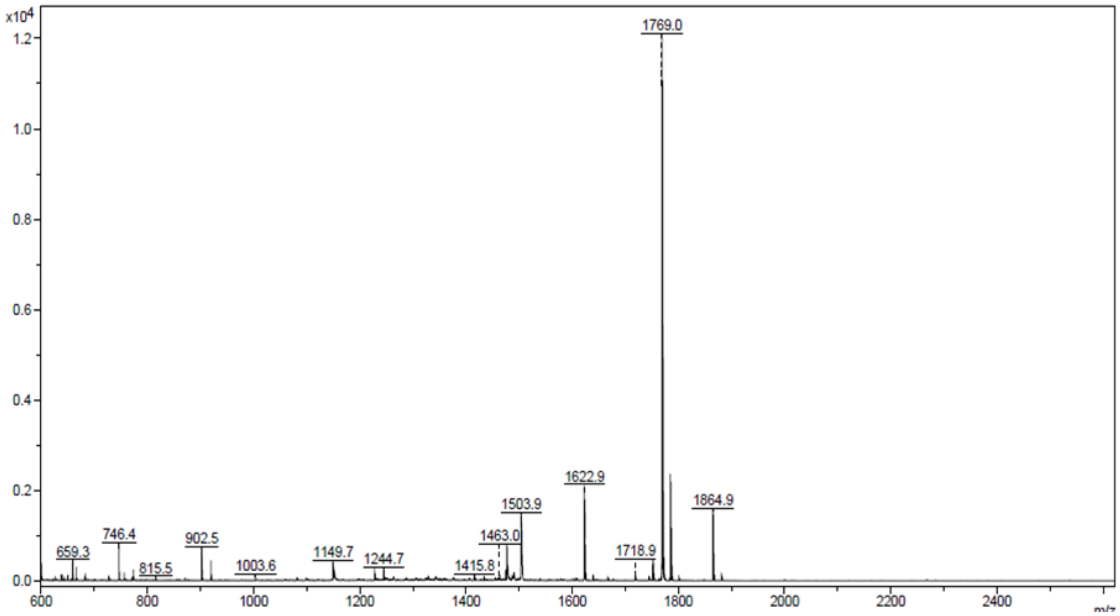

Figure S18: MALDI TOF MS spectra of Fuc(1,3)-5 (**3**).

Fuc(1,4)-5 (4)

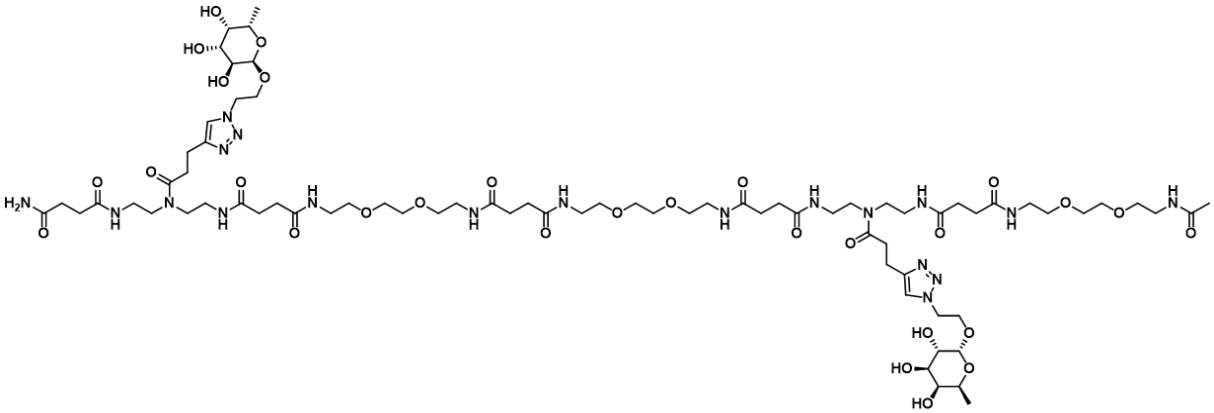

Compound **4** was synthesized in a batch size of 0.234 mmol. 266 mg (0.152 mmol) of crude product (310 mg) were purified by ion exchange resin and preparative RP-HPLC. The purified product **4** was obtained as lyophilized white powder (145 mg, 0.083 mmol, 55%).

^{1}H NMR (600 MHz, D_2O): δ = 7.92 (s, 2H, N=N-N-C*H*), 4.85 (d, ^{3}J = 3.8 Hz, 2H, Fuc-H-1), 4.69-4.62 (m, 4H, N=N-N-CH_2), 4.05-4.02 (m, 2H, N=N-N-CH$_2$-CH_2), 3.94 (dt, $^{2,3}J$ = 10.8, 3.7 Hz, 2H, N=N-N-CH$_2$-CH_2), 3.73 (dd, $^{3,3}J$ = 10.3, 3.8 Hz, 2H, Fuc-H-2), 3.69-3.66 (m, 14H, O-CH_2-CH_2-O, Fuc-H-3), 3.64-3.61 (m, 14H, CH_2-O-(CH$_2$)$_2$-O-CH_2, Fuc-H-4), 3.50-3,45 (m, 8H, N-*CH*$_2$-CH$_2$-NH), 3.40-3.33 (m, 20H, O=C-NH-CH_2), 3.09 (q, ^{3}J = 6.6 Hz, 2H, Fuc-H-5), 3.01 (t, ^{3}J = 7.2 Hz, 4H, N-N=N-C-CH_2), 2.79 (t, ^{3}J = 7.3 Hz, 4H, N-N=N-C-CH$_2$-CH_2), 2.54-2.46 (m, 20H,

O=C-CH_2-CH_2-C=O), 2.00 (s, 3H, O=C-CH_3), 1.04 (d, ^3J = 6.6 Hz, 6H, Fuc-H-6). MALDI TOF MS: *m/z* calcd for $C_{74}H_{127}N_{19}O_{29}Na$ $[M+Na]^+$ 1769.92; found 1769.0. HR-ESI/MS: *m/z* calcd for $C_{74}H_{127}N_{19}O_{29}$ (monoisotopic mass 1745.9047): $[M+2H]^{2+}$ 873.9596, found 873.9596. RP-HPLC: (gradient from 100% to 50% eluent A in 30 min, 25°C): t_R = 11.2 min, determined purity 99%.

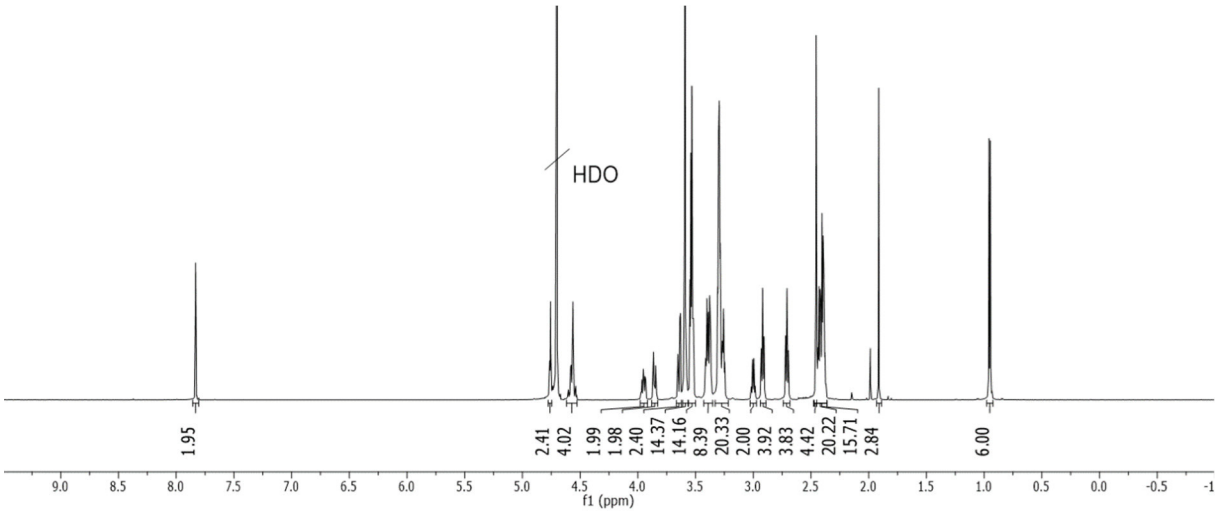

Figure S19: ^{1}H NMR (600 MHz, D_2O) spectra of Fuc(1,4)-5 (**4**).

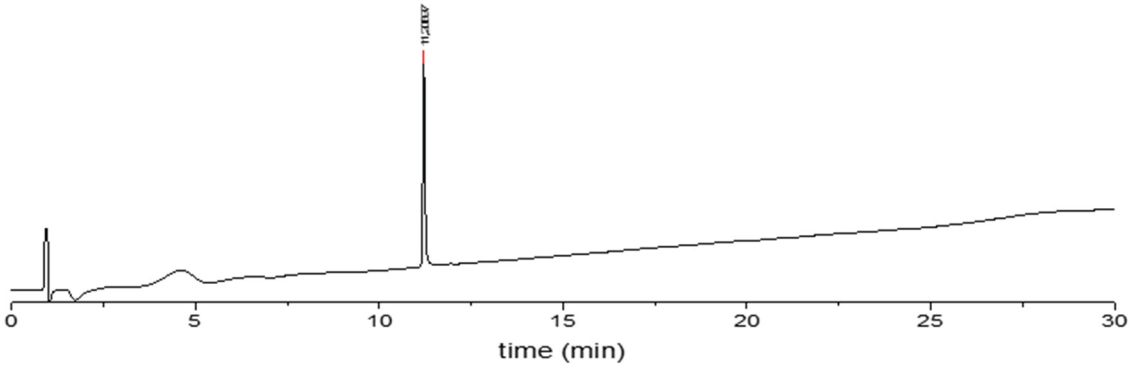

Figure S20: RP-HPLC spectra of Fuc(1,4)-5 (**4**).

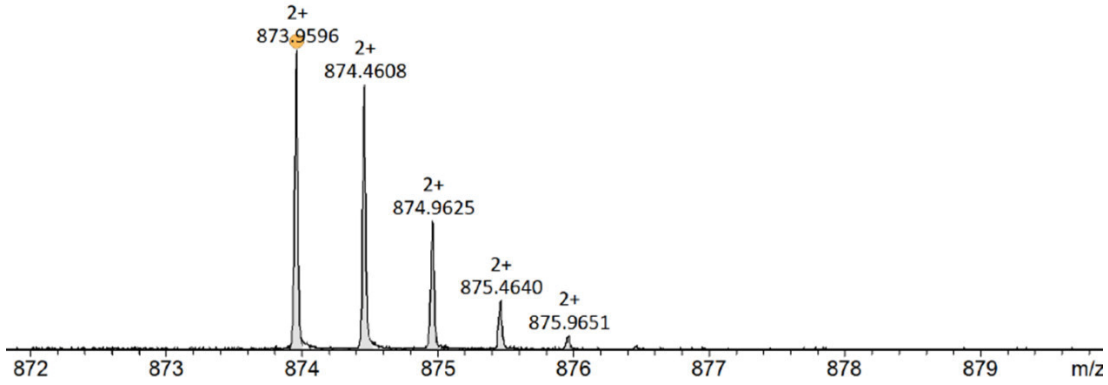

Figure S21: HR/ESI-MS spectra of Fuc(1,4)-5 (**4**).

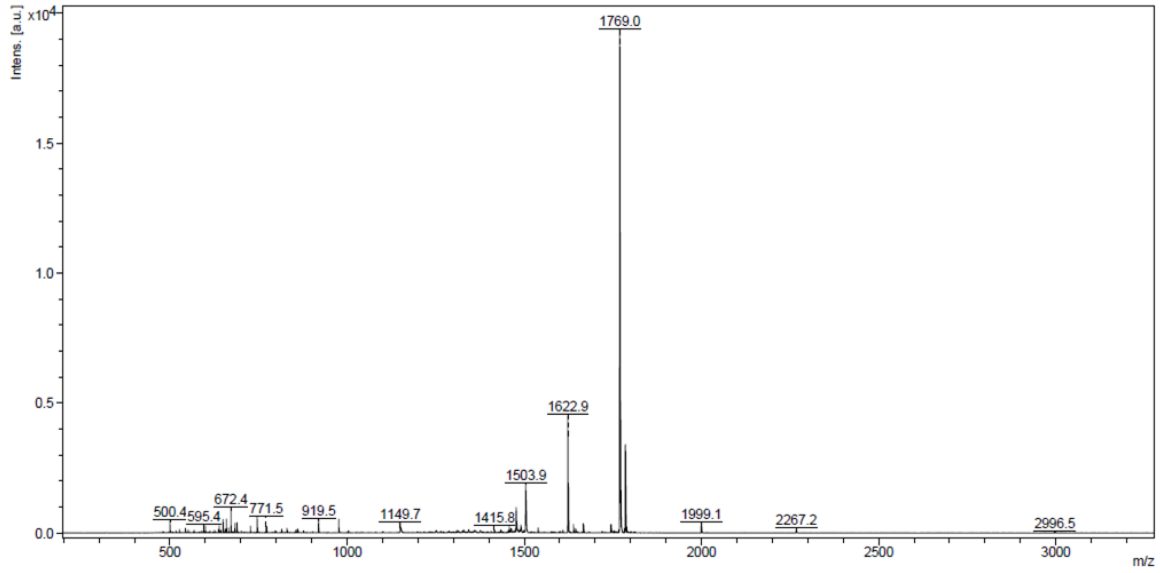

Figure S22: MALDI TOF MS spectra of Fuc(1,4)-5 (**4**).

Fuc(1,5)-5 (5)

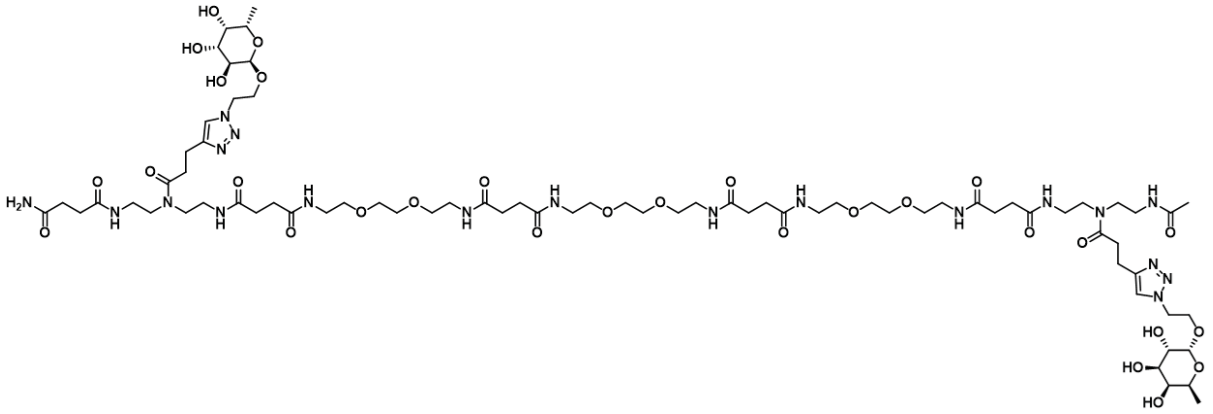

Compound **5** was synthesized in a batch size of 0.234 mmol. 291 mg (0.167 mmol) of crude product (325 mg) were purified by ion exchange resin and preparative RP-HPLC. The purified product **5** was obtained as lyophilized white powder (144 mg, 0.0824 mmol, 49%).

^{1}H NMR (600 MHz, D_2O): δ = 7.92 (s, 2H, N=N-N-C*H*), 4.85 (d, ^{3}J = 3.8 Hz, 2H , Fuc-H-1), 4.69-4.62 (m, 4H, N=N-N-CH_2), 4.06-4.02 (m, 2H, N=N-N-CH$_2$-CH_2), 3.94 (dt, $^{2,3}J$ = 10.8, 3.7 Hz, 2H, N=N-N-CH$_2$-CH_2), 3.73 (dd, $^{3,3}J$ = 10.3, 3.8 Hz, 2H, Fuc-H-2), 3.69-3.66 (m, 15H, O-CH_2-CH_2-O, Fuc-H-3), 3.63-3.61 (m, 14H, CH_2-O-(CH$_2$)$_2$-O-CH_2, Fuc-H-4), 3.50-3.45 (m, 8H, N-CH_2-CH$_2$-NH), 3.40-3.32 (m, 21H, O=C-NH-CH_2), 3.09 (q, ^{3}J = 6.6 Hz, 2H, Fuc-H-5), 3.01 (t, ^{3}J = 7.2 Hz, 4H, N-N=N-C-CH_2), 2.81-2.78 (m, 4H, N-N=N-C-CH$_2$-CH_2), 2.54-2.47 (m, 20H, O=C-CH_2-CH_2-C=O),

1.94, 1.93 (s, s, 3H, O=C-CH_3), 1.04 (d, ^3J = 6.6 Hz, 6H, Fuc-H-6). MALDI TOF MS: *m/z* calcd for $C_{74}H_{127}N_{19}O_{29}Na$ $[M+Na]^+$ 1769.92; found 1769.0. HR-ESI/MS: *m/z* calcd for $C_{74}H_{127}N_{19}O_{29}$ (monoisotopic mass 1745.9047): $[M+2H]^{2+}$ 873.9596, found 873.9598. RP-HPLC: (gradient from 100% to 50% eluent A in 30 min, 25°C): t_R = 11.2 min, determined purity 99%.

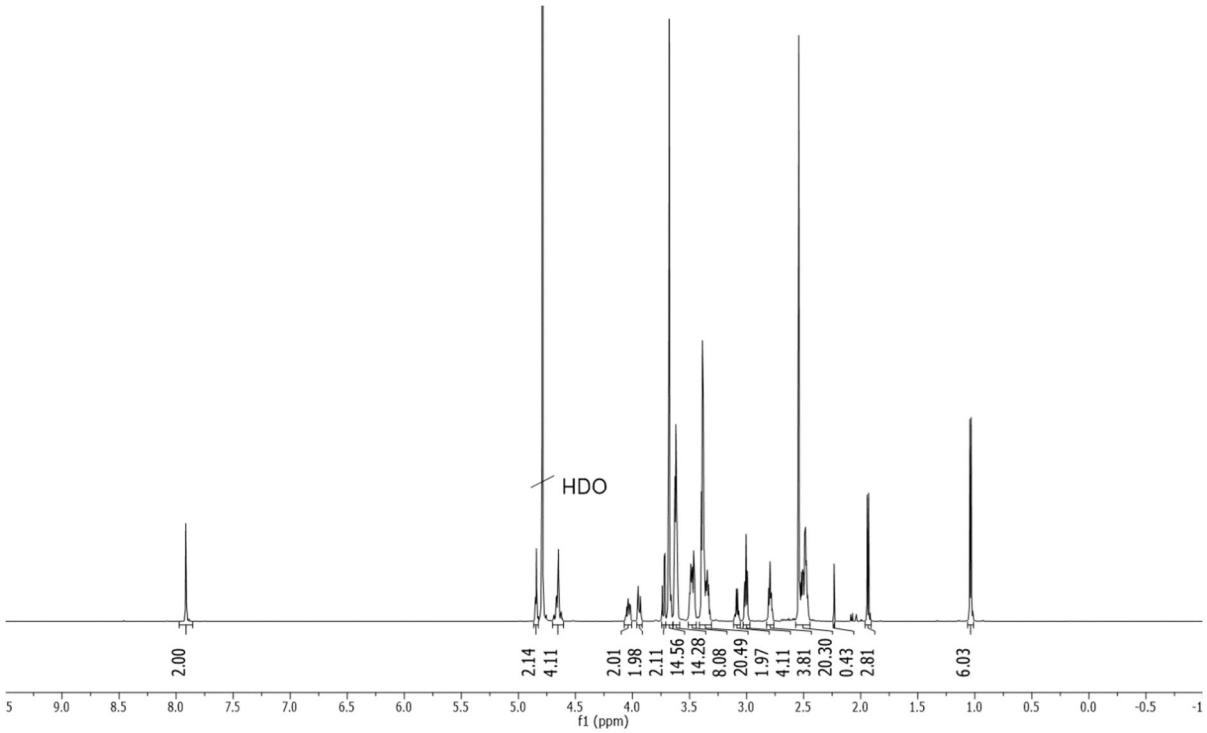

Figure S23: ^{1}H NMR (600 MHz, D_2O) spectra of Fuc(1,5)-5 (**5**).

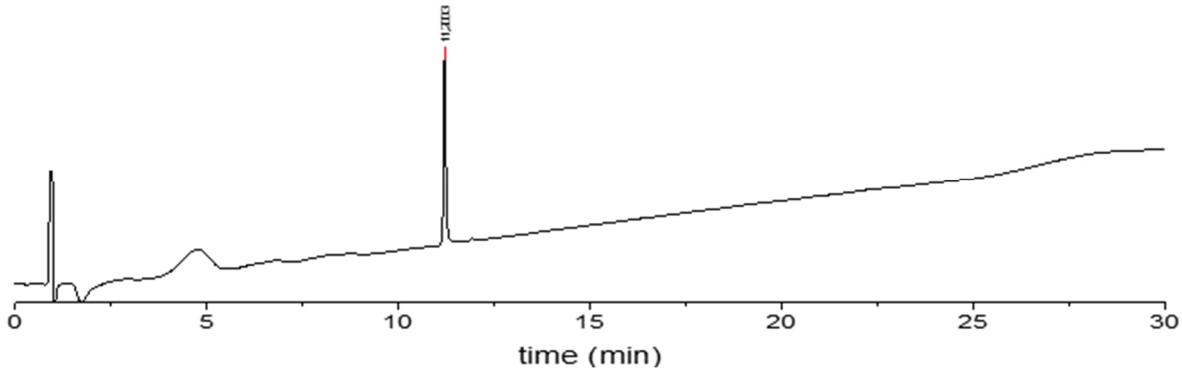

Figure S24: RP-HPLC spectra of Fuc(1,5)-5 (**5**).

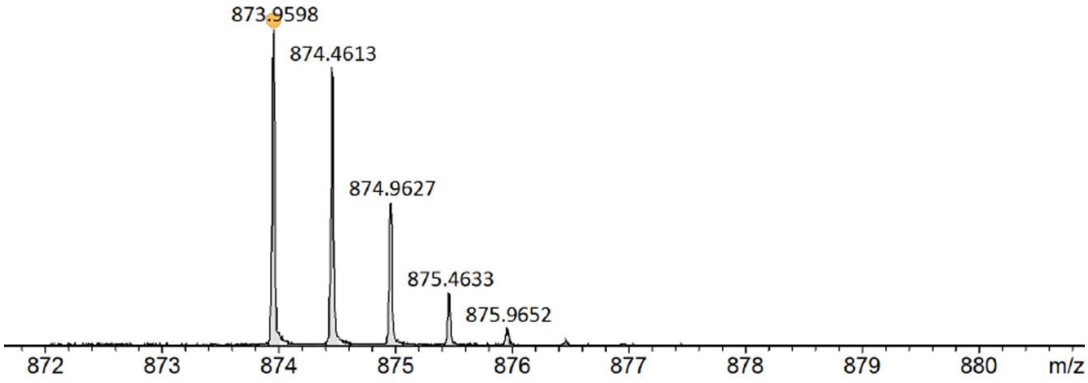

Figure S25: HR/ESI-MS spectra of Fuc(1,5)-5 (**5**).

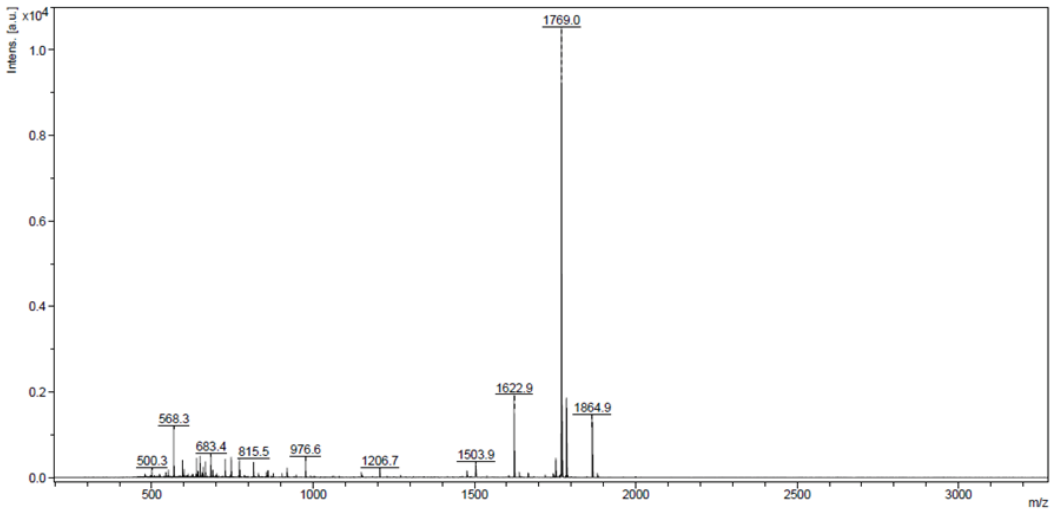

Figure S26: MALDI TOF MS spectra of Fuc(1,5)-5 (**5**).

Fuc(1,2,3,4)-4 (6)

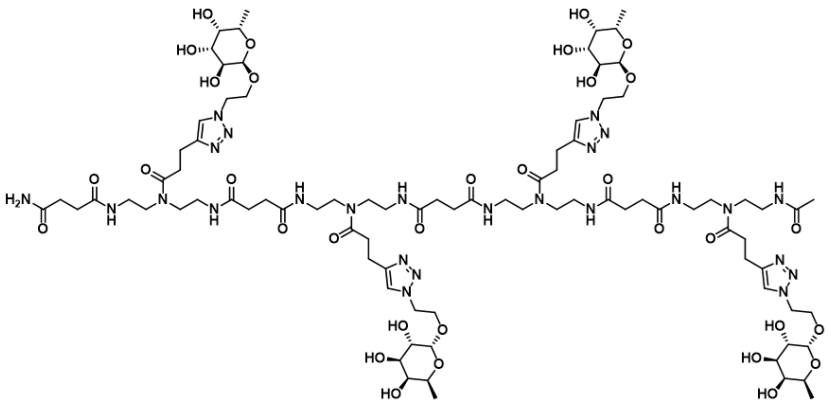

Compound **6** was synthesized in a batch size of 0.1 mmol. The crude product (282 mg, 0.137 mmol) was purified by ion exchange resin and preparative RP-HPLC. 133 mg (0.0648 mmol, 47%) of purified product **6** was obtained as lyophilized white powder.

^{1}H NMR (300 MHz, D_2O): δ = 7.91 (s, 4H, N=N-N-C*H*), 4.84 (d, ^{3}J = 3.5 Hz, 4H , Fuc-H-1), 4.67-4.62 (m, 8H, N=N-N-CH_2), 4.07-3.99 (m, 4H, N=N-N-CH_2-CH_2), 3.96-3.90 (m, 4H, N=N-N-CH_2-CH_2), 3.75-3.62 (m, 12H, Fuc-H-2, Fuc-H-3, Fuc-H-4), 3.50-3.44 (m, 16H, N-*C*H_2-CH_2-NH), 3.38-3.31 (m, 16H, O=C-NH-CH_2), 3.08 (q, ^{3}J = 6.6 Hz, 4H, Fuc-H-5), 3.01-2.97 (m, 8H, N-N=N-C-CH_2), 2.80-2.75 (m, 8H, N-N=N-C-CH_2-CH_2), 2.55-2.43 (m, 16H, O=C-CH_2-CH_2-C=O), 1.94, 1.92 (s, s, 3H, O=C-CH_3), 1.03 (d, ^{3}J = 6.6 Hz, 12H, Fuc-H-6). MALDI TOF MS: *m/z* calcd for $C_{86}H_{141}N_{25}O_{33}$ $[M+Na]^+$ 2075.01, found 2075.02; $[M-Fuc+Na]^+$ 1928.95, found 1928.95. HR-ESI/MS: *m/z* calcd for $C_{86}H_{141}N_{25}O_{33}$ (monoisotopic mass 2052.0124): $[M+3H]^{3+}$ 685.0114, found 685.0113. RP-HPLC: (gradient from 100% to 50% A in 30 min, 25°C): t_R = 10.4 min, determined purity ≥ 99%.

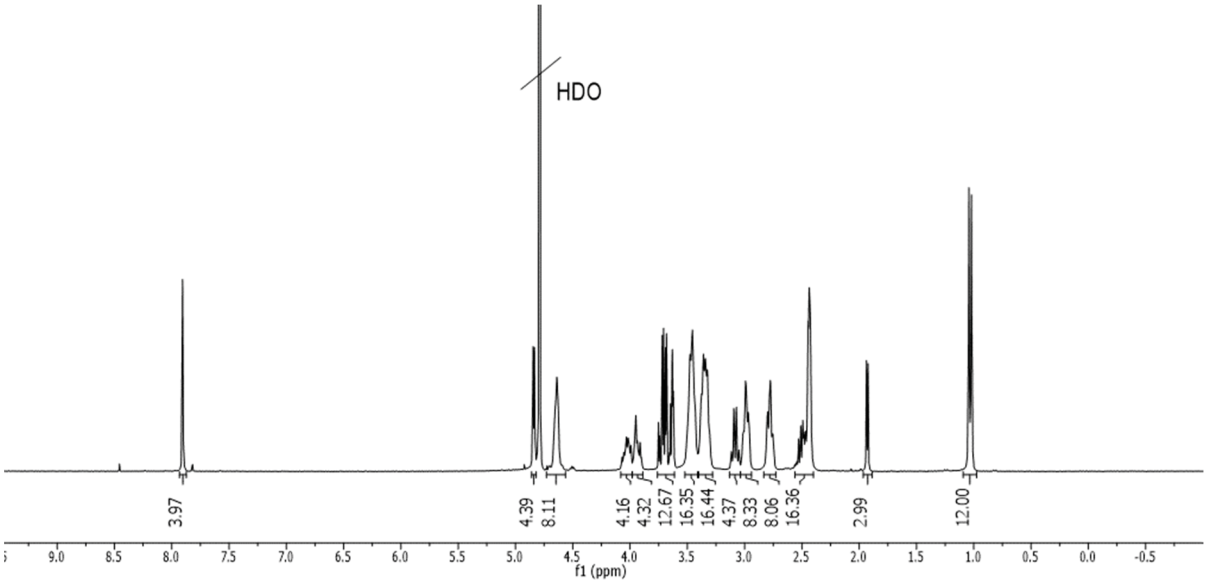

Figure S27: ^{1}H NMR (300 MHz, D_2O) spectra of Fuc(1,2,3,4)-4 (**6**).

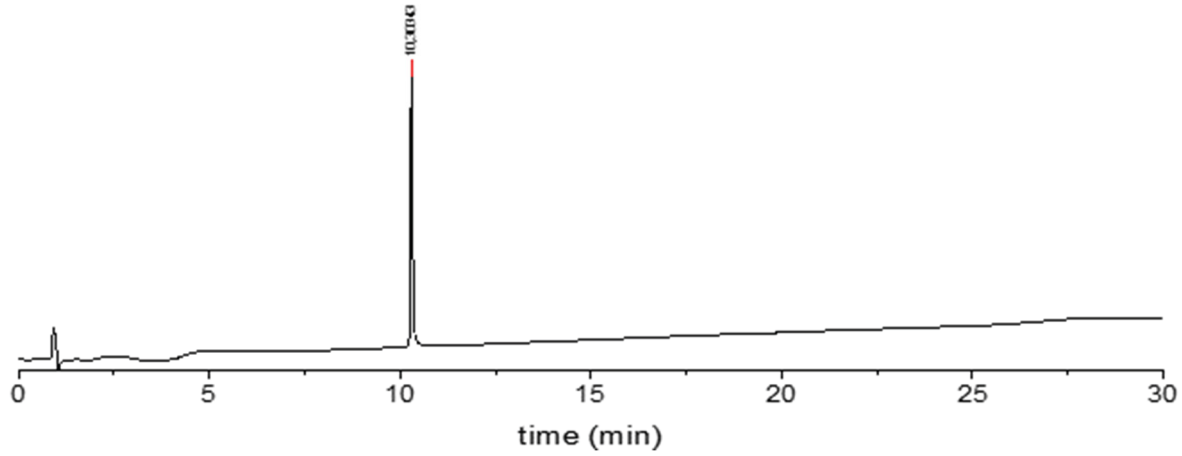

Figure S28: RP-HPLC spectra of Fuc(1,2,3,4)-4 (**6**).

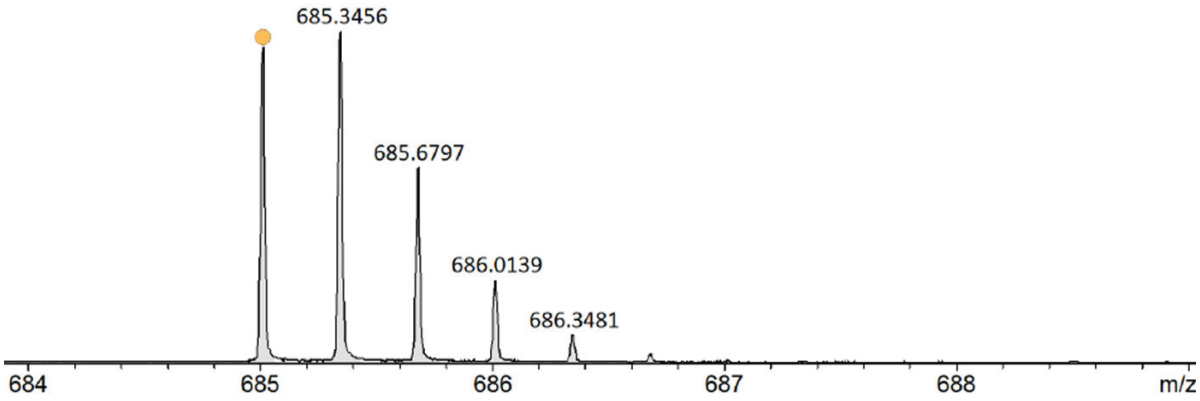

Figure S29: HR/ESI-MS spectra of Fuc(1,2,3,4)-4 (**6**).

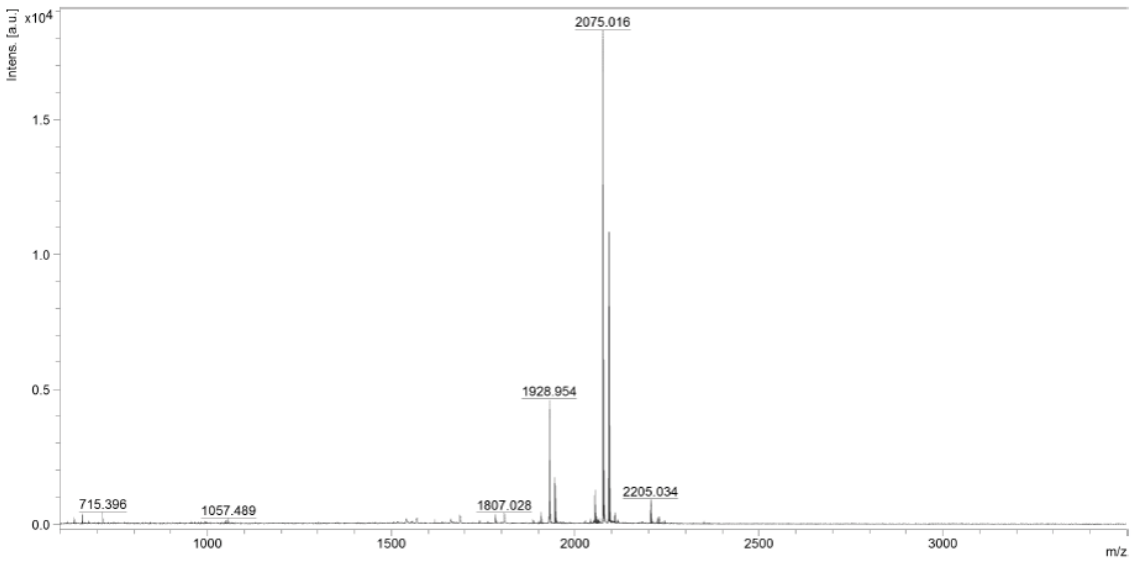

Figure S30: MALDI TOF MS spectra of Fuc(1,2,3,4)-4 (**6**).

Fuc(1,3,5,7)-7 (7)

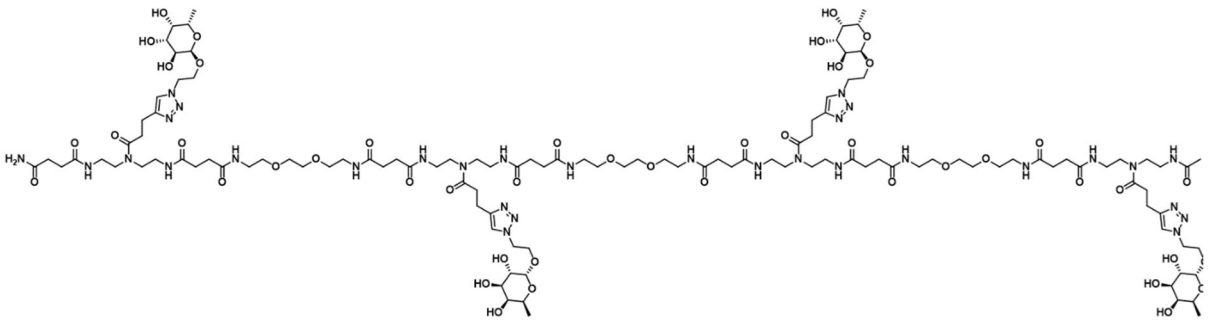

Compound **7** was synthesized in a batch size of 0.1 mmol. 106 mg (0.0386 mmol) of crude product (298 mg) were purified by ion exchange resin and preparative RP-HPLC. The purified product **7** was obtained as lyophilized white powder (31 mg, 0.011 mmol, 28%).

^{1}H NMR (300 MHz, D_2O): δ = 7.92 (s, 4H, N=N-N-C*H*), 4.84 (d, ^{3}J = 3.6 Hz, 4H , Fuc-H-1), 4.67-4.64 (m, 8H, N=N-N-CH_2), 4.08-4.00 (m, 4H, N=N-N-CH_2-CH_2), 3.97-3.91 (m, 4H, N=N-N-CH_2-CH_2), 3.75-3.59 (m, 38H, O-CH_2-CH_2-O, Fuc-H-2, Fuc-H-3, CH_2-O-$(CH_2)_2$-O-CH_2, Fuc-H-4), 3.51-3.44 (m, 16H, N-CH_2-CH_2-NH), 3.39-3.34 (m, 28H, O=C-NH-CH_2), 3.08 (q, ^{3}J = 6.6 Hz, 4H, Fuc-H-5), 3.00 (t, ^{3}J = 7.1 Hz, 8H, N-N=N-C-CH_2), 2.79 (t, ^{3}J = 7.2 Hz, 8H, N-N=N-C-CH_2-CH_2), 2.53-2.46 (m, 28H, O=C-CH_2-CH_2-C=O), 1.94, 1.93 (s, s, 3H, O=C-CH_3), 1.04 (d, ^{3}J = 6.6 Hz, 12H, Fuc-H-6). MALDI TOF MS: *m/z* calcd for $C_{116}H_{195}N_{31}O_{45}Na$ $[M+Na]^+$ 2765.39, found 2765.4; $[M-Fuc+Na]^+$ 2619.33, found 2619.3. HR-ESI/MS: *m/z* calcd for $C_{116}H_{195}N_{31}O_{45}$ (monoisotopic mass 2742.3923): $[M+3H]^{3+}$ 915.1381, found 915.1382. RP-HPLC: (gradient from 100% to 50% eluent A in 30 min, 25°C): t_R = 11.7 min, determined purity 97%.

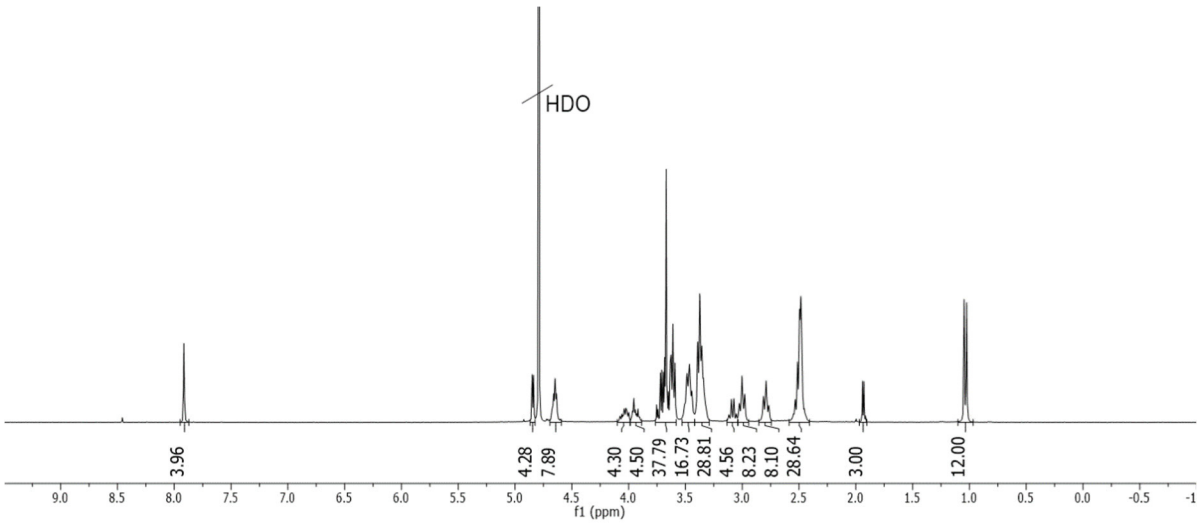

Figure S31: ^{1}H NMR (300 MHz, D_2O) spectra of Fuc(1,3,5,7)-7 (**7**).

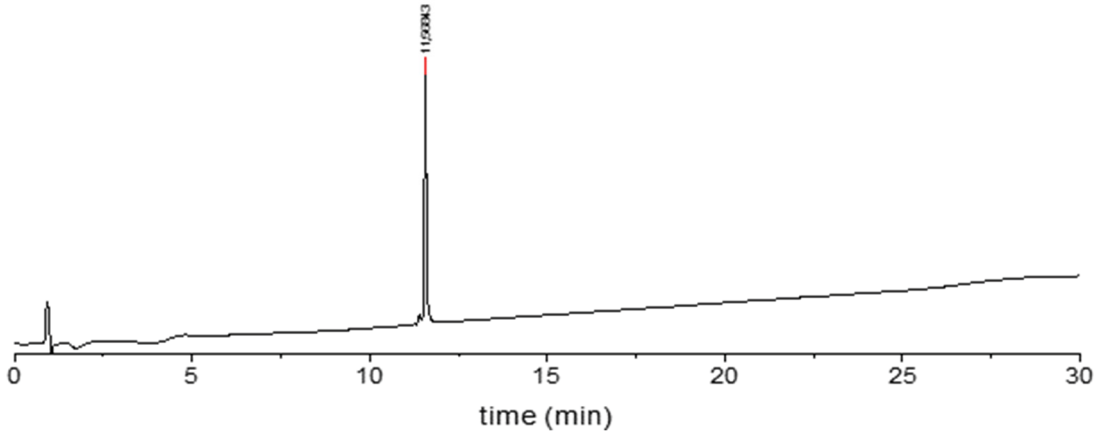

Figure S32: RP-HPLC spectra of Fuc(1,3,5,7)-7 (**7**).

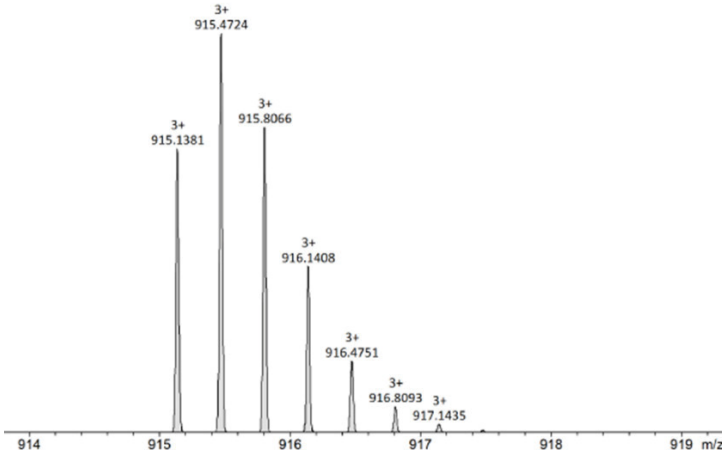

Figure S33: HR/ESI-MS spectra of Fuc(1,3,5,7)-7 (**7**).

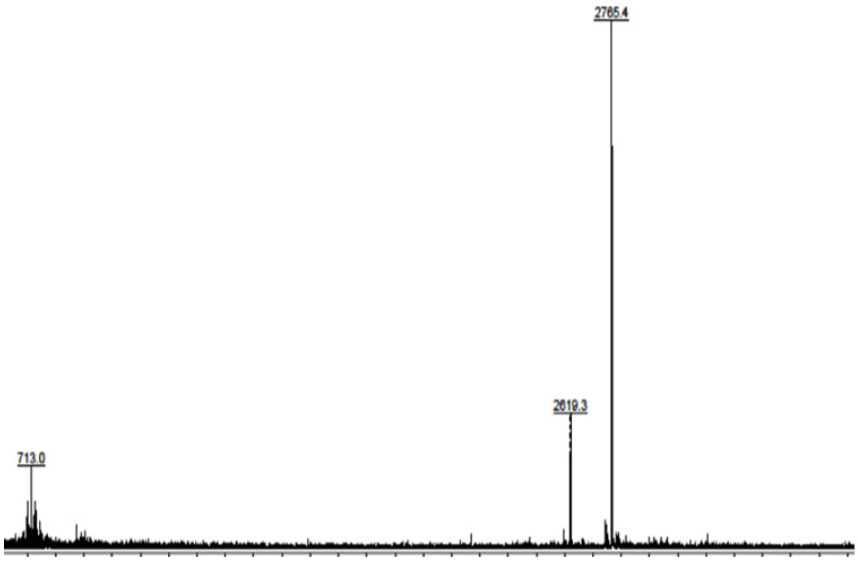

Figure S34: MALDI TOF MS spectra of Fuc(1,3,5,7)-7 (**7**).

Gal(4)-7 (8)

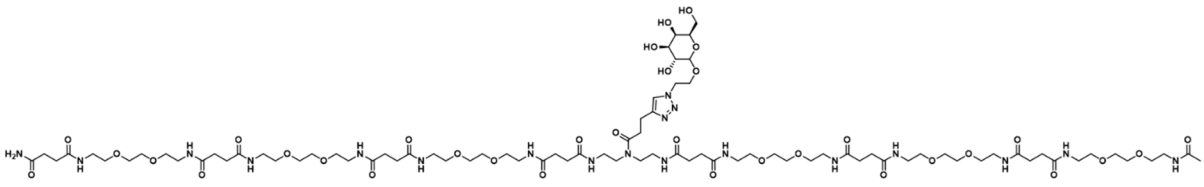

Compound **8** was synthesized in a batch size of 0.1 mmol. The crude product (80 mg, 0.04 mmol) was purified by ion exchange resin and preparative RP-HPLC. 53 mg (0.03 mmol, 30%) of purified product **8** was obtained as lyophilized white powder.

^{1}H NMR (600 MHz, D_2O): δ = 8.46, 7.90, 7.87 (s, s, s 1H, N=N-N-CH), 4.93 (d, ^3J = 1.4 Hz, 0.2H, α-Gal-H-1), 4.66-4.61 (m, 2H, N=N-N-CH_2), 4.37 (d, ^3J = 7.9 Hz, 0.8H, β-Gal-H-1), 4.31-4.27 (m, 0.8H, N=N-N-CH_2-CH_2 (*β-Gal*)), 4.11-4.08 (m, 1H, N=N-N-CH_2-CH_2), 4.03-4.00 (m, N=N-N-CH_2-CH_2, 0.5H (*α-Gal*)), 3.91 (d, ^3J = 3.4 Hz, 0.8H, β-Gal-H-2), 3.80-3.60 (m, 56H, α-Gal-H-2, Gal-H-3, -H-4, -H-5, -H-6, O-CH_2-CH_2-O, CH_2-O-$(CH_2)_2$-O-CH_2,), 3.51-3.45 (m, 6H, N-CH_2-CH_2-NH, Gal-H-6), 3.41-3.33 (m, 29H, O=C-NH-CH_2), 3.01 (t, ^3J = 7.2 Hz, 2H, N-N=N-C-CH_2), 2.80 (t, ^3J = 7.3 Hz, 2H, N-N=N-C-CH_2-CH_2), 2.59-2.46 (m, 29H, O=C-CH_2-CH_2-C=O), 2.00 (s, O=C-CH_3). MALDI TOF MS: *m/z* calcd for $C_{83}H_{147}N_{19}O_{34}Na$ $[M+Na]^+$ 1977.04, found 1977.07. HR-ESI/MS: *m/z* calcd for $C_{83}H_{147}N_{19}O_{34}$ (monoisotopic mass 1954.0358): $[M+3H]^{3+}$ 652.3453, found 652.3524, $[M+4H]^{4+}$ 489.5090, found 489.5164. RP-HPLC: (gradient from 100% to 50% eluent A in 30 min, 25°C): t_R = 12.6 min, 12.7 min determined purity ≥99%.

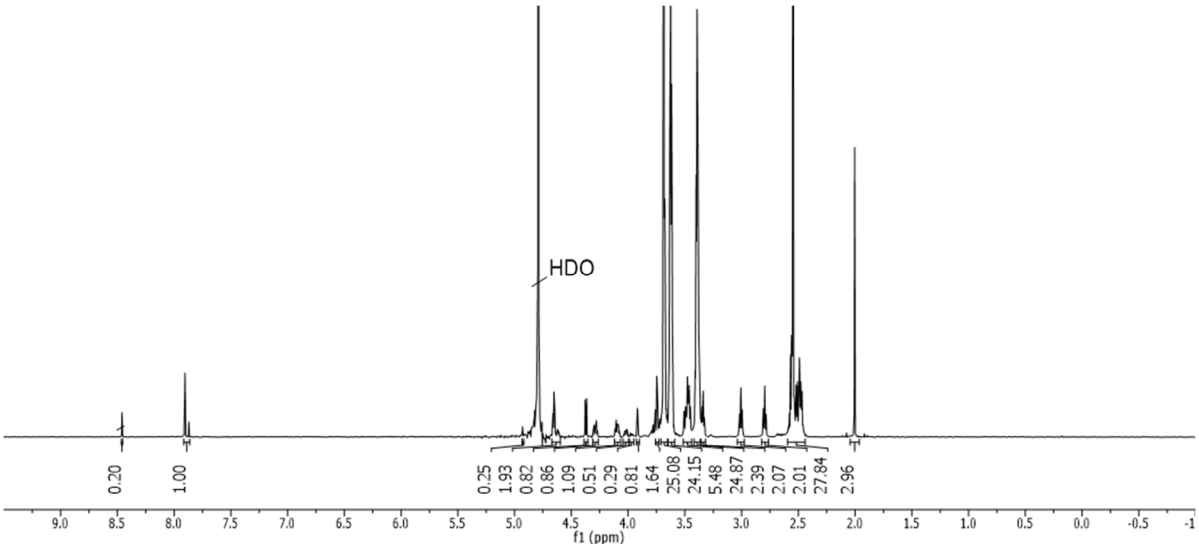

Figure S35: ^{1}H NMR (600 MHz, D_2O) spectra of Gal(4)-7 (**8**).

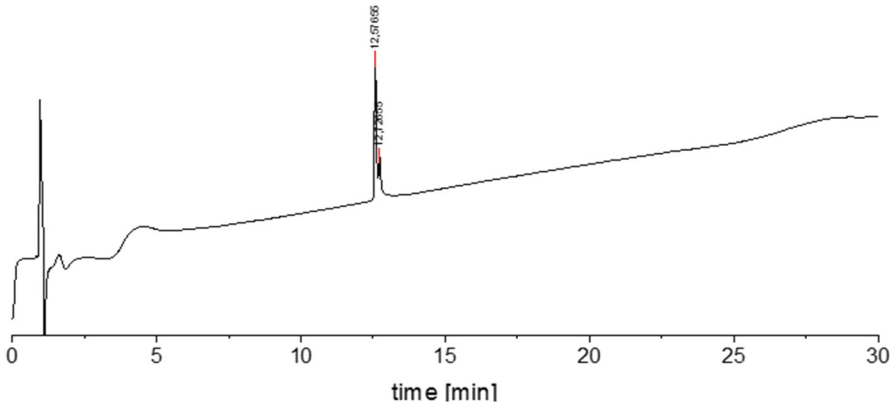

Figure S36: RP-HPLC spectra of Gal(4)-7 (**8**).

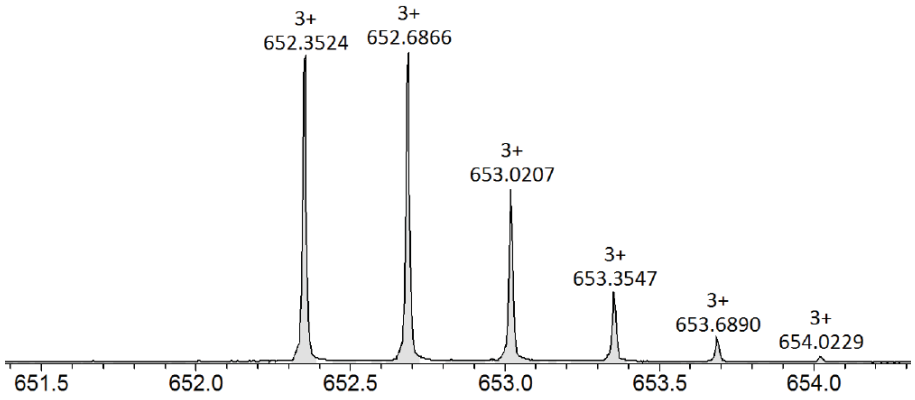

Figure S37: HR/ESI-MS spectra of Gal(4)-7 (**8**).

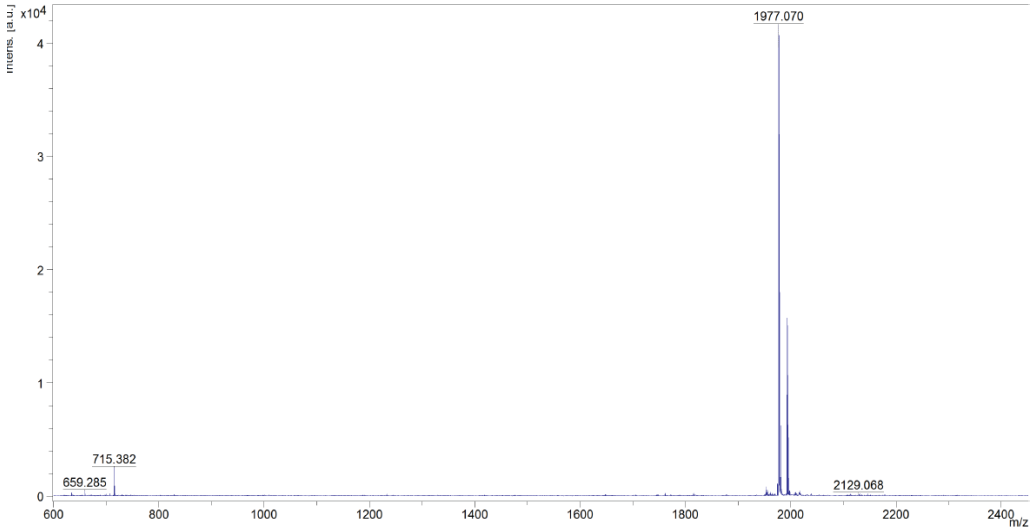

Figure S38: MALDI TOF MS spectra of Gal(4)-7 (**8**).

Fuc(1)Gal(4)-5 (9)

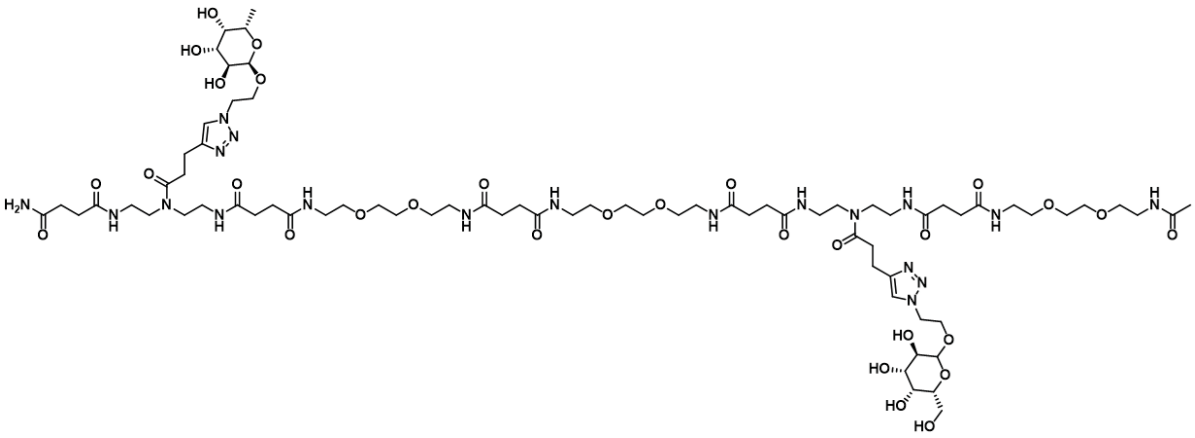

Compound **9** was synthesized in a batch size of 0.15 mmol. The crude product (301 mg, 0.171 mmol) was purified by ion exchange resin and preparative RP-HPLC. 152 mg (0.0862 mmol, 51%) of purified product **9** was obtained as lyophilized white powder.

^{1}H NMR (600 MHz, D_2O): δ = 7.92 (s, 1H, N=N-N-C*H (Fuc)*), 7.90 (s, 0.8H, N=N-N-C*H (β-Gal)*), 7.87 (s, 0.2H, N=N-N-C*H (α-Gal)*), 4.93 (d, ^{3}J = 1.6 Hz, 0.2H, α-Gal-H-1), 4.84 (d, ^{3}J = 3.8 Hz, 1H, Fuc-H-1), 4.69-4.61 (m, 4H, N=N-N-CH_2), 4.37 (d, ^{3}J = 7.9 Hz, 0.8H, β-Gal-H-1), 4.31-4.27 (m, 0.8H, N=N-N-CH_2-CH_2 (*β-Gal*)), 4.11-4.08 (m, 1H, N=N-N-CH_2-CH_2 (*β-Gal*)), 4.06-4.00 (m, 1.4H, N=N-N-CH_2-CH_2 (*Fuc*, *α-Gal*)), 3.94 (dt, $^{2,3}J$ = 10.8, 3.8 Hz, 1H, N=N-N-CH_2-CH_2 (*Fuc*)), 3.91 (d, ^{3}J = 3.8 Hz, 0.8H, β-Gal-H-2), 3.80-3.70 (m, 3.5H, α-Gal-H-2, Gal-H-3, Gal-H-4, Fuc-H-2), 3.69-3.66 (m, 14H, O-CH_2-CH_2-O, Fuc-H-3, Gal-H-5), 3.63-3.61 (m, 14H, CH_2-O-$(CH_2)_2$-O-CH_2, Fuc-H-4, Gal-H-6), 3.51-3.45 (m, 9H, N-*C*H_2-CH_2-NH), 3.39-3.33 (m, 20H, O=C-NH-CH_2), 3.09 (q, ^{3}J = 6.5 Hz, 1H, Fuc-H-5), 3.00 (t, ^{3}J = 7.2 Hz, 4H, N-N=N-C-CH_2), 2.79 (t, ^{3}J = 7.3 Hz, 4H, N-N=N-C-CH_2-CH_2), 2.54-2.47 (m, 20H, O=C-CH_2-CH_2-C=O), 2.00, 1.92 (s, s, 3H, O=C-CH_3), 1.04 (d, ^{3}J = 6.6 Hz, 3H, Fuc-H-6). MALDI TOF MS: *m/z* calcd for $C_{74}H_{127}N_{19}O_{30}Na$ $[M+Na]^+$ 1784.90, found 1784.89; $[M+K]^+$ 1800.90, found 1800.87. HR-ESI/MS: *m/z* calcd for $C_{74}H_{127}N_{19}O_{30}$ (monoisotopic mass 1761.8996): $[M+2H]^{2+}$ 881.9571, found 881.9561. RP-HPLC: (gradient from 100% to 50% eluent A in 30 min, 25°C): t_R = 10.8min, 11.0 min determined purity ≥99%.

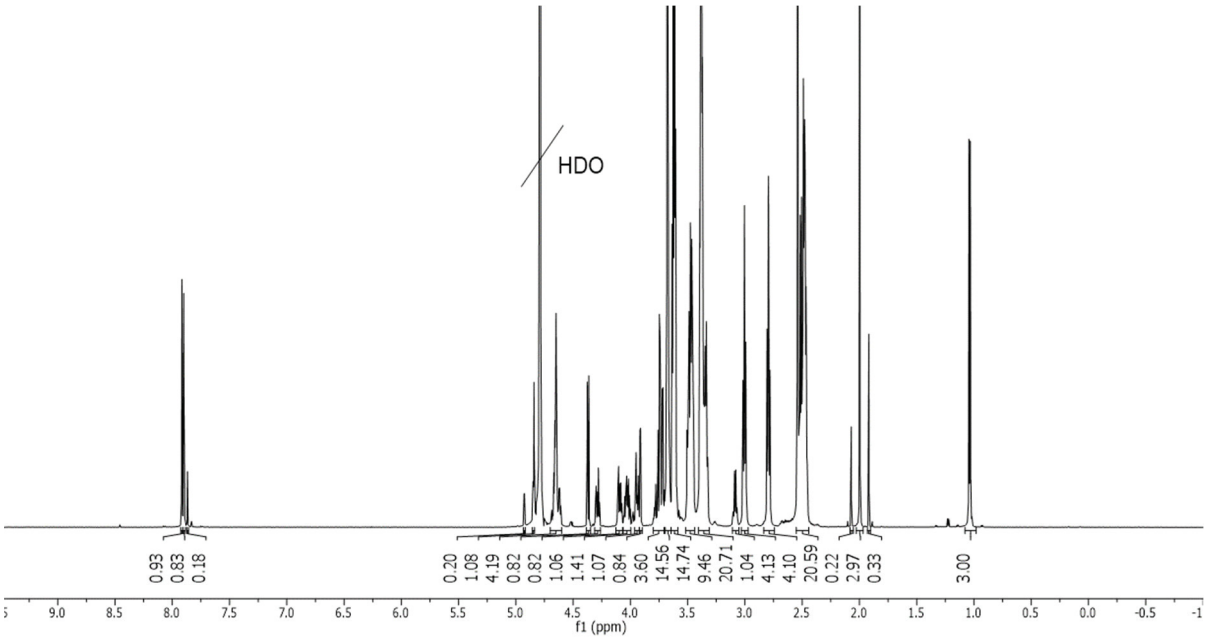

Figure S39: ^{1}H NMR (600 MHz, D_2O) spectra of Fuc(1)Gal(4)-5 (**9**).

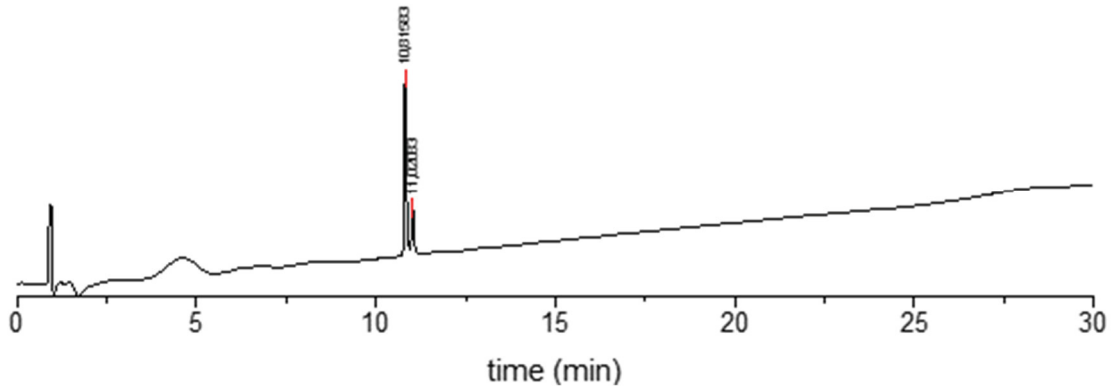

Figure S40: RP-HPLC spectra of Fuc(1)Gal(4)-5 (**9**).

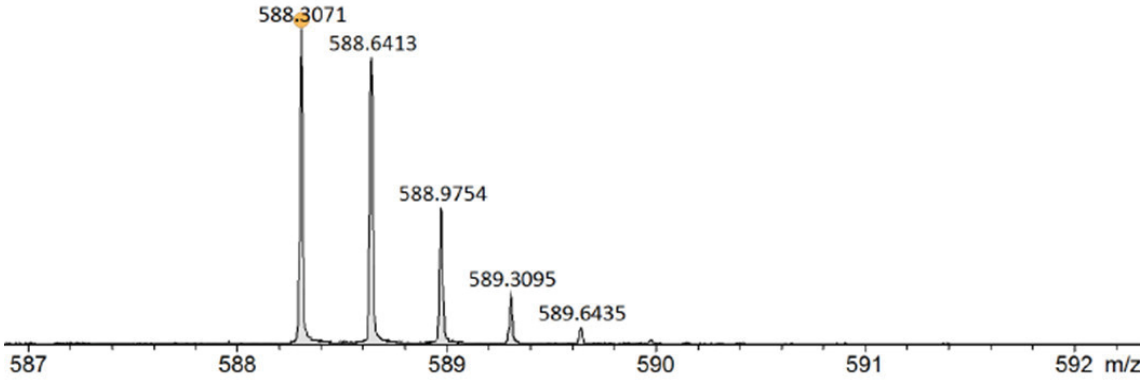

Figure S41: HR/ESI-MS spectra of Fuc(1)Gal(4)-5 (**9**).

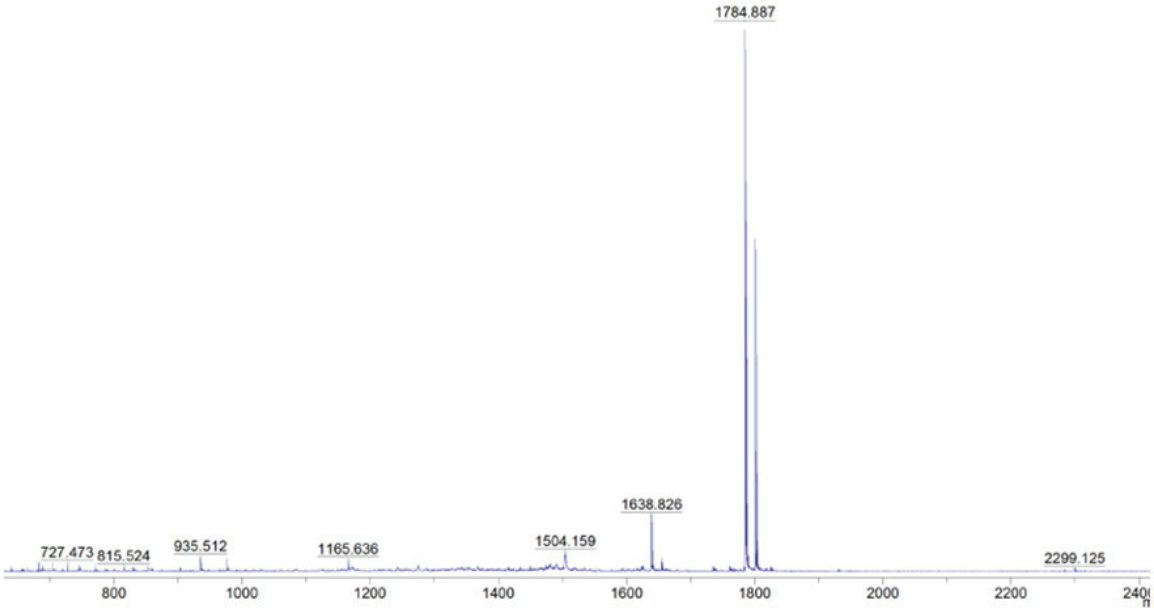

Figure S42: MALDI TOF MS spectra of Fuc(1)Gal(4)-5 (**9**).

Fuc(1,5)-TEMPO(2,6)-6 (10)

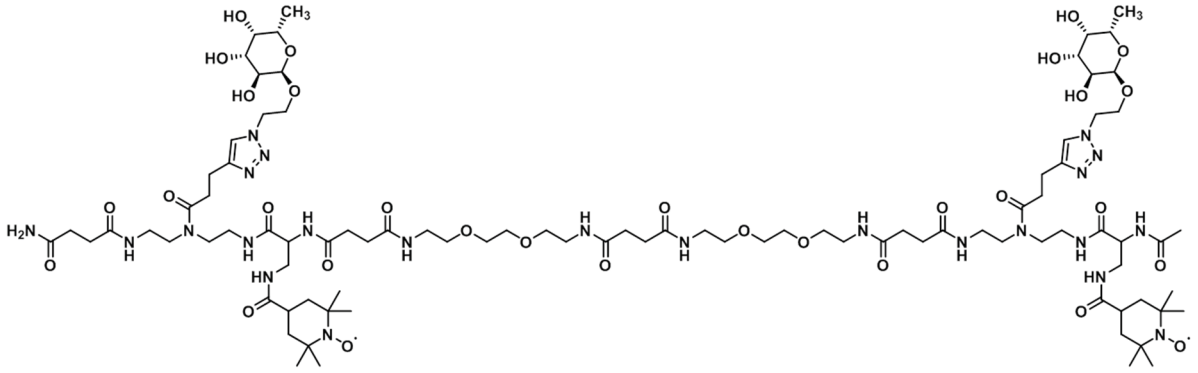

Compound **10** was synthesized in a batch size of 0.05 mmol. The product was obtained as lyophilized white powder.

^{1}H NMR (500 MHz, D_2O): δ = 7.98 (s, 2H, N=N-N-C*H*), 4.91-4.89 (m, 2H, Fuc-H-1), 4.75-4.71 (m, 4H, N=N-N-CH_2), 4.55 (s, br, 2H, C=O-NH-C*H*), 4.10-4.01 (m, 4H, N=N-N-CH_2-CH_2), 3.75-3.45 (m, 52H, (CH_2)$_2$-O-(CH_2)$_2$-O-(CH_2)$_2$, N-*CH*$_2$-CH_2-NH, C=O-NH-CH-CH_2, Fuc-H-2, H-3, H-4), 3.19 (s, br, 2H, Fuc-H-5), 3.06 (s, br, 4H, N-N=N-C-CH_2), 2.86 (s, br, 4H, N-N=N-C-CH_2-CH_2), 2.61-2.56 (m, 16H, O=C-CH_2-CH_2-C=O), 2.10 (s, 3H, O=C-CH_3), 2.01 (s, br, 2H, TEMPO), 1.52 (s, br, 9H, TEMPO), 1.27-1.23 (m, 1H, TEMPO), 1.11 (s, 6H, Fuc-H-6). HR-ESI/MS: *m/z* calcd for $C_{90}H_{153}N_{23}O_{33}$ $[M+3H]^{3+}$ 695.707, found 695.706. RP-HPLC: (gradient from 100% eluent A to 100% eluent B in 17 min, 25°C): t_R = 8.21 min, determined purity ≥ 87 %.

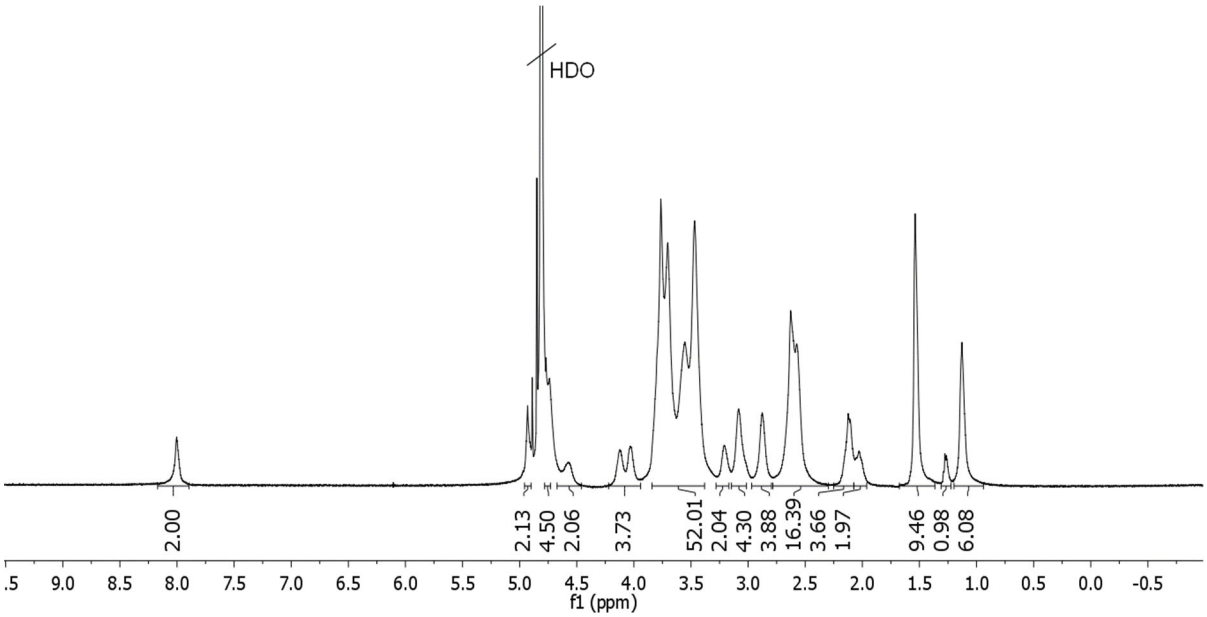

Figure S43: ^{1}H NMR (500 MHz, D_2O) spectra of Fuc(1,5)TEMPO(2,6)-6 (**10**).

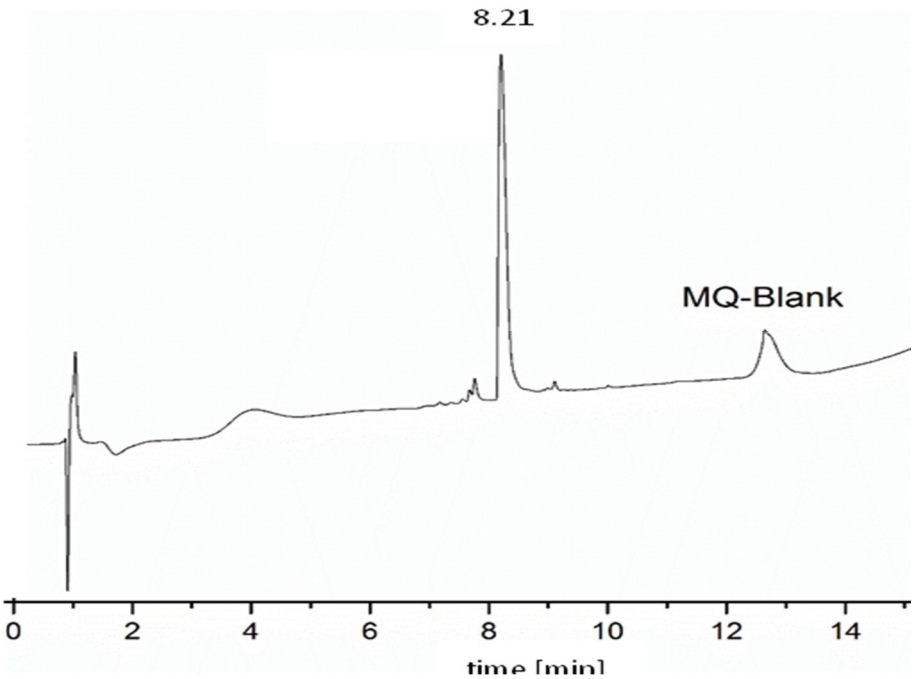

Figure S44: RP-HPLC spectra of Fuc(1,5)TEMPO(2,6)-6 (**10**).

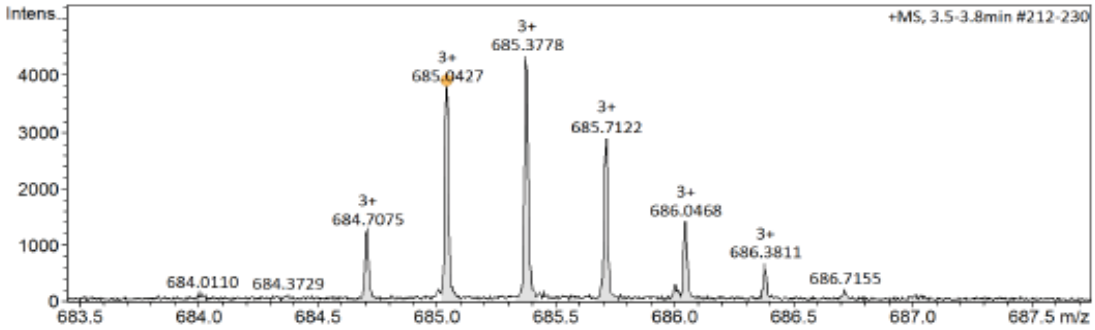

Figure S45: HR/ESI-MS spectra of Fuc(1,5)TEMPO(2,6)-6 (**10**).

Gal(1,2,3,4)-4 (11)

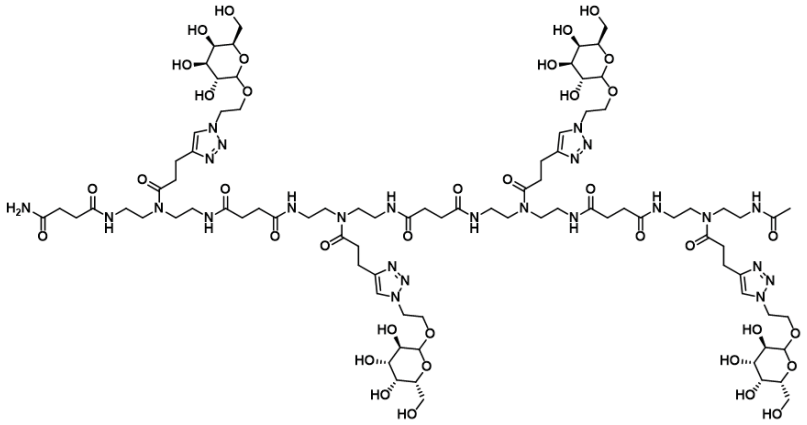

Compound **11** was synthesized in a batch size of 0.1 mmol. The crude product (300 mg, 0.142 mmol) was purified by ion exchange resin and preparative RP-HPLC. 137 mg (0.0647 mmol, 46%) of purified product **11** was obtained as lyophilized white powder.

^{1}H NMR (300 MHz, D_2O): δ = 7.88 (s, 3H, N=N-N-C*H*), 7.85 (s, 1H, N=N-N-C*H*), 4.92 (m, 1H, α-Gal-H-1), 4.66-4.58 (m, 8H, N=N-N-C*H*$_2$), 4.36 (d, ^3J = 7.8 Hz, 3H, β-Gal-H-1), 4.31-4.25 (m, 3H, N=N-N-CH$_2$-C*H*$_2$), 4.12-4.05 (m, 4H, N=N-N-CH$_2$-C*H*$_2$), 4.04-3.93 (m, 2H, N=N-N-CH$_2$-C*H*$_2$), 3.91 (d, ^3J = 3.3 Hz, 3H, β-Gal-H-2), 3.81-3.59 (m, 17H, α-Gal-H-2, Gal-H-3,-H-4,-H-5,-H-6), 3.52-3.45 (m, 20H, N-*CH*$_2$-CH$_2$-NH, Gal-H-6), 3.35-3.32 (m, 16H, O=C-NH-C*H*$_2$), 3.01-2.95 (m, 8H, N-N=N-C-C*H*$_2$), 2.79-2.75 (m, 8H, N-N=N-C-CH$_2$-C*H*$_2$), 2.56-2.42 (m, 16H, O=C-C*H*$_2$-C*H*$_2$-C=O), 1.93, 1.91 (s, s, 3H, O=C-C*H*$_3$). MALDI TOF MS: *m/z* calcd for $C_{86}H_{141}N_{25}O_{37}Na$ $[M+Na]^+$ 2138.99, found 2139.01. HR-ESI/MS: *m/z* calcd for $C_{86}H_{141}N_{25}O_{33}$ (monoisotopic mass 2115.9920): $[M+3H]^{3+}$ 706.3379, found 706.3375. RP-HPLC: (gradient from 100% to 50% eluent A in 30 min, 25°C): t_R = 9.0 min, 9.1 min, 9.3 min determined purity 99%.

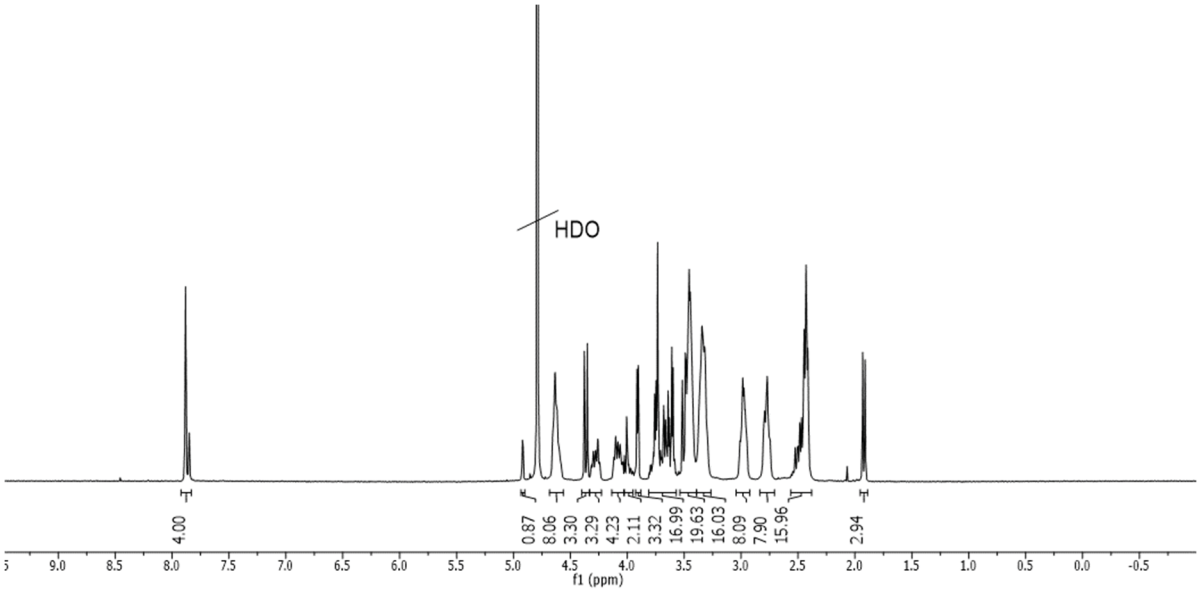

Figure S46: ^{1}H NMR (300 MHz, D_2O) spectra of Gal(1,2,3,4)-4 (**11**).

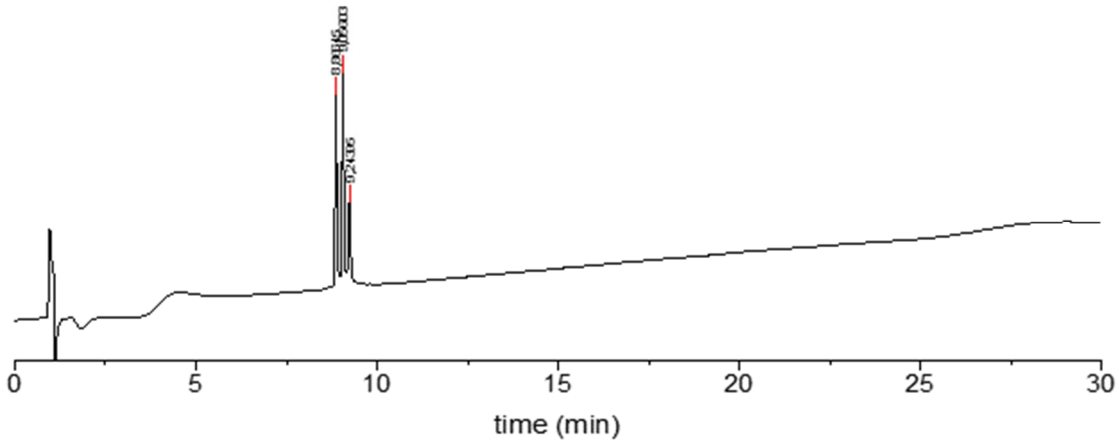

Figure S47: RP-HPLC spectra of Gal(1,2,3,4)-4 (**11**).

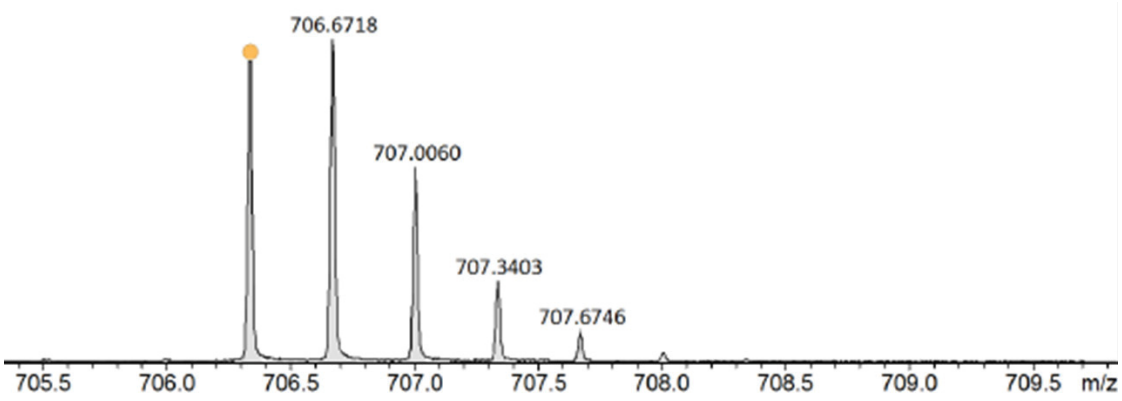

Figure S48: HR/ESI-MS spectra of Gal(1,2,3,4)-4 (**11**).

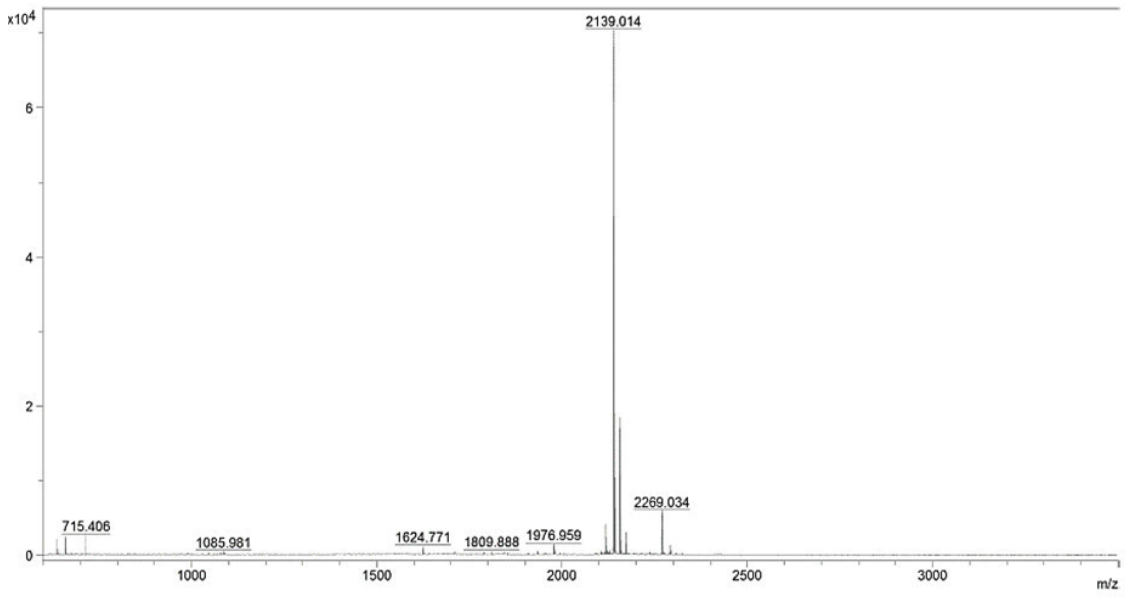

Figure S49: MALDI TOF MS spectra of Gal(1,2,3,4)-4 (**11**).

3. Native mass spectrometry

Native mass spectrometry (MS) measurements were performed according to the previously described reference protein method to analyze glycan binding[5–7] using 3 μM purified NoV GII.4 P-dimer and 10 μM reference protein cytochrome c (C7752 Sigma-Aldrich). P-dimer was subjected to buffer exchange to 300 mM ammonium acetate and 20 mM triethylammonium acetate (TEAA) (90358 Sigma) at pH 7.0 via centrifugal filter units at 13000 g, 4°C (Vivaspin 500, MWCO 10000, Sartorius). The reference protein was directly dissolved in the same buffer. Glycan mimetics were dissolved in MilliQ and binding was measured at final concentrations varying from 100 μM to 200 μM. Mass spectra were acquired at room temperature (25 °C) in positive ion mode on a Liquid Chromatography Time of Flight (LCT Premier) MS instrument modified for high mass (Waters, UK and MS Vision, the Netherlands) with a nano-electrospray ionization (ESI) source. Gold-coated electrospray capillaries were produced in house for direct sample infusion without any accessory chromatographic separation. The voltages and pressures were optimized for non-covalent protein complexes.[8] Capillary and sample cone voltages were 1.20 kV to 1.30 kV and 120 V, respectively. Pressures were 7 mbar in the source region and 6.2 x 10^{-2} to 6.5 x 10^{-2} mbar argon in the hexapole region. Under these conditions, no ligand dissociation from target or reference protein were observed, which is easily detected due to lower protein charge states arising upon loss of the ligand charged on the free backbone amine. A spectrum of a 25 mg/ml cesium iodide solution from the same day was applied for calibration of raw data using the MassLynx software (Waters, UK). OriginPro 2016 SR2 software (United States) was used to determine binding and non-binding peak areas. The non-specific protein-ligand clustering and specific binding were interpreted as described.[5,7] The corrected signal was averaged over at least three independent measurements. The data was summed over all charge states and renormalized to the unbound protein peak. The law of mass action was employed to analyze the binding events of glycan mimetics on P-dimer and determine the macroscopic dissociation constant K_{D1}. Glycan mimetic **8** (Table 2) was designed as a non-binding control with a single galactose, which indeed showed no binding above experimental error (as defined in comparison with NMR data) and therefore confirmed that the backbone has little contribution to glycan mimetic binding.

At equilibrium conditions, the dissociation constant K_D can be determined from the concentrations of free ligand [L], free protein [P], and protein ligand complex [PL] (1). The peak areas observed for protein and protein ligand complexes observed in native MS relate well to in solution concentrations assuming that a small ligand has negligible effect on ionization efficiency. Therefore, titrations are not required and K_D values can in principle be obtained from single point measurements. Our data indeed show that determined K_Ds are in good agreement at varying ligand concentrations (Table 2).

$$K_D = \frac{[P][L]}{[PL]} \qquad (\mathbf{1})$$

For multiple ligand binding events:

$$\begin{aligned} P + L &\rightleftharpoons PL \\ PL + L &\rightleftharpoons PL_2 \\ PL_2 + L &\rightleftharpoons PL_3 \\ &\vdots \\ PL_{n-1} + L &\rightleftharpoons PL_n \end{aligned}$$

Scheme 2: Theoretical multiple binding events between protein (P) and n ligands (L).

$$v = \frac{[\text{Bound ligand PL}]}{[\text{ Protein of interest P}]} = \frac{[PL] + 2[PL_2] + 3[PL_3] \cdots + n[PL_n]}{[P] + [PL] + [PL_2] + [PL_3] \cdots + [PL_n]} \qquad (\mathbf{2})$$

The ratio of bound ligand PL to the total protein of interest P equals to the degree of binding v.

$$v_1 = \frac{[PL]}{[P] + [PL]} = \frac{[L]}{K_D + [L]} \qquad (\mathbf{3})$$

The dissociation constant with one binding event v_1 is described by equation (3) and retrieves equation (2) again when solved to K_D.

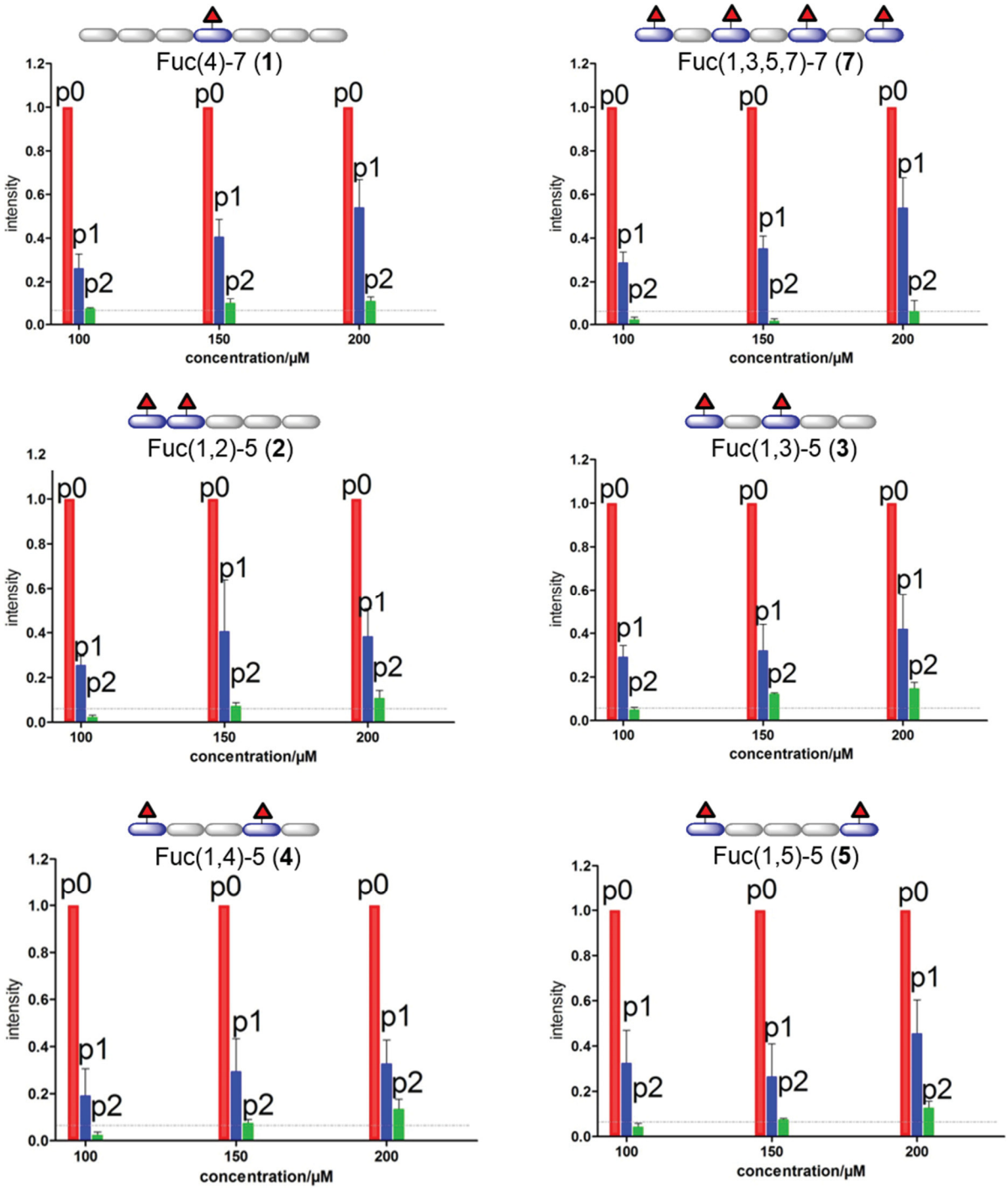

Figure S50: Native MS results from glycomacromolecules **1**-**5** and **7**.

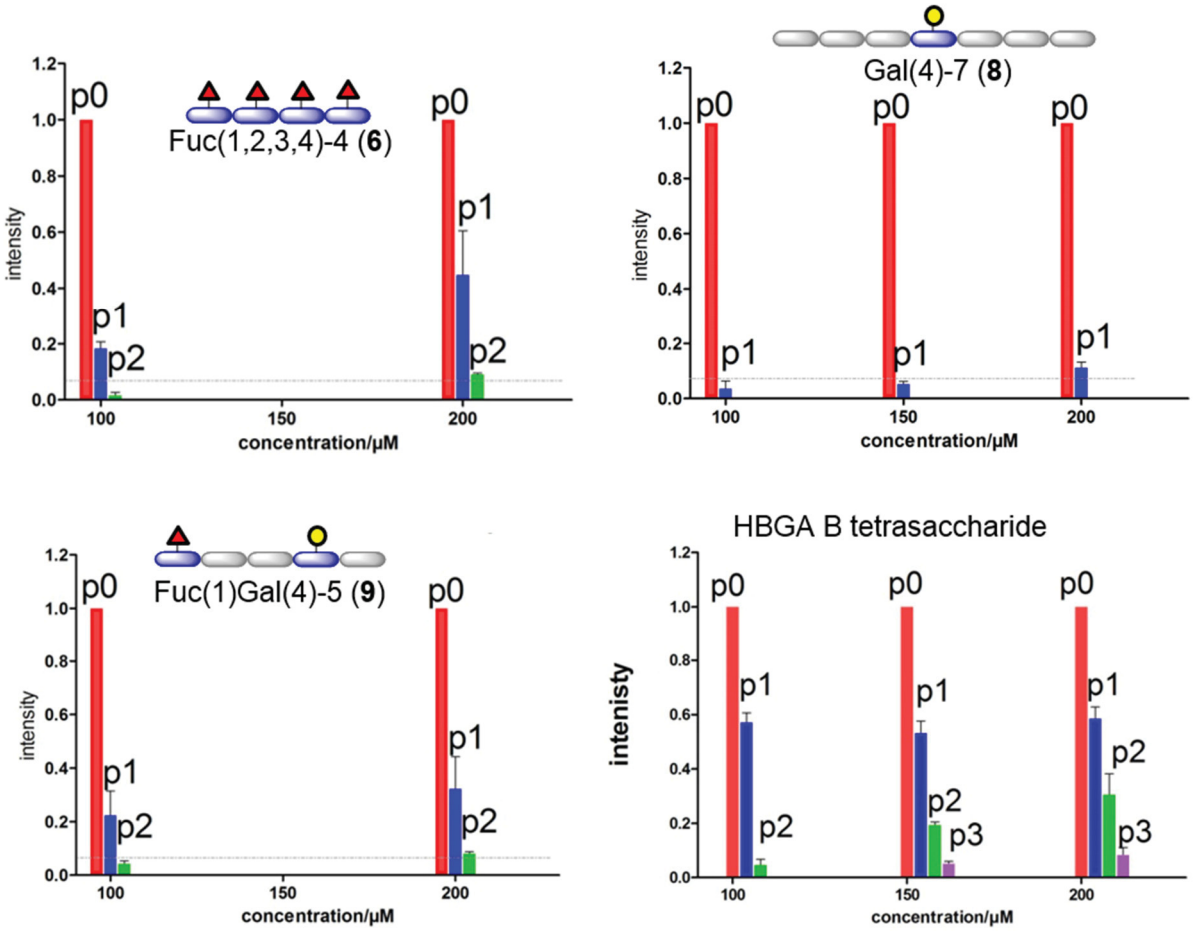

Figure S51: Native MS results from glycomacromolecules **6, 8** and **9** and HBGA B tetrasaccharide.

To reveal the specific binding and correct for unspecific clustering during native MS measurements, a reference protein was mixed with P dimer and glycomacromolecules in solution. The reference protein does not bind to target protein or ligand of interest. Therefore, glycans observed on the surface of the reference protein during the experiment is regarded as non-specific clustering. Clustering is an inherent process during electrospray ionization[8,9], the initially formed droplets also contain free ligand, which dries down onto the protein upon desolvation. A ratio of peak areas is obtained for reference protein plus unspecific clustering of ligand to free reference protein. In contrast, target proteins exhibit both specific binding and non-specific clustering. The unspecific clustering is eliminated via the ratio obtained from unspecific clustering to the reference protein revealing the specific binding to the target protein, which then allows further K_D calculation and stoichiometry determination.

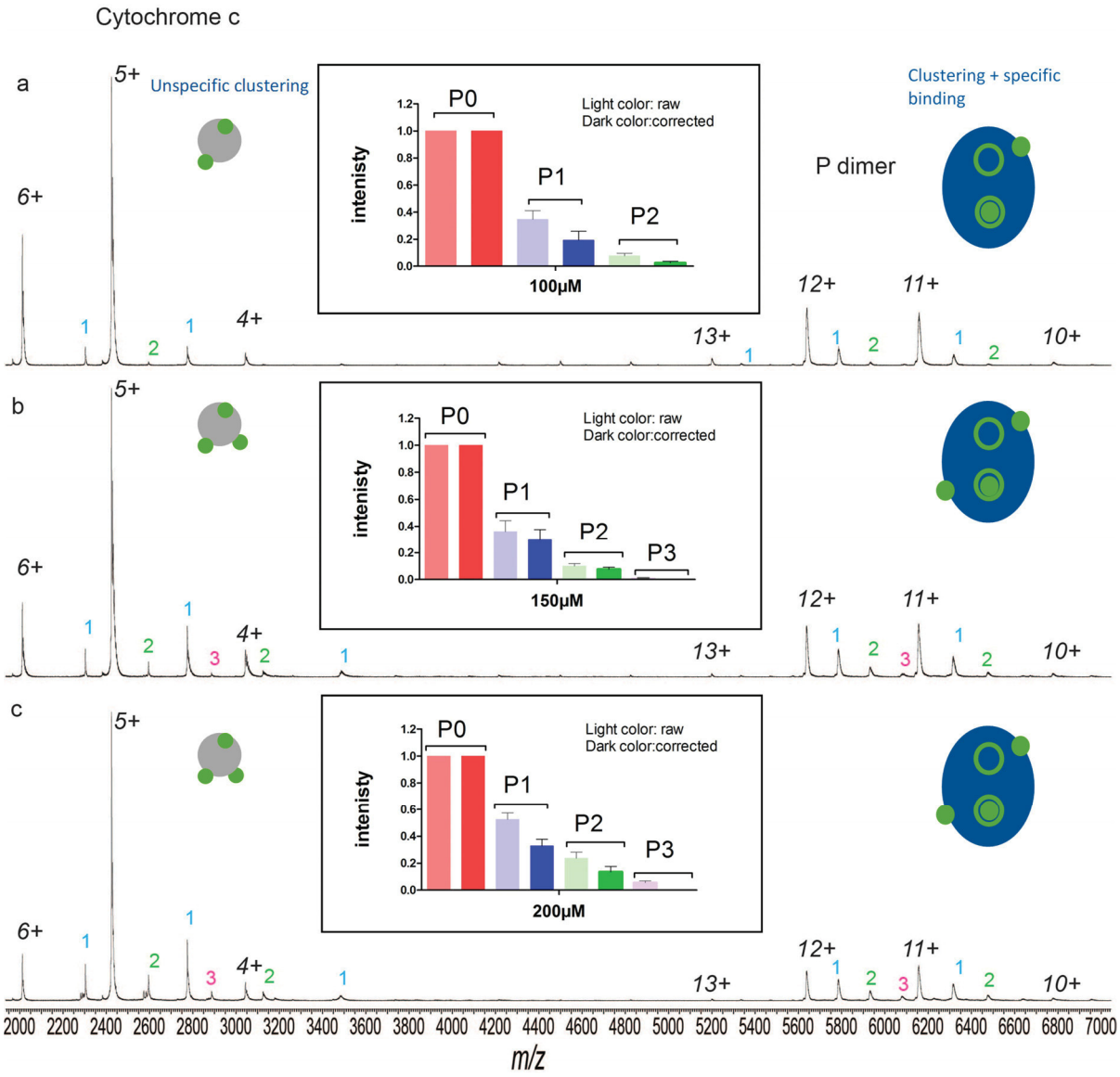

Figure S52. Native mass spectra of glycomacromolecule **5** binding to GII.4 Saga P-dimers. Cytochrome c (reference protein) was used for unspecific clustering correction. a)–c) show raw data at 100 μM, 150 μM and 200 μM glycomacromolecule **5** concentration, respectively. Raw (light color) and corrected (dark color) intensities for free and glycomacromolecule **5** bound P dimer is plotted as inset in bar graphs. All charge states of P dimers were summarized and intensity normalized to non-binding P dimer peaks. Schematically, green, grey and oval blue dots represent glycomacromolecules, cytochrome c and P dimer, respectively, and green circle on the oval blue dots are conveyed as binding pockets to show the unspecific clustering and binding at different ligand concentrations.

4. STD NMR and CSP NMR

4.1 Protein biosynthesis of GII.4 Saga P-dimers

Biosynthesis and purification of unlabeled and U-[^{2}H,^{15}N] GII.4 Saga P-dimers have been described previously.[7]

4.2 STD NMR

NMR samples contained 30 µM P-dimers, 100 µM DSS-d_6 and 1 mM of either compound **7** or **11** in 20 mM deuterated sodium phosphate buffer, pH* 7.4. A train of 50 ms Gaussian-shaped radio frequency pulses with a field strength of 67 Hz separated by 1 ms for a total duration of 2 s was used for protein irradiation. Off and on-resonance experiments were performed at 200 ppm and -2 ppm, respectively. A 40 ms spinlock filter was used for suppression of protein signals. 640 and 720 scans have been acquired for compounds **7** and **11**, respectively.

4.3 Chemical shift perturbation experiments

Compound **6** has been titrated to a sample containing 85 µM U-[^{2}H,^{15}N] P-dimers, 100 mM DSS-d_6 and 400 µM imidazole in 75 mM sodium phosphate buffer, 100 mM NaCl, pH* (uncorrected pH) 7.30, 10 % D_2O. HSQC TROSY spectra were acquired with 128 ms and 121 ms acquisition time as well as 16 ppm and 35 ppm sweep width in the respective proton or nitrogen dimension. 24 scans were measured. Methyl α-L-fucopyranoside (Carbosynth) was added to a sample containing 100 µM U-[^{2}H,^{15}N] P-dimers in the same buffer as described above. 20 scans were acquired. Spectra were processed using Topspin 3.5 (Bruker) and analyzed with the CCPNMR 2.4.0 software suite.[10]

5. Protein expression, purification and crystallization of the norovirus P- dimer

The norovirus Vietnam026 GII.10 strain (GenBank accession number AF504671) was purified as previously published.[11] Briefly, the near-full-length GII.10 P domain (residues 224 to 538) was cloned in a modified pMal-c2x expression vector and transformed into BL21 cells. Transformed cells were grown in LB medium (supplemented with 100 μg/ml ampicillin) for 4 h at 37°C. Expression was induced with 0.7 mM IPTG at an OD_{600} = 0.7 for 18 h at 22°C. Cells were harvested by centrifugation and disrupted by sonication on ice. A His-tagged fusion-P domain protein was purified from a Ni-NTA column (Qiagen) and digested with HRV-3C protease (Novagen) overnight at 4°C. The cleaved P-domain was separated on the Ni-NTA column and dialyzed in gel filtration buffer (GFB: 25 mM Tris-HCl pH 7.6 and 300 mM NaCl) overnight at 4°C. The P domain was further purified by size exclusion chromatography, concentrated to 2 mg/ml in GFB and stored at 4°C. Crystals of the P domain were obtained by the hanging-drop vapor diffusion method in a mother solution containing 0.2 M sodium nitrate, 0.1 M bis-tris propane (pH7.5), 20% (w/v) PEG3350. Crystals were grown in a 1:1 mixture of the protein sample and mother liquor at 18°C for 2 days. A single crystal was then soaked briefly with multivalent fucose-macromolecule in a cryoprotectant containing the mother liquor with 30% ethylene glycol and was flash frozen before data collection. X-ray diffraction data were collected at the European Synchrotron Radiation Facility, France at beamline ID23-1 and ID29 and processed with XDS.[12] The structure was solved using molecular replacement in PHASER[13] using the previously solved norovirus P domain (3ONU) as a search model. The structure was refined in multiple rounds of manual model building in COOT[14] with subsequent refinement with PHENIX[15]. The structure was validated with COOT and Molprobity.[16] Figures were generated using PyMOL. Atomic coordinates and structure factors have been deposited in the Protein Data Bank (PDB) with the accession code of 6GY9.

Table S1. Data collection and refinement statistics of human norovirus GII.10 P domain complex structure.

	GII.10 and Glycomacromolecule 6 (PDB ID: 6GY9)
Data collection	
Space group	$P2_1$
Cell dimensions	
a, *b*, *c* (Å)	66.28 80.37 71.51
α, β, γ (°)	90 101.66 90
Resolution range (Å)	35.02-1.83 (1.89-1.83)*
R_{merge}	4.11 (51.86)*
$I/\sigma I$	15.92 (2.03)*
Completeness (%)	93.55 (92.57)*
Redundancy	2.7 (2.7)*
Refinement	
Resolution range (Å)	34.17-1.83 (1.89-1.83)*
No. of reflections	60919
R_{work}/R_{free}	20.04/23.23
No. of atoms	4981
Protein	4654
Ligand/ion	30
Water	297
Average *B* factors (Å^2)	
Protein	31.56
Ligand/ion	40.72
Water	32.59
RMSD	
Bond lengths (Å)	0.007
Bond angles (°)	1.160

Data set was collected from a single crystal.
*Values in parentheses are for highest-resolution shell.

6. Molecular dynamics simulations

Molecular Dynamics simulations were performed at a constant temperature of 310° and constant pressure of 1 bar using gromacs 4.5.5.[17] Each molecule was simulated for 100 ns after a 20 ns equilibration run. Electrostatics were calculated using the particle mesh Ewald method,[18] and water molecules were kept rigid with SETTLE.[19]

Interaction parameters for the building blocks of the macromolecules were obtained from the amber SB99 force field[20,21] for the backbone and the general amber force field[22] for the triazole linker and partial charges were derived using the R.E.D. tools scripts.[23] Structure optimization for the charge derivation was performed with Gaussian at the HF/6-31G* level of theory. The final set of charges for

each molecular fragment was obtained from an ensemble average of 50 structures generated from 20 ns MD trajectories. The fucose ligands were modeled using the GLYCAM06$^{TIP5P}_{OSMO,r14}$ force field,[24,25] and the system was solvated with TIP5P[26] water molecules to avoid excessive interactions between the fucose ligands.

7. Dynamic light scattering

Dynamic light scattering was conducted with a PSS Nicomp ZLS Z3000 equipped with a 500 mW laser and an avalanche photodetector at a scattering angle of 90°. The concentration of the glycomacromolecule samples were 10 mg/ml. Twofold dilution of the sample gave the same results and plots of decay rate versus the square of the scattering vector for different scattering angles were linear showing that the sample and setup were overall well-behaved. Autocorrelation functions were evaluated by single exponential fitting with cumulant. DLS polydispersities were on the order of 0.2-0.3 probably due to fluctuations of the chains. The error of the hydrodynamic radii given here is the standard deviation from at least three different measurements.

8. EPR measurements

Spin-labeled glycomacromolecule **10** stock solutions (10 mM) were prepared in D_2O and stored under N_2 gas at -20 °C until further use. For all EPR measurements, dilutions thereof were prepared in sodium phosphate buffered solution (75 mM sodium phosphate buffer, pH 7.3, 100 mM NaCl). The spin label concentration was determined by EPR spectroscopy using the reference free spin counting function of the EMXnano (Bruker Biospin).

For DEER experiments, samples containing spin-labeled ligand in the absence and presence of the P-dimer were prepared in partially deuterated sodium phosphate buffered solution (75 mM sodium phosphate buffer, pH 7.3, 100 mM NaCl). Concentration of P-dimer was 75 µM for all samples containing protein, while ligand was added at 300 µM and 75 µM concentration, resulting in samples with a molar ratio of P-dimer to ligand of 1:4 and 1:1, respectively. Pure ligand was measured at 90 µM concentration. As a cryoprotectant 20% (v/v) of deuterated glycerol were added to each sample. The

samples were transferred into quartz glass tubes (ER 221 TUB-Q-10; Bruker, I.D. 1 mm), shock-frozen in liquid nitrogen to trap the conformational ensemble and subsequently measured.

DEER experiments were performed using an ELEXSYS E580 spectrometer equipped with an EN5107D2 Q-band EPR probe head (both Bruker Biospin) and a 10 W solid state amplifier. A CF935 helium gas flow system (Oxford Instruments) was used for temperature control. Experiments were performed at T = 50 K. DEER experiments were performed using a dead-time free four-pulse sequence.[27] The echo amplitude was recorded as a function of the dipolar evolutions time t. The corresponding EPR spectrum was obtained by field-swept echo acquisition and the pump and observer pulses were positioned on the global maximum and close to the most intense local maximum (shifted by 50 MHz) of the spectrum, respectively. The pump pulse length was adjusted in order to obtain a flip angle of π resulting in pulse length between 22 and 28 ns. The pulse separation time τ_1 was 400 ns and the dipolar evolution time τ_2 was 5000 ns. Nuclear modulation artifacts were suppressed by variation of the interpulse delay τ_1 and averaging 8 traces with $\Delta\tau_1$ = 16 ns. An eight-step phase cycle was used. For a complete DEER experiment individual scans were recorded, subjected to phase correction individually, and subsequently summarized (Figure S53).

DEER data sets were analyzed using the DeerAnalysis 2016 software package for MATLAB.[28] Extraction of the dipolar evolution function was achieved by background correction with a 3-dimensional homogeneous background function (Figure S53). Modulation depth scaling was used to take different pump pulse lengths into account. Background-corrected data were analyzed by a worm-like chain model.[28] The DEER data in the absence of the Norovirus P-dimer can be well described by a worm-like chain model (contour length 3.8 nm, persistence length 2.0 nm, and standard deviation due to label flexibility 0.22 nm, Figures S54).

The DEER data upon background correction for the spin-labeled fucose- ligand in the absence and presence of the P-dimer (molar ratio P-dimer/Fucose- ligand 1:4 and 1:1) is shown in Figure S55 (raw data see Figure S53). No significant differences are observed for the data obtained in these three experiments suggesting that the conformational ensemble of the fucose-ligand remains unaltered in the presence of the P-dimer.

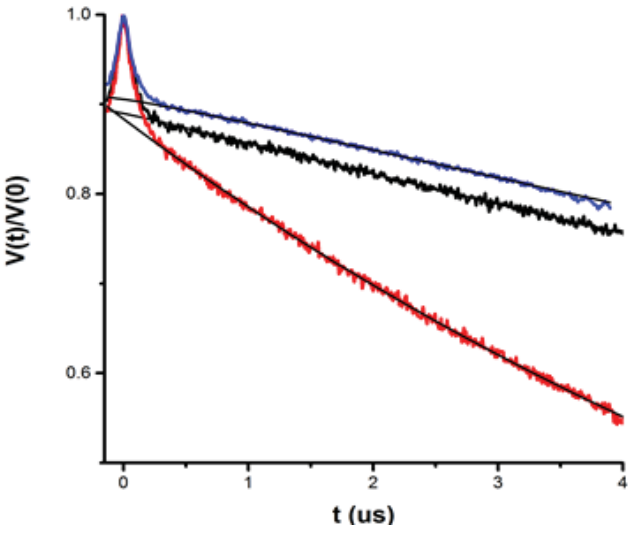

Figure S53: DEER raw data of the doubly spin-labelled ligand **10** in the absence (blue) and in the presence of P-dimer (molar ratio P-dimer/ligand 1:4 (red) and 1:1 (black)) and corresponding background-functions (thin solid lines).

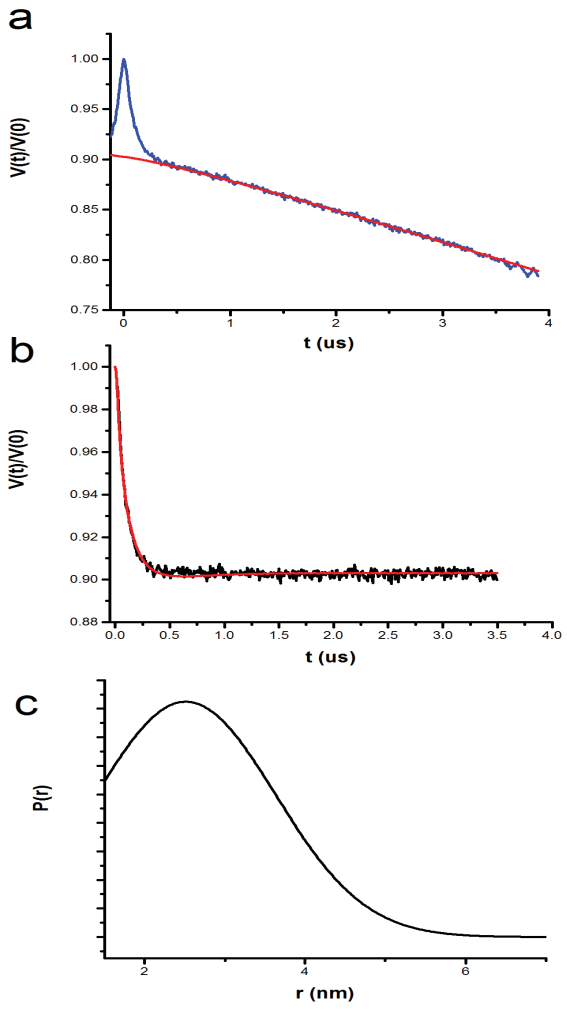

Figure S54: DEER distance measurements of the doubly spin-labeled ligand **10** in the absence of the P-dimer: a) experimental EPR raw data (blue) and background fit (red); b) corresponding form factor after background correction (black) and fit with a worm-like chain model (red); c) corresponding distance distribution (worm-like chain model).

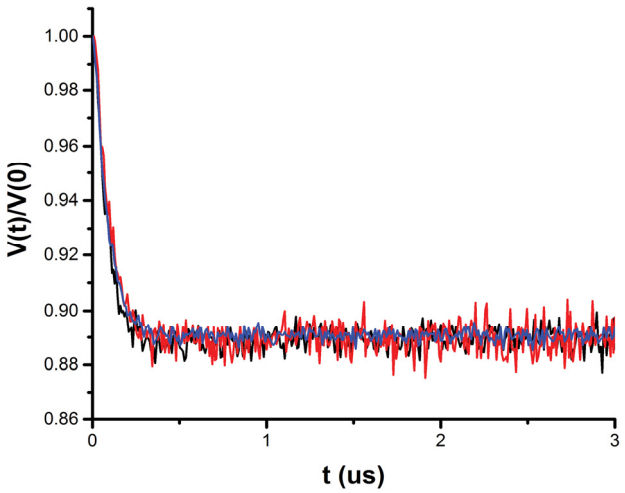

Figure S55: DEER distance measurements of the doubly spin-labeled ligand **10**. Experimental EPR data in the absence (blue) and in the presence (molar ratio P-dimer/Fucose- ligand 1:4 (red) and 1:1 (black)).

9. References

(1) Roux, S.; Zékri, E.; Rousseau, B.; Paternostre, M.; Cintrat, J.-C.; Fay, N. Elimination and exchange of trifluoroacetate counter-ion from cationic peptides: A critical evaluation of different approaches. *J. Peptide Sci.* **2008**, *14*, 354–359.

(2) Ponader, D.; Wojcik, F.; Beceren-Braun, F.; Dernedde, J.; Hartmann, L. Sequence-Defined Glycopolymer Segments Presenting Mannose: Synthesis and Lectin Binding Affinity. *Biomacromolecules* **2012**, *13*, 1845–1852.

(3) Ponader, D.; Maffre, P.; Aretz, J.; Pussak, D.; Ninnemann, N. M.; Schmidt, S.; Seeberger, P. H.; Rademacher, C.; Nienhaus, G. U.; Hartmann, L. Carbohydrate-Lectin Recognition of Sequence-Defined Heteromultivalent Glycooligomers. *J. Am. Chem. Soc.* **2014**, *136*, 2008–2016.

(4) Roy, B.; Mukhopadhyay, B. Sulfuric acid immobilized on silica: An excellent catalyst for Fischer type glycosylation. *Tetrahedron Lett.* **2007**, *48*, 3783–3787.

(5) Sun, J.; Kitova, E. N.; Wang, W.; Klassen, J. S. Method for Distinguishing Specific from Nonspecific Protein−Ligand Complexes in Nanoelectrospray Ionization Mass Spectrometry. *Anal. Chem.* **2006**, *78*, 3010–3018.

(6) Han, L.; Kitov, P. I.; Kitova, E. N.; Tan, M.; Wang, L.; Xia, M.; Jiang, X.; Klassen, J. S. Affinities of recombinant norovirus P dimers for human blood group antigens. *Glycobiology* **2012**, *23*, 276–285.

(7) Mallagaray, A.; Lockhauserbäumer, J.; Hansman, G.; Uetrecht, C.; Peters, T. Attachment of Norovirus to Histo Blood Group Antigens: A Cooperative Multistep Process. *Angew. Chem.* **2015**, *127*, 12182–12187.

(8) Tahallah, N.; Pinkse, M.; Maier, C. S.; Heck, A. J. R.; Loo, J. A. The effect of the source pressure on the abundance of ions of noncovalent protein assemblies in an electrospray ionization orthogonal time-of-flight instrument. *Rapid Commun. Mass Spectrom.* **2001**, *15*, 596–601.

(9) Leney, A. C. ; Heck, A. J., Native mass spectrometry: what is in the name?, J. Am. Soc. Mass Spectrom. 2017, 28(1), 5-13.

(10) F, Vranken, Wim; Wayne, B.; J. Stevens, T.; H, Fogh, Rasmus; Anne, P.; Miguel, L.; L. Ulrich, E.; L. Markley, J.; John, I.; D. Laue, E. The CCPN data model for NMR spectroscopy: Development of a software pipeline. *Proteins* **2005**, *59*, 687–696.

(11) Hansman, G. S.; Biertümpfel, C.; Georgiev, I.; McLellan, J.S.; Chen, L.; Zhou, T.; Katayama, K.; Kwong, P.D. Crystal Structures of GII.10 and GII.12 Norovirus Protruding Domains in Complex with Histo-Blood Group Antigens Reveal Details for a Potential Site of Vulnerability. J. Virol. 2011, 85(13), 6687-6701.

(12) Kabsch, W. Automatic processing of rotation diffraction data from crystals of initially unknown symmetry and cell constants. *J. Appl. Crystallogr.* **1993**, *26*, 795–800.

(13) McCoy, A. J.; Grosse-Kunstleve, R. W.; Adams, P. D.; Winn, M. D.; Storoni, L. C.; Read, R. J. Phaser crystallographic software. *J. Appl. Crystallogr.* **2007**, *40*, 658–674.

(14) Emsley, P.; Lohkamp, B.; Scott, W. G.; Cowtan, K. Features and development of Coot. *Acta Crystallogr D* **2010**, *66*, 486–501.

(15) Adams, P. D.; Afonine, P. V.; Bunkóczi, G.; Chen, V. B.; Davis, I. W.; Echols, N.; Headd, J. J.; Hung, L.-W.; Kapral, G. J.; Grosse-Kunstleve, R. W. *et al.* PHENIX: A comprehensive Python-based system for macromolecular structure solution. *Acta Crystallogr D* **2009**, *66*, 213–221.

(16) Chen, V. B.; Arendall, W. B.; Headd, J. J.; Keedy, D. A.; Immormino, R. M.; Kapral, G. J.; Murray, L. W.; Richardson, J. S.; Richardson, D. C. MolProbity: All-atom structure validation for macromolecular crystallography. *Acta Crystallogr D* **2009**, *66*, 12–21.

(17) van der Spoel, D.; Lindahl, E.; Hess, B.; Groenhof, G.; Mark, A. E.; Berendsen, H. J. C. GROMACS: Fast, flexible, and free. *J. Comput. Chem.* **2005**, *26*, 1701–1718.

(18) Darden, T.; York, D.; Pedersen, L. Particle mesh Ewald: An N·log(N) method for Ewald sums in large systems. *J. Chem. Phys.* **1993**, *98*, 10089–10092.

(19) Miyamoto, S.; Kollman, P. A. Settle: An analytical version of the SHAKE and RATTLE algorithm for rigid water models. *J. Comput. Chem.* **1992**, *13*, 952–962.

(20) Hornak, V.; Abel, R.; Okur, A.; Strockbine, B.; Roitberg, A.; Simmerling, C. Comparison of multiple AMBER force fields and development of improved protein backbone parameters. *Proteins* **2006**, *65*, 712–725.

(21) Wang, J.; Cieplak, P.; Kollman, P. A. How well does a restrained electrostatic potential (RESP) model perform in calculating conformational energies of organic and biological molecules? *J. Comput. Chem.* **2000**, *21*, 1049–1074.

(22) Wang, J.; Wolf, R. M.; Caldwell, J. W.; Kollman, P. A.; Case, D. A. Development and testing of a general amber force field. *J. Comput. Chem.* **2004**, *25*, 1157–1174.

(23) Dupradeau, F.-Y.; Pigache, A.; Zaffran, T.; Savineau, C.; Lelong, R.; Grivel, N.; Lelong, D.; Rosanski, W.; Cieplak, P. The R.E.D. tools: Advances in RESP and ESP charge derivation and force field library building. *Phys. Chem. Chem. Phys.* **2010**, *12*, 7821–7839.

(24) Kirschner, K. N.; Yongye, A. B.; Tschampel, S. M.; Gonzalez-Outeirino, J.; Daniels, C. R.; Foley, B. L.; Woods, R. GLYCAM06: A Generalizable Biomolecular Force Field. Carbohydrates. *J. Comput. Chem.* **2008**, *29*, 622–655.

(25) Sauter, J.; Grafmüller, A. Predicting the Chemical Potential and Osmotic Pressure of Polysaccharide Solutions by Molecular Simulations. *J. Chem. Theory Comput.* **2016**, *12*, 4375–4384.

(26) Mahoney, M. W.; Jorgensen, W. L. A five-site model for liquid water and the reproduction of the density anomaly by rigid, nonpolarizable potential functions. *J. Chem. Phys.* **2000**, *112*, 8910–8922.

(27) Pannier, M.; Veit, S.; Godt, A.; Jeschke, G.; Spiess, H. W. Dead-time free measurement of dipole–dipole interactions between electron spins. *J. Magn. Reson.* **2011**, *213*, 316–325.

(28) Jeschke, G.; Chechik, V.; Ionita, P.; Godt, A.; Zimmermann, H.; Banham, J.; Timmel, C. R.; Hilger, D.; Jung, H. DeerAnalysis2006—a comprehensive software package for analyzing pulsed ELDOR data. *Appl. Magn. Reson.* **2006**, *30*, 473–498.

5.2 Monodisperse sequence-controlled α-L-fucosylated glycooligomers and their multivalent inhibitory effects on LecB

Katharina Susanne Bücher, Nikolina Babic, Tanja Freichel, Filip Kovacic, Laura Hartmann

Macromolecular Biosciences **2018**, *18* (12), 1800337 (1-8)

DOI: 10.1002/mabi.201800337
Received 4 September 2018
Published version of record online 8 November 2018
Published issue online 10 September 2018

https://doi.org/10.1002/mabi.201800337

Own Contribution (first author)

Synthesis of building blocks, synthesis of azidoethyl-2,3,4-tri-*O*-acetyl-α-L-fucopyranoside, synthesis of glycomacromolecules, characterization of all compounds by conducting HPLC-MS measurements and analyzing results of NMR, MALDI-TOF-MS and HR-ESI-MS, full characterization of carbohydrate derivatives, collaborative design of glycomacromolecules, collaborative development of a setup for surface plasmon resonance (SPR) measurements, performance and analysis of all SPR experiments, collaborative writing of manuscript.

Macromolecular Bioscience
www.mbs-journal.de

Monodisperse Sequence-Controlled α-L-Fucosylated Glycooligomers and Their Multivalent Inhibitory Effects on LecB

Katharina Susanne Bücher, Nikolina Babic, Tanja Freichel, Filip Kovacic, and Laura Hartmann**

The opportunistic bacterium *Pseudomonas aeruginosa*, often exhibiting multiresistance against conventional antibiotics, expresses the lectin LecB that is suspected to be an important factor during biofilm formation via interactions with cell-surface presented carbohydrate ligands such as the blood group antigens. Therefore, carbohydrate-based ligands interfering with LecB binding have the potential to lead to new anti-biofilm and anti-adhesion therapies. This study explores in vitro binding potencies of glycomimetic ligands containing up to six α-L-fucose ligands on a monodisperse, sequence-controlled oligoamide scaffold interacting with LecB. Surface plasmon resonance (SPR) and a modified enzyme-linked lectin assay (mELLA) revealed an increasing affinity to LecB with increasing fucose valency. Furthermore, fucosylated glycooligomers were shown to inhibit the formation of *P. aeruginosa* biofilm up to 20%. Overall these results show the potential of fucosylated oligoamides to be further developed as inhibitors of LecB binding and biofilm formation.

1. Introduction

Pseudomonas aeruginosa is a Gram-negative, rod-shaped bacterium with a high viability in even antibacterial environments. It can colonize almost all kinds of tissues and organs where it forms biofilms.[1] Biofilm-conditioned, decreased availability of the bacteria is one of the main factors in often-observed resistance against common antibiotics.[2] This becomes particularly problematic in immune-suppressed individuals, for example, suffering from AIDS, cancer, or cystic fibrosis. *P. aeruginosa* infections are symptomized by serious secondary acute and chronic pneumonia or otitis externa diffusa.[2,3] Therefore it is of great importance to understand the mechanisms leading to biofilm formation and develop compounds that are able to interfere with biofilm formation while being nontoxic for the patient. Two multivalent lectins of *P. aeruginosa* are believed to play key roles in the recognition and adhesion to human cells, biofilm formation as well as epithelial tissue damages. These are the galactose-specific LecA (PA-IL) and the fucose-specific LecB (PA-IIL).[1,4] In this work we study LecB, a 11.9 kDa calcium-dependent lectin forming homotetramers extracellularly. With four fucose binding sites at 40–50 Å distances, it is involved in the cross-linking of *P. aeruginosas'* own extracellular glycans or host surface exposed glycolipids and glycoproteins.[2] Due to the involvement of carbohydrate-lectin interactions in biofilm formation, the inhibition or blocking of the lectin has been investigated in a number of studies aiming to prevent or disrupt biofilm formation.[1,2,5–7] Considering natural monosaccharides as ligands, LecB has the highest affinity for L-fucose with a K_D of 2.9 μM, while mannose and fructose are weaker binding partners.[8,9] The effect of monosaccharides on LecB binding was for example shown by Hauber et al., where the amount of *P. aeruginosa* in sputum of infected cystic fibrosis patients was reduced after inhalation with a mixture of galactose and fucose.[10] LecB binding affinities could be improved by functionalizing L-fucose with methyl (MeFuc) or *p*-nitrophenyl groups.[7,9,11] As LecB also binds oligosaccharides, for example, blood group antigens A, B, H, Le^x and Le^a, the latter with highest affinity of 210 nM,[12] multivalent fucosylated glycoclusters,[13,14] –oligomers,[15] and –dendrimers[16–19] were designed for LecB inhibition. Synthetic multivalent dendrimers[16,18] and complex dendritic glycoclusters[17] with up to 16 fucose units showed up to 86 times higher binding potency per sugar unit in comparison to MeFuc. Similar to other multivalent glycomimetic structures, effects of the scaffold, for example, in terms of its architecture and distances between the ligands, were shown to have an effect on LecB binding.[14,15]

Recently, we have reported the synthesis of a novel class of multivalent glycomimetics based on monodisperse and sequence-controlled oligo(amidoamines) (see **Figure 1**). Through the step-wise assembly of tailor-made building blocks

K. S. Bücher, T. Freichel, Prof. L. Hartmann
Institute of Organic and Macromolecular Chemistry
Heinrich-Heine-University Duesseldorf
Universitaetsstraße 1, 40225 Duesseldorf, Germany
E-mail: laura.hartmann@hhu.de

N. Babic, Dr. F. Kovacic
Institute of Molecular Enzyme Technology
Heinrich-Heine-University Duesseldorf and
Forschungszentrum Jülich GmbH
Wilhelm Johnen Straße, 52428 Jülich, Germany
E-mail: f.kovacic@fz-juelich.de

The ORCID identification number(s) for the author(s) of this article can be found under https://doi.org/10.1002/mabi.201800337.

DOI: 10.1002/mabi.201800337

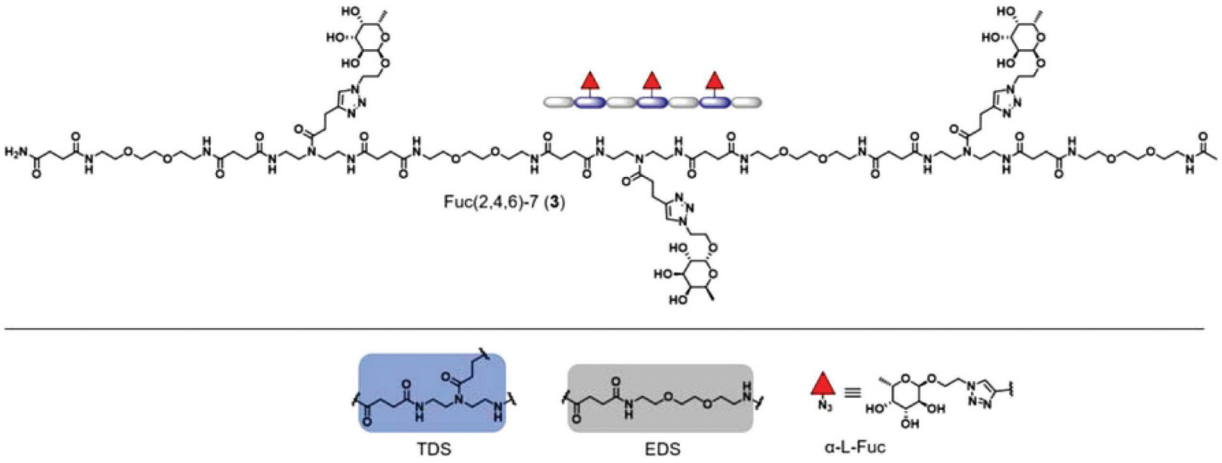

Figure 1. Structure and schematic representation of fucosylated glycooligomer Fuc(2,4,6)-7 (see Table 1, entry 3) and building block units.

on solid support, full control over the scaffold's composition as well as the presentation of carbohydrate ligands at defined positions along the scaffold is possible.[20] Thus an important advantage of such precision glycooligomers is their highly variable, yet controlled synthesis giving access to chemically defined glycomimetics of different valencies, different architectures, different ligand densities, going from lower to higher molecular weights or combining different carbohydrate ligands within one macromolecule.[21,22] Using this platform, we have previously demonstrated the synthesis of precision glycomacromolecules carrying fucose ligands varying in the number and spacing of ligands.[22] Here we now study such fucosylated glycooligomers (Figure 1) as ligands of LecB and explore their potential as inhibitors of biofilm formation.

2. Experimental Section

2.1. Synthesis of Fucosylated Glycooligomers

Building blocks TDS and EDS were synthesized following known procedures.[20] Fucosylated oligoamides were synthesized according to the previously established protocols via solid phase polymer synthesis (SPPoS) on a Tentagel S-RAM resin with a loading of 0.22–0.25 mmol g^{-1} (for detailed information, see Supporting Information).[20,23] In short, via alternating coupling and deprotection steps with EDS as spacer and TDS as functional building block, the targeted scaffold structures were build-up. The following attachment of azidated monosaccharides by solid supported copper click cycloaddition reaction (CuAAC) with a twofold excess of carbohydrate azide derivative per alkyne group applying previously published protocols gave the final glycooligomers.[20] 2-Azidoethyl-2,3,4-tri-*O*-acetyl-α-L-fucose was synthesized using a sulfuric acid catalyst for Fischer-glycosylation to gain pure α-functionalization.[24] 2-Azidoethyl-2,3,4,6-tetra-*O*-acetyl-D-galactose was used as α/β-mixture.[25] Glycooligomers were cleaved off the resin with a solution of 95% trifluoro acetic acid (TFA) and isolated by precipitation in diethyl ether. After decanting the ether, dissolving the product in water and lyophilization, all glycooligomers were purified by ion exchange resin and preparative HPLC (with a gradient of water/acetonitrile). Overall, seven fucose and one galactose functionalized glycooligomers were synthesized and characterized by means of ^{1}H-NMR, RP-HPLC/MS, MALDI-TOF-MS, and high resolution ESI-MS (see Supporting Information). Synthesis and analysis of glycooligomers **1** and **4** has been previously reported.[23]

2.2. Surface Plasmon Resonance

In SPR experiments, the inhibitory potential of glycooligomers **1**–**8** toward LecB were analyzed and compared to MeFuc during an inhibition competition assay on a highly fucosylated streptavidin (SA)-sensor chip. Measurements were performed in two experiments, investigating the binding of glycooligomers **1**–**5** and the galactosylated negative control **8** in the first experiment on two different sensor chips and applying glycooligomers **3**, **6**, and **7** on a freshly prepared third sensor chip.

Measurements were conducted on a Biacore X100 instrument from GE Healthcare Life Sciences in a two-flow cell system. Biacore X100 control software was used for recording and analysis was performed with Biacore X100 evaluation software. All buffers and water were filtered in vacuum through membrane filters with 0.2 µm pore size before usage on the instrument. To a sensor chip functionalized with streptavidin (SA-chip) biotinylated fucose-polyacrylamide (biotinylated Fuc-PAA, 4.2 µg mL^{-1} in HBS-P+ buffer, pH 7.4) as positive control (flow cell 2) and biotinylated galactose-polyacrylamide (biotinylated Gal-PAA, 4.2 µg mL^{-1} in HBS-P+ buffer, pH 7.4) as negative control (flow cell 1) were immobilized via biotin-streptavidin capturing method[26] with a contact time of 500 s and a flow rate of 5 µL min^{-1}. Sodium chloride, isopropanol, and sodium hydroxide were prepared as denoted from the manufacturer and HSB-P+ buffer was used as running buffer during the immobilization procedure. Immobilisation levels, expressed in response units (RU), reached for the first (1) and second (2) experiment were 1054.2 $RU^{(1)}$ and 1206.6 $RU^{(1)}$ and 1102.4 $RU^{(2)}$ for the fucosylated flow cells 2 and 1067.8 $RU^{(1)}$ and 1247.0 $RU^{(1)}$ and 1135.9 $RU^{(2)}$ for the galactosylated reference cells 1, respectively.

The measurements were carried out with tris(hydroxymethyl) aminomethane (TRIS) buffer (20 mM TRIS, 100 mM NaCl, 0.1 mM $CaCl_2$, pH 7.5) as running buffer. During the measurements the interaction of injected LecB to the fucosylated sensor chip was monitored as response units (RU) of the difference spectra (flow cell 2–flow cell 1). After preincubation of LecB with a dilution series of a specific ligand for 1 h the inhibitory effect of the ligand was observed by the decrease of LecB signal (RU) on the sensor chip correlated with increasing amount of ligand in the dilution series. Within one experiment the inhibition assay of each ligand was repeated in at least three independent measurements whereas repetitions of MeFuc were carried out at the beginning, in the middle and at the end of the whole experiment to ensure reproducibility.

For the inhibition competition assay, a series of eight to nine different concentrations of a specific ligand in TRIS buffer were produced in a 1:3-dilutions series starting with 3600 nM. 40 µL of each dilution was incubated with 40 µL of LecB in TRIS buffer (400 nM) to obtain final concentrations of 200 nM for LecB and 1800, 600, 200, 100 (additional dilution), 66.66, 22.22, 7.41, 2.47, and 0.82 nM for the ligands (dilution series of glycooligomers **4** and **5** 600 nM–0.27 nM). Dilutions of MeFuc differed because of lower affinities and led to final concentrations of 10.0 µM, 3.33 µM, 1.11 µM, 370 nM, 123 nM, 41 nM, 14 nM, 4.6 nM, and 1.5 nM. LecB and ligand were incubated for 1 h at room temperature and the series was measured subsequently by automated injection to both flow cells in a multi cycle measurement. One inhibition competition assay for a specific ligand included two startup cycles of running buffer as negative control, the series of incubated LecB with the desired ligand dilutions, one duplicate measurement of a LecB-ligand complex with a ligand concentration close to the IC_{50} value as internal standard of each series and additionally one cycle of LecB (200 nM) without inhibitor as positive control and one cycle of inhibitor (C_{max}) without LecB as negative control.

Each sample was injected with a flow rate of 20 µL min^{-1}, a contact time of 100 s and a dissociation phase of 60 s. Regeneration of the sensor chip by washing off the protein–oligomer complex was not successful (see Supporting Information). Hence, after sample injection, a solution of 1 M NaCl and 0.05% sodium dodecyl sulfate (SDS) in water was injected two times at a flow rate of 30 µL min^{-1} in order to denature LecB still attached to the sensor chip surface. The first denaturation phase took 60 s and the second denaturation was conducted with a contact time of 30 s. Every measurement cycle was completed by washing with running buffer with a contact time of 120 s and a flow rate of 10 µL min^{-1}.

As binding signal of each cycle the report point was set to 165 s after cycle start at the end of the association phase whereas the baseline before injection was adjusted to 0 RU. The relative response unit at this report point obtained from the 200 nM LecB solution in TRIS buffer without inhibitor was set to 100% binding. The binding signals gained from LecB incubated with the dilutions of the corresponding ligand were referred to LecB and calculated for relative binding in %. Half maximum inhibitory concentration (IC_{50}) values were calculated as concentration of the ligand resulting in 50% inhibition of LecB binding to the fucosylated sensor chip surface by reciprocal binding curves. Calculations were carried out with OriginPro 9.0G. Representative inhibition curves were set to 0% inhibition for binding of LecB (without inhibitor) whereas the concentration of inhibitor was set to 0.01 nM to realize the presentation of the value at the logarithmic scale. Maximal inhibition by glycooligomers was extrapolated to 10 µM (100%). The signal of LecB/inhibitor mixture with lowest inhibitor concentration was set to 100% inhibition. The relative inhibitory potencies (RIP) of the ligands were calculated by correlating their IC_{50} values with the IC_{50} value of MeFuc measured on the same sensor chip (IC_{50} (α-MeFuc)/IC_{50} (ligand)).

2.3. Modified Enzyme-Linked Lectin Assay

As second binding assay, the enzyme-linked lectin assay (ELLA) modified according Schwarbroch (2017) was used.[27] In short, hydrophobic nunc-immuno maxi-sorp plates (Thermo Fisher Scientific, Darmstadt) were coated with α-L-fucose-polyacrylamid-biotin (FPA) conjugate (100 µL, 5 µg mL^{-1}) (GlycoTech, Canada) dissolved in sodium phosphate buffer (0.3 M, pH 7.4) by agitating the plates (150 rpm) for 1 h at 37 °C. FPA solution was discarded and the plates were agitated (150 rpm) for 1 h at 37 °C with blocking buffer (100 µL, 137 mM NaCl, 1.4 mM KH_2PO_4, 8.1 mM Na_2HPO_4, 2.7 mM KCl, 0.2% (v/v) Tween 20, bovine serum albumin (BSA) 3% (w/v), pH 7.4) containing BSA to saturate unbound sites in order to prevent unspecific LecB binding. BSA solution was discard and the inhibitor (50 µL) dissolved in sodium phosphate buffer (0.3 M, pH 7.4) was added in a 2×10^{-7}–9 mM concentration range. Subsequently, *P. aeruginosa* lectin LecB (50 µl, 15 ng mL^{-1}, Elicityl OligoTech) dissolved in Tris/HCl buffer (100 mM, 0.1 mM $CaCl_2$, pH 8) was added and the plates were agitated (150 rpm) for 1 h at 37 °C. The liquid was discarded and the excess of unbound LecB was removed by agitating (150 rpm) the plate for 20 min at 37 °C with blocking buffer. Washing step was repeated three times and bound LecB was detected by agitating (150 rpm) the plate overnight at 4 °C with anti-LecB antiserum (100 µL) diluted 5000 fold with blocking buffer. The excess of unbounded antibody was removed by agitating (150 rpm) the plate in three cycles of 20 min at 37 °C with the blocking buffer followed by the incubation with secondary goat anti-rabbit IgG antibodies couplet to horseradish peroxidase (100 µL, Bio-Rad, Munich) according manufacturer's recommendations. The excess of unbounded antibody was removed by agitating (150 rpm) the plate in three cycles of 20 min at 37 °C with the blocking buffer. Peroxidase substrate (100 µL, hydrogen peroxide 0.0095% (v/v), luminol 1.28 mM, Tris/HCl 0.1 mM, pH 8.6, *p*-hydroxycoumaric acid 0.1 g L^{-1}, dimethyl sulfoxide 9.1% (v/v)) was added and the chemoluminescence was measured using a microtiter plate reader (Infinite M1000 Pro, Tecan trading AG, Switzerland). The percentage of inhibition was calculated according to Equation (1) and IC_{50} values were calculated using logistic fit of sigmoidal curves. All results are mean ± standard deviation of three independent experiments each measured three times.

$$\left[\frac{\left(A_{\text{without inhibitor}} - A_{\text{with inhibitor}}\right)}{A_{\text{without inhibitor}}}\right] \times 100 \quad (1)$$

2.4. Biofilm Assay

The *P. aeruginosa* PA01[28] overnight culture was diluted with LB medium to an OD_{580nm} = 1.4 and aliquots of 48 µL were incubated with 2 µL of each oligomer solution (50 mM) in sterile water using 96-well microtiter plate for 21 h at 37 °C. After discarding the culture, the plate was washed two times with distilled water and air-dried. The bounded cells were stained with 80 µL of 1% crystal violet (w/v) for 15 min at room temperature. After removing unbounded crystal violet, the plate was washed with distilled water and air-dried. Cell-bounded crystal violet was dissolved in 100 µL of 30% acetic acid (v/v) by agitating for 30 min at 300 rpm and room temperature. Finally, aliquots of 80 µL were transferred to the new microtiter plate and absorbance was measured at wavelength of 550 nm. Negative control contained 48 µL of LB medium and 2 µL of sterile water. Positive control containing 48 µL of *P. aeruginosa* PA01 culture and 2 µL of sterile water was taken as 100%. The issue of unequal evaporation from the plate during incubation, so-called "edge effect," was minimized as described previously.[29]

3. Results and Discussion

3.1. Synthesis of Fucosylated Glycooligomers

In total, seven sequence-controlled L-fucose-functionalized oligoamides (**1–7**) as well as a galactose-functionalized oligoamide (**8**) were synthesized according to previously presented protocols (**Table 1**).[20] In short, two tailor-made building blocks, EDS and TDS, were iteratively coupled on solid support using standard Fmoc-coupling protocols. EDS is used as so-called spacer building block introducing a diethylene glycol unit in the backbone of the oligomer while TDS is used as functional building block introducing an alkyne side chain allowing for CuAAC of azido-functionalized carbohydrate ligands (Figure 1). Through the sequence of building blocks during assembly, the positions of alkyne moieties and thereby the carbohydrate ligands along the scaffold are controlled. This sequence is also represented in the nomenclature of such glycooligomers where first the kind of carbohydrate ligand is given (e.g., Fuc), followed by the position of ligands along the scaffold (e.g., 1,3,5) followed by the overall number of building blocks in the scaffold (e.g., 5) (see also Figure 1). After successful assembly of the scaffold, fucose or galactose ligands were introduced via established CuAAC protocols and glycooligomers were isolated after cleavage from the solid support. All glycooligomers were further purified by ion exchange and reversed phase semi-preparative RP-HPLC in order to obtain the final products in high purity (see Table 1 and Supporting Information).

Fucosylated glycooligomers in this series vary in valency (oligomers **1–5**) with one up to six fucose ligands per oligomer. Additionally, three trivalent structures (**3**, **6**, and **7**) were synthesized containing one, two, or three EDS spacer building blocks between the fucose units, respectively. It should be noted that the fucosylated glycooligomers in solution most likely adapt a coiled conformation as was previously shown, for example, by dynamic light scattering experiments.[23] The hydrodynamic volume of such coiled structures would be expected to also depend on the overall length of the scaffold. Therefore, in order to keep this parameter relatively constant, all glycooligomers are about seven building blocks long. The exceptions are hexavalent oligomer **5** with no EDS spacing and a total of 6 building blocks and trivalent oligomer **7** with three EDS spacer units and thus a total of nine building blocks. As negative control, glycooligomer **8** was constructed in analogy to divalent structure **2** using galactose as ligand known to bind weak to LecB.

Table 1. Analytical data of glycooligomers **1–8**.

Entry	Schematic structures	MW [g mol^{-1}]	n[a] Fucose [Galactose]	Retention time[b] [min]	Yield [%][c]	Relative purity [%][b]
1	 Fuc(4)-7	1938.0	1	12.3	55	98
2	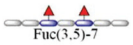 Fuc(3,5)-7	2206.2	2	12.1	38	98
3	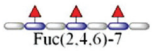 Fuc(2,4,6)-7	2474.3	3	11.8	47	99
4	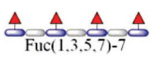 Fuc(1,3,5,7)-7	2742.4	4	11.6	28	97
5	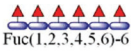 Fuc(1,2,3,4,5,6)-6	3048.5	6	10.9	48	99
6	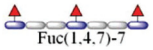 Fuc(1,4,7)-7	2474.3	3	11.9	30	98
7	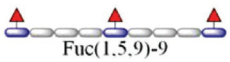 Fuc(1,5,9)-9	2934.5	3	12.5	80	99
8	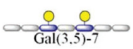 Gal(3,5)-7	2238.2	0 (2)	11.5, 11.7	57	99

[a]Number of fucose units on the scaffold; [b]As determined by integration of the UV signal at 214 nm in reversed phase HPLC (gradient water/acetonitrile (95/5) to water/acetonitrile (1:1) in 30 min) after purification with ion exchange resin and RP semi-preparative HPLC; [c]Isolated yield after purification with ion exchange resin and RP semi-preparative HPLC.

3.2. Competition Studies of Fucosylated Glycooligomers toward LecB with SPR

To investigate the inhibitory effects of precision glycooligomers **1–8** on LecB, SPR experiments were performed applying a competition assay. Therefore, a sensor chip was functionalized with commercially available polydisperse fucosylated polyamide. Glycooligomers as well as MeFuc as reference inhibitor were incubated with LecB and subsequently injected onto the SPR chip to test binding of LecB to the fucosylated chip surface. Depending on the affinity of the inhibitor to LecB, more or less LecB is blocked through binding to the glycooligomer and will not bind to the chip surface. In order to determine half maximum inhibitory concentrations, all glycooligomers and MeFuc were applied in series of different concentrations. As negative control,

a galactose-functionalized polyamide (Gal-PAA) was immobilized on a reference cell on the chip and galactose-functionalized oligomer (**8**) was tested as inhibitor in the assay. Within the competition assay, the main challenge was the regeneration of the SPR chip after each measurement due to the pronounced interaction of LecB with the highly fucosylated chip surface. However, we were able to show that via multicycle test measurements with several subsequent injections and denaturation steps using SDS and sodium chloride, reproducible IC_{50} values are derived (see Supporting Information). Reproducibility was further monitored by a duplicate measurement with a ligand concentration close to the IC_{50} value at the end of each assay. All oligomers were measured in three independent assays. Additionally, MeFuc was measured at the beginning, in the middle, and at the end of every series of experiments, again confirming reproducibility.

Following this procedure, all glycooligomers were tested for their inhibitory potential against LecB giving the according IC_{50} values (see **Figure 2**). No binding of LecB and fucosylated glycooligomers on the reference cell functionalized with Gal-PAA was observed. Similarly, galactose functionalized oligomer **8** showed only low influence on the binding of LecB to the cell functionalized with Fuc-PAA (see Supporting Information).

Figure 2B,D comprises the results of the SPR measurements also giving the relative inhibitory potential (RIP) as the obtained IC_{50} values (see Supporting Information) normalized to the IC_{50} value of MeFuc and the RIP divided by the number of fucose ligands per oligomer (RIP/n). In agreement with previous results we observe that already the monovalent glycooligomer **1** shows an increased inhibitory potential in comparison to MeFuc.[20] When looking at the higher valent structures, in general higher valency leads to an increase in the inhibitory potential indicating higher affinity. Thus hexavalent glycooligomer **5** exhibits the best inhibitory potential in this study with a 17 times better binding (IC_{50} = 22 nM) in comparison to MeFuc (IC_{50} = 381 nM). These results display a good binding enhancement comparable to other similar fucosylated oligomers in literature, for example fucosylated phosphodiesters from the group of Vidal with an enhancement in binding of 14 for a hexavalent structure in comparison to L-fucose that itself binds about seven times less than MeFuc.[15] Looking at the RIP normalized to the number of fucose ligands, we see that for all glycooligomers the inhibitory potential per carbohydrate moiety is similar. This indicates that the increase in binding is most likely related to statistical effects where more fucose ligands attached to the oligomer lead to an increased probability of binding to the receptor. This is again in agreement with previous observations from other groups investigating the binding of linear fucosylated oligomers toward LecB.[14,15]

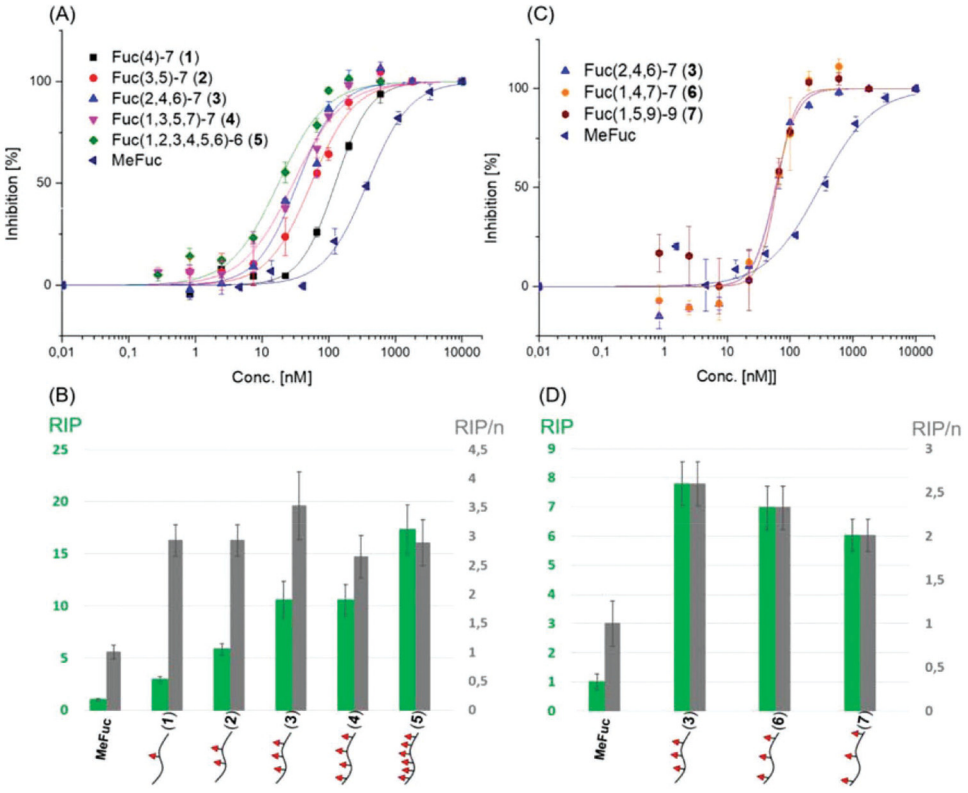

Figure 2. Inhibition of LecB binding measured by SPR with LecB (200 nM) and glycooligomers **1**–**5** with different fucose valency (A, B) and trivalent glycooligomers **3**, **6**, and **7** with different spacing between the fucose side chains (C, D): IC_{50} curves (A, C), maximal inhibition by glycooligomers was extrapolated to 10 μM (100%); relative binding potencies (RIP) (green) and binding potencies per fucose unit (RIP/n) (grey) (B, D), schematic structures are depicted underneath diagrams. Values were expressed relative to MeFuc (RIP = 1). Errors are standard errors of the mean (SEM) of three independent measurements. MeFuc served as reference in both experiments.

3.3. Binding Studies with Modified Enzyme-Linked Lectin Assay

All fucosylated glycooligomers **1–7** and the negative control **8** were further investigated for their binding affinity toward LecB in an inhibition competition assay by a modified form of ELLA, a version of the enzyme-linked immunosorbent assay[30] that allows quantification of the lectin LecB using an anti-LecB antiserum.[31] The competitive inhibition of LecB binding to a highly fucosylated solid surface was assayed by introducing a specific fucosylated oligomer simultaneously to the plate. To determine LecB concentration suitable for the inhibition assays the mELLA was performed in the absence of an inhibitor with the protein in concentration range 0.13–1000 ng mL^{-1}, and luminescence, which is proportional to the amount of LecB, was measured (Figure S41, Supporting Information). From the obtained saturation curve, we determined a linear relationship of the signal intensity with the LecB up to 19 ng mL^{-1}. Therefore, using 15 ng mL^{-1} LecB in inhibition experiments allowed sensitive determination of free LecB (LecB not in the complex with the inhibitor). To exclude interference of the inhibitors with mELLA assay, biotinylated Fuc-PAA coated surface was incubated (1 h, 37 °C) with glycooligomers **2** and **7** (1.2 and 33 μM) followed by washing and incubation with LecB (Figure S42, Supporting Information). Very similar chemoluminescence intensities detected with mELLA indicate that glycooligomer inhibitors do not disrupt fucosylated surface of the plate. Under these conditions, all glycooligomers were tested for competitive inhibition of LecB binding giving the respective IC_{50} values (Figures S43, S45–S52, and Table S2, Supporting Information). Galactose-functionalized glycooligomer (**8**) could not bind LecB (Figure S44, Supporting Information) which is in agreement with low affinity of LecB for galactose.[6]

Figure 3 shows relative inhibitory potencies (RIP) and RIP per fucose side chain (RIP/n) derived from IC_{50} values from mELLA (Table S2, Supporting Information). In agreement with results from the SPR assay, we observe that the inhibitory potencies of glycooligomers increase with the number of fucose moieties. However, while for the SPR experiments a continues increase in RIP with increasing number of fucose ligands was observed, in the mELLA RIP of glycooligomers with 1 and 2 fucose moieties is at the level of MeFuc while inhibition is strongly enhanced for glycooligomers with 3 or more fucose moieties (RIP > 18), with the highest RIP = 31 for tetravalent structure **4** ($n = 4$). Interestingly, differences in RIP ranging from 5 to 24 for the trivalent glycooligomers, structures **3**, **6**, and **7** with different spacing between fucose moieties was observed. In SPR experiments, only minor effects of ligand spacing were observed. It should be noted that in the SPR experiment inhibitors and LecB were preincubated in solution providing the chance to reach an equilibrium prior binding to fucosylated surface of the chip. In the mELLA assay, the inhibitor was added to the fucosylated surface followed by addition of LecB to achieve the competition between two binding partners. While the latter setup could be expected to be more sensitive against the availability of fucose side chains and the kinetics within the binding process, it also mimics the situation that might occur during in vivo inhibition of biofilm formation. Here biotic surfaces presenting fucose ligands would compete for binding to LecB with the potential inhibitors, such as our glycooligomers. Overall, results from mELLA suggest that the structure of glycooligomers, especially the arrangement of fucose units on the scaffold, play an important role for LecB inhibition. Thus, these molecules offer an interesting blueprint for further design of multivalent polymer-based LecB inhibitors.

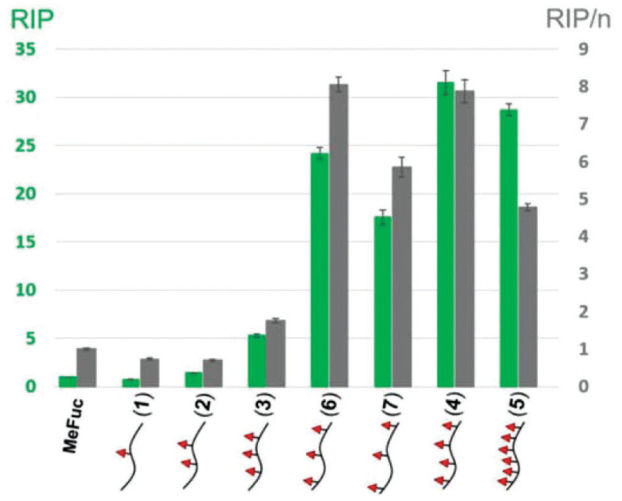

Figure 3. Inhibition of LecB binding measured with mELLA. A) Relative binding potencies (RIP) and B) binding potencies per fucose unit (RIP/n) of glycooligomers **1–7,** schematic structures are depicted underneath diagram. All values were expressed relative to MeFuc (RIP = 1). Errors are standard errors of the mean (SEM) of nine independent measurements.

3.4. Biofilm Formation Assay

All glycooligomers were tested for their ability to inhibit formation of *P. aeruginosa* PA01 biofilm in vivo. LecB is considered an essential protein for the formation of biofilm as was shown by a *P. aeruginosa* strain with the *LecB* gene deleted[31] and to be possibly involved in linking extracellular polysaccharides forming the biofilm matrix.[2,31] Therefore, inhibitors bound to LecB as seen in the previous binding studies of the glycooligomers might prevent efficient assembly of biofilm. To test this effect, staining *P. aeruginosa* PA01 cells attached to the plastic surface of microtiter plate in presence of 2 mM glycooligomer inhibitors **1–7** was performed showing reduction of biofilm amount (15–20%) for all fucosylated glycooligomers as shown in **Figure 4**. The galactose-functionalized glycooligomer as negative control did not influence biofilm formation. The effect of MeFuc as reference was much weaker (7% inhibition) in comparison to the fucosylated glycooligomers. However, we did not observe a correlation of the number or spacing of fucose ligands and the resulting effect on biofilm formation. It is clear that biofilm formation and inhibition is a complex process depending on multiple virulence factors and might not only depend on the inhibition of LecB. This is in agreement with other studies of *Pseudomonas* lectin inhibitors, for example, complex glycopeptide dendrimers (IC_{50} = 0.14 μM by ELLA)[16] and mannose-centered galactoclusters (IC_{50} = 10 μM by ELLA)[32] that inhibited biofilm formation for 40–55% at IC_{50} concentrations.

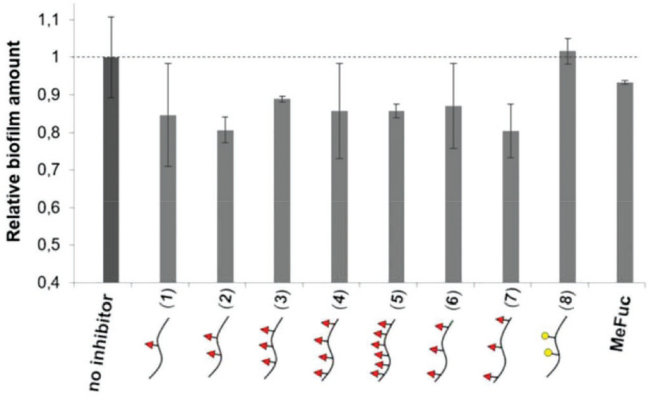

Figure 4. Biofilm formation assay with *P. aeruginosa* incubated with glycoamidoamine inhibitors. Inhibitory effect of glycooligomers **1**–**7** (2 mM) on formation of *P. aeruginosa* PA01 biofilm in a microtiterplate after 21 h incubation. Attached biofilm was quantified with crystal violet. The mean ± standard errors of three independent experiments are normalized to cultures grown without an inhibitor.

Therefore, in order to understand the mechanism of biofilm inhibition using fucoslyated glycooligomers and designing even more potent inhibitors based on the precision oligoamide scaffolds, further studies are required. Nevertheless, this first generation of glycooligomers shows the potential to further develop such multivalent LecB inhibitors and investigate both, their lectin binding behavior and effect in biofilm inhibition.

4. Conclusions

A series of fucosylated glycooligomers was successfully tested for their potential to act as inhibitors in LecB binding. SPR results show enhanced inhibitory potential against LecB with increasing valency of the glycooligomers while mELLA results also indicate an influence of the spacing of ligands along the oligomeric backbone. Reduction of biofilm formation by *P. aeruginosa* PA01 in presence of the glycooligomers shows the potential of such glycooligomers for the further development toward novel antivirulence drugs. Ongoing studies are concerned with the more detailed structural analysis of ligand–receptor complex binding and the further improvement of inhibitory potential by using glycooligomers as building blocks to assemble even higher valent ligands, for example, by attachment of glycooligomers onto nanoparticles[33] or polymerization of glycooligomer-based macromonomers.[22]

Supporting Information

Supporting Information is available from the Wiley Online Library or from the author.

Acknowledgement

L. H. acknowledges support from the Boehringer Ingelheim Foundation through the Plus3 program. N. B. thanks the Jürgen Manchot Stiftung for funding. The authors thank Prof. Karl-Erich Jaeger from the Institute of Molecular Enzyme Technology (Heinrich Heine University Duesseldorf) for valuable discussions.

Conflict of Interest

The authors declare no conflict of interest.

Keywords

fucose, glycomacromolecules, LecB, multivalent inhibitor, solid phase synthesis

Received: September 4, 2018
Revised: October 4, 2018
Published online: November 8, 2018

[1] C. Chemani, A. Imberty, S. de Bentzmann, M. Pierre, M. Wimmerová, B. P. Guery, K. Faure, *Infect. Immun.* **2009**, *77*, 2065.
[2] A. V. Grishin, M. S. Krivozubov, A. S. Karyagina, A. L. Gintsburg, *Acta Naturae* **2015**, *7*, 29.
[3] J. Sundström, K. Jacobson, E. Munck-Wikland, S. Ringertz, *Archives of Otolaryngology - Head and Neck Surgery* **1996**, *122*, 833.
[4] a) D. Avichezer, N. Gilboa-Garber, *FEBS Lett.* **1987**, *216*, 62; b) R. J. Pieters, *Org. Biomol. Chem.* **2009**, *7*, 2013.
[5] a) R. Sommer, S. Wagner, K. Rox, A. Varrot, D. Hauck, E.-C. Wamhoff, J. Schreiber, T. Ryckmans, T. Brunner, C. Rademacher, R. W. Hartmann, M. Brönstrup, A. Imberty, A. Titz, *J. Am. Chem. Soc.* **2018**, *140*, 2537; b) S. Cecioni, A. Imberty, S. Vidal, *Chem. Rev.* **2015**, *115*, 525.
[6] A. Bernardi, J. Jimenez-Barbero, A. Casnati, C. de Castro, T. Darbre, F. Fieschi, J. Finne, H. Funken, K.-E. Jaeger, M. Lahmann, T. K. Lindhorst, M. Marradi, P. Messner, A. Molinaro, P. V. Murphy, C. Nativi, S. Oscarson, S. Penadés, F. Peri, R. J. Pieters, O. Renaudet, J. L. Reymond, B. Richichi, J. Rojo, F. Sansone, C. Schäffer, W. B. Turnbull, T. Velasco-Torrijos, S. Vidal, S. Vincent, T. Wennekes, H. Zuilhof, A. Imberty, Chem. *Chem. Soc. Rev.* **2013**, *42*, 4709.
[7] N. Garber, U. Guempel, N. Gilboa-Garber, R. J. Royle, *FEMS Microbiol. Lett.* **1987**, *48*, 331.
[8] R. Loris, D. Tielker, K.-E. Jaeger, L. Wyns, *J. Mol. Biol.* **2003**, *331*, 861.
[9] C. Sabin, E. P. Mitchell, M. Pokorná, C. Gautier, J.-P. Utille, M. Wimmerová, A. Imberty, *FEBS Lett.* **2006**, *580*, 982.
[10] H.-P. Hauber, M. Schulz, A. Pforte, D. Mack, P. Zabel, U. Schumacher, *Int. J. Med. Sci.* **2008**, *5*, 371.
[11] D. Hauck, I. Joachim, B. Frommeyer, A. Varrot, B. Philipp, H. M. Möller, A. Imberty, T. E. Exner, A. Titz, *ACS Chem. Biol.* **2013**, *8*, 1775.
[12] a) N. Gilboa-Garber, D. Sudakevitz, M. Sheffi, R. Sela, C. Levene, *Glycoconj. J.* **1994**, *11*, 414; b) L. Cooling, *Clin. Microbiol. Rev.* **2015**, *28*, 801.
[13] N. Galanos, E. Gillon, A. Imberty, S. E. Matthews, S. Vidal, *Org. Biomol. Chem.* **2016**, *14*, 3476.
[14] B. Gerland, A. Goudot, G. Pourceau, A. Meyer, V. Dugas, S. Cecioni, S. Vidal, E. Souteyrand, J.-J. Vasseur, Y. Chevolot, F. Morvan, *Bioconjugate Chem.* **2012**, *23*, 1534.
[15] F. Morvan, A. Meyer, A. Jochum, C. Sabin, Y. Chevolot, A. Imberty, J.-P. Praly, J.-J. Vasseur, E. Souteyrand, S. Vidal, *Bioconjugate Chem.* **2007**, *18*, 1637.

[16] E. M. Johansson, S. A. Crusz, E. Kolomiets, L. Buts, R. U. Kadam, M. Cacciarini, K.-M. Bartels, S. P. Diggle, M. Cámara, P. Williams, R. Loris, C. Nativi, F. Rosenau, K. E. Jaeger, T. Darbre, J. L. Reymond, *Chem. Biol.* **2008**, *15*, 1249.
[17] N. Berthet, B. Thomas, I. Bossu, E. Dufour, E. Gillon, J. Garcia, N. Spinelli, A. Imberty, P. Dumy, O. Renaudet, *Bioconjugate Chem.* **2013**, *24*, 1598.
[18] E. Kolomiets, E. M. V. Johansson, O. Renaudet, T. Darbre, J.-L. Reymond, *Org. Lett.* **2007**, *9*, 1465.
[19] I. Deguise, D. Lagnoux, R. Roy, *New J. Chem.* **2007**, *31*, 1321.
[20] D. Ponader, F. Wojcik, F. Beceren-Braun, J. Dernedde, L. Hartmann, *Biomacromolecules* **2012**, *13*, 1845.
[21] a) D. Ponader, P. Maffre, J. Aretz, D. Pussak, N. M. Ninnemann, S. Schmidt, P. H. Seeberger, C. Rademacher, G. U. Nienhaus, L. Hartmann, *J. Am. Chem. Soc.* **2014**, *136*, 2008; b) M. Baier, M. Giessler, L. Hartmann, *Chem. - Eur. J.* **2018**, *24*, 1619; c) T. Freichel, S. Eierhoff, N. L. Snyder, L. Hartmann, *J. Org. Chem.* **2017**, *82*, 9400; d) S. Igde, S. Röblitz, A. Müller, K. Kolbe, S. Boden, C. Fessele, T. K. Lindhorst, M. Weber, L. Hartmann, *Macromol. Biosci.* **2017**, *17*, 1700198 (1-13); e) F. Wojcik, S. Mosca, L. Hartmann, *J. Org. Chem.* **2012**, *77*, 4226.
[22] C. Gerke, M. F. Ebbesen, D. Jansen, S. Boden, T. Freichel, L. Hartmann, *Biomacromolecules* **2017**, *18*, 787.
[23] K. S. Bücher, H. Yan, R. Creutznacher, K. Ruoff, A. Mallagaray, A. Grafmueller, J. S. Dirks, T. Kilic, S. Weickert, A. Rubailo, M. Drescher, S. Schmidt, G. Hansman, T. Peters, C. Uetrecht, L. Hartmann, *Biomacromolecules* **2018**, *19* (9), 3714.
[24] B. Roy, B. Mukhopadhyay, *Tetrahedron Lett.* **2007**, *48*, 3783.
[25] J. Geng, G. Mantovani, L. Tao, J. Nicolas, G. Chen, R. Wallis, D. A. Mitchell, B. R. G. Johnson, S. D. Evans, D. M. Haddleton, *J. Am. Chem. Soc.* **2007**, *129*, 15156.
[26] S. Lrofas, B. Johnsson, Å. Edström, A. Hansson, G. Lindquist, R.-M. M. Hillgren, L. Stigh, *Biosens. Bioelectron.* **1995**, *10*, 813.
[27] T. Schwabroch, *PhD Thesis*, Heinrich Heine University (Düsseldorf), 06, **2017**.
[28] B. W. Holloway, V. Krishnapillai, A. F. Morgan, *Microbiol. Rev.* **1979**, *43*, 73.
[29] S. K. Shukla, T. S. Rao, *An Improved Crystal Violet Assay for Biofilm Quantification in 96-Well Microtitre Plate*, can be found under https://www.biorxiv.org/content/biorxiv/early/2017/01/13/100214.full.pdf.
[30] E. Engvall, P. Perlmann, *Immunochemistry* **1971**, *8*, 871.
[31] D. Tielker, S. Hacker, R. Loris, M. Strathmann, J. Wingender, S. Wilhelm, F. Rosenau, K.-E. Jaeger, *Microbiology* **2005**, *151*, 1313.
[32] C. Ligeour, O. Vidal, L. Dupin, F. Casoni, E. Gillon, A. Meyer, S. Vidal, G. Vergoten, J.-M. Lacroix, E. Souteyrand, A. Imberty, J.-J. Vasseur, Y. Chevolot, F. Morvan, *Org. Biomol. Chem.* **2015**, *13*, 8433.
[33] S. Boden, K. G. Wagner, M. Karg, L. Hartmann, *Polymers* **2017**, *9*, 1.

Supporting Information

for *Macromol. Biosci.*

Monodisperse sequence-controlled α-L-fucosylated glycooligomers and their multivalent inhibitory effects on LecB

Katharina Susanne Bücher, Nikolina Babic, Tanja Freichel, Filip Kovacic* and Laura Hartmann*

1 Experimental methods

1.1 Materials

Diethyl ether (with BHT as inhibitor, ≥ 99.8%), triisopropylsilane (TIPS) (98%), (+)-sodium-L-ascorbate (≥ 99.0%), citric acid (≥ 99.5%), D-galactose (≥ 99%), sodium diethyldithiocarbamat trihydrate, sodium methanolate (95%) and all deuterated solvents were all purchased from Sigma-Aldrich. Dimethylformamide (DMF) (99.8%, for peptide synthesis), piperidine (99%), copper(II)sulfate (98%), 2-bromoethanole (97%), sodium azide (99%), isopropanol (99.5%), TRIS (≥ 99.8%) and trityl chloride (98%) were purchased from Acros Organics. Methanol (100%), sulfuric acid (95-98%) and acetic anhydride (Ac_2O) (99.7%) were purchased from VWR Prolabo Chemicals. *N*,*N*-Diisopropylethylamine (DIPEA) (≥ 99%) was purchased from Carl Roth. Dichloromethane (DCM) (99.99%), acetonitrile (≥ 99.9%) and NaCl (≥ 99.0%) were purchased from Fisher Scientific. Trifluoroacetic acid (TFA) (99%) was purchased from Fluorochem. Tentagel S RAM® (Rink Amide) resin was purchased from Rapp Polymere and had a loading of 0.22 mmol, 0.23 mmol or 0.25 mmol of Fmoc-protected amine groups per gram of resin. L-Fucose was purchased from Jennewein Biotechnologie GmbH. Silica gel (60 M, 0.04-0.063 mm) was purchased from Machery-Nagel. Succinic anhydride was purchased from Carbolution. Benzotriazol-1-yl-oxytripyrrolidinophosphonium hexafluorophosphate (PyBOP) was purchased from NovaBiochem. The ion exchange resin (AG1-X8, quarternary ammonium, 100-200 mesh, acetate form) was purchased from BioRad. Syringe filters, 4 mm, 0.45 µm PTFE were purchased from Restek. Filter syringes with a

polypropylene frit were purchased from Multisyntech GmbH. Streptavidin sensor chips (SA-chips), sodium chloride solution (1 M), sodium hydroxide solution (0.2 M) and HSB-P+ buffer for SPR measurements were purchased from GE Healthcare Life Sciences. LecB was perchased from OligoTech. α-L-methylfucose (> 98.0%) was purchased TCI. $CaCl_2$ (min. 97%) was purched from AppliChem. Biotinylated fucose- and galactose-polyacrylamide (Fuc-PAA, Gal-PAA) were purchased from GlycoTech.

1.2 Instrumentation

Nuclear magnetic resonance spectroscopy (NMR)

Spectra of ^{1}H NMR and ^{13}C NMR were recorded on a Bruker AVANCE III – 300 (for 300 MHz) and a Bruker AVANCE III – 600 (for 600 MHz). As internal standard residual, non-deuterated solvent was used. Chemical shifts were reported in delta (δ) expressed in units of parts per million (ppm).

Semi-preparative reverse-phase high-performance liquid chromatography (semi-preparative RP-HPLC)

Preparative RP-HPLC for purification of glycomacromolecules was performed on an Agilent 1200 HPLC System at 25 °C. Product separation was realized on a Varian Persuit semi-preparative column (C_{18}, 250x10.0 mm). The glycomacromolecules were eluted with a linear gradient of water (A) and acetonitrile (B) at a flow rate of 20 mL/min. The product fractions were collected and combined. After concentration in vacuum the glycomacromolecules were dissolved in milliQ-water, filtered through syringe filters and lyophilized.

Reversed phase - high performance liquid chromatography - mass spectrometry (RP-HPLC/MS)

Analytical RP-HPLC/MS was performed at 25 °C with a RP-HPLC system from Agilent (Agilent 1260 Infinity) equipped with an Agilent Poroshell 120 EC-C18 (3.0×50 mm, 2.5 µm) RP column. As mobile phases H_2O/ACN (95/5) (A) and H_2O/ACN (5/95) (B) with 0.1% formic acid were used. A variable wavelength detector (VWD) was coupled that was set to 214 nm. It was combined with a 6120 Quadrupole LC/MS with Electrospray Ionization (ESI) source operating in positive ionization mode in a m/z range of 200 to 2000. Oligomer analysis was conducted applying a linear gradient of mobile

phases A and B starting with 100% A and reaching 50% of mobile phase A in 30 min with a flow rate of 0.4 mL/min. UV and MS signals were analyzed with the OpenLab ChemStation software for LC/MS from Agilent Technologies.

High resolution –electrospray ionization - mass spectrometry (HR-ESI/MS)

HR-ESI/MS spectra were recorded on an Agilent 6210 (Electrospray Ionization) ESI-TOF from Agilent Technologies (Santa Clara, CA, USA) with a flow rate of 4 µL/min and a spray voltage of 4 kV. The desolvation gas was set to 15 psi (1 bar).

Matrix-assisted laser desorption ionization- time of flight – mass spectrometry (MALDI-TOF-MS)

MALDI TOF MS spectra were recorded on a Bruker MALDI-TOF Ultraflex I system using 2,5-dihydroxybenzoic acid (DHB) as matrix in a 10 fold excess compared to the compound. The spectra were generated in linear mode for a m/z range of 1000-4000 (calibrated with a protein mixture) or in reflector mode for a m/z range 2000-20000 without calibration.

Lyophilization

The lyophilization was performed with an Alpha 1-4 LD plus instrument from Martin Christ Freeze Dryers GmbH at -42 °C and 0.1 mbar with an.

Peptide synthesizer

Automated synthesis of oligomeric backbones was performed on a peptide synthesizer from CS Bio (CS136XT). The batch sizes varied between 0.085 mmol and 0.13 mmol. All protocols for automated synthesis were written with CSPEPM software from CS Bio.

1.3 General methods

Synthesis of azidoethyl-2,3,4-tri-*O*-acetyl-α-L-fucopyranoside and azidoethyl-2,3,4,6-tetra-*O*-acetyl-α/β-D-galactopyranoside was performed according to literature.[1,2] EDS and TDS building blocks were synthesized using previously reported protocols.[2]

Solid phase polymer synthesis of glycooligomers

Solid phase synthesis of glycooligomers was conducted according to literature.[2,3] As solid support commercial available Tentagel S RAM® resin (Rink amide) was used (loading 0.22-0.25 mmol/g). The detailed batch sizes are described for each compound separately. Glycooligomers **1** and **4** were reported earlier.[2]

The resin was swollen for 1 h at room temperature by shaking with DCM and washing 10 times with DMF. By alternating Fmoc-deprotection steps and coupling steps the oligomeric backbones were elongated either in 10 mL filter syringes or automated on a peptide synthesizer. Fmoc deprotection was realized by shaking 3 times with 5 mL of 25% piperidine in DMF for 10 min and washing 10 times with DMF afterwards. Coupling was conducted with 5 eq. of corresponding building block (TDS or EDS) in 3 mL DMF mixed with 5 eq. of PyBOP. After adding 10 eq. DIPEA, the mixture was flushed with nitrogen, added to the resin and shaken for 1.5 h and washed 10 times with DMF afterwards. After capping of scaffolds with 3 mL acetic anhydride for 15 min twice and washing with 5 times with DMF and 5 times with DCM the azidated α-L-fucose or D-galactose derivatives were coupled by CuAAC reaction on solid support. CuAAC was performed by mixing 2 eq. 2-azidoethylpyranoside in 2 mL DMF with 50mol% sodium ascorbate (aqueous solution, c = 33 mg/mL) per alkyne group, degassing with nitrogen and adding to the resin. Afterwards 25mol% $CuSO_4$ per alkyne group (aqueous solution, c = 20 mg/mL) was degassed and added to the resin. CuAAC proceeded with exclusion of light at RT for overnight. Azidated carbohydrates were recovered by extraction with ethyl acetate and water. The resin was washed with sodium diethyldithiocarbamate in DMF (23 mM), water, DMF and DCM. Carbohydrates were de-acetylated twice by adding 5 mL NaOMe in methanol (0.2 M), shaking for 30 min and washing with DCM (3 times) and methanol (3 times). Cleavage of final glycooligomers was performed by adding 3 mL 95% TFA (containing 2.5% TIPS and 2.5% DCM) twice for 1.5 h and precipitation from diethyl ether. Ether was centrifuged, decanted and the solid was dried in nitrogen stream. It was dissolved in MilliQ-water and lyophilized. Crude product oligomers were purified with ion exchange resin with 1 g resin per 100 mg oligomer according to literature followed by preparative RP-HPLC.[4] Completeness of the reaction steps were monitored using microcleavages and analytical RP-LC/MS.

2 Glycooligomer analysis

Fuc(3,5)-7 (2)

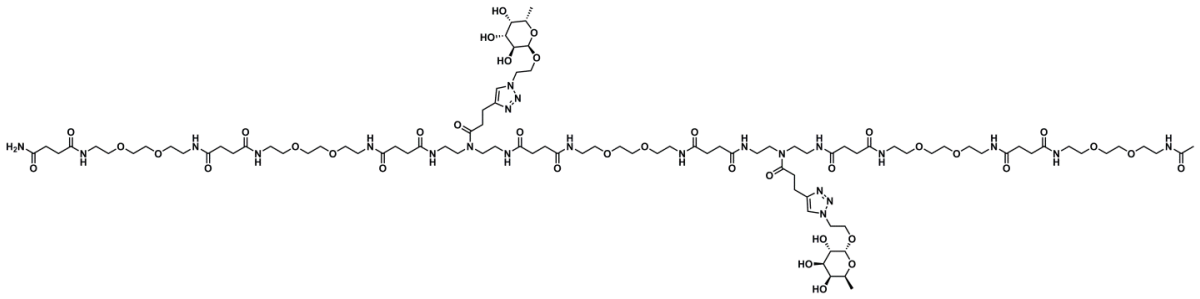

Compound **2** was synthesized in a batch size of 0.12 mmol. 132 mg (0.06 mmol) of crude product (295 mg) were purified by ion exchange resin and preparative RP-HPLC. The purified product **2** was obtained as lyophilized white powder (51 mg, 0.023 mmol, 38%).

^{1}H NMR (600 MHz, D_2O): δ = 7.92 (s, 2H, N=N-N-C*H*), 4.84 (d, ^{3}J = 3.8 Hz, 2H , Fuc-H-1), 4.69-4.62 (m, 4H, N=N-N-CH_2), 4.06-4.02 (m, 2H, N=N-N-CH_2-CH_2), 3.94 (dt, $^{2,3}J$ = 10.8, 3.7 Hz, 2H, N=N-N-CH_2-CH_2), 3.73 (dd, $^{3,3}J$ = 10.3, 3.8 Hz, 2H, Fuc-H-2), 3.70-3.67 (m, 22H, O-CH_2-CH_2-O, Fuc-H-3), 3.64-3.60 (m, 22H, CH_2-O-(CH_2)$_2$-O-CH_2, Fuc-H-4), 3.50-3.45 (m, 8H, N-*CH*$_2$-CH_2-NH), 3.41-3.33 (m, 28H, O=C-NH-CH_2), 3.09 (q, ^{3}J = 6.6 Hz, 2H, Fuc-H-5), 3.00 (t, ^{3}J = 7.3 Hz, 4H, N-N=N-C-CH_2), 2.79 (t, ^{3}J = 7.3 Hz, 4H, N-N=N-C-CH_2-CH_2), 2.57-2.46 (m, 28H, O=C-CH_2-CH_2-C=O), 2.00 (s, 3H, O=C-CH_3), 1.04 (d, ^{3}J = 6.6 Hz, 6H, Fuc-H-6). MALDI TOF MS*:* *m/z* calcd for $C_{94}H_{163}N_{23}O_{37}$ $[M+Na]^+$ 2230.46; found 2229.2. HR-ESI/MS: *m/z* calcd for $C_{94}H_{163}N_{23}O_{37}$ (monoisotopic mass 2206.1580): $[M+3H]^{3+}$ 736.3933, found 736.3941. RP-HPLC: (gradient from 100% to 50% eluent **A** in 30 min, 25°C): t_R = 12.1 min, determined purity 98%.

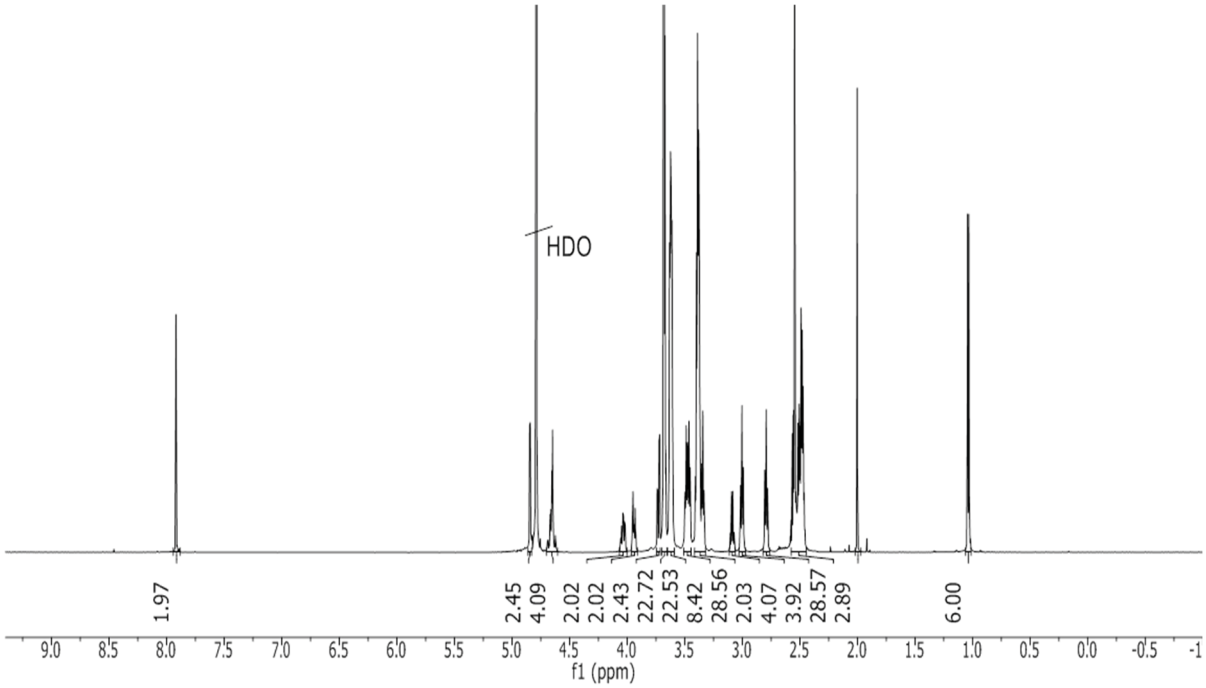

Figure S1: ^{1}H NMR (600 MHz, D_2O) spectrum of Fuc(3,5)-7 (**2**).

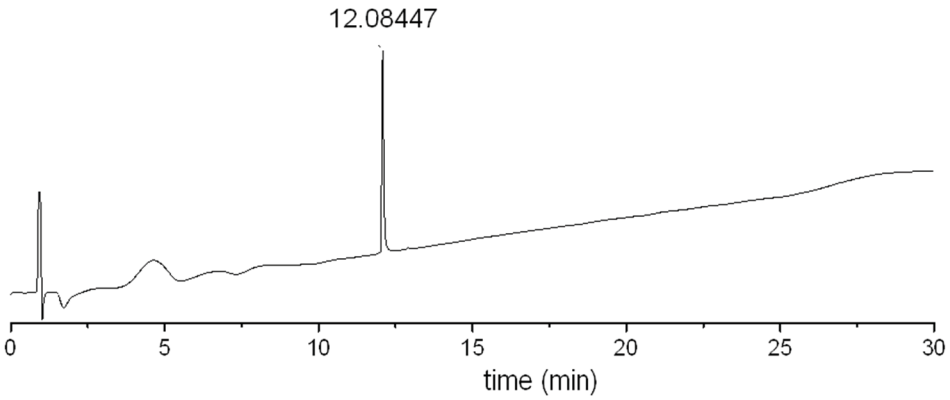

Figure S2: RP-HPLC spectrum of Fuc(3,5)-7 (**2**).

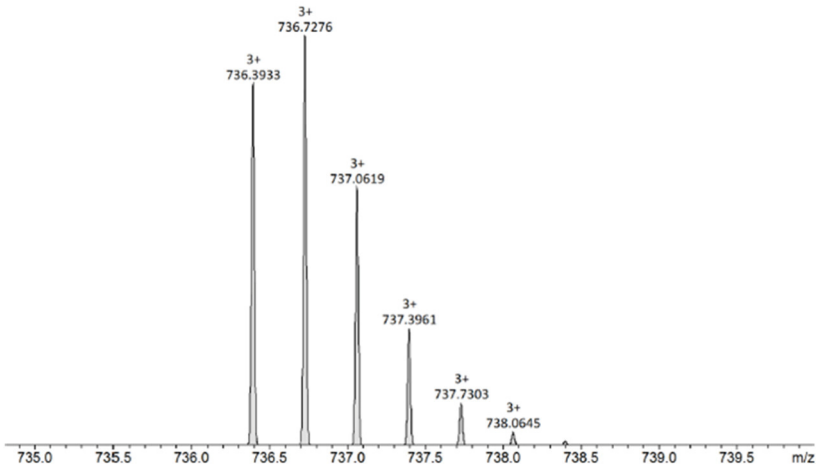

Figure S3: HR/ESI-MS spectrum of Fuc(3,5)-7 (**2**).

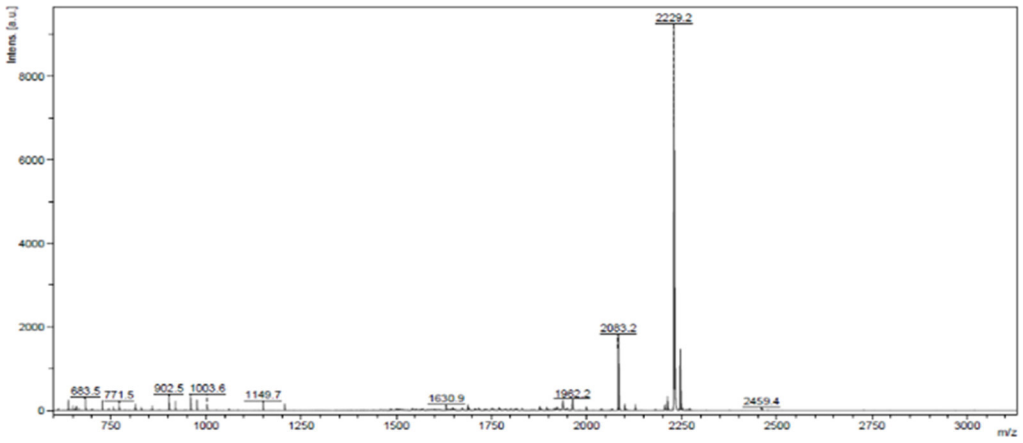

Figure S4: MALDI TOF MS spectrum of Fuc(3,5)-7 (**2**).

Fuc(2,4,6)-7 (3)

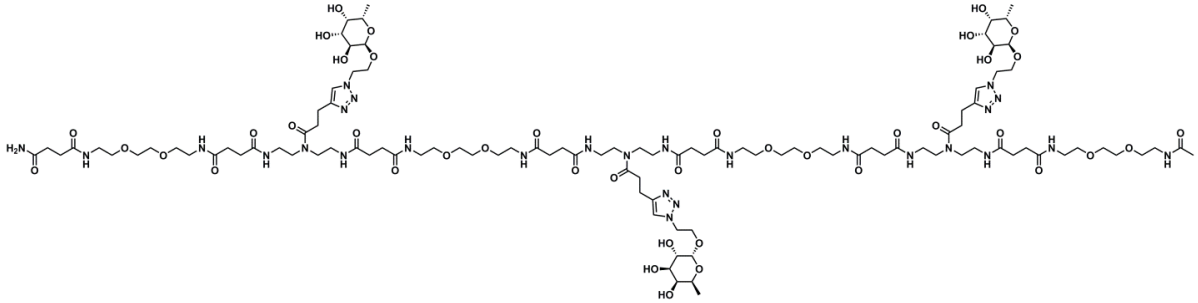

Compound **3** was synthesized in a batch size of 0.1 mmol. 116 mg (0.047 mmol) of crude product (272 mg) were purified by ion exchange resin and preparative RP-HPLC. The purified product **3** was obtained as lyophilized white powder (54 mg, 0.022 mmol, 47%).

^{1}H NMR (600 MHz, D_2O): δ = 7.92 (s, 3H, N=N-N-C*H*), 4.84 (d, ^{3}J = 3.8 Hz, 3H , Fuc-H-1), 4.69-4.62 (m, 6H, N=N-N-CH_2), 4.06-4.02 (m, 3H, N=N-N-CH$_2$-CH_2), 3.94 (dt, $^{2,3}J$ = 10.8, 3.7 Hz, 3H, N=N-N-CH$_2$-CH_2), 3.73 (dd, $^{3,3}J$ = 10.3, 3.8 Hz, 3H, Fuc-H-2), 3.69-3.66 (m, 19H, O-CH_2-CH_2-O, Fuc-H-3), 3.63-3.60 (m, 19H, CH_2-O-(CH$_2$)$_2$-O-CH_2, Fuc-H-4), 3.50-3.45 (m, 12H, N-*CH*$_2$-CH$_2$-NH), 3.40-3.33 (m, 28H, O=C-NH-CH_2), 3.09 (q, ^{3}J = 6.6 Hz, 3H, Fuc-H-5), 3.00 (t, ^{3}J = 7.3 Hz, 6H, N-N=N-C-CH_2), 2.79 (t, ^{3}J = 7.3 Hz, 6H, N-N=N-C-CH$_2$-CH_2), 2.56-2.46 (m, 28H, O=C-CH_2-CH_2-C=O), 2.00 (s, 3H, O=C-CH_3), 1.04 (d, ^{3}J = 6.6 Hz, 9H, Fuc-H-6). MALDI TOF MS*: m/z* calcd for $C_{105}H_{179}N_{27}O_{41}Na$ $[M+Na]^+$ 2497.27, found 2497.39. HR-ESI/MS: *m/z* calcd for $C_{105}H_{179}N_{27}O_{41}$ (monoisotopic mass 2474.2752): $[M+3H]^{3+}$ 825.7657, found 825.7669. RP-HPLC: (gradient from 100% to 50% eluent **A** in 30 min, 25°C): t_R = 11.8 min, determined purity 99%.

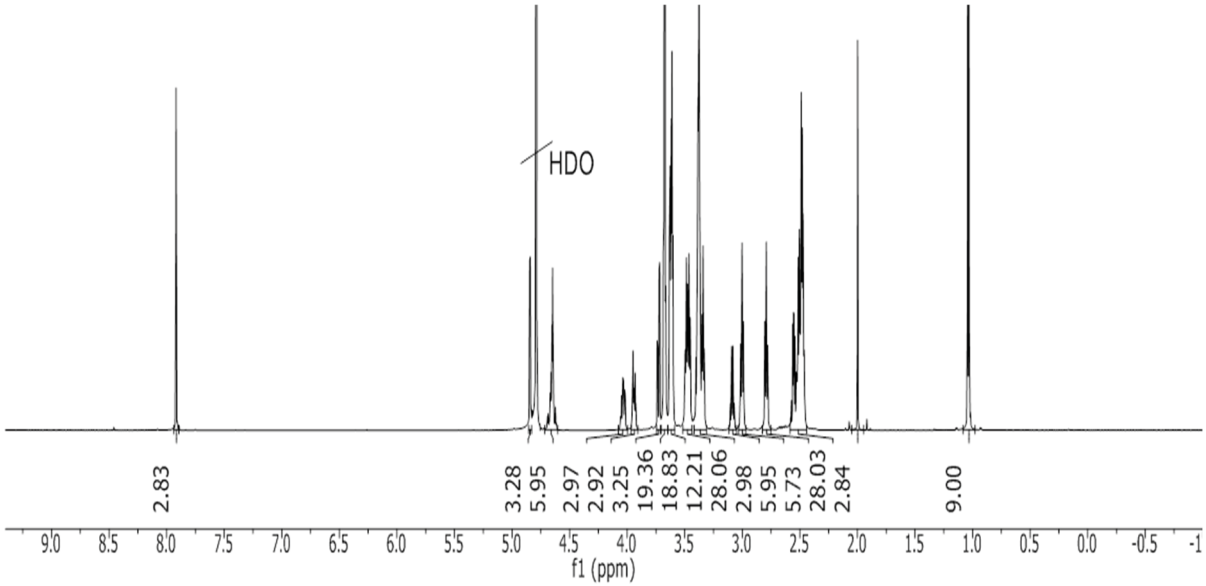

Figure S5: ^{1}H NMR (600 MHz, D_2O) spectrum of Fuc(2,4,6)-7 **(3)**.

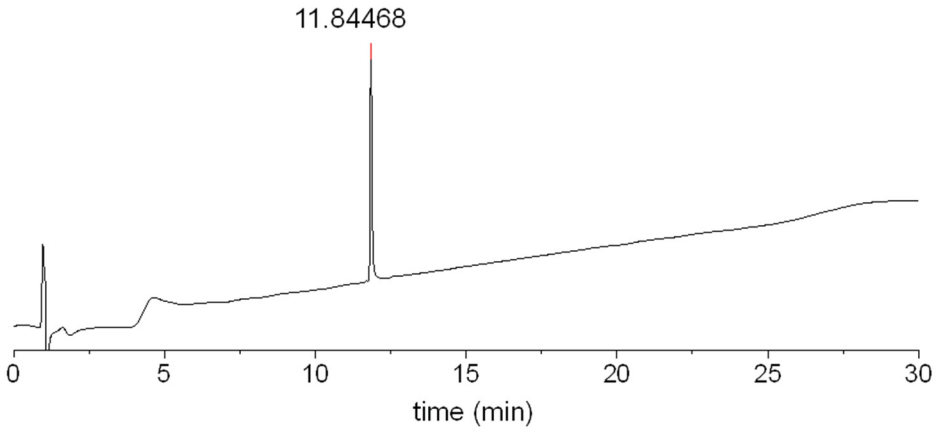

Figure S6: RP-HPLC spectrum of Fuc(2,4,6)-7 (**3**).

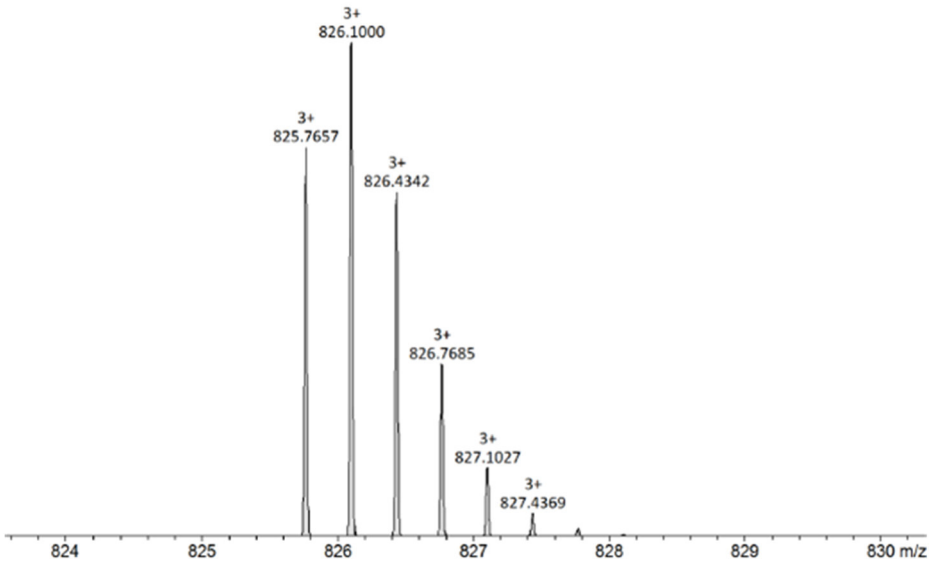

Figure S7: HR/ESI-MS spectrum of Fuc(2,4,6)-7 (**3**).

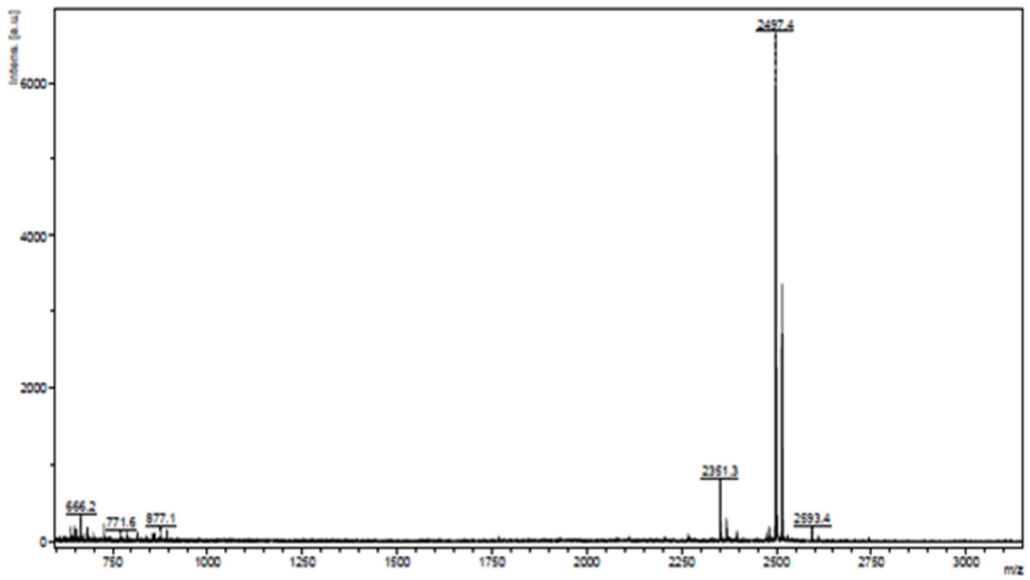

Figure S8: MALDI TOF MS spectrum of Fuc(2,4,6)-7 (**3**).

Fuc(1,2,3,4,5,6)-6 (5)

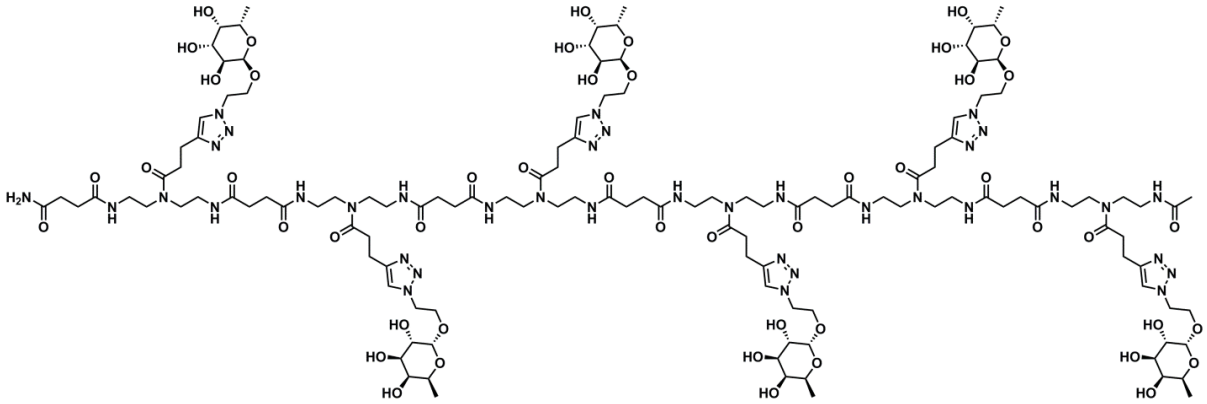

Compound **5** was synthesized in a batch size of 0.1 mmol. The crude product (284 mg, 0.093 mmol) was purified by ion exchange resin and preparative RP-HPLC. 137 mg (0.045 mmol, 48%) of purified product **5** was obtained as lyophilized white powder.

^{1}H NMR (600 MHz, D_2O): δ = 7.91 (s, 6H, N=N-N-C*H*), 4.84 (d, ^{3}J = 3.7 Hz, 6H, Fuc-H-1), 4.68-4.61 (m, 12H, N=N-N-CH_2), 4.05-4.01 (m, 6H, N=N-N-CH_2-CH_2), 3.95-3.92 (m, 6H, N=N-N-CH_2-CH_2), 3.73 (dd, $^{3,3}J$ = 10.3, 3.8 Hz, 6H, Fuc-H-2), 3.67 (dd, $^{3,3}J$ = 10.3, 3.3 Hz, 6H, Fuc-H-3), 3.63-3.62 (m, 6H, Fuc-H-4), 3.48-3.44 (m, 24H, N-*CH*$_2$-CH_2-NH), 3.37-3.31 (m, 24H, O=C-NH-CH_2), 3.08 (q, ^{3}J = 6.6 Hz, 6H, Fuc-H-5), 3.00-2.97 (m, 12H, N-N=N-C-CH_2), 2.80-2.76 (m, 12H, N-N=N-C-CH_2-CH_2), 2.54-2.42 (m, 24H, O=C-CH_2-CH_2-C=O), 1.94, 1.92 (s, s, 3H, O=C-CH_3), 1.03 (d, ^{3}J = 6.6 Hz, 18H, Fuc-H-6). MALDI TOF MS: *m/z* calcd for $C_{128}H_{209}N_{37}O_{49}Na$ $[M+Na]^+$ 3071.50, found 3071.52;

$[M+K]^+$ 3087.50, found 3087.5. HR-ESI/MS: *m/z* calcd for $C_{128}H_{213}N_{37}O_{49}$ (monoisotopic mass 3048.5000): $[M+4H]^{4+}$ 763.1323, found 763.1325. RP-HPLC: (gradient from 100% to 50% **A** in 30 min, 25°C): t_R = 10.9 min, determined purity 99%.

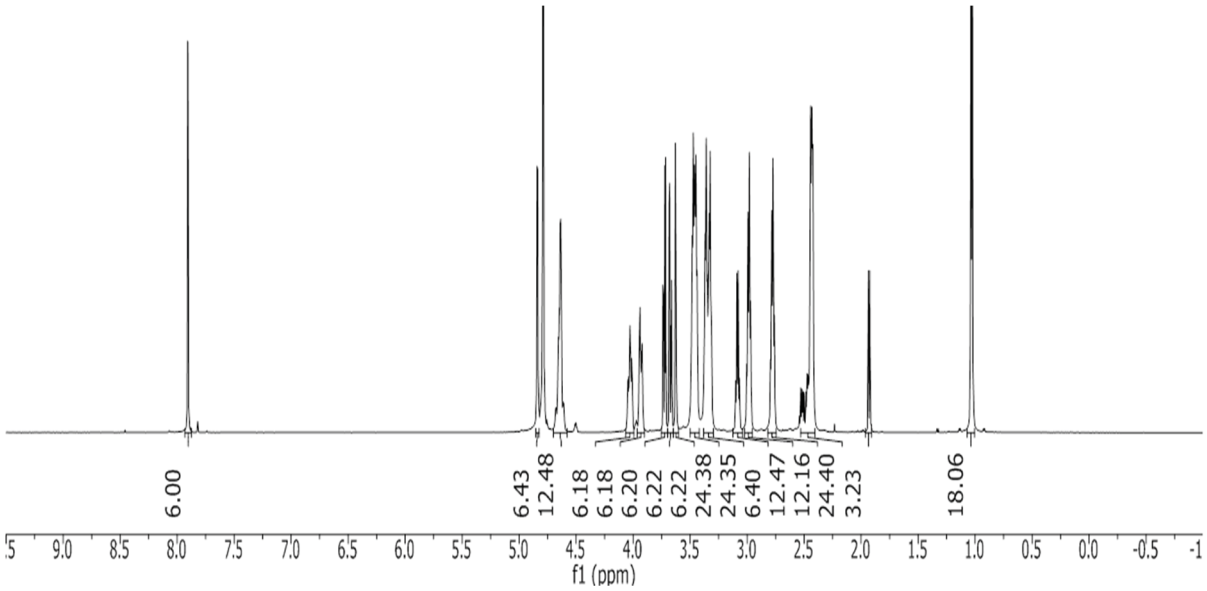

Figure S9: ^{1}H NMR (300 MHz, D_2O) spectrum of Fuc(1,2,3,4,5,6)-6 (**5**).

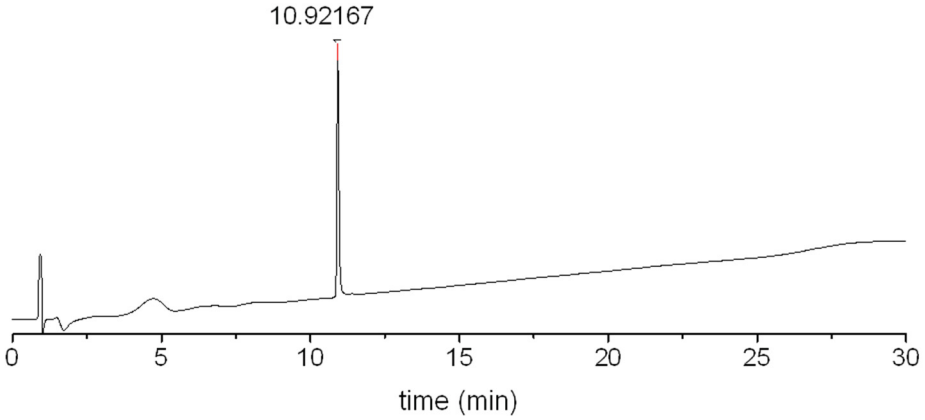

Figure S10: RP-HPLC spectrum of Fuc(1,2,3,4,5,6)-6 (**5**).

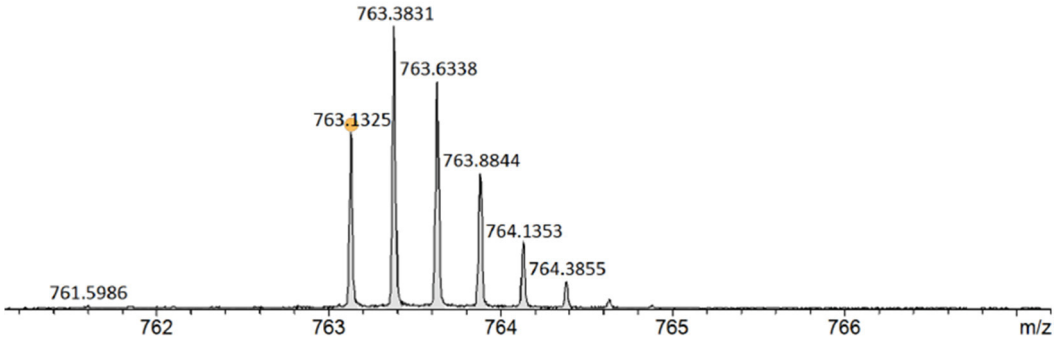

Figure S11: HR/ESI-MS spectrum of Fuc(1,2,3,4,5,6)-6 (**5**).

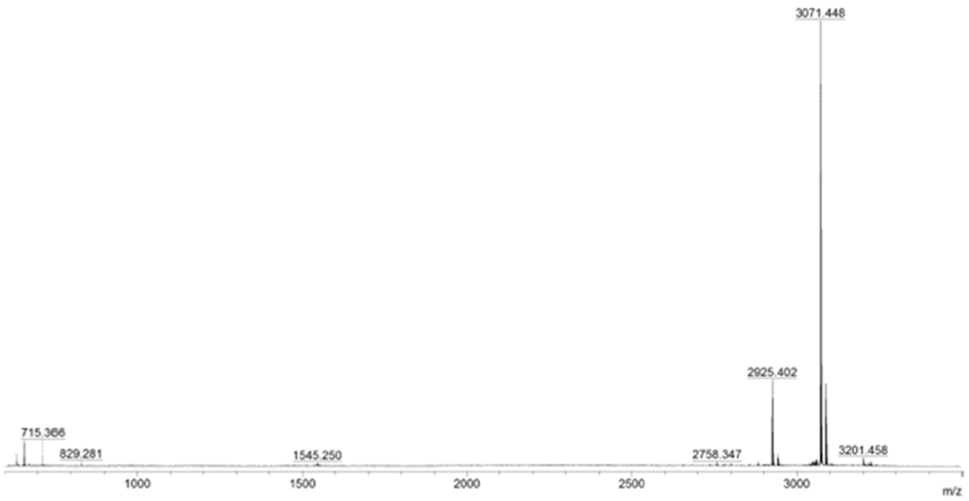

Figure S12: MALDI TOF MS spectrum of Fuc(1,2,3,4,5,6)-6 (**5**).

Fuc(1,4,7)-7 (6)

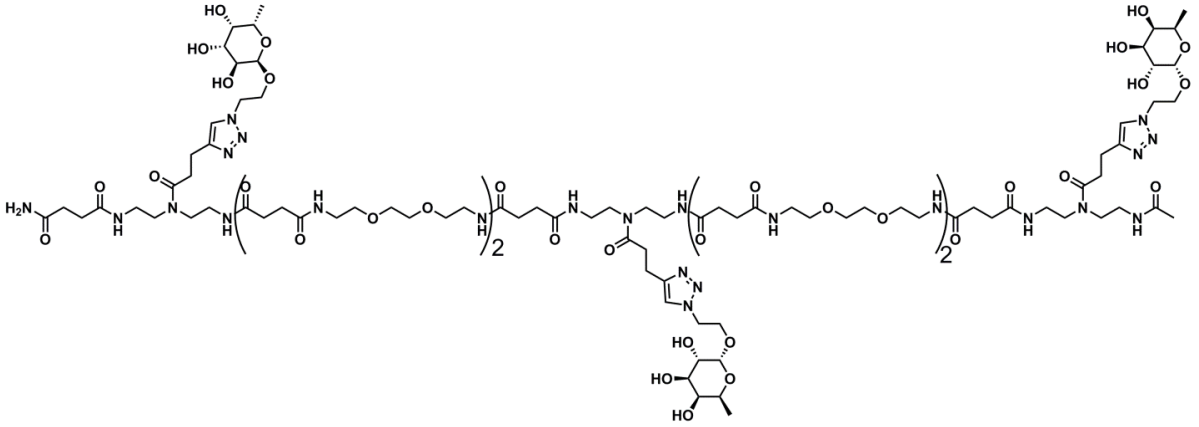

Compound **6** was synthesized in a batch size of 0.1 mmol. 256 mg (0.103 mmol) of crude product (288 mg) were purified by ion exchange resin and preparative RP-HPLC. The purified product **6** was obtained as lyophilized white powder (77 mg, 0.031 mmol, 30%).

^{1}H NMR (600 MHz, D_2O): δ = 7.92 (s, 3H, N=N-N-C*H*), 4.84 (d, ^{3}J = 3.8 Hz, 3H , Fuc-H-1), 4.69-4.62 (m, 6H, N=N-N-CH_2), 4.06-4.02 (m, 3H, N=N-N-CH$_2$-CH_2), 3.94 (dt, $^{2,3}J$ = 10.7, 3.6 Hz, 3H, N=N-N-CH$_2$-CH_2), 3.73 (dd, $^{3,3}J$ = 10.3, 3.8 Hz, 3H, Fuc-H-2), 3.69-3.66 (m, 19H, O-CH_2-CH_2-O, Fuc-H-3), 3.63-3.60 (m, 19H, CH_2-O-(CH$_2$)$_2$-O-CH_2, Fuc-H-4), 3.50-3.45 (m, 12H, N-*CH*$_2$-CH$_2$-NH), 3.39-3.32 (m, 29H, O=C-NH-CH_2), 3.09 (q, ^{3}J = 6.5 Hz, 3H, Fuc-H-5), 3.00 (t, ^{3}J = 7.2 Hz, 6H, N-N=N-C-CH_2), 2.81-2.78 (m, 6H, N-N=N-C-CH$_2$-CH_2), 2.54-2.47 (m, 28H, O=C-CH_2-CH_2-C=O), 1.94, 1.93 (s, s, 3H, O=C-CH_3), 1.04 (d, ^{3}J = 6.6 Hz, 9H, Fuc-H-6). MALDI TOF MS: *m/z* calcd for $C_{105}H_{179}N_{27}O_{41}Na$ $[M+Na]^+$ 2497.28, found 2497.3. HR-ESI/MS: *m/z* calcd for $C_{105}H_{179}N_{27}O_{41}$ (monoisotopic mass

2474.2752): $[M+3H]^{3+}$ 825.7657, found 825.7660. RP-HPLC: (gradient from 100% to 50% eluent **A** in 30 min, 25°C): t_R = 11.9 min, determined purity 98%.

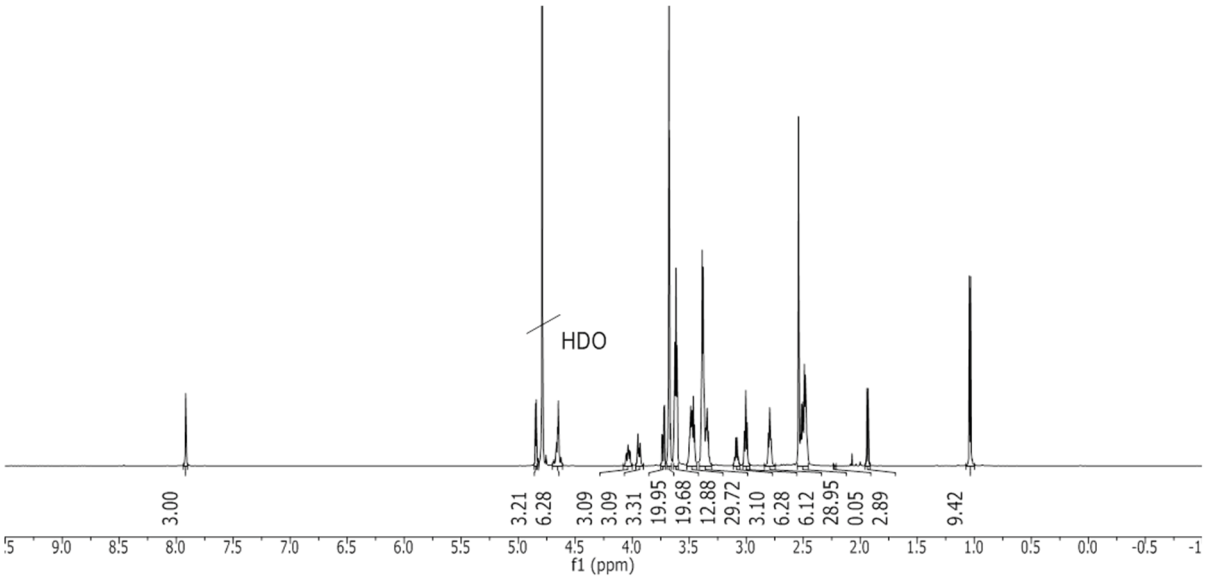

Figure S13: ^{1}H NMR (600 MHz, D_2O) spectrum of Fuc(1,4,7)-7 (**6**).

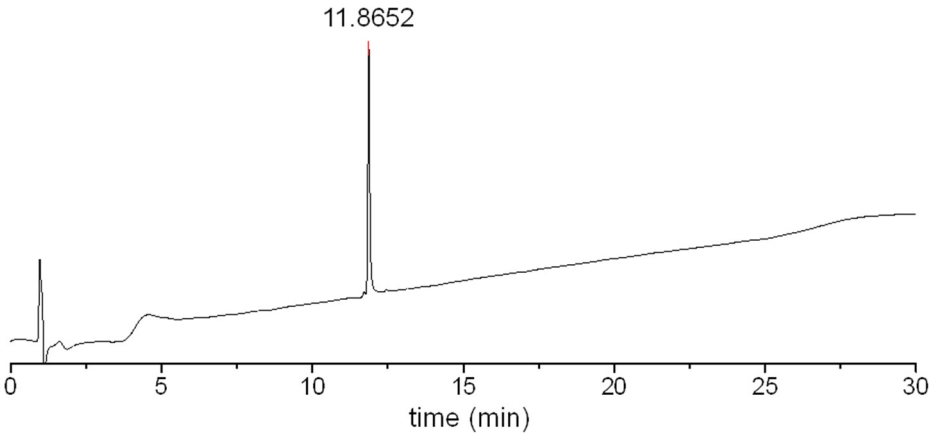

Figure S14: RP-HPLC spectrum of Fuc(1,4,7)-7 (**6**).

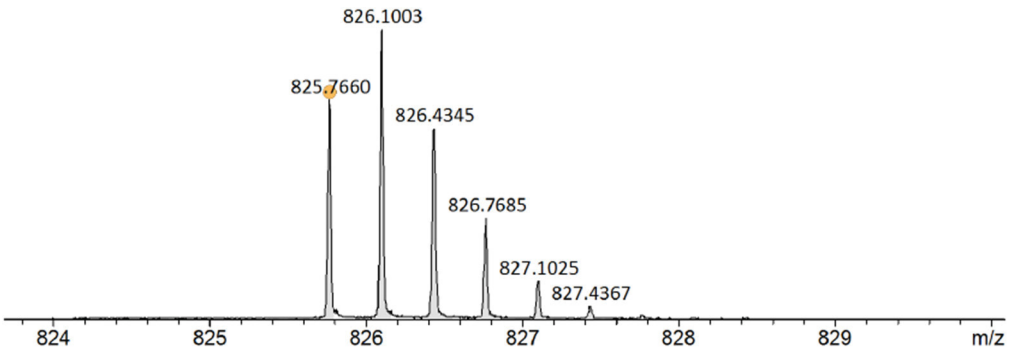

Figure S15: HR/ESI-MS spectrum of Fuc(1,4,7)-7 (**6**).

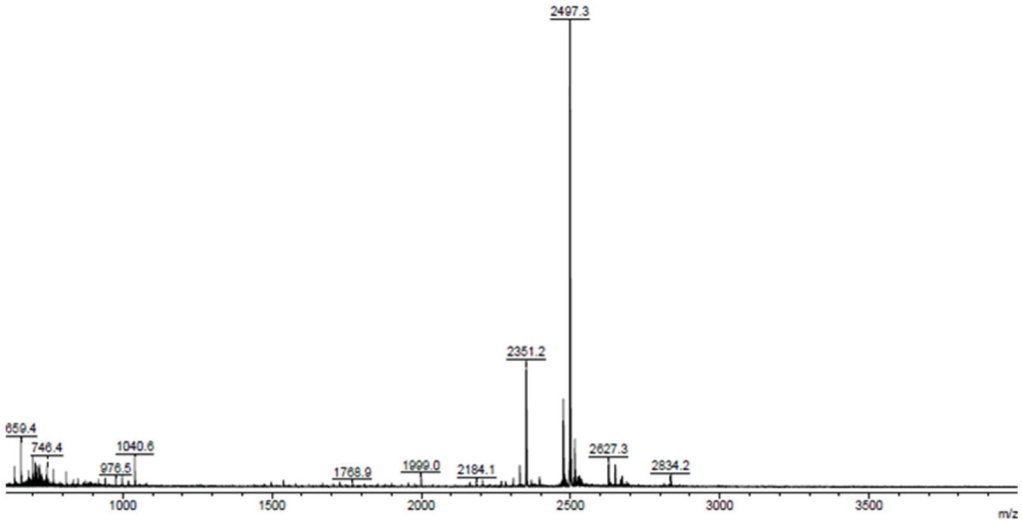

Figure S16: MALDI TOF MS spectrum of Fuc(1,4,7)-7 (**6**).

Fuc(1,5,9)-9 (7)

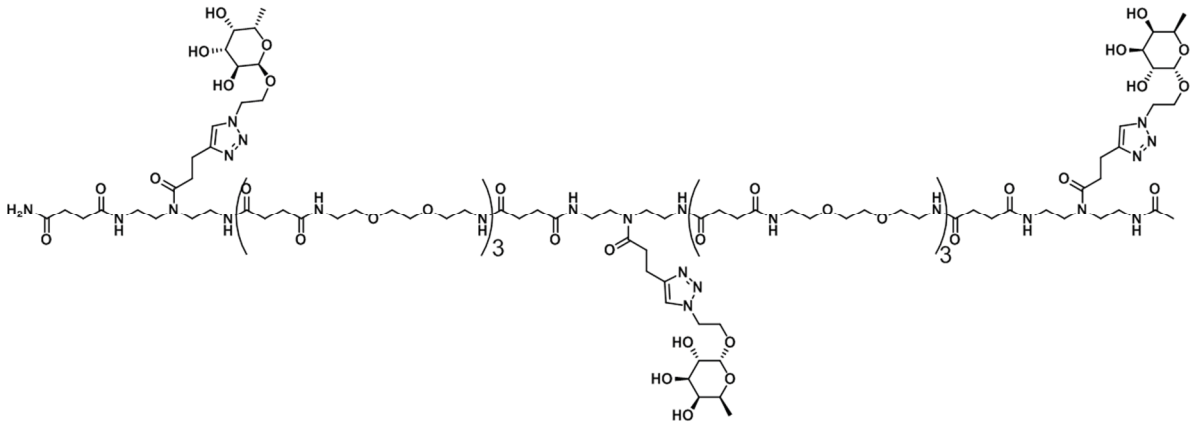

Compound **7** was synthesized in a batch size of 0.085 mmol. 74 mg (0.025 mmol) of crude product (246 mg) were purified by ion exchange resin and preparative RP-HPLC. The purified product **7** was obtained as lyophilized white powder (60 mg, 0.020 mmol, 80%).

^{1}H NMR (300 MHz, D_2O): δ = 7.91 (s, 3H, N=N-N-C*H*), 4.84 (d, ^3J = 3.5 Hz, 3H, Fuc-H-1), 4.67-4.63 (m, 6H, N=N-N-CH_2), 4.07-4.00 (m, 3H, N=N-N-CH_2-CH_2), 3.96-3.90 (m, 3H, N=N-N-CH_2-CH_2), 3.75-3.66-3.60 (m, 59H, O-CH_2-CH_2-O, Fuc-H-2, Fuc-H-3, CH_2-O-$(CH_2)_2$-O-CH_2, Fuc-H-4), 3.51-3.34 (m, 49H, N-CH_2-CH_2-NH, O=C-NH-CH_2), 3.08 (q, ^3J = 6.8 Hz, 3H, Fuc-H-5), 3.00 (t, ^3J = 7.1 Hz, 6H, N-N=N-C-CH_2), 2.79 (t, ^3J = 7.2 Hz, 6H, N-N=N-C-CH_2-CH_2), 2.54-2.48 (m, 36H, O=C-CH_2-CH_2-C=O), 2.23 (s, 6H, O=C-CH_3), 1.94, 1.93 (s, s, 3H, O=C-CH_3), 1.03 (d, ^3J = 6.6 Hz, 9H, Fuc-H-6). MALDI TOF MS: *m/z* calcd for $C_{125}H_{215}N_{31}O_{49}Na$ $[M+Na]^+$ 2957.5, found 2957.5. HR-ESI/MS: *m/z*

calcd for $C_{125}H_{215}N_{31}O_{49}$ (monoisotopic mass 2934.5285): $[M+4H]^{4+}$ 734.6394, found 734.6394. RP-HPLC: (gradient from 100% to 50% eluent **A** in 30 min, 25°C): t_R = 12.3 min, determined purity 99%.

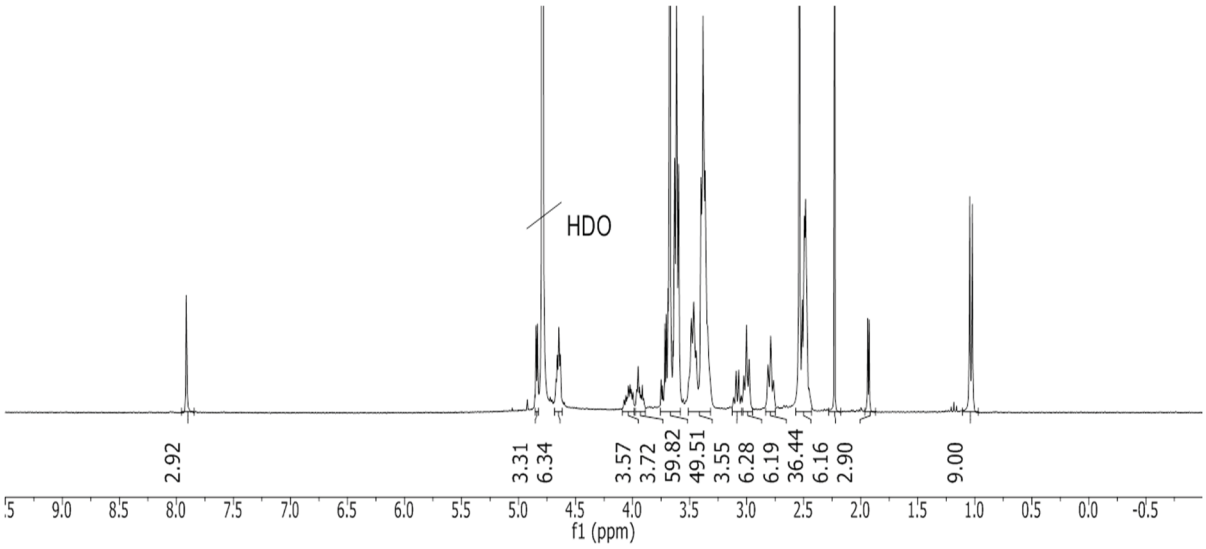

Figure S17: ^{1}H NMR (600 MHz, D_2O) spectrum of Fuc(1,5,9)-9 (**7**).

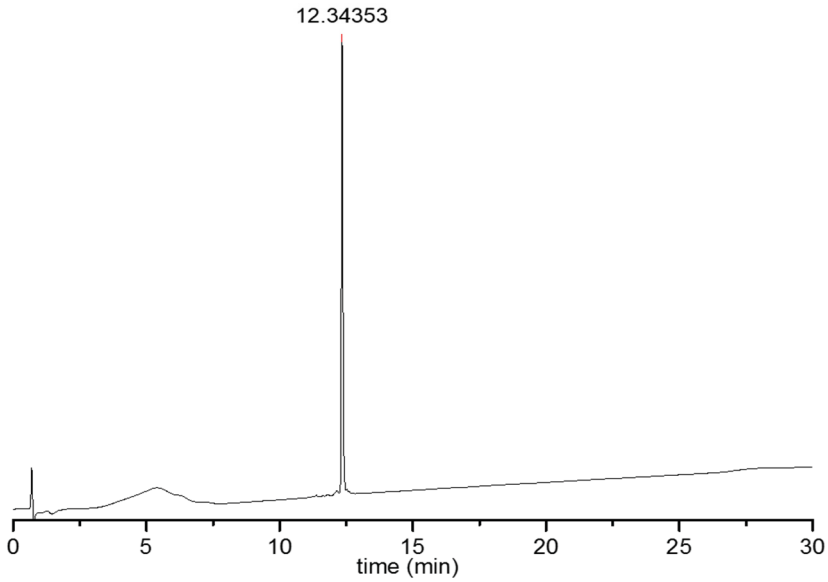

Figure S18: RP-HPLC spectrum of Fuc(1,5,9)-9 (**7**).

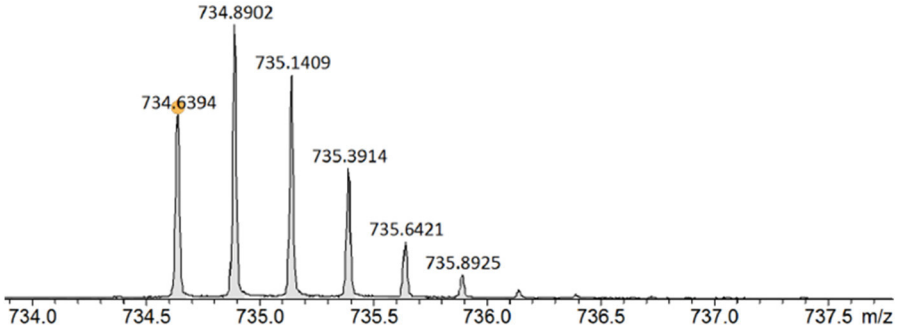

Figure S19: HR/ESI-MS spectrum of Fuc(1,5,9)-9 (**7**).

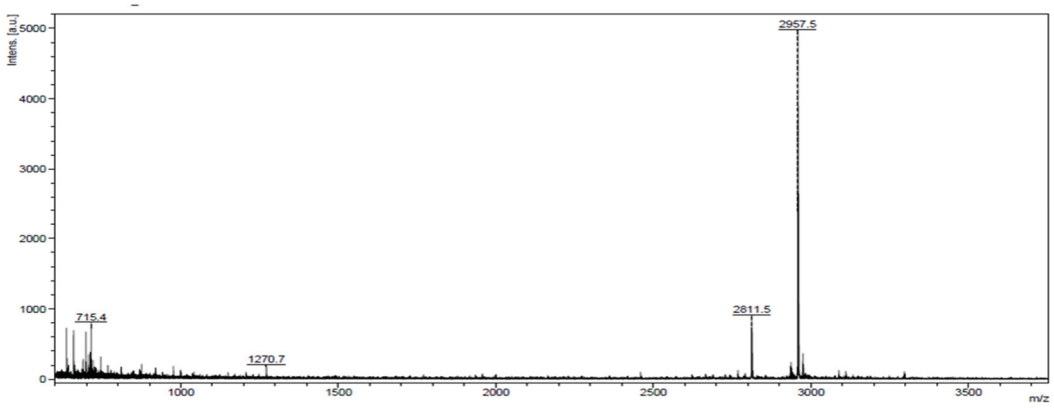

Figure S20: MALDI TOF MS spectrum of Fuc(1,5,9)-9 (**7**).

Gal(3,5)-7 (8)

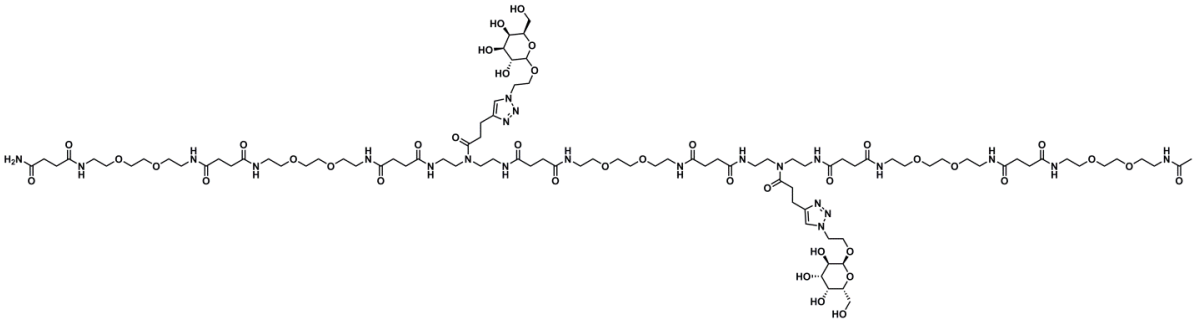

Compound **8** was synthesized in a batch size of 0.176 mmol. 134 mg (0.060 mmol) of crude product (321 mg) was purified by ion exchange resin and preparative RP-HPLC. 76 mg (0.034 mmol, 57%) of purified product **8** was obtained as lyophilized white powder.

^{1}H NMR (600 MHz, D_2O): δ = 7.90 (s, 1.5H, N=N-N-C*H*), 7.87 (s, 0.4H, N=N-N-C*H*), 4.93 (d, ^{3}J = 1.3 Hz, 0.5H, α-Gal-H-1), 4.65 (t, ^{3}J = 5.1 Hz, 3H, N=N-N-CH_2), 4.62 (t, ^{3}J = 5.1 Hz, 1H, N=N-N-CH_2), 4.37 (d, ^{3}J = 7.9 Hz, 1.6H, β-Gal-H-1), 4.31-4.27 (m, 1.6H, N=N-N-CH_2-CH_2), 4.11-4.07 (m, 2H, N=N-N-CH_2-CH_2), 4.03-4.00 (m, 0.8 H, N=N-N-CH_2-CH_2), 3.98-3.95 (m, 0.5H, N=N-N-CH_2-CH_2), 3.91 (d, ^{3}J = 3.3 Hz, 1.6 H, β-Gal-H-2), 3.80-3.60 (m, 50H, α-Gal-H-2, Gal-H-3,-H4,-H-5,-H-6, O-CH_2-CH_2-O, CH_2-O-$(CH_2)_2$-O-CH_2), 3.51-3.45 (m, 10H, N-CH_2-CH_2-NH, Gal-H-6), 3.41-3.33 (m, 28H, O=C-NH-CH_2), 3.00 (t, ^{3}J = 7.2 Hz, 4H, N-N=N-C-CH_2), 2.97 (t, ^{3}J = 7.3 Hz, 4H, N-N=N-C-CH_2-CH_2), 2.56-2.46 (m, 28H, O=C-CH_2-CH_2-C=O), 2.00 (s, 3H, O=C-CH_3). MALDI TOF MS: *m/z* calcd for $C_{94}H_{163}N_{23}O_{39}Na$ $[M+Na]^+$ 2261.1, found 2261.1. HR-ESI/MS: *m/z* calcd for $C_{94}H_{166}N_{23}O_{39}$ (monoisotopic mass 2238.1497): $[M+3H]^{3+}$ 747.0566, found 747.0573. RP-HPLC: (gradient from 100% to 50% eluent A in 30 min, 25°C): t_R = 11.5 min, 11.7 min, determined purity 99%.

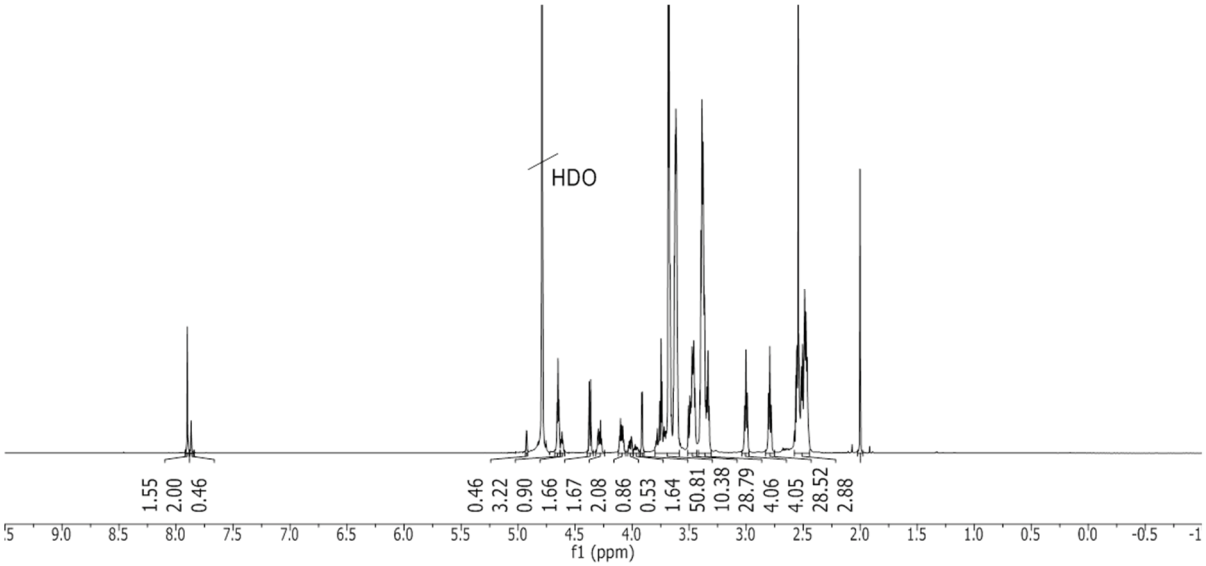

Figure S21: ^{1}H NMR (300 MHz, D_2O) spectrum of Gal(3,5)-7 (**8**).

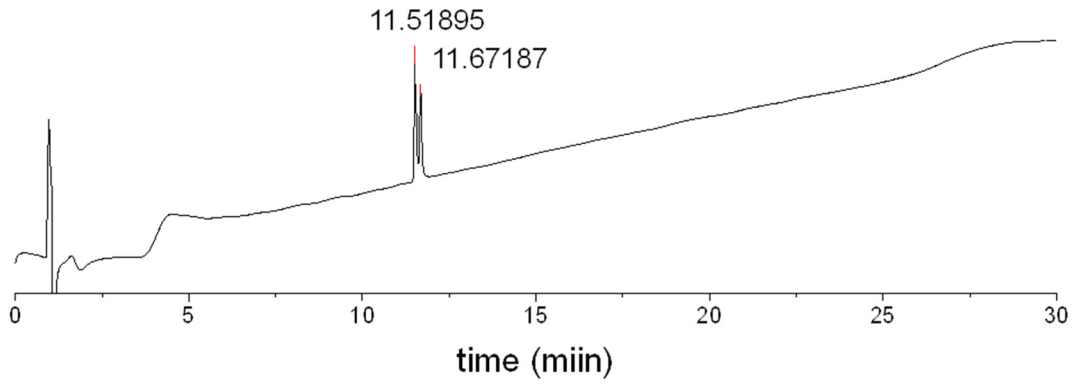

Figure S22: RP-HPLC spectrum of Gal(3,5)-7 (**8**).

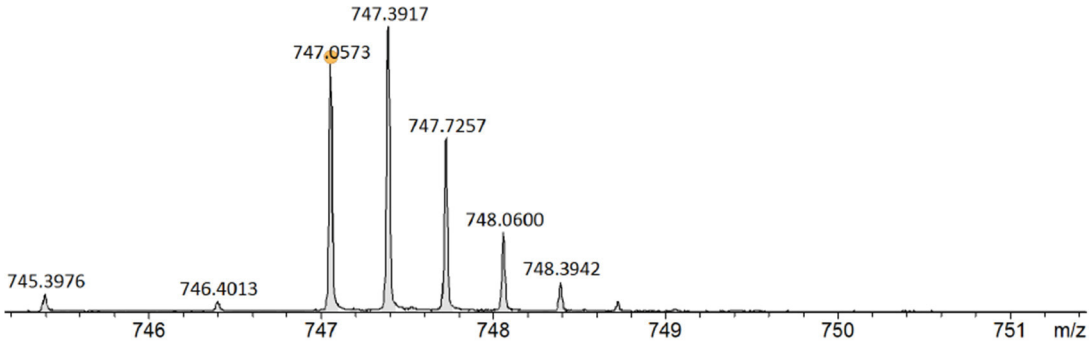

Figure S23: HR/ESI-MS spectrum of Gal(3,5)-7 (**8**).

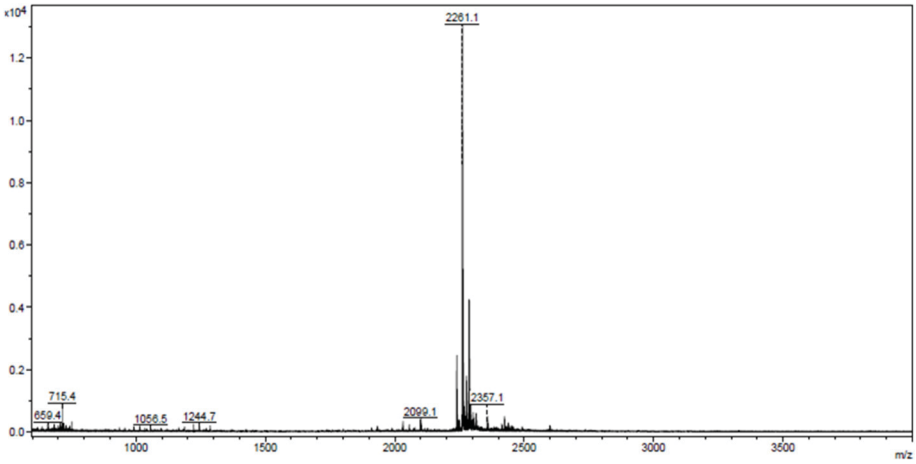

Figure S24: MALDI TOF MS spectrum of Gal(3,5)-7 (**8**).

3 Surface plasmon resonance spectroscopy (SPR)

Table S1: IC_{50} values and relative inhibitory potencies (RIP) from SPR measurements.

Glycooligomer	n[a]	IC_{50} [nM][b]	RIP[c]	RIP/n[c,d]
MeFuc	1	381 ± 47	1	1
1	1	130 ± 12	2.9	2.9
2	2	65 ± 6	5.9	2.9
3	3	36 ± 6	10.6	3.5
4	4	36 ± 5	10.6	2.6
5	6	22 ± 3	17.3	2.9
MeFuc	1	397 ± 103	1	1
3	3	51 ± 5	7.8	2.6
6	3	57 ± 6	7.0	2.3
7	3	66 ± 6	6.0	2.0

[a]Number of fucose units on the oligomeric backbone. [b]IC_{50} values determined by three independent measurements with standard error of the mean value (SEM). [c]Relative inhibitory potencies based on MeFuc, RIP = IC_{50} (MeFuc)/IC_{50} (glycooligomer). [d]Relative inhibitory potency per fucose unit of oligomer (RIP/n).

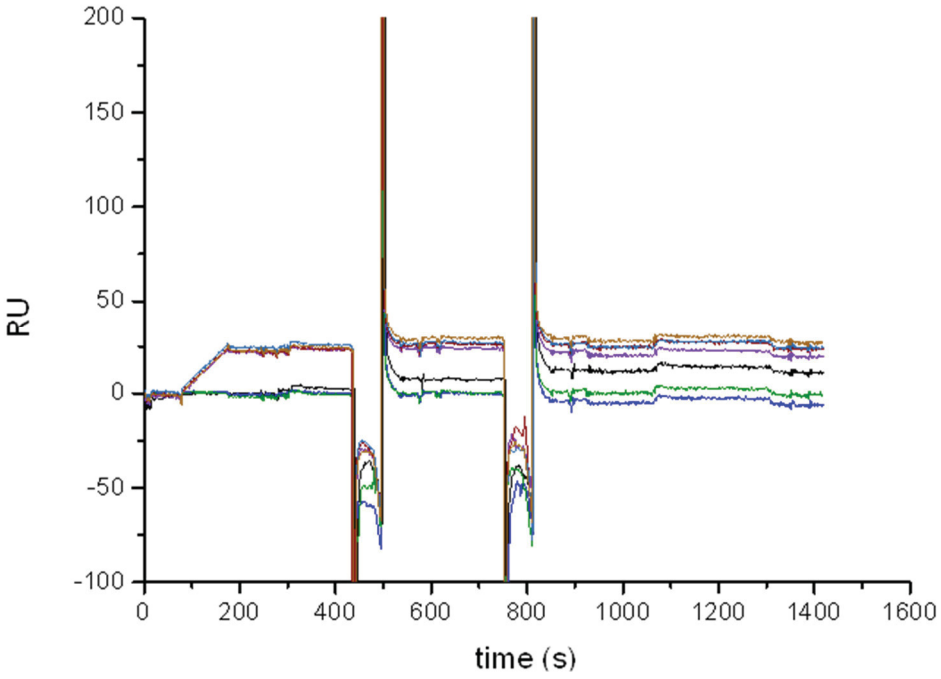

Figure S25: 4-cycle test measurement with LecB (200 nM) and buffer run (3x)

3.1 Sensograms and evaluated binding curves from SPR

In following section raw data of SPR multicycle measurements are shown for each ligand separately. One inhibition competition assay for a specific ligand usually included: two startup cycles of Tris buffer (cycle 1 and 2), the series of incubated LecB (200 nM) with increasing amount of ligand dilutions (usually cycles 3-11), a solution of LecB only (200 nM) in Tris buffer (cycle 12), one duplicate measurement of a LecB-ligand complex (cycle 13), a solution of ligand only (maximal ligand conc.) in Tris buffer (cycle 14).

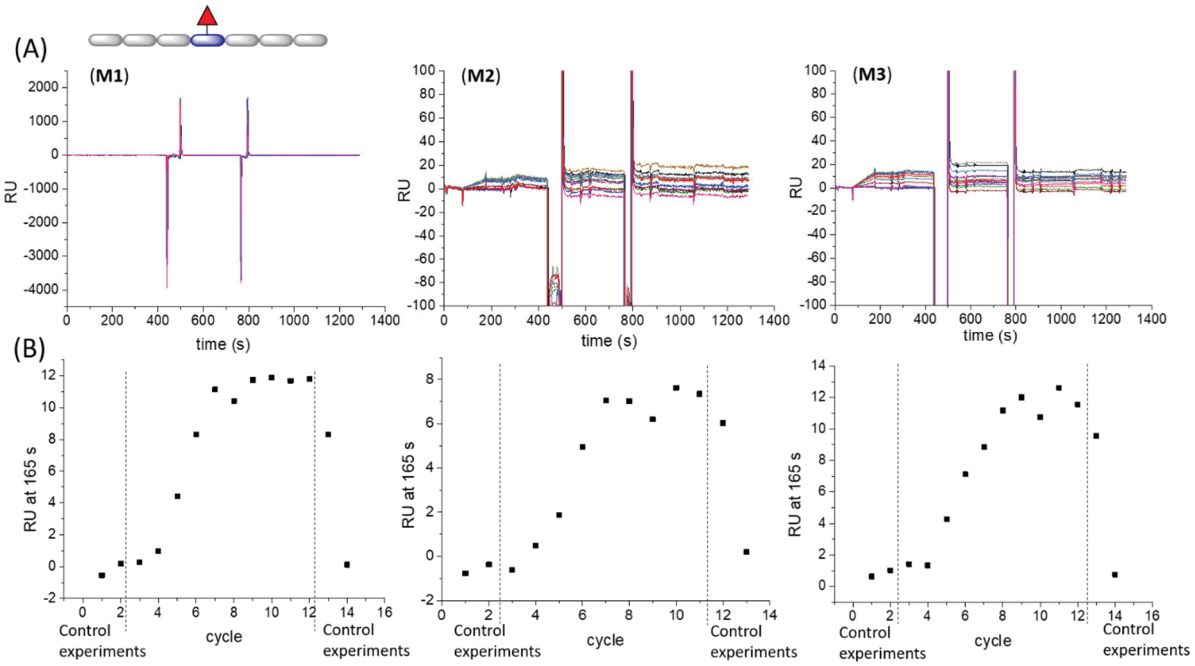

Figure S26: Raw data of three independent measurements (M1-M3) with Fuc(4)-7 (**1**) (1800 nM, 600 nM, 200 nM, 100 nM, 66.66 nM, 22.22 nM, 7.41 nM, 2.47 nM, 0.82 nM) (**A**) and corresponding evaluated binding at 165 sec (**B**) from first experiment.

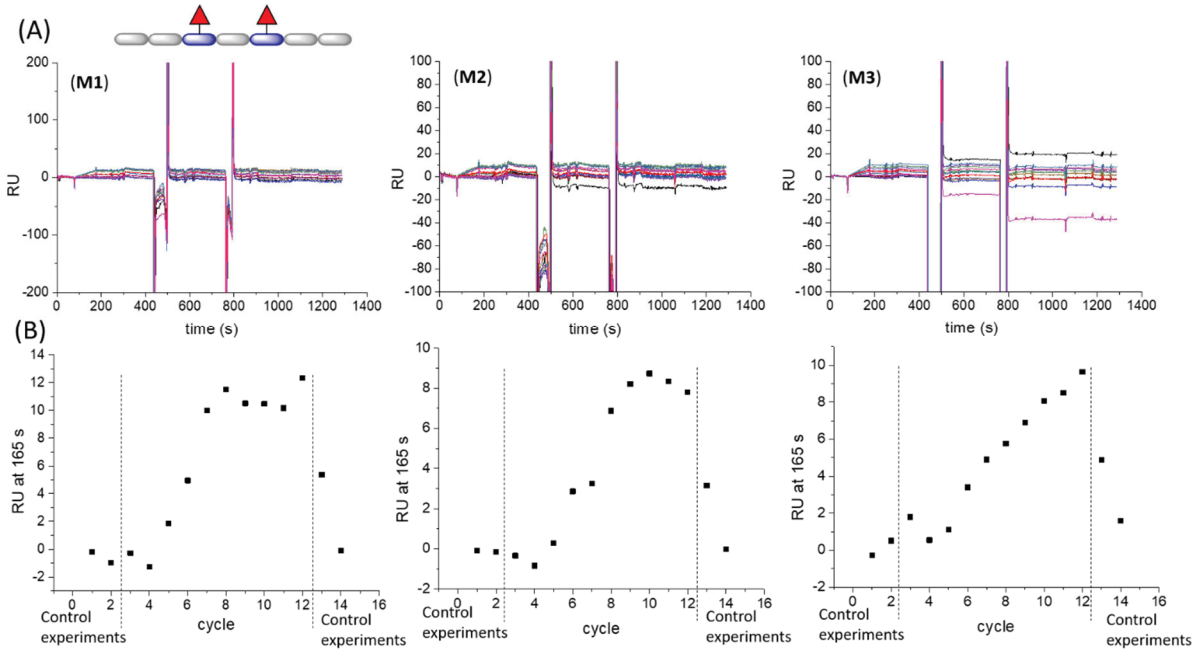

Figure S27: Raw data of three independent measurements (M1-M3) with Fuc(3,5)-7 (**2**) (1800 nM, 600 nM, 200 nM, 100 nM, 66.66 nM, 22.22 nM, 7.41 nM, 2.47 nM, 0.82 nM) (**A**) and corresponding evaluated binding at 165 sec (**B**) from first experiment.

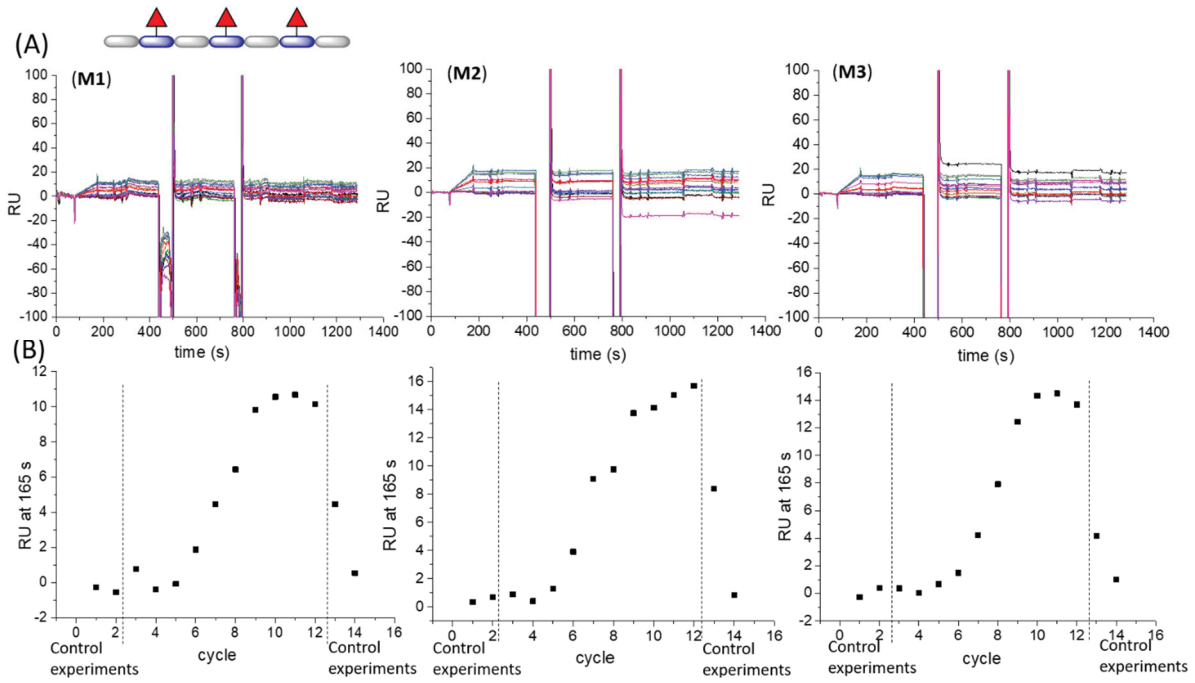

Figure S28: Raw data of three independent measurements (M1-M3) with Fuc(2,4,6)-7 (**3**) (1800 nM, 600 nM, 200 nM, 100 nM, 66.66 nM, 22.22 nM, 7.41 nM, 2.47 nM, 0.82 nM) (**A**) and corresponding evaluated binding at 165 sec (**B**) from first experiment.

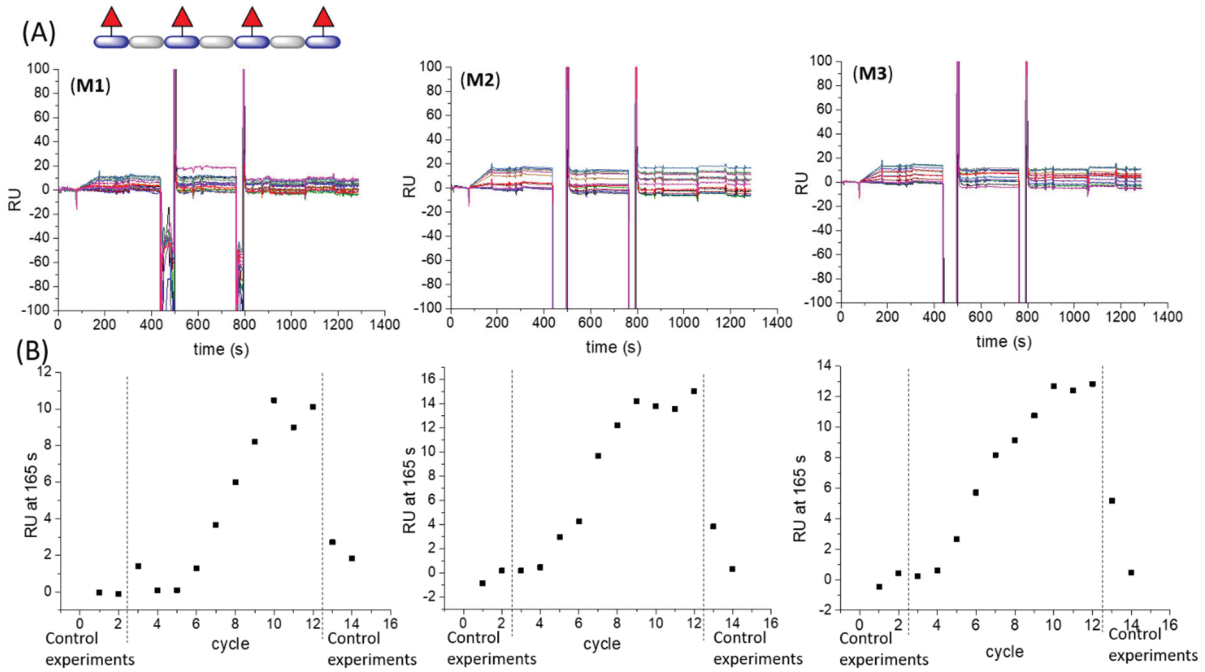

Figure S29: Raw data of three independent measurements (M1-M3) with Fuc(1,3,5,7)-7 (**4**) (600 nM, 200 nM, 100 nM, 66.66 nM, 22.22 nM, 7.41 nM, 2.47 nM, 0.82 nM, 0.28 nM) (**A**) and corresponding evaluated binding at 165 sec (**B**) from first experiment.

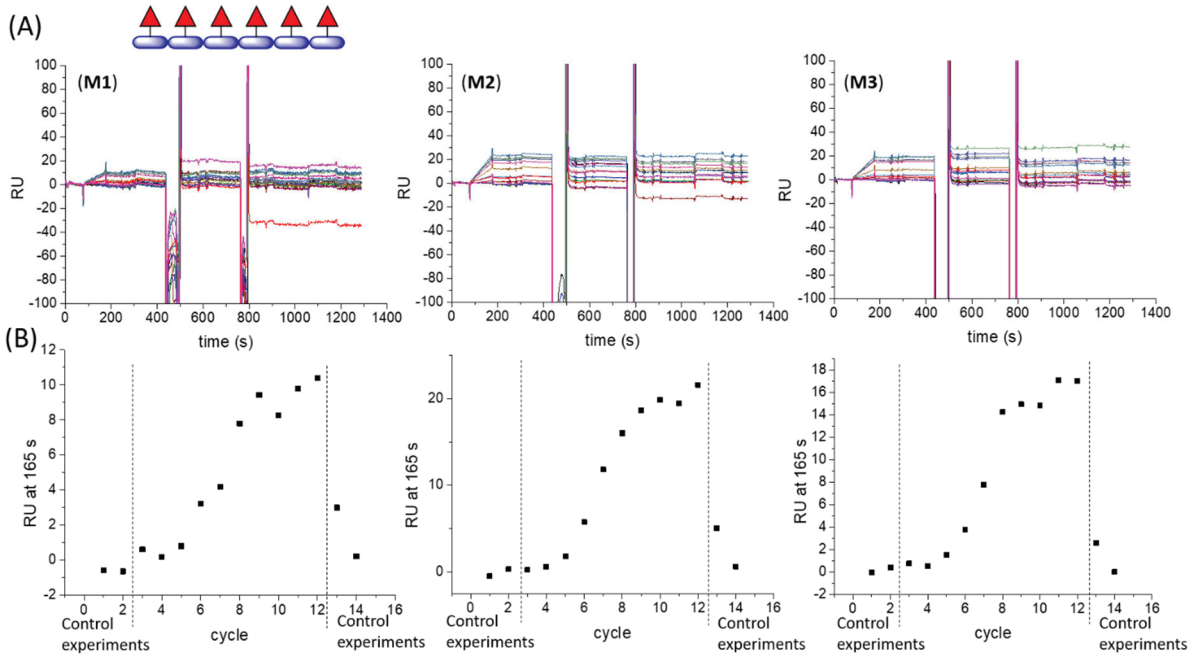

Figure S30: Raw data of three independent measurements (M1-M3) with Fuc(1,2,3,4,5,6)-6 (**5**) (600 nM, 200 nM, 100 nM, 66.66 nM, 22.22 nM, 7.41 nM, 2.47 nM, 0.82 nM, 0.28 nM) (**A**) and corresponding evaluated binding at 165 sec (**B**) from first experiment.

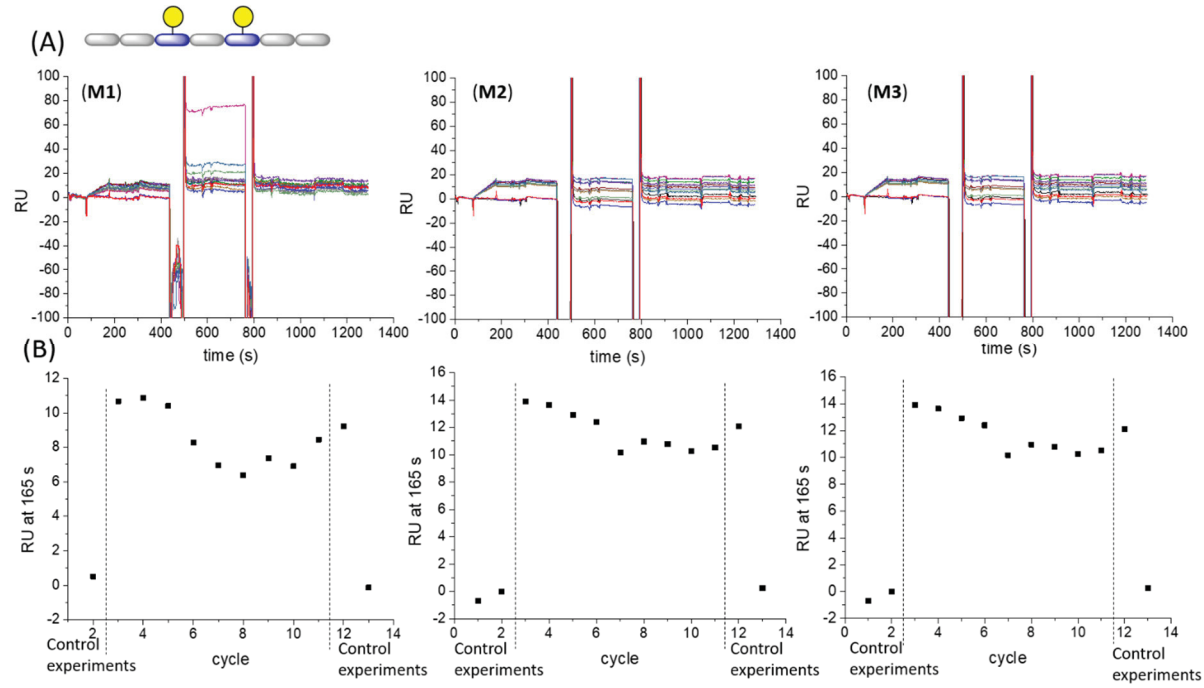

Figure S31: Raw data of three independent measurements (M1-M3) with Gal(3,5)-7 (**8**) (1800 nM, 600 nM, 200 nM, 66.66 nM, 22.22 nM, 7.41 nM, 2.47 nM, 0.82 nM) (**A**) and corresponding evaluated binding at 165 sec (**B**) from first experiment.

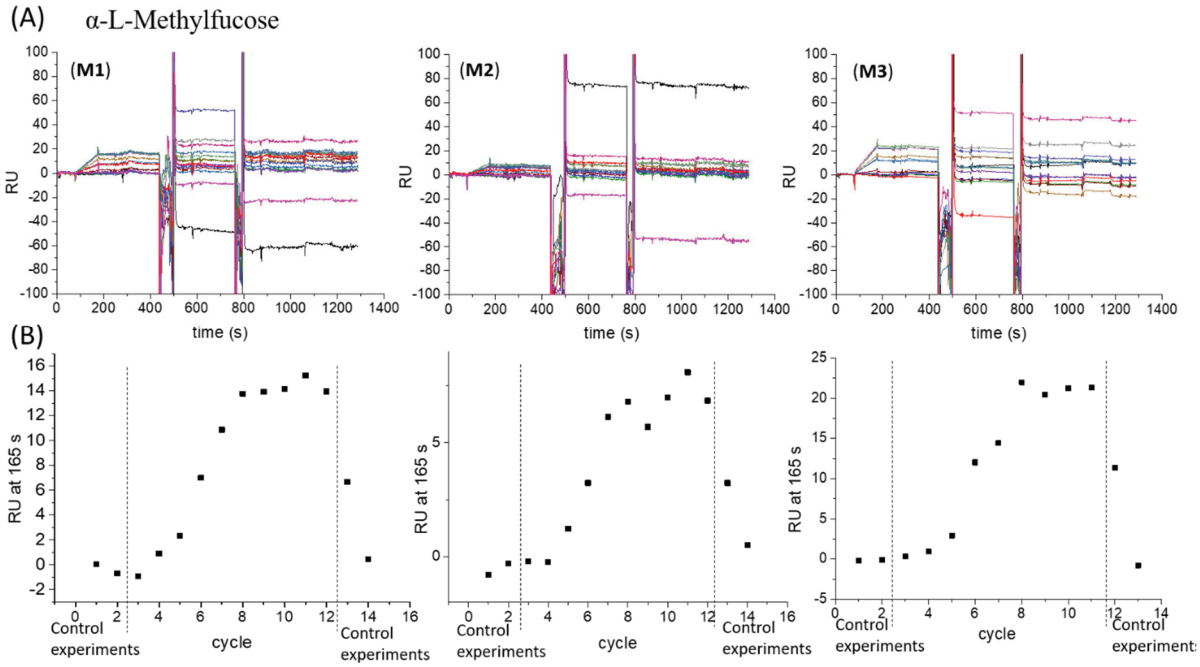

Figure S32: Raw data of three independent measurements (M1-M3) with methylfucose (10.0 µM, 3.33 µM, 1.11 µM, 370 nM, 123 nM, 41 nM, 14 nM, 4.6 nM, 1.5 nM) (**A**) and corresponding evaluated binding at 165 sec (**B**) from first experiment.

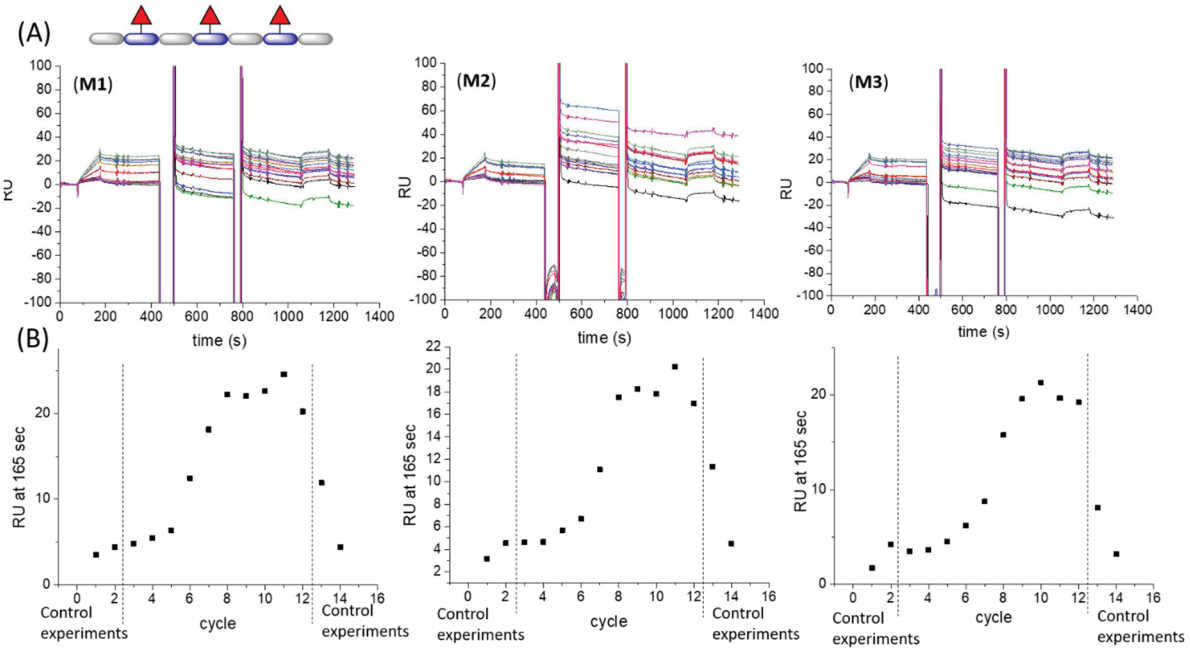

Figure S33: Raw data of three independent measurements (M1-M3) with Fuc(2,4,6)-7 (**3**) (1800 nM, 600 nM, 200 nM, 100 nM, 66.66 nM, 22.22 nM, 7.41 nM, 2.47 nM, 0.82 nM) (**A**) and corresponding evaluated binding at 165 sec (**B**) from second experiment.

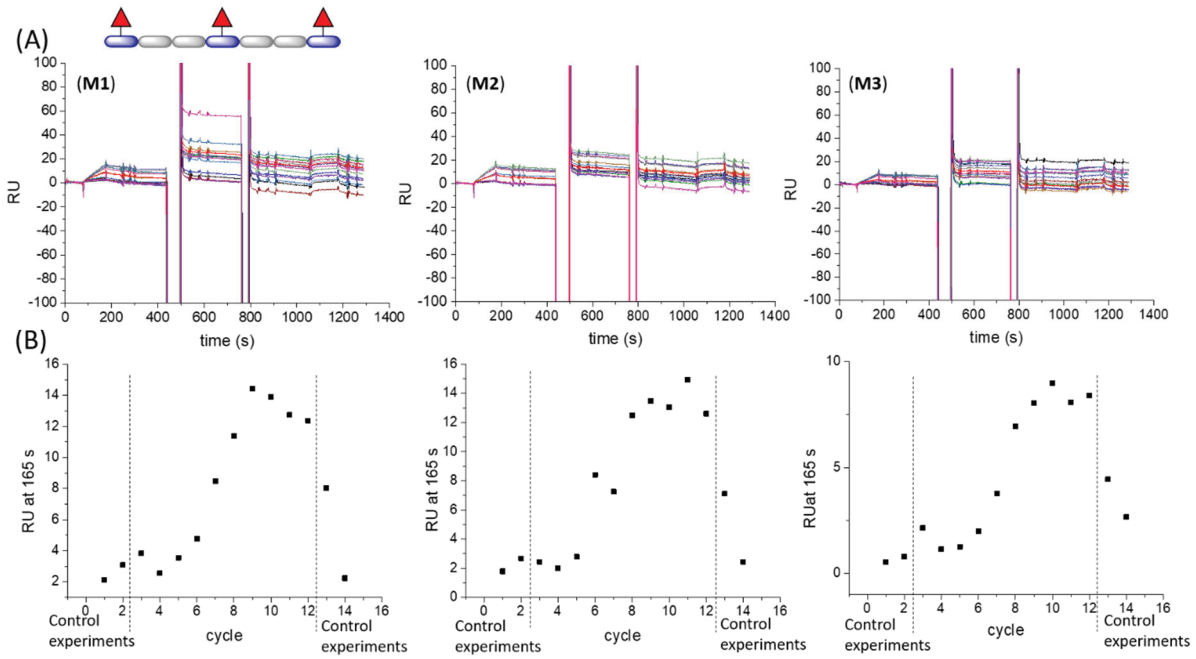

Figure S34: Raw data of three independent measurements (M1-M3) with Fuc(1,4,7)-7 (**6**) (1800 nM, 600 nM, 200 nM, 100 nM, 66.66 nM, 22.22 nM, 7.41 nM, 2.47 nM, 0.82 nM) (**A**) and corresponding evaluated binding at 165 sec (**B**) from second experiment.

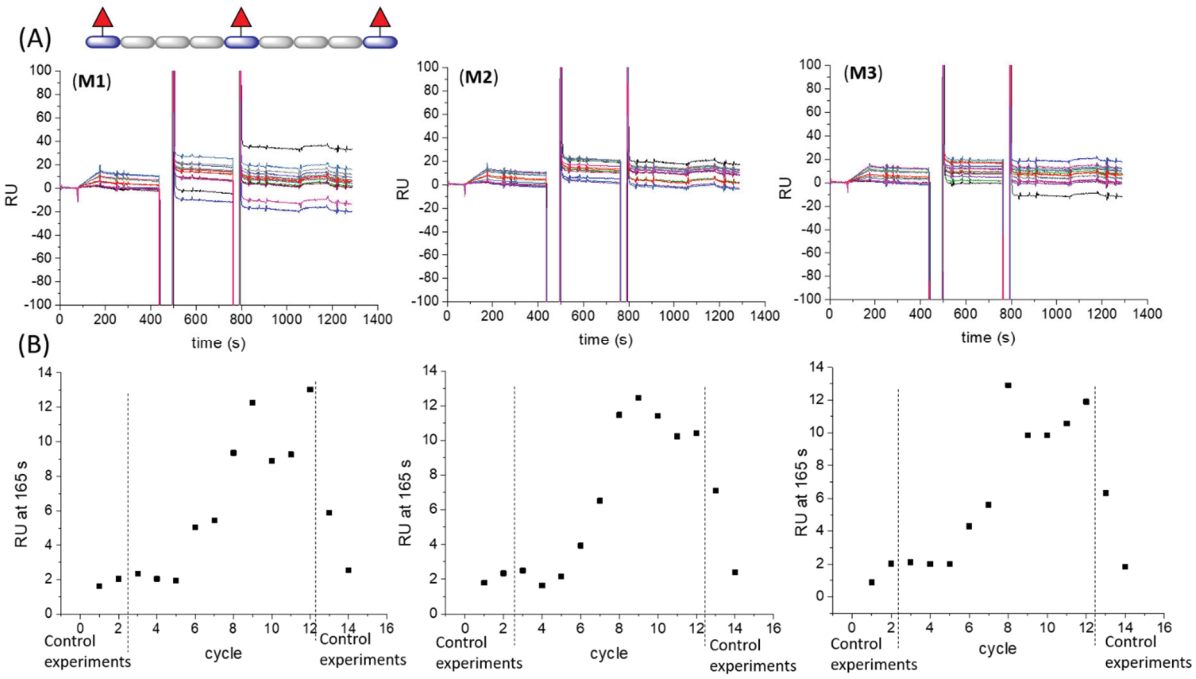

Figure S35: Raw data of three independent measurements (M1-M3) with Fuc(1,5,9)-9 (**7**) (1800 nM, 600 nM, 200 nM, 100 nM, 66.66 nM, 22.22 nM, 7.41 nM, 2.47 nM, 0.82 nM) (**A**) and corresponding evaluated binding at 165 sec (**B**) from second experiment.

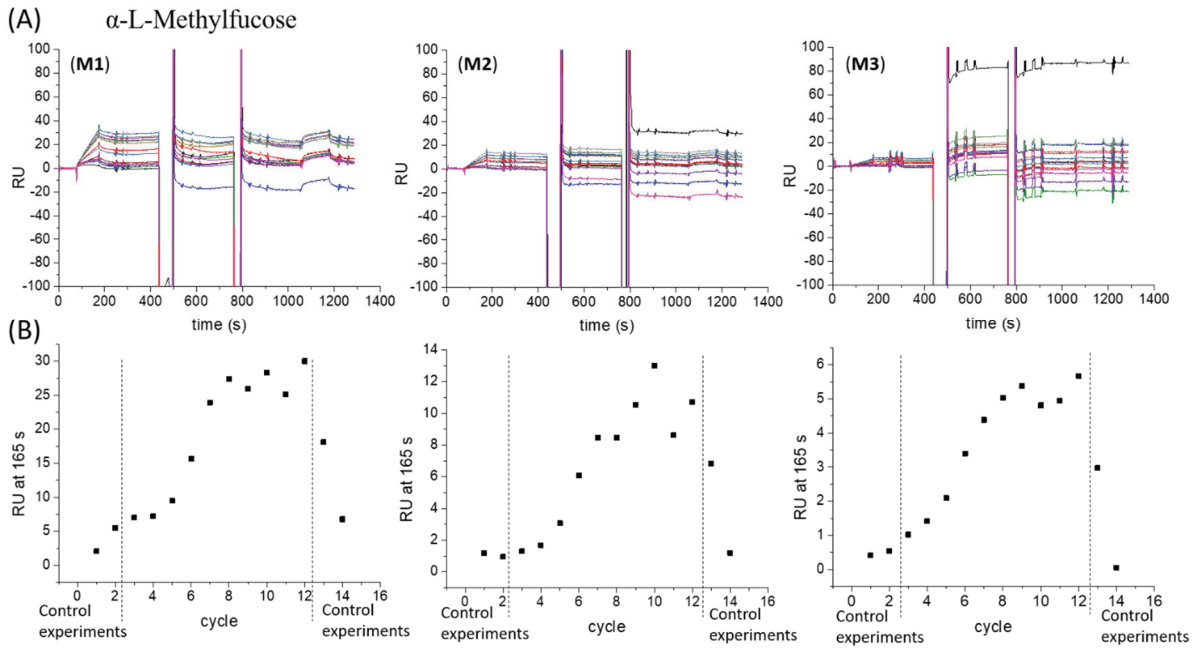

Figure S36: Raw data of three independent measurements (M1-M3) with methylfucose (10.0 µM, 3.33 µM, 1.11 µM, 370 nM, 123 nM, 41 nM, 14 nM, 4.6 nM, 1.5 nM) (**A**) and corresponding evaluated binding at 165 sec (**B**) from second experiment.

3.2 IC_{50} curves of independent SPR measurements

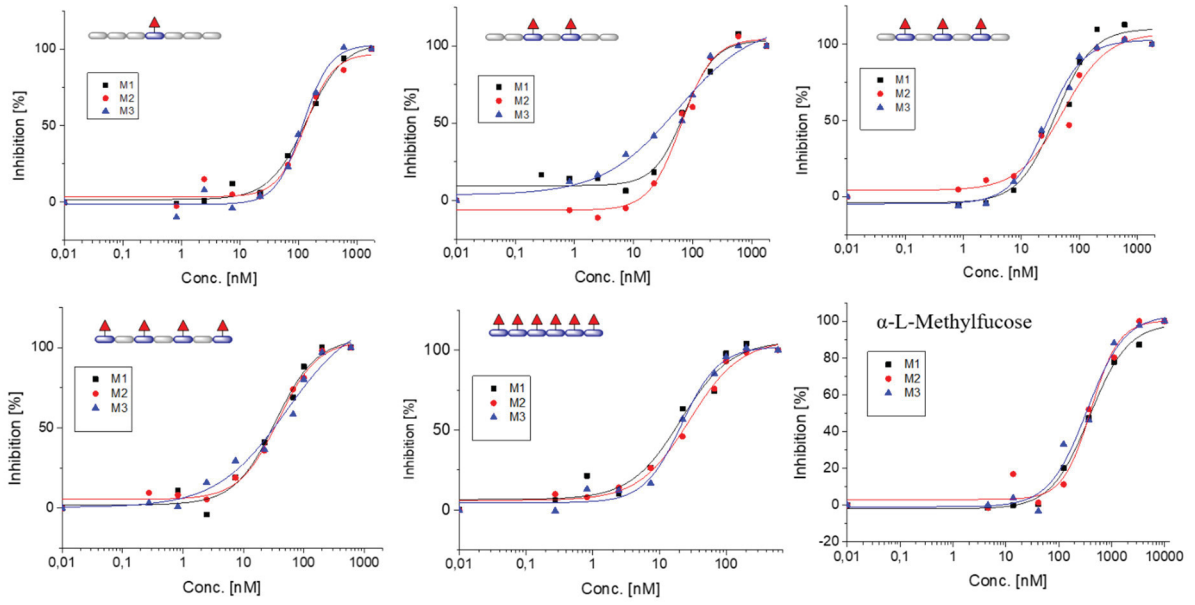

Figure S37: IC_{50} curves of triplicate measurements (M1-M3) from experiment 1, evaluating influence of valency.

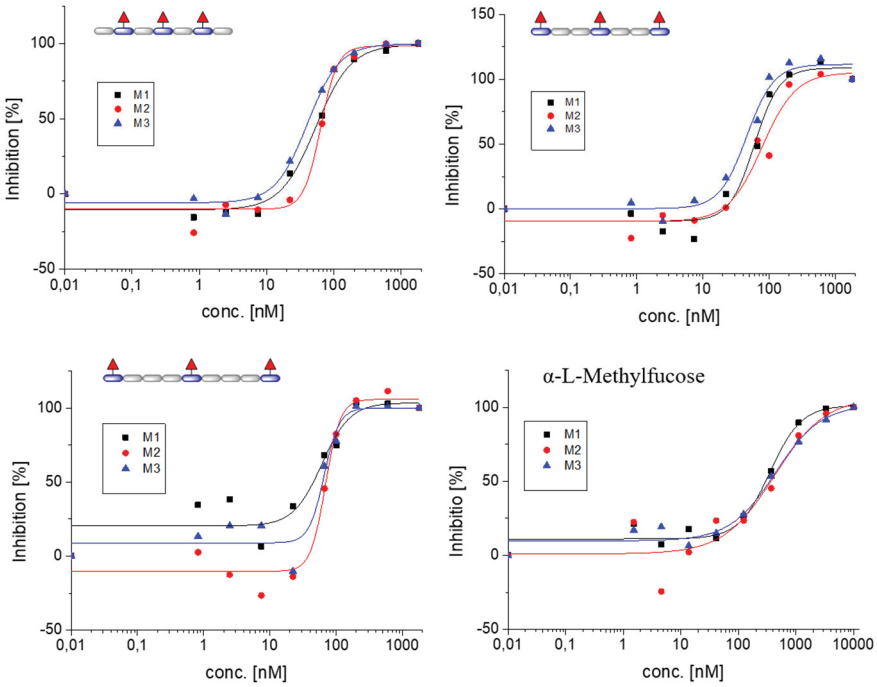

Figure S38: IC_{50} curves of triplicate measurements (M1-M3) from experiment 2, evaluating influence of fucose spacing.

3.3 IC_{50} curves of SPR measurement

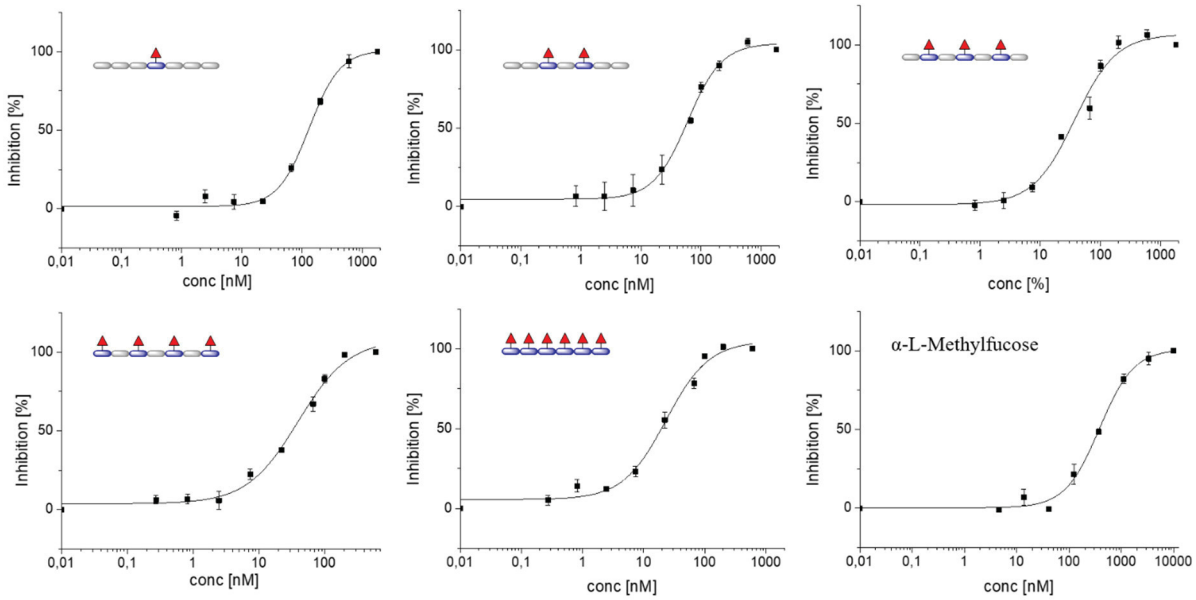

Figure S39: final IC_{50} curves of mean values from experiment 1, evaluating influence of valency.

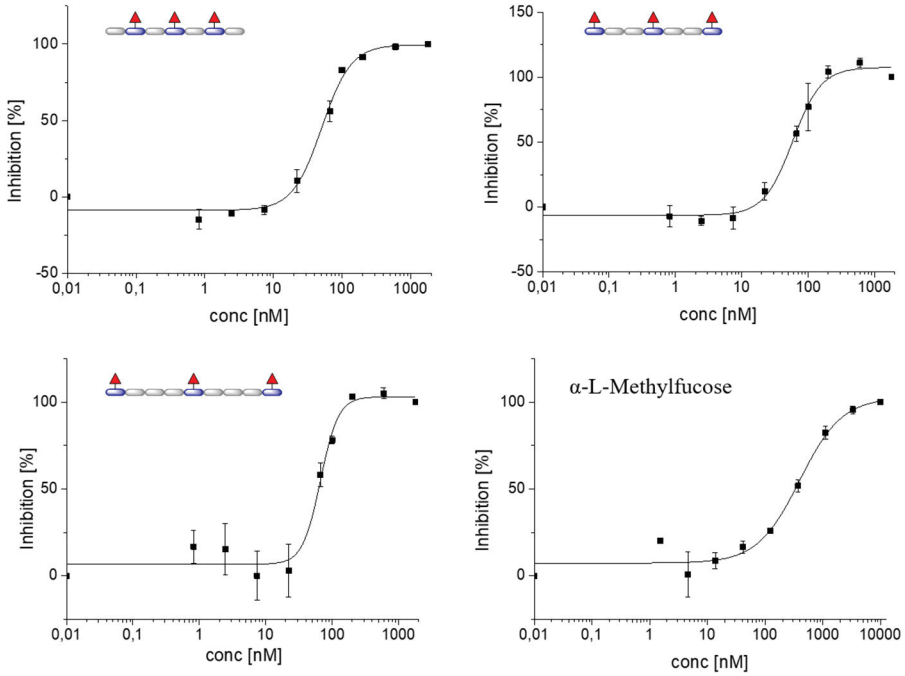

Figure S40: Final IC_{50} curves of mean values from experiment 2, evaluating influence of fucose spacing.

4. Modified Enzyme Linked Lectin Assay (mELLA)

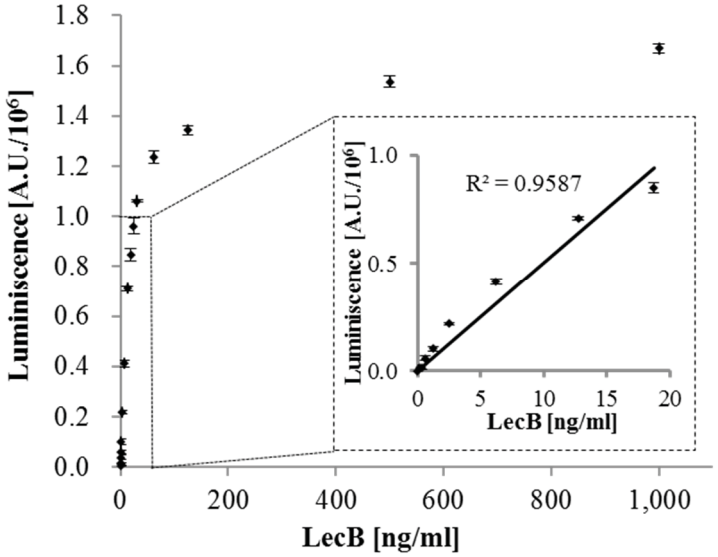

Figure S41: Saturation curve of LecB obtained by mELLA. Microtiter plate with fucosylated surface was incubated with 0.13-1000 ng/mL LecB followed by washing of unbound LecB and quantification of bound LecB with anti-LecB antiserum. Inset show enlarged linear part of the saturation curve. The results are mean ± standard deviation of three experiments each performed with three samples.

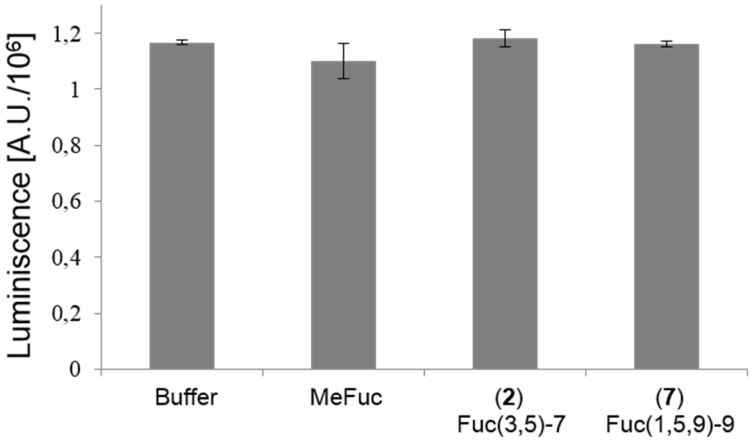

Figure S42: Stability of fucosylated solid surface in presence of the inhibitors. Microtiterplate was coated with FPA as described above and binding of LecB (15 ng/mL) to the FPA-plate was tested after incubation (1 h, 37°C) with 1.2 – 33 µM inhibitor.

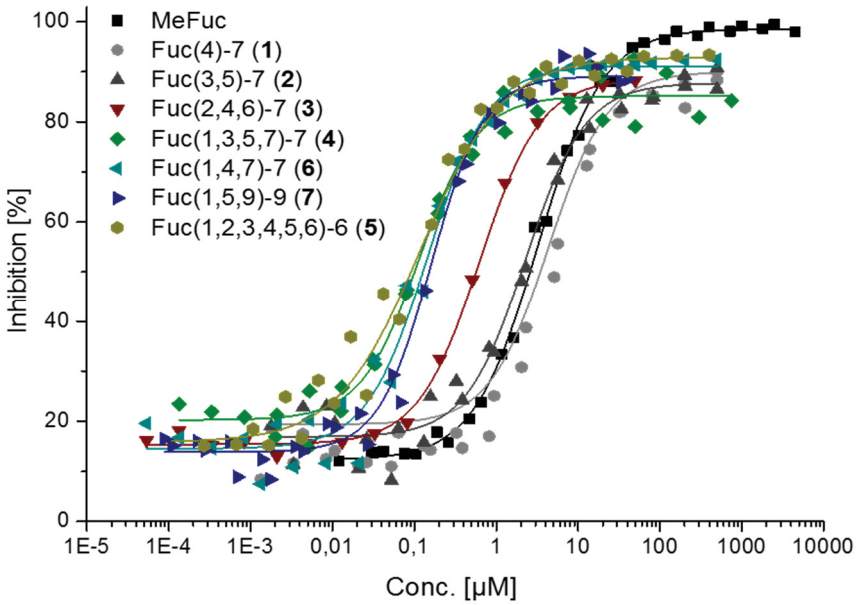

Figure S43: Competitive inhibitory effect of fucosylated glycooligomers and α-L-methylfucose on LecB binding to α-L-fucose-PAA-biotin was tested by mELLA assay. Sigmoidal curves represent averaged three independent experiments performed in triplicates.

Table S2: IC_{50} values and relative inhibitory potencies (RIP) of MeFuc and glycooligomers **1-7** determined by mELLA.

Glycooligomer	n[a]	IC_{50} [µM][b]	RIP[c]	RIP/n[c,d]
MeFuc	1	3.21 ± 0.21	1.0	1.0
1	1	4.41 ± 0.49	0.7	0.7
2	2	2.29 ± 0.33	1.4	0.7
3	3	0.61 ± 0.06	5.3	1.8
4	4	0.10 ± 0.01	31.4	7.9
5	6	0.11 ± 0.02	28.6	4.8
6	3	0.13 ± 0.01	24.1	8.0
7	3	0.18 ± 0.01	17.6	5.9

[a]Number of fucose units on the oligomeric backbone. [b]IC_{50} values determined by three independent measurements with standard error of the mean value (SEM). [c]Relative inhibitory potencies based on MeFuc, RIP = IC_{50} (MeFuc)/IC_{50} (glycooligomer). [d]Relative inhibitory potency per fucose unit of oligomer (RIP/n).

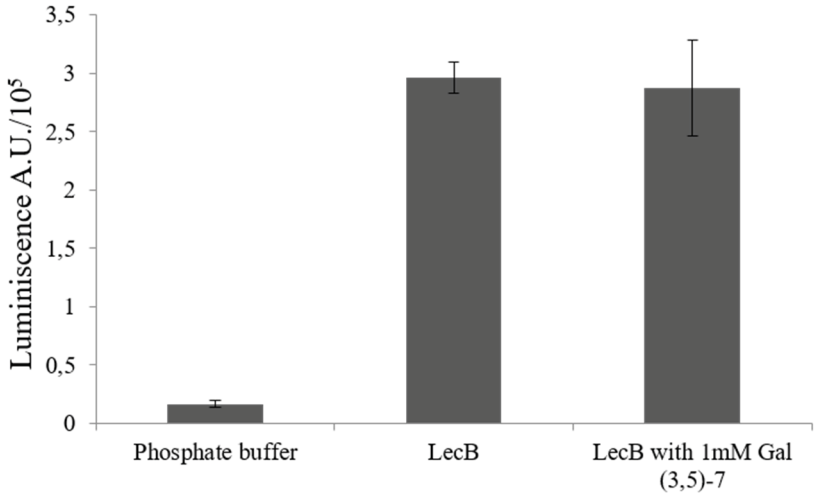

Figure S44: Effect of galactose functionalized glycooligomer (**8**) onto binding of LecB measured with mELLA. The sample without any LecB (phosphate buffer) represent the blank. The absolute luminescence value for LecB incubated with Gal(3,5)-7 (**8**) inhibitor was comparable with the value for LecB without added inhibitor (LecB). Results are mean ± standard errors of three measurements.

4.1 IC_{50} curves of mELLA assays

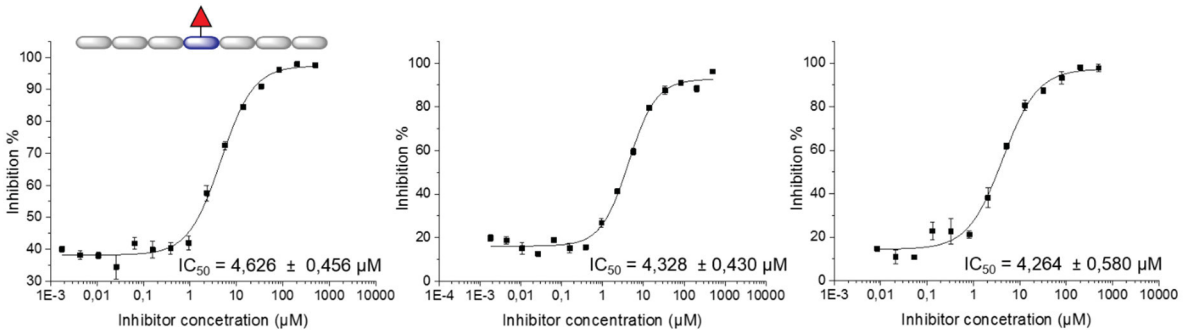

Figure S45: IC_{50} curves and corresponding IC_{50} values of three mELLA measurements (triplicates) with Fuc(4)-7 (**1**).

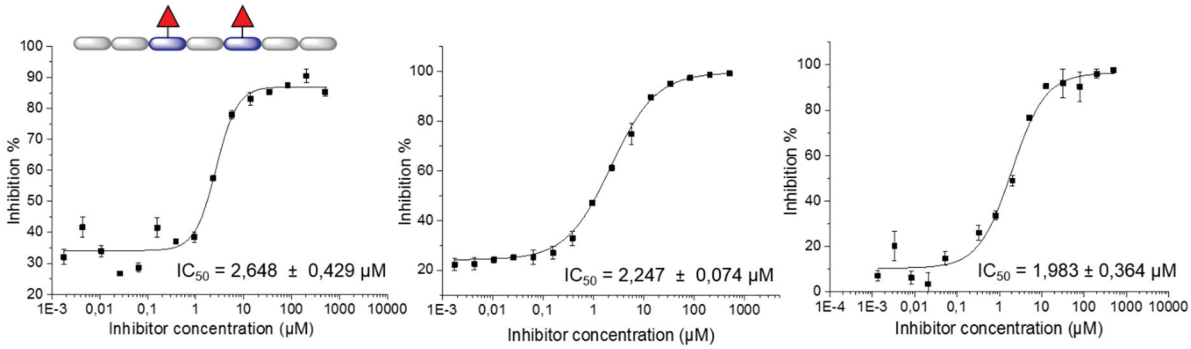

Figure S46: IC_{50} curves and corresponding IC_{50} values of three mELLA measurements (triplicates) with Fuc(3,5)-7 (**2**).

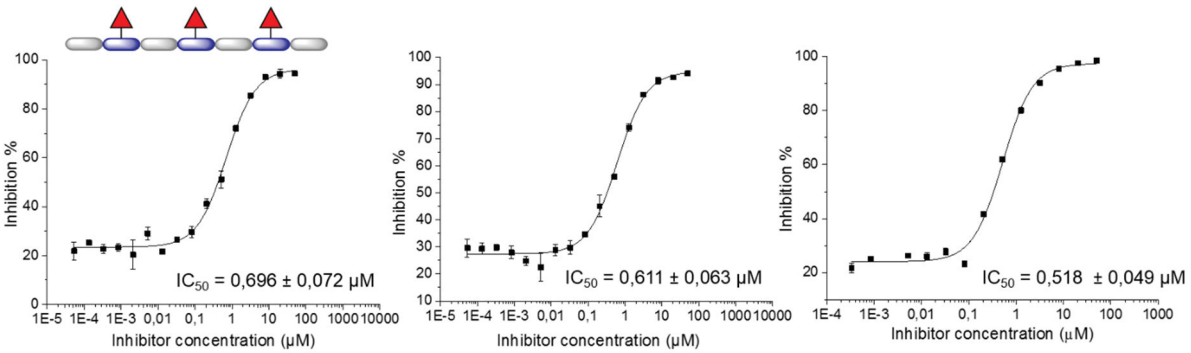

Figure S47: IC_{50} curves and corresponding IC_{50} values of three mELLA measurements (triplicates) with Fuc(2,4,6)-7 (**3**).

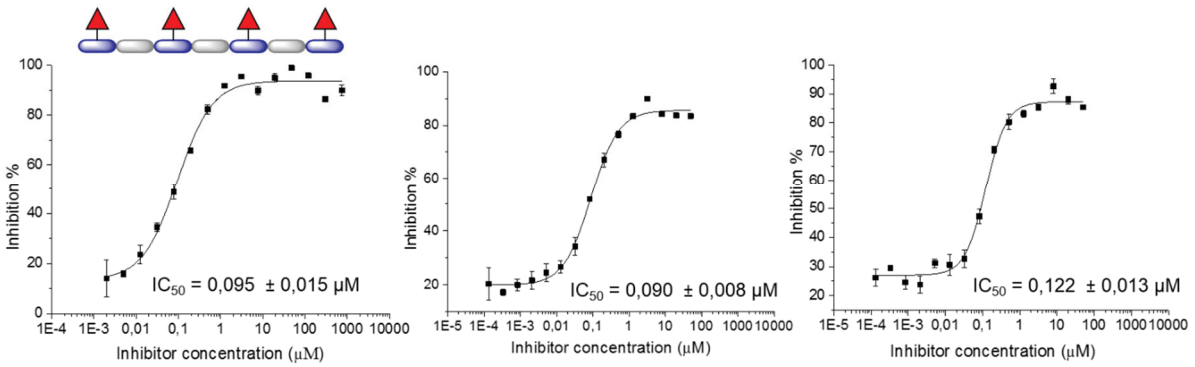

Figure S48: IC_{50} curves and corresponding IC_{50} values of three mELLA measurements (triplicates) with Fuc(1,3,5,7)-7 (**4**).

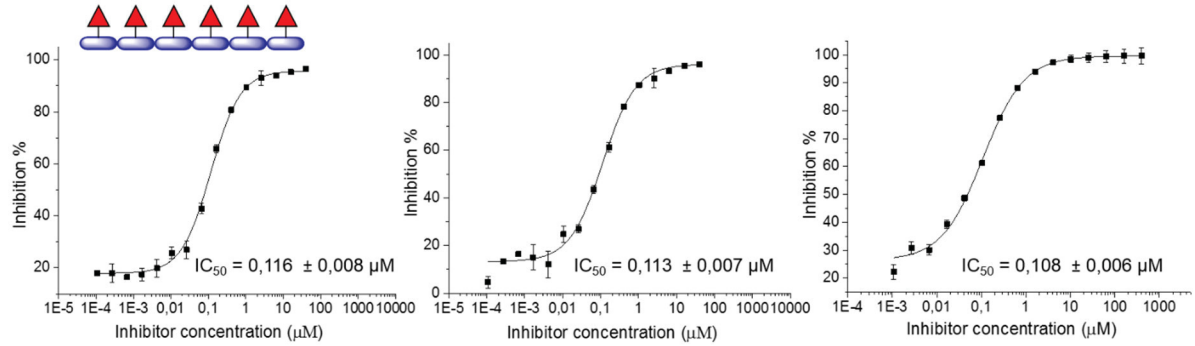

Figure S49: IC_{50} curves and corresponding IC_{50} values of three mELLA measurements (triplicates) with Fuc(1,2,3,4,5,6)-6 (**5**).

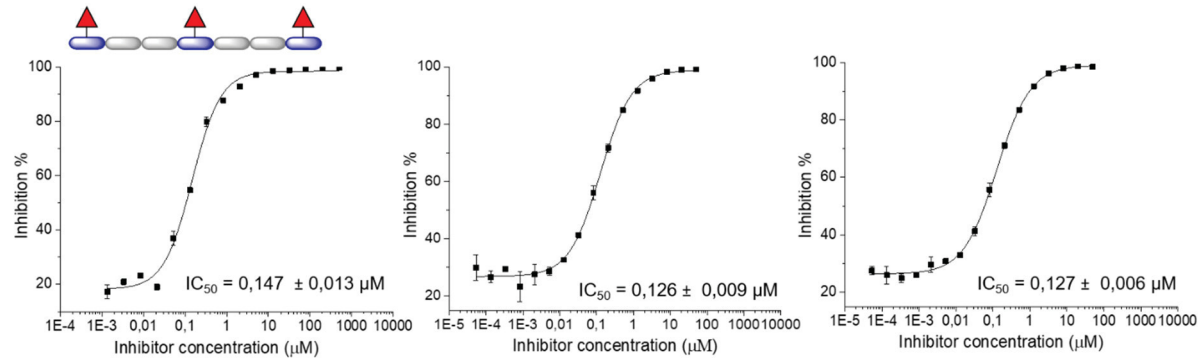

Figure S50: IC_{50} curves and corresponding IC_{50} values of three mELLA measurements (triplicates) with Fuc(1,4,7)-7 (**6**).

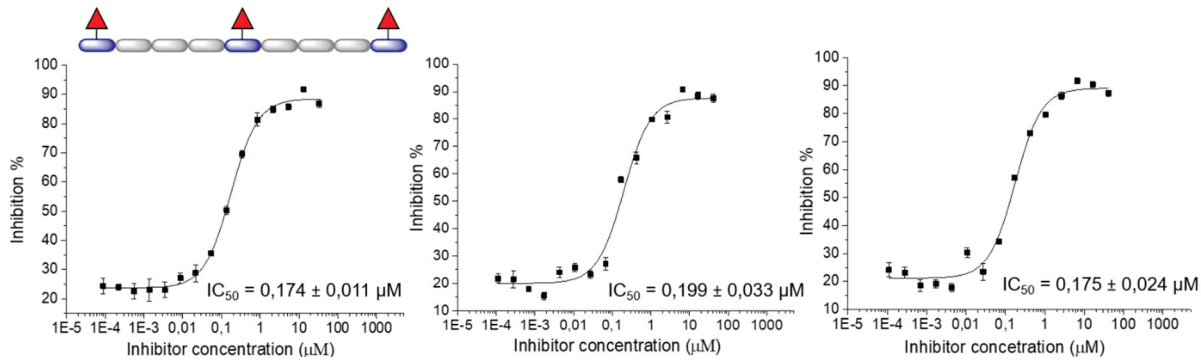

Figure S51: IC_{50} curves and corresponding IC_{50} values of three mELLA measurements (triplicates) with Fuc(1,5,9)-9 (**7**).

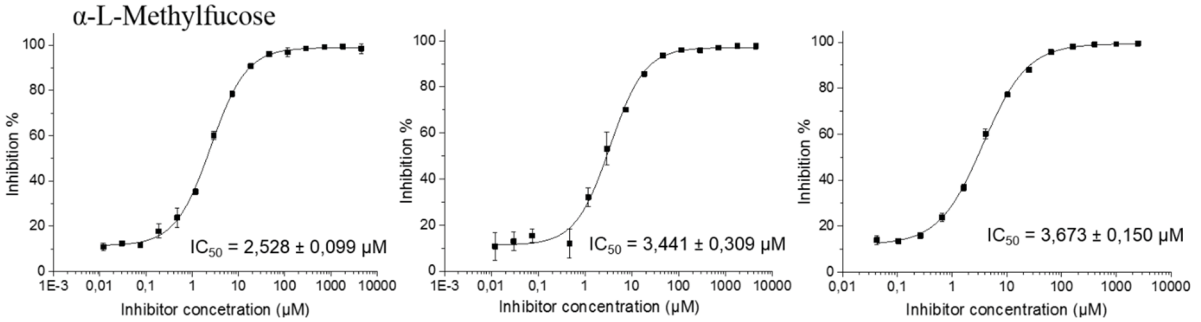

Figure S52: IC_{50} curves and corresponding IC_{50} values of three mELLA measurements (triplicates) with methylfucose.

4. References

[1] J. Geng, G. Mantovani, L. Tao, J. Nicolas, G. Chen, R. Wallis, D. A. Mitchell, B. R. G. Johnson, S. D. Evans, D. M. Haddleton, *J. Am. Chem. Soc.* **2007**, *129*, 15156-15163.

[2] K. S. Bücher, H. Yan, R. Creutznacher, K. Ruoff, A. Mallagaray, A. Grafmueller, J. S. Dirks, T. Kilic, S. Weickert, A. Rubailo, M. Drescher, S. Schmidt, G. Hansman, T. Peters, C. Uetrecht, L. Hartmann, Biomacromolecules **2012**, *13*, 1845-1852.

[3] D. Ponader, F. Wojcik, F. Beceren-Braun, J. Dernedde, L. Hartmann, *Biomacromolecules* **2012**, *13*, 1845.

[4] S. Roux, E. Zékri, B. Rousseau, M. Paternostre, J.-C. Cintrat, N. Fay, *J. Peptide Sci.* **2008**, *14*, 354-359.

5.3 Heteromultivalent glycooligomers as mimetics of blood group antigens

Katharina Susanne Bücher, Patrick Benjamin Konietzny, Nicole L. Snyder, Laura Hartmann

Chemistry a European Journal **2019**, *25* (13), 3301-3309

DOI: 10.1002/chem.201804505
Received 4 September 2018
First published (accepted manuscript) 15 November 2018
Published version of record online 07 February 2019
Published issue online 01 March 2019

https://doi.org/10.1002/chem.201804505

Own Contribution (first author)

Design and synthesis of *iso*-DTDS, synthesis of EDS and of alpha-functionalized carbohydrate ligands except azido-2,3,6,2´,3´4´,6´-hepta-*O*-acetyl-β-D-lactose (15) and step 1-2 of 2-azidoethyl-2,3,4,6-tetra-*O*-acetyl-α-D-galactopyranoside (14c) (2-Bromoethyl-α/β-D-galactopyranoside (14a) and 2-bromoethyl-2,3,4,6-tetra-*O*-acetyl-α-D-galactopyranoside (14b)). Synthesis of all glycooligomers. Characterization of all compounds by conducting HPLC-MS measurements and analyzing results of NMR, MALDI-TOF-MS and HR-ESI-MS, performance and analysis of SPR experiments, collaborative writing of manuscript.

ChemPubSoc Europe

DOI: 10.1002/chem.201804505

CHEMISTRY A European Journal Full Paper

Oligosaccharides |*Hot Paper*|

Heteromultivalent Glycooligomers as Mimetics of Blood Group Antigens

Katharina S. Bücher,[a] Patrick B. Konietzny,[a] Nicole L. Snyder,[b] and Laura Hartmann*[a]

Abstract: Precision glycomacromolecules have proven to be important tools for the investigation of multivalent carbohydrate–lectin interactions by presenting multiple glycan epitopes on a highly-defined synthetic scaffold. Herein, we present a new strategy for the versatile assembly of heteromultivalent glycomacromolecules that contain different carbohydrate motifs in proximity within the side chains. A new building block suitable for the solid-phase polymer synthesis of precision glycomacromolecules was developed with a branching point in the side chain that bears a free alkyne and a TIPS-protected alkyne moiety, which enables the subsequent attachment of different carbohydrate motifs by on-resin copper-mediated azide–alkyne cycloaddition reactions. Applying this synthetic strategy, heteromultivalent glycooligomers presenting fragments of histo-blood group antigens and human milk oligosaccharides were synthesized and tested for their binding behavior towards bacterial lectin LecB.

Introduction

Glycoconjugates are ubiquitous in nature and are important components of the extracellular matrix and glycocalyx, a dense layer of carbohydrate-based molecules on the cell surface. Their specific interactions with carbohydrate recognition receptors, such as lectins, play important roles in many biochemical processes,[1] including cell–cell communication, immune response, fertilization, cell migration,[2,3] and cancer metastasis.[3,4] Furthermore, they are known to mediate interactions with pathogens[5,6] such as viruses and bacteria that engage specific carbohydrates within the glycocalyx to attach, enter, and infect these cells. In particular, histo-blood group antigens (HBGAs), including ABO blood groups and Lewis antigens, represent important target structures for many pathogenic lectins.[6,7] While there are still many open questions concerning the biological function and role of HBGAs, such as their specificity towards selected pathogens, it has already been shown that glycomimetic structures[8] can be used as suitable model compounds to study the role of HBGAs, which in turn, may be used to develop new inhibitors for use in antibacterial or antiviral treatment.[9]

In principle, glycomimetic structures of HBGAs are built from a specific epitope fragment of the HBGA; in the simplest case, a fucose unit is presented in a multivalent fashion on a synthetic scaffold.[10] There are numerous reports of glycosylated macromolecular scaffolds and their binding interactions with pathogen-related lectins, such as LecB from *Pseudomonas aeruginosa*.[11,12] However, the question remains as to how the affinity and selectivity of HBGA mimetics might be altered by including not only one but several different glycan fragments that imitate more closely the natural ligand's heterofunctional structure.[13–15] Indeed, it has been shown that the combination of different carbohydrate moieties in heterofunctional glycoconjugates and glycomimetic structures strongly affects their recognition process.[16] Therefore, we introduce here a new strategy towards obtaining glycomimetic ligands by using an oligo(amidoamine) scaffold with sequence-controlled divalent heterofunctional glycan side chains that are based on different fragments of HBGA and human milk oligosaccharide (HMO) ligands.

Previously, we reported the synthesis of sequence-controlled glycooligo(amidoamines), the so-called precision glycomacromolecules, and their use as multivalent glycomimetic ligands.[17] In short, tailor-made building blocks were assembled in a stepwise fashion on a solid support to introduce functional moieties in the side chains at defined positions within the scaffold that enabled the attachment of different carbohydrate ligands. The straightforward exchange of building blocks during synthesis provided us with access to a library of glycomacromolecules that varied by, for example, the number and position of carbohydrates, the overall length or architecture of the scaffold, the nature of the linkage between the carbohydrate and the scaffold and/or main-chain motifs.[18,19,20] Furthermore, we developed different methods to obtain heteromultivalent glycomacromolecules by using orthogonal coupling

[a] *K. S. Bücher, P. B. Konietzny, Prof. Dr. L. Hartmann*
Institute of Organic and Macromolecular Chemistry
Heinrich Heine University Düsseldorf
Düsseldorf (Germany)
E-mail: laura.hartmann@hhu.de

[b] *Prof. Dr. N. L. Snyder*
Department of Chemistry
Davidson College, Davidson, NC (USA)

Supporting information and the ORCID identification number(s) for the author(s) of this article can be found under:
https://doi.org/10.1002/chem.201804505.

strategies or throughthe sequential introduction of ligands during scaffold assembly.[21] Copper-mediated azide–alkyne cycloaddition (CuAAC) proved to be an important tool for the introduction of carbohydrate ligands, both for homo- and heteromultivalent glycomacromolecules, yielding highly efficient coupling directly on solid support. The required alkyne and azido functional groups can be placed either on the building block, such as TDS (triple bond diethylenetriamine succinyl; 1-(fluorenyl)-3,11-dioxo-7-(pent-4-ynoyl)-2-oxa-4,7,10-triazatetradecan-14-oic acid)[17] or BADS (*p*-(azidomethyl)benzoyl diethylenetriamine succinyl),[19] or on the carbohydrate ligand. In this study, we extended this approach by introducing a new building block that contained two alkyne groups (one free and one protected) that allowed for the controlled introduction of different carbohydrates by using CuAAC. After coupling of a first carbohydrate ligand using the free alkyne, the second, protected alkyne moiety was deprotected and conjugated with a second carbohydrate ligand by using the same reaction conditions (Scheme 1).

Results and Discussion

Building block synthesis: *iso*-DTDS (7)

To mimic the heteromultivalent presentation of neighboring monosaccharide motifs in branched oligosaccharide structures more closely, a new building block *iso*-DTDS (*iso*-di-triple-bond diethylenetriamine succinic acid) (**7**) was developed. *iso*-DTDS is based on a previously established key intermediate:[17,20] a diethylenetriamine with asymmetrically protected primary amine groups (Scheme 2) that allows for the introduction of functional side chains at the central secondary amine position. For *iso*-DTDS, the functional side chain exhibits a rigid phenylene linker as a branching point with two acetylene units, one of which is protected with a TIPS (triisopropylsilyl) group (Scheme 1). TIPS was selected because it is a well-established alkyne protecting group that can be selectively cleaved on solid support,[22] and allows for sequential CuAAC-based functionalization in the presence of another alkyne, in this case with azido functionalized carbohydrates.

Scheme 2 depicts the synthesis of *iso*-DTDS, and begins with compound **1**, in accordance to literature protocols,[23] from asymmetrically *meta*-halogenized benzoic acid **1a** (see the Supporting Information for synthesis details). After methyl protection of the acid group to give compound **1b**, thermoselective double Sonogashira reactions were conducted using a $Pd[P(Ph_3)]_4$/CuI catalytic system: initial substitution of the TIPS acetylene at C3 on the benzene ring (compound **1c**) was followed by trimethylsilyl(TMS)acetylene substitution at the C5 position. The resultant compound **1d** was then treated with KOH in THF to remove the TMS group and the methyl protecting groups simultaneously to give compound **1** in 71% overall yield.

The synthesis of *iso*-DTDS is based on previous reports for key intermediate **2** (trityl- and TFA-protected diethylenetriamine).[17,20] Compound **1** was coupled to the free secondary

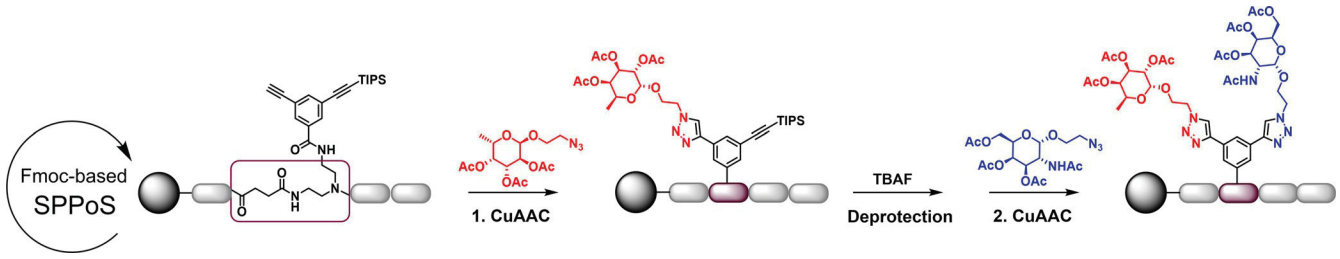

Scheme 1. Introduction of a new building block during solid-phase polymer synthesis provides for the asymmetrical conjugation of ligands by coupling a carbohydrate ligand to the free alkyne by using CuAAC (e.g., fucose in red) followed by deprotection of the second alkyne moiety and coupling of a second carbohydrate ligand (e.g., GalNAc in blue).

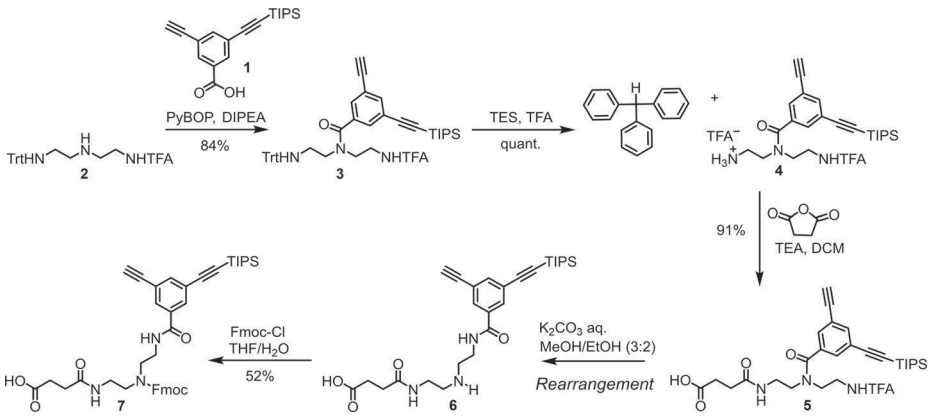

Scheme 2. Synthetic route for new building block *iso*-DTDS **7**, which combines precursor **1**[23] and key intermediate **2**.[17,20]

amine of compound **2** by using PyBOP (benzotriazol-1-yl-oxy-tripyrrolidinophosphonium hexafluorophosphate) and DIPEA (*N*,*N*-diisopropylethylamine). The resulting intermediate **3** was treated with TFA and triethylsilane (TES) as a scavenger to cleave the trityl protecting group providing a mixture of compound **4** and triphenylmethane. Crude product **4** was used in the next reaction step without further purification. The C-terminal carboxylic acid group was introduced using succinic anhydride. Compound **5** was isolated by precipitation into aqueous citric acid solution. In the next step, the TFA-protecting group was removed. As previously described by Baier et al., a rearrangement can occur during this step.[19] Formation of the primary amine and the rearrangement product was monitored by LC-MS (see the Supporting Information). Running the reaction at 60 °C for 8 h followed by stirring at room temperature for 16 h afforded only isomerized product **6** with minor impurities from the TIPS-cleaved side product. After removal of the solvent, crude product **6** was treated with Fmoc chloride, which yielded the final *iso*-DTDS building block **7** after purification. *iso*-DTDS was obtained in 40% overall yield from compound **2** and 98% purity, as determined by integration of UV signals in RP(reversed-phase)-HPLC (see the Supporting Information). ^{1}H NMR spectra of *iso*-DTDS were recorded in [D_6]DMSO and [D_4]MeOH (Figure 1; see the Supporting Information). In [D_6]DMSO, the characteristic amide protons of isomerized building block **7** were observed at $\delta = 8.77$ and 7.90 ppm as well as the carboxylic acid proton at $\delta =$ 12.01 ppm (Figure 1A). Unfortunately, the broad solvent peak at $\delta = 3.38$ ppm complicates the analysis of the methylene protons of *iso*-DTDS (see the Supporting Information). Therefore, additional analysis was performed in [D_4]MeOH (Figure 1B). As a result, signals for the TIPS protecting group at $\delta = 1.12$ ppm and the Fmoc protecting group between $\delta = 7.0$–8.0 ppm for aromatic protons and $\delta = 4.39$ and 4.16 ppm for aliphatic protons were clearly visible in the ^{1}H NMR spectrum (for detailed analysis, see the Supporting Information).

Synthesis of glycooligomers

Syntheses of precision glycooligo(amidoamines) were performed by applying previously reported procedures of Fmoc-based solid-phase polymer synthesis.[17] *iso*-DTDS was combined with the previously established ethylenedioxy-bis(ethylamine) succinyl building block (EDS)[17] by using PyBOP as a coupling reagent (Scheme 3). Coupling efficiency of *iso*-DTDS was evaluated by Fmoc quantification that was based on UV/Vis measurements of the cleavage solution for test sequence (EDS–*iso*-DTDS–EDS) for both single and double coupling with 5 and 3 equivalents of building block, respectively. Coupling efficiencies for the introduction of *iso*-DTDS were about 86% for the single coupling and 95% for the double coupling. The use of alternative coupling reagents did not improve the coupling efficiency: coupling with DIC and HATU showed 21 and 80% product formation, respectively, for a single coupling (PyBOP: 86%). EDS building block coupling onto the *iso*-DTDS chain end yielded 96% efficiency under standard coupling conditions (see the Supporting Information), which shows that chain elongation is successful after introduction of *iso*-DTDS. On the basis of these results, further glycooligo(amidoamines) were synthesized by using standard coupling conditions for EDS (see the Supporting Information) and double coupling for *iso*-DTDS (3 equiv of building block and PyBOP with 30 equiv of DIPEA in DMF for 1.5 h).

Scheme 3 shows the solid-phase synthesis of heteromultivalent glycooligomers using *iso*-DTDS. After assembly of the oligomer backbone and acetylation of the final amine group, carbohydrate ligands were conjugated to the *iso*-DTDS side chain. As a first step for all glycooligomers, acetylated α-L-fucopyra-

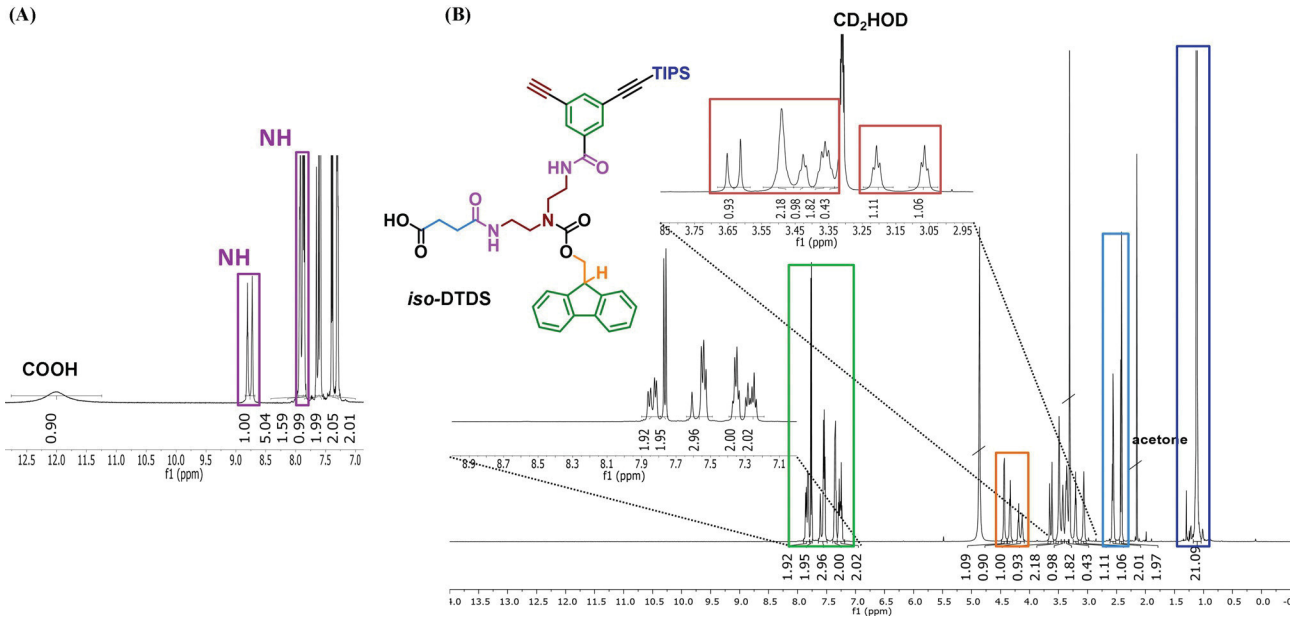

Figure 1. ^{1}H NMR spectra of *iso*-DTDS: A) excerpt of spectrum in [D_6]DMSO; B) full spectrum in [D_4]MeOH.

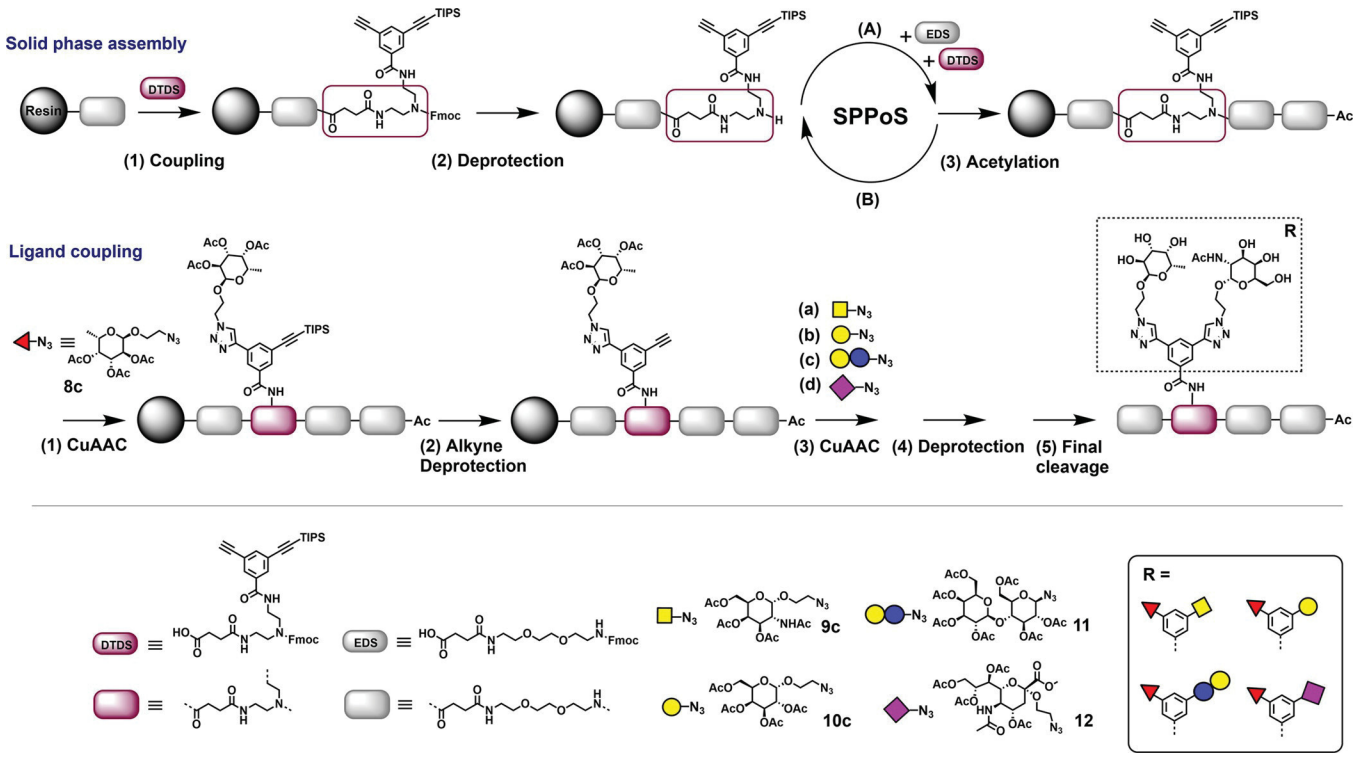

Scheme 3. Strategy for the synthesis of heteromultivalent glycooligomers by applying *iso*-DTDS; the introduction of different carbohydrate units by consecutive CuAAC on solid support.

nosylazide (**8c**, Fuc) was coupled in accordance with previously established CuAAC conditions. After removing excess reagents by successive washing, the TIPS-protecting group was cleaved with TBAF in DMF.[24] The corresponding glycooligomer could then be subjected to a second CuAAC reaction with another azido-functionalized carbohydrate derivative (e.g., GalNAc (**9c**), Gal (**10c**), Lac (**11**), or Sia (**12**)). In the final step, carbohydrate side chains were deacetylated on resin, and the crude final glycooligomers were cleaved off the resin under acidic conditions and isolated by precipitation and lyophilization.

Following this protocol, a first generation of homo- and heteromultivalent glycooligomers that introduce two *iso*-DTDS building blocks and thereby four carbohydrate ligands were synthesized (Figure 2). In total, six glycooligomers were synthesized by using a scaffold with the sequence EDS–*iso*-DTDS–EDS–EDS–*iso*-DTDS–EDS. We first introduced Fuc, a common monosaccharide motif found in different HBGAs, through CuAAC conjugation to the unprotected alkyne on the side chains of the DTDS. The corresponding glycooligomer was then split into four batches and further functionalized with either a GalNAc, Gal, Lac, or Sia residue after TIPS deprotection to generate glycooligomers **13**–**16** (Figure 2). In addition, a homomultivalent all-Fuc glycooligomer **17** and an all-Gal glycooligomer **18** were synthesized for comparison in later binding studies. The aromatic unit in the glycomimetic structures was installed with the aim of mimicking the branching sugar unit in the natural trisaccharide.An additional ethyl linker was introduced via the functionalized monosaccharides in an effort to balance the rigidity of the aromatic branching unit.

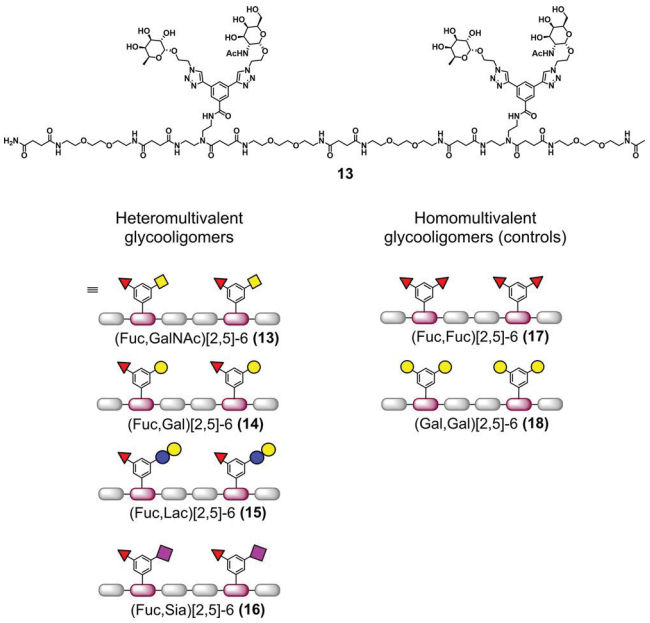

Figure 2. Hetero- and homomultivalent glycooligomer structures as HBGA and HMO mimicry.

Nomenclature of glycooligomers follows previously introduced systematics: the carbohydrates attached to a single branching unit (*iso*-DTDS) are written in brackets (e.g., (Fuc,Gal)) followed by the position of *iso*-DTDS within the oligomer chain and the overall chain length, as given by the total

number of building blocks; for example, (Fuc,Gal)[2,5]-6 for glycooligomer **14**.

Crude glycooligomers were directly analyzed by RP-HPLC/MS (see the Supporting Information) after cleavage off the resin. The results demonstrate that the glycooligomers are synthesized in good purity (72–85%). Nevertheless, all structures were further purified by using an ion-exchange resin and semi-preparative RP-HPLC to give the final structures in high purities (>99%) (see the Supporting Information). Glycooligomer **16**, which contained two Sia ligands, was isolated bearing a methyl protecting group (**16-Me**). After purification, glycooligomer **16-Me** was subjected to cleavage of the methyl group to give glycooligomer **16** (Table 1). Final analysis of glycooligomer structures was performed by ^{1}H NMR, RP-HPLC/MS, HRMS (ESI), and MALDI-TOF MS (see the Supporting Information).

Table 1. Analytical data of glycooligomers **13**–**18**.

Glycooligomer	Type of sugar	Natural model fragment	MW [g mol^{-1}]	Yield[a] [%]
13	Fuc/GalNAc	HBGA A	2701.88	40
14	Fuc/Gal	Lewis^a	2619.78	49
15	Fuc/Lac	2'Fucosyllactose (2'FL)	2855.95	46
16-Me	Fuc/Sia(Me)	–	2906.06	40
16	Fuc/Sia	Sialyl-Lewis^a	2878.01	36
17	Fuc/Fuc	Control	2587.78	26
18	Gal/Gal[b]	Negative control	2651.77	36

[a] Overall yield after purification by ion-exchange resin and semi-preparative HPLC with a gradient of water/acetonitrile. [b] Alpha/beta mixture of galactose.

Lectin binding studies of heteromultivalent glycooligomers towards LecB

After the successful synthesis of the first generation of heteromultivalent glycooligomers that imitate fragments of HBGAs, we investigated their potential to act as HBGA mimetics by studying their binding behavior towards LecB from *Pseudomonas aeruginosa*. It is well known that LecB binds to different HBGAs and HMOs, of which Lewis^a shows higher affinity (K_D = 210 nM) than the monovalent ligand L-fucose (K_D = 2.9 μM).[25,12] We have previously reported a surface plasmon resonance (SPR) inhibition competition assay that allows for the measurement of half maximum inhibitory concentration (IC_{50}) values of glycooligomers binding to LecB.[26] In short, a commercially available streptavidin-coated sensor chip was functionalized with commercially available biotinylated polyacrylamide that contained either fucose (PAA-Fuc) as a positive control or galactose (PAA-Gal) as a negative control at the reference cell. Glycooligomers were preincubated for 1 h at different concentrations with LecB (200 nM) in TRIS-buffer, and the ligand/LecB complex was injected into the SPR sensor chip. Inhibitory potencies of glycooligomers were measured as the reduction of LecB adhesion to the fucosylated sensor chip surface with increasing amounts of glycooligomer. α-L-Methylfucose (MeFuc) was measured as a reference compound. Galactosylated oligomer **18** was used as a negative control, whereas homomultivalent fucosylated oligomer **17** served as a positive control for comparison of the effect of heteromultivalency in the HBGA mimetics **13**–**16**. Negative control glycooligomer **18** showed no binding to LecB (see the Supporting Information). Table 2 shows the results of the inhibition competition assay of glycooligomers **13**–**17** and α-L-methylfucose.

Table 2. Results from SPR inhibition competition assay of glycooligomers **13**–**17** and LecB (200 nM).

Ligand	n[a]	IC_{50} [nM][b]	RIP[c]	RIP/n[c,d]
MeFuc	1	300 ± 28	1 ± 0.1	1
	2	61 ± 16	4.9 ± 0.3	2.5
	2	35 ± 9	8.6 ± 0.3	4.3
	2	60 ± 11	5.0 ± 0.2	2.5
	2	76 ± 8	3.9 ± 0.1	2.0
	4	54 ± 8	5.6 ± 0.2	1.4

[a] Number of fucose units within the ligand. [b] IC_{50} values determined by two independent measurements with standard error of the mean (SEM). [c] Relative inhibitory potencies (RIP) based on α-L-methylfucose (MeFuc), RIP = IC_{50}(MeFuc)/ IC_{50}(glycooligomer). [d] Relative inhibitory potency normalized on fucose units per oligomer (RIP/n).

Compared with α-L-methylfucose, all glycooligomers showed increased inhibition of LecB (Table 2). Previously, we showed that binding to LecB increased with an increasing number of fucose units on the oligomeric backbone.[26] Surprisingly, positive control **17**, exhibiting a total of four fucose side chains, did not show an increase in binding compared with the heteromultivalent glycooligomers that present only two fucose ligands. For further comparison, we normalized the IC_{50} values on the IC_{50} value of α-L-methylfucose to provide relative inhibitory potencies (RIP) that can be further normalized to the number of fucose ligands (RIP/n) (Table 2). Indeed, RIP values fit well with previously investigated homomultivalent glycooligomers binding to LecB, for which an RIP/n of about 2–3 was observed.[26] Similar values for heteromultivalent glycooligomers **13**, **15**, and **16** indicate that the second carbohydrate motif seems to play no role in improving the overall binding to LecB. Only glycooligomer **14** with an additional galactose ligand in close proximity to the fucose ligand showed a lower IC_{50} value, and thereby, an increased binding. One possible ex-

planation could be a partial mimicking of the Lewis[a] ligand. Interestingly, Sialyl-Lewis[a] mimetic **16** did not show increased binding, although Sialyl-Lewis[a] is also known as a potent binder of LecB.[12] Therefore, further studies are required to investigate participation of the different carbohydrate motifs in LecB binding in more detail, for example, by STD-NMR or crystallography. Ongoing studies also include the analysis of the glycooligomer conformation, and thereby, the distance between carbohydrate side chains attached through the *iso*-DTDS building block, for example, by means of molecular modelling and light scattering.

Conclusion

A new building block, *iso*-DTDS, suitable for solid-phase polymer synthesis was used to introduce closely neighboring carbohydrate ligands in the side chains of precision glycomacromolecules. *iso*-DTDS can be used to create heteromultivalent glycooligomeric constructs that combine different carbohydrate motifs, and thereby, more closely mimic complex oligosaccharide ligands. In this report, *iso*-DTDS was applied to the synthesis of glycooligomers that contain fragments of HBGAs. Inhibitory potencies of these glycomimetic oligomers towards LecB were investigated. Interestingly, a glycooligomer with only Fuc ligands showed similar inhibitory effects as glycooligomers that combined Fuc ligands with GalNAc, Lac, or Sia moieties. Only the glycooligomer that combined Fuc and Gal residues showed a slight increase in the inhibitory potential, which indicates additional binding of the Gal ligands within the structure that is based on fragments of the natural Lewis[a] ligand. Overall, this strategy gives straightforward access to a variety of heteromultivalent glycooligomers and extends our platform of precision glycomacromolecules. Following the presented concept, macromolecular mimetics of other oligosaccharides or combinations of carbohydrates with additional non-carbohydrate binding motifs are now accessible.

Experimental Section

Synthesis of *iso*-DTDS

Key intermediate **2**[17,20] and precursor intermediate **1**[23] were synthesized according to literature procedures.

3-Ethynyl-5-[(triisopropylsilyl)ethynyl]benzoic acid (1): Aqueous KOH solution (15 mL, 0.2 g mL^{-1}, 3 g, 53 mmol, 3.7 equiv) was added to a solution of methyl-3-((triisopropylsilyl)ethynyl)-5-((trimethylsilyl)ethynyl)benzoate (**1d**) (5.98 g, 14.5 mmol, 1 equiv) in THF (15 mL), and the reaction mixture was stirred for 24 h at room temperature. Upon completion, 15 mL of water were added and a precipitate formed. The THF was evaporated, and the remaining aqueous suspension was cooled with an ice bath. Aqueous HCl (58 mL, 174 mmol, 3 M, 12 equiv) was added, and the mixture was stirred for at least 1 h. The obtained solid precipitate was isolated by vacuum filtration and dried under high vacuum overnight to afford 3-ethynyl-5-((triisopropylsilyl)ethynyl)benzoic acid (**1**) as a colorless solid (4.35 g, 13.3 mmol, 92%). ^{1}H NMR (600 MHz, $CDCl_3$): $\delta = 8.15$ (p, $^4J = 1.6$ Hz, 2H, H_{Ar}-2, H_{Ar}-6), 7.8 (t, $^4J = 1.6$ Hz, 1H, H_{Ar}-4), 3.15 (s, 1H, C≡C-*H*), 1.15–1.13 ppm (m, 21H, -C*H*-(CH_3)$_2$); ^{13}C NMR (75.5 MHz, $CDCl_3$): $\delta = 170.7$ (-COOH), 140.3 (C_{Ar}-4), 133.8 (C_{Ar}-2), 133.4 (C_{Ar}-6), 129.9 (C_{Ar}-1), 124.8 (C_{Ar}-5), 123.2 (C_{Ar}-3), 104.7 (*C*≡C-TIPS), 93.6 (C≡*C*-TIPS), 81.7 (*C*≡C-H), 79.1 (C≡*C*-H), 18.8 (CH_3), 11.4 ppm (*C*H(CH_3)$_2$); $R_f = 0.46$ (CH_2Cl_2/MeOH, 10:1); LRMS (ESI): *m/z* calcd for $C_{20}H_{26}O_2Si$: 327.2 $[M+H]^+$; found: 327.2; HRMS (ESI): *m/z* calcd for $C_{20}H_{26}O_2Si$: 327.1775 $[M+H]^+$; found: 327.1772; RP-HPLC: (eluent **B,** for composition of eluent B see Supporting Information, gradient from 80–100% over 10 min, then eluent **B**, 100%, for 17 min, 25 °C): $t_R = 5.8$ min, determined purity 98%.

3-Ethynyl-*N*-[2-(2,2,2-trifluoroacetamido)ethyl]-5-[(triisopropylsilyl)ethynyl]-*N*-[2-(tritylamino)ethyl]benzamide (3): Dialkyne acid **1** (2 g, 6.13 mmol, 1.05 equiv), PyBOP (3.19 g, 6.13 mmol, 1.05 equiv), HOBt (hydroxybenzotriazole, 0.89 g, 5.84 mmol, 1 equiv), and DIPEA (1.66 mL, 17.52 mmol, 3 equiv) were added to a solution of 2,2,2-trifluoro-*N*-(2-((2-(tritylamino)ethyl)amino)ethyl)acetamide (key intermediate **2**) (2.58 g, 5.84 mmol, 1 equiv) in DMF (40 mL). The mixture was stirred for 16 h at room temperature. The resulting yellowish solution was poured into water (400 mL) and left to stand overnight. The suspension was centrifuged, and the water was decanted. The solid product was redissolved in ethyl acetate and extracted three times with water. The organic phase was dried over $MgSO_4$, filtered, and concentrated in vacuum. Column chromatography (hexane/ethyl acetate, 3:1–2:1) afforded the product as colorless crystals (3.68 g, 4.9 mmol, 84%). ^{1}H NMR (600 MHz, $CDCl_3$): $\delta = 7.85$ (s, 1H, NH), 7.66 (s, 1H, H_{Bz}), 7.53 (s, 1H, H_{Bz}), 7.46 (s, 1H, H_{Bz}), 7.37 (d, $^3J = 7.8$ Hz, 6H, C(C_6H_5)$_3$), 7.28 (t, $^3J = 7.7$ Hz, 6H, C(C_6H_5)$_3$), 7.19 (t, $^3J = 7.3$ Hz, 3H, C(C_6H_5)$_3$), 3.63–3.61 (m, 2H, (C=O)NH-CH_2-CH_2), 3.51–3.48 (m, 2H, (C=O)NH-CH_2-CH_2), 3.43 (t, $^3J = 5.9$ Hz, 2H, C(Ph)$_3$-NH-CH$_2$-CH_2), 3.13 (s, 1H, C≡C-H), 2.25 (t, $^3J = 5.9$ Hz, 2H, C(Ph)$_3$-NH-CH_2), 1.13–1.12 ppm (m, 21H, -C*H*-(CH_3)$_2$); ^{13}C NMR (151 MHz, $CDCl_3$): $\delta = 172.6$ ((C=O)Ph), 157.8 ((C=O)CF_3), 157.6, 145.3 (C-1$_{Phenyl}$), 136.8 (C-4$_{Bz}$), 136.0 (C-1$_{Bz}$), 130.4 (C-2$_{Bz}$, C-6$_{Bz}$), 129.8 (C-2$_{Bz}$, C-6$_{Bz}$), 128.4 (*o*-C$_{Phenyl}$, *m*-C$_{Phenyl}$), 128.1 (*o*-C$_{Phenyl}$, *m*-C$_{Phenyl}$), 126.6 (*p*-C$_{Phenyl}$), 124.8 (C-5$_{Bz}$), 123.0 (C-3$_{Bz}$), 116.7 (CF_3), 104.7 (C-TIPS), 93.5 (C≡C-TIPS), 81.8 (*C*≡C-H), 79.2 (C≡*C*-H), 71.0 (*C*-Ph$_3$), 60.4 (*residual ethyl acetate*), 50.4 (N(CH$_2$)$_2$), 44.2 (N(CH$_2$)$_2$), 42.2 (NH-CH$_2$), 39.5 (NH-CH$_2$), 21.1 (*residual ethyl acetate*), 18.6 (CH_3), 14.2 (*residual ethyl acetate*), 11.3 ppm (*C*H(CH_3)$_2$); HRMS (ESI): *m/z* calcd for $C_{45}H_{50}F_3N_3O_2Si$ (monoisotopic mass 749.3624): 750.3697 $[M+H]^+$; found: 750.3699; RP-HPLC: (eluent **B**, gradient from 80–100% over 10 min, then eluent **B**, 100% for 17 min, 25 °C): $t_R = 11.2$ min, determined purity 99%. $R_f = 0.79$ (hexane/ethyl acetate, 1:1).

2,2,2-trifluoroacetaldehyde,2-{3-ethynyl-*N*-[2-(2,2,2-trifluoroacetamido)-ethyl]-5-[(triisopropylsilyl)ethynyl]benzamido}ethan-1-aminium salt (4): TES (10.8 mL, 68 mmol, 2.8 equiv) and TFA (26 mL, 337 mmol, 10% v/v) were added to a solution of compound **3** (18.09 g, 24.1 mmol, 1 equiv) in CH_2Cl_2 (240 mL). The colorless solution was stirred for 1 h at room temperature, and the reaction progress was determined by TLC (hexane/ethyl acetate, 1:1) until complete. The TFA was co-evaporated with toluene. The crude product, which contained triphenylmethane as a side product (1:1 mixture as determined by ^{1}H NMR), was obtained as a white solid (20.86 g crude mixture calcd to contain product: 14.9 g, 24 mmol, quant.). Remaining triphenylmethane was not successfully separated but could be removed in the next reaction step. The obtained crude product was used without further purification. $R_f = 0.72$ (CH_2Cl_2/MeOH, 5:1); ^{1}H NMR (600 MHz, $CDCl_3$): $\delta = 8.18$ (s, 3H, NH), 7.96 (s, 1H, (CO)NH), 7.63 (s, 1H, H_{Bz}), 7.43 (s, 1H, H_{Bz}), 7.38 (s, 1H, H_{Bz}), 7.30–7.27 (m, 6H, C_5H_6), 7.25 (*residual toluene*), 7.23–7.20 (m, 3H, C_5H_6), 7.17 (*residual toluene*), 7.13–7.11 (m, 6H, C_5H_6), 5.56 (s, 1H, C*H*$_3$-Ph$_3$), 3.81 (s, 2H, CH$_2$), 3.72 (s, 2H, NH), 3.55 (s, 2H, CH$_2$), 3.36–3.31 (m, 4H, CH$_2$), 3.15 (s, 1H, C≡C-H), 2.36 (*residual toluene*), 1.14–1.09 ppm (m, 21H, C*H*(CH_3)$_2$); LRMS (ESI): *m/z* calcd for

$C_{26}H_{36}F_3N_3O_2Si$: 508.3 $[M+H]^+$; found: 508.2; HRMS (ESI): *m/z* calcd for $C_{26}H_{36}F_3N_3O_2Si$: 508.2602 $[M+H]^+$; found: 508.2607.

4-[(2-{3-ethynyl-*N*-[2-(2,2,2-trifluoroacetamido)ethyl]-5-[(triisopropylsilyl)ethynyl]benzamido} ethyl)amino]-4-oxobutanoic acid (5): Succinic anhydride (2.411 g, 24 mmol, 1 equiv) and NEt_3 (10 mL, 72 mmol, 3 equiv) were added to a solution of crude product **4** (20.86 g, which equates to about 14.97 g, 24 mmol, 1 equiv of product **4**) in CH_2Cl_2 (240 mL, 0.1 M). The reaction mixture was stirred for 2 h at room temperature. The reaction progress was determined by TLC (CH_2Cl_2/MeOH, 10:1 v/v, acetic acid 1 droplet). After complete consumption of the starting material, the reaction mixture was concentrated to a total volume of 100 mL under reduced pressure. The mixture was precipitated in aq. citric acid (10%, 2 L) and stirred for 1 h. The precipitate was isolated by vacuum filtration, washed extensively with water to remove excess citric acid, then washed with cold CH_2Cl_2. The product was obtained as a white solid (13.30 g, 22 mmol, 91%). R_f = 0.52 (CH_2Cl_2/MeOH, 9:1+one droplet AcOH); ^{1}H NMR (300 MHz, CD_3OD, $CDCl_3$): δ = 7.57 (t, ^4J = 1.5 Hz, 1H, *p*-H_{Bz}), 7.37 (s, 2H, *o*-H_{Bz}), 3.72–3.67 (m, 1H, NCH_2CH_2), 3.63–3.56 (m, 2H, NCH_2CH_2), 3.52–3.44 (m, 2H, NCH_2CH_2), 3.40–3.33 (m, 3H, NCH_2CH_2, C≡CH, *overlapping with signal from CD_2HOD signal*), 3.25–3.20 (m, 1H, *N*-CH_2CH_2), 2.63–2.53 (m, 2H, $(CO)CH_2$), 2.48–2.37 (m, 2H, $(CO)CH_2$), 1.09 ppm (s, 21H, $CH(CH_3)_2$); LRMS (ESI): *m/z* calcd for $C_{30}H_{40}F_3N_3O_5Si$: 608.3 $[M+H]^+$, 630.3 $[M+Na]^+$; found: 608.3, 630.2; HRMS (ESI): *m/z* calcd for $C_{30}H_{40}F_3N_3O_5Si$: 608.2762 $[M+H]^+$; found: 608.2753; RP-HPLC: (gradient: 40–100% eluent **B** in 30 min, 25 °C): t_R = 15.6 min, determined purity 87%.

4-({2-[(2-{3-ethynyl-5-[(triisopropylsilyl)ethynyl]benzamido}-ethyl)amino]ethyl}amino)-4-oxobutanoic acid (6): Compound **5** (10.0 g, 16.5 mmol, 1 equiv) was suspended in a mixture of MeOH (250 mL) and EtOH (180 mL) and stirred at 40 °C until the starting material was dissolved completely. K_2CO_3 (16 g, 116 mmol, 7 equiv) in water (100 mL) was added, and the mixture was heated to 60 °C and allowed to stir at 60 °C for 8 h, and then at room temperature overnight. Remaining solvents were removed under reduced pressure at 40 °C. The crude product was analyzed by RP-HPLC and used without further purification. HRMS (ESI): *m/z* calcd for $C_{28}H_{41}N_3O_4Si$: 512.29 $[M+H]^+$; found: 512.04; RP-HPLC: (gradient: 100–50% eluent **A** over 0–5 min, 50–0% eluent **A** over 5–12 min, 0% eluent **A** over 12–17 min, 25 °C): t_R = 8.8 min, determined purity 92%.

4-{[2-({[(9H-fluoren-9-yl)methoxy]carbonyl}(2-{3-ethynyl-5-[(triisopropyl-silyl)ethynyl]benzamido}ethyl)amino)ethyl]amino}-4-oxobutanoic acid (7): The slurry of compound **6** was redissolved in THF (200 mL) and water (200 mL). Fmoc-Cl (4.67 g, 18 mmol, 1.1 equiv) was added, and the reaction mixture was stirred for 18 h at room temperature. The emulsion was evaporated under reduced pressure. The pH was tested to be pH > 7 (if the pH < 7 adjust). The gel-like residue was redissolved in ethyl acetate (50 mL), water (300 mL), and brine (200 mL). The aqueous layer was washed two times with ethyl acetate to remove remaining Fmoc-based byproducts. Citric acid (1 L, 10% solution in water) was added to the aqueous layer to adjust to pH < 4. The product was extracted three times from the aqueous solution with ethyl acetate. The collected organic layers were dried over $MgSO_4$, filtered, and concentrated under reduced pressure. Crude product (11.69 g, 15.9 mmol, 96%) was further purified by silica gel column chromatography (CH_2Cl_2/MeOH, 20:1) to afford pure product **7** (6.3 g, 8.5 mmol, 52%). R_f = 0.71 (CH_2Cl_2/MeOH, 10:1+droplet AcOH); ^{1}H NMR (600 MHz, CD_3OD): δ = 7.84 (dd, $^{4,4}J$ = 21.4, 8.0 Hz, 2H, *o*-H_{Bz}), 7.76 (d, ^3J = 7.6 Hz, 2H, H_{Ar} (Fmoc)), 7.64–7.49 (m, 3H, *p*-H_{Bz}, H_{Ar} (Fmoc)), 7.35 (m, 2H, H_{Ar} (Fmoc)), 7.27 (dt, $^{3,4}J$ = 21.5, 7.3 Hz, 2H, H_{Ar} (Fmoc)), 4.44 (d, ^3J = 5.8 Hz, 1H, OCH_2CH), 4.34 (d, ^3J = 6.1 Hz, 1H, OCH_2CH), 4.16 (dt, $^{3,4}J$ = 36.4, 5.7 Hz, 1H, OCH_2CH), 3.63 (d, ^5J = 23.9 Hz, 1H, C≡C-H), 3.49 (s, br, 2H, $NHCH_2CH_2$), 3.45–3.40 (m, 1H, $NHCH_2CH_2$), 3.39–3.34 (m, 2H, $NHCH_2CH_2$), 3.34–3.30 (m, *overlapping with [D_4]MeOH*, $NHCH_2CH_2$), 3.21 (t, ^3J = 5.9 Hz, 1H, $NHCH_2CH_2$), 3.06 (t, ^3J = 5.8 Hz, 1H, $NHCH_2CH_2$), 2.56 (t, ^3J = 6.9 Hz, 2H, $(CO)CH_2$), 2.42 (t, ^3J = 7.0 Hz, 2H, $(CO)CH_2$), 1.15–1.08 ppm (m, 21H, $CH(CH_3)_2$); ^{13}C NMR (151 MHz, [D_6]DMSO): δ = 173.8 (CO_2H), 172.0 ($CH_2(CO)NH$), 171.1 ($CH_2(CO)NH$), 164.5 (PhCO), 155.6 (O(CO)NH), 155.5 (O(CO)NH), 143.8 (C_{Ar} (Fmoc)), 143.8 (C_{Ar} (Fmoc)), 140.7 (C_{Ar} (Fmoc)), 136.7, 136.6 (*o*-C_{Bz}), 135.5, 135.4 (*o*-C_{Bz}), 130.7, 130.5 (C-1_{Bz}), 127.6 (C_{Ar} (Fmoc)), 127.6 (C_{Ar} (Fmoc)), 127.1 (C_{Ar} (Fmoc)), 125.1 (C_{Ar} (Fmoc)), 125.0 (C_{Ar} (Fmoc)), 123.1 (C-5_{Bz}), 123.0 (C-5_{Bz}), 122.6 (C-3_{Bz}), 122.5 (C-3_{Bz}), 120.1 (C_{Ar} (Fmoc)), 120.1 (C_{Ar} (Fmoc)), 105.1 (C≡C-TIPS), 92.0 (C≡C-TIPS), 91.9 (C≡C-TIPS), 82.5 (C≡C-H), 82.3 (C≡C-H), 81.7 (C≡C-H), 67.9 (Fmoc-CH-CH_2), 66.9 (Fmoc-CH-CH_2), 46.9, 46.7, 46.6, 46.5, 38.1, 37.5, 36.8 (all $HNCH_2CH_2$), 30.1 (succinyl-CH_2), 30.0 (succinyl-CH_2), 29.1 (succinyl-CH_2), 21.1 ($CH(CH_3)_2$), 18.5 (CH_3), 10.6 ppm; LRMS (ESI): *m/z* calcd for $C_{43}H_{51}N_3O_6Si$: 734.4 $[M+H]^+$, 756.3 $[M+Na]^+$; found: 734.3, 756.2; HRMS (ESI): *m/z* calcd for $C_{43}H_{51}N_3O_6Si$ (monoisotopic mass 733.3547): 734.3620 $[M+H]^+$; found: 734.3623; RP-HPLC: (gradient: 80–100% eluent **B** over 0–10 min, 100% eluent **B** over 10–17 min, 25 °C): t_R = 6.1 min, determined purity 98%.

Glycooligomers analysis

(Fuc,GalNAc)[2,5]-6 (13): ^{1}H NMR (600 MHz, D_2O): δ = 8.50–8.48 (m, 2H, N=*N-N-CH*), 8.46–8.44 (m, 2H, N=*N-N-CH*), 8.12–8.09 (m, 2H, *p*-H_{Ph}), 7.94–7.90 (m, 4H, *o*-H_{Ph}), 4.88 (d, ^3J = 3.6 Hz, 2H, Fuc-H1α), 4.84–4.82 (m, 2H, GalNAc-H1α), 4.75–4.69 (m, 8H, N=*N-N-*CH_2), 4.16 (dt, $^{2,3}J$ = 10.1, 4.5 Hz, 2H, N=*N-N-*CH_2-CH_2), 4.10–4.00 (m, 6H, N=*N-N-*CH_2-CH_2 GalNAc-H3), 3.95 (dt, $^{2,3}J$ = 10.5, 4.8 Hz, 2H, N=*N-N-*CH_2-CH_2), 3.87 (d, ^3J = 2.9 Hz, 2H, GalNAc-H2), 3.82–3.79 (m, 2H, GalNAc-H4), 3.74–3.44 (m, 62H, CH_2-*O*-$(CH_2)_2$-*O*-CH_2, *N*-CH_2-CH_2-NH, Fuc-H2, GalNAc-H6, Fuc-H3, Fuc-H4), 3.40–3.26 (m, 16H, O=C-NH-CH_2-CH_2-O), 3.22 (dt, $^{3,3}J$ = 17.7, 5.4 Hz, 2H, Fuc-H5), 3.14–3.09 (m, 2H, GalNAc-H5), 2.76–2.69 (m, 4H, O=C-CH_2-CH_2-C=O), 2.55–2.47 (m, 20H, O=C-CH_2-CH_2-C=O), 1.96, 1.95 (s, s, 3H, $(CH_2$-NH)-(O=)C-CH_3), 1.78–1.77 (m, 6H, NH-(O=)C-CH_3) (*GalNAc*)), 0.93–0.91 ppm (m, 6H, Fuc-H6); MALDI-TOF-MS: *m/z* calcd for $C_{116}H_{181}N_{29}O_{45}$: 2723.28 $[M+Na]^+$; found 2723.34; HRMS (ESI): *m/z* calcd for $C_{116}H_{181}N_{29}O_{45}$ (monoisotopic mass 2700.2766): 901.0995 $[M+3H]^{3+}$; found: 901.0988; RP-HPLC: (gradient: 100–50% eluent **A** over 30 min, 25 °C): t_R = 14.0 min, determined purity 99%.

(Fuc,Gal)[2,5]-6 (14): ^{1}H NMR (600 MHz, D_2O): δ = 8.47–8.44 (m, 4H, N=*N-N-CH*), 8.05–8.03 (m, 2H, *p*-H_{Ph}), 7.89–7.86 (m, 4H, *o*-H_{Ph}), 4.98 (d, ^3J = 3.7 Hz, 2H, Gal-H1α), 4.88 (d, ^3J = 3.5 Hz, 2H, Fuc-H1α), 4.75–4.68 (m, 8H, N=*N-N-*CH_2), 4.17–4.15 (m, 2H, N=*N-N-*CH_2-CH_2), 4.10–4.07 (m, 2H, N=*N-N-*CH_2-CH_2), 4.02–3.98 (m, 4H, N=*N-N-*CH_2-CH_2), 3.83–3.79 (m, 4H, Gal-H2, Gal-H4), 3.76–3.69 (m, 6H, Fuc-H2, Gal-H3, Gal-H6), 3.67–3.43 (m, 55H, CH_2-*O*-$(CH_2)_2$-*O*-CH_2, *N*-CH_2-CH_2-NH, Fuc-H3, Fuc-H4), 3.41–3.24 (m, 18H, O=C-NH-CH_2-CH_2-O, Gal-H6), 3.20 (dt, $^{3,3}J$ = 19.6, 5.1 Hz, 2H, Fuc-H5), 3.16–3.13 (m, 2H, Gal-H5), 2.75–2.69 (m, 4H, O=C-CH_2-CH_2-C=O), 2.54–2.48 (m, 20H, O=C-CH_2-CH_2-C=O), 1.95, 1.94 (s, s, 3H, O=C-CH_3), 0.94–0.92 ppm (m, 6H, Fuc-H6); MALDI-TOF-MS: *m/z* calcd for $C_{112}H_{175}N_{27}O_{45}$: 2641.2 $[M+Na]^+$; found: 2641.3; HRMS (ESI): *m/z* calcd for $C_{112}H_{175}N_{27}O_{45}$ (monoisotopic mass 2618.2235): 873.7485 $[M+3H]^{3+}$; found 873.7479; RP-HPLC: (gradient: 100–50% eluent **A** over 30 min, 25 °C): t_R = 13.7 min, determined purity 99%.

(Fuc,Lac)[2,5]-6 (15): ^{1}H NMR (600 MHz, D_2O): δ = 8.58 (s, 2H, N=*N-N-CH*), 8.40–8.39 (m, 2H, N=*N-N-CH*), 8.01–7.09 (m, 2H, *p*-H_{Ph}),

7.88–7.79 (m, 4H, *o*-H_{Ph}), 5.87 (dd, $^{3,4}J$ = 9.1, 1.7 Hz, 2H, Glc-H1β), 4.87 (d, ^{3}J = 3.4 Hz, 2H, Fuc-H1α), 4.73–4.64 (m, 4H, N=*N*-*N*-CH_2), 4.57 (d, ^{3}J = 7.7 Hz, 2H, Gal-H1β), 4.15 (dt, $^{2,3}J$ = 8.9, 2.0 Hz, 2H, N=*N*-*N*-CH_2-CH_2), 4.08–4.05 (m, 4H, N=*N*-*N*-CH_2-CH_2, Glc-H), 4.00–3.94 (m, 12H, Glc-H, Gal-H), 3.88–3.84 (m, 2H, Glc-H), 3.82–3.79 (m, 4H, Gal-H2, Gal-H4), 3.74–3.69 (m, 6H, Fuc-H2, Gal-H3, Gal-H6), 3.64–3.44 (m, 51H, CH_2-*O*-$(CH_2)_2$-*O*-CH_2, *N*-CH_2-CH_2-NH, Fuc-H3, Fuc-H4), 3.42–3.27 (m, 17H, O=C-NH-CH_2-CH_2-O), 3.24–3.12 (m, 6H, Gal-H6, Fuc-H5, Gal-H5), 2.73–2.68 (m, 4H, O=C-CH_2-CH_2-C=O), 2.55–2.45 (m, 20H, O=C-CH_2-CH_2-C=O), 1.94, 1.93 (s, s, 3H, O=C-CH_3), 0.95–0.93 ppm (m, 6H, Fuc-H6); MALDI-TOF-MS: *m/z* calcd for $C_{120}H_{187}N_{27}O_{53}$: 2877.3 $[M+Na]^+$; found 2877.3; HRMS (ESI): *m/z* calcd for $C_{120}H_{187}N_{27}O_{53}$ (monoisotopic mass 2854.2768): 952.4329 $[M+3H]^{3+}$; found: 952.4325; RP-HPLC: (gradient: 100–50% eluent **A** over 30 min, 25 °C): t_R = 12.8 min, determined purity ≥99%.

[Fuc,Sia(methyl-protected)][2,5]-6 (16-Me): ^{1}H NMR (600 MHz, D_2O): δ = 8.48–8.46 (m, 2H, N=*N*-*N*-C*H*), 8.37–8.36 (m, 2H, N=*N*-*N*-C*H*), 8.08–8.06 (m, 2H, *p*-H_{Ph}), 7.92–7.88 (m, 4H, *o*-H_{Ph}), 4.88 (d, ^{3}J = 3.5 Hz, 2H, Fuc-H1α), 4.76–4.62 (m, 11H, COO-CH_3, N=*N*-*N*-CH_2, *overlapping with HDO-signal*), 4.24–4.22 (m, 2H, N=*N*-*N*-CH_2-CH_2), 4.10–4.07 (m, 2H, N=*N*-*N*-CH_2-CH_2), 4.02–3.98 (m, 4H, N=*N*-*N*-CH_2-CH_2), 3.83 (t, ^{3}J = 10.2 Hz, 2H, Sia-H8), 3.76–3.43 (m, 73H, CH_2-*O*-$(CH_2)_2$-*O*-CH_2, *N*-CH_2-CH_2-NH, Fuc-H2, Fuc-H3, Fuc-H4, Sia-H4-H7, Sia-H9), 3.41–3.25 (m, 17H, O=C-NH-CH_2-CH_2-O), 3.20 (dt, $^{3,3}J$ = 18.7, 5.2 Hz, 2H, Fuc-5), 3.16–3.11 (m, 2H, Sia-H), 2.76–2.70 (m, 4H, O=C-CH_2-CH_2-C=O), 2.62 (dd, $^{2,3}J$ = 12.9, 4.6 Hz, 2H, Sia-H_e3), 2.55–2.47 (m, 21H, O=C-CH_2-CH_2-C=O), 2.00 (s, 6H, (NH)CO-CH_3 (*Sia*)), 1.95, 1.95 (s, s, 3H, O=C-CH_3), 1.79 (t, $^{2,3}J$ = 12.4 Hz, 2H, Sia-H_a3), 0.94–0.93 ppm (m, 6H, Fuc-H6). MALDI-TOF-MS: *m/z* calcd for $C_{124}H_{193}N_{29}O_{51}$: 2927.34 $[M+Na]^+$; found: 2927.47; HRMS (ESI): *m/z* calcd for $C_{124}H_{193}N_{29}O_{51}$ (monoisotopic mass 2904.3400): 969.1206 $[M+3H]^{3+}$; found: 969.1191; RP-HPLC: (gradient: 100–50% eluent **A** over 30 min, 25 °C): t_R = 14.6 min, determined purity 99%.

(Fuc,Sia)[2,5]-6 (16): ^{1}H NMR (300 MHz, D_2O): δ = 8.46–8.43 (m, 2H, N=*N*-*N*-C*H*), 8.38–8.34 (m, 2H, N=*N*-*N*-C*H*), 8.05–8.01 (m, 2H, *p*-H_{Ph}), 7.89–7.82 (m, 4H, *o*-H_{Ph}), 4.88 (d, ^{3}J = 3.0 Hz, 2H, Fuc-H1α), 4.74–4.60 (m, 8H, N=*N*-*N*-CH_2), 4.25–4.20 (m, 2H, N=*N*-*N*-CH_2-CH_2), 4.13–3.95 (m, 8H, N=*N*-*N*-CH_2-CH_2, Sia-H8), 3.85–3.11 (m, 94H, CH_2-*O*-$(CH_2)_2$-*O*-CH_2, *N*-CH_2-CH_2-NH, Fuc-H2, Fuc-H3, Fuc-H4, Sia-H4-H7, Sia-H9, O=C-NH-CH_2-CH_2-O, Fuc-H-5), 2.77–2.49 (m, 28H, O=C-CH_2-CH_2-C=O, Sia-$H3_{eq}$), 2.00 (s, 6H, NC(=O)CH_3 (*Sia*)), 1.95, 1.94 (s, s, 3H, O=C-CH_3), 1.75 (t, $^{2,3}J$ = 12.1 Hz, 2H, Sia-$H3_{ax}$), 0.93 ppm (d, ^{3}J = 6.6 Hz, 6H, Fuc-H6); HRMS (ESI): *m/z* calcd for $C_{122}H_{189}N_{29}O_{51}$ (monoisotopic mass 2878.3087): 959.7769 $[M+3H]^{3+}$; found: 959.7761; RP-HPLC: (gradient: 100–50% eluent **A** over 30 min, 25 °C): t_R = 13.6 min, 13.8 min, determined purity 96%.

(Fuc,Fuc)[2,5]-6 (17): ^{1}H NMR (600 MHz, D_2O): δ = 8.39 (s, 4H, N=*N*-*N*-C*H*), 7.99–7.97 (m, 2H, *p*-H_{Ph}), 7.82–7.79 (m, 4H, *o*-H_{Ph}), 4.78 (d, ^{3}J = 3.1 Hz, 4H, Fuc-H1α), 4.67–4.56 (m, 8H, N=*N*-*N*-CH_2), 4.04–3.89 (m, 8H, N=*N*-*N*-CH_2-CH_2), 3.63–3.09 (m, 76H, Fuc-H2, Fuc-H3, Fuc-H4, CH_2-*O*-$(CH_2)_2$-*O*-CH_2, *N*-CH_2-CH_2-NH, O=C-NH-CH_2-CH_2-O), 3.06–2.99 (m, 4H, Fuc-H5), 2.68–2.59 (m, 4H, O=C-CH_2-CH_2-C=O), 2.47–2.36 (m, 20H, O=C-CH_2-CH_2-C=O), 1.86, 1.86 (s, s, 3H, O=C-CH_3), 0.82 ppm (d, ^{3}J = 6.5 Hz, 12H, Fuc-H6). MALDI-TOF-MS: *m/z* calcd for $C_{112}H_{175}N_{27}O_{43}$ 2609.2 $[M+Na]^+$; found: 2609.3. HRMS (ESI): *m/z* calcd for $C_{112}H_{175}N_{27}O_{43}$ (monoisotopic mass 2586.2337): 863.0852 $[M+3H]^{3+}$; found: 863.0851; RP-HPLC: (gradient: 100–50% eluent **A** over 30 min, 25 °C): t_R = 14.3 min, determined purity 99%.

(Gal,Gal)[2,5]-6 (18): Negative control **18** exhibits galactose units of an α/β-mixture (3:1). ^{1}H NMR (600 MHz, D_2O): δ = 8.38–8.34 (m, 4H, N=*N*-*N*-C*H*), 7.97–7.91 (m, 2H, *p*-H_{Ph}), 7.81–7.75 (m, 4H, *o*-H_{Ph}), 5.00 (d, ^{3}J = 1.4 Hz, 1H, Gal-H1α), 4.74–4.65 (m, 8H, N=*N*-*N*-CH_2), 4.45 (d, ^{3}J = 7.4 Hz, Gal-H1β), 4.39–4.32 (m, 3H, N=*N*-*N*-CH_2-CH_2), 4.19–4.12 (m, 4H, N=*N*-*N*-CH_2-CH_2), 4.08–4.01 (m, 3H, N=*N*-*N*-CH_2-CH_2, Gal-H2α), 3.92 (d, *J* = 3.2 Hz, 4H, Gal-H2β), 3.79–3.12 (m, 89H, Gal-H2, Gal-H4, Gal-H5, Gal-H3, Gal-H6, CH_2-*O*-$(CH_2)_2$-*O*-CH_2, *N*-CH_2-CH_2-NH, O=C-NH-CH_2-CH_2-O), 2.76–2.68 (m, 4H, O=C-CH_2-CH_2-C=O), 2.52–2.47 (m, 20H, O=C-CH_2-CH_2-C=O), 1.94–1.92 ppm (m, 3H, O=C-CH_3); MALDI-TOF-MS: *m/z* calcd for $C_{112}H_{175}N_{27}O_{47}$ 2673.2134 $[M+Na]^+$; found: 2673.294; HRMS (ESI): *m/z* calcd for $C_{112}H_{175}N_{27}O_{47}$ (monoisotopic mass 2650.2134): 884.4117 $[M+3H]^{3+}$; found: 884.4114; RP-HPLC: (gradient: 100–50% eluent **A** over 30 min, 25 °C): t_R = 12.9, 13.1, 13.3 min; determined purity 99%.

Acknowledgements

The authors would like to thank Mirko Lindic for his help with synthesizing azidoethyl-2,3,4,6-tetra-*O*-acetyl-α-D-galactopyranoside and Mischa Baier for helpful discussions. L.H. thanks the DFG for support through the FOR 2327 ViroCarb (HA 5950/5-1) and large equipment grant INST 208/735-1. N.L.S. thanks the Davidson College VPAA and the Dean Rusk International Studies Program for sabbatical support.

Conflict of interest

The authors declare no conflict of interest.

Keywords: carbohydrates · glycomimetics · oligosaccharides · precision glycomacromolecules · solid-phase synthesis

[1] H. Rüdiger, *Chem. unserer Zeit* **1981**, *15*, 155.
[2] a) P. M. Drake, W. Cho, B. Li, A. Prakobphol, E. Johansen, N. L. Anderson, F. E. Regnier, B. W. Gibson, S. J. Fisher, *Clin. Chem.* **2010**, *56*, 223; b) D. J. Becker, J. B. Lowe, *Glycobiology* **2003**, *13*, 41R–53R; c) J. C. Hoving, G. J. Wilson, G. D. Brown, *Cell. Microbiol.* **2013**, *15*, 185.
[3] R. Kannagi, *Glycoconjugate J.* **1997**, *14*, 577.
[4] a) E. M. Vestergaard, H. O. Hein, H. Meyer, N. Grunnet, J. Jørgensen, H. Wolf, T. F. Ørntoft, *Clin. Chem.* **1999**, *45*, 54;b) E. Miyoshi, K. Noda, Y. Yamaguchi, S. Inoue, Y. Ikeda, W. Wang, J. H. Ko, N. Uozumi, W. Li, N. Taniguchi, *Biochim. Biophys. Acta Gen. Subj.* **1999**, *1473*, 9.
[5] a) A. V. Grishin, M. S. Krivozubov, A. S. Karyagina, A. L. Gintsburg, *Acta Naturae* **2015**, *7*, 29; b) B. Fiege, C. Rademacher, J. Cartmell, P. I. Kitov, F. Parra, T. Peters, *Angew. Chem. Int. Ed.* **2012**, *51*, 928; *Angew. Chem.* **2012**, *124*, 952; c) A. Koromyslova, S. Tripathi, V. Morozov, H. Schroten, G. S. Hansman, *Virology* **2017**, *508*, 81; d) N. Sriwilaijaroen, Y. Suzuki, H. Kida, *Proc. Jpn. Acad. Ser. B* **2012**, *88*, 226.
[6] L. Cooling, *Clin. Microbiol. Rev.* **2015**, *28*, 801.
[7] a) J. Topin, M. Lelimousin, J. Arnaud, A. Audfray, S. Pérez, A. Varrot, A. Imberty, *ACS Chem. Biol.* **2016**, *11*, 2011; b) J. E. Heggelund, A. Varrot, A. Imberty, U. Krengel, *Curr. Opin. Struct. Biol.* **2017**, *44*, 190.
[8] T. K. Lindhorst, in Cracking the Sugar Code by Navigating the Glycospace: Glycomimetics: Tools for Investigation of Functional Diversity in the Carbohydrate Regime, Vol. 1, Proceedings of the 2nd Beilstein Glyco-Bioinformatics Symposium, Beilstein Institut, Potsdam, Germany, **2011**, 147–164.
[9] a) B. Ernst, J. L. Magnani, *Nat. Rev. Drug Discovery* **2009**, *8*, 661; b) D. Hauck, I. Joachim, B. Frommeyer, A. Varrot, B. Philipp, H. M. Möller, A. Imberty, T. E. Exner, A. Titz, *ACS Chem. Biol.* **2013**, *8*, 1775.
[10] a) A. M. Wands, J. Cervin, H. Huang, Y. Zhang, G. Youn, C. A. Brautigam, M. Matson Dzebo, P. Björklund, V. Wallenius, D. K. Bright, C. S. Bennett, P. Wittung-Stafshede, N. S. Sampson, U. Yrlid, J. J. Kohler, *ACS Infect. Dis.* **2018**, *4*, 758; b) D. Goyard, V. Baldoneschi, A. Varrot, M. Fiore, A. Imberty, B. Richichi, O. Renaudet, C. Nativi, *Bioconjugate Chem.* **2018**, *29*, 83.
[11] For example: a) E. M. V. Johansson, S. A. Crusz, E. Kolomiets, L. Buts, R. U. Kadam, M. Cacciarini, K.-M. Bartels, S. P. Diggle, M. Cámara, P. Wil-

liams, R. Loris, C. Nativi, F. Rosenau, K. E. Jaeger, T. Darbre, J. L. Reymond, *Chem. Biol.* **2008**, *15*, 1249; b) B. Gerland, A. Goudot, G. Pourceau, A. Meyer, V. Dugas, S. Cecioni, S. Vidal, E. Souteyrand, J.-J. Vasseur, Y. Chevolot, F. Morvan, *Bioconjugate Chem.* **2012**, *23*, 1534; c) E. Kolomiets, E. M. V. Johansson, O. Renaudet, T. Darbre, J.-L. Reymond, *Org. Lett.* **2007**, *9*, 1465; d) K. Buffet, I. Nierengarten, N. Galanos, E. Gillon, M. Holler, A. Imberty, S. E. Matthews, S. Vidal, S. P. Vincent, J.-F. Nierengarten, *Chem. Eur. J.* **2016**, *22*, 2955; e) G. Michaud, R. Visini, M. Bergmann, G. Salerno, R. Bosco, E. Gillon, B. Richichi, C. Nativi, A. Imberty, A. Stocker, T. Darbre, J.-L. Reymond, *Chem. Sci.* **2016**, *7*, 166; K. Marotte, C. Sabin, C. Préville, M. Moumé-Pymbock, M. Wimmerová, E. P. Mitchell, A. Imberty, R. Roy, *ChemMedChem* **2007**, *2*, 1328; Review article: A. Bernardi, J. Jimenez-Barbero, A. Casnati, C. De Castro, T. Darbre, F. Fieschi, J. Finne, H. Funken, K.-E. Jaeger, M. Lahmann, T. K. Lindhorst, M. Marradi, P. Messner, A. Molinaro, P. V. Murphy, C. Nativi, S. Oscarson, S. Penadés, F. Peri, R. J. Pieters, O. Renaudet, J. L. Reymond, B. Richichi, J. Rojo, F. Sansone, C. Schäffer, W. B. Turnbull, T. Velasco-Torrijos, S. Vidal, S. Vincent, T. Wennekes, H. Zuilhof, A. Imberty, *Chem. Soc. Rev.* **2013**, *42*, 4709; R. J. Pieters, *Org. Biomol. Chem.* **2009**, *7*, 2013; A. Imberty, Y. M. Chabre, R. Roy, *Chem. Eur. J.* **2008**, *14*, 7490; V. Wittmann, R. J. Pieters, *Chem. Soc. Rev.* **2013**, *42*, 4492.

[12] K. Marotte, C. Préville, C. Sabin, M. Moumé-Pymbock, A. Imberty, R. Roy, *Org. Biomol. Chem.* **2007**, *5*, 2953.

[13] J. Guiard, B. Fiege, P. I. Kitov, T. Peters, D. R. Bundle, *Chem. Eur. J.* **2011**, *17*, 7438.

[14] M. L. Huang, S. C. Purcell, S. Verespy III, Y. Wang, K. Godula, *Biomater. Sci.* **2017**, *5*, 1537.

[15] G. C. Daskhan, H.-T. T. Tran, P. J. Meloncelli, T. L. Lowary, L. J. West, C. W. Cairo, *Bioconjugate Chem.* **2018**, *29*, 343.

[16] For example: a) C. Pifferi, B. Thomas, D. Goyard, N. Berthet, O. Renaudet, *Chem. Eur. J.* **2017**, *23*, 16283; b) M. Abellán Flos, M. I. G. Moreno, O. Mellet, Carmen; J. M. G. Fernandez, J.-F. Nierengarten, S. P. Vincent, *Chem. Eur. J.* **2016**, *22*, 11450; J. M. G. Fernandez, J.-F. Nierengarten, S. P. Vincent, *Chem. Eur. J.* **2016**, *22*, 11450; c) K. E. Moog, M. Barz, M. Bartneck, F. Beceren-Braun, N. Mohr, Z. Wu, L. Braun, J. Dernedde, E. A. Liehn, F. Tacke, T. Lammers, H. Kunz, R. Zentel, *Angew. Chem. Int. Ed.* **2017**, *56*, 1416; *Angew. Chem.* **2017**, *129*, 1438; d) Y. Gou, J. Geng, S. J. Richards, J. Burns, R. Becer, D. M. Haddleton, *J. Polym. Sci. Part A* **2013**, *51*, 2588; A. Patel, T. K. Lindhorst, *Eur. J. Org. Chem.* **2002**, *1*, 79; T. K. Lindhorst, K. Bruegge, A. Fuchs, O. Sperling, *Beilstein J. Org. Chem.* **2010**, *6*, 801; I. Deguise, D. Lagnoux, R. Roy, *New J. Chem.* **2007**, *31*, 1321. Review article: J. L. Jiménez Blanco, C. Ortiz Melleta, J. M. García Fernández, *Chem. Soc. Rev.* **2013**, *42*, 4518.

[17] D. Ponader, F. Wojcik, F. Beceren-Braun, J. Dernedde, L. Hartmann, *Biomacromolecules* **2012**, *13*, 1845.

[18] a) S. Boden, K. G. Wagner, M. Karg, L. Hartmann, *Polymer* **2017**, *9*, 716; b) S. Igde, S. Röblitz, A. Müller, K. Kolbe, S. Boden, C. Fessele, T. K. Lindhorst, M. Weber, L. Hartmann, *Macromol. Biosci.* **2017**, *17*, 1700198.

[19] M. Baier, M. Giessler, L. Hartmann, *Chem. Eur. J.* **2018**, *24*, 1619 – 1630.

[20] F. Wojcik, S. Mosca, L. Hartmann, *J. Org. Chem.* **2012**, *77*, 4226.

[21] a) F. Wojcik, A. G. O'Brien, S. Götze, P. H. Seeberger, L. Hartmann, *Chem. Eur. J.* **2013**, *19*, 3090; b) D. Ponader, P. Maffre, J. Aretz, D. Pussak, N. M. Ninnemann, S. Schmidt, P. H. Seeberger, C. Rademacher, G. U. Nienhaus, L. Hartmann, *J. Am. Chem. Soc.* **2014**, *136*, 2008; c) T. Freichel, S. Eierhoff, N. L. Snyder, L. Hartmann, *J. Org. Chem.* **2017**, *82*, 9400.

[22] C. Toonstra, M. N. Amin, L.-X. Wang, *J. Org. Chem.* **2016**, *81*, 6176.

[23] F. Ishiwari, K.-I. Fukasawa, T. Sato, K. Nakazono, Y. Koyama, T. Takata, *Chem. Eur. J.* **2011**, *17*, 12067.

[24] M. Galibert, V. Piller, F. Piller, V. Aucagne, A. F. Delmas, *Chem. Sci.* **2015**, *6*, 3617.

[25] N. Garber, U. Guempel, N. Gilboa-Garber, R. J. Royle, *FEMS Microbiol. Lett.* **1987**, *48*, 331.

[26] K. S. Bücher, N. Babic, T. Freichel, F. Kovacic, L. Hartmann, *Macromol. Biosci.* **2018**, *18*, 1800337.

Manuscript received: September 4, 2018
Revised manuscript received: October 26, 2018
Accepted manuscript online: November 15, 2018
Version of record online: February 7, 2019

CHEMISTRY
A European Journal

Supporting Information

Heteromultivalent Glycooligomers as Mimetics of Blood Group Antigens

Katharina S. Bücher,[a] Patrick B. Konietzny,[a] Nicole L. Snyder,[b] and Laura Hartmann*[a]

chem_201804505_sm_miscellaneous_information.pdf

Supporting Information

Heteromultivalent glycooligomers as mimetics of blood group antigens

Katharina Susanne Bücher[a], Patrick Benjamin Konietzny[a], Nicole L. Snyder[b], Laura Hartmann*[a]

[a]Institute of Organic and Macromolecular Chemistry, Universitätsstraße 1, Heinrich Heine University Düsseldorf, Germany
[b]Department of Chemistry, Davidson College, Davidson, NC, USA

1. Materials

Diethyl ether (with BHT as inhibitor, ≥ 99.8%), triisopropylsilane (TIPS) (98%), (+)-sodium-L-ascorbate (≥ 99.0%), citric acid (≥ 99.5%), D-galactose (Gal) (≥ 99%), sodium diethyldithiocarbamat trihydrate, sodium methanolate (95%), diethylene triamine (≥ 99%), 2,2′-(ethylenedioxy)bis(ethylamine) (98%), Amberlite (IR120, hydrogen form), 1-hydroxybenzotriazole (HOBt) (≥ 97%), D-lactose (Lac) (≥ 98%), triethylsilane (99%), 3-bromo-5-iodobenzoic acid (97%), copper iodide (CuI) (≥ 99.5%), bis(triphenylphosphine)palladium(II)chloride ($Pd(PPh_3)_2Cl_2$) (≥ 99%), tetrabutylammoniumfluoride trihydrate (TBAF) (98%), silver carbonate (Ag_2CO_3) (99%), acetyl chloride (98%) and all deuterated solvents were purchased from Sigma-Aldrich. *N*,*N*-Dimethylformamide (DMF) (99.8%, for peptide synthesis), piperidine (99%), copper(II)sulfate (98%), 2-bromoethanol (97%), sodium azide (99%), isopropanol (99.5%), TRIS (≥ 99.8%) and trityl chloride (98%) were purchased from Acros Organics. Methanol (100%), ethyl acetate (≥ 99%), magnesium sulfate ($MgSO_4$) (≥ 99.5%), hydrochloric acid (HCl) (conc.), potassium carbonate (K_2CO_3) (98-100%), *n*-hexane (≥ 95%), sulfuric acid (95-98%) and acetic anhydride (Ac_2O) (99.7%) were purchased from VWR Prolabo Chemicals. *N*,*N*-Diisopropylethylamine (DIPEA) (≥ 99%) was purchased from Carl Roth. Dichloromethane (DCM) (99.99%), acetonitrile (ACN) (≥ 99.9%) and sodium chloride (NaCl) (≥ 99.0%) were purchased from Fisher Scientific. Trifluoroacetic acid (TFA) (99%), triisopropylsilylacetylene (TIPS-acetylene) (97%) and trimethylsilylacetylene (TMS-acetylene) (98%) were purchased from Fluorochem. Tentagel S RAM (Rink Amide) resin was purchased from Rapp Polymere and had a loading of 0.25 mmol of Fmoc-protected amine groups per gram of resin. L-Fucose (Fuc) (≥ 95%) and *N*-acetylneuraminic acid (Neu5Ac or here Sia) were purchased from Jennewein Biotechnologie GmbH. Silica gel (60 M, 0.04-0.063 mm) was purchased from Macherey-Nagel. Succinic anhydride was purchased from Carbolution. (HATU) Benzotriazol-1-yl-oxytripyrrolidinophosphonium hexafluorophosphate (PyBOP) was purchased from NovaBiochem. The ion exchange resin (AG1-X8, quarternary ammonium, 100-200 mesh, acetate form) was purchased from BioRad. Syringe filters, 4 mm, 0.45 µm PTFE were purchased from Restek. Filter syringes with a polypropylene frit were purchased from Multisyntech GmbH. Streptavidin sensor chips (SA-chips), sodium chloride solution (1 M), sodium hydroxide solution (0.2 M) and HSB-P+ buffer for SPR

measurements were purchased from GE Healthcare Life Sciences. LecB was purchased from OligoTech. α-L-Methylfucose (> 98.0%) was purchased from TCI. Calcium chloride ($CaCl_2$) (min. 97%), potassium hydroxide (KOH) (90%) and calcium hydroxide ($Ca(OH)_2$) were purchased from AppliChem. Biotinylated fucose- and galactose-polyacrylamide (Fuc-PAA, Gal-PAA) were purchased from GlycoTech. Triethylamine (NEt_3) (> 99.5%), tetrahydrofuran (THF) (99.0%), toluene (Tol) (99.8%) and acidic catalyst LewatitK2629 were purchased from Fluka. *N*-Acetyl-D-galactosamine (GalNAc) was purchased from CarboSynth. *p*-Toluene sulfonic acid monohydrate (*p*-TsOH) (≥ 98%) was purchased from Merck.

2. Instrumentation

Attenuated Total Reflectance Fourier Transform Infrared Spectroscopy (ATR FTIR)

The IR spectrum was recorded with a Nicolet 6700, attenuated total reflectance Fourier transform infrared spectroscopy (ATR FTIR) spectrometer from Thermo Scientific. The spectrum was analyzed with Omnic software 7.4.

Nuclear magnetic resonance spectroscopy (NMR)

^{1}H NMR and ^{13}C NMR spectra were measured on a Bruker AVANCE III – 300 (300 MHz) and a Bruker AVANCE III – 600 (600 MHz). Chemical shifts were obtained in delta (δ) expressed in units of parts per million (ppm). Residual, non-deuterated solvent was utilized as internal standard.

Reverse-phase semi-preparative high-performance liquid chromatography (preparative RP-HPLC)

All glycooligomers were purified by semi-preparative RP-HPLC performed on an Agilent 1200 HPLC system using a Varian Pursuit semi-preparative column (C_{18}, 250x10.0 mm). Separation of glycooligomers was realized applying a linear gradient of milliQ-water (**A**) and acetonitrile (**B**) at a flow rate of 20 mL/min at 25 °C. The product fractions were combined, concentrated in vacuum to dryness, dissolved in milliQ-water, filtered through syringe filters and lyophilized to obtain the purified glycooligomers.

Reversed Phase - High Performance Liquid Chromatography - Mass Spectrometry (RP-HPLC/MS)

Analysis of glycooligomers was conducted on an analytical RP-HPLC system (Agilent 1260 Infinity) with a Poroshell 120 EC-C18 (3.0×50 mm, 2.5 µm) RP column from Agilent. The instrument was coupled to a variable wavelength detector (VWD) which was set to 214 nm and was combined with a 6120 Quadrupole LC/MS with an Electrospray Ionization (ESI) source (operating in positive ionization mode in a m/z range of 200 to 2000). A gradient of mobile phase **A** (H_2O/ACN (95:5) + 0.1% formic acid) and mobile phase **B** (H_2O/ACN (5:95) + 0.1% formic acid) was used for the analysis of building blocks and glycooligomers at 25 °C with a flow rate of 0.4 mL/min. Furthermore, successful couplings in SPPoS and purities of final glycooligomers were determined from the obtained chromatograms. The measurements were performed with a linear gradient starting with 100% of mobile phase **A** reaching

50% mobile phase **A** after 30 min. Methods for measurements of the building block intermediates are given for each individual step (see below). Analyses of UV and MS signals were performed with OpenLab ChemStation software for LC/MS from Agilent Technologies.

High Resolution –Electrospray Ionization - Mass Spectrometry (HR-ESI-MS)

HR-ESI-MS spectra were recorded on an Agilent 6210 (Electrospray Ionization) ESI-TOF from Agilent Technologies (Santa Clara, CA, USA) with a flow rate of 4 µL/min. The spray voltage was set to 4 kV and the desolvation gas had 15 psi (1 bar).

Matrix-Assisted Laser Desorption Ionization – Time Of Flight – Mass Spectrometry (MALDI-TOF-MS)

MALDI-TOF-MS spectra were recorded on a Bruker MALDI-TOF Ultraflex I system using 2,5-dihydroxybenzoic acid (DHB) as matrix in 10-fold excess compared to the compound. Spectra were obtained either in linear mode for m/z range of 1000-4000, calibrated with a protein mixture or in reflector mode for a m/z range 2000-20000 without calibration.

Lyophilization

Glycooligomers were dried by lyophilization on a freeze-dryer (Alpha 1-4 LD plus) from Martin Christ Freeze Dryers GmbH at -42 °C and 0.1 mbar.

3. General methods

3.1 Solid phase polymer synthesis of glycooligomers

The spacer building block EDS was synthesized according to literature.[1] Solid phase synthesis is based on previously reported protocols.[2] The synthesis of the backbone structure was conducted in two batches. The first batch size was 0.317 mmol and was split after the first CuAAC reaction into four aliquots (0.08 mmol each) for the synthesis of heteromultivalent glycooligomers. The second batch was 0.08 mmol and was split after backbone construction into two aliquots (0.04 mmol each) for the synthesis of homomultivalent control structures. Detailed procedures are described for batch 1 (see below).

Prior to the synthesis of glycooligomers, Tentagel S RAM resin (1.27 g, 0.317 mmol, loading 0.25 mmol/g) was swollen in DCM by washing three times with DCM (3 mL) and shaking for 1 h in DCM (10 mL). Afterwards the resin was washed 10 times with DMF.

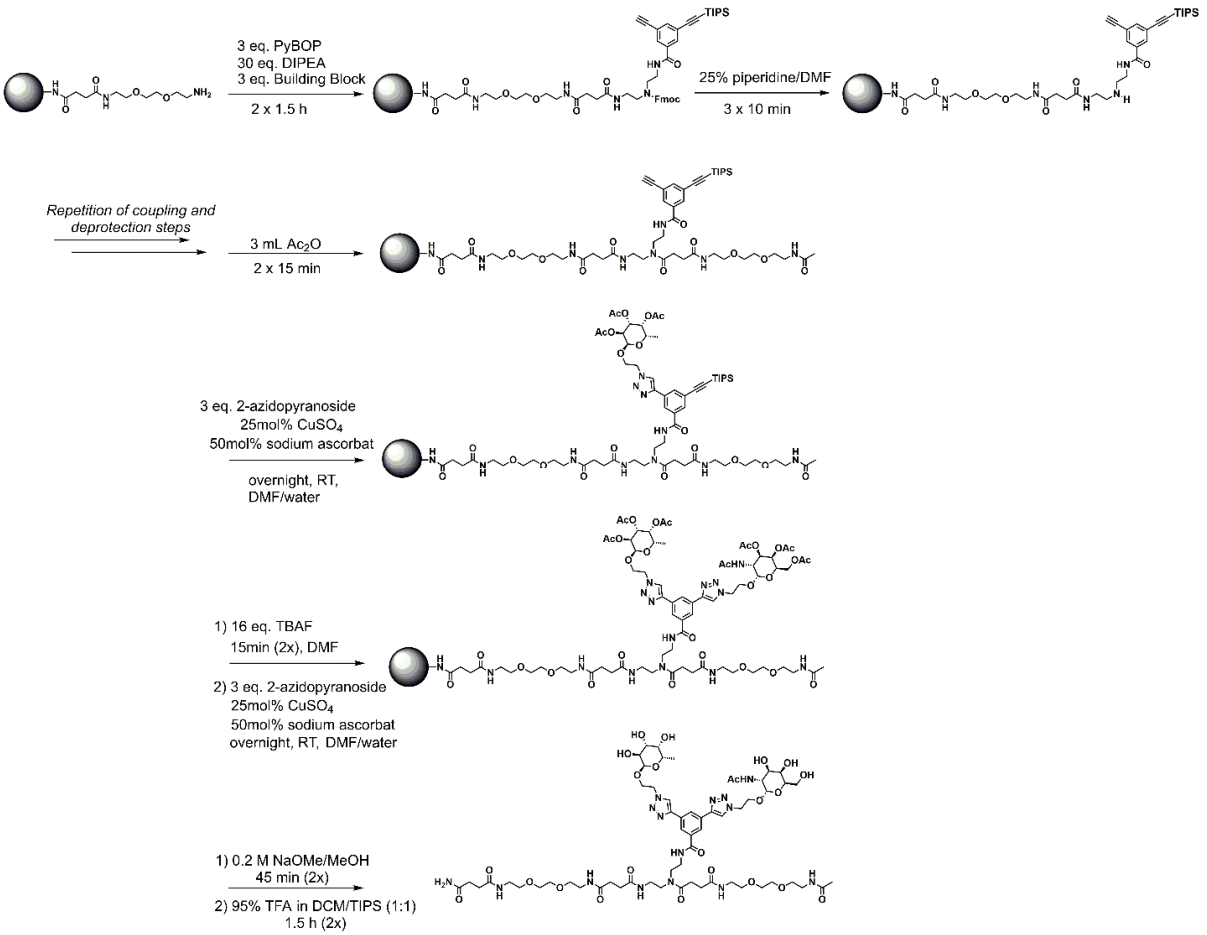

Scheme S1: Synthesis of a heteromultivalent glycooligomer applying *iso*-DTDS, exemplarily with α-L-fucose and *N*-acetyl-α-D-galactosamine on solid support.

Fmoc cleavage

Cleavage of the Fmoc-protecting group was performed by adding 25% piperidine in DMF (10 mL) and shaking for 10 min. The resin was washed three times with DMF afterwards. This procedure was repeated twice and then the resin was washed 20 times with DMF.

Coupling procedure

The following protocol describes the coupling of *iso*-DTDS for the batch size of 0.317 mmol. The initial coupling of an EDS building block required 5 eq. (0.745 g, 1.59 mmol) of EDS, 5 eq. (0.825 g, 1.59 mmol) of PyBOP and 10 eq. (0.54 mL, 3.17 mmol) of DIPEA with a reaction period of 1.5 h. For *iso*-DTDS the coupling procedure was performed twice (double coupling).

Iso-DTDS (697 mg, 0.951 mmol, 3 eq.) and PyBOP (495 mg, 0.951 mmol, 3 eq.) were dissolved in DMF (3 mL). After addition of DIPEA (1.62 mL, 9.51 mmol, 30 eq.) the mixture was subsequently flushed with nitrogen for 1 min. The solution was added to the resin and shaken for 1.5 h. Afterwards the resin was washed 10 times with DMF.

Capping

After full assembly of the backbones, the *N*-terminal side was capped by addition of acetic anhydride (10 mL) to the resin. The resin was shaken for 15 min and washed three times with DMF. The procedure was repeated once more, followed by washing 10 times with DMF and 10 times with DCM.

CuAAC reaction of carbohydrates

Azidated carbohydrate (0.793 mmol, 3 eq. per alkyne group, total 1.585 mmol, 6 eq.) were dissolved in DMF (2.5 mL) and mixed with aqueous sodium ascorbate solution (1 mL water, 30 mg sodium ascorbate, c = 30 mg/mL, 50 mol% per free alkyne group, total: 2 mL). The mixture was degassed with nitrogen and added to 0.317 mmol of resin loaded with oligomer under nitrogen flow. Aqueous $CuSO_4$ solution (0.6 mL water, 15 mg $CuSO_4$, c = 20 mg/mL, 25 mol% per alkyne group, total: 1.2 mL) were degassed and added to the resin under nitrogen flow. The reaction mixture was shaken overnight. Afterward the reaction mixture was collected to recover the azidated carbohydrate with acetyl-protecting groups by extraction with 50 mL ethyl acetate and washing with 50 mL water (five times). The organic layer was then dried over $MgSO_4$, filtered and the solvent was evaporated in vacuum. The recovered azidated carbohydrates could be used again without further purification. After the coupling the resin was washed extensively with a solution of sodium diethyldithiocarbamate in DMF (23 mM), followed by water, DMF and DCM until the DMF washing solution showed no coloration.

TIPS-deprotection

The resin with oligomer was washed with anhydrous, degassed DMF four times in a filter syringe and then degassed with nitrogen three times. A solution of TBAF in anhydrous DMF (600 mM) was added to the resin (16 eq. per protected alkyne group) and the reaction mixture was shaken for 15 min at room temperature. The reaction mixture was poured into an aqueous $Ca(OH)_2$ solution to avoid formation of HF. The resin was washed three times with DMF. This protocol was repeated for a second time, and then the resin was then extensively washed with DMF, water, 0.1% aqueous TFA solution and water. Washing solutions were collected in the aqueous $Ca(OH)_2$ solution. After quartering the batch, a second CuAAC reaction was performed applying the same procedure as described before, but with different azidated carbohydrates for each batch (Gal, GalNAc, Lac, Sia).

Deacetylation of carbohydrates

A 0.2 M solution of NaOMe in MeOH was added to the resin and shaken for 30 min. The resin was then washed three times with MeOH and three times with DCM. The procedure was repeated once and at the end the washing steps were repeated three times.

Final cleavage

The final glycooligomers were cleaved from the resin by adding 3 mL of cleavage solution (95% TFA, 2.5% TIPS and 2.5% DCM) and shaking for 1 h. Afterwards the reaction mixture was purged in cold Et_2O to precipitate the glycooligomer. The heterogeneous mixture was centrifuged, the ether was decanted and the product was dried in a nitrogen stream. The cleavage procedure was repeated once and the combined crude product fractions were dissolved in 5 mL MilliQ-water each, combined and lyophilized overnight.

Purification

The final glycooligomers were purified by ion exchange resin using 1 g resin per 100 mg glycooligomer according to literature.[3] Afterwards the glycooligomers were further purified by preparative HPLC with a gradient of water and acetonitrile. Glycooligomer analysis was performed by ^{1}H NMR, HR-ESI-MS, MALDI-TOF-MS and RP-HPLC/MS (gradient from 100% to 50% **A** in 30 min, 25 °C).

De-methylation of sialylated glycooligomer 16-Me

To sialylated oligomer (10 mg) 1mL LiOH solution (0.1 M in H_2O/MeOH 1:1) was transfered. The mixture was shaken for 1.5 h. Afterwards the pH of the reaction mixture was monitored and acidic ion exchange resin (Amberlite) was added until reaching a neutral pH. The oligomer solution was collected with the help of a syringe and filtered into a test tube. Water was added to the oligomer solution (5 mL). The resin was washed three times with 2 mL of water and the washing solutions were combined through a filter syringe with the main oligomer solution. The water/methanol solution of sialylated oligomer was lyophilized on a high vacuum pump at ~0.01 mbar overnight.

3.2 Syntheses of azido-functionalized carbohydrates

Azido-2,3,6,2´,3´4´,6´-hepta-*O*-acetyl-β-D-lactose **11**[4], azidoethyl-per-*O*-acetyl-α/β-D-galactopyranoside[5] and azidoethyl-functionalized *N*-acetylneuraminic acid **12**[6,7] were synthesized according to literature. The synthesis of azidoethyl-2,3,4-tri-*O*-acetyl-α-L-fucopyranoside (**8c**), azidoethyl-2,3,4,6-tetra-*O*-acetyl-*N*-acetyl-α-D-galactosamine (**9c**) and azidoethyl-2,3,4,6-tetra-*O*-acetyl-α-D-galactopyranoside (**10c**) were performed in three steps starting from the commercially available monosaccharides, applying a modified protocol by *Roy et al.* (Scheme S2).[8] The synthesis and analytical data of **8c** was previously published.[9]

General procedure for the synthesis of 8c (Fuc-N3), 9c (GalNAc-N3) and 10c (Gal-N3)

In the first step the corresponding monosaccharide was reacted neat with 2-bromoethanol and H_2SO_4-silica catalyst at 65 °C (for catalyst preparation see below). After purification by column chromatography, the functionalized products were obtained as α/β-mixtures in a ratio of 7:1 (**8a**, Fuc) and 17:3 (**9a**, GalNAc) as determined from ^{1}H NMR. In case of **10a** (Gal) the α/β-ratio was not determined and the α/β-mixture was used without further purification. After acetylation in acetic anhydride with H_2SO_4-silica catalyst and work up, pure α-anomeric products were obtained by column chromatography affording **8b** (48% yield), **9b** (24% yield) and **10b** (10% yield). Final substitution with sodium azide in DMF was performed generating **8c, 9c** and **10c**.

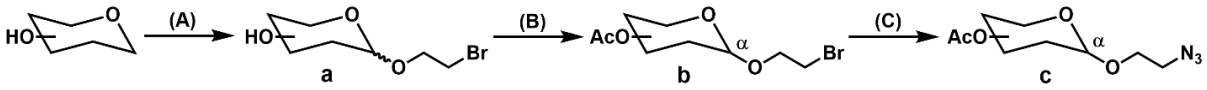

Scheme S2: Synthesis of azidoethyl-functionalized monosaccharides in α-conformation. *Reagents and conditions*: (**A**) 2-bromoethanol (5 eq.), H_2SO_4-silica catalyst, 65 °C, 6 h/RT, 16 h; (**B**) Ac_2O (48 eq.), H_2SO_4-silica catalyst, RT; (**C**) NaN_3 (4 eq.), DMF, 50 °C, 36 h.

Preparation of H_2SO_4–silica catalyst

The catalyst was prepared as described in literature[8]: Briefly, Et_2O (50 mL) and silica gel (10 g) were mixed and conc. H_2SO_4 (3 mL) was added carefully. The suspension was shaken for 5 min and the solvent was evaporated under reduced pressure. The remaining functionalized silica catalyst was dried for 3 h at 110 °C and was used without further purification.

2-Bromoethyl-α/β-pyranosides (a)

O-Acetyl protected monosaccharide (122 mmol, 1 eq.) was suspended in 2-bromoethanol (44 mL, 620 mmol, 5 eq.) and was heated to 65 °C. Subsequently H_2SO_4–silica catalyst (0.61 g) was added. All material was dissolved after 6 h. If starting material was still visible additional catalyst was added. Stirring at 65 °C was continued until TLC reaction control showed complete conversion. The reaction mixture was allowed to cool to room temperature and stirred for additional 16 h. The crude product was separated from excess 2-bromoethanol by silica gel column chromatography with DCM. Product pyranosides were isolated as anomeric mixtures with a gradient of DCM/MeOH in case of **8a** (fucose) and **10a** (Gal) and with DCM/MeOH (6:1) in case of GalNAc (**9a**) and used without further purification.

2-Bromoethyl-α/β-L-fucopyranoside (8a) was afforded as a colorless to yellowish solid (19.45 g, 71.89 mmol) in 59% yield as α/β-mixture (7:1).

2-Bromoethyl-*N*-acetyl-α/β-D-galactosamine (9a) was afforded as a colorless solid (2.88 g, 8.8 mmol) in 28% yield as α/β-mixture (17:3). ^{1}H NMR (300 MHz, CD_3OD): δ [ppm] = 4.93 (d, ^3J = 1.9 Hz, 0.2H, H-1, *starting material*), 4.91 (d, ^3J = 3.7 Hz, 1H, αH-1), 4.58 (s, br, 0.2H, NH), 4.27 (dd, $^{3,3}J$ = 11.6, 4.3 Hz, 1H, H-3), 4.17 (dd, $^{3,3}J$ = 4.1, 2.0 Hz, 0.2H, H-3, *starting material*), 4.02-3.95 (m, 1H, H-2), 3.90 (d, ^3J = 4.4 Hz, 2H, H-6), 3.84-3.70 (m, 4H, H-4, H-5, OCH_2CH_2Br), 3.64-3.56 (m, 2H, OCH_2CH_2Br), 1.97 (s, 3H, CH_3), 1.97 (s, 0.5H, CH_3, *starting material*). ESI-MS: *m/z* for $C_{10}H_{18}BrNO_6$ (exact monoisotopic mass 327.0): $[M+H]^+$ calcd. 328.0, found 328.2. R_f = 0.48 (DCM/MeOH (4:1)).

2-Bromoethyl-α/β-D-galactopyranoside (10a) was afforded as colorless solid (4.65 g, 16.3 mmol) in 29% yield as a α/β-mixture and was used without further purification.

2-Bromoethyl-per-O-acetyl-α-pyranosides (b)

To a suspension of 2-bromoethylpyranoside (8.8 mmol, 1 eq.) in acetic anhydride (40 mL, 423 mmol, 48 eq.) was added 880 mg H_2SO_4-silica catalyst (100 mg per mmol starting material) and the reaction mixture was stirred at room temperature for 16-24 h (see details for each compound). After completion of the reaction as determined by TLC, the mixture was diluted with 20 mL DCM and washed with saturated $NaHCO_3$ aq. solution and water twice. The organic layers were combined, dried over $MgSO_4$ and the solvent was removed under reduced pressure. Anomeric mixtures of **8b**, **9b** and **10b** were separated by silica gel column chromatography as described below.

2-Bromoethyl-2,3,4-tri-*O*-acetyl-α-L-fucopyranoside (8b) was obtained as white solid (210 mg, 0.53 mmol, 48 %). Reaction time was 24 h. Silica gel column chromatography was performed with a gradient of toluene/ethyl acetate (50:1 – 8:1).

2-Bromoethyl-2,3,4,6-tetra-*O*-acetyl-*N*-acetyl-α-D-galactosamine (**9b**) was obtained as white solid (0.967 g, 2.1 mmol, 24 %). Reaction time was 16 h. Silica gel column chromatography was performed with a gradient of toluene/ethyl acetate (50:1 – 8:1). ^{1}H NMR (600 MHz, $CDCl_3$): δ [ppm] = 5.73 (d, ^3J = 9.7 Hz, 1H, NH), 5.39 (dd, $^{3,3}J$ = 3.3, 1.3 Hz, 1H, H-4), 5.18 (dd, $^{3,3}J$ = 11.3, 3.2 Hz, 1H, H-3), 4.93 (d,

^{3}J = 3.7 Hz, 1H, H-1α), 4.60 (ddd, $^{3,3,3}J$ = 11.3, 9.7, 3.7 Hz, 1H, H-2), 4.31-4.21 (m, 1H, H-5), 4.17-3.98 (m, 3H, H-6, OCH_2CH$_2$Br), 3.80 (dt, $^{2,3}J$ = 11.6, 6.0 Hz, 1H, OCH_2CH$_2$Br), 3.54 (dd, $^{3,3}J$ = 5.9, 5.0 Hz, 2H, OCH$_2$CH_2Br), 2.22 (s, 3H, CH$_3$), 2.16 (s, 3H, CH$_3$), 2.05 (s, 3H, CH$_3$), 2.00 (s, 3H, CH$_3$), 1.97 (s, 3H, CH$_3$). ^{13}C NMR (151 MHz, CDCl$_3$): δ [ppm] = 171.1 (NH(C=O)), 170.5 (C=O), 170.4 (C=O), 170.3 (C=O), 166.5 (NHCO), 98.3 (C-1α), 68.5, 68.4, 67.4, 67.4 (C-3, C-4, C-5, C-6), 62.1 (CH$_2$CH$_2$Br), 47.9 (C-2), 30.9 (CH$_2$Br), 23.4, 22.3 ((NH)(CO)CH$_3$), 20.9 (CH$_3$), 20.9 (CH$_3$), 20.8(CH$_3$). ESI-MS: *m/z* for $C_{16}H_{24}BrNO_9$ (exact monoisotopic mass 453.1): $[M+H]^+$ calcd. 454.1, found 456. R_f = 0.66 (α) and 0.57 (β) (DCM/MeOH (8:1)).

2-Bromoethyl-2,3,4,6-tetra-*O*-acetyl-α-D-galactopyranoside (**10b**) was obtained as white solid (720 mg, 1.6 mmol, 10 %). Reaction time was 24 h. Silica gel column chromatography was performed with a gradient of *n*-hexane/ethyl acetate (50:1 – 3:1). ^{1}H NMR (600 MHz, CDCl$_3$): δ [ppm] = 5.47-5.46 (m, 1H, H-4), 5.36 (dd, $^{3,3}J$ = 10.9, 3.4 Hz, 1H, H-3), 5.19 (d, ^{3}J = 3.7 Hz, 1H, α-H-1), 5.11 (dd, $^{3,3}J$ = 10.9, 3.7 Hz, 1H, H-2), 4.33 (t, ^{3}J = 6.9 Hz, 1H, H-5), 4.10 (qd, $^{2,3}J$ = 11.3, 6.6 Hz, 2H, H-6), 3.99 (dt, $^{2,3}J$ = 11.5, 5.8 Hz, 1H, OCH_2CH$_2$Br), 3.83 (dt, $^{2,3}J$ = 11.6, 5.9 Hz, 1H, OCH_2CH$_2$Br), 3.50 (t, ^{3}J = 5.9 Hz, 2H, OCH$_2$CH_2Br), 2.14 (s, 3H, CH_3), 2.09 (s, 3H, CH_3), 2.05 (s, 3H, CH_3), 1.99 (s, 3H, CH_3). ^{13}C NMR (151 MHz, CDCl$_3$): δ [ppm] = 170.6 (C=O), 170.5 (C=O), 170.3 (C=O), 170.1 (C=O), 96.6 (C-1α), 68.8, 68.2, 67.6, 66.9 (C-2, C-3, C-4, C-5, C-6), 61.9 (CH$_2$-CH$_2$-Br), 30.1 (CH$_2$-Br), 21.0 (CH$_3$), 20.9 (CH$_3$), 20.8 (CH$_3$), 20.8 (CH$_3$). ESI-MS: *m/z* for $C_{16}H_{23}BrNO_{10}$ (exact monoisotopic mass 454.0): $[M+H_3O]^+$ calcd. 473.1, found 474. R_f = 0.53 (*n*-hexane/ethyl acetate (6:4)).

2-Azidoethyl-per-O-acetyl-α-pyranosides (c)

2-Bromoethyl-per-*O*-acetyl-α-pyranoside (5 mmol, 1 eq.) dissolved in DMF (40 mL) was treated with sodium azide (1.3 g, 20 mmol, 4 eq.). The reaction mixture was heated to 50 °C and stirred for 36 h. Conversion was monitored by TLC. To the crude product 10 mL of water was added and the reaction mixture was concentrated to almost dryness under reduced pressure at 55 °C (9 mbar). Remark: the mixture should not be dried completely to avoid any risk of explosion (organic azides). The resulting crude product was dissolved in ethyl acetate and washed three times with water, three times with saturated NaHCO$_3$ aq. solution and three times with water again. The organic layer was dried over MgSO$_4$, filtered and the solvent was removed under reduced pressure. The corresponding product was dried in high vacuum.

2-Azidoethyl-2,3,4-tri-*O*-acetyl-α-L-fucopyranoside (**8c**) was obtained as white crystals (1.61 g, 4.48 mmol, 90 %).

2-Azidoethyl-2,3,4,6-tetra-*O*-acetyl-*N*-acetyl-α-D-galactosamine (**9c**) was obtained as colorless crystals (450 mg, 1.08 mmol, 61 %). ^{1}H NMR (300 MHz, CDCl$_3$): δ [ppm] = 5.66 (d, ^{3}J = 9.6 Hz, 1H, NH), 5.39 (d, ^{3}J = 2.9 Hz, 1H, H-4), 5.17 (dd, $^{3,3}J$ = 11.4, 3.2 Hz, 1H, H-3), 4.94 (d, ^{3}J = 3.6 Hz, 1H, H-1α), 4.62 (ddd, $^{3,3,3}J$ = 11.2, 9.9, 3.6 Hz, 1H, H-2), 4.18 (t, ^{3}J = 6.5 Hz, 1H, H-5), 4.13-4.07 (m, 3H, H-6, *overlapping with residual ethyl acetate*), 3.91 (ddd, $^{2,3,3}J$ = 10.8, 5.4, 2.9 Hz, 1H, OCH_2CH$_2$N$_3$), 3.66 (ddd, $^{2,3,3}J$ = 10.8, 8.0, 2.8 Hz, 1H, OCH$_2$CH_2N$_3$), 3.54 (ddd, $^{2,3,3}J$ = 13.4, 8.0, 2.9 Hz, 1H, OCH$_2$CH_2N$_3$), 3.35 (ddd, $^{2,3,3}J$ = 13.5, 5.4, 2.8, 1H, OCH_2CH$_2$N$_3$), 2.16 (s, 3H, CH$_3$), 2.04 (s, 3H, CH$_3$), 2.03 (*residual ethyl acetate*), 1.99 (s, 3H, CH$_3$), 1.96 (s, 3H, CH$_3$), 1.25 (*residual ethyl acetate*). ^{13}C NMR (151 MHz, CDCl$_3$): δ [ppm] =207.1 (*residual acetone*), 171.0 (NH(CO), 170.5 (C=O), 170.4 (C=O), 170.4 (C=O), 98.2 (C-1α), 68.3, 67.7, 67.4, 67.2 (C-3, C-4, C-5, C-6), 62.0 (OCH$_2$CH$_2$N$_3$), 60.5 (*residual ethyl acetate*),

50.6 (C-2), 47.7 (CH_2N_3), 31.0 (*residual acetone*), 23.3 (NH(CO)$\underline{C}H_3$), 21.2 (*residual ethyl acetate*), 20.9 (CH_3), 20.8 (CH_3), 20.8 (CH_3), 14.3 (*residual ethyl acetate*). ESI-MS: *m/z* for $C_{16}H_{24}N_4O_9$ (exact monoisotopic mass 416.2): $[M+H]^+$ calcd. 417.2, found 417.2.

2-Azidoethyl-2,3,4,6-tetra-*O*-acetyl-α-D-galactopyranoside (**10c**) was obtained as white crystals (0.486 g, 1.16 mmol, 87 %). ^{1}H NMR (300 MHz, $CDCl_3$): δ [ppm] = 5.46 (dd, $^{3,3}J$ = 3.4, 1.3 Hz, 1H, H-4), 5.35 (dd, $^{3,3}J$ = 10.3, 3.4 Hz, 1H, H-3), 5.18-5.08 (m, 2H, H-1α, H-2), 4.24 (dt, $^{3.3}J$ = 6.6, 6.2, 1.1 Hz, 1H, H-5), 4.09 (d, ^3J = 6.4 Hz, 2H, H-6), 3.86 (m, 1H, OCH_2CH$_2$N$_3$), 3,62 (m, 1H, OCH_2CH$_2$N$_3$), 3.51-3.34 (m, 2H, OCH$_2$CH_2N$_3$), 2.13 (s, CH_3), 2.07 (s, CH_3), 2.04 (s, CH_3), 1.97 (s, CH_3). ^{13}C NMR (75.5 MHz, $CDCl_3$): δ [ppm] = 170.7 (C=O), 170.5 (C=O), 170.3 (C=O), 170.1 (C=O), 96.6 (C-1α), 68.1, 68.0, 67.5, 67.5, 66.7 (C-2, C-3, C-4, C-5, C-6), 61.9 (O$\underline{C}$H$_2$CH$_2$N$_3$), 50.5 (CH_2N_3), 20.9 (CH_3), 20.8 (CH_3), 20.8 (CH_3). HR-ESI-MS: *m/z* for $C_{16}H_{23}N_3O_{10}$ (exact monoisotopic mass 417.1383): $[M+NH_4]^+$ calcd. 435.1727, found 435.1725. R_f = 0.79 (*n*-hexane/ethyl acetate (6:4)).

General procedure for the synthesis of 12 (Sia-N3)

The synthesis of *N*-acetyl-α-neuraminic acid (α-sialic acid) with an azidoethyl-linker (**12**) is shown in Scheme 3 and was realized by a modified procedure from literature (Scheme S3) affording the α-functionalized product in an overall yield of 16 %.[6,7] The reaction sequence started with the methylation of the acid group using dry methanol in the presence of Dowex as an acidic resin. The resulting crude α/β-mixture of **A** was suspended and stirred in acetyl chloride. After distillation of the excess acetyl chloride the crude peracetylated **B** was used in the next step without further purification. The chloride was substituted with 2-bromoethanol in a S_N2 reaction promoted by Ag_2CO_3. Product **C** was obtained as α/β-mixture (2:1) and converted into the desired azido-glycoside **D** with NaN_3 in DMF. Unfortunately, azide-functionalized acetylated sialic acid **D** and the corresponding bromoethyl-functionalized **C** could not be distinguished in TLC for reaction control. Therefore, IR was conducted to monitor formation of **D** by the appearance of a peak at 2107 cm^{-1} (Figure S46). To separate the α/β-mixture, azidated acetyl-protected sialic acid **D** was deprotected with sodium methanolate in methanol. Column chromatography of crude neutralized product **E** led to 66% of the α-product. The α-anomer was re-acetylated afterwards with Ac_2O because the peracetylated product exhibits a higher stability in the CuAAC reaction on solid support and enables a simple recovery of the anomerically pure sialic acid azide derivative **12α** after CuAAC by extraction with ethyl acetate and washing with water.

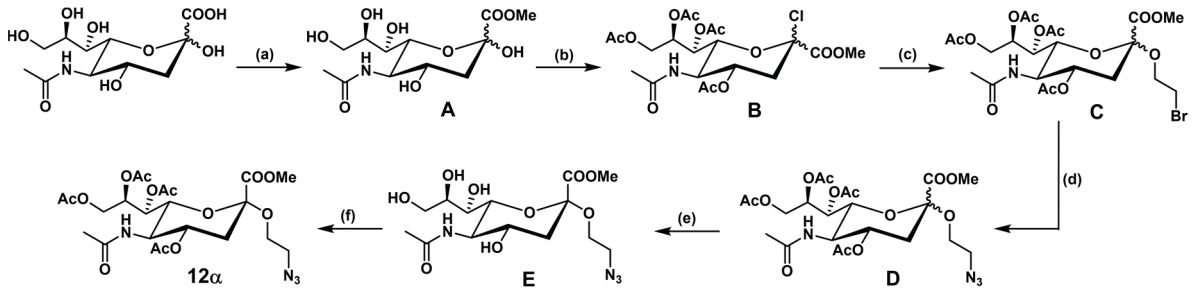

Scheme S3: Synthesis of azidoethyl-functionalized sialic acid **12α**. *Reagents and conditions*: (**a**) dry MeOH, acidic catalyst Dowex, 16 h, RT, 98 %; (**b**) acetyl chloride (90 eq.), 2 d, RT, N_2-atm.; (**c**) 2-bromoethanol (41 eq.), molecular sieves, Ag_2CO_3 (2 eq.), N_2-atm, 20 h, RT, 47 %; (**d**) NaN_3, DMF, 36 h, 50 °C, 81 %; (**e**) MeONa in MeOH (0.2 M, 3.9 eq.), 4 h, RT, AcOH, 66 % α-product; (**f**) *Re-acetylation of α-product*: Ac_2O, *p*-TsOH x H_2O, 0 °C/RT, 18 h, 72 %.

N-Acetylneuraminic acid methyl ester (A)

Methanol was dried with molecular sieves for 16 h and freshly distilled prior to use. *N*-Acetylneuraminic acid (10 g, 32.4 mmol, 1 eq.) was stirred with LewatitK2629 acid catalyst (2.5 g) in 750 mL dry methanol for 16 h at room temperature. The suspension became a clear solution as the reaction equilibrium shifted towards product formation. The catalyst was removed by filtration and the reaction mixture was concentrated to dryness under reduced pressure affording methyl ester (**A**) as white solid (10.22 g, 31.5 mmol, 98 %). The resulting product was used without further purification.

^{1}H NMR (600 MHz, DMSO-d_6): δ [ppm] = 8.09 (d, ^{3}J = 8.3 Hz, 1H, NH), 6.42 (d, ^{3}J = 2.3 Hz, 1H, OH), 4.83 (d, ^{3}J = 6.3 Hz, 1H, OH), 4.55 (d, ^{3}J = 4.6 Hz, 1H, OH), 4.33 (d, ^{3}J = 5.5 Hz, 1H, OH), 4.21 (t, ^{3}J = 6.0 Hz, 1H, OH), 3.90-3.79 (m, 1H, H-8), 3.76-3.71 (m, 4H, H-9, $COOCH_3$), 3.63-3.45 (m, 3H, H-5, H-4, H-9), 3.31-3.25 (m, 1H, H-6), 3.18 (ddd, $^{3,3,3}J$ = 9.3, 4.6, 1.3 Hz, 1H, H-7), 2.03 (dd, $^{2,3}J$ = 12.8, 4.9 Hz, 1H, H-3_{eq}), 1.89 (s, 3H, NC(=O)CH_3), 1.76-1.67 (m, 1H, H-3_{ax}). ^{13}C NMR (151 MHz, DMSO-d_6): δ [ppm] = 171.9 (NH(C=O)), 170.2 ($\underline{C}OOCH_3$), 94.9 (C-2), 70.5, 69.7, 69.1 (C-6, C-7, C-8), 65.5 (C-4), 63.6 (C-9), 53.0 (C-5), 52.3 (O-$\underline{C}H_3$), 48.6 (C-3), 22.6 ((CO$\underline{C}H_3$).

2-Chloro-4,7,8,9-tetra-O-acetyl-N-acetylneuraminic acid methyl ester (B)

N-Acetylneuraminic acid methyl ester (7 g, 22 mmol, 1 eq.) was suspended in acetyl chloride (140 mL, 1.96 mol, 90 eq.) and the mixture was stirred at room temperature for 2 d under nitrogen. The progress of the reaction was monitored by TLC (*n*-hexane/ethyl acetate (1:4)). After completion of the reaction, the solution became clear. Distillation to dryness and drying on high vacuum pump 12 g of a white to yellowish solid of crude product **B that** was used without further purification.

^{1}H NMR (300 MHz, $CDCl_3$): δ [ppm] = 5.60 (d, ^{3}J = 10.0 Hz, 1H, NH), 5.47 (dd, $^{3,3}J$ = 6.9, 2.3 Hz, 1H, H-7), 5.39 (ddd, $^{3,3,3}J$ = 10.2, 6.2, 4.8 Hz, 1H, H-4), 5.16 (ddd, $^{3,3,3}J$ = 7.0, 5.9, 2.7 Hz, 1H, H-8), 4.42 (dd, $^{2,3}J$ = 12.5, 2.7 Hz, 1H, H-9), 4.35 (dd, $^{3,3}J$ = 10.8, 2.4 Hz, 1H, H-6), 4.20 (q, ^{3}J = 10.4 Hz, 1H, H-5), 4.06 (dd, $^{2,3}J$ = 12.5, 5.9 Hz, 1H, H-9), 3.87 (s, 3H, $COOCH_3$), 2.77 (dd, $^{2,3}J$ = 13.9, 4.8 Hz, 1H, H-3_e), 2.31-2.22 (m, 1H, H-3_a), 2.11 (s, 3H, C(=O)CH_3), 2.07 (s, 3H, C(=O)CH_3), 2.05, 2.04 (s, s, 6H, C(=O)CH_3), 1.90 (s, 3H, C(=O)CH_3). ESI-MS: *m/z* for $C_{20}H_{28}ClNO_{12}$ (exact monoisotopic mass 509.1): $[M+H]^+$ calcd. 510.1, found 510.1; $[M-H_2O+H]^+$ calcd. 492.1, found 492.2; $[M-HCl+H]^+$ calcd. 474.2, found 474.2; $[M-HOAc+H]^+$ calcd. 450.1, found 450.1; $[M-HOAc-H_2O+H]^+$ calcd. 432.1, found 432.2; $[M-HOAc-HCl+H]^+$ calcd. 414.1, found 414.1; $[M-2HOAc+H]^+$ calcd. 390.1, found 390.1; [M(*hydrolyzed prod*)+K]$^+$ calcd. 362.08, found 362.2. R_f = 0.34 (ethyl acetate/*n*-hexane (4:1).

2-Bromoethyl-4,7,8,9-tetra-O-acetyl-N-acetylneuraminic acid methyl ester (C)

Sialyl chloride **B** (3 g, 5.9 mmol, 1 eq.) was dissolved in 2-bromoethanol (17 mL, 240 mmol, 41 eq.) and the solution was flushed with nitrogen. Molecular sieves (amount 3.75 g, 4 Å, 1.25 mg per mg sialyl chloride **B**) were added and the reaction mixture was stirred at room temperature. After 1 h Ag_2CO_3 (3.25 g, 11.8 mmol, 2 eq.) was added and the reaction mixture was stirred for additional 20 h at room temperature in the dark. The solid was filtered, washed with ethyl acetate and the yellow filtrate was washed three times with H_2O. The organic layer was dried over $MgSO_4$, filtered and concentrated to dryness under reduced pressure. Column chromatography DCM/ethyl acetate (1:1) afforded the α/β-mixture of product glycoside **C** as yellow oil (1.67 g, 2.8 mmol, 47 %). IR: ν (cm^{-1}) = 1741, 1664, 1369, 1213, 1126, 1070, 1034, 947, 601, 569, 405. ESI-MS: *m/z* for $C_{22}H_{32}BrNO_{13}$ (exact monoisotopic mass

597.1) $[M+Na]^+$ calcd. 620.1, found, 620.0; $[M+H]^+$ calcd. 598.1, found 600.0; $[M-Br(CH_2)_2OH]^+$ calcd. 474.2, found 474.2. R_f = 0.51 (ethyl acetate).

2-Azidoethyl-4,7,8,9-tetra-O-acetyl-N-acetylneuraminic acid methyl ester (D)

In a 250 mL round bottom flask, a solution of **C** (4.12 g, 6.9 mmol) in DMF (55 mL) was treated with sodium azide (1.79 g, 27.6 mmol) and the reaction mixture (yellow dispersion). The reaction was stirred for 36 h at 50 °C and monitored via TLC (ethyl acetate/toluene (3:2)). After 24 h, the reaction mixture was concentrated to almost dryness under reduced pressure at 55 °C. The resulting yellow product was redissolved in 250 mL ethyl acetate and water and the organic layer was washed three times with 250 mL water, three times with 250 mL saturated $NaHCO_3$ and again three times with 250 mL water. The organic layer was dried over magnesium sulfate, filtered and concentrated to dryness under reduced pressure affording **D** as a white to yellowish solid in a 2:1 α/β-mixture (3.14 g, 5.6 mmol, 81 %). For analytical details see anomerically pure compound **12α**.

2-Azidoethyl-N-acetyl-α-neuraminic acid methyl ester (E)

To peracetylated sialoside **D** (2 g, 3.57 mmol, 1 eq) a solution of sodium methoxide in methanol (70 mL, 0.2 M, 14 mmol, 3.9 eq) was added. The mixture was stirred for 4 h at room temperature. The reaction was monitored by TLC (ethyl acetate/MeOH/H_2O (4:1:0.1)). After completion the solution was neutralized by drop-wise addition of 0.8 mL glacial AcOH (pH should be approximately 7). The solvent was removed under reduced pressure. Column chromatography afforded α-anomeric compound **E** (0.916 g, 2.34 mmol, 66 %).

^{1}H NMR (600 MHz, Methanol-d_4): δ [ppm] = 3.98 (ddd, $^{2,3,3}J$ = 10.6, 5.7, 3.4 Hz, 1H, OCH_2CH_2N_3), 3.85 (s, 3H, COOCH_3), 3.85-3.82 (m, 2H, H-8, H-9), 3.78 (t, ^3J = 10.2, 1H, H-5), 3.69-3.62 (m, 3H, H-4, H-9, OCH_2CH_2N_3), 3.59 (dd, $^{3,3}J$ = 10.5, 1.6 Hz, 1H, H-6), 3.51 (dd, $^{3,3}J$ = 8.9, 1.5 Hz, 1H, H-7), 3.39 (ddd, $^{2,3,3}J$ = 13.3, 7.4, 3.4 Hz, 1H, CH_2N_3), 3.33-3.29 (m, ~1H, *overlapping with solvent peak,* CH_2N_3), 2.72 (dd, $^{2,3}J$ = 12.8, 4.7 Hz, 1H, H-3$_{eq}$), 2.00 (s, 3H, NC(=O)CH_3), 1.98 (s, 1H, residual acetic acid), 1.77 (m, 1H, H-3$_{ax}$). ^{13}C NMR (151 MHz, Methanol-d_4): δ [ppm] = 175.20 (NHC=O), 170.64 (C-1), 100.14 (C-2), 74.94, 72.31, 70.13, 68.40 (C-4, C-6, C-7, C-8), 64.66 (C-6), 64.44 (CH_2CH_2N_3), 53.70 (C-5), 53.48 (OCH_3), 51.68 (CH_3N_3), 41.50 (C-3), 22.71 ((C=O)CH_3). R_f = 0.41 (alpha) (DCM/MeOH/H_2O (9:2:0.2)).

Re-acetylation: 2-Azidoethyl-4,7,8,9-tetra-O-acetyl-N-acetyl-α-neuraminic acid methyl ester (12α)

Sialic acid azide **E** (0.5 g, 1.27 mmol, 1 eq.) was suspended in acetonitrile (20 mL) to give a white suspension. The mixture was cooled to 0 °C and acetic anhydride (8 mL, 85 mmol, 67 eq.) was added drop-wise. Then *p*-toluene sulfonic acid monohydrate (200 mg, 1.05 mmol, 0.8 eq.) was added and the reaction mixture was stirred for 18 h at room temperature. Reaction control was performed with TLC (ethyl acetate/MeOH/H_2O (4:1:0.2)). After complete conversion the solvent was removed under reduced pressure. The yellow oil was dissolved in ethyl acetate and washed three times with water and six times with saturated aqueous $NaHCO_3$. The organic layer was separated, dried over $MgSO_4$, filtered and the solvent was removed under reduced pressure. Product **12α** was obtained as colorless oil (0.506 g, 0.903 mmol, 71 % yield).

^{1}H NMR (600 MHz, $CDCl_3$): δ [ppm] = 5.39 (ddd, *J* = 8.6, 5.7, 2.7 Hz, 1H, H-4), 5.31 (dd, *J* = 8.7, 2.1 Hz, 1H, H-7), 5.22 (d, ^{3}J = 9.8 Hz, 1H, NH), 4.87 (ddd, *J* = 12.3, 10.0, 4.6 Hz, 1H, H-8), 4.29 (dd, *J* = 12.5, 2.7 Hz, 1H, H-9), 4.08 (m, 3H, H-9, H-5, H-6), 3.97 (ddd, $^{2,3,3}J$ = 10.7, 5.6, 3.1 Hz, 1H, C*H*$_2$CH$_2$N$_3$), 3.81 (s, 3H, COOCH$_3$), 3.47 (ddd, $^{2,3,3}J$ = 10.7, 7.5, 3.1 Hz, 1H, C*H*$_2$CH$_2$N$_3$), 3.38 (ddd, $^{2,3,3}J$ = 13.3, 7.5, 3.1 Hz, 1H, CH$_2$N$_3$), 3.29 (ddd, $^{2,3,3}J$ = 13.3, 5.6, 3.1 Hz, 1H, CH$_2$N$_3$), 2.62 (dd, *J* = 12.9, 4.6 Hz, 1H, H-3$_e$), 2.14, 2.13 (s, s, C(=O)CH3), 2.03, 2.02 (s, s, C(=O)CH3), 1.97 (m, 1H, H-3$_a$), 1.87 (s, N-C(=O)CH3). ^{13}C NMR (151 MHz, $CDCl_3$): δ [ppm] = 171.12, 170.79, 170.37, 170.29, 170.21 (CO(CH$_3$)), 168.27 (COO-CH$_3$), 98.81 (C-2), 72.65 (C-6), 69.04, 68.40, 67.31 (C-4, C-7, C-8), 64.27 (C-9), 62.55 (OCH$_2$CH$_2$N$_3$), 53.00 (C-5), 50.65 (COO-CH$_3$), 49.53 (OCH$_2$CH$_2$N$_3$), 38.08 (C-3), 23.33 (NC(=O)CH$_3$), 21.26, 20.98, 20.94, 20.89 (OC(=O)CH$_3$). IR: ν (cm^{-1}) = 2107, 1741, 1664, 1369, 1213, 1126, 1034, 947, 601. HR-ESI-MS: *m/z* for $C_{22}H_{32}N_4O_{13}$ (exact monoisotopic mass 560.1966) $[M+H]^+$ calcd. 561.2044, found 561.2037. R_f = 0.30 (α) (ethyl acetate/MeOH/H_2O (9:2:0.2)).

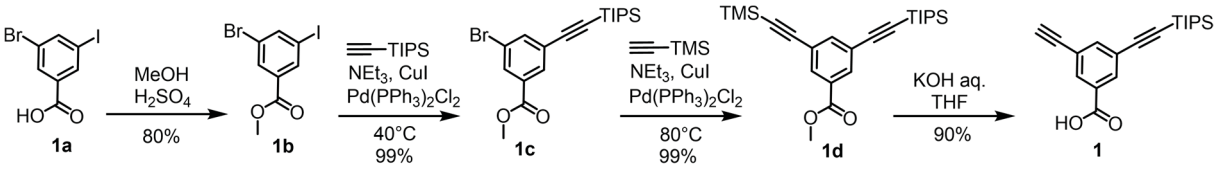

Scheme S4: Synthesis of compound **1** as precursor for the synthesis of *iso*-DTDS, according to literature.[10]

4. *Iso*-DTDS reactivity studies

4.1 Kinetic studies of TFA-deprotection of compound **5**

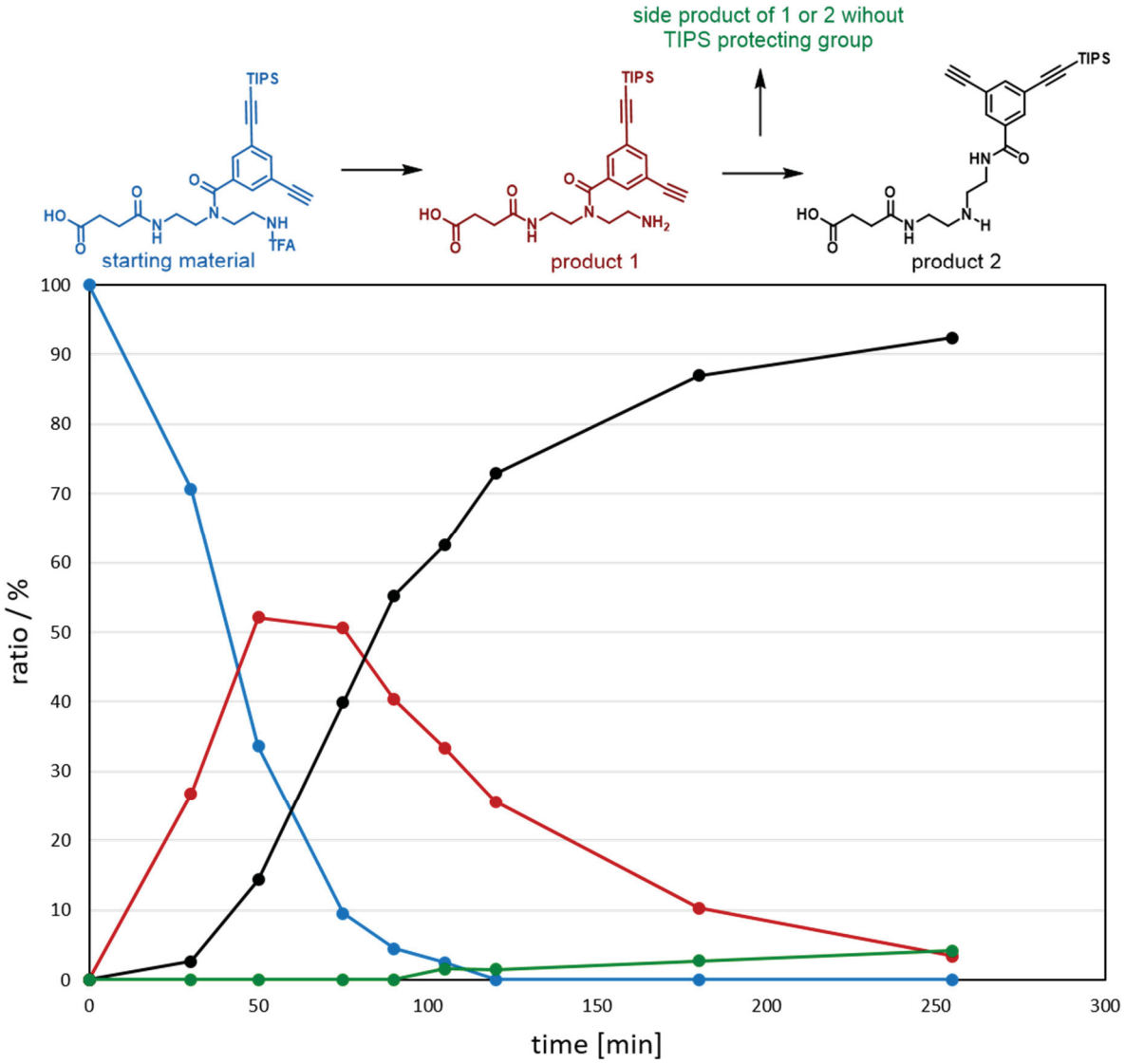

Figure S1: Kinetic study of TFA-deprotection (product 1, red) and rearrangement (product 2 = compound **6**, black) of starting material (compound **5**, blue) and side product (green), determined by integration of corresponding peak areas from RP-HPLC/MS spectra (from 100 % to 50 % eluent **A** in 5 min, decreasing to 0 % **A** until 12 min, proceeding at 0 % **A**, 17 min, 25 °C).

Table S1: Kinetic study of TFA-deprotection: relative amounts of starting material (**5**), product 1 (rearrangement product), product 2 (**6**) and side product during the reaction process. [a]Determined by integration of peak areas from RP-HPLC/MS spectra (from 100 % to 50 % eluent **A** in 5 min, decreasing to 0 % **A** until 12 min, proceeding at 0 % **A**, 17 min, 25 °C).

Time [min]	Amount Starting material[a]	Amount product 1[a]	Amount product 2[a]	Amount side product[a]
0	100.0	0.0	0.0	0.0
30	70.7	26.7	2.6	0.0
50	33.6	52.1	14.3	0.0
75	9.5	50.6	39.9	0.0
90	4.5	40.3	55.2	0.0
105	2.5	33.4	62.5	1.6
120	0.0	25.6	72.9	1.5
180	0.0	10.3	87.0	2.7
255	0.0	3.4	92.4	4.2
1360	0.0	0.0	92.4	7.6

4.1 Coupling efficiencies

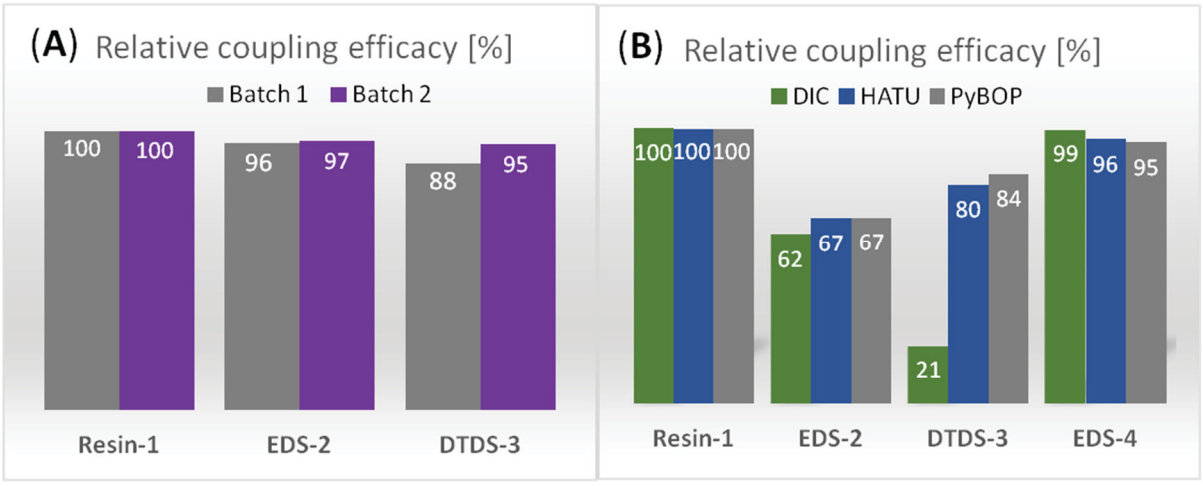

Figure S2: Efficiencies of Fmoc-deprotection and coupling steps of test sequence [Resin(1)-EDS(2)-DTDS(3)-EDS(4)], determined by UV/Vis measurements (301 nm) of Fmoc-cleavage solution after deprotection with UV-signal of cleavage solution from resin set to 100 %: (A) for batch 1 (monocoupling) and batch 2 (double coupling in case of *iso*-DTDS) using PyBOP as coupling reagent, (B) monocoupling for three different coupling reagents (DIC, HATU, PyBOP).

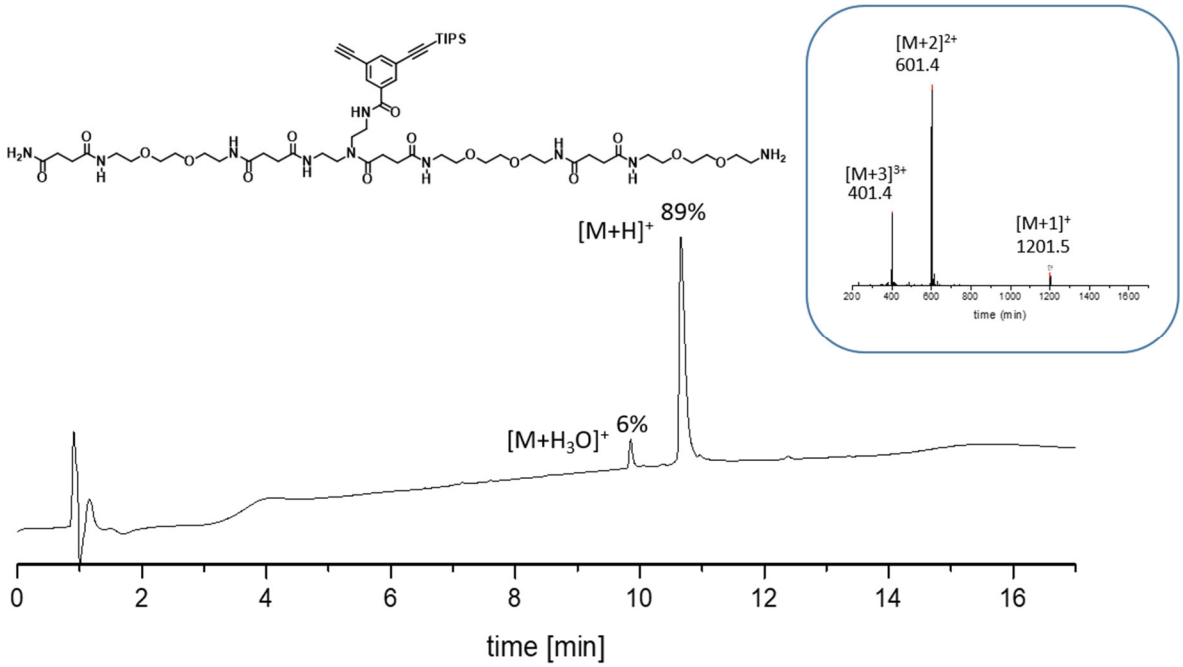

Figure S3: RP-HPLC chromatogram (gradient from 80 % to 100 % eluent **B** in 10 min, proceeding at 100% **B**, 17 min, 25 °C) of crude product of test structure [EDS-DTDS-EDS-EDS] and corresponding mass spectrum (after microcleavage with 95 % TFA in DCM/TIPS (1:1)).

5. Spectral analysis

5.1 Building blocks

Iso-DTDS

3-Bromo-5-iodobenzoic acid methyl ester (1b)

^{1}H NMR (300 MHz, $CDCl_3$): δ [ppm] = 8.28 (t, $^{3,3}J$ = 1.5 Hz, 1H, H_{Ar}-4), 8.11 (t, $^{4,4}J$ = 1.6 Hz, 1H, H_{Ar}-2), 8.02 (t, $^{4,4}J$ = 1.7 Hz, 1H, H-6$_{Ar}$), 3.92 (s, 3H, COCH_3). R_f = 0.74 (*n*-hexane/ethyl acetate (5:1)).

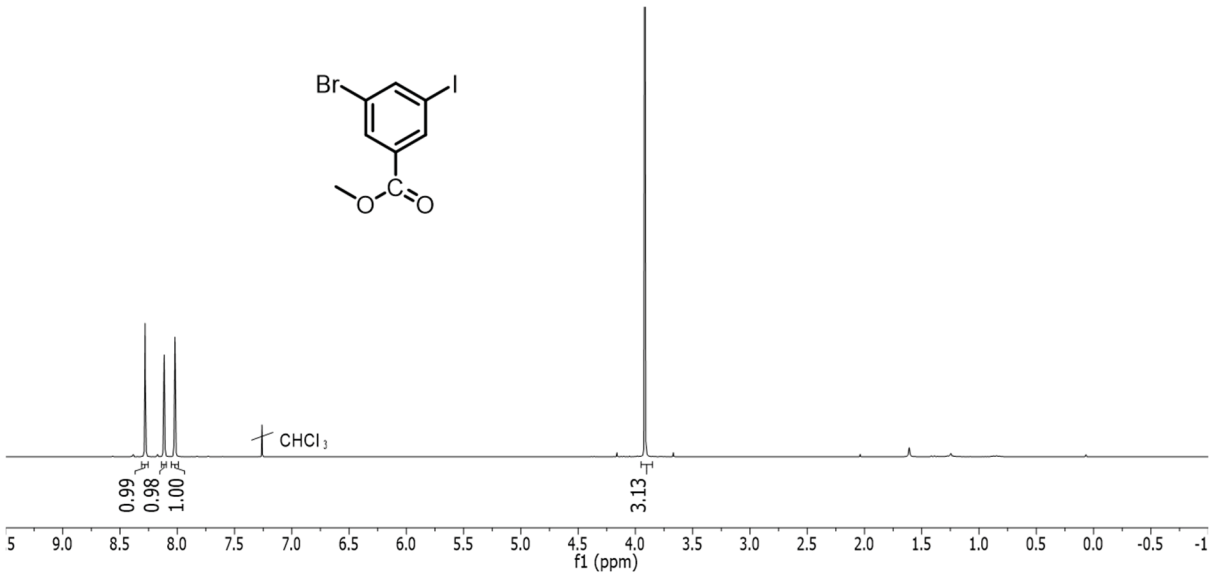

Figure S4: ^{1}H NMR spectrum (300 MHz, $CDCl_3$) of compound **1b**.

3-Bromo-5-((triisopropylsilyl)ethynyl)benzoic acid methyl ester (1c)

^{1}H NMR (300 MHz, $CDCl_3$): δ [ppm] = 8.10 (s, 1H, H_{Ar}-2), 8.03 (s, 1H, H_{Ar}-6), 7.77 (s, 1H, H_{Ar}-4), 3.93 (s, 3H, COCH_3), 1.13 (s, 21H, CH-(CH_3)$_2$). HR-ESI-MS: *m/z* for $C_{19}H_{27}BrO_4Si$ (exact monoisotopic mass 394.0964) $[M+H]^+$ calcd. 395.1042, found 395.1029. R_f = 0.57 (*n*-hexane).

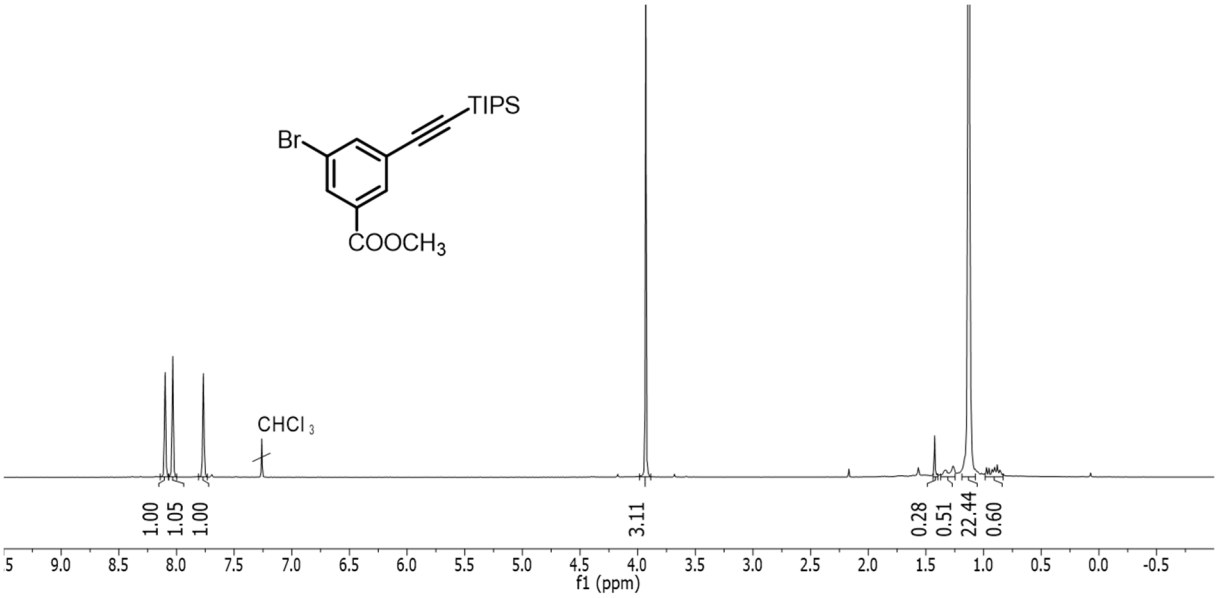

Figure S5: ^{1}H NMR spectrum (300 MHz, $CDCl_3$) of compound **1c**.

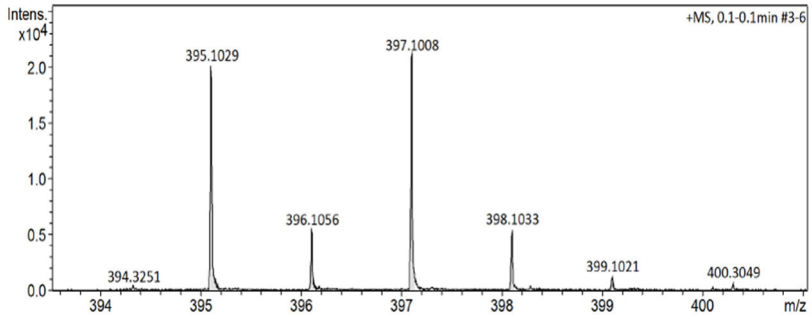

Figure S5: HR-ESI-MS spectrum of compound **1c**.

3-((Triisopropylsilyl)ethynyl)-5-((trimethylsilyl)ethynyl)benzoic acid methyl ester (1d)

^{1}H NMR (300 MHz, $CDCl_3$): δ [ppm] = 8.04 (p, ^4J = 1.6 Hz, 2H, H_{Ar}-2, H_{Ar}-6), 7.72 (t, ^4J = 1.6 Hz, 1H, H_{Ar}-4), 3.92 (s, 3H, COCH_3), 1.13 (s, 21H, Si-CH-(CH_3)$_2$), 0.25 (s, 9H, Si-CH_3). HR-ESI-MS: *m/z* for $C_{24}H_{36}O_2Si_2$ (exact monoisotopic mass 412.2254) $[M+H]^+$ calcd. 413.2332, found 413.2329. R_f = 0.49 (*n*-hexane).

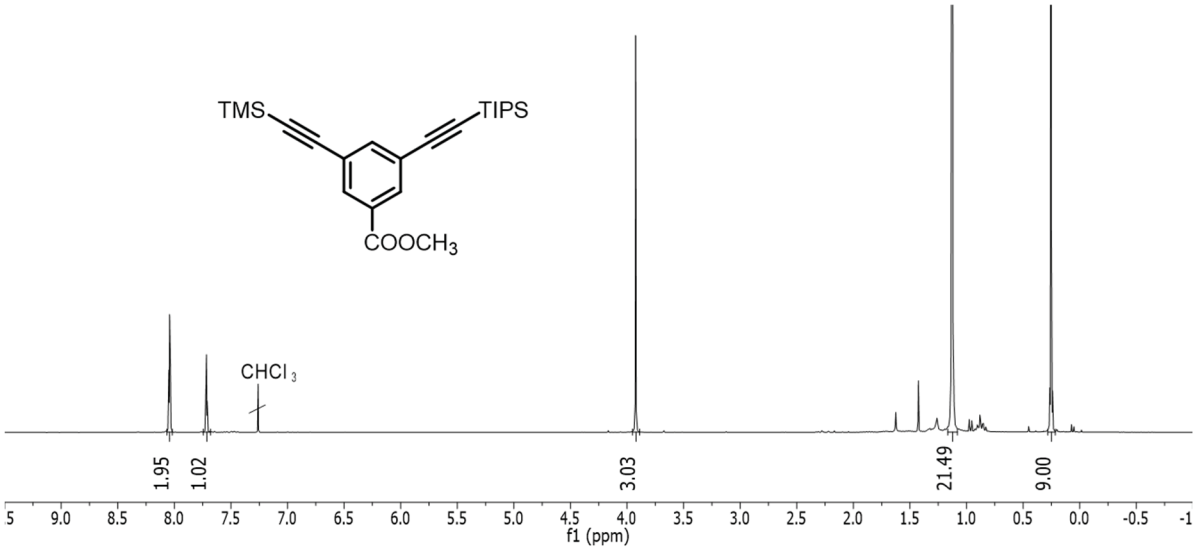

Figure S6: ^{1}H NMR spectrum (300 MHz, $CDCl_3$) of compound **1d**.

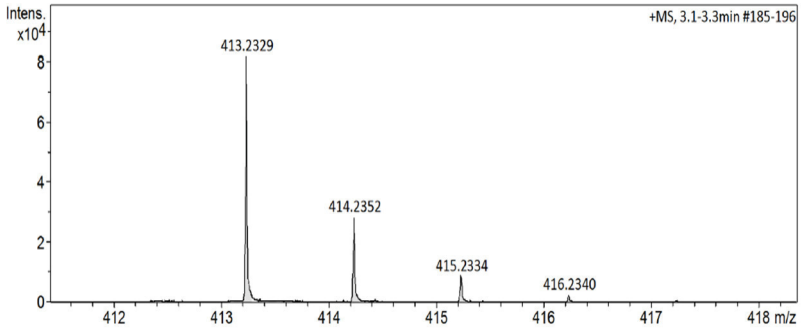

Figure S7: HR-ESI-MS spectrum of compound **1d**.

3-Ethynyl-5-((triisopropylsilyl)ethynyl)benzoic acid (1)

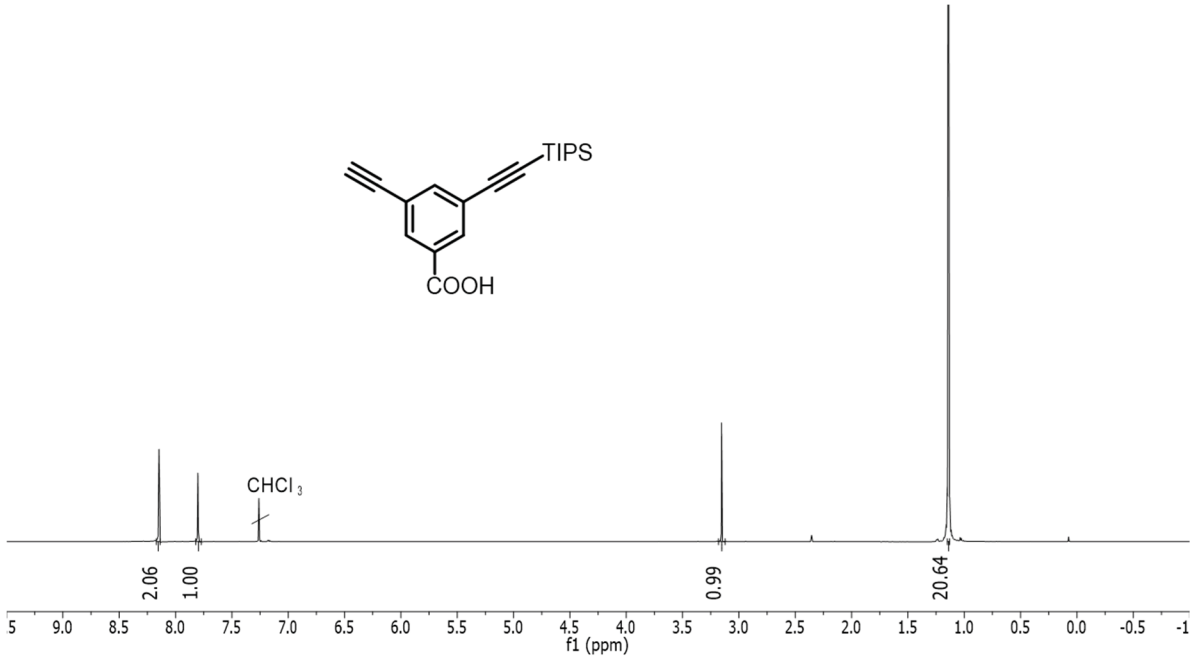

Figure S8: ^{1}H NMR spectrum (600 MHz, $CDCl_3$) of compound **1**.

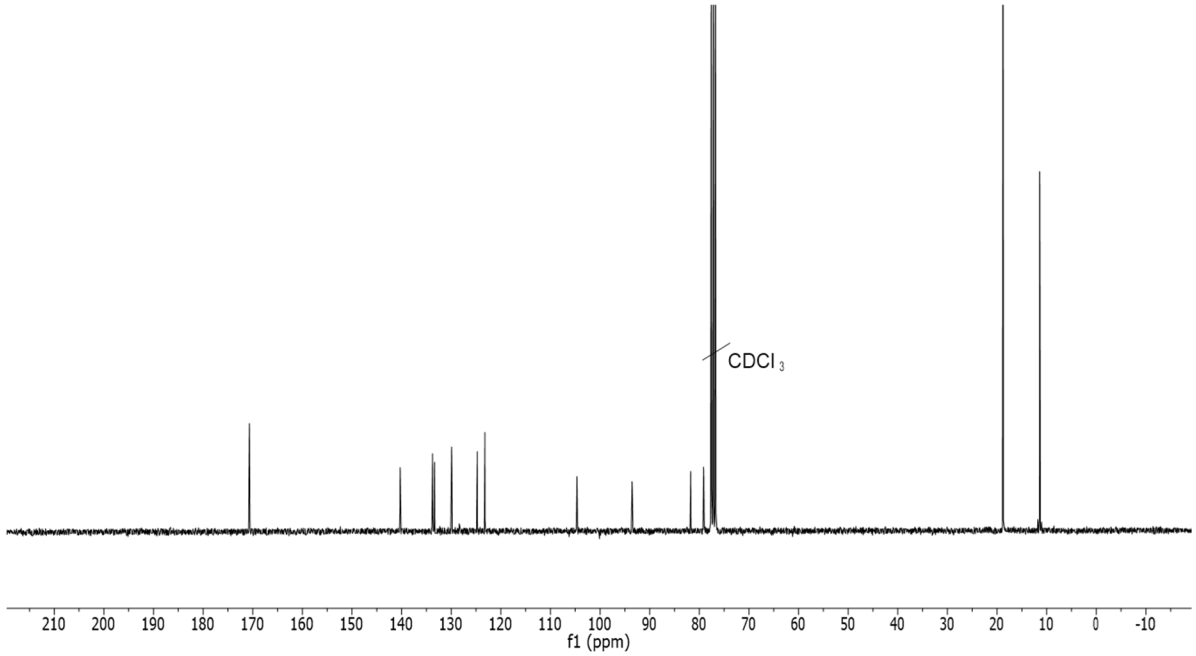

Figure S9: ^{13}C NMR spectrum (75.5 MHz, $CDCl_3$) of compound **1**.

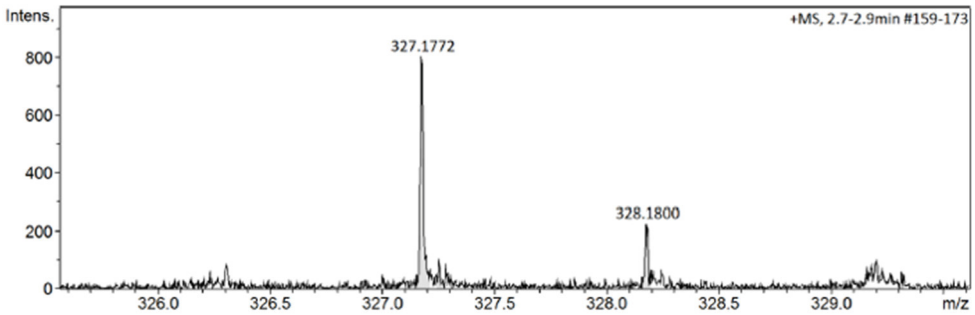

Figure S10: HR-ESI-MS spectrum of compound **1**.

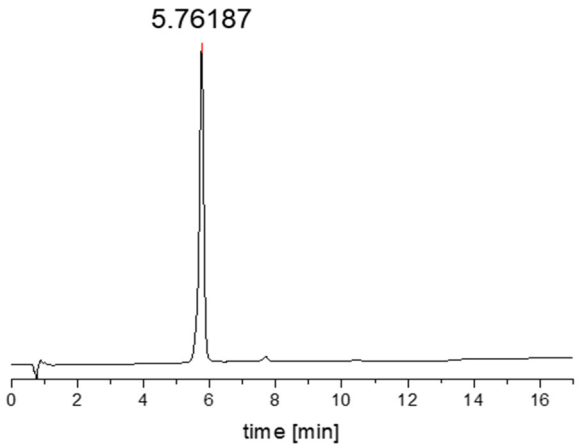

Figure S11: RP-HPLC chromatogram of compound **1** (gradient from 80 % to 100 % eluent **B** in 10 min, proceeding at 100 % **B**, 17 min, 25 °C.

2,2,2-Trifluoro-*N*-(2-((2-(tritylamino)ethyl)amino)ethyl)acetamide (2)

^{1}H NMR (300 MHz, $CDCl_3$): δ [ppm] = 7.46-7.42 (m, 6H, H_{Ph}), 7.29-7.23 (m, 6H, H_{Ph}), 7.20-7.14 (m, 3H, H_{Ph}), 3.40-3.36 (m, 2H, C(=O)NH-CH_2), 2.80-2.72 (m, 2H, NH-CH_2), 2.69 (dd, $^{2,3}J$ = 6.5, 5.1 Hz, 2H, NH-CH_2), 2.31-2.27 (m, 2H, NH-CH_2).

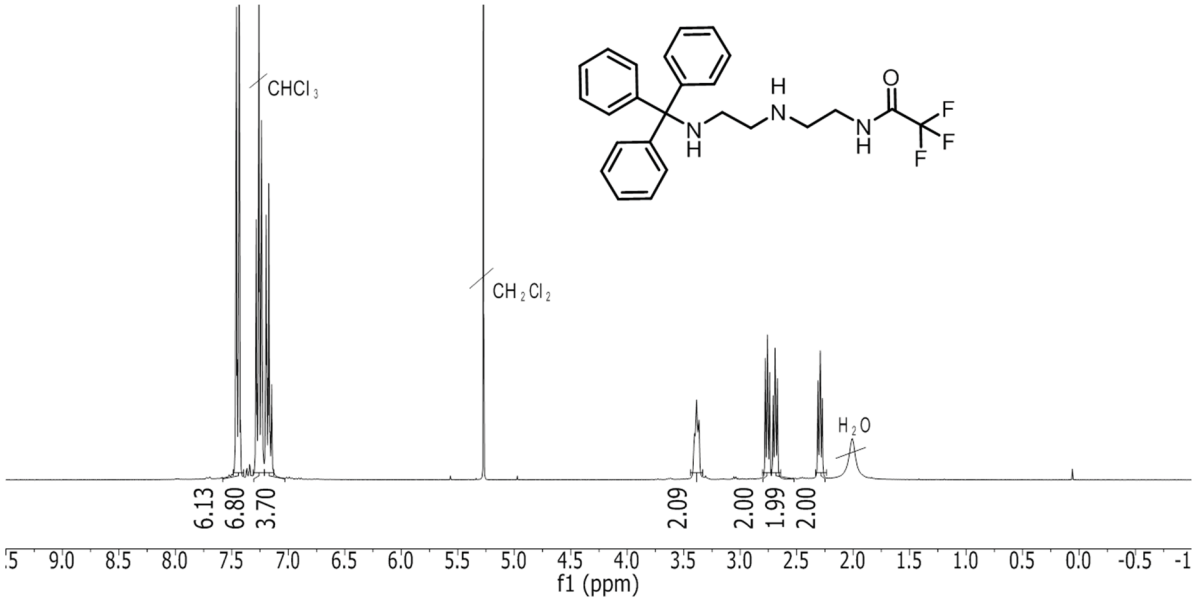

Figure S12: ^{1}H NMR spectrum (300 MHz, $CDCl_3$) of compound **2**.

3-Ethynyl-*N*-(2-(2,2,2-trifluoroacetamido)ethyl)-5-((triisopropylsilyl)ethynyl)-*N*-(2-(tritylamino)-ethyl)benzamide (3)

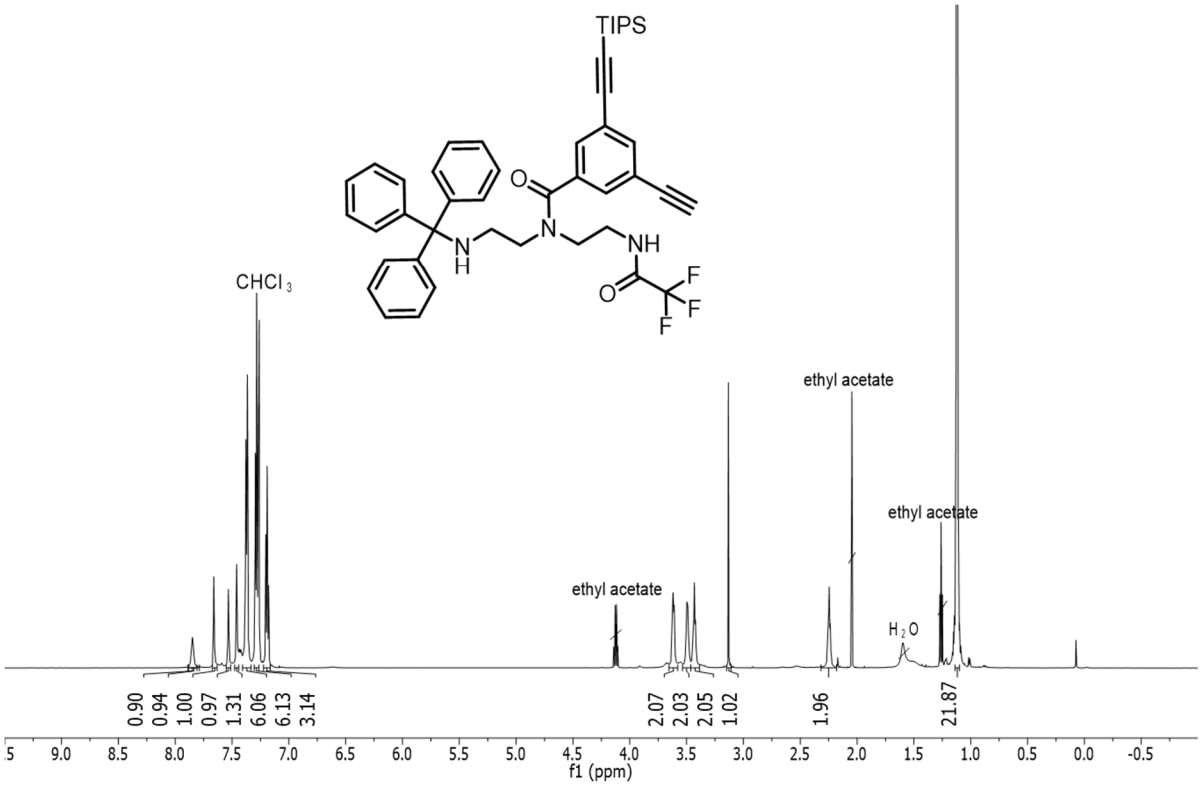

Figure S13: ^{1}H NMR spectrum (600 MHz, $CDCl_3$) of compound **3**.

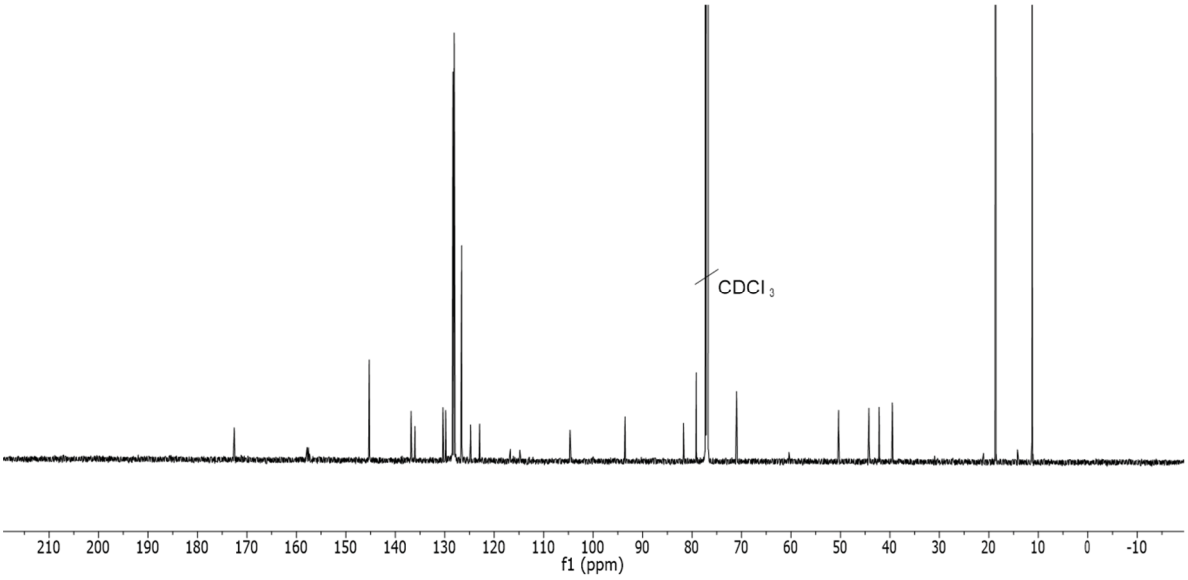

Figure S14: ^{13}C NMR spectrum (151 MHz, $CDCl_3$) of compound **3**.

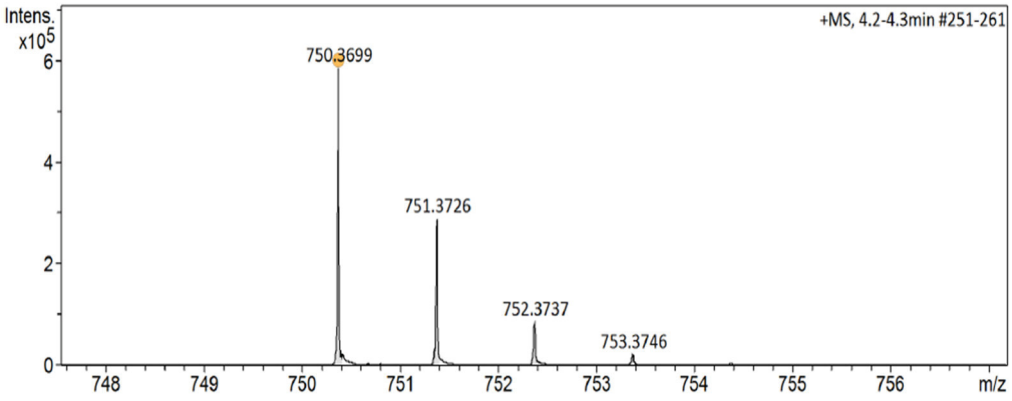

Figure S15: HR-ESI-MS spectrum of compound **3**.

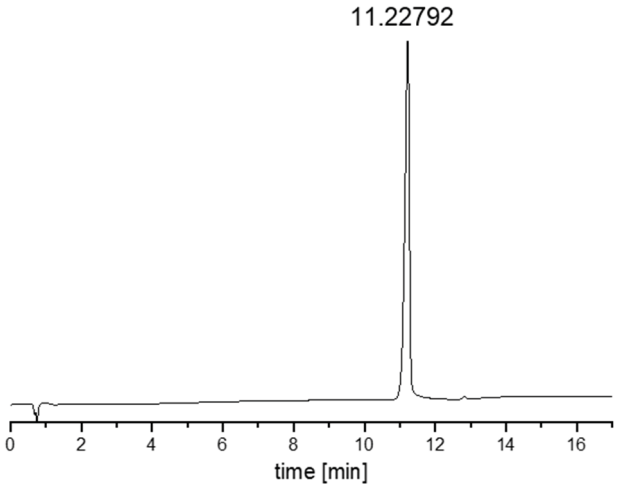

Figure S16: RP-HPLC chromatogram of compound **3** (gradient from 80 % to 100 % eluent **B** in 10 min, proceeding at 100 % **B**, 17 min, 25 °C).

2,2,2-trifluoroacetaldehyde,2-(3-ethynyl-*N*-(2-(2,2,2-trifluoroacetamido)ethyl)-5-((triisopropylsilyl)-ethynyl)benzamido)ethan-1-aminium salt (4)

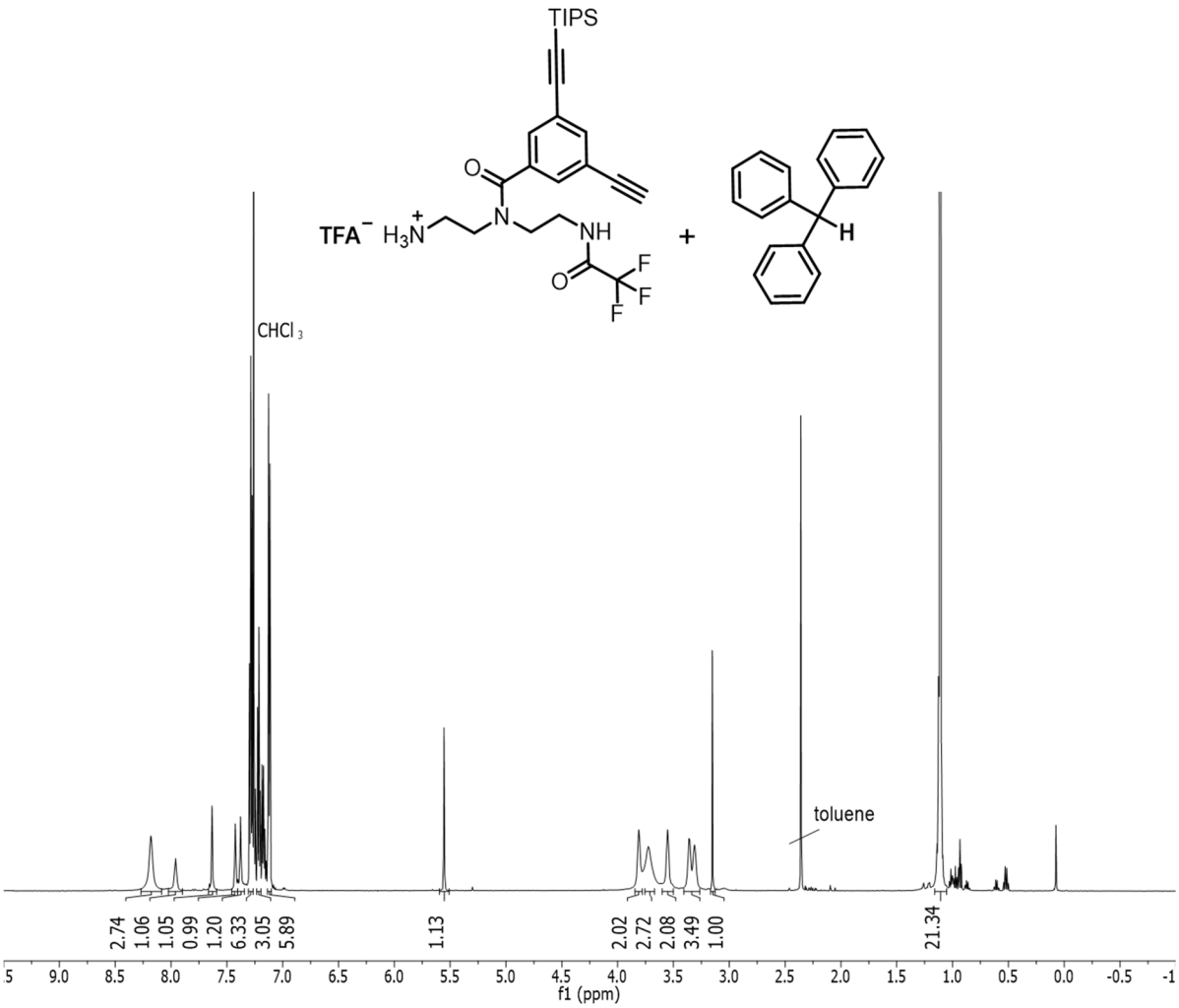

Figure S17: ^{1}H NMR spectrum (600 MHz, $CDCl_3$) of compound **4**.

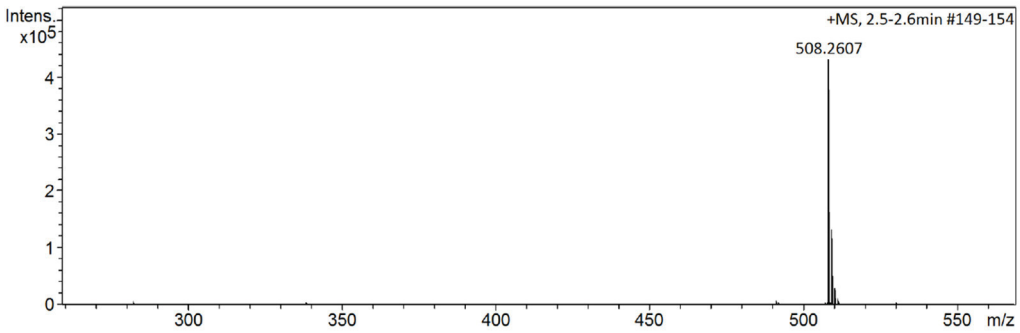

Figure S18: HR-ESI-MS spectrum of compound **4**.

4-((2-(3-Ethynyl-*N*-(2-(2,2,2-trifluoroacetamido)ethyl)-5-((triisopropylsilyl)ethynyl)benzamido) ethyl)amino)-4-oxobutanoic acid (5)

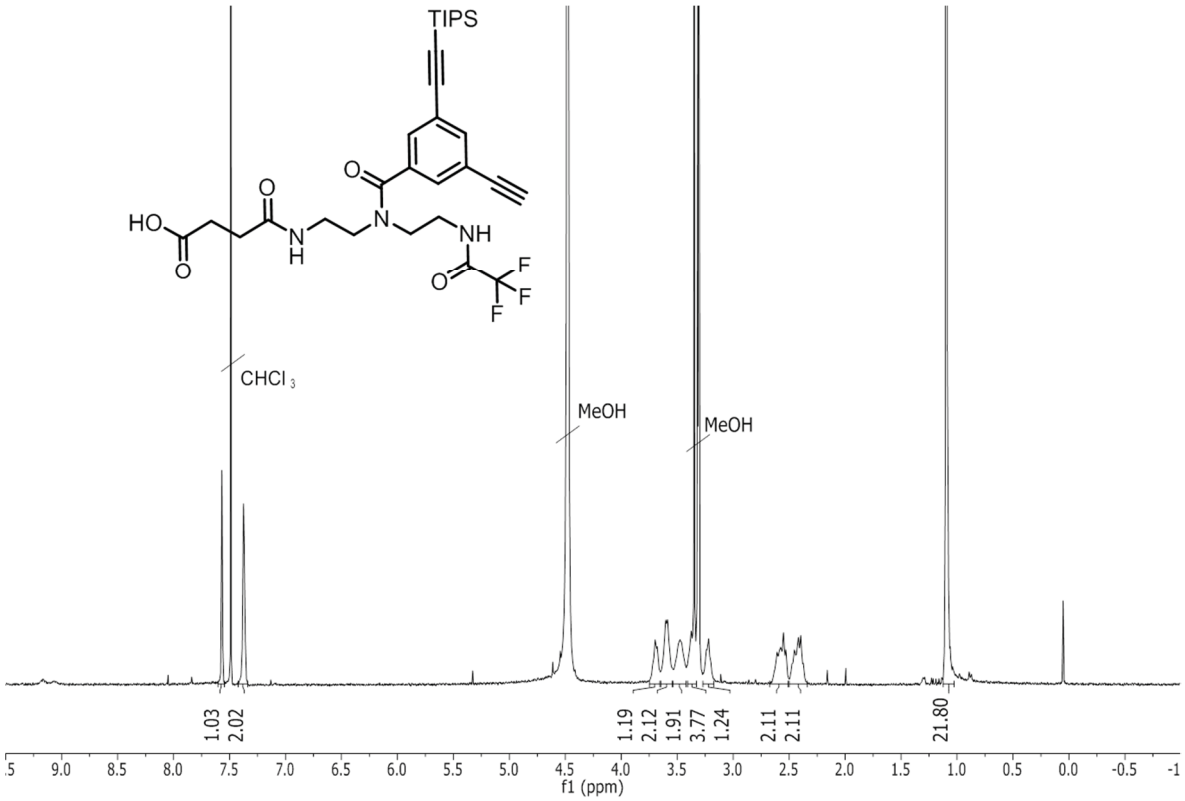

Figure S19: ^{1}H NMR spectrum (300 MHz, CD_3OD, $CDCl_3$) of compound **5**.

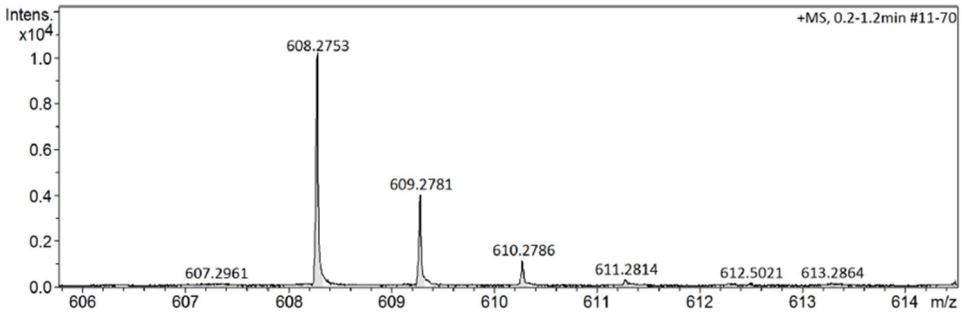

Figure S20: HR-ESI-MS spectrum of compound **5**.

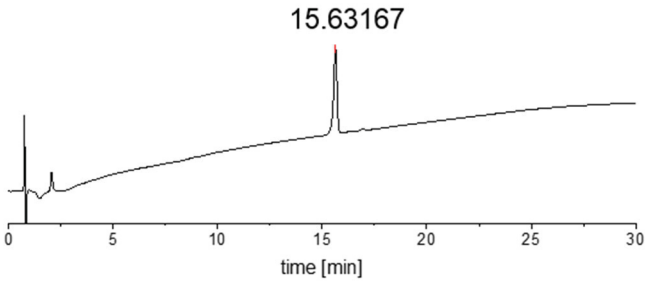

Figure S21: RP-HPLC chromatogram of compound **5** (gradient from 40 % to 100 % eluent **B** in 30 min, 25 °C).

4-((2-((2-(3-Ethynyl-5-((triisopropylsilyl)ethynyl)benzamido)ethyl)amino)ethyl)amino)-4-oxobutanoic acid (6)

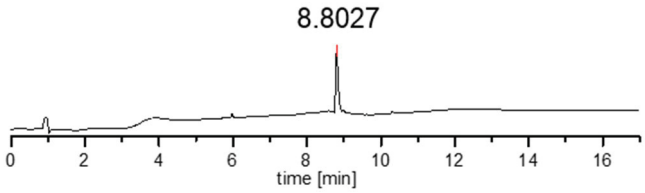

Figure S22: RP-HPLC chromatogram of compound **6** (gradient from 100 % to 50 % eluent **A** in 5 min, decreasing to 0 % **A** until 12 min, proceeding at 0 % **A**, 17 min, 25 °C).

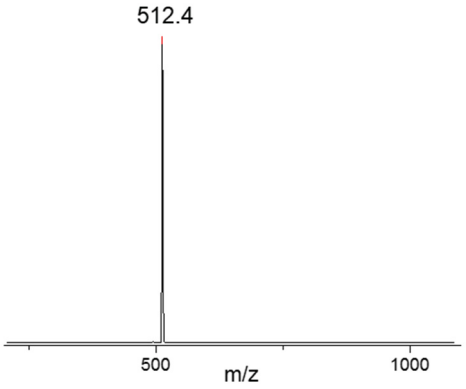

Figure S23: ESI-MS spectrum of compound **6**.

4-((2-((((9H-fluoren-9-yl)methoxy)carbonyl)(2-(3-ethynyl-5-((triisopropylsilyl)ethynyl)benzamido)-ethyl)amino)ethyl)amino)-4-oxobutanoic acid (7)

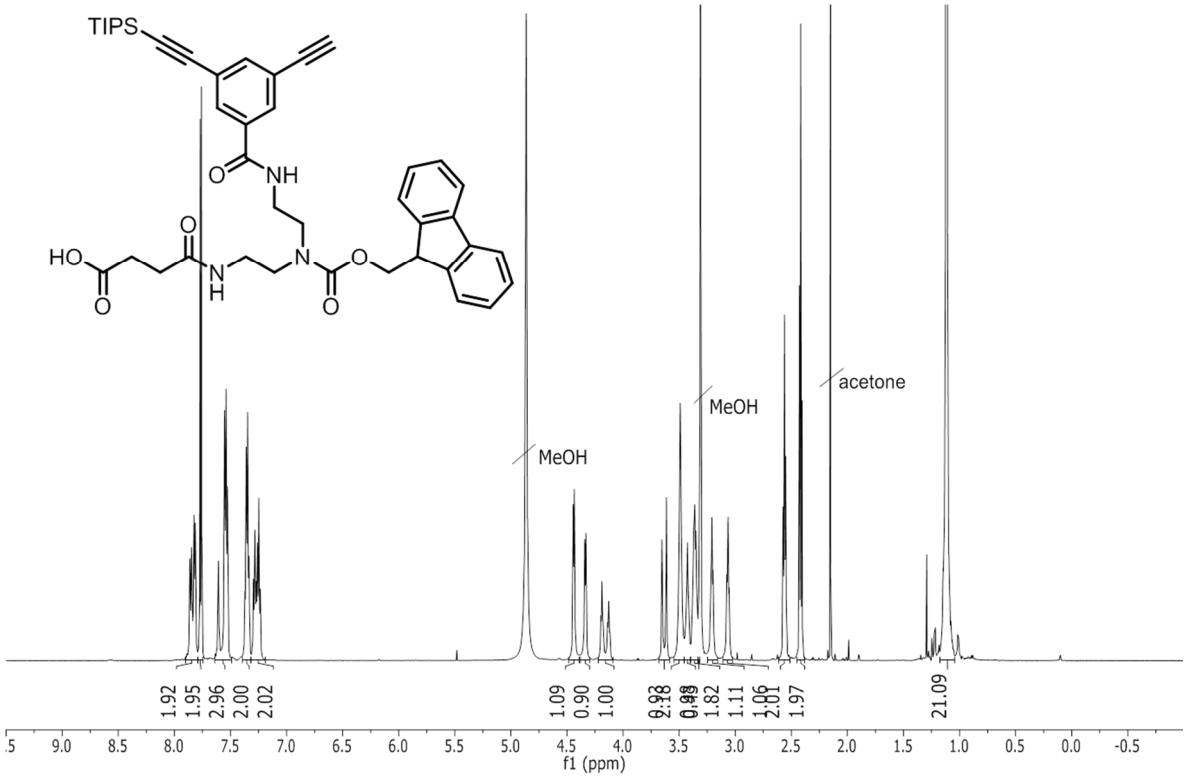

Figure S24: ^{1}H NMR spectrum (600 MHz, CD_3OD) of compound **7**.

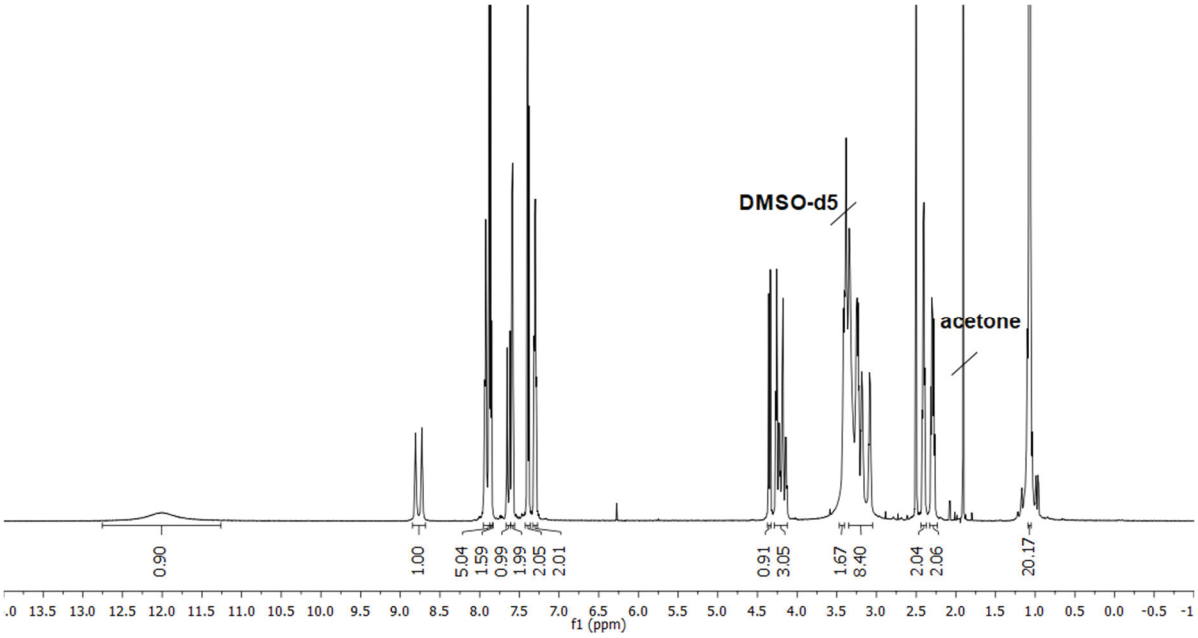

Figure S25: ^{1}H NMR spectrum (600 MHz, DMSO-d_6) of compound **7**.

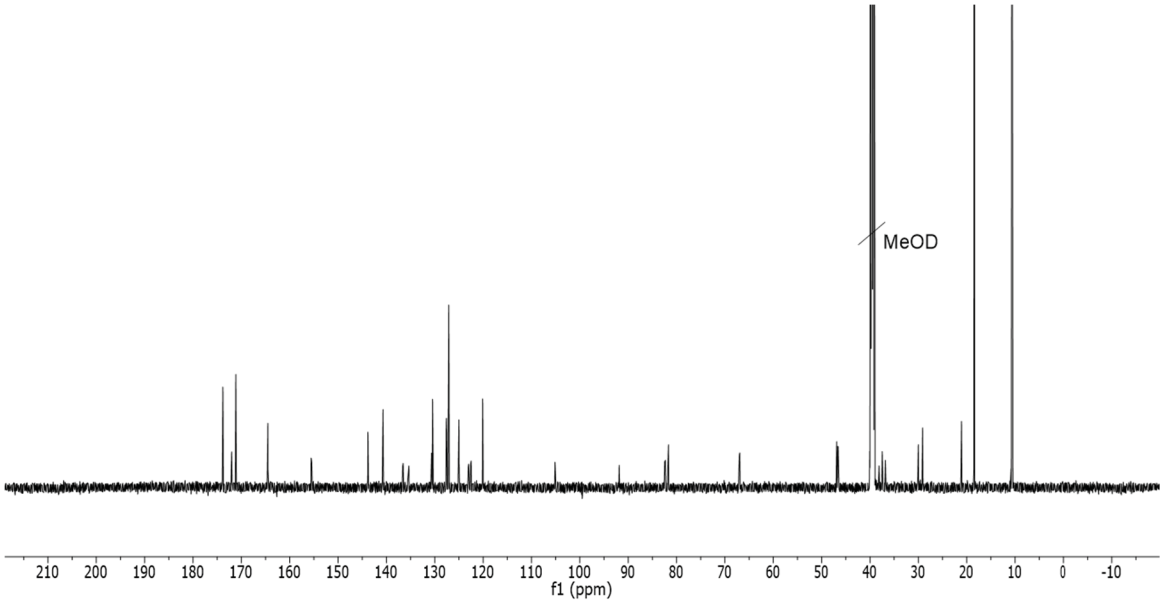

Figure S26: ^{13}C NMR spectrum (151 MHz, DMSO-d_6) of compound **7**.

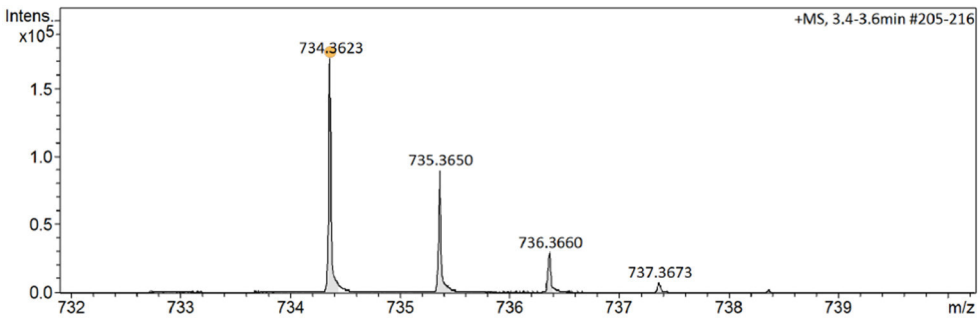

Figure S27: HR-ESI-MS spectrum of compound **7**.

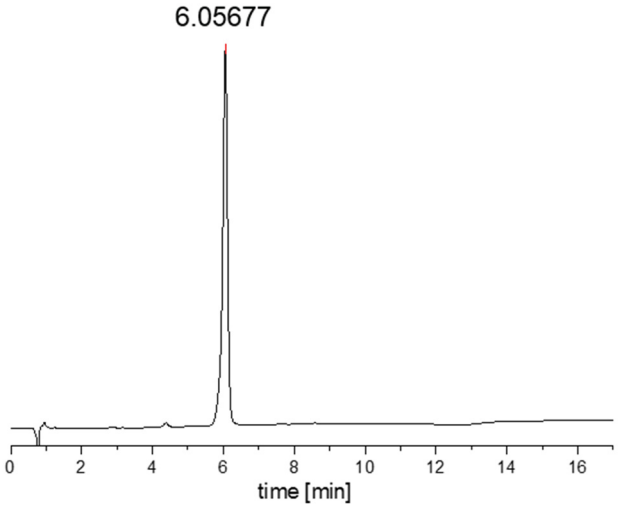

Figure S28: RP-HPLC chromatogram of compound **7** (gradient from 80 % to 100 % eluent **B** in 10 min, proceeding at 100 % **B**, 17 min, 25 °C).

(9H-fluoren-9-yl)-3,14-dioxo-2,7,10-trioxa-4,13-diazaheptadecan-17-oic acid (EDS)

^{1}H NMR (300 MHz, DMSO-d_6): δ [ppm] = 7.89 (d, ^{3}J = 7.5 Hz, 2H, H_{Ph}), 7.69 (d, ^{3}J = 7.5 Hz, 2H, H_{Ph}), 7.44-7.39 (m, 2H, H_{Ph}), 7.35-7.30 (m, 2H, H_{Ph}), 4.30-4.18 (m, 3H, Fmoc-C*H*-C*H*$_2$), 3.50 (s, 4H, OC*H*$_2$C*H*$_2$O), 3.42-3.37 (m, 4H, OC*H*$_2$CH$_2$NH), 3.21-3.10 (m, 4H, OCH$_2$C*H*$_2$NH), 2.43-2.38 (m, 2H, C(=O)CH$_2$CH$_2$C(=O)), 2.33-2.28 (m, 2H, C(=O)CH$_2$CH$_2$C(=O)). ^{13}C NMR (75.5 MHz, DMSO-d_6): δ [ppm] = 173.9 (COOH), 171.1 (CH$_2$-C=O), 156.2 (O-C=O), 143.9, 140.7, 127.6, 127.1, 125.2, 120.1 (all C_{Ar}), 69.6 (OCH$_2$CH$_2$), 69.1 (OCH$_2$CH$_2$), 65.3 (OCH$_2$CH), ~40 (NH-CH$_2$, *overlapping with residual DMSO*), 46.7 (OCH$_2$CH), 30.0 (CH$_2$-C=O), 29.2 (CH$_2$-C=O). ESI-MS: *m/z* for $C_{25}H_{30}N_2O_7$ (exact monoisotopic mass 470.2) $[M+H]^+$ calcd. 471.2, found 471.2.

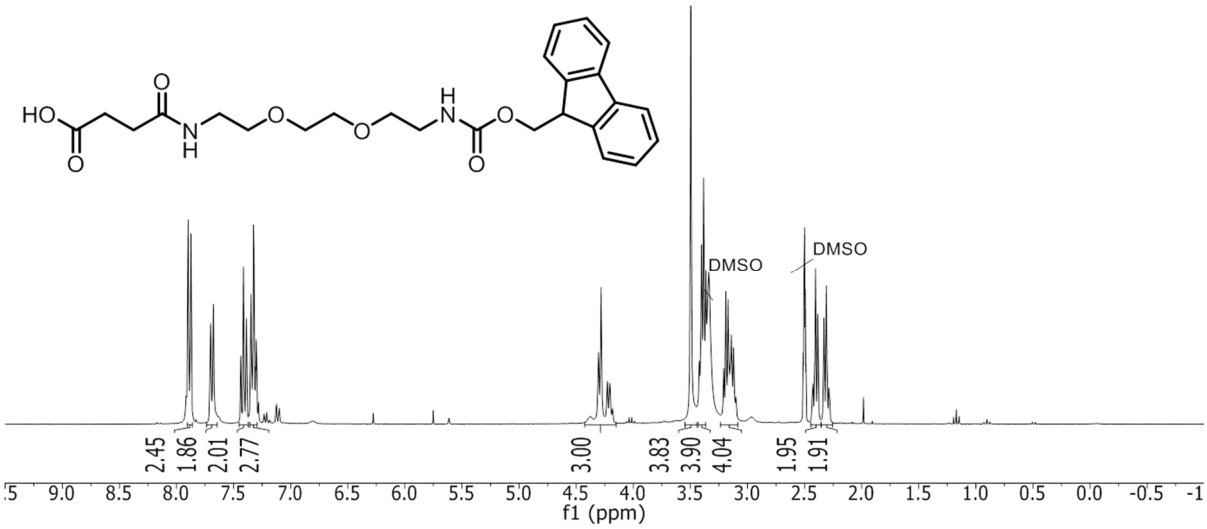

Figure S29: ^{1}H NMR spectrum (300 MHz, DMSO-d_6) of EDS.

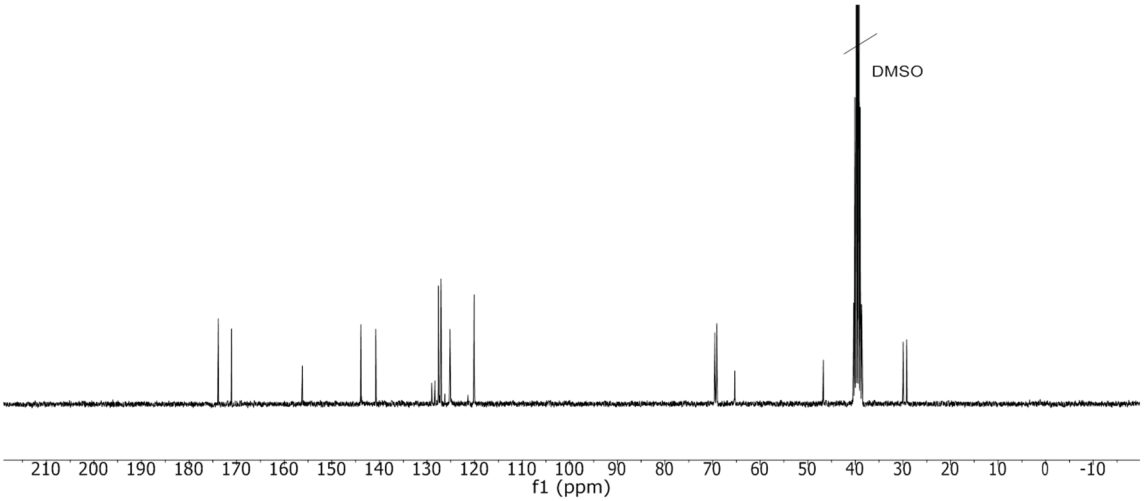

Figure S30: ^{13}C NMR spectrum (75.5 MHz, DMSO-d_6) of EDS.

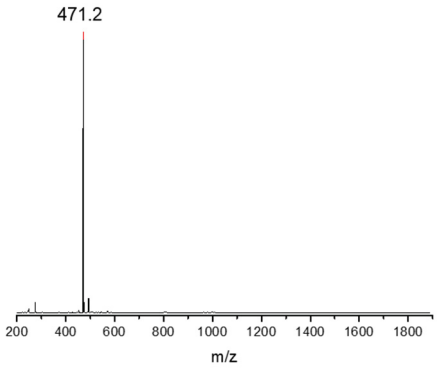

Figure S31: ESI-MS spectrum of EDS.

5.2 Carbohydrate derivatives

2-Azidoethyl-2,3,4,6-tetra-O-acetyl-N-acetyl-α-D-galactosamine

2-Bromoethyl-*N*-acetyl-D-galactosamine (9a)

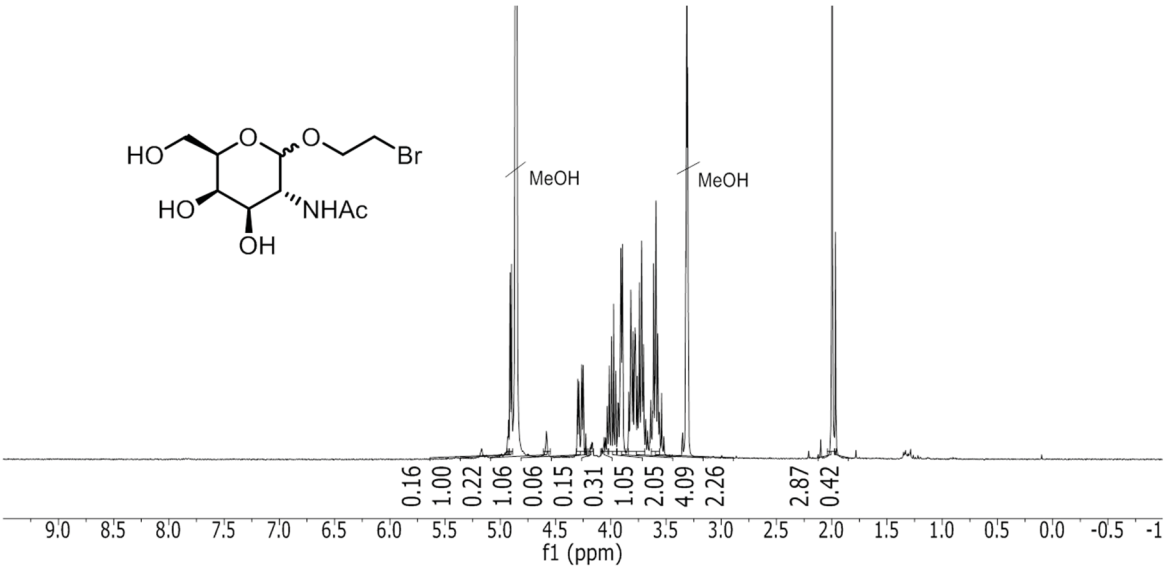

Figure S32: ^{1}H NMR spectrum (300 MHz, CD_3OD) of **9a**.

2-Bromoethyl-2,3,4,6-tetra-*O*-acetyl-*N*-acetyl-α-D-galactosamine (9b)

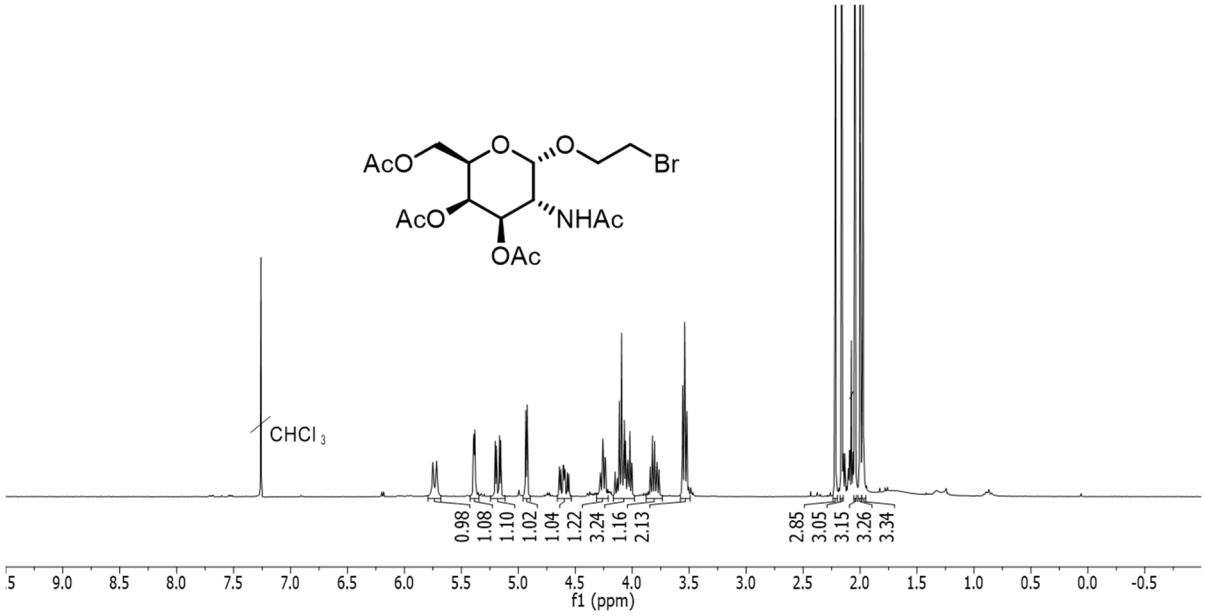

Figure S33: ^{1}H NMR spectrum (600 MHz, $CDCl_3$) of **9b**.

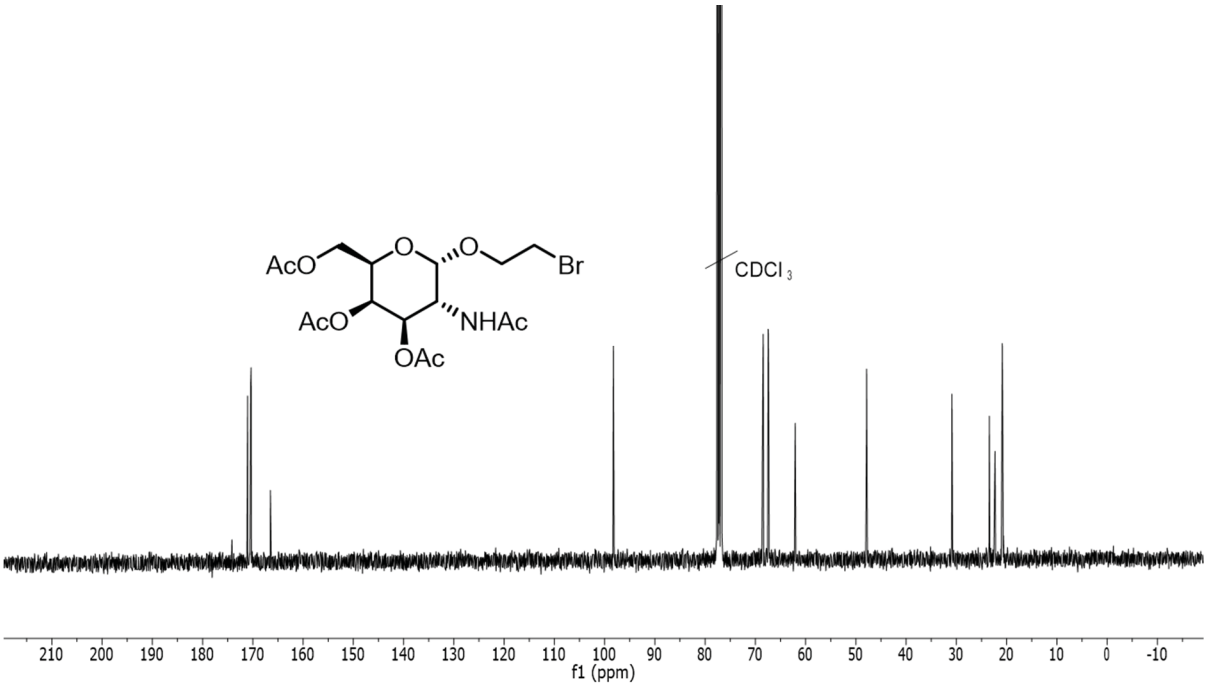

Figure S34: ^{13}C NMR spectrum (151 MHz, $CDCl_3$) of **9b**.

2-Azidoethyl-2,3,4,6-tetra-*O*-acetyl-*N*-acetyl-α-D-galactosamine (9c)

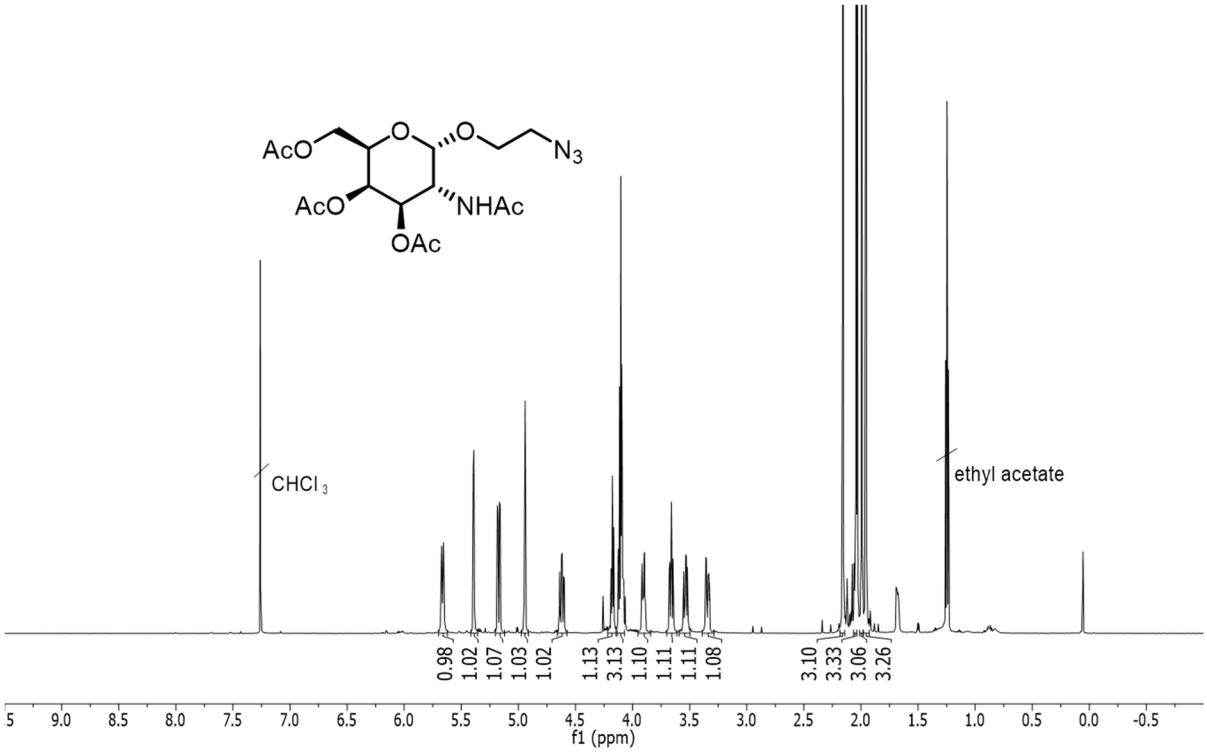

Figure S35: ^{1}H NMR spectrum (300 MHz, $CDCl_3$) of **9c**.

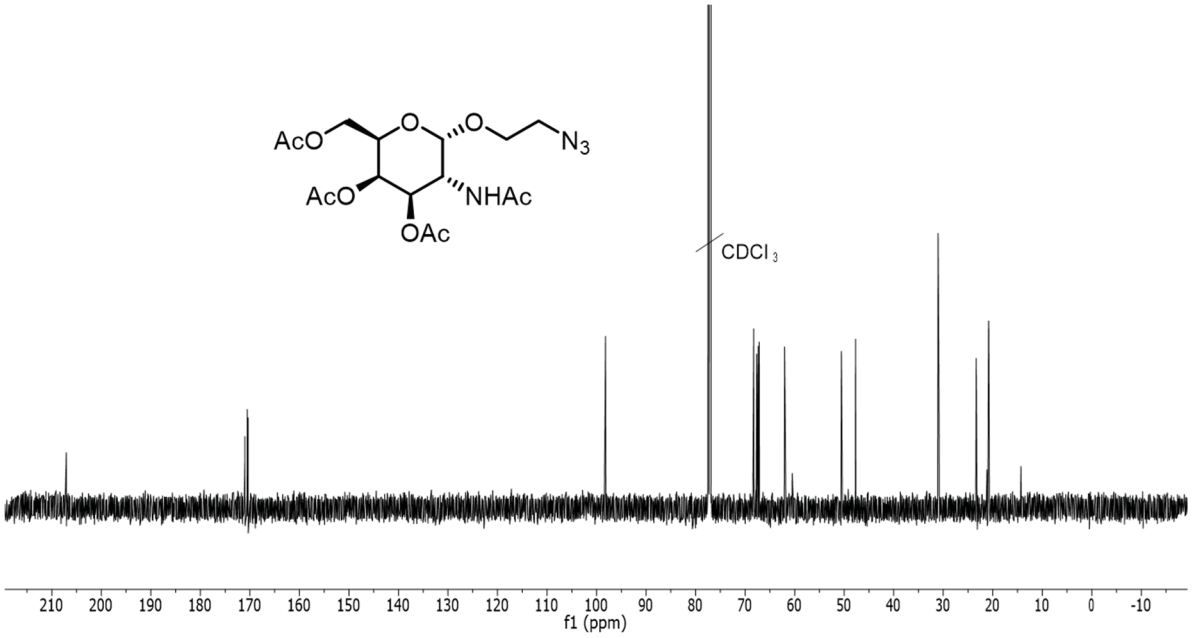

Figure S36: ^{13}C NMR spectrum (151 MHz, $CDCl_3$) of **9c**.

2-Azidoethyl-2,3,4,6-tetra-O-acetyl-α-D-galactopyranoside

2-Bromoethyl-2,3,4,6-tetra-*O*-acetyl-α-D-galactopyranoside (10b)

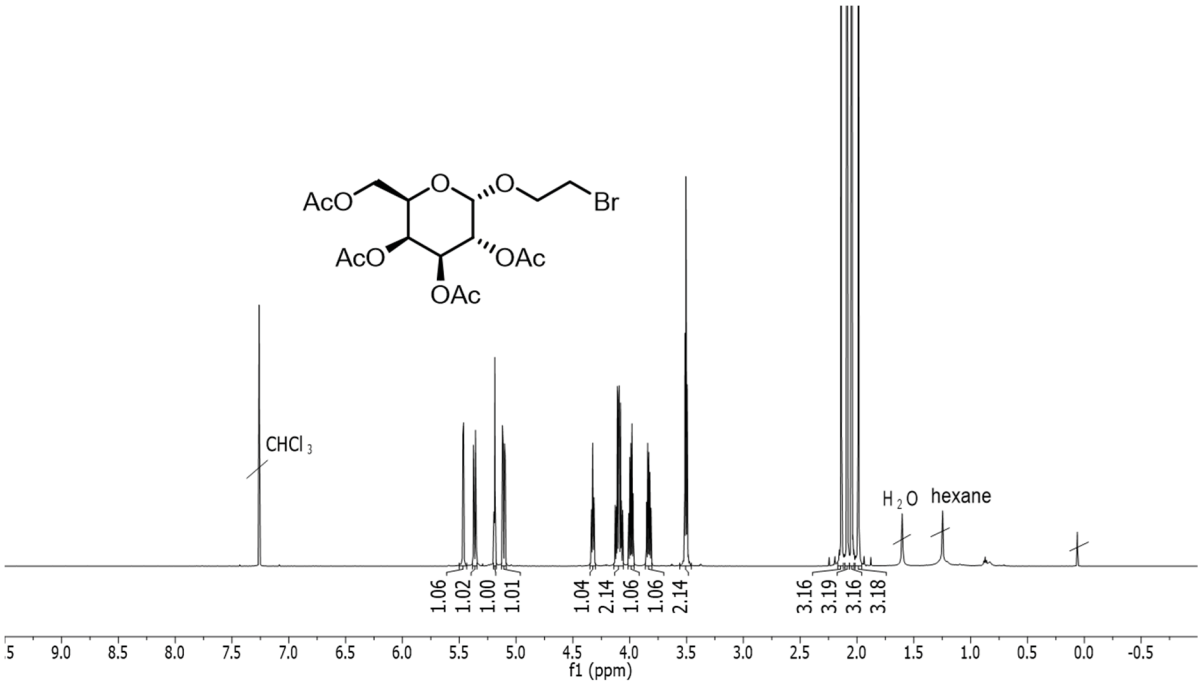

Figure S37: ^{1}H NMR spectrum (600 MHz, $CDCl_3$) of **10b**.

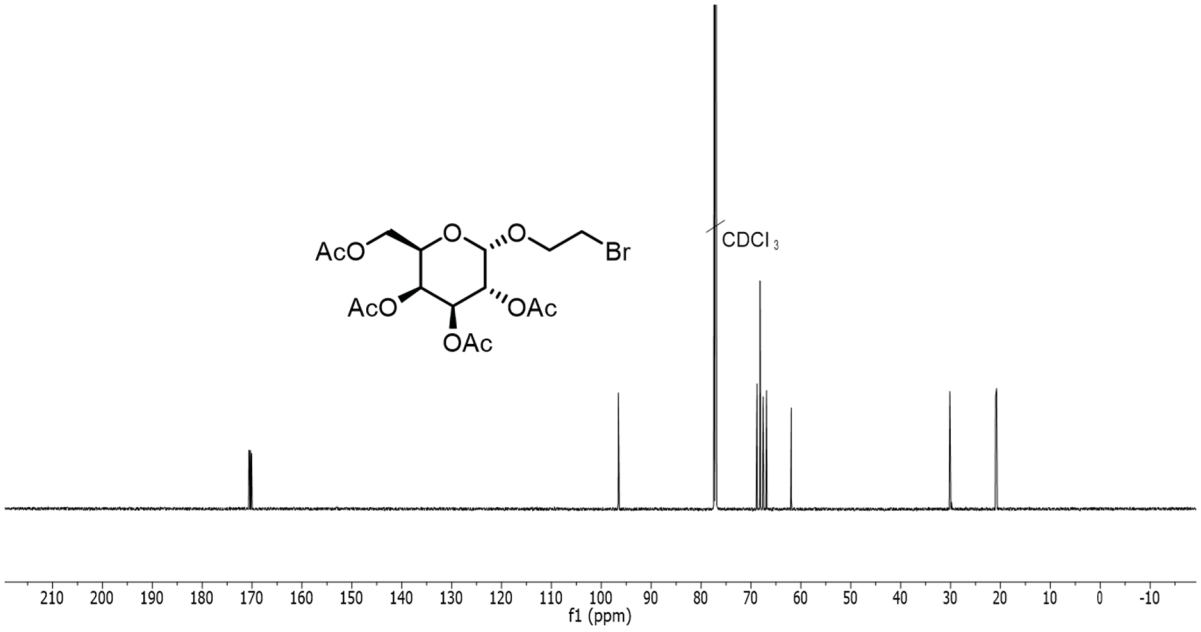

Figure S38: ^{13}C NMR spectrum (151 MHz, $CDCl_3$) of **10b**.

2-Azidoethyl-2,3,4,6-tetra-*O*-acetyl-α-D-galactopyranoside (10c)

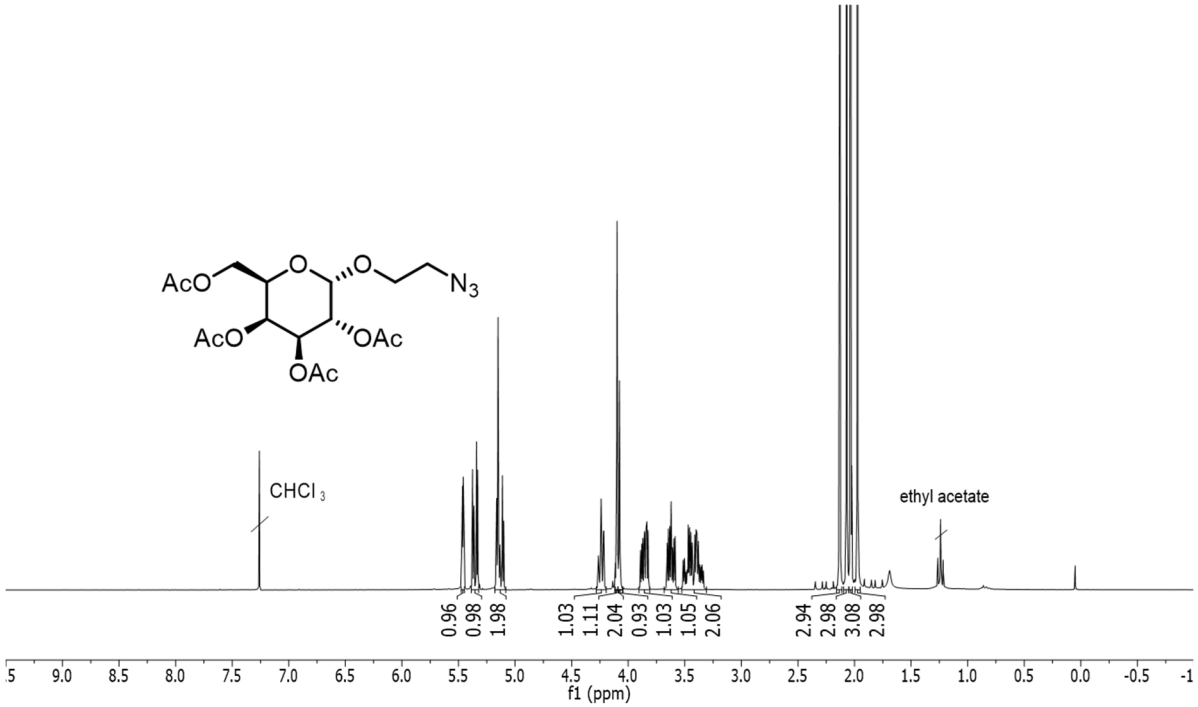

Figure S39: ^{1}H NMR spectrum (300 MHz, $CDCl_3$) of **10c**.

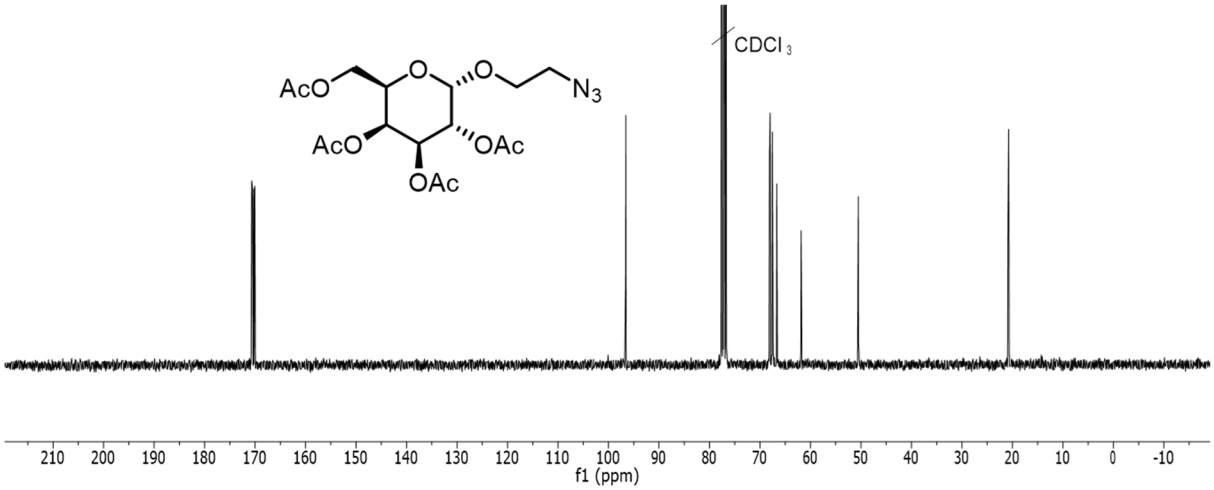

Figure S40: ^{13}C NMR spectrum (75.5 MHz, $CDCl_3$) of **10c**.

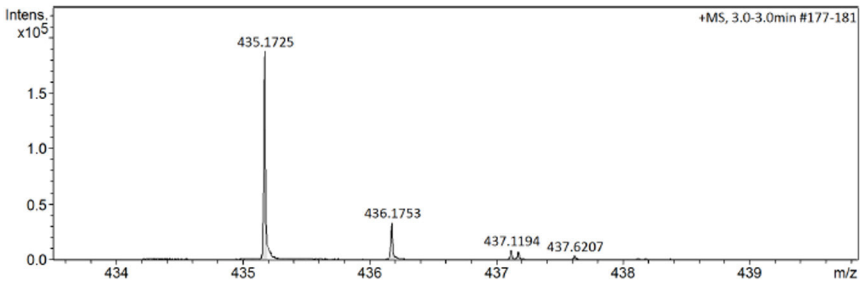

Figure S41: HR-ESI-MS spectrum of **10c**.

2-Azidoethyl-4,7,8,9-tetra-O-acetyl-N-acetyl-α-neuraminic acid methyl ester

***N*-Acetylneuraminic acid methyl ester (A)**

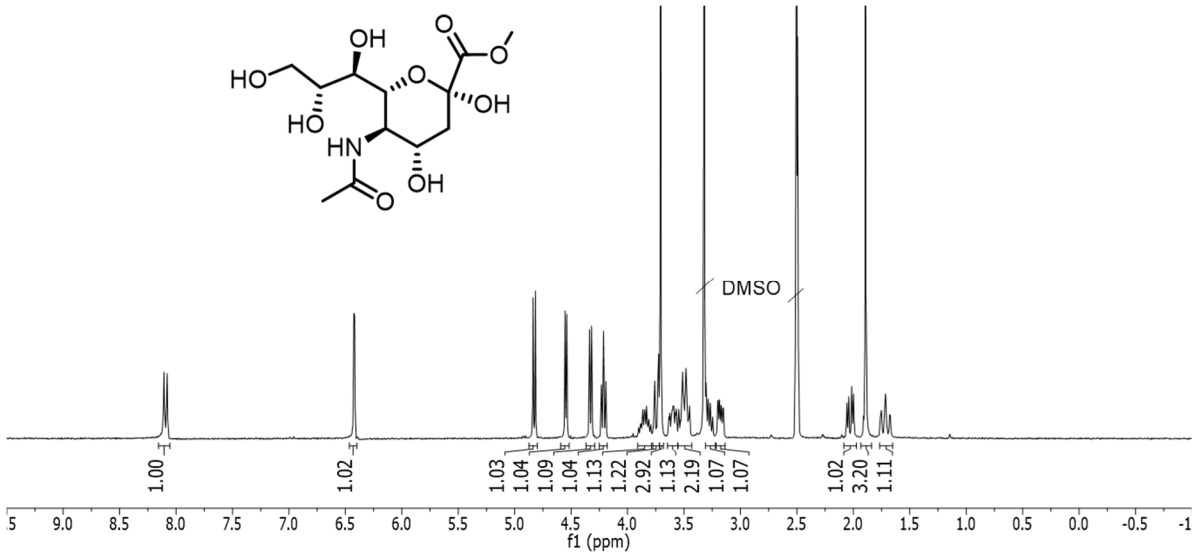

Figure S42: ^{1}H NMR spectrum (600 MHz, DMSO-d_6) of **A**.

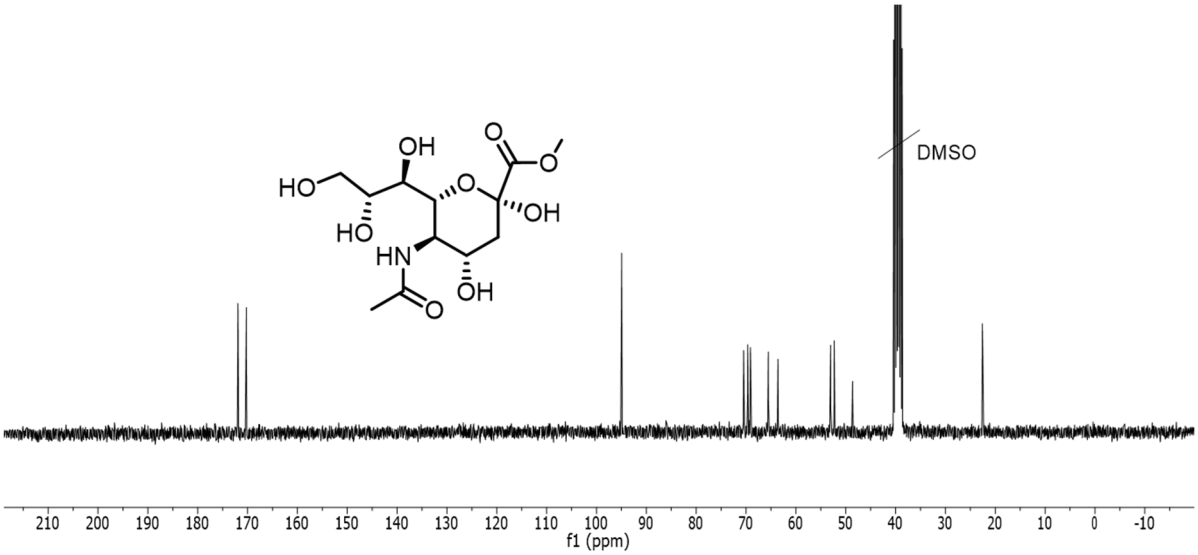

Figure S43: ^{13}C NMR spectrum (151 MHz, DMSO-d_6) of **A**.

2-Chloro-4,7,8,9-tetra-*O*-acetyl-*N*-acetyl-neuraminic acid methyl ester (B)

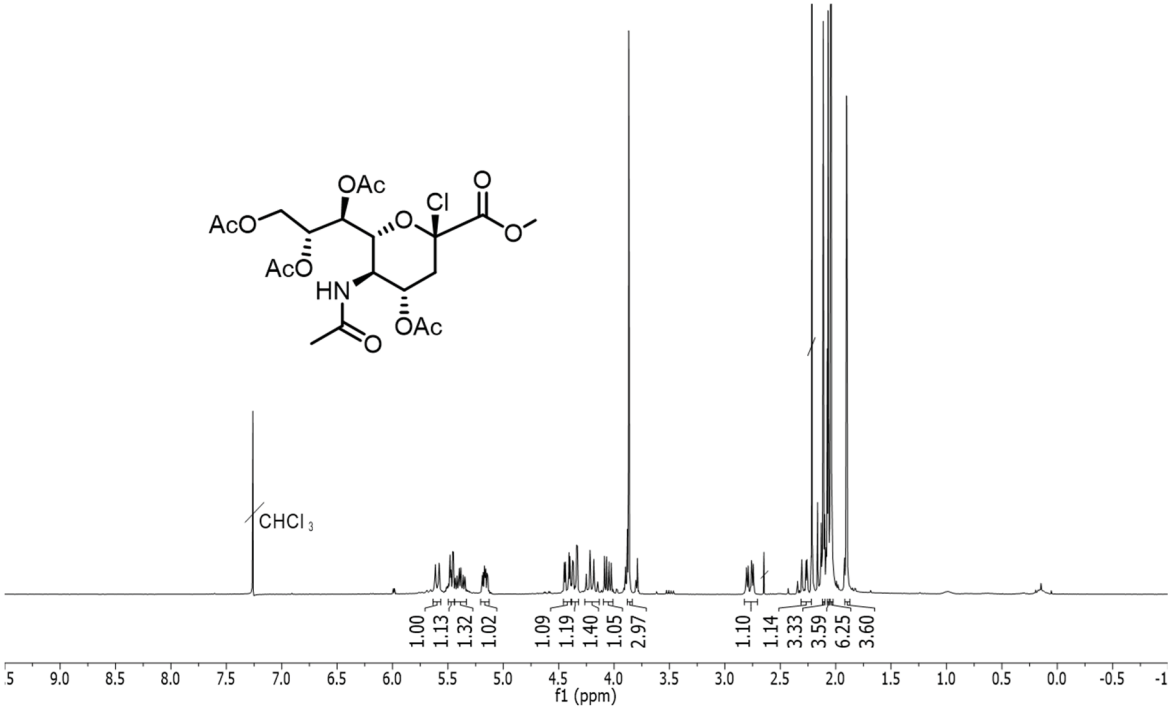

Figure S44: ^{1}H NMR spectrum (300 MHz, $CDCl_3$) of **B**.

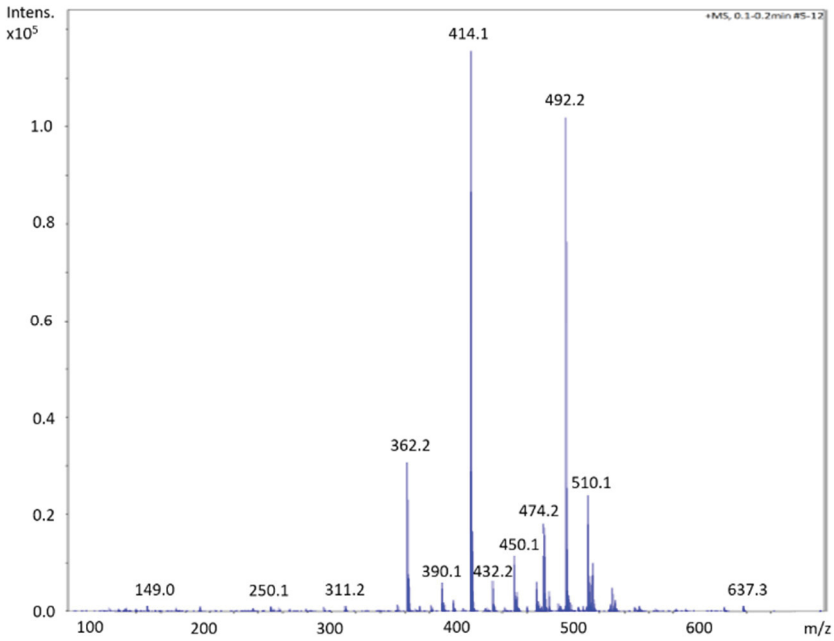

Figure S45: ESI-MS spectrum of **B**.

2-Bromoethyl-4,7,8,9-tetra-*O*-acetyl-*N*-acetyl-neuraminic acid methyl ester (C)

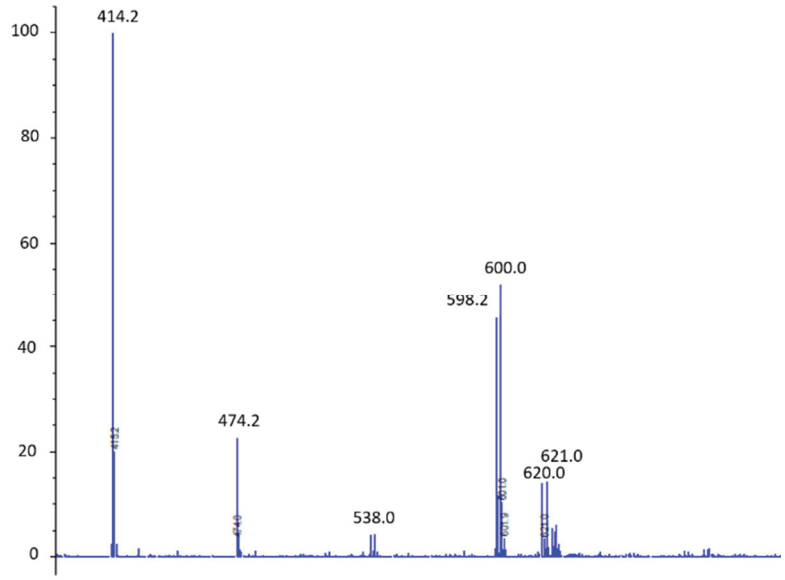

Figure S46: ESI-MS spectrum of **C**.

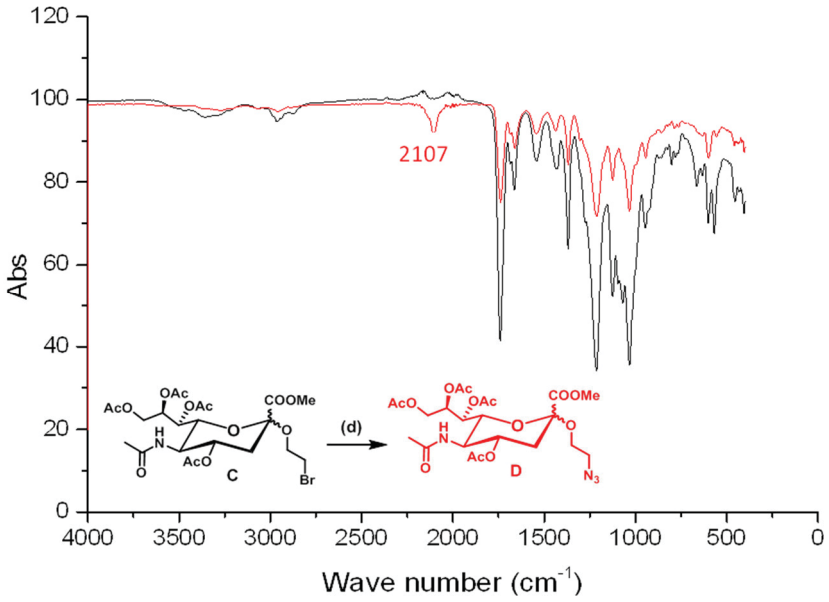

Figure S47: ATR-FTIR spectra of **C** and **D**.

2-Azidoethyl-*N*-acetyl-α-neuraminic acid methyl ester (E)

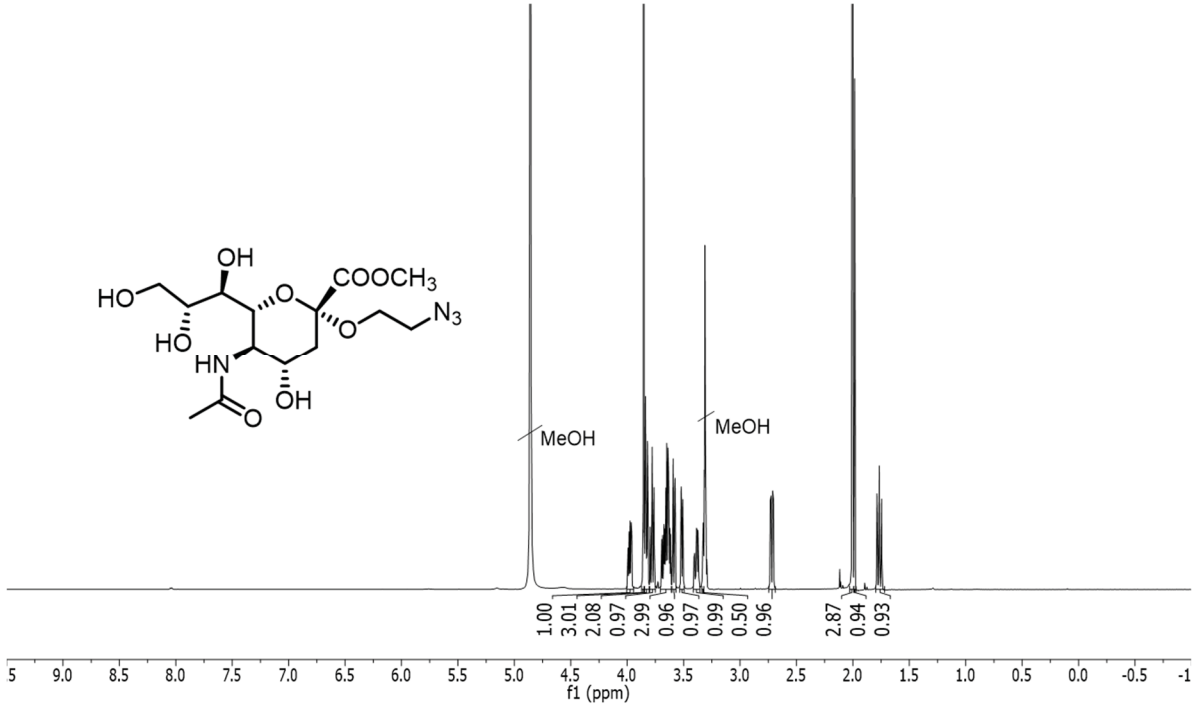

Figure S48: ^{1}H NMR spectrum (600 MHz, CD_3OD) of **E**.

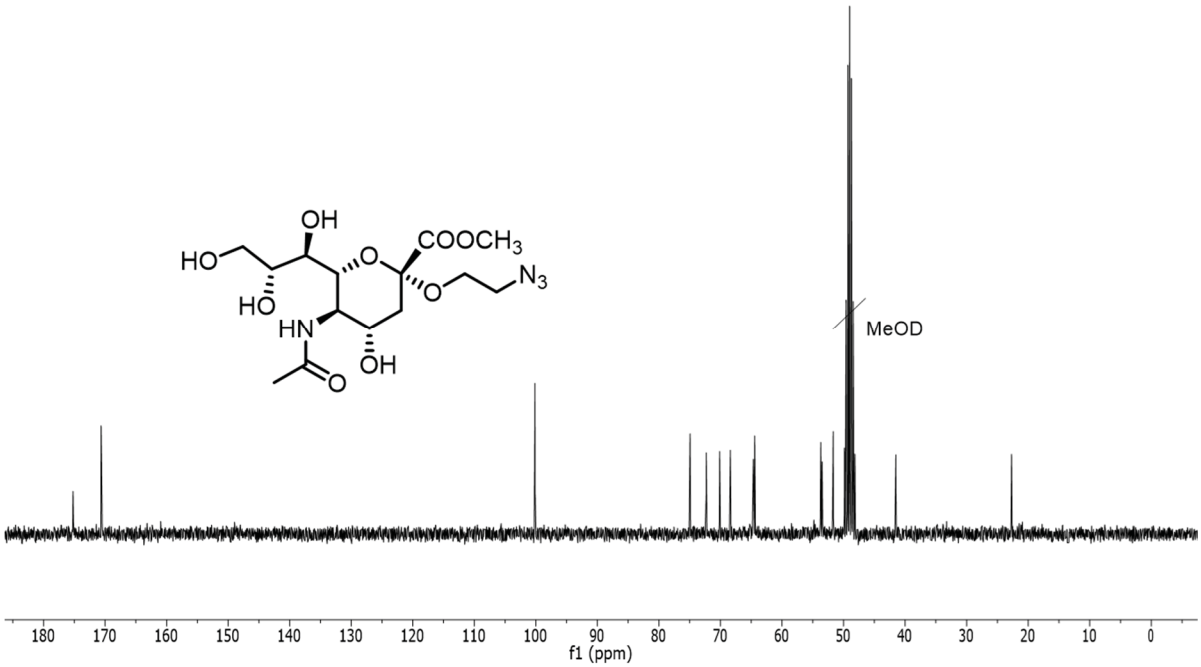

Figure S49: ^{13}C NMR spectrum (151 MHz, CD_3OD) of **E**.

2-Azidoethyl-4,7,8,9-tetra-*O*-acetyl-*N*-acetyl-α-neuraminic acid methyl ester (12α)

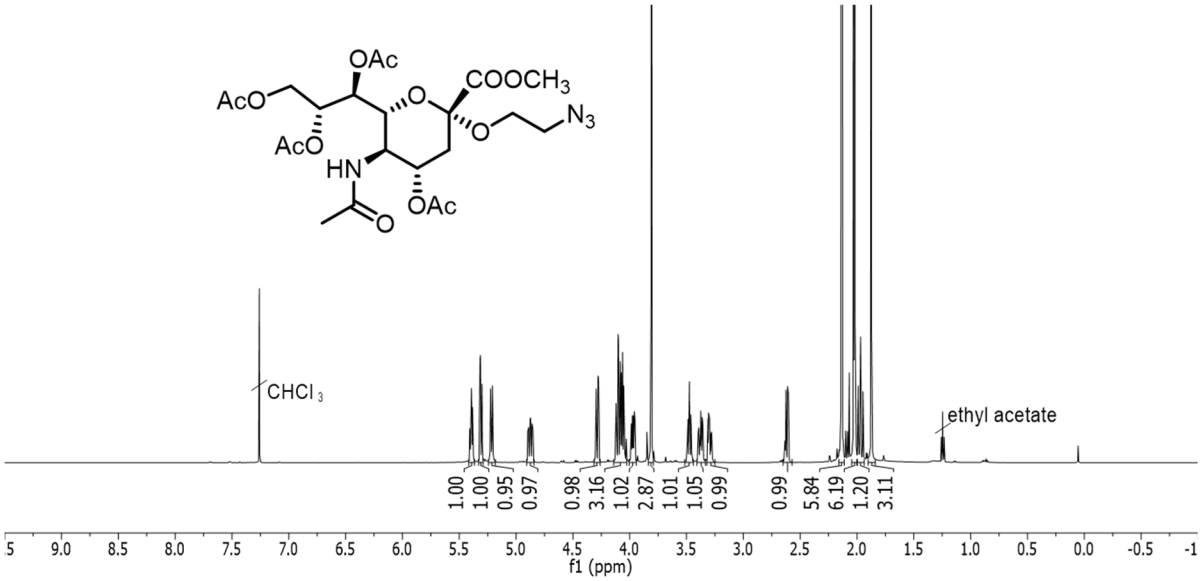

Figure S50: ^{1}H NMR spectrum (600 MHz, $CDCl_3$) of **12α**.

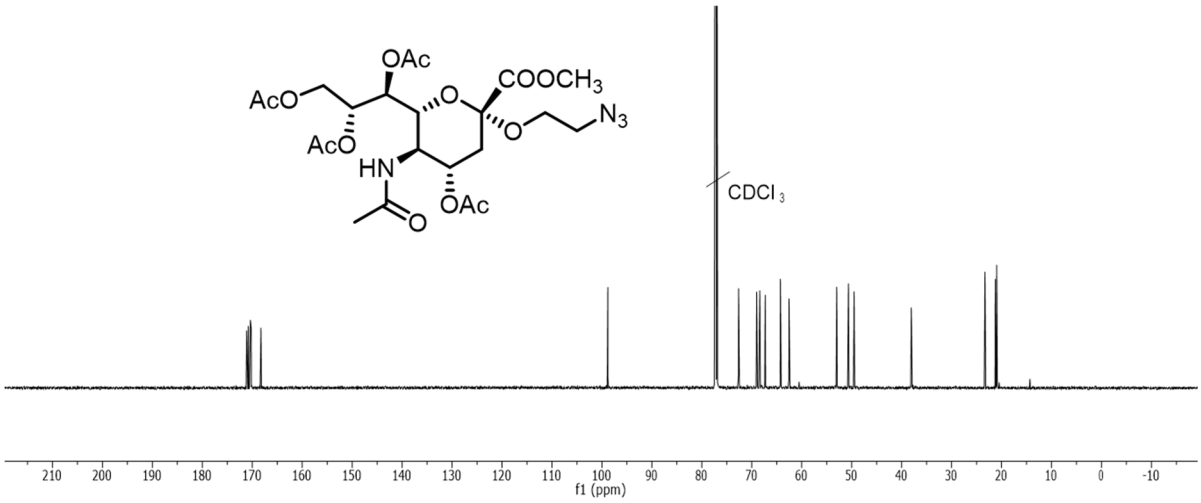

Figure S51: ^{13}C NMR spectrum (151 MHz, $CDCl_3$) of **12α**.

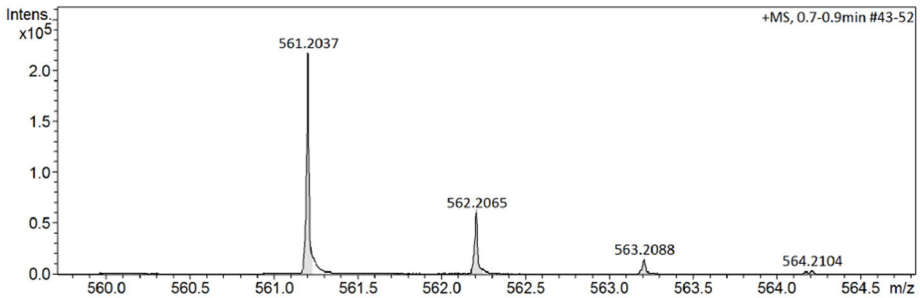

Figure S52: HR-ESI-MS spectrum of **12α**.

Azido-2,3,6,2´,3´4´,6´-hepta-O-acetyl-β-D-lactose (11)

^{1}H NMR (600 MHz, $CDCl_3$): δ [ppm] = 5.33 (dd, $^{3,3}J$ = 3.4, 0.8 Hz, 1H, H-4), 5.19 (t, $^{3,3}J$ = 9.3 Hz, 1H, H-3), 5.09 (dd, $^{3,3}J$ = 10.4, 7.9 Hz, 1H, H-2), 4.94 (dd, $^{3,3}J$ = 10.4, 3.5 Hz, 1H, H-3), 4.84 (t, $^{3,3}J$ = 8.9 Hz, 1H, H-2), 4.61 (d, ^{3}J = 8.8 Hz, 1H, H-1), 4.49 (dd, $^{2,3}J$ = 8.0, 2.0 Hz, 1H, H-6a), 4.47 (d, ^{3}J = 10.2 Hz, 1H, H-1), 4.14-4.03 (m, 3H, H-6b, H-6a), 3.86 (dt, $^{3,3}J$ = 6.8, 0.8 Hz, 1H, H-5), 3.80 (t, $^{3,3}J$ = 9.5 Hz, 1H, H-4), 3.69 (ddd, $^{3,3,3}J$ = 9.9, 5.1, 2.0 Hz, 1H, H-5), 2.13 (s, 1H, H-8), 2.12 (s, 1H, H-8), 2.05 (s, 1H, H-8), 2.05 (s, 1H, H-8), 2.03 (s, 1H, H-8), 2.03 (s, 1H, H-8), 1.95 (s, 1H, H-8). ^{13}C NMR (151 MHz, $CDCl_3$): δ [ppm] = 170.44 (C-7), 170.40 (C-7), 170.21 (C-7), 170.14 (C-7), 169.73 (C-7), 169.58 (C-7), 169.17 (C-7), 101.21 (C-1), 87.81 (C-1), 75.88 (C-4), 74.91 (C-5), 72.63 (C-3), 71.09 (C-2), 71.03 (C-3), 70.86 (C-5), 69.16 (C-2), 66.69 (C-4), 61.84 (C-6), 60.90 (C-6), 20.91 (C-8), 20.84 (C-8), 20.74 (C-8), 20.74 (C-8), 20.72 (C-8), 20.71 (C-8), 20.61 (C-8). HR-ESI-MS: *m/z* for $C_{26}H_{35}N_3O_{17}$ (exact monoisotopic mass 661.1966) $[M+NH_4]^+$ calcd. 679.2305, found 679.2299. ESI-MS: *m/z* for $C_{26}H_{35}N_3O_{17}$ $[M+NH_4]^+$ calcd. 679.2, found 679.2; $[M+Na]^+$ calcd. 684.2, found 684.2; $[M\text{-}GlcN_3]^+$ calcd. 331.1, found 331.0.

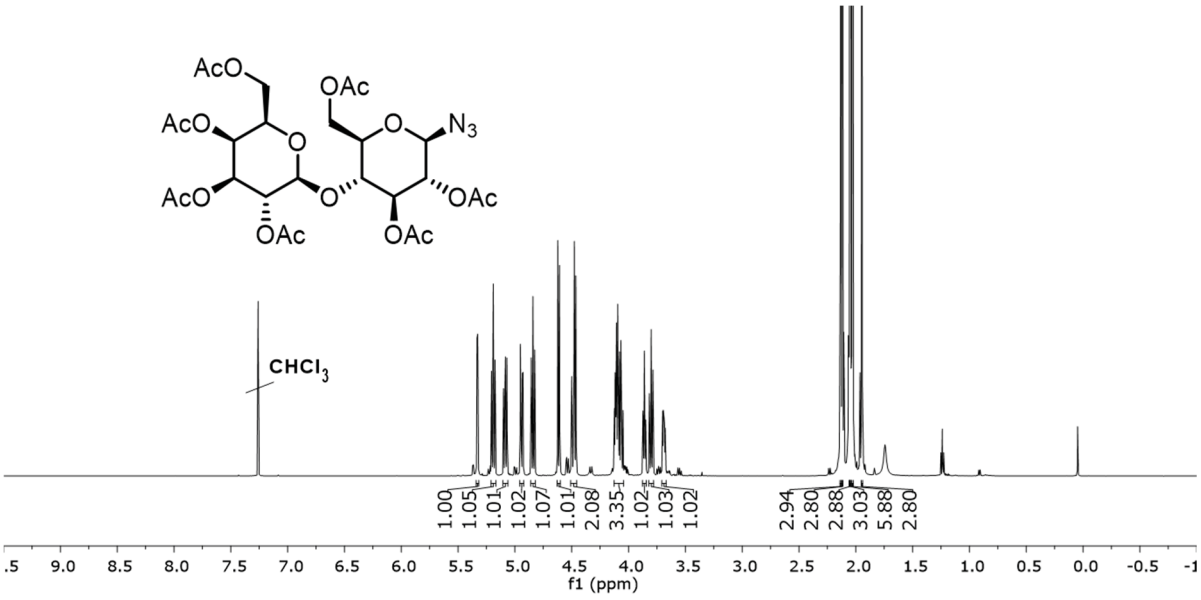

Figure S53: ^{1}H NMR spectrum (600 MHz, $CDCl_3$) of **11**.

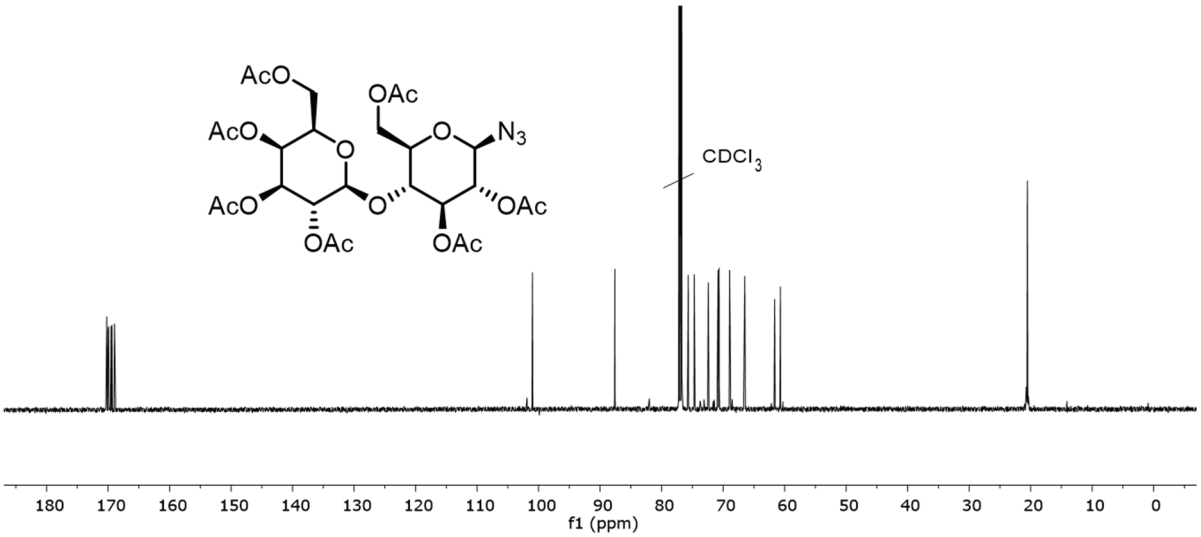

Figure S54: ^{13}C NMR spectrum (151 MHz, $CDCl_3$) of **11**.

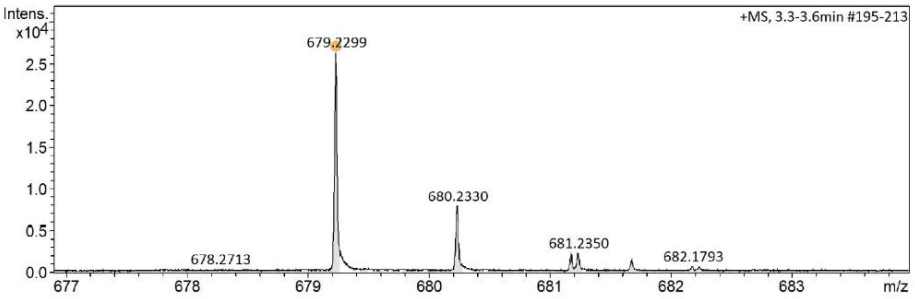

Figure S55: HR-ESI-MS spectrum of **11**.

5.3 Glycooligomer analysis

(Fuc,GalNAc)[2,5]-6 (13)

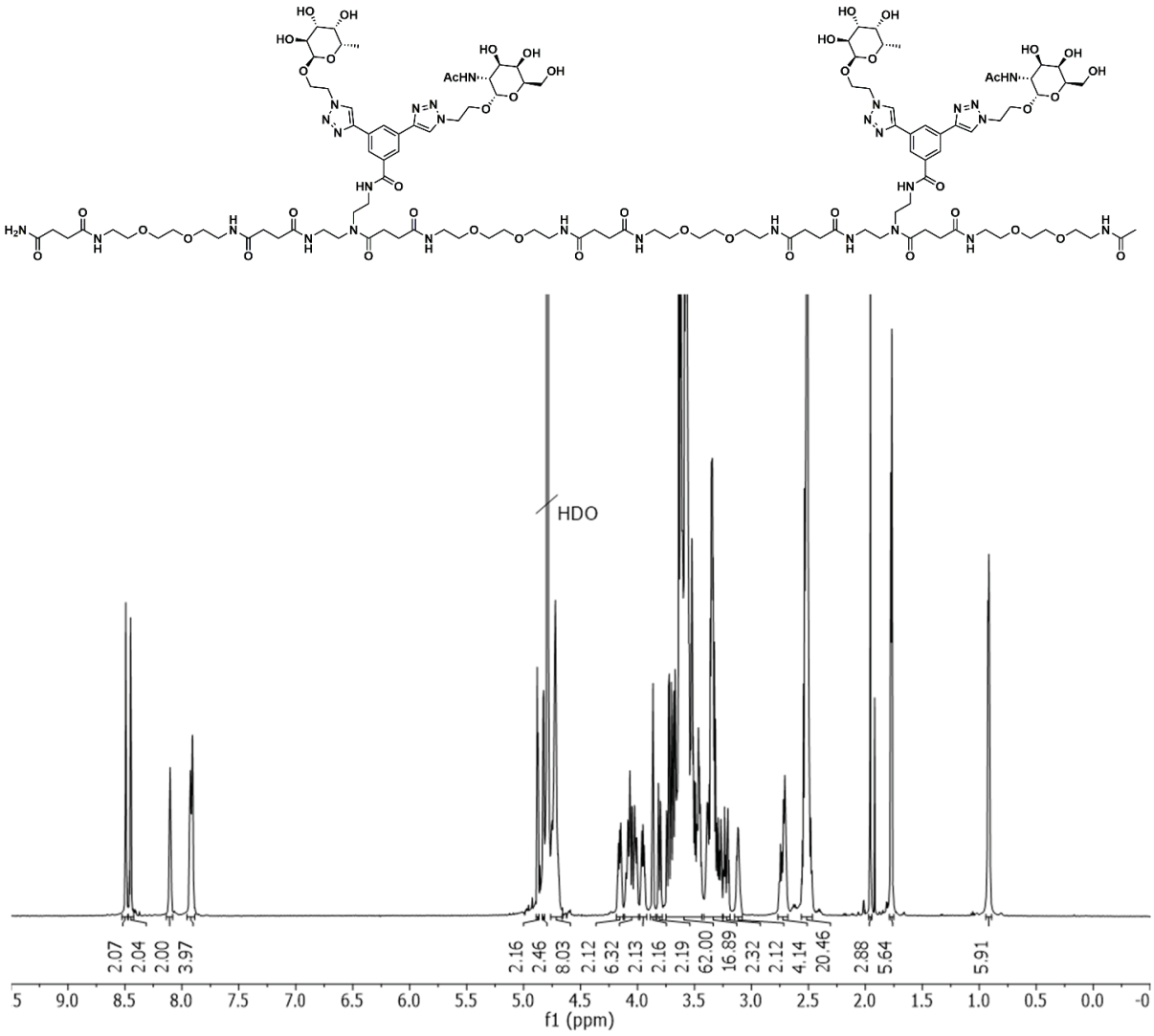

Figure S56: ^{1}H NMR (600 MHz, D_2O) spectrum of (Fuc,GalNAc)[2,5]-6 (**13**).

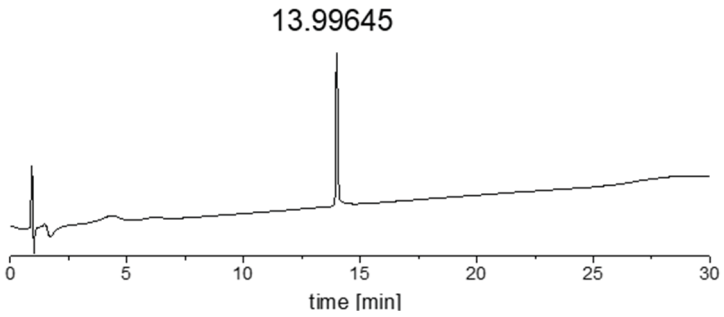

Figure S57: RP-HPLC chromatogram of (Fuc,GalNAc)[2,5]-6 (**13**).

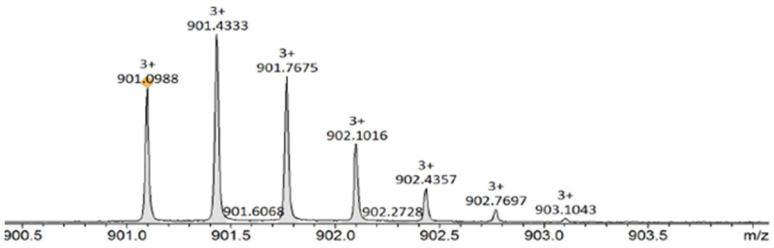

Figure S58: HR-ESI-MS spectrum of (Fuc,GalNAc)[2,5]-6 (**13**).

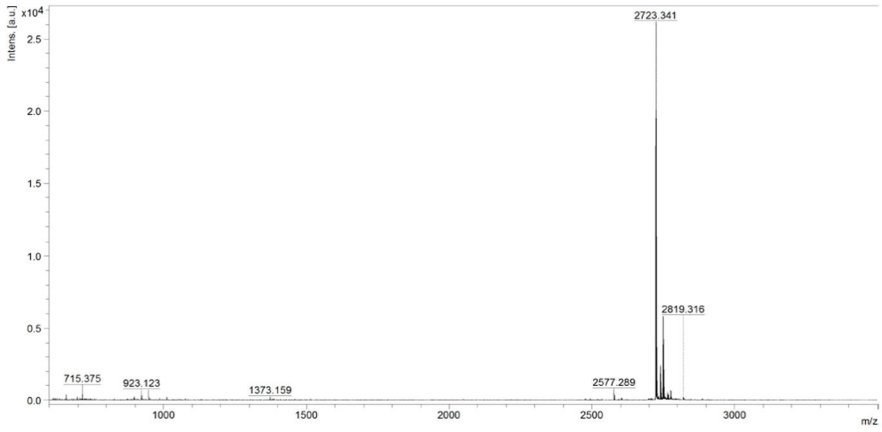

Figure S59: MALDI-TOF-MS spectrum of (Fuc,GalNAc)[2,5]-6 (**13**).

(Fuc,Gal)[2,5]-6 (14)

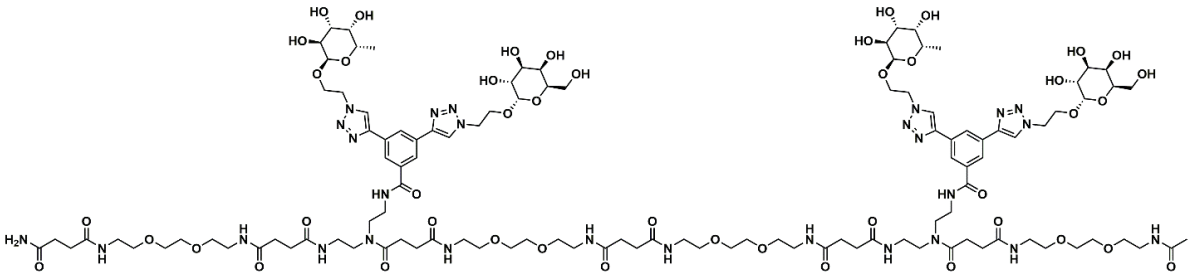

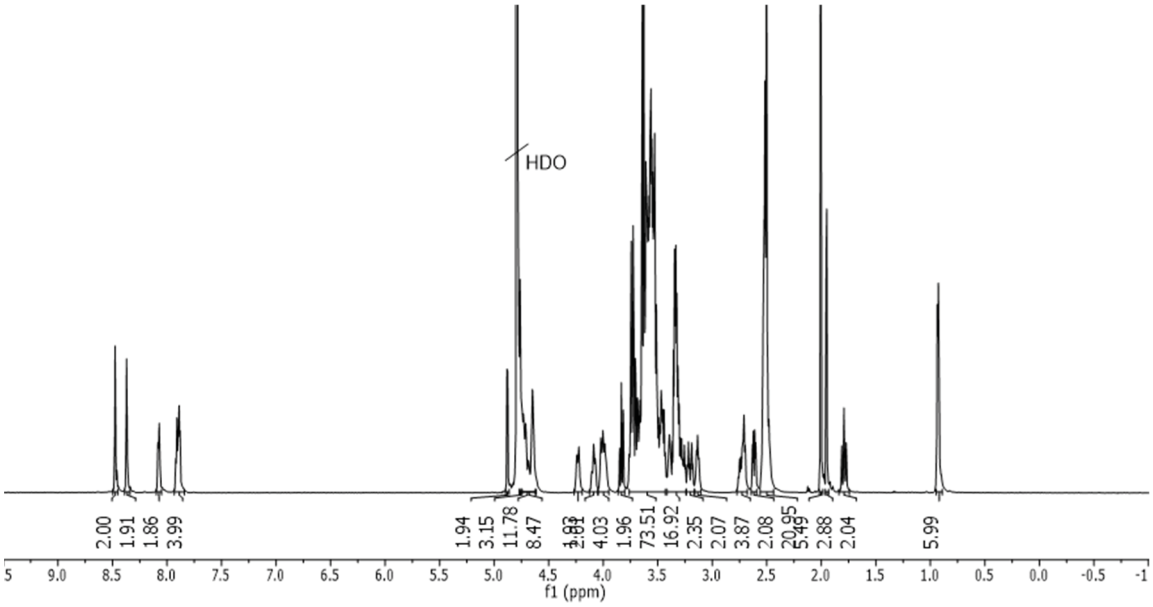

Figure S60: ^{1}H NMR (600 MHz, D_2O) spectrum of (Fuc,Gal)[2,5]-6 (**14**).

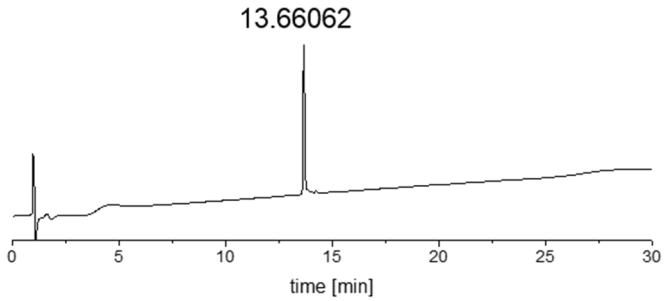

Figure S61: RP-HPLC chromatogram of (Fuc,Gal)[2,5]-6 (**14**).

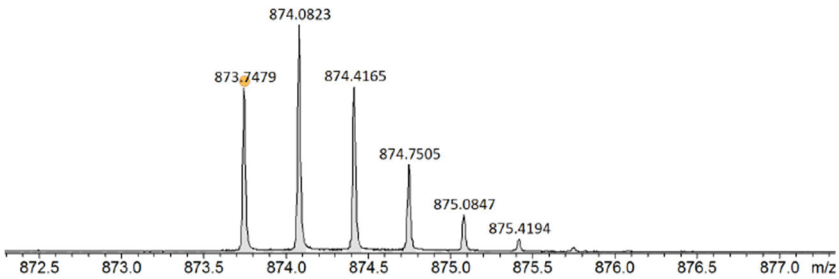

Figure S62: HR-ESI-MS spectrum of (Fuc,Gal)[2,5]-6 (**14**).

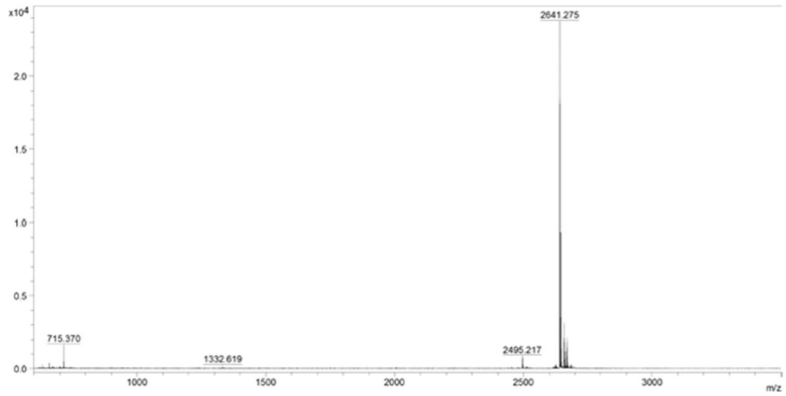

Figure S63: MALDI-TOF-MS spectrum of (Fuc,Gal)[2,5]-6 (**14**).

(Fuc,Lac)[2,5]-6 (15)

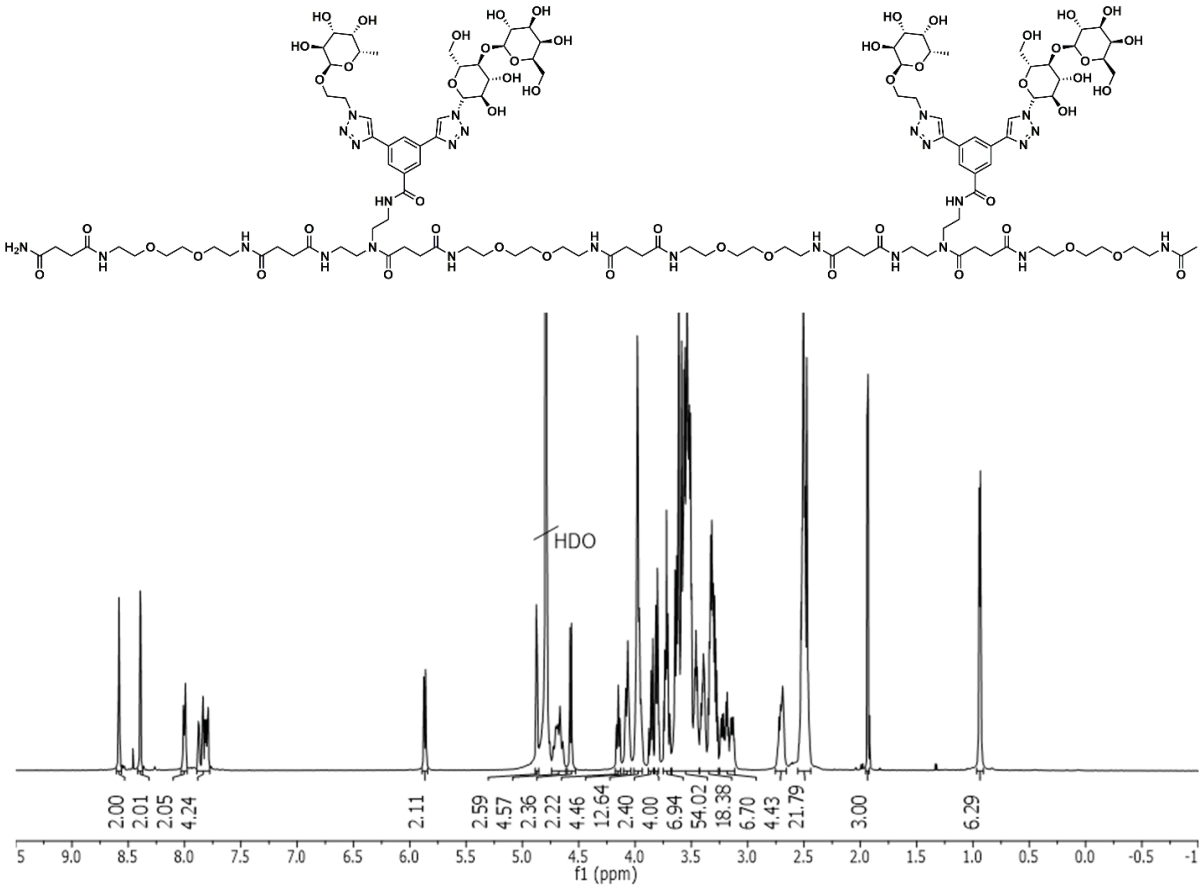

Figure S64: ^{1}H NMR (600 MHz, D_2O) spectrum of (Fuc,Lac)[2,5]-6 (**15**).

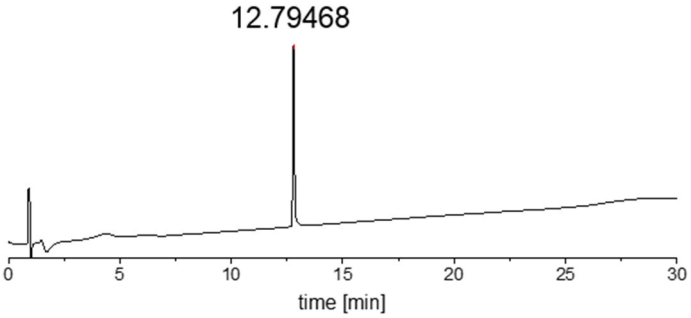

Figure S65: RP-HPLC chromatogram of (Fuc,Lac)[2,5]-6 (**15**).

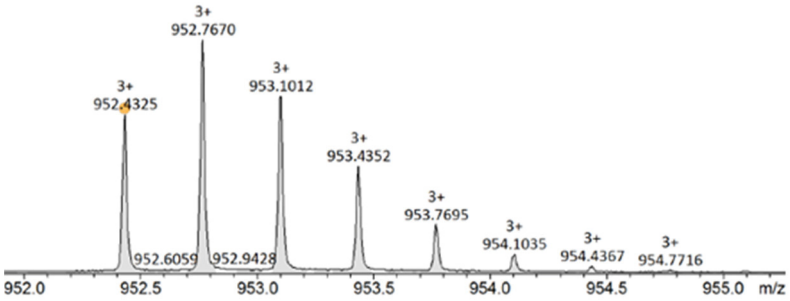

Figure S66: HR-ESI-MS spectrum of (Fuc,Lac)[2,5]-6 (**15**).

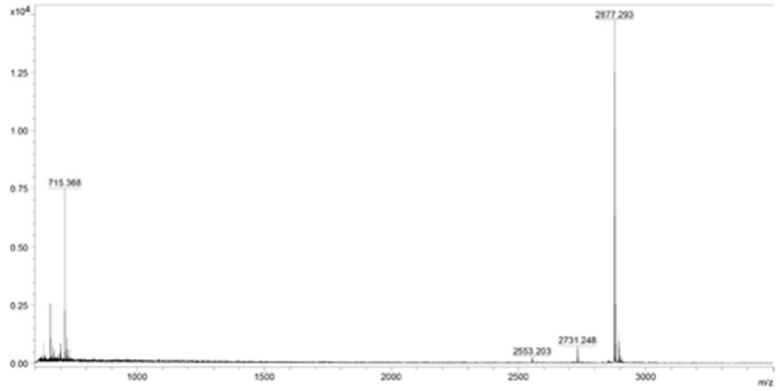

Figure S67: MALDI-TOF-MS spectrum of (Fuc,Lac)[2,5]-6 (**15**).

(Fuc,Sia-methyl protected)[2,5]-6 (16-Me)

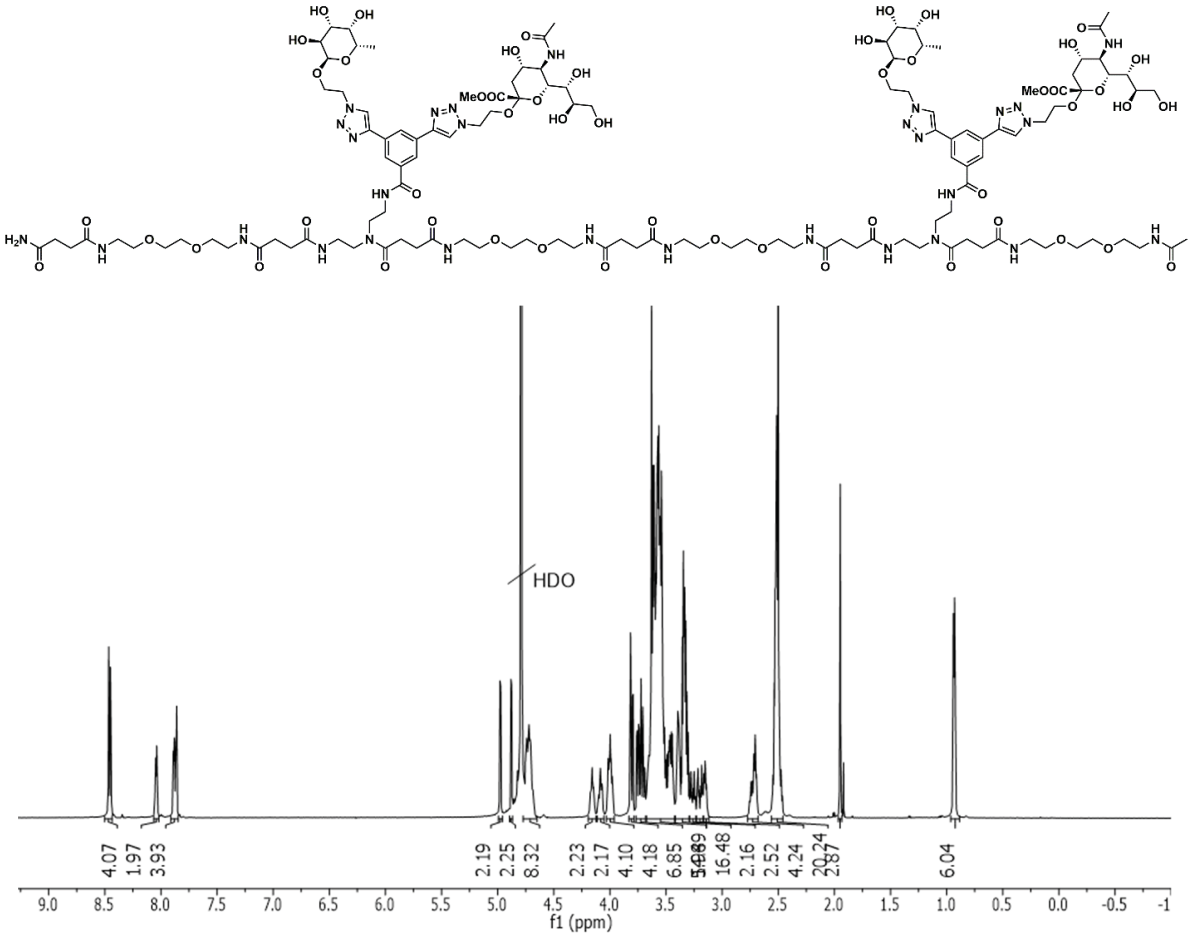

Figure S68: ^{1}H NMR (600 MHz, D_2O) spectrum of (Fuc,Sia-Me)[2,5]-6 (**16-Me**).

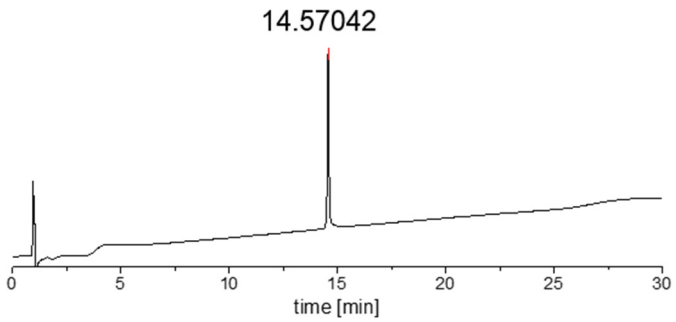

Figure S69: RP-HPLC chromatogram of (Fuc,Sia-Me)[2,5]-6 (**16-Me**).

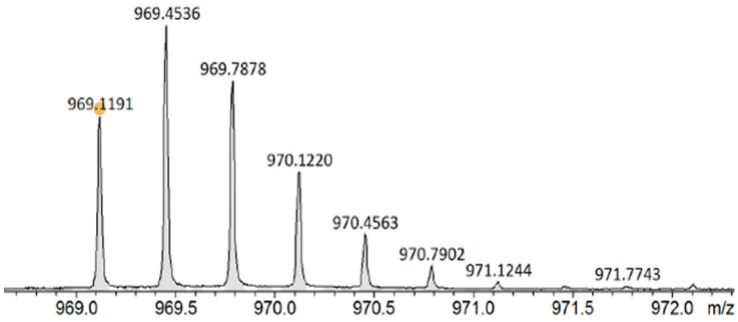

Figure S70: HR-ESI-MS spectrum of (Fuc,Sia-Me)[2,5]-6 (**16-Me**).

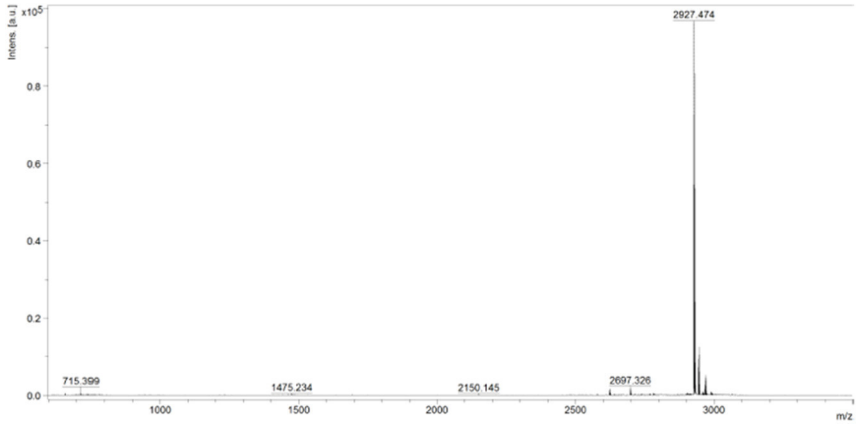

Figure S71: MALDI-TOF-MS spectrum of (Fuc,Sia-Me)[2,5]-6 (**16-Me**).

(Fuc,Sia)[2,5]-6 (16)

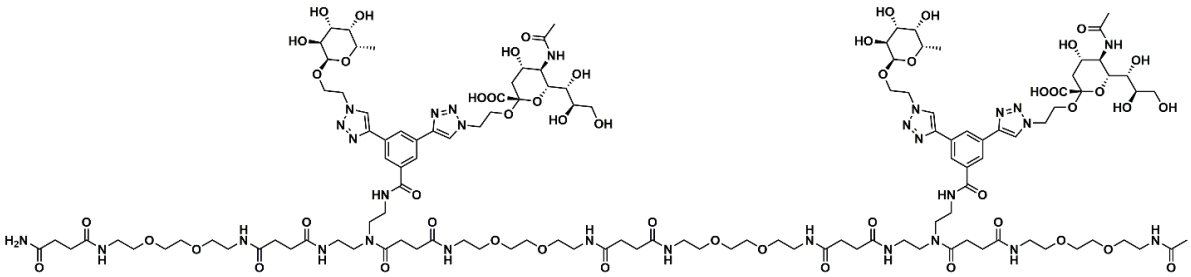

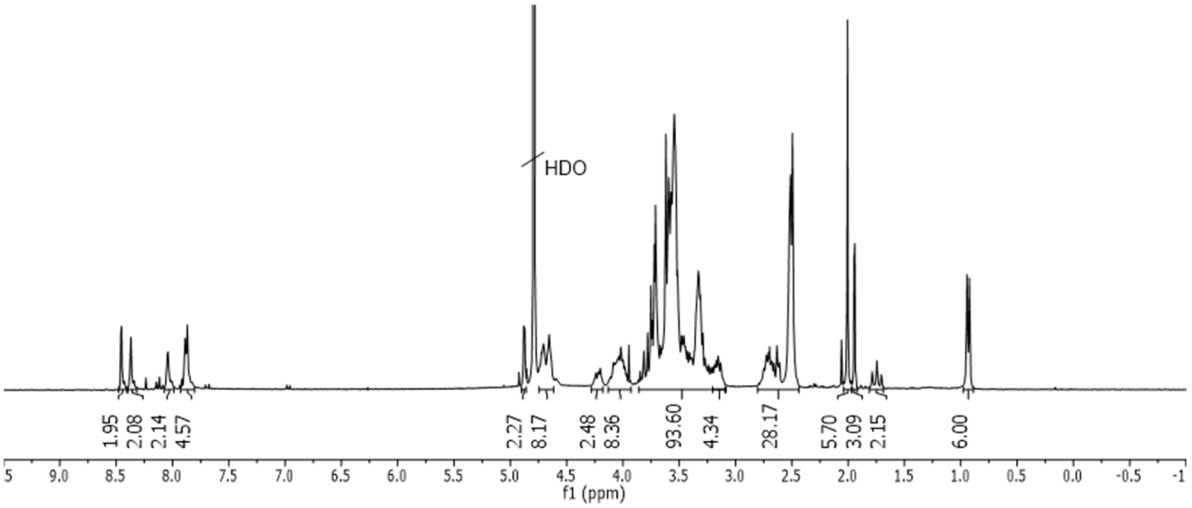

Figure S72: ^{1}H NMR (600 MHz, D_2O) spectrum of (Fuc,Sia)[2,5]-6 (**16**).

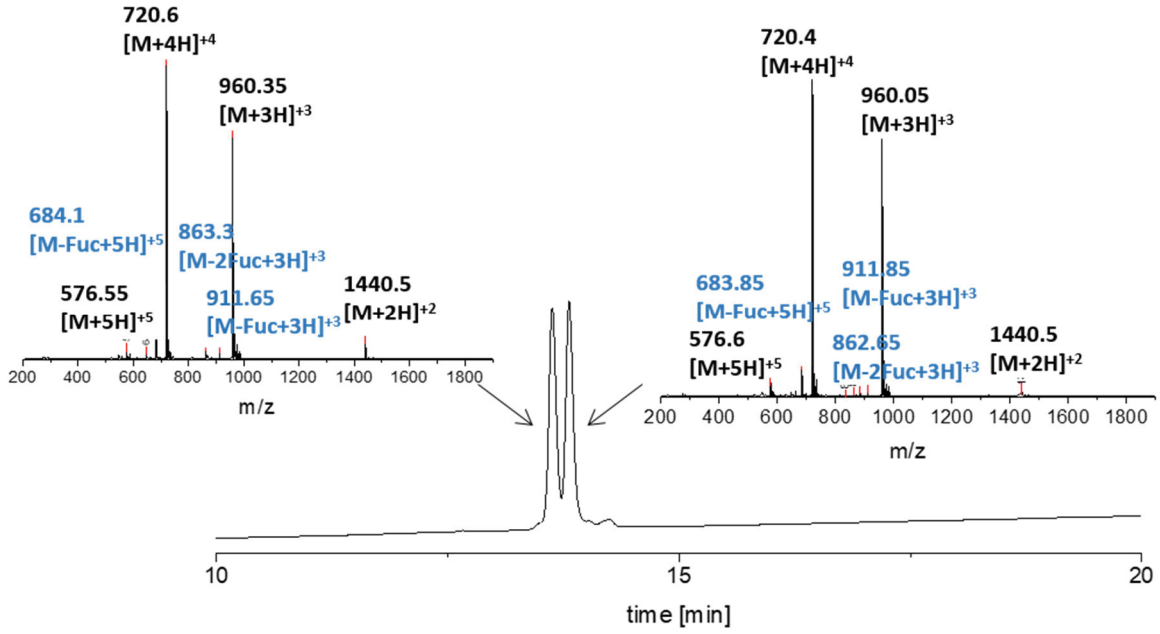

Figure S73: RP-HPLC chromatogram and corresponding mass spectra of (Fuc,Sia)[2,5]-6 (**16**).

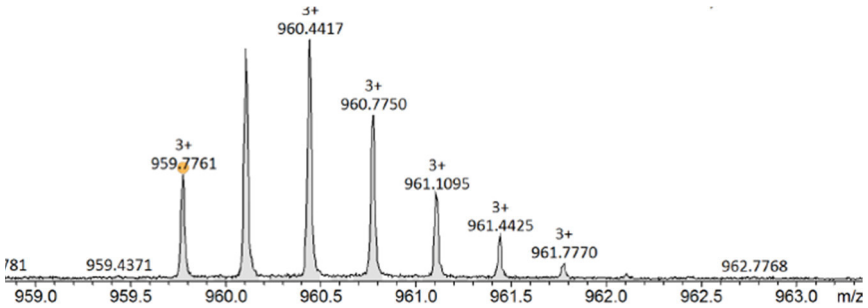

Figure S74: HR-ESI-MS spectrum of (Fuc,Sia)[2,5]-6 (**16**).

(Fuc,Fuc)[2,5]-6 (17)

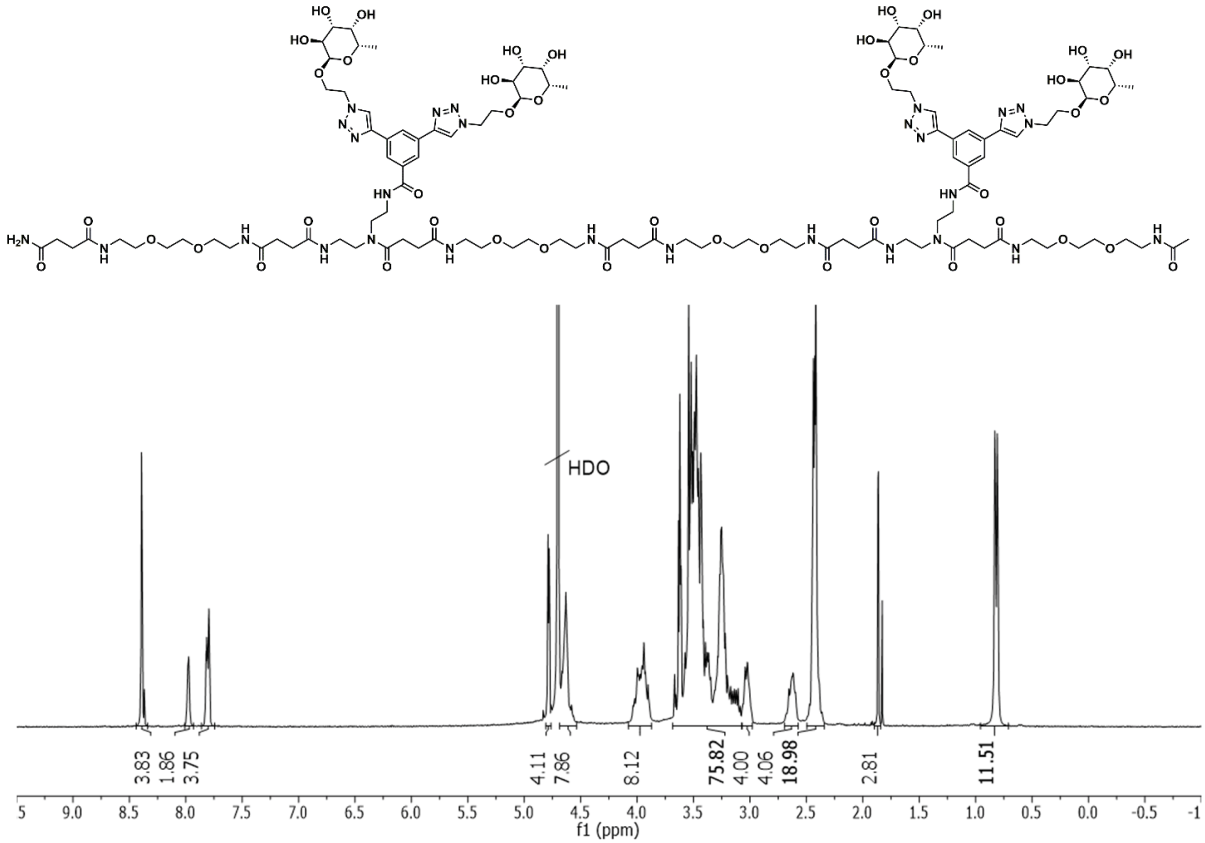

Figure S75: ^{1}H NMR (600 MHz, D_2O) spectrum of (Fuc,Fuc)[2,5]-6 (**17**).

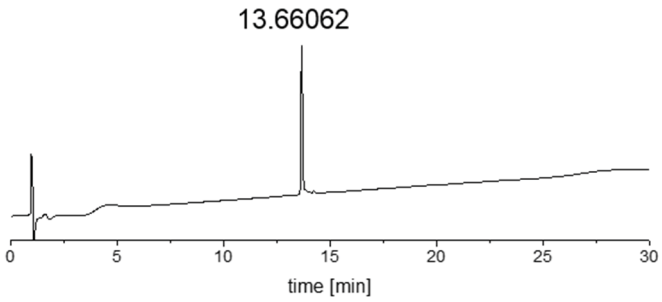

Figure S76: RP-HPLC chromatogram of (Fuc,Fuc)[2,5]-6 (**17**).

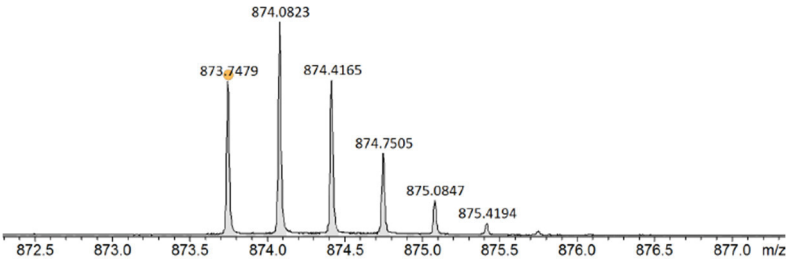

Figure S77: HR-ESI-MS spectrum of (Fuc,Fuc)[2,5]-6 (**17**).

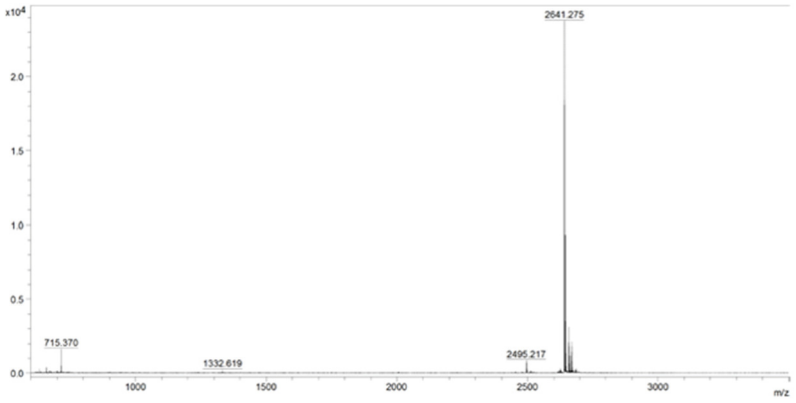

Figure S78: MALDI-TOF-MS spectrum of (Fuc,Fuc)[2,5]-6 (**17**).

(Gal,Gal)[2,5]-6 (18)

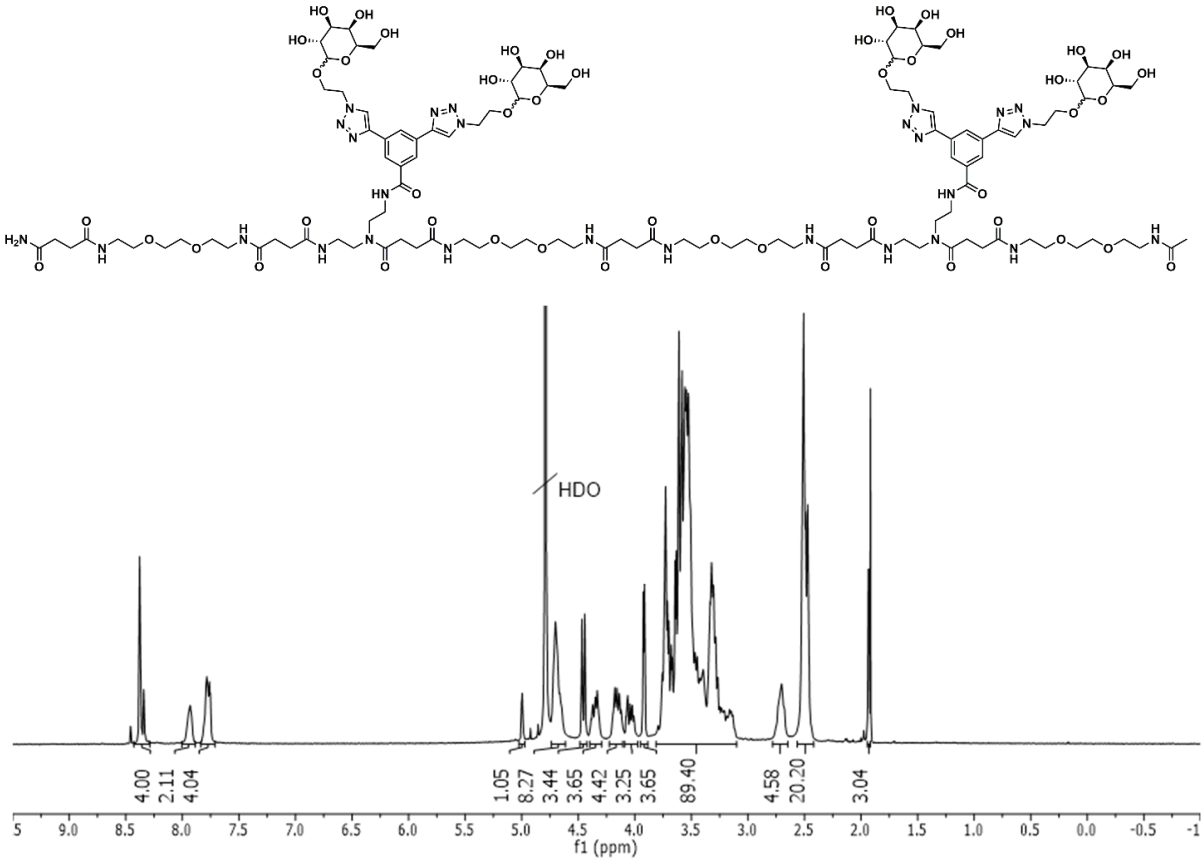

Figure S79: ^{1}H NMR (600 MHz, D_2O) spectrum of (Gal,Gal)[2,5]-6 (**18**).

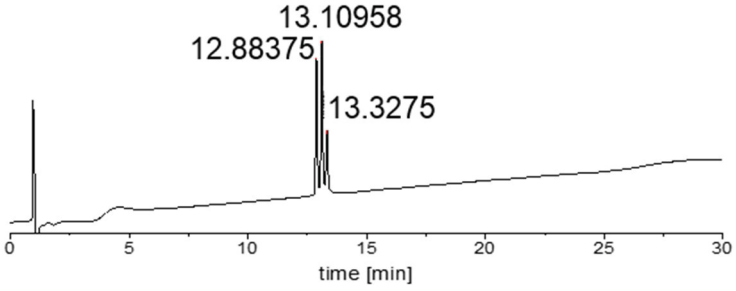

Figure S80: RP-HPLC chromatogram of (Gal,Gal)[2,5]-6 (**18**). The three observed peaks could be explained due to the α/β-mixture of the attached galactose units.

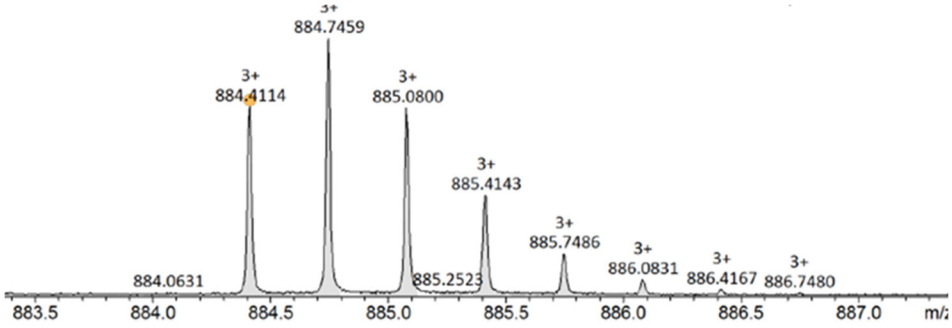

Figure S81: HR-ESI-MS spectrum of (Gal,Gal)[2,5]-6 (**18**).

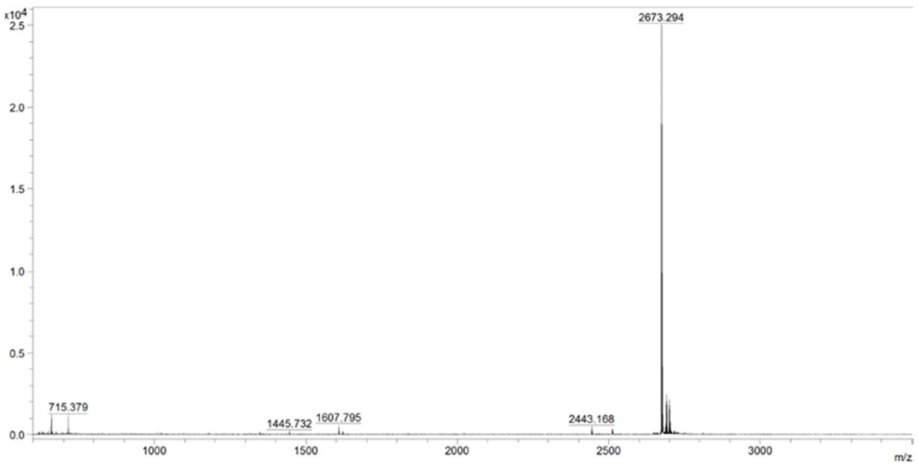

Figure S82: MALDI-TOF-MS spectrum of (Gal,Gal)[2,5]-6 (**18**).

6. Surface Plasmon Resonance (SPR)

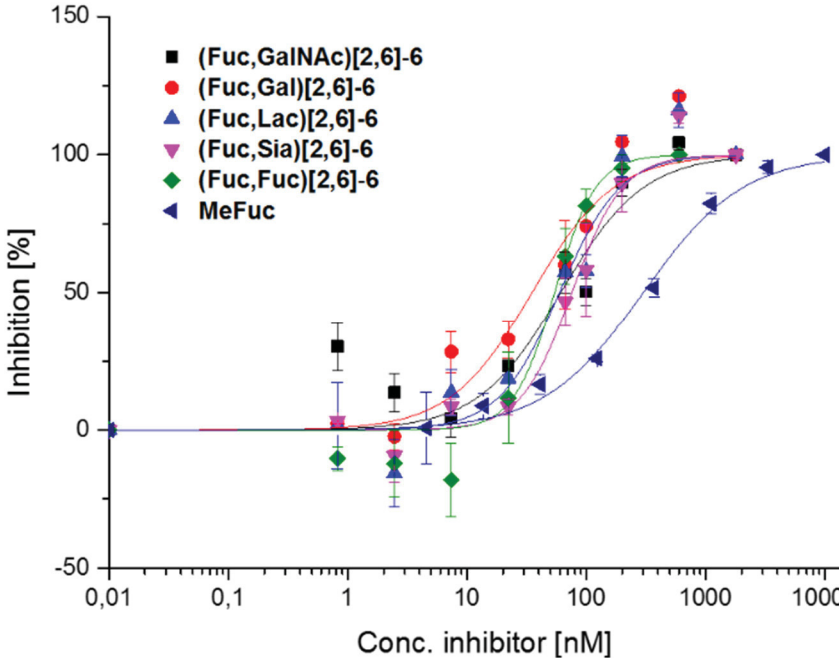

Figure S83: Inhibition-competition curves of fucosylated inhibitors **13**-**18** and α-L-methylfucose with only LecB (200 nM) set to 0 % inhibition and maximal inhibitor concentration set to 100 % inhibition.

6.1 SPR sensograms

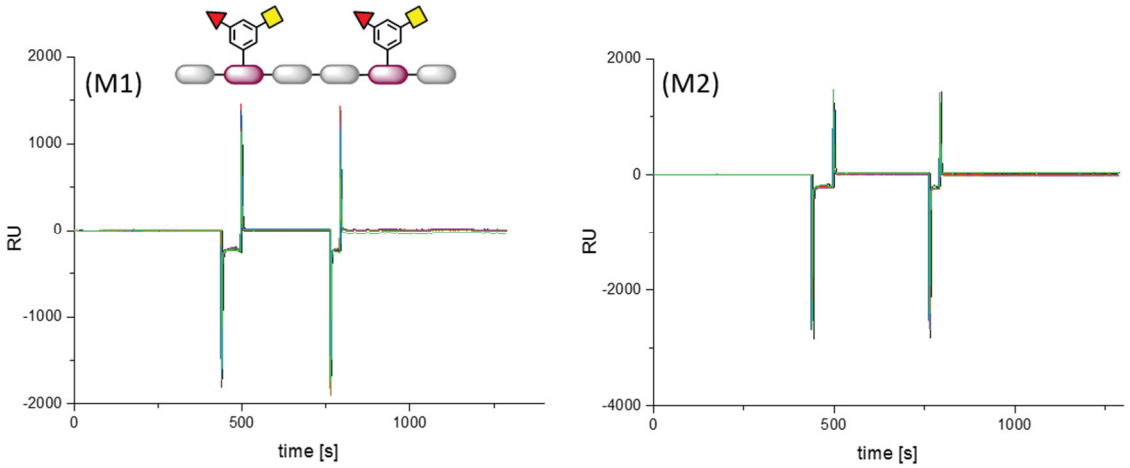

Figure S84: Raw data of measurement 1 (left) and 2 (right) from SPR inhibition-competition assay with LecB and (Fuc,GalNAc)[2,5]-6 (**13**).

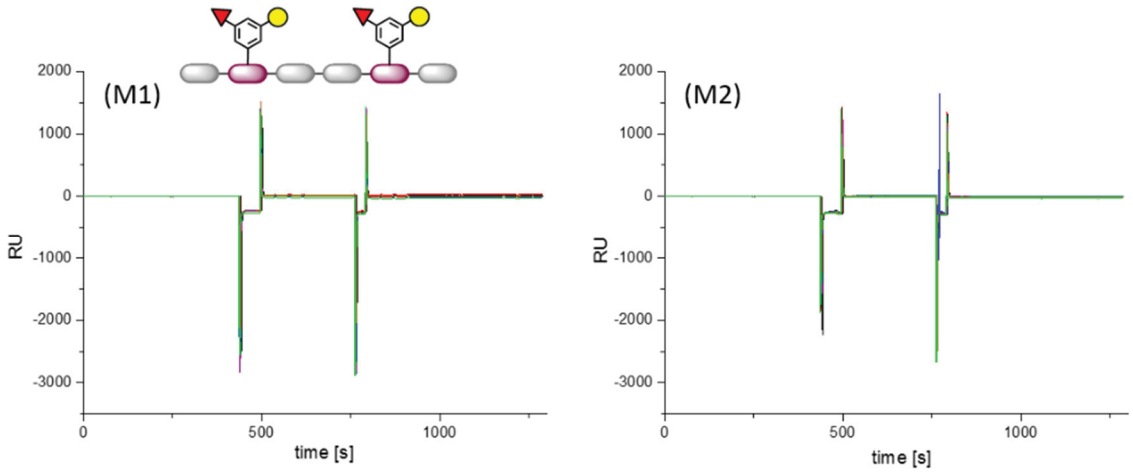

Figure S85: Raw data of measurement 1 (left) and 2 (right) from SPR inhibition-competition assay with LecB and (Fuc,Gal)[2,5]-6 (**14**).

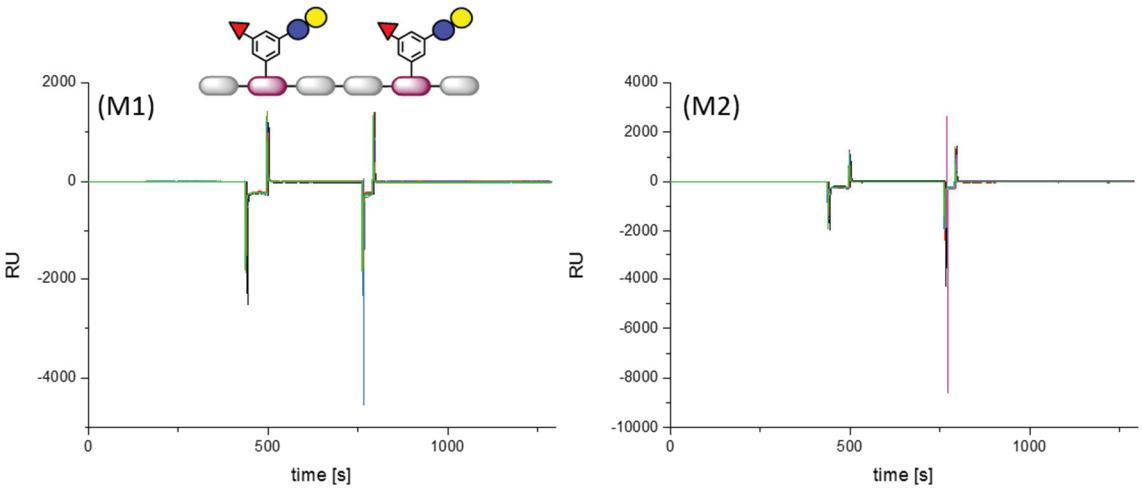

Figure S86: Raw data of measurement 1 (left) and 2 (right) from SPR inhibition-competition assay with LecB and (Fuc,Lac)[2,5]-6 (**15**).

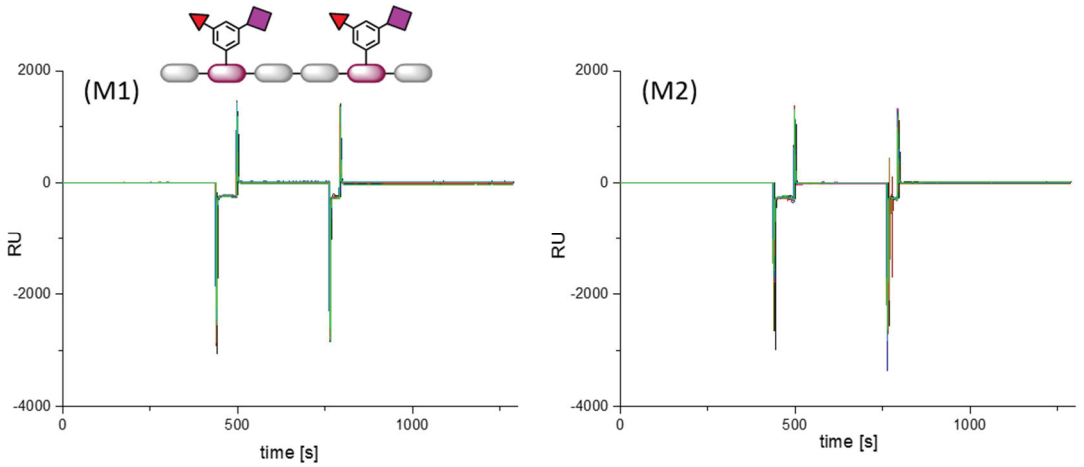

Figure S87: Raw data of measurement 1 (left) and 2 (right) from SPR inhibition-competition assay with LecB and (Fuc,Sia)[2,5]-6 (**16**).

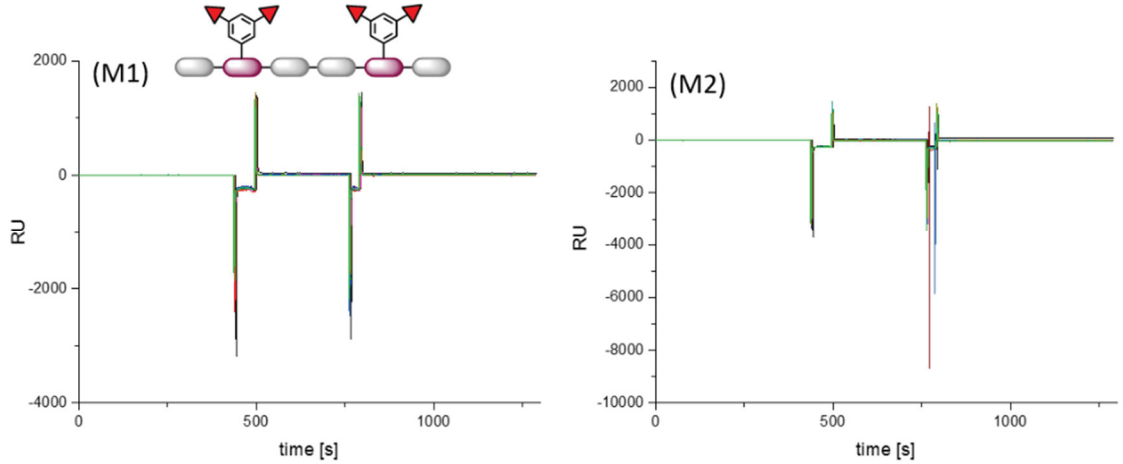

Figure S88: Raw data of measurement 1 (left) and 2 (right) from SPR inhibition-competition assay with LecB and (Fuc,Fuc)[2,5]-6 (**17**).

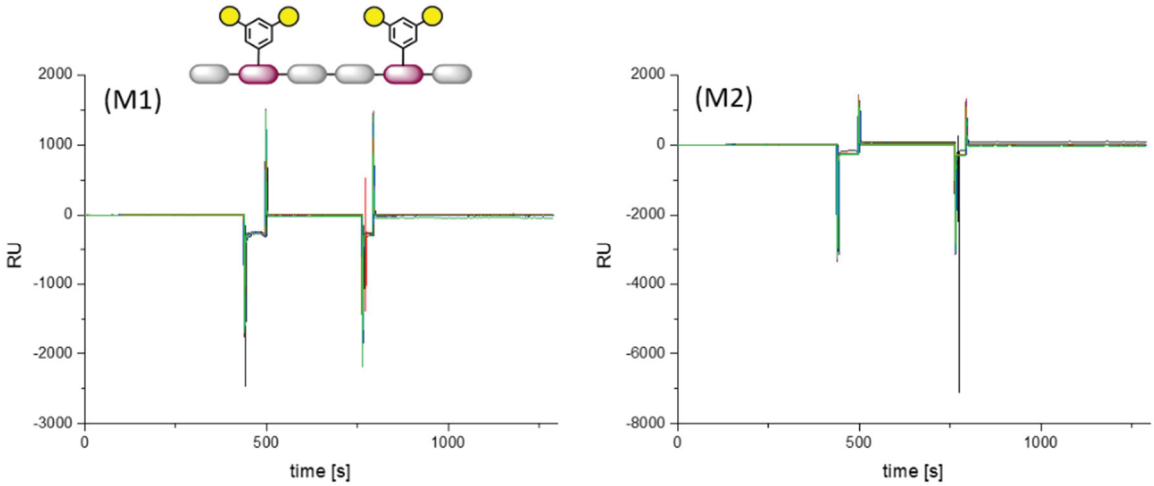

Figure S89: Raw data of measurement 1 (left) and 2 (right) from SPR inhibition-competition assay with LecB and (Gal,Gal)[2,5]-6 (**18**).

6.2 IC_{50} curves

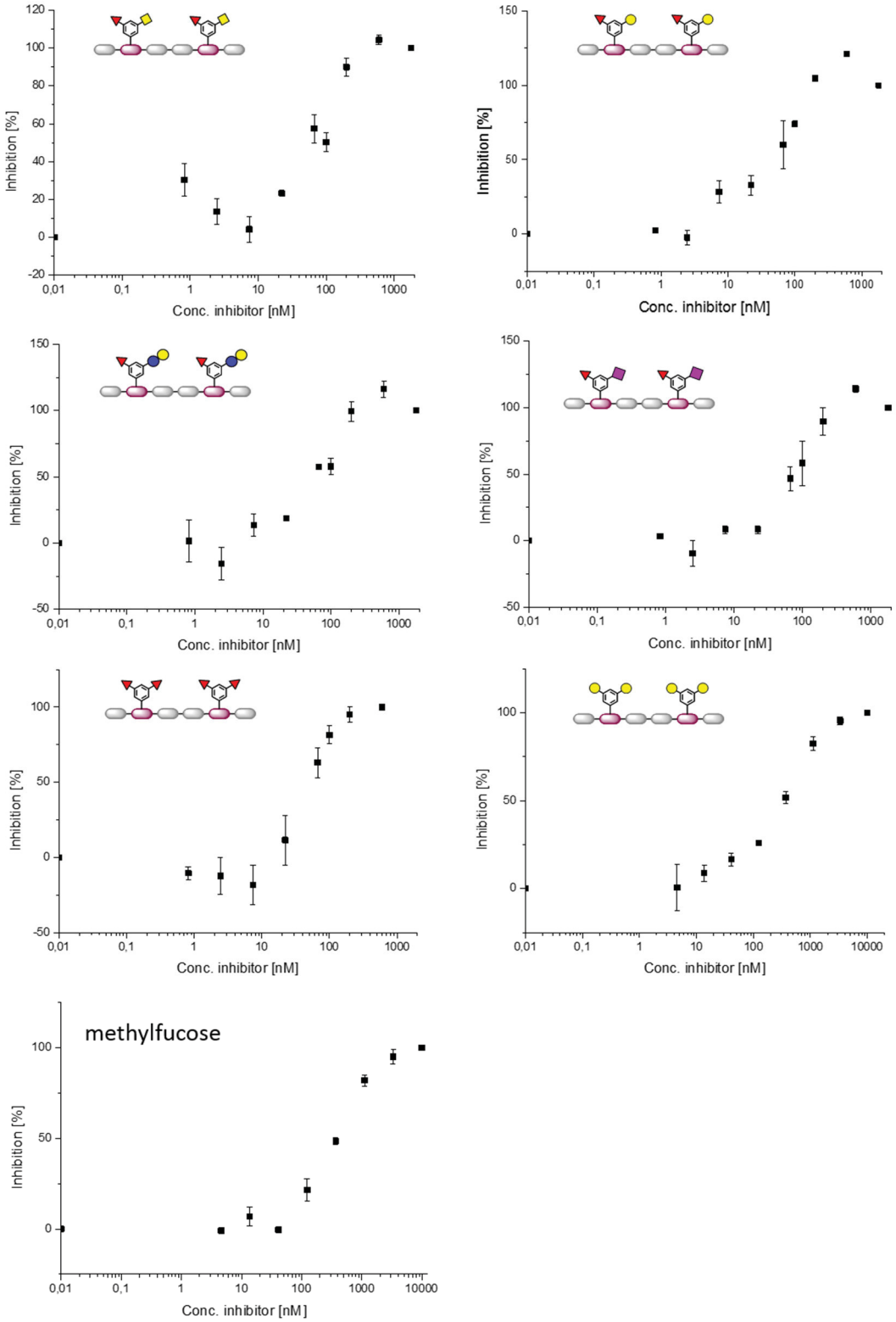

Figure S90: Increasing inhibition of LecB-binding with increasing amount of inhibitors **13**-**18** and methylfucose. The curves result from editing attended raw data from SPR inhibition-competition assay.

7. Literature

[1] D. Ponader, F. Wojcik, F. Beceren-Braun, J. Dernedde, L. Hartmann, *Biomacromolecules* **2012**, *13*, 1845.
[2] C. Gerke, M. F. Ebbesen, D. Jansen, S. Boden, T. Freichel, L. Hartmann, *Biomacromolecules* **2017**, *18*, 787.
[3] S. Roux, E. Zékri, B. Rousseau, M. Paternostre, J.-C. Cintrat, N. Fay, *J. Peptide Sci.* **2008**, *14*, 354.
[4] S. Cecioni, D. Goyard, J.-P. Praly, S. Vidal in *Carbohydrate Microarrays: Methods and Protocols* (Ed.: Y. Chevolot), Humana Press, Totowa, NJ, **2012**, pp. 57–68.
[5] J. Geng, G. Mantovani, L. Tao, J. Nicolas, G. Chen, R. Wallis, D. A. Mitchell, B. R. G. Johnson, S. D. Evans, D. M. Haddleton, *J. Am. Chem. Soc.* **2007**, *129*, 15156.
[6] R. Šardzík, G. T. Noble, M. J. Weissenborn, A. Martin, S. J. Webb, S. L. Flitsch, *Beilstein J. Org. Chem.* **2010**, *6*, 699.
[7] R. Caraballo, M. Saleeb, J. Bauer, A. M. Liaci, N. Chandra, R. J. Storm, L. Frangsmyr, W. Qian, T. Stehle, N. Arnberg, M. Elofsson, *Org. Biomol. Chem.* **2015**, *13*, 9194.
[8] B. Roy, B. Mukhopadhyay, *Tetrahedron Lett.* **2007**, *48*, 3783.
[9] K. S. Bücher, H. Yan, R. Creutznacher, K. Ruoff, A. Mallagaray, A. Grafmueller, J. S. Dirks, T. Kilic, S. Weickert, A. Rubailo, M. Drescher, S. Schmidt, G. Hansman, T. Peters, C. Uetrecht, L. Hartmann, *Biomacromolecules*, **2018**, *19* (9), 3714.
[10] F. Ishiwari, K.-I. Fukasawa, T. Sato, K. Nakazono, Y. Koyama, T. Takata*, Chem. Eur. J.* **2011**, *17*, 12067.

6 Conclusion and Perspectives

The synthesis of fucose-functionalized glycooligo(amidoamines) has been shown for the investigation of carbohydrate-lectin interaction of two pathogenic lectins, the viral capsid protein P-dimer of human Norovirus and the bacterial LecB from hospital-acquired *Pseudomonas aeruginosa*. These lectins seem to be responsible for the bacterial and viral adhesion to the host cell surfaces and first steps of infection. Although they are fast mutating microbs they exhibit overall four conserved binding sites towards fucosylated structures that might be suitable attachment factors for future antibacterials and antivirals. Therefore, in this thesis, the synthesis of monodisperse fucosylated glycooligo(amidoamines) was developed and they were applied as model structures to gain information about structure-function relations during the binding processes towards the targeted lectins in different functional assays together with collaboration partners from virology and enzymology. Previously established protocols for the solid phase polymer synthesis (SPPoS) enable the synthesis of so-called precision glycooligomers, a novel class of glycomimetics suitable for the investigation of structure-function relations in lectin binding.[1] After subsequent assembly of tailor-made building blocks on a solid support and following carbohydrate attachment by solid supported CuAAC monodisperse glycooligo(amidoamines) can be generated.

In this thesis, fucose as important carbohydrate motif for the targeting of bacterial and viral lectins was introduced for the first time during SPPoS. A set of monodisperse α-L-fucosylated glycooligomers was synthesized with varying structural parameters based on known building blocks EDS and TDS as well as an α-L-fucose derivative functionalized with an azidoethyl-linker (see Figure 15).

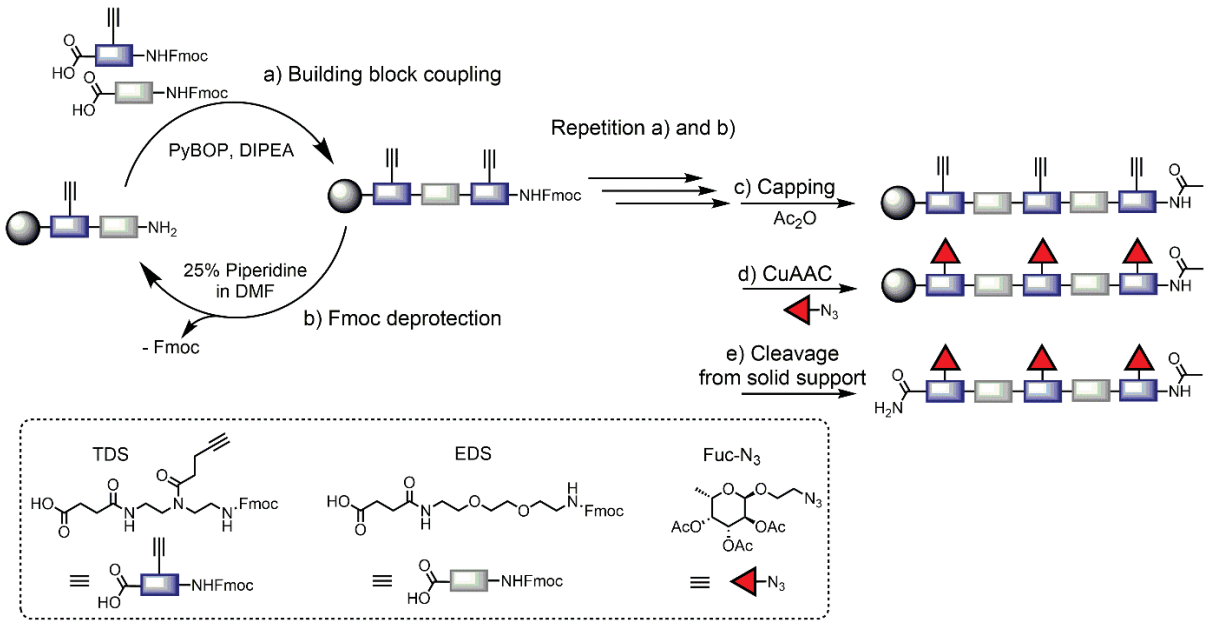

Figure 15: Schematic representation of solid phase polymer synthesis of fucosylated glycooligo(amidoamines).

The fucose side chains were attached through *O*-glycosidic bonds as can be found also in natural glycoconjugates. Due to the overall biological function of fucosylation that serves as marker strategy and depends on the fast and efficient attachment and removal of fucose moieties on glycoconjugates, the fucose glycosidic bond is sensitive and therefore partial cleavage of fucose side chains of the glycomimetic structures were observed in ESI MS and MALDI TOF MS measurements (see Figure 17). However, the completeness of fucosylation of glycooligomers was proven by ^{1}H NMR and the stability of fucosylated glycomimetics in aqueous solution could be observed even after several months by RP-HPLC and ^{1}H NMR.

In the first part of this work, homomultivalent fucosylated glycooligo(amidoamines) were successfully generated adjusting precisely their valency, chain length and fucose-spacing for the potential attachment to the binding sites of P-dimer and LecB (see Figure 16). These fucosylated oligomers have been synthesized varying in only one or two parameters for good comparability of their binding behavior towards the lectins. A first series of fucose-oligomers have been synthesized, differing in valency but keeping the number of spacer building blocks the same to evaluate potential statistical rebinding effects. In addition, fucose-oligomers were generated that bear only two fucose units with different number of EDS-units in between to examine the influence of spacing onto binding towards P-dimer. Spacing was also varied between fucose units of trivalent oligomers. Different spacing was expected to impact potential clustering effects since the availability of fucose side chains as well as the overall size of the fucose-oligomers might influence bridging between several receptor molecules. Fucose-oligomers exhibiting a high fucose density on the oligomeric scaffolds but different sizes were produced to give information about steric shielding effects and to evaluate the influence of fucose distance but also the effect of increased fucose/scaffold ratio on potential statistical rebinding. In addition, four negative control structures were generated presenting galactose instead of fucose side chains due to low binding affinities of galactose towards the targeted lectins P-dimer and LecB.

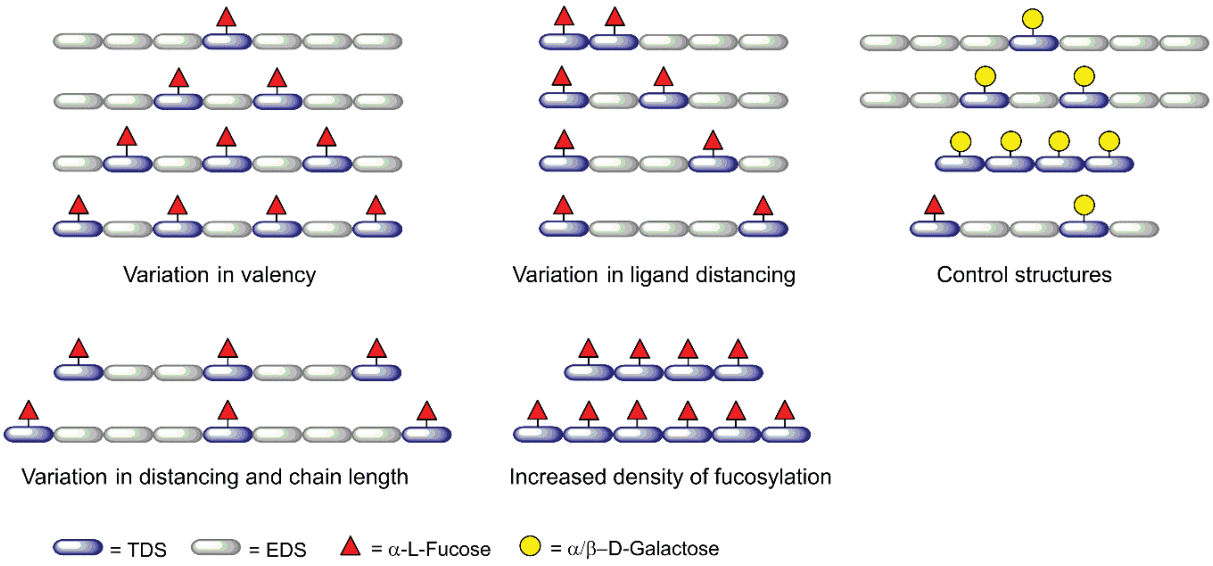

Figure 16: Synthesized fucosylated glycooligomers with varying valency, spacing and chain length.

The primary structures of the glycooligomers were designed based on the receptor proteins structures and distancing of their carbohydrate recognition domains. In an all-stretched conformation, the length between two fucose units attached to the backbone with no EDS-spacer-units in between would be 31 Å. However, such a stretched conformation is not expected for the glycooligomers in aqueous solution as their backbones should be rather flexible. Indeed, MD-simulations, conducted by Dr. Andrea Grafmüller, propose a coiled conformation for the glycooligomers which was also shown previously for similar structures by fluorescence correlation spectroscopy.[2] Furthermore, the distribution of distance between two neighboring fucose side chains was calculated to be about 10-20 Å in coiled-conformation, independent of the number of included EDS-spacer units (see Figure 17). Dynamic light scattering, performed in collaboration with Jun-Prof. Dr. Stephan Schmidt, provided hydrodynamic radii of about 12-13 Å in salt or buffered solution, confirming the calculations from MD-simulations. Surprisingly glycooligomers show much increased hydrodynamic radii in ultrapure water of about 100 nm, most likely due to self-aggregation effects. The glycooligomers represent non-charged glycomimetics with a predominantly hydrophilic character. Interestingly the addition of salt prevents this phenomenon leading to the assumption that indeed hydrophilic contacts play a role during these interactions. This self-aggregation behavior could be observed by several techniques but is not fully understood to date. Nevertheless, the interactions of fucose-oligomers towards P-dimer and LecB were conducted in buffered solution thus self-aggregation should not affect the investigation of binding processes.

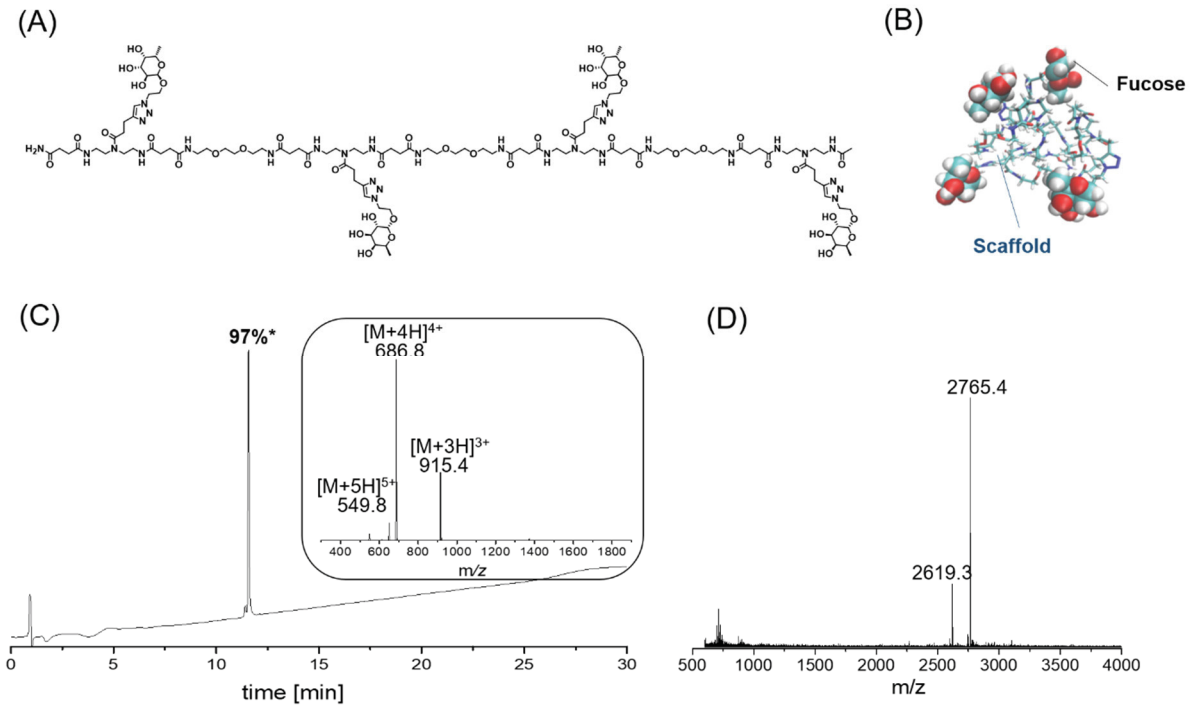

Figure 17: *Exemplary analytical data of tetravalent fucose-oligomer Fuc(1,3,5,7)-7: (A) chemical structure; (B) MD-simulations of coiled conformation (calculated by Dr. Andrea Grafmüller); (C) RP-HPLC and MS spectra (water/acetonitrile (95/5) to water/acetonitrile (1:1) in 30 min); (D) MALDI TOF MS spectra with m/z for $[M+Na]^+$ and corresponding $[M+Na-Fuc]^+$ lacking one fucose. *Relative purity as determined by integration of UV signal.*

While the generated homomultivalent fucosylated glycooligomers already provide multivalent glycomimetics suitable to address different bacterial and viral lectins, the natural attachment factor of P-dimer and LecB is not fucose itself but these are fucosylated glycans like the histo-blood group antigens (HBGA). In case of P-dimer the main binding motifs are the blood group antigens.[3] In addition, human milk oligosaccharides (HMO) are known to be bound from various human Norovirus strains[4] while sLe^a is thought to be the natural binding factor of LecB.[5] Unfortunately, the synthesis of more complex carbohydrates is very time-consuming affording only low amounts of target glycans. Especially the synthesis of natural glycans bearing additional functional groups for multiple-attachment to synthetic macromolecules is very laborious.

Therefore, in the second part of this work, heteromultivalent fucosylated glycooligo(amidoamines) have been generated to mimic more complex carbohydrate ligands, specifically the blood group antigens A and B, sLe^a and fucosyllactose. Due to the high flexibility of the oligo(amidoamine)-backbones and the resulting undefined distances between the attached carbohydrate side chains a new building block was developed. It reduces the flexibility between two linked carbohydrates to each other within a linker unit while keeping the overall flexibility of the backbone the same. The new functional building block *iso*-DTDS exhibits a carboxyl group and an Fmoc-protected amine group for the introduction in Fmoc-based solid phase polymer synthesis. As side chain *iso*-DTDS possesses a phenylene-branching unit with two alkyne moieties in meta-position with one of the alkyne groups

carrying a TIPS-protecting group. The developed synthetic route is based on the synthesis of previously introduced functional building blocks using an asymmetrical protected diethylene triamine derivative (key intermediate) (see Figure 18).[6] This was used for the attachment of a precursor benzoic acid derivative equipped with TIPS-acetylene and an alkyne functionality in meta-position. During the synthesis a rearrangement step occurs when exchanging the protecting groups. It was possible to drive this isomerization to completeness. Thereby the rearrangement could be incorporated into the synthetic strategy resulting in the final building block with defined stereochemistry, suitable for solid phase synthesis. The chemical definition of building block structure is essential for the synthesis of sequence-controlled monodisperse glycooligomers and further structure-function-relations during their binding towards lectins. One disadvantage in the synthesis of *iso*-DTDS is the requirement of column chromatography for two steps during the synthesis. Therefore, a major improvement of the synthesis could be to evaluate suitable parameters for the purification *e.g.* by crystallization.

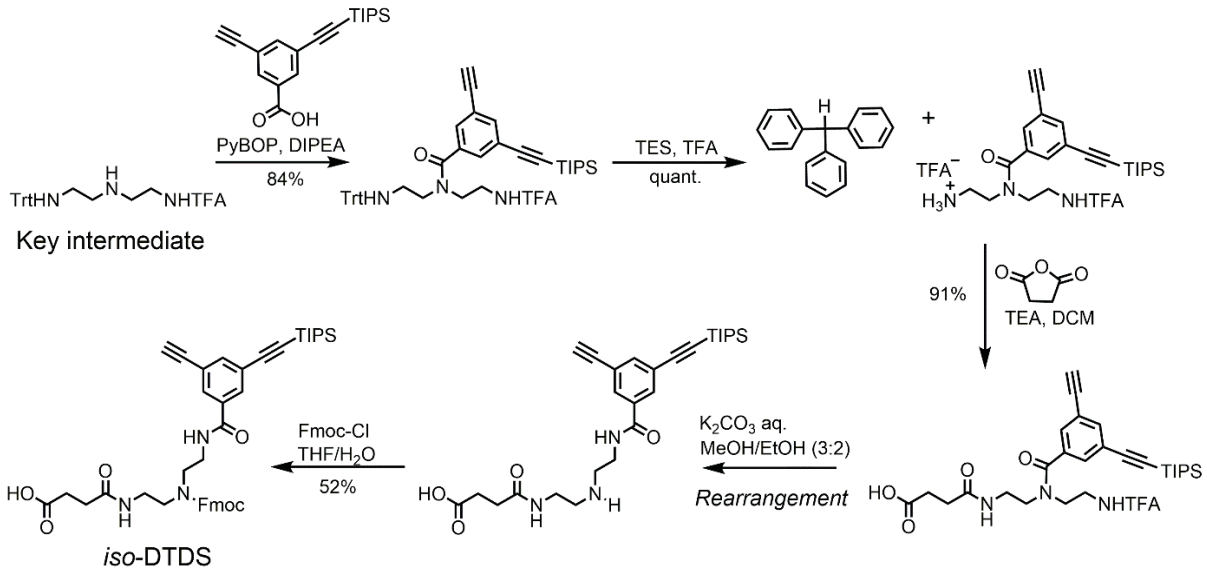

Figure 18: Synthesis of bi-functional building block iso-DTDS. Reprinted with permission from K. S. Bücher, P. B. Konietzny, N. L. Snyder, L. Hartmann, Chem. Eur. J. ***2019****, 25* (13), 3301-3309*. Copyright © 2019 Wiley-VCH Verlag GmbH & Co. KGaA, Weinheim.*

Iso-DTDS was then successfully applied in Fmoc-based SPPoS with 95% coupling efficacy by a double coupling procedure to generate oligo(amidoamine)-backbones. To gain heteromultivalent glycosylated oligomers, in the following a consecutive carbohydrate(1)-coupling, TIPS-deprotection and again carbohydrate(2)-coupling procedure was performed. The synthetic strategy gives simplified access to heteromultivalent glycomimetics, requiring only low amounts of the azidated carbohydrates (2-3 eq.). A cleavage procedure for TIPS was already described by Toonstra in 2016, in this case using a self-constructed resin.[7] The group of J.-F. Lutz reported a similar method for the construction of functionalized DNA-analogs but only post-functionalization could be accomplished. Due to the harsh

cleavage conditions during TIPS-deprotection this was not performed on commercial available solid supports in phosphoramidite-chemistry.[8] In this work, for the first time, TIPS-deprotection was performed on a commercially available Tentagel-resin with Rinkamide-linker.

With this method, six glycooligomers were synthesized applying *iso*-DTDS and EDS consisting of four heteromultivalent oligomers with fucose and an additional carbohydrate (Gal, GalNAc, Lac, Sia) per side chain and two homomultivalent control structures with either fucose or galactose units (see Figure 19). The overall geometry was kept the same for all heteromultivalent glycooligomers to examine the influence of each additional carbohydrate in combination with neighboring fucose. Indeed, fucose is the main binding epitope but a general assumption is that during HBGA and HMO binding to P-dimer and LecB other carbohydrates make further contacts in the binding pockets.

This versatile methodology for the synthesis of heteromultivalent glycooligomers enables the attachment of different carbohydrates at the end of the synthesis. An advantage of the generated structures is the high proximity of the carbohydrate units as mimicry of more complex glycans.

Previously heteromultivalent glycooligomers were achieved by sequential building block coupling and carbohydrate attachment steps or by the usage of different types of functional building blocks that could be used for the orthogonal introduction of carbohydrate side chains at the end of the synthesis. These concepts allow for the defined positioning of different carbohydrates along the oligomeric scaffold but due to the coiled conformation of glycooligomers with flexible backbones and linker structures the overall relative positioning of carbohydrates remains undefined.

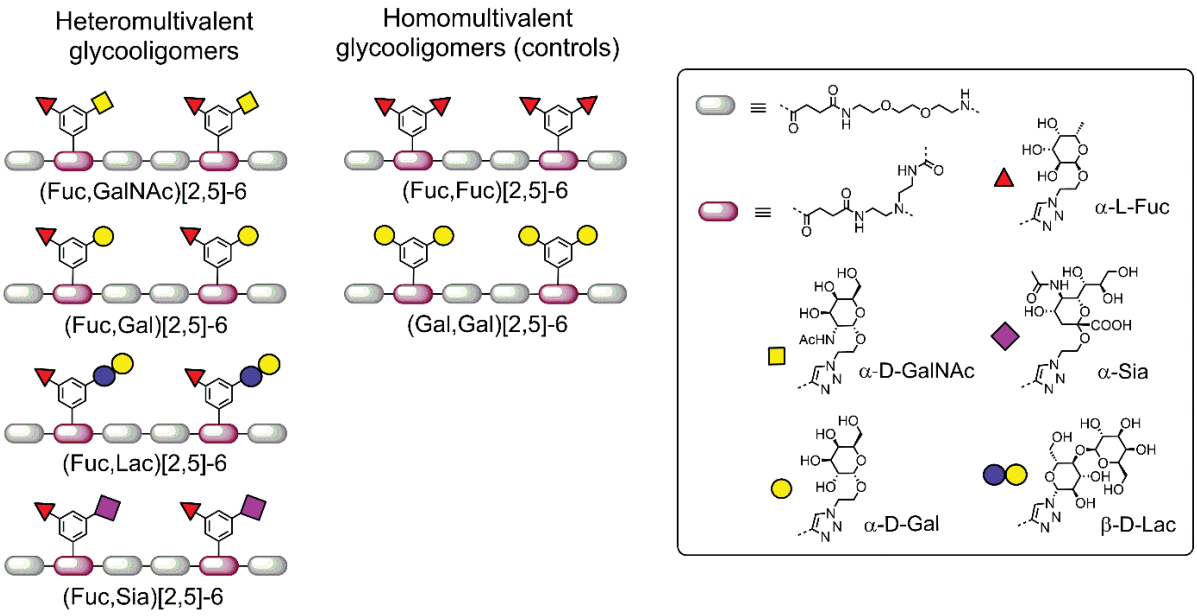

Figure 19: Synthesized glycooligomers using iso-DTDS as functional building block. Adapted with permission from K. S. Bücher, P. B. Konietzny, N. L. Snyder, L. Hartmann, Chem. Eur. J. ***2019****, 25* (13), 3301-3309*. Copyright © 2019 Wiley-VCH Verlag GmbH & Co. KGaA, Weinheim.*

With the new building block *iso*-DTDS the introduction of more rigid linkers, shared by two different carbohydrate ligands, enables the more defined relative presentation of carbohydrates multivalently on the oligomeric scaffold. Similar ideas are known from literature for hetero-functionalized polydisperse glycomimetics.[9] In most cases they used very flexible linker structures that do not avoid the local separation of the carbohydrate side chains causing undefined distancing between the attached carbohydrates hampering structure-function-relations.

In future the developed strategy could advance the synthesis of sequence-controlled glycooligomers by generating a TIPS-protected TDS-building block. This could improve the synthetic effort of heteromultivalent oligomers and enable simple access towards specific functionalization patterns with various carbohydrates along the glycooligomer scaffold. The new building block could further be used for non-carbohydrate ligands or in combination with these. This might be an opportunity to influence binding in a new fashion, since a first ligand could trigger binding of the neighboring second ligand as it is known that lectin binding sites can also interact with non-carbohydrate units. In addition, potent non-carbohydrate moieties evaluated by fragment-based screenings for binding partners towards the corresponding lectins could be attached and combined. The fragment-based presentation might further simplify the evaluation of capable inhibitors.

After their successful synthesis, all homo- and heteromultivalent glycooligomers were subjected to different binding studies with P-dimer and LecB in close collaboration with other working groups from virology and enzymology. Both lectins possess four known binding pockets for fucosylated carbohydrates with different and relatively low binding affinities (K_D ~ mM) towards α-L-methylfucose in case of P-dimer (distances of binding pockets about 11 Å, 6 Å and 10 Å) whereas LecB exhibits a higher affinity towards α-L-methylfucose (K_D = 0.43 µM) and larger distances between the binding pockets with up to ~40-50 Å (35-37 Å for neighboring binding sites respectively).

To begin with, the interaction between homomultivalent fucose-oligomers and the viral P-dimer has been investigated by native MS measurements performed by Hao Yan and Dr. Charlotte Uetrecht, STD and CSP NMR conducted by Robert Creutznacher, Dr. Alvaro Mallagaray and Prof. Dr. Thomas Peters and co-crystallization experiments performed by Kerstin Ruoff, Dr. Turgay Kilic and Dr. Grant Hansman. The major finding, confirmed by all binding studies with P-dimer, was that only one fucose unit of glycooligomers can bind to the receptor, independent of the valency, spacing between fucose side chains and overall size of the oligomer. However, the interaction of glycooligomers with the P-dimer takes place with a fucose side chain and not with the oligomeric backbone as determined *e.g.* by epitope mapping (see Figure 20, left side), evaluating the glycooligo(amidoamines) again as suitable tools for the research in multivalent binding mechanisms towards lectins.

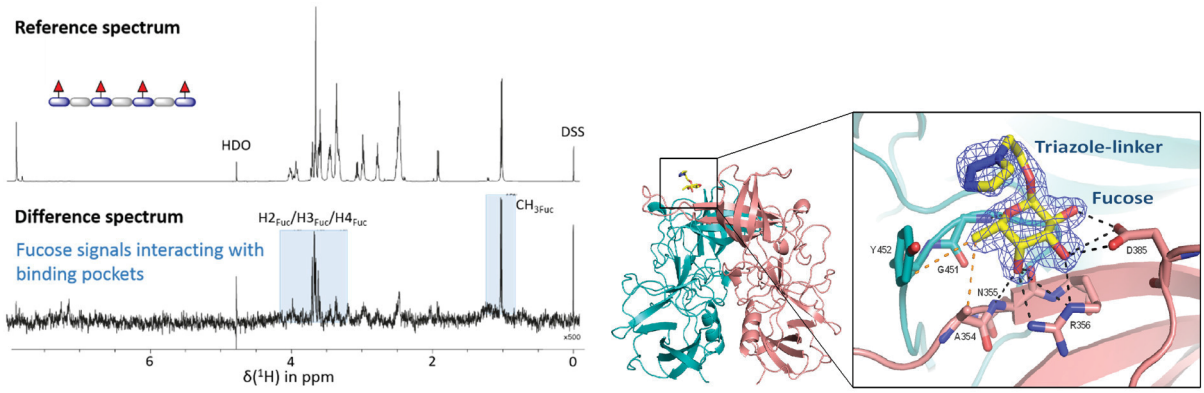

Figure 20: Results from STD NMR epitope mapping with tetravalent fucose-oligomer and P-dimer, performed by R. Creutznacher and Dr. A. Mallagaray (left); co-crystallization with P-dimer, conducted from K. Ruoff and Dr. T. Kilic (right). A*dapted with permission from K. S. Bücher et al, Biomacromolecules* ***2018****, 19 (9), 3714–3724. Copyright © 2018 American Chemical Society.*

Furthermore, monovalent negative control with one galactose side chain did not show binding to P-dimer as expected. CSP NMR measurements showed that the interaction of fucose units takes place with the same amino acids in the binding pocket of P-dimer as in case of natural ligands like pure α-L-methylfucose.

Although binding of P-dimer towards fucose is generally weak, most fucosylated glycooligomers bind strong enough to the lectin receptor to be successfully crystallized in complex with P-dimer (see Figure 20, right side). The dissociation constants of all homomultivalent fucose-oligomers are determined to be 200-400 µM by native mass spectrometry, exhibiting a 2-3 times lower binding affinity compared to the natural ligand HBGA B tetrasaccharide (110 µM) (see Table 1). In comparison, STD NMR results have shown that α-L-methylfucose binds about 40 times less than HBGA B tetrasaccharide. That leads to the assumption that the glycooligomers might enhance the overall binding towards P-dimer. Due to the fact that even monovalent fucose-oligomer binds as good as multivalently functionalized oligomers no statistical rebinding or chelation effects seem to promote the interaction with P-dimer. At higher concentrations of divalent fucose-oligomers the binding of a second glycooligomer molecule to the receptor could be partially observed. These oligomers exhibit a smaller size in comparison to most other tested fucose-oligomers due to the overall smaller chain length but also to less valency as proposed by MD-simulations. Overall, these studies showed that fucosylated glycooligomers are able to bind P-dimer, however, glycooligomers could not yet make use of any multivalent effects creating higher affinity glycomimetics. Based on the current findings, this is mainly attributed to sterical hindrance and therefore next generation glycooligomers could be based on smaller *e.g.* branched scaffolds.

*Table 1: Results from native MS measurements with fucose-oligomers and P-dimer, performed by H. Yan. Reprinted with permission from K. S. Bücher et al, Biomacromolecules **2018**, 19 (9), 3714–3724. Copyright © 2018 American Chemical Society.*

Glycooligomer	K_{D1} (µM)[a]	Concentration glycomacromolecule (µM)		
		100	150	200
Schematic structures		Averaged number of glycooligomers bound to one P-dimer		
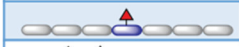	230 ± 50	1	1	1
	310 ± 90	1	1	2
	240 ± 60	1	2	2
	340 ± 130	1	1	2
	290 ± 90	1	1	2
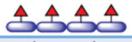	380 ± 100	1		1
	330 ± 80	1	1	1
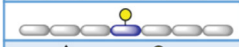	2400 ± 600	1	1	1
	370 ± 90	1		1
HBGA B	110 ± 30	2	3	3

Fucosylated glycooligomers have been further investigated in their binding towards LecB by surface plasmon resonance (SPR) and a modified form of ELLA (mELLA) in collaboration with Nikolina Babic and Dr. Filip Kovacic. For this purpose, first a suitable setup for an inhibition-competition assay in SPR measurements had to be developed. The main problem is the strong interaction of LecB towards fucosylated structures. During a direct binding assay, conjugating LecB to the chip surface and incubating with different concentrations of fucosylated glycooligomer, the oligomers could not be removed afterwards. This strong interaction reflects the difficulties to dissolve the hardly disruptive biofilms from *Pseudomonas aeruginosa*. The opposite assay allows for the complete destruction of LecB on the chip and enables reproducible measurements, though the life-time of sensor chip is much reduced in this assay due to accumulation of LecB and LecB-oligomer-complex. The applied inhibition-competition assay is a versatile method to investigate the binding of glycomimetic constructs towards LecB and has been shown the first time with SPR measurements.

The main result from binding studies is the enhanced inhibitory potential of fucosylated homomultivalent glycooligomers with increasing amount of fucose side chains on the binding of LecB to a polymeric fucosylated surface. In SPR measurements, a linear binding enhancement could be observed with an about 2-3 times increase in inhibitory potential per fucose unit compared to methylfucose while the variation of spacing with one up to three EDS-units within the three trivalent oligomers did not influence the inhibition (see Table 2). These findings are in agreement with results from literature, also confirming the validity of the SPR assay.[10,11]

Table 2: Results from inhibition competition assay of SPR with homomultivalent fucose-oligomers and LecB. Adapted *with permission from K. S. Bücher, N. Babic, T. Freichel, F. Kovacic, L. Hartmann, Macromol. Biosci.* ***2018****, 18 (12), 1800337 (1-8). Copyright © 2018 Wiley-VCH Verlag GmbH & Co. KGaA, Weinheim.*

Glycooligomer	n[a]	IC_{50} [nM][b]	RIP[c]	RIP/n[c,d]
MeFuc	1	381 ± 47	1	1
1	1	130 ± 12	2.9	2.9
2	2	65 ± 6	5.9	2.9
3	3	36 ± 6	10.6	3.5
4	4	36 ± 5	10.6	2.6
5	6	22 ± 3	17.3	2.9
MeFuc	1	397 ± 103	1	1
3	3	51 ± 5	7.8	2.6
6	3	57 ± 6	7.0	2.3
7	3	66 ± 6	6.0	2.0

[a]Number of fucose units on the oligomeric backbone. [b]IC_{50} values determined by three independent measurements with standard error of the mean value (SEM). [c]Relative inhibitory potencies (RIP) based on MeFuc, RIP = IC_{50} (MeFuc)/IC_{50} (glycooligomer). [d]Relative inhibitory potency per fucose unit of oligomer (RIP/n).

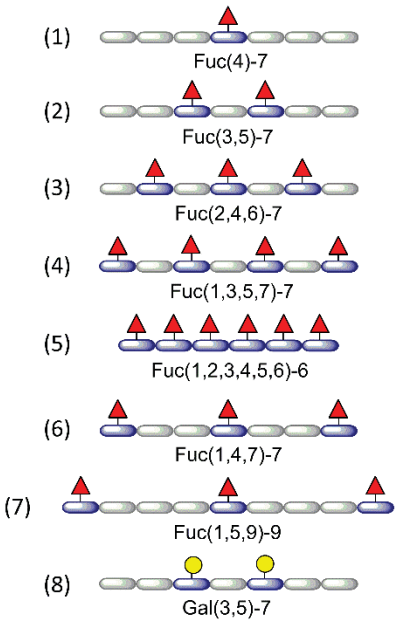

Results from mELLA assays show an about 30 times increased inhibition by the hexavalent oligomer (**5**). However, a trivalent (**6**) and a tetravalent (**4**) fucose-oligomer exhibit the highest inhibitory potential per fucose. These oligomers have one and two EDS-spacer units between the fucose-side chains and the same overall oligomer length. Although MD-simulations predict no influence of EDS-spacing on the presentation and distancing of fucose side chains in the secondary structure of flexible oligomers, these three tested trivalent oligomers showed significant differences in binding behavior in mELLA. At this point, this finding is attributed to the different set-ups of the binding assays with the SPR assay looking at preincubated ligand-receptor complexes while the mELLA assay looks at in situ competition between the glycooligomers and the glyco-functionalized surface. Further studies *e.g.* by light scattering should be performed to further evaluate these findings and the potential influence of the oligomer conformation on receptor binding.

SPR binding studies with LecB and fucosylated heteromultivalent glycooligomers with two fucose units and two moieties of a second carbohydrate (galactose, *N*-acetyl-galactosamine, lactose or sialic acid) did not show further enhancement in inhibition towards LecB. Homomultivalent control structure with four fucose side chains surprisingly did not further increase the inhibitory effect compared to homodivalent fucose-oligomer (**2**). At this point, this is attributed to a decreased availability of fucose side chains of the heteromultivalent oligomers, hampering the interaction with LecB. The overall observed increased inhibitory effects, especially in case of homomultivalent fucose-oligomers, are not attributed to chelate binding as this would lead to higher binding avidities per fucose unit but might be reasoned by statistical rebinding and by the influence of released water from the binding pockets

during the binding process. In literature especially dendritic fucosylated glycooligomers have been identified as high affinity ligands for LecB.[10,12] Nevertheless, the presented homomultivalent fucosylated glycooligomers exhibit higher inhibitory potencies than similar flexible oligomers previously presented in literature.[11] Therefore the presented studies of glycooligomer binding behavior towards LecB give important information for the development of next generation glycooligomers as potential LecB inhibitors. Finally, to gain first insights into their potential antibacterial properties, a first *in vivo* test looking at biofilm formation of *P. aeruginosa* in presence of the glycooligomers was conducted by Nikolina Babic and Dr. Fillip Kovacic. All fucosylated glycooligomers could reduce the amounts of biofilms of about 15-20% and showed a 2-3 times better efficacy than methylfucose (7%).

Overall, applying solid phase polymer synthesis glycooligo(amidoamines) presenting fucose in their side chains have been created giving access to precision fucosylated glycomimetics. In addition, a new building block was developed that enables the introduction of different carbohydrates in close proximity and thus generating an additional parameter to mimic complex glycans on the oligomeric scaffold. The here synthesized fucose-oligomers showed high potential not only as model structures to evaluate glycomimetic binding mechanisms but also in biomedical applications as shown by their interactions with viral and bacterial lectins.

Further developments based on the findings of this thesis should aim at increasing overall affinities. Fucosylated precision glycooligomers could be polymerized or attached to nanoparticles generating higher valent systems with different structural characteristics that could be tested for their binding behavior towards virus like particles (VLPs) of Norovirus. To further investigate binding mechanisms of single P-dimer the affinities and potential specificities of heteromultivalent HBGA-mimetics should be evaluated. The fucosylated glycooligomers can furthermore be transferred to multivalent HBGA tri- and tetrasaccharides presenting glycomimetics by enzymatic extension. To reduce the degree of freedom for the glycomimetics during the binding process the investigation of more rigid structures is in progress, thus fucosylated oligoproline helices can be tested. To explore the interaction of new compounds, a hemagglutination test might be an applicable binding assay for both lectins. For the successful disruption of biofilms of *P. aeruginosa* degradable fucosylated glycooligomers could be generated that might incorporate into the biofilms and dissolve them after an external trigger. The generated knowledge about structural influence for binding can subsequently benefit the development of suitable antibacterial or antiviral drugs. Their requirements would in addition demand further chemical transformations, as *e.g.* their stability against enzymatic degradation could be achieved by substitution of the glycosidic bond. In addition, the effective targeting of infected tissues could be induced. Furthermore, it would be necessary to evaluate if the backbone structures are metabolically harmless and investigate their pharmacokinetic behavior.

References

[1] D. Ponader, F. Wojcik, F. Beceren-Braun, J. Dernedde, L. Hartmann, *Biomacromolecules* **2012**, *13*, 1845.

[2] D. Ponader, P. Maffre, J. Aretz, D. Pussak, N. M. Ninnemann, S. Schmidt, P. H. Seeberger, C. Rademacher, G. U. Nienhaus, L. Hartmann, *J. Am. Chem. Soc.* **2014**, *136*, 2008.

[3] M. Tan, R. Hegde, X. Jiang, *J. Virol.*, **2004**, *78*, 6233.

[4] H. Schroten, F.-G. Hanisch, G. S. Hansman, *J. Virol.* **2016**, *90*, 5855.

[5] K. Marotte, C. Preville, C. Sabin, M. Moume-Pymbock, A. Imberty, R. Roy, *Org. Biomol. Chem.* **2007**, *5*, 2953.

[6] F. Wojcik, S. Mosca, L. Hartmann, *J. Org. Chem*. **2012**, *77*, 4226.

[7] C. Toonstra, M. N. Amin, L.-X. Wang, *J. Org. Chem.* **2016**, *81*, 6176.

[8] N. F. König, A. Al Ouahabi, S. Poyer, L. Charles, J.-F. Lutz, *Angew. Chem. Int. Ed.* **2017**, *56*, 7297.

[9] a) R. Loka, M. S. McConnell, H. M. Nguyen, *Biomacromolecules* **2015**, *16*, 4013. b) J. Guiard, B. Fiege, P. I. Kitov, T. Peters, D. R. Bundle, *Chem. Eur. J.* **2011**, *17*, 7438.

[10] B. Gerland, A. Goudot, G. Pourceau, A. Meyer, V. Dugas, S. Cecioni, S. Vidal, E. Souteyrand, J.-J. Vasseur, Y. Chevolot, F. Morvan, *Bioconjugate Chem.* **2012**, *23*, 1534.

[11] F. Morvan, A. Meyer, A. Jochum, C. Sabin, Y. Chevolot, A. Imberty, J.-J. Vasseur, E. Souteyrand, s. Vidal, *Bioconjugate Chem.* **2007**, *18*, 1637.

[12] a) E. M. V. Johansson, S. A. Crusz, E. Kolomiets, L. Buts, R. U. Kadam, M, Cacciarini, K.-M. Bartels, S. P. Diggle, M. Cámara, P. Williams, R. Loris, C. Nativi, F. Rosenau, K.-E. Jaeger, T. Darbre, J.-L. Reymond, *Chem. Biol.* **2008**, *15*, 1249. b) N. Berthet, B. Thomas, I. Bossu, E. Dufour, E. Gillon, J. Garcia, N. Spinelli, A. Imberty, P. Dumy, O. Renaudet, *Bioconjugate Chem.* **2013**, *24*, 1598.

Erklärung

Ich versichere an Eides Statt, dass die Dissertation von mir selbständig und ohne unzulässige fremde Hilfe unter Beachtung der Grundsätze zur Sicherung guter wissenschaftlicher Praxis an der Heinrich-Heine-Universität Düsseldorf erstellt worden ist. Diese Dissertationsschrift wurde in der vorliegenden oder einer ähnlichen Form noch bei keiner anderen Fakultät eingereicht. Ich habe bisher keine erfolglosen Promotionsversuche unternommen.

Frankfurt am Main, den 17.09.2018

Ort, Datum

Katharina Bücher